

UNIVERSITY OF MONS
NUCLEAR AND SUBNUCLEAR UNIT

UNIVERSITAT DE BARCELONA
DEPARTAMENT DE FÍSICA QUÀNTICA I ASTROFÍSICA AND INSTITUT DE CIÈNCIES DEL
COSMOS

THE QUANTUM THREE-BODY PROBLEM

BARYONS AND GLUEBALLS AS PIVOTAL EXAMPLES

CYRILLE CHEVALIER

SUPERVISOR:

PROF. CLAUDE SEMAY
PROF. VINCENT MATHIEU



Contents

Preface	vii
I The Three-body Problem in Non-Relativistic Quantum Mechanics	1
1 Framework: Equations and Properties	3
1.1 Schrödinger Equation and the Quantum Formalism	3
1.1.1 Quantum States and Observables	4
1.1.2 Hamiltonians for Three-body Systems	7
1.1.3 Eigenstates of Observables and Complete Sets of States	12
1.1.4 Symmetry and Identical Particles	16
1.1.5 Hamiltonian Eigenstates and the Time-Independent Schrödinger Equation	19
1.2 The Variational Theorems as Powerful Tools	20
1.2.1 The Rayleigh-Ritz Variational Theorem	20
1.2.2 The MacDonald Theorem	23
1.2.3 Convergence of the Upper Bounds	25
1.3 Miscellaneous Results	27
2 Oscillator Bases Expansions: a Versatile Resolution Method	33
2.1 The Theory of the Oscillator Bases Expansion	34
2.1.1 The Harmonic Oscillator Eigenstates	34
2.1.2 Three-body Hamiltonians and Jacobi Coordinates	40
2.1.3 Setup of the bases	42
2.1.4 Calculation of Matrix Elements	45
2.2 Including Spin Management	53
2.3 Tests of the Method	58
2.3.1 Tests with Two-body Interactions	59
2.3.2 Tests with Three-body Interactions	63

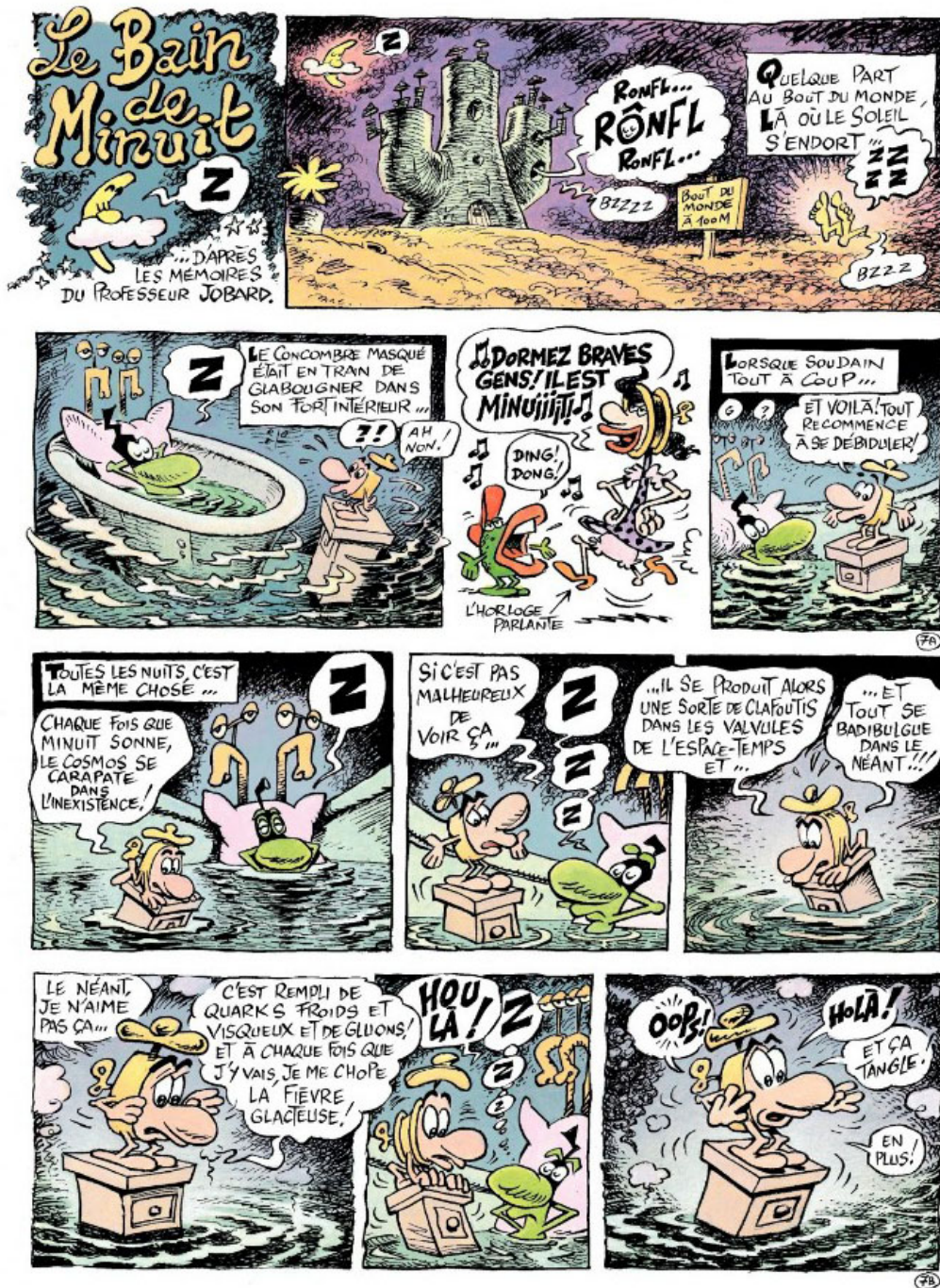
2.3.3	Tests with Two- and Three-body Interactions	65
2.4	Conclusion: Why the OBE?	67
	Complements	68
3	The Envelope Theory: a Step Toward Many-Body Systems	75
3.1	Envelope Theory for Systems of Identical Particles	77
3.1.1	The envelope theory as an auxiliary field method	77
3.1.2	Compact equations	81
3.1.3	Variational properties	85
3.1.4	Improvement of the envelope theory	88
3.1.5	Generalisations	99
3.1.6	Approximations of eigenstates and relation with the OBE	101
3.1.7	Accuracy tests	104
3.2	Envelope Theory for Systems of Different Particles	112
3.2.1	Auxiliary fields for systems of different particles	112
3.2.2	Compact equations for $N_a + N_b$ particles	115
3.2.3	Improvement for $N_a + 1$ particles	117
3.2.4	Tests of the ET for $N_a + 1$ particles	120
3.3	Conclusion: why the ET?	123
	Complements	124
II	Constituent Approaches of QCD and the Baryon Spectrum	129
4	Hadronic Physics: From Discovery to Quantum Chromodynamics	131
4.1	A short historical review of early hadron detections	131
4.2	Hadron classification and the quark hypothesis	134
4.2.1	Hadron classification	134
4.2.2	The quark hypothesis	139
4.3	Colour confinement and QCD	146
4.3.1	The QCD Lagrangian	147
4.3.2	Perturbation theory and Feynman diagrams	149
4.3.3	Miscellaneous QCD properties and non-perturbative approaches	152
4.3.4	Exotic particles	154
5	The Baryon Spectrum : an Example of Three-body Bound States	159
5.1	Modern constituent approaches	159

5.1.1	Short-range QCD potential	159
5.1.2	Long-range QCD potential	164
5.1.3	Mid-range behaviour and kinematics	167
5.2	The baryon spectrum	168
5.2.1	Nucleon-like baryons	168
5.2.2	Broader baryon spectrum	169
5.3	Conclusion: why constituent approaches ?	173

III The Helicity Formalism and Glueball Spectroscopy 179

6	Toward Relativistic Quantum Mechanics : the Helicity Formalism	181
6.1	The Poincaré group	182
6.1.1	The Poincaré algebra	182
6.1.2	Special Poincaré group transformations	184
6.2	One-body Helicity States	187
6.2.1	The one-body canonical states	187
6.2.2	The one-body helicity states	189
6.3	Two-body Helicity States	192
6.3.1	Helicity bases for two-body systems	192
6.3.2	Decomposition of a physical two-body state in J -helicity states	196
	Complements	197
7	Two-gluon Glueballs: Set Up of a Methodology	201
7.1	Calculations with physical two-body states	202
7.2	Two-gluon Glueballs	206
	Complements	212
8	Three-body Helicity Formalism: A Technical Extension	217
8.1	Berman's Definition	218
8.2	Wick's definition	223
	Complements	227
9	Three-gluon Glueballs: Broadening the Spectrum	241
9.1	Berman's basis for three-gluon systems	241
9.1.1	Three-gluon glueball states	244
9.1.2	Low-lying three-gluon Glueballs with negative charge conjugation	245

9.1.3	Selection of trial helicity-momentum wave functions	249
9.2	Evaluation of matrix elements	250
9.2.1	Evaluation on unsymmetrical states	251
9.2.2	Evaluation on symmetrical states	254
9.3	Determination of the low-lying Glueball Spectrum	257
9.4	Outlooks for the glueball spectrum	271
	Complements	271
	Conclusion and Outlooks	277
	List of Abbreviations	279



Extract from the comic book "Le concombre masqué" written by N. Mandryka. The special album is entitled "Le Bain de minuit". This work aims at demonstrating that quarks and gluons are warmer than announced in the strip.

Preface

Dear reader, let me begin this document by welcoming you and thanking you in advance for the time you will spend reading this work (or so I hope). As a soft introduction, let us begin with a brief meta-discussion about what this document is, what it is not, and the context in which it was written. This may not be as trivial as it seems, as the following chapters were written with several perspectives in mind. For this reason, the document can be approached from two different angles: as the keystone of a PhD thesis or as an introduction to hadronic physics. Both aspects are outlined in turn below.

This Document as the Keystone of a PhD Thesis

This document represents the culmination of a PhD thesis initiated at the University of Mons (UMONS) in September 2021. The original project, funded by the F.R.S.-FNRS, was titled *Study of Two-Gluon and Three-Gluon Glueballs within Constituent Models*. Glueballs are particles theoretically predicted in the early 1970s [1]. Despite this long-standing prediction, their experimental identification remains a topic of debate within the scientific community, primarily for two reasons [2]. First, theoretical predictions for glueballs are inherently challenging. Although different resolution methods exist, they generally struggle to produce consistent predictions beyond the energy spectrum [3]. Second, the lowest-lying glueballs are so similar to mesons that the actual physical states are most likely mixtures of glueballs and mesons. This makes the analysis of experimental data highly intricate and difficult to disentangle. Additional mesonic states, particularly within the f_0 - and η -meson families, have been observed in experimental spectra, yet interpreting these states with clarity remains extremely difficult. Significant efforts are underway at facilities such as PANDA, Crystal Barrel, WA102 and BESIII. Although promising evidence has already emerged [4], the results continue to be subject to debate within the community. The aforementioned project aims to help clarify this situation within its scope by providing new theoretical predictions. Moreover, extending the description to include three-gluon glueballs may open new experimental pathways for their detection, as

these prove less similar to mesons than the two-gluon ones.

However, the path taken to reach this goal was not a straight one, as with many research projects. Rather than a smooth journey, it involved many turns and unexpected detours. After four dedicated years, it became more appropriate to broaden the scope of the thesis from a narrow focus on glueballs to the wider topic of the three-body problem in quantum mechanics. This shift allows for a more cohesive treatment of the various aspects explored during the research, including those not ultimately applied to glueballs. That is why glueballs now feature only in the subtitle of the present document. It also made it possible to create a comprehensive text that can be approached with minimal prerequisites. This aspect is further detailed below in this preface.

Despite this broadening, the original research question remained a central guideline throughout the thesis. The goal of studying two-gluon, and especially three-gluon, glueballs motivated the majority of the calculations. Some approaches proved less relevant or more challenging to apply directly within a glueball context, while others succeeded in shedding light on these enigmatic particles. Small boxed texts at the end of each chapter summarize the role of the preceding chapter within the PhD project. These are entitled *"This chapter in the context of a thesis"*. Without spoiling the conclusion, I can already say that most of the project's objectives were at least approached. This does not imply that the present work brings the study of glueballs within constituent approaches to a close. On the contrary, the framework developed herein opens up new possibilities for deeper analysis and future research on these intriguing states.

The thesis also unfolded within a broader research environment. It was supervised by C. Semay in the Nuclear and Subnuclear Physics Unit at UMONS, and by V. Mathieu in the Departament de Física Quàntica i Astrofísica and Institut de Ciències del Cosmos at the universitat de Barcelona. Many aspects of this work were, and will continue to be, used by other members of these research teams. In particular, I would like to acknowledge L. Cimino, J. Viseur, C. Tourbez and C.T. Willemys who are helping to extend this research into other areas of hadronic physics. At various points in the following discussion, I attempt to pay tribute to their contributions by referencing their work and how it intersects with mine.

This Document as a Primer of Hadronic Physics

As mentioned earlier, beyond its purpose as a PhD dissertation, this document also aims to be self-contained and pedagogical as it could serve as starting point for further works. It is written with the assumption that the reader has at least a three-year undergraduate education in physical sciences. Such a background should be sufficient for understanding the first part of

the document, I hope this also holds true for the other two parts, despite the technical nature of some of the topics covered. As an introduction, let us briefly review the common tread running through each chapter.

- Chapter 1 introduces the subject by reviewing fundamental concepts from quantum mechanics, outlining key definitions, and introducing the notations used throughout the document. It does not aim to provide an exhaustive treatment of quantum mechanics, as can be found in references [5, 6, 7]. Rather, it emphasises certain aspects that are sometimes relegated to later chapters, such as the variational theorem. This chapter illustrates the pedagogical intent of the text.
- Chapter 2 builds on the previous section by presenting a resolution method known as the oscillator bases expansion (OBE). Consistent with the title of the document, it focuses on three-body systems. The method is illustrated and tested on various examples.
- Chapter 3 introduces a second resolution method, the envelope theory (ET), which is more user-friendly but also more approximate. As its computational cost is independent of the number of particles, calculations are presented for systems of N identical particles. A generalisation to systems containing two different kinds of particles is also proposed. This concludes the first part of the document, devoted to non-relativistic and semi-relativistic quantum mechanics in general.
- Chapter 4 introduces hadronic physics from several perspectives. It begins with a historical overview of the emergence of this field, followed by discussions on hadron classification and the quark hypothesis. The chapter concludes with a brief review of the modern theory of the strong interaction, namely quantum chromodynamics (QCD). Rather than being exhaustive, this chapter aims to summarize the concepts necessary for understanding the subsequent developments.
- Chapter 5 applies the previously introduced methods and concepts to the study of hadrons, and particularly baryons. It presents the framework of constituent approaches, which will be used throughout the remainder of the document. The chapter frequently refers back to concepts introduced in the previous one. Constituent models are also illustrated through the derivation of a baryon spectrum and a discussion on the emergence of internal diquarks. This concludes the second part of the text, which introduced hadron physics and constituent approaches.
- Chapter 6 opens a new perspective on constituent approaches by partially reconciling them with special relativity. It introduces the definitions and properties of the different Lorentz

covariant complete sets of states from the helicity formalism. These are then employed to decompose two-body bound states, including those containing massless constituents.

- Chapter 7 builds on the results of the previous chapter to develop a methodology for deriving spectra from the aforementioned Lorentz-covariant states. These calculations are applied to two-gluon glueballs and compared with results obtained from other resolution methods.
- Chapter 8 generalises the helicity formalism to three-body systems. It echoes Chapter 6, as it also introduces definitions and properties necessary for later developments. Relevant properties are demonstrated in complementary sections.
- Finally, Chapter 9 applies the previously established methodology to three-body systems, focusing on the study of three-gluon glueballs. The chapter concludes with a discussion of the resulting spectrum and a comparison with results obtained using other resolution methods.

I hope that reading this document will provide sufficient foundation for entering the intricate field of hadronic physics. While not exhaustive, this work aims to present the main theoretical approaches used to study hadrons in the context of effective theories. Technical resolution methods are consistently illustrated with numerous examples. Most of the models discussed strive to reproduce experimental data in a concise and economical manner, by identifying and highlighting the essential physical mechanisms relevant to each system. Although the resulting theories are phenomenological in nature, attention is given to justifying their components by referring to more fundamental, although more complex, approaches.

Only the final two chapters depart somewhat from this editorial approach, offering a slightly more technical discussion on three-gluon glueballs. These chapters can be seen as an introduction to, or illustration of, more advanced topics, providing a perspective on how the tools and descriptions developed earlier can be generalised to more complex systems.

This Document as the Conclusion of Four Years

As a final aspect beyond the academic content, this text also marks the conclusion of four years during which I had the opportunity to meet many people and receive from many others. I would like to take this moment to thank all of these invaluable, though sometimes indirect, contributors. I will switch to my native language when appropriate.

Sur le plan professionnel, je me dois avant tout de remercier mes promoteurs, Claude et Vincent qui ont eu la patience de m'encadrer tout du long de ces quatre années. Je ne les remercierai jamais assez pour m'avoir permis d'avancer, à mon rythme, et en m'apportant à intervalles réguliers l'aide et les réponses dont j'avais besoin. Outre leur rôle d'encadrants, leur supervision m'a énormément appris, tant concernant la physique que la gestion d'un projet. Si je termine cette thèse avec un tel bagage, c'est avant tout grâce à eux. Je retiens également plus simplement les moments passés hors du cadre professionnel, autour d'un bon repas par exemple. Outre mes promoteurs, je me dois aussi de remercier mes collaborateurs, plus ou moins proches. Je commencerai par mentionner Lorenzo avec qui j'aurai passé au total trois ans de co-doctorat. Merci pour toutes ces discussions enrichissantes sur les nombreuses zones de recouvrement entre nos thèses respectives. Dans ce même ordre d'idée, je me dois également de remercier Fabien pour nos échanges réguliers et constructifs quant aux boules de glue. Au rang des retours instructifs, j'aimerais également remercier Jérémy pour le temps qu'il a consacré à la relecture d'un de mes articles, contribuant ainsi largement à sa publication. De retour au sein du service, je souhaite saluer Cintia qui, même si moins directement concernée par mon projet, aura elle aussi contribué à un environnement de travail agréable et positif. Je terminerai en citant les différents étudiants qui sont venus travailler dans notre service. Dans l'ordre d'ancienneté, il y a Ethan, Joachim, Thomas, Clara, Selma, Amaël et enfin Lucie. Merci à tous pour la confiance que vous nous avez accordé en nous laissant prendre part à votre formation. Puisque la majorité d'entre vous se lancent également dans l'aventure d'un doctorat, je suppose que ce passage chez nous ne s'avéra pas trop traumatisant. Particulièrement, je lègue tous mon courage et ma motivation à Joachim et Clara qui tentent cette aventure dans le même service que moi.

Dans un autre registre, mes pensées vont également aux membres de ma famille, qui m'ont soutenu chacun à leur manière durant ces quatre années. Comment ne pas commencer par Mo avec qui je partage ma vie depuis sept ans maintenant. Nous vivons d'autant plus cette aventure à deux, qu'elle s'est également lancée dans une thèse, en biologie moléculaire en ce qui la concerne. Nous nous soutenons mutuellement, partageant joies et angoisses, pour le meilleur et pour le pire. Mes parents ont évidemment eux aussi une place privilégiée dans cette section. Dire qu'ils m'ont soutenu durant ma thèse n'est qu'un doux euphémisme, puisque c'est depuis ma naissance qu'ils remplissent un tel rôle. Puisqu'il y aurait bien trop à dire pour tenir en un si petit paragraphe, je me contenterai d'un sobre "merci", faisant office pour sous-entendre tout ce que j'ai dans le cœur. Mon frère mérite également une mention particulière. C'est sûrement en suivant inconsciemment ses traces que je me retrouve en ce moment même à écrire ces quelques lignes. Il me berçait en me récitant ses leçons de rétho, il y a de cela 27 ans. Aujourd'hui, c'est en préparant mes communications orales que je berce son merveilleux fils, Alexandre, qui nous a

fait le plaisir d'entrer dans notre famille, il y a un mois à peine. Sans oublier Jackie, je souhaite à leur petite famille le meilleur pour l'avenir.

Enfin, un doctorat est aussi parsemé de rencontres et d'amis. Suivant une hiérarchie chronologique, je mentionnerai tout d'abord mes amis du collège qui m'ont soutenu, chacun à leur manière. Entre parcs d'attraction et restaurants, entre blagues et discussions de vieux, entre whist et dofus, vous avez extirpé mon esprit de ses réflexions scientifiques en des moments parfois très opportuns. Outre ces amitiés de longue date, l'université et le doctorat m'ont fait rencontrer énormément de personnes d'horizons divers et variés. À ce titre, je me dois de mentionner la table des physiciens à la cantine dont les membres les plus récurrents furent Alice, Antoine, Florent, Ludo, Lorenzo, Seb, Steve et Thomas. Qu'on la tente, qu'on appelle le chien ou qu'on propose cœur, cette table n'a eu de cesse de générer des instants tous plus mémorables les uns que les autres. Outre la team physicien, je me dois de citer également la team jeudi-jeu dont les réunions ont le don de rompre la routine quotidienne, et ce malgré le parfum latent de biologie-médicale qu'il y règne. Une de mes pensées va également à tous les étudiants à qui j'ai eu le plaisir d'enseigner la physique statistique et/ou la mécanique quantique. Vous avez toujours été bienveillants et respectueux, si bien que je n'ai, en quatre ans, jamais dû élever la voix. Pensez bien que je suis fier de chacun d'entre vous. Finally, and certainly not least, I return to English to acknowledge all the people I met at conferences and doctoral training schools. How could I forget Enrico? Thank you for your joy, your energy, and the nice project we worked on together in Trento. It is perhaps one of the achievements I am most proud of. Many thanks also to Andre and Guilherme, we met on several occasions, and it was always a pleasure. I also had the chance to meet many other kind and inspiring people in Trento, Sevilla, Mainz, Salamanca, Barcelona and Osaka. Unfortunately, my memory for names is not the best, so I may not recall every name individually, but please know that your warm welcome and support have not gone unnoticed.

I could surely continue this list for another full page of acknowledgements. However, I think it is time to return to more physics-oriented discussions. Let me close with a heartfelt thank you to everyone who contributed to my work, directly or indirectly, even if I could not mention you all by names.

Part I

The Three-body Problem in Non-Relativistic Quantum Mechanics

Chapter 1

Framework: Equations and Properties

This first chapter reviews the foundation principles underlying what is commonly referred to as *the three-body problem in non-relativistic quantum mechanics*. A reader already acquainted with this theory may not encounter many new concepts in this chapter, but even for such an audience, revisiting the essential ideas and terminologies related to this topic seems worthwhile. Conversely, for readers with only a basic understanding of the quantum domain, this chapter aims to introduce, as precisely and concisely as possible, the indispensable concepts necessary to approach the rest of this document. Section 1.1 summarizes the key notions of the quantum formalism, with particular attention to systems of three particles. Following the approach found in many textbooks [5, 6] (though not all [7]), this chapter primarily relies on the Schrödinger equation. Section 1.2 presents a less conventional perspective on this equation, leading to a family of results collectively known as *variational theorems*. The chapter concludes in Section 1.3 with a non-exhaustive list of miscellaneous properties which will be referenced at various points throughout the document.

1.1 Schrödinger Equation and the Quantum Formalism

In 1926, Erwin Schrödinger formulated an equation that became a cornerstone of the discipline latter known as quantum mechanics. In its modern formulation, this equation is expressed as follows,

$$i\hbar \frac{\partial}{\partial t} |\Psi(t)\rangle = H |\Psi(t)\rangle. \quad (1.1)$$

The Schrödinger equation will serve here as a natural starting point to introduce and discuss the fundamental concepts underlying the quantum formalism. The two primary objects to define in (1.1) are $|\Psi(t)\rangle$ and H . Both are addressed in the following section.

1.1.1 Quantum States and Observables

The Schrödinger equation governs the time evolution of the system's state, denoted in (1.1) as $|\Psi(t)\rangle$. For a given system of particles, the set of all possible states is formally endowed with the structure of a Hilbert space over the field of complex numbers, \mathbb{C} . An Hilbert space refers to a vector space equipped with an inner product and complete under the norm induced by that product. In the language of physicists, introducing the structure of a vector space for quantum states is often referred to as the superposition principle in quantum mechanics. The inner product of two states, say $|\Psi_1\rangle$ and $|\Psi_2\rangle$, is a complex number denoted $\langle\Psi_1|\Psi_2\rangle$. This operation allows to define, for any state $|\Psi_1\rangle$, an application, denoted $\langle\Psi_1|$, corresponding to taking the inner product with it,

$$\begin{aligned} \langle\Psi_1| : \mathcal{H} &\longrightarrow \mathbb{C}, \\ |\Psi_2\rangle &\longmapsto \langle\Psi_1|\Psi_2\rangle. \end{aligned} \tag{1.2}$$

Above, \mathcal{H} denotes the aforementioned Hilbert space of all the quantum states. According to the terminology introduced by Paul Dirac, the system's state $|\Psi_1\rangle$ is referred to as a *ket*, while the corresponding operation $\langle\Psi_1|$ is termed a *bra*. Combining both terminologies gives rise to the word *bracket*, which refers to the notation used for the inner product. Dirac's notation is clever in the sense it makes very natural to apply bras on kets¹,

$$\langle\Psi_1|(|\Psi_2\rangle) = \langle\Psi_1|\Psi_2\rangle. \tag{1.3}$$

Before to move on to the description of H , let us mention that, to be considered as *physical*, a quantum state must satisfy a normalisation condition requiring that its modulus always equals one. This requirement is tied to the way quantum states are interpreted, a topic addressed in a few paragraphs.

Because equation (1.1) rules the evolution of the system's state, it logically incorporates at some point the nature of the system's components and, if relevant, their interaction with one another and with the environment. These aspects are encapsulated in a linear Hermitian operator acting on the system's states, known as the Hamiltonian and typically denoted by H . A given linear operator \mathcal{O} on \mathcal{H} is said to be *Hermitian* if, in an inner product, its action on

¹ However, this apparent easiness of use may lead to some mathematical misconceptions and/or inconsistencies [8]. As soon as this danger increases, the user should rely on the true mathematical nature of $\langle\Psi|$ and $|\Psi\rangle$ more than on any notation trick.

the ket is equivalent to its action on the bra,

$$(\langle \Psi_1 | \mathcal{O} | \Psi_2 \rangle = \langle \Psi_1 | (\mathcal{O} | \Psi_2 \rangle). \quad (1.4)$$

Above, the notation $(\langle \Psi_1 | \mathcal{O})$ refers to the bra associated to the ket $\mathcal{O} | \Psi_1 \rangle$. Hermiticity can also be defined referring to *Hermitian adjoint operators*. Let \mathcal{O} be a linear operator, its Hermitian adjoint is denoted \mathcal{O}^\dagger and satisfies

$$(\langle \Psi_1 | \mathcal{O} | \Psi_2 \rangle = \langle \Psi_1 | (\mathcal{O}^\dagger | \Psi_2 \rangle). \quad (1.5)$$

Therefore, an operator \mathcal{O} is Hermitian as soon as $\mathcal{O} = \mathcal{O}^\dagger$. Physically, observable quantities are represented in the formalism by Hermitian operators². For instance, the Hamiltonian is associated with the observable that is the total energy of the system. Observables and their associated operators are endowed with an important operation called the *commutator*. For two Hermitian operators \mathcal{A} and \mathcal{B} corresponding to different observables, the commutator $[\mathcal{A}, \mathcal{B}]$ is defined via the usual sum and composition of operators as follows,

$$[\mathcal{A}, \mathcal{B}] = \mathcal{A}\mathcal{B} - \mathcal{B}\mathcal{A}. \quad (1.6)$$

This operation can reveal important information about the relationship between observables, sometimes unveiling underlying group structures. It also characterises the extent to which the operators associated with two observables fail to commute. The significance of the commutator should become even clearer in Section 1.1.3.

The fundamental objects of the quantum formalism having been introduced, it is time to briefly discuss their interpretation. As seen in the previous paragraphs, compared to classical mechanics, the quantum formalism assigns a fundamentally different nature to states and observables. For that matter, interpreting quantum mechanics remains a controversial topic, deserving its own dedicated chapter. However, the scientific community agrees on a minimal interpretation known as *Born rule*. This rule explains how to deduce the outcomes of a measurement performed on a system from the state of the system, $|\Psi(t)\rangle$, and the Hermitian operator associated with the measured observable, \mathcal{O} . To start with, the rule identifies states for which a measurement of \mathcal{O} yields a definite value $f(o) \in \mathbb{R}$ with certainty. Such determinate

² The relationship between classical observables and Hermitian operators is highly non-trivial. Readers interested in an in-depth introduction to this topic are referred to [9].

states, denoted $|o; \alpha\rangle$, satisfy by definition the following equation,

$$\mathcal{O} |o; \alpha\rangle = f(o) |o; \alpha\rangle. \quad (1.7)$$

Concerning terminology, $|o; \alpha\rangle$ is called an *eigenvector* or *eigenstate* of \mathcal{O} , and $f(o)$ is its corresponding *eigenvalue*. The set of all the eigenvalues of an operator \mathcal{O} is named its *spectrum* and solving equation (1.7) to determine all eigenvalue-eigenvector pairs constitutes an *eigenvalue problem*. The Hermitian nature of \mathcal{O} ensures that its spectrum is real [5, 6]. A few comments regarding eigenstates $|o; \alpha\rangle$ are worth noting. In the following, eigenstates are assumed to be normalised.

- The label o in $|o; \alpha\rangle$ serves to indicate that this state is, by definition, an eigenvector of \mathcal{O} with eigenvalue $f(o)$. Such labels are typically referred to as *quantum numbers*³. Eigenstates with different eigenvalues are known to be orthogonal [5, 6].
- The label α differentiates linearly independent eigenstates that share the same eigenvalue o . These eigenstates are described as *degenerate*. If two eigenstates are degenerate, then any linear combinations of these states is also an eigenstate of \mathcal{O} with the same eigenvalue [5, 6]. This property can be exploited, for instance, to orthogonalise degenerate states. The orthogonalisation process is assumed to be carried out in what follows.
- To be physical, like any state, an eigenvector must be normalised. In general, only a countable number of eigenvalues yield normalisable eigenstates. For continuous eigenvalues, it is impossible for the system to access a normalisable state for which any measurement of the observable would yield that value with certainty. However, it does not imply that the associated eigenstates should be disregarded entirely; rather, they cannot independently describe physical systems. In such case, the notation is somewhat misleading: although the eigenvectors are not genuine quantum states, they are still denoted as such.
- The complete definition of observable actually requires its eigenvectors span the entire Hilbert space. As a result, for any state $|\Psi\rangle$, there exist coefficients $c_{o;\alpha}$ such that⁴

$$|\Psi\rangle = \sum_o \sum_\alpha c_{o;\alpha} |o; \alpha\rangle. \quad (1.8)$$

³ In some cases, the eigenvalue is directly used as the quantum number (that is, $f(o) = o$), but in most cases, for notational convenience, the quantum number simply indicates the eigenvalue.

⁴ In some cases, all or part of these sums may turn into integrals if labels σ or α are continuous. Such situations are not treated for now and will be encountered later.

These coefficients are obtained as the inner product of $|\Psi\rangle$ with the eigenvectors: $c_{o;\alpha} = \langle o; \alpha | \Psi \rangle$. This expansion is related to the concept of *completeness relation* for $|o; \alpha\rangle$,

$$|\Psi\rangle = \sum_o \sum_\alpha |o; \alpha\rangle \langle o; \alpha | \Psi \rangle \implies \sum_o \sum_\alpha |o; \alpha\rangle \langle o; \alpha| = \mathbb{1}. \quad (1.9)$$

Concrete examples of completeness relations are discussed in Section 1.1.3.

Let $|\Psi\rangle$ denote a generic state, the Born rule states that the probability $\mathcal{P}(o)$ of obtaining a value o upon measuring \mathcal{O} is given by

$$\mathcal{P}(o) = \sum_\alpha |\langle o; \alpha | \Psi \rangle|^2. \quad (1.10)$$

In cases where $|o\rangle$ is non-normalisable, o belongs to a continuum, and $\mathcal{P}(o)$ represents the probability density associated with a measurement of \mathcal{O} . Such situations will be encountered in Section 1.1.3. The probabilistic interpretation (1.10) leads to a compact expression for the expectation value for the measurement of \mathcal{O} on the state $|\Psi\rangle$,

$$\begin{aligned} \langle \Psi | \mathcal{O} | \Psi \rangle &= \sum_{\bar{o}, \bar{\alpha}} \sum_{o, \alpha} \langle \Psi | \bar{o}; \bar{\alpha} \rangle \langle o; \alpha | \Psi \rangle \langle \bar{o}; \bar{\alpha} | \mathcal{O} | o; \alpha \rangle \\ &= \sum_{o, \alpha} |\langle o; \alpha | \Psi \rangle|^2 o = \sum_o \mathcal{P}(o) o = \langle \mathcal{O} \rangle. \end{aligned} \quad (1.11)$$

Evaluating the expression $\langle \Psi | \mathcal{O} | \Psi \rangle$ is sometimes referred to as evaluating \mathcal{O} on $|\Psi\rangle$. Apart from computing expectation values, combining equations (1.8) and (1.10) also justifies the normalisation condition: normalisation ensures that the total probability of all the possible outcomes sums to one.

So far, the notions introduced have remained fully general. To explore more concrete aspects, the next section delves deeper into the description of Hamiltonian operators. Along the way, introducing additional observables and their corresponding operators will be necessary.

1.1.2 Hamiltonians for Three-body Systems

Being related to the energy of the system, Hamiltonian operators are often expressed in terms of more fundamental observables, such as the positions and momenta of the particles. Since this document is devoted to three-body systems, let us illustrate this statement within that context.

Hamiltonian operators for three particles are typically structured as follows,

$$H = T(\mathbf{p}_1, \mathbf{p}_2, \mathbf{p}_3) + \sum_{i < j=1}^3 V_{ij}(|\mathbf{r}_i - \mathbf{r}_j|) + W(\mathbf{r}_1, \mathbf{r}_2, \mathbf{r}_3) \quad (1.12)$$

Above, \mathbf{r}_i serves as a shorthand notation for (r_{ix}, r_{iy}, r_{iz}) , the three Hermitian operators corresponding to the components of the i^{th} particle's position. Similarly, \mathbf{p}_i represents (p_{ix}, p_{iy}, p_{iz}) , the components of the i^{th} particle's momentum. Combinations of these vectors, such as $|\mathbf{r}_i - \mathbf{r}_j|$, must be understood as compact notations for the corresponding combinations of the components. Operators r_{ia} and p_{jb} with $i, j \in \{1, 2, 3\}$ and $a, b \in \{x, y, z\}$ are, by definition, related through the following commutators⁵,

$$[r_{ia}, p_{jb}] = i\hbar\delta_{ij}\delta_{ab}, \quad [r_{ia}, r_{jb}] = 0, \quad [p_{ia}, p_{jb}] = 0. \quad (1.13)$$

From these commutators, most of the properties of r_{ia} and p_{jb} can be deduced and any set of variables satisfying similar commutation relations will exhibit analogous properties. Such sets of variables are referred to as *conjugate variables*.

In expression (1.12), T_i , V_{ij} and W are arbitrary functions of the operators on which they depend⁶. These functions decompose the Hamiltonian into four distinct sets of terms. Terms involving a V function account for the possibility of pairwise particle interactions. Due to the requirement of translational invariance, these so-called *two-body interactions* depend only on the relative position between the two particles. In this work, two-body interactions are assumed to depend solely on the modulus of this relative position. Systems in which the orientation of the relative position affects the interaction, such as those involving tensor forces, do exist but are not considered here. The second contribution to the potential energy involves a function W . This generic interaction depends simultaneously on the position of three particles and is referred to as a *three-body interaction*. As with two-body interactions, they are generally assumed to be translation invariant. Genuine three-body interactions occur in many physical systems, such as helium clusters [10], atomic nuclei [11] or hadrons [12, 13, 14, 15, 16]. However, these interactions are generally challenging to handle. In the following, W will be assumed to

⁵ An informed reader may recognise in these relations the fundamental Poisson bracket from Hamiltonian mechanics. This resemblance reflects the foundational principles behind the introduction of position and momentum operators in quantum mechanics.

⁶ The definition of functions of operators acting on an Hilbert space is beyond the scope of this discussion. Interested readers are referred to [6] for further details.

depend on the particle positions through a specific combination, denoted by ρ ,

$$\rho = \sqrt{(\mathbf{r}_1 - \mathbf{r}_2)^2 + (\mathbf{r}_1 - \mathbf{r}_3)^2 + (\mathbf{r}_2 - \mathbf{r}_3)^2}. \quad (1.14)$$

This specific structure, while less common in theoretical models, may serve as an approximation for a more complex three-body interaction. For example, such three-body forces have been successfully used to describe physical systems like baryons [13, 14, 15, 12] and helium clusters [10]. It is also possible to include other interaction potentials, such as *one-body interactions*, defined as follows,

$$\sum_{i=1}^3 U_i(|\mathbf{r}_i - \mathbf{R}_{\text{CM}}|). \quad (1.15)$$

Above, $\mathbf{R}_{\text{CM}} = (m_1\mathbf{r}_1 + m_2\mathbf{r}_2 + m_3\mathbf{r}_3)/M$ and $M = m_1 + m_2 + m_3$ represent the centre-of-mass position and the total mass of the system, respectively, in a non-relativistic framework. The inclusion of the centre-of-mass position \mathbf{R}_{CM} is required by translational invariance. However, one-body interactions are less common than two- and three-body ones and are typically employed as approximations for more sophisticated potentials. Such interactions will not be further explored in the following.

The term involving the function T in (1.12), which represents the relative kinetic energy of the system, still remains to be discussed. For non-relativistic particles with respective masses m_i , it is typically expressed as follows,

$$T(\mathbf{p}_1, \mathbf{p}_2, \mathbf{p}_3) = m_1c^2 + m_2c^2 + m_3c^2 + \frac{\mathbf{p}_1^2}{2m_1} + \frac{\mathbf{p}_2^2}{2m_2} + \frac{\mathbf{p}_3^2}{2m_3} - \frac{\mathbf{P}^2}{2M}. \quad (1.16)$$

Above, $\mathbf{P} = \mathbf{p}_1 + \mathbf{p}_2 + \mathbf{p}_3$ is the total momentum of the system. For further applications in particle physics, the mass energy of each particle has been incorporated into the kinetic energy, and contribution from the centre-of-mass motion is subtracted to ensure Galilean invariance. For light particles, a semi-relativistic version is sometimes used in phenomenological models,

$$T(\mathbf{p}) = \sqrt{m_1^2c^4 + \mathbf{p}_1^2c^2} + \sqrt{m_2^2c^4 + \mathbf{p}_2^2c^2} + \sqrt{m_3^2c^4 + \mathbf{p}_3^2c^2}. \quad (1.17)$$

In this case, the energy due to the centre-of-mass motion is not explicitly subtracted. To eliminate any contamination of the energy from the global motion of the system, occurrences of \mathbf{P} in this expression must be manually removed, by imposing $\mathbf{P} = \mathbf{0}$. While definition (1.17) provides better agreement with experimental results for relativistic particles, it should not, under any circumstances, be interpreted as an attempt to make Schrödinger's equation covariant.

The previous description was limited to spatial components. Beyond position variables, a

quantum particle may also be characterised by other degrees of freedom, such as spin, isospin, or color. For the remainder of this section, we will focus on spin. Spin was first introduced to explain the splitting of certain energy levels in atomic spectra under the influence of magnetic fields. Wolfgang Pauli proposed that the electron possesses a new intrinsic degree of freedom that spans a two-dimensional vector space [17]. According to Pauli, this property, later named spin, is responsible for the observed splitting through its interaction with the external magnetic field. This hypothesis was subsequently validated by the Stern-Gerlach experiment and through observations of the hyperfine structure in atomic spectra. Formally, the introduction of spin expands the set of fundamental operators available to construct a Hamiltonian. The fundamental spin-related operators correspond to the spin components along the three spatial directions, S_{ix} , S_{iy} , and S_{iz} . These operators satisfy the following commutation relations,

$$[S_{ia}, S_{jb}] = i\hbar\delta_{ij} \sum_{c \in \{x,y,z\}} \epsilon_{abc} S_{ic} \quad (1.18)$$

where $i, j \in \{1, 2, 3\}$, $a, b \in \{x, y, z\}$, and ϵ_{abc} is the fully antisymmetric Levi-Civita symbol with $\epsilon_{xyz} = 1$. For notational convenience, the spin operators of each particle are often represented as three-vectors \mathbf{S}_i . Up to a factor of \hbar , commutation relations (1.18) reveal that the spin operators of each particle obey the same structure as the algebra of the group $SO(3)$. While no two spin components of a given particle commute, it is possible to construct an operator for each particle that commutes with all spin components. These operators are known as the spin Casimirs and are denoted S_i^2 ,

$$S_i^2 = \mathbf{S}_i^2 = S_{ix}^2 + S_{iy}^2 + S_{iz}^2. \quad (1.19)$$

By either direct computation from (1.18) or through group-theoretical considerations, one can verify that

$$[S_i^2, S_{ja}] = 0. \quad (1.20)$$

The action of a spin Casimir characterises the total spin of the corresponding particle. Specifically, a particle is said to have a total spin s if its state is an eigenstate of S_i^2 with eigenvalue $\hbar^2 s(s+1)$. In light of the Born rule, this definition ensures that any measurement of the particle's spin yields its total spin value with certainty. The total spin also determines the possible eigenvalues of the spin component operators. For a spin- s particle, there are $2s+1$ spin component eigenvalues, ranging from $-s\hbar$ to $s\hbar$ in steps of \hbar . In Pauli's theory, the electron is described as having spin $1/2$ which, as noted earlier, endows the particle with a two-dimensional intrinsic vector space spanned by the two possible spin projections, $+\hbar/2$ and $-\hbar/2$. The fundamental nature of spin

will be explored in greater depth in Part III.

Spin operators can appear in Hamiltonians in various forms. One such form, encountered for example in the description of the baryon spectrum, involves a two-body interaction proportional to the inner product of the spin operators in order to form a scalar,

$$V_{ij}^{SS} = V_{ij}(|\mathbf{r}_i - \mathbf{r}_j|) \mathbf{S}_i \cdot \mathbf{S}_j \quad (1.21)$$

Above, V_{ij} is an arbitrary function of the operator associated with the relative distance between particle i and j . More generally, spin degrees of freedom can also interact with other observables, such as orbital angular momentum through so-called spin-orbit couplings. While such interactions are not explored further in this document, the corresponding observable plays a fundamental role in the following discussions and deserves a minimal introduction. For each particle, the orbital angular momentum is again represented by three operators corresponding to its three components. Unlike spin, orbital angular momentum operators are derived from position and momentum operators, as per the classical definitions,

$$L_{ix} = r_{iy}p_{iz} - r_{iz}p_{iy} \quad L_{iy} = r_{iz}p_{ix} - r_{ix}p_{iz} \quad L_{iz} = r_{ix}p_{iy} - r_{iy}p_{ix}. \quad (1.22)$$

These relations, which are often summed up as $\mathbf{L}_i = \mathbf{r}_i \times \mathbf{p}_i$, can be used to demonstrate that the orbital angular momentum operators satisfy commutation relations analogous to those of spin operators,

$$[L_{ia}, L_{jb}] = i\hbar\delta_{ij} \sum_{c \in \{x,y,z\}} \epsilon_{abc} L_{ic}. \quad (1.23)$$

As a result, spin and orbital angular momentum share the same $SO(3)$ algebraic structure, which justifies the common interpretation that they possess similar natures. As with spin, the orbital angular momentum of each particles also has a Casimir operator that commutes with all its components,

$$L_i^2 = L_{ix}^2 + L_{iy}^2 + L_{iz}^2. \quad (1.24)$$

Angular momentum components and their corresponding Casimirs play a crucial role in solving the Schrödinger equation. As noted earlier, the former are sometimes included in Hamiltonians through spin-orbit interactions (proportional to $\mathbf{L}_i \cdot \mathbf{S}_i$), while the latter naturally emerge when the equation is expressed in spherical coordinates. Before concluding this section, it is worth mentioning that the above definitions describe orbital angular momenta for individual particles. Equivalent definitions for any combination of particle positions can be derived by replacing \mathbf{r}_i and \mathbf{p}_i in definitions (1.22) with the appropriate conjugate variables. For example,

the angular momentum associated with the relative position between two particles is obtained by substituting $\mathbf{r}_i - \mathbf{r}_j$ and $(\mathbf{p}_i - \mathbf{p}_j)/2$ for \mathbf{r}_i and \mathbf{p}_i in (1.22).

Finally, other internal degrees of freedom, such as the aforementioned isospin and color, will not be addressed in the current work. Briefly, the underlying principle is similar to that of spin: an intrinsic vector space is introduced, on which new operators act, and interactions involving these operators are explicitly incorporated into the Hamiltonian. For additional information, the interested reader is referred to [18, 19].

1.1.3 Eigenstates of Observables and Complete Sets of States

During the discussion of three-body Hamiltonians, various observables have been introduced. Exploring the associated eigenvalue equations (1.7) is particularly valuable, as the eigenstates they define provide the fundamental building blocks for interpreting quantum states. To achieve the most precise interpretation, one might ask whether it is possible to define a common set of eigenstates for multiple observables simultaneously. This proves indeed possible, provided that all the observables commute with one another. Constructing a set of common eigenstates for the maximum number of independent observables leads to the concept of complete sets of states. The associated completeness relations provides tools for concretely representing quantum states. These complete sets and completeness will be introduced in this section through a few examples.

To start with, let us temporarily freeze the spatial variables and illustrate the aforementioned concepts using spin degrees of freedom. Since spin component operators of a given particle do not commute with one another (see equations (1.18)), it is impossible to define common eigenstates for all these operators simultaneously. Consequently, no quantum state can be defined where the result of measuring any spin component is certain. However, the Casimir operators introduced in relation (1.19) have been shown to commute with all spin components, thereby enabling the construction of common eigenstates for all the S_i^2 Casimirs and for one component of each spin, such as S_{iz} ,

$$S_i^2 |s_1 m_1; s_2 m_2; s_3 m_3\rangle = \hbar^2 s_i(s_i + 1) |s_1 m_1; s_2 m_2; s_3 m_3\rangle, \quad (1.25a)$$

$$S_{iz} |s_1 m_1; s_2 m_2; s_3 m_3\rangle = \hbar m_i |s_1 m_1; s_2 m_2; s_3 m_3\rangle. \quad (1.25b)$$

Group theory considerations show that $s_i \in \{0, 1/2, 1, \dots\}$ and $m_i \in \{-s_i, -s_i + 1, \dots, s_i\}$. Notably, as long as the spatial degrees of freedom remain frozen, the states $|s_1 m_1; s_2 m_2; s_3 m_3\rangle$ are uniquely defined by relations (1.25). In other words, introducing additional labels α , as in equation (1.7), is unnecessary because the current set of quantum numbers already fully specifies the state. As with any eigenstates of observables, the states (1.25) span the entire Hilbert space. These

observations establish the set $\{|s_1 m_1; s_2 m_2; s_3 m_3\rangle\}$ as a *complete set of states*, which satisfies a completeness relation that, in the current case, is expressed as follows,

$$\sum_{s_1, s_2, s_3} \sum_{m_1, m_2, m_3} |s_1 m_1; s_2 m_2; s_3 m_3\rangle \langle s_1 m_1; s_2 m_2; s_3 m_3| = \mathbb{1} \quad (1.26)$$

This relation illustrates equation (1.9). In most practical cases, the summations over s_i labels can be omitted, as the three particles are assumed to have fixed total spins. This simplification corresponds to freezing the total spin degrees of freedom while leaving only the spin projection quantum numbers unconstrained. Property (1.26) ensures that any spin state can be represented as a linear combination of the spin eigenvectors (1.25). For instance, let us assume a system of particles with respective spins s_1 , s_2 and s_3 , the spin state of the system being denoted $|\chi; s_1 s_2 s_3\rangle$. This spin state can indeed be decomposed as a linear combination of the spin eigenvectors using relation (1.26),

$$\begin{aligned} |\chi; s_1 s_2 s_3\rangle &= \left(\sum_{m_1, m_2, m_3} |s_1 m_1; s_2 m_2; s_3 m_3\rangle \langle s_1 m_1; s_2 m_2; s_3 m_3| \right) |\chi; s_1 s_2 s_3\rangle \\ &= \sum_{m_1, m_2, m_3} \langle s_1 m_1; s_2 m_2; s_3 m_3 | \chi; s_1 s_2 s_3 \rangle |s_1 m_1; s_2 m_2; s_3 m_3\rangle \end{aligned} \quad (1.27)$$

In the expression, one may recognise the inner product that provides, according to Born rule, the probability of observing the state with spin projections $\hbar m_1$, $\hbar m_2$ and $\hbar m_3$. Notably, providing all these complex coefficients $\langle s_1 m_1; s_2 m_2; s_3 m_3 | \chi; s_1 s_2 s_3 \rangle$ completely determines the spin state of the system. This observation forms the foundation of the concept of state representation which will be fully addressed in the next example.

Let us now turn to the description of spatial degrees of freedom, using position and momentum operators for one spinless particle. To avoid notation ambiguities, operators will temporarily be distinguished from their corresponding eigenvalues by placing hats over their symbols. Since all position component operators commute with one another (see equation (1.13)), a common set of position eigenstates exists. These eigenstates are denoted $|\mathbf{r}_1; \mathbf{r}_2; \mathbf{r}_3\rangle$ and satisfy

$$\hat{\mathbf{r}}_1 |\mathbf{r}_1; \mathbf{r}_2; \mathbf{r}_3\rangle = \mathbf{r}_1 |\mathbf{r}_1; \mathbf{r}_2; \mathbf{r}_3\rangle, \quad (1.28a)$$

$$\hat{\mathbf{r}}_2 |\mathbf{r}_1; \mathbf{r}_2; \mathbf{r}_3\rangle = \mathbf{r}_2 |\mathbf{r}_1; \mathbf{r}_2; \mathbf{r}_3\rangle, \quad (1.28b)$$

$$\hat{\mathbf{r}}_3 |\mathbf{r}_1; \mathbf{r}_2; \mathbf{r}_3\rangle = \mathbf{r}_3 |\mathbf{r}_1; \mathbf{r}_2; \mathbf{r}_3\rangle. \quad (1.28c)$$

Above, eigenvalues \mathbf{r}_1 , \mathbf{r}_2 and \mathbf{r}_3 range continuously over \mathbb{R}^3 , representing all possible positions accessible to each of the three particles. Position eigenstates are an example of non-normalisable

eigenstates with continuous eigenvalues. Despite that, the precise definition of position eigenstate is fixed by imposing the following adapted orthonormalisation condition (in the Dirac sense),

$$\langle \mathbf{r}'_1; \mathbf{r}'_2; \mathbf{r}'_3 | \mathbf{r}_1; \mathbf{r}_2; \mathbf{r}_3 \rangle = \delta^3(\mathbf{r}'_1 - \mathbf{r}_1) \delta^3(\mathbf{r}'_2 - \mathbf{r}_2) \delta^3(\mathbf{r}'_3 - \mathbf{r}_3) \quad (1.29)$$

where $\delta^3(\mathbf{r}' - \mathbf{r}) = \delta(r'_x - r_x) \delta(r'_y - r_y) \delta(r'_z - r_z)$ is the product of three Dirac deltas. Other normalisation conventions are, of course, possible. As in the case of spin, position eigenstates are unequivocally defined by equations (1.28). These also satisfy a completeness relation,

$$\int d^3r_1 d^3r_2 d^3r_3 | \mathbf{r}_1; \mathbf{r}_2; \mathbf{r}_3 \rangle \langle \mathbf{r}_1; \mathbf{r}_2; \mathbf{r}_3 | = \mathbb{1} \quad (1.30)$$

This relation enables the decomposition of any state as an integral over position eigenstates. For instance, let $|\Psi\rangle$ be the state of a three-body system. Using relation (1.30), $|\Psi\rangle$ can be expressed as

$$|\Psi\rangle = \int d^3r_1 d^3r_2 d^3r_3 \langle \mathbf{r}_1; \mathbf{r}_2; \mathbf{r}_3 | \Psi \rangle | \mathbf{r}_1; \mathbf{r}_2; \mathbf{r}_3 \rangle. \quad (1.31)$$

This decomposition is referred to as the position representation of $|\Psi\rangle$. The integration kernel $\langle \mathbf{r}_1; \mathbf{r}_2; \mathbf{r}_3 | \Psi \rangle$ is called the position wave function of the system and is commonly denoted by $\Psi(\mathbf{r}_1, \mathbf{r}_2, \mathbf{r}_3)$. In most cases, when a state is labelled $|\Psi\rangle$, the symbol Ψ implicitly represents its position wave function. Equation (1.31) illustrates a statement made at the beginning of the section: although $| \mathbf{r}_1; \mathbf{r}_2; \mathbf{r}_3 \rangle$ are not normalisable and therefore do not correspond to physical states themselves, they can be used for decomposing any physical state. Regarding interpretation, as mentioned earlier, the squared modulus $|\langle \mathbf{r}_1; \mathbf{r}_2; \mathbf{r}_3 | \Psi \rangle|^2$ provides the probability density of measuring the three particles at positions \mathbf{r}_1 , \mathbf{r}_2 and \mathbf{r}_3 . Once again, specifying the position wave function completely defines the state of the system, meaning that any operation performed on the state can be mapped onto its position wave function. For instance, the action of $\hat{\mathbf{p}}_i$ corresponds to differentiation with respect to \mathbf{r}_i ,

$$\hat{\mathbf{p}}_i | \Psi_1 \rangle \implies -i\hbar \nabla_{\mathbf{r}_i} \Psi_1(\mathbf{r}_1, \mathbf{r}_2, \mathbf{r}_3). \quad (1.32)$$

This relation between $\hat{\mathbf{p}}_i$ and differentiation can be derived directly from property (1.13) [6].

A similar discussion applies to momentum component operators. These commuting operators

possess a set of common eigenstates, denoted $|\mathbf{p}_1; \mathbf{p}_2; \mathbf{p}_3\rangle$, satisfying

$$\hat{\mathbf{p}}_1 |\mathbf{p}_1; \mathbf{p}_2; \mathbf{p}_3\rangle = \mathbf{p}_1 |\mathbf{p}_1; \mathbf{p}_2; \mathbf{p}_3\rangle, \quad (1.33a)$$

$$\hat{\mathbf{p}}_2 |\mathbf{p}_1; \mathbf{p}_2; \mathbf{p}_3\rangle = \mathbf{p}_2 |\mathbf{p}_1; \mathbf{p}_2; \mathbf{p}_3\rangle, \quad (1.33b)$$

$$\hat{\mathbf{p}}_3 |\mathbf{p}_1; \mathbf{p}_2; \mathbf{p}_3\rangle = \mathbf{p}_3 |\mathbf{p}_1; \mathbf{p}_2; \mathbf{p}_3\rangle. \quad (1.33c)$$

The eigenvalues \mathbf{p}_1 , \mathbf{p}_2 , and \mathbf{p}_3 again range continuously in \mathbb{R}^3 , representing all possible momenta accessible to each of the three particles. These states are conventionally normalised as follows,

$$\langle \mathbf{p}'_1; \mathbf{p}'_2; \mathbf{p}'_3 | \mathbf{p}_1; \mathbf{p}_2; \mathbf{p}_3 \rangle = \delta^3(\mathbf{p}'_1 - \mathbf{p}_1) \delta^3(\mathbf{p}'_2 - \mathbf{p}_2) \delta^3(\mathbf{p}'_3 - \mathbf{p}_3). \quad (1.34)$$

and they satisfy the following completeness relation,

$$\int d^3r_1 d^3r_2 d^3r_3 |\mathbf{p}_1; \mathbf{p}_2; \mathbf{p}_3\rangle \langle \mathbf{p}_1; \mathbf{p}_2; \mathbf{p}_3| = \mathbb{1}. \quad (1.35)$$

This property enables the decomposition of any physical state into the so-called momentum representation. For a three-body system in a state $|\Psi\rangle$, one can write

$$|\Psi\rangle = \int d^3p_1 d^3p_2 d^3p_3 \langle \mathbf{p}_1; \mathbf{p}_2; \mathbf{p}_3 | \Psi \rangle |\mathbf{p}_1; \mathbf{p}_2; \mathbf{p}_3\rangle. \quad (1.36)$$

where $\langle \mathbf{p}_1; \mathbf{p}_2; \mathbf{p}_3 | \Psi \rangle$ is referred to as the momentum wave-function of the state. Once again, specifying the momentum wave function fully determines the state of the system. Since momentum and position operators do not commute, it is impossible to define common eigenstates for all these operators simultaneously. This limitation is directly related to the well-known Heisenberg indeterminacy principle.

Complete sets of states for spatial degrees of freedom do not necessarily require continuous spectra. For instance, eigenstates of confining Hamiltonians⁷ can always be normalised, resulting in a discrete spectrum. Concrete examples of such Hamiltonians and spectra will be provided in Chapter 2 but the associated representation for quantum states can already be introduced. For the current paragraph, let us assume the existence of a discrete complete set of states. The corresponding eigenstates are denoted $|o_1 \dots o_a\rangle$, where o_i belongs to a subset of \mathbb{Z} and is the quantum number associated with the eigenvalue of the observable \mathcal{O}_i . It is assumed that specifying all the eigenvalues $o_1 \dots o_a$ uniquely determines the corresponding eigenstate without ambiguity. As a result, these eigenstates satisfy the following orthonormality and completeness

⁷ Hamiltonian with potentials that do not saturate at large distance.

relations,

$$\langle o'_1 \dots o'_a | o_1 \dots o_a \rangle = \delta_{o'_1 o_1} \dots \delta_{o'_a o_a}, \quad \sum_{o_1} \dots \sum_{o_a} |o_1 \dots o_a\rangle \langle o_1 \dots o_a| = \mathbb{1}. \quad (1.37)$$

Using completeness, any state $|\Psi\rangle$ for the system can be expressed as follows

$$|\Psi\rangle = \sum_{o_1} \dots \sum_{o_a} \langle o_1 \dots o_a | \Psi \rangle |o_1 \dots o_a\rangle. \quad (1.38)$$

Coefficients $\langle o_1 \dots o_a | \Psi \rangle$ represent the state $|\Psi\rangle$ in the discrete complete basis $\{|o_1 \dots o_a\rangle\}$. Decomposing quantum states in such a basis enables their representation as infinite column vectors. In this formulation, linear operators acting on quantum states are expressed as infinite matrices, which act via matrix multiplication. Let $|\Phi\rangle$ denote $\mathcal{O}|\Psi\rangle$. In the basis $\{|o_1 \dots o_a\rangle\}$, the state $|\Phi\rangle$ is represented via its components $\langle o_1 \dots o_a | \Phi \rangle$,

$$\langle o_1 \dots o_a | \Phi \rangle = \langle o_1 \dots o_a | \mathcal{O} | \Psi \rangle = \sum_{o'_1} \dots \sum_{o'_a} \langle o_1 \dots o_a | \mathcal{O} | o'_1 \dots o'_a \rangle \langle o'_1 \dots o'_a | \Psi \rangle. \quad (1.39)$$

To make the matrix structure of this equation more explicit, let us impose an ordering in the complete labeling $o_1 \dots o_a$. This ordering replaces the detailed set of quantum numbers with a single natural number n and the expression becomes

$$\langle n | \Phi \rangle = \sum_{n' \in \mathbb{N}} \langle n | \mathcal{O} | n' \rangle \langle n' | \Psi \rangle \implies \begin{pmatrix} \langle 0 | \Phi \rangle \\ \langle 1 | \Phi \rangle \\ \vdots \end{pmatrix} = \begin{pmatrix} \langle 0 | \mathcal{O} | 0 \rangle & \langle 0 | \mathcal{O} | 1 \rangle & \dots \\ \langle 1 | \mathcal{O} | 0 \rangle & \langle 1 | \mathcal{O} | 1 \rangle & \dots \\ \vdots & \vdots & \ddots \end{pmatrix} \begin{pmatrix} \langle 0 | \Psi \rangle \\ \langle 1 | \Psi \rangle \\ \vdots \end{pmatrix} \quad (1.40)$$

Matrices explicitly appear in the last formulation. In this representation, the coefficients $\langle n | \mathcal{O} | n' \rangle$ are referred to as the *matrix elements* of \mathcal{O} . Notice that the Hermitian character of \mathcal{O} implies that the matrix associated to \mathcal{O} is equal to its conjugate transpose.

1.1.4 Symmetry and Identical Particles

Since two sections, the system considered includes three generic particles. Many-body problems in quantum mechanics are intrinsically linked to the concept of symmetry in quantum states, particularly in the presence of identical particles. Specifically, the quantum state of any system must be either symmetric or antisymmetric under the exchange of any pair of identical particles. The exchange of particles i and j is represented by a linear operator denoted \mathbb{P}_{ij} . The exchange operators are designated as *unitary operators* because $\mathbb{P}_{ij}^\dagger \mathbb{P}_{ij} = \mathbb{1}$ and *involutions*

because $\mathbb{P}_{ij}^2 = \mathbf{1}$. The symmetry and antisymmetry conditions for particles i and j in a state $|\Psi\rangle$ are expressed as follows,

$$\mathbb{P}_{ij} |\Psi\rangle = |\Psi\rangle, \quad \mathbb{P}_{ij} |\Psi\rangle = -|\Psi\rangle. \quad (1.41)$$

This constraint arises from the fundamental indistinguishability of identical quantum particles. The allowance for both symmetry and antisymmetry stems from the interpretation of quantum states via the squared moduli of their coefficients. In particular, two quantum states that differ only by a global phase factor are physically equivalent. Consequently, encoding the indistinguishability of particles i and j in a system state $|\Psi\rangle$ requires that $|\Psi\rangle$ and $\mathbb{P}_{ij} |\Psi\rangle$ differ only by a global phase factor. In three spatial dimensions⁸, the only permissible phase factors are $+1$ or -1 , thereby leading to symmetric and antisymmetric states, respectively.

The choice between symmetry and antisymmetry is dictated by the spin of the particles. Particles with integer spins, known as bosons, obey symmetry conditions, whereas particles with half-integer spins, called fermions, obey antisymmetry conditions. The connection between spin and symmetry is a consequence of the spin-statistics theorem in quantum field theory [21], a topic beyond the scope of this work. From a non-symmetric state, symmetric or antisymmetric states can be constructed using operators known as symmetrisers, \mathbb{S} , and antisymmetrisers, \mathbb{A} . For two particles, these operators are defined in terms of \mathbb{P}_{ij} as follows,

$$\mathbb{S} = \mathbf{1} + \mathbb{P}_{12}, \quad \mathbb{A} = \mathbf{1} - \mathbb{P}_{12}. \quad (1.42)$$

For three particles, the definitions extend to

$$\mathbb{S} = \mathbf{1} + \mathbb{P}_{12} + \mathbb{P}_{13} + \mathbb{P}_{12}\mathbb{P}_{13}\mathbb{P}_{12} + \mathbb{P}_{13}\mathbb{P}_{12} + \mathbb{P}_{12}\mathbb{P}_{13}, \quad (1.43)$$

$$\mathbb{A} = \mathbf{1} - \mathbb{P}_{12} - \mathbb{P}_{13} - \mathbb{P}_{12}\mathbb{P}_{13}\mathbb{P}_{12} + \mathbb{P}_{13}\mathbb{P}_{12} + \mathbb{P}_{12}\mathbb{P}_{13}. \quad (1.44)$$

The application of these operators does not preserve the normalisation.

To illustrate the role of symmetry, let us again consider a system of three spinless particles in a generic state $|\Psi\rangle$. This state is decomposed in the position representation via a position wave function $\Psi(\mathbf{r}_1, \mathbf{r}_2, \mathbf{r}_3) = \langle \mathbf{r}_1; \mathbf{r}_2; \mathbf{r}_3 | \Psi \rangle$,

$$|\Psi\rangle = \int d^3r_1 d^3r_2 d^3r_3 \Psi(\mathbf{r}_1, \mathbf{r}_2, \mathbf{r}_3) |\mathbf{r}_1; \mathbf{r}_2; \mathbf{r}_3\rangle. \quad (1.45)$$

⁸ In two-dimensional systems, intermediate phases factors can occur, leading to symmetries referred to as *anyonic* [20].

This description is valid for distinguishable particles. In the presence of three identical particles, however, the state $|\Psi\rangle$ must be fully symmetrised. Permutation operators acting on position eigenstates logically swap the corresponding position eigenvalues. This statement allows to evaluate the action of the symmetriser on $|\Psi\rangle$,

$$\begin{aligned} \mathbb{S}|\Psi\rangle = \int d^3r_1 d^3r_2 d^3r_3 \Psi(\mathbf{r}_1, \mathbf{r}_2, \mathbf{r}_3) & (|\mathbf{r}_1; \mathbf{r}_2; \mathbf{r}_3\rangle + |\mathbf{r}_2; \mathbf{r}_1; \mathbf{r}_3\rangle + |\mathbf{r}_3; \mathbf{r}_2; \mathbf{r}_1\rangle \\ & + |\mathbf{r}_1; \mathbf{r}_3; \mathbf{r}_2\rangle + |\mathbf{r}_3; \mathbf{r}_1; \mathbf{r}_2\rangle + |\mathbf{r}_2; \mathbf{r}_3; \mathbf{r}_1\rangle). \end{aligned} \quad (1.46)$$

By performing appropriate changes of variables for each of the six terms, the sum over position eigenstates can be reorganised as sum over position wave functions,

$$\begin{aligned} \mathbb{S}|\Psi\rangle = \int d^3r_1 d^3r_2 d^3r_3 & (\Psi(\mathbf{r}_1, \mathbf{r}_2, \mathbf{r}_3) + \Psi(\mathbf{r}_2, \mathbf{r}_1, \mathbf{r}_3) + \Psi(\mathbf{r}_3, \mathbf{r}_2, \mathbf{r}_1) \\ & + \Psi(\mathbf{r}_1, \mathbf{r}_3, \mathbf{r}_2) + \Psi(\mathbf{r}_3, \mathbf{r}_1, \mathbf{r}_2) + \Psi(\mathbf{r}_2, \mathbf{r}_3, \mathbf{r}_1)) |\mathbf{r}_1, \mathbf{r}_2, \mathbf{r}_3\rangle. \end{aligned} \quad (1.47)$$

The state symmetry condition translates into a symmetry condition for the position wave function under exchanges of its variables. This justifies the common view that symmetry acts directly on wave functions. Similar results hold for momentum representation and/or for antisymmetry conditions. In general, for particles with spin or other intrinsic degrees of freedom, symmetry applies to the entire system. This enables the combination of symmetries from different components to construct a symmetric total state. For instance, an antisymmetric spatial component can yield a symmetric total state when combined with an antisymmetric spin component. Moreover, partially symmetric components can also be combined to achieve a symmetric global state. For instance, partially symmetric space and spin components can be superposed to obtain a symmetric global state.

Symmetry can be challenging to establish, but once achieved, it can significantly simplify many calculations. Let us exemplify it with the evaluation of two-body potential matrix elements. Let $|\Psi\rangle$ denote the state of a system of identical particles, and let $V(|\mathbf{r}_i - \mathbf{r}_j\rangle)$ be a two-body interaction acting between the particles. Due to symmetry, evaluating the corresponding matrix element for one pair of particles is equivalent to evaluating it for any other pair,

$$\begin{aligned} \langle\Psi| V(|\mathbf{r}_i - \mathbf{r}_j\rangle) |\Psi\rangle & = (\pm \langle\Psi| \mathbb{P}_{ik}) V(|\mathbf{r}_i - \mathbf{r}_j\rangle) (\pm \mathbb{P}_{ik} |\Psi\rangle) \\ & = \langle\Psi| \left(\mathbb{P}_{ik}^\dagger V(|\mathbf{r}_i - \mathbf{r}_j\rangle) \mathbb{P}_{ik} \right) |\Psi\rangle \\ & = \langle\Psi| \left(\mathbb{P}_{ik}^{-1} V(|\mathbf{r}_i - \mathbf{r}_j\rangle) \mathbb{P}_{ik} \right) |\Psi\rangle \\ & = \langle\Psi| V(|\mathbf{r}_k - \mathbf{r}_j\rangle) |\Psi\rangle. \end{aligned} \quad (1.48)$$

The plus and minus signs account for bosonic and fermionic systems, respectively. The final equality identifies the successive actions $\mathbb{P}_{ik}^{-1}V(|\mathbf{r}_i - \mathbf{r}_j|)\mathbb{P}_{ik}$ with $V(|\mathbf{r}_k - \mathbf{r}_j|)$. A similar argument can be applied to change the label j as well. Equalities like (1.48) will be employed extensively throughout this document.

1.1.5 Hamiltonian Eigenstates and the Time-Independent Schrödinger Equation

Beyond the commonly referred Schrödinger equation (1.1), a central equation in many quantum mechanical applications is the time-independent Schrödinger equation,

$$H|\Psi\rangle = E|\Psi\rangle. \quad (1.49)$$

One may recognize this equation as the eigenvalue problem associated with the Hamiltonian of the system. This equation holds significant importance for two main reasons. First, in cases of time-independent interactions, such as those discussed in Section 1.1.2, solving the time-independent equation provides the necessary information to address the time-dependent one. If equation (1.49) is fully solved, meaning that all Hamiltonian eigenvectors $|\Psi_i\rangle$ and their corresponding eigenvalues E_i are known, the time evolution of a system with an initial state $|\Psi(0)\rangle$ can be expressed as,

$$|\Psi(t)\rangle = \sum_i \langle\Psi_i|\Psi(0)\rangle e^{-iE_it/\hbar} |\Psi_i\rangle. \quad (1.50)$$

A demonstration of this result can be found in any standard quantum mechanics textbook, such as [5, 6]. Solving the time-dependent Schrödinger equation is perhaps the most frequently cited motivation for solving the time-independent one. While this is undoubtedly valid, let us broaden this perspective slightly. In many quantum mechanical problems, including those addressed in this work, the explicit time evolution of the system is not considered. Nonetheless, solving equation (1.49) remains essential. This equation defines a critical class of states: those resulting from energy measurements. By solving (1.49), one determines the system's accessible energy levels and the corresponding eigenstates. In atomic physics, determining atomic spectra is often an end goal in itself. Similarly, in particle physics, particle states are typically defined as energy eigenstates. Thus, solving the time-independent equation yields key information about a particle's properties.

Although the full Schrödinger equation retains its elegance and generality, the applications discussed in this work focus primarily on solving the time-independent equation for the second

reason mentioned above. In both Parts II and III, the primary objectives will be the computation of energy spectra for baryons and glueballs, respectively. Establishing the properties of energy eigenstates, such as spin or parity, will also be a primary concern. Solving (1.49) is a challenging task and various resolution methods exist, each with its advantages and limitations. Two methods will be detailed in this work: the oscillator bases expansion and the envelope theory. The former is rooted in a family of results known as variational theorems, which will be introduced in the next chapter. Beyond offering a practical method for obtaining approximate solutions to (1.49), these theorems provide a different perspective on the equation, a perspective that is often under-emphasised.

1.2 The Variational Theorems as Powerful Tools

The previous section concluded by emphasising the importance of solving the time-independent Schrödinger equation. Analytical resolutions of this equation exist only for very specific forms of the Hamiltonian. For N particles, one of the few (if not the only) completely exactly solvable Hamiltonians is the non-relativistic harmonic oscillator. For illustration, the isotropic harmonic oscillator, H_{oh} , is defined as follows considering N vectorial degrees-of-freedom in three spatial dimensions, \mathbf{x}_i ,

$$H_{\text{oh}} = \frac{1}{2m} \sum_{i=1}^N \mathbf{p}_i^2 + \frac{m\omega^2}{2} \sum_{i=1}^N \mathbf{x}_i^2. \quad (1.51)$$

Above, \mathbf{p}_i is the variable conjugate to \mathbf{x}_i . Anisotropic versions of (1.51) where the parameters m and ω depend on the particle labels (and therefore related to systems of different particles) can also be solved analytically [22]. The analytical spectrum of the harmonic oscillator lays the groundwork for the approximation methods developed in Chapters 2 and 3. However, let us defer the discussion of the N -body harmonic oscillator spectrum to the sections dedicated to it.

At this stage, it seems that tackling equation (1.49) directly for general Hamiltonians is a challenging task. Nevertheless, this can be overcome by changing the perspective and examining the time-independent Schrödinger equation through the lens of variational theorems, to which this section is devoted. This section is heavily inspired by the Chapter 3 of the comprehensive book from Y. Suzuki and K. Varga [23].

1.2.1 The Rayleigh-Ritz Variational Theorem

Let us consider a generic system of any number of particles in any number of dimensions. This system is subjected to a generic Hamiltonian H . In the following, the (normalised) eigenstates

and eigenvalues of H will be denoted $|\phi_i\rangle$ and E_i , respectively,

$$H |\phi_i\rangle = E_i |\phi_i\rangle. \quad (1.52)$$

The index i is assumed to start at $i = 0$ and to increase with energy. Only the discrete part of the spectrum is considered. Let $|\Psi\rangle$ be a normalised quantum state that the system may occupy. The Rayleigh-Ritz variational theorem states that, regardless of the choice of $|\Psi\rangle$, the energy expectation value is smaller when evaluated with $|\phi_0\rangle$ than with $|\Psi\rangle$,

$$\langle\Psi| H |\Psi\rangle \geq \langle\phi_0| H |\phi_0\rangle = E_0. \quad (1.53)$$

Equality holds if $|\Psi\rangle = |\phi_0\rangle$.

Proof. This proof is inspired by the one provided in reference [5] – Since H is an observable, its spectrum spans the entire Hilbert space. Therefore, there exist coefficients c_i such that

$$|\Psi\rangle = \sum_i c_i |\phi_i\rangle. \quad (1.54)$$

Using this decomposition, evaluating the Hamiltonian on $|\Psi\rangle$ gives

$$\langle\Psi| H |\Psi\rangle = \sum_j \sum_i c_j^* c_i \langle\phi_j| H |\phi_i\rangle = \sum_i |c_i|^2 E_i. \quad (1.55)$$

In each term of this sum, one may replace E_i by the lowest eigenenergy, E_0 . By doing so, each term is underestimated,

$$\langle\Psi| H |\Psi\rangle = \sum_i |c_i|^2 E_i \geq \left(\sum_i |c_i|^2 \right) E_0. \quad (1.56)$$

As a result, as long as $|\Psi\rangle$ is normalised, it follows that $\langle\Psi| H |\Psi\rangle \geq E_0$. \square

Theorem (1.53) provides the expected new perspective on the time-independent Schrödinger equation. Essentially, this equation seeks the state that minimises the energy expectation value and defines it as its lowest energy solution. This lowest energy solution is often referred to as the *ground-state*, while higher energy solution are referred to as *excited states*. Theorem (1.53) can be exploited to derive approximations for the ground-state eigenvalue. By repeatedly evaluating H on various different states $|\Psi\rangle$, referred to as *trial states*, the Rayleigh-Ritz theorem provides various upper bounds to this energy eigenvalue. Among these upper bounds, the smallest one

(that is, the most constraining) can be used as an approximation for E_0 . The approximation becomes more accurate as the set of trial states covers a larger portion of the Hilbert space.

Most of the time, instead of evaluating the Hamiltonian state by state, parameters are added to $|\Psi\rangle$, and the expectation value is minimised with respect to these parameters. Two types of parameters should be distinguished. Let us assume that, for any value of a given set of parameters a_1, \dots, a_q , a specific procedure provides a corresponding set of Q orthonormal states, denoted $|\varphi_i(a_1 \dots a_q)\rangle$. This set can be used to construct a trial state that depends on $2Q + q$ real parameters,

$$|\Psi(a_1 \dots a_q; c_1 \dots c_Q)\rangle = \sum_{i=1}^Q c_i |\varphi_i(a_1 \dots a_q)\rangle. \quad (1.57)$$

Each complex-valued c_i parameters account for two real ones. These parameters, included as coefficients in the linear combinations, are referred to as *linear variational parameters*, while the others are called *non-linear variational parameters*. If the minimisation with respect to non-linear variational parameters requires a true optimisation process, the optimisation with respect to the linear variational parameters is easier to perform. To minimise $\langle \Psi(a_1 \dots a_q; c_1 \dots c_Q) | H | \Psi(a_1 \dots a_q; c_1 \dots c_Q) \rangle$ with respect to the c_i , the corresponding derivatives are constrained to vanish,

$$\begin{cases} \frac{\partial}{\partial c_i} \langle \Psi(a_1 \dots a_q; c_1 \dots c_Q) | H | \Psi(a_1 \dots a_q; c_1 \dots c_Q) \rangle = 0, \\ \frac{\partial}{\partial c_i^*} \langle \Psi(a_1 \dots a_q; c_1 \dots c_Q) | H | \Psi(a_1 \dots a_q; c_1 \dots c_Q) \rangle = 0. \end{cases} \quad (1.58)$$

Above, c_i and c_i^* are treated as independent variables to account for the fact that each c_i encodes two real parameters. It can be shown that imposing these minimisation conditions together with the normalisation constraint $\sum_i |c_i|^2 = 1$ is equivalent to solving the following matrix eigenvalue problem,

$$\begin{pmatrix} \langle \varphi_1(a_1 \dots a_q) | H | \varphi_1(a_1 \dots a_q) \rangle & \cdots & \langle \varphi_1(a_1 \dots a_q) | H | \varphi_Q(a_1 \dots a_q) \rangle \\ \vdots & \ddots & \vdots \\ \langle \varphi_Q(a_1 \dots a_q) | H | \varphi_1(a_1 \dots a_q) \rangle & \cdots & \langle \varphi_Q(a_1 \dots a_q) | H | \varphi_Q(a_1 \dots a_q) \rangle \end{pmatrix} \begin{pmatrix} c_1 \\ \vdots \\ c_Q \end{pmatrix} = \epsilon \begin{pmatrix} c_1 \\ \vdots \\ c_Q \end{pmatrix}. \quad (1.59)$$

The many eigenvalues ϵ that solve this equation correspond to local minima. The upper bound that serves as an approximation for the true lowest eigenenergy is the minimal eigenvalue in (1.59). To summarise, obtaining an approximation for the ground-state eigenvalue of a given Hamiltonian H is generally structured in the following four-step procedure.

1. Choose a set of Q orthonormal⁹ trial states $|\varphi_i(a_1 \dots a_q)\rangle$ that incorporates as many non-

linear variational parameters as desired.

2. Compute all the matrix elements of H on $\{|\varphi_i(a_1\dots a_q)\rangle\}$ for a given set of non-linear variational parameters.
3. Solve the eigenvalue problem (1.59) and identify the lowest eigenvalue (note that some algorithms only compute the lowest one).
4. Repeat steps 2 and 3 for different non-linear variational parameters until a minimum is found. This minimum serves as an approximation for the true ground-state eigenenergy.

Although the Rayleigh-Ritz variational theorem discusses only the eigenvalue, it is also frequently used to approximate the corresponding eigenstate. The trial state that achieves the minimum is assumed to, at least approximately, resemble the true eigenstate, especially if the eigenenergy is accurately reproduced.

1.2.2 The MacDonald Theorem

The Rayleigh-Ritz theorem, and especially the subsequent procedure, appears to be limited to the study of ground-states. However, this theorem can be extended to describe excited states as well. This extension is known as the MacDonald theorem [24]. The context is analogous to that presented in the previous section. Let us consider a general system of any number of particles in any number of dimensions, subjected to a general Hamiltonian H , and let $\{|\varphi_i\rangle\}$ be a set of Q orthonormal states that the system may occupy. The MacDonald theorem states that ϵ_i , the i^{th} eigenvalue of the Hamiltonian matrix restricted to $\{|\varphi_i\rangle\}$, is an upper bound of E_i , the i^{th} true eigenvalue of H ,

$$E_0 \leq \epsilon_0, \quad E_1 \leq \epsilon_1, \quad \dots, \quad E_Q \leq \epsilon_Q \quad (1.60)$$

where $\epsilon_0 \leq \epsilon_1 \leq \dots \leq \epsilon_Q$ and

$$\begin{pmatrix} \langle \varphi_1 | H | \varphi_1 \rangle & \cdots & \langle \varphi_1 | H | \varphi_Q \rangle \\ \vdots & \ddots & \vdots \\ \langle \varphi_Q | H | \varphi_1 \rangle & \cdots & \langle \varphi_Q | H | \varphi_Q \rangle \end{pmatrix} \begin{pmatrix} c_{i1} \\ \vdots \\ c_{iQ} \end{pmatrix} = \epsilon_i \begin{pmatrix} c_{i1} \\ \vdots \\ c_{iQ} \end{pmatrix}. \quad (1.61)$$

⁹ In full generality, the orthonormality condition on $|\varphi_i(a_1\dots a_q)\rangle$ is not necessary. In the presence of non-orthogonal trial states, the eigenvalue problem (1.59) becomes a generalised eigenvalue problem, which can also be addressed. This situation will not be encountered initially.

Proof. This proof is inspired by the one provided in reference [23] – The result is demonstrated iteratively. Let us define \mathcal{V}_Q as the subspace spanned by the set of orthonormal states $\{|\varphi_i\rangle\}$, and \mathcal{W}_Q as the subspace spanned by the Q first eigenstates of H . The following lemma is first established: there always exists a state $|\Psi\rangle$ in \mathcal{V}_Q such that $\langle\Psi|H|\Psi\rangle \geq E_Q$. We begin by defining P , the projector onto the subspace \mathcal{W}_Q . Denoting $|\phi_i\rangle$ as the eigenstates of H , one has

$$P = \sum_{i=1}^Q |\phi_i\rangle \langle\phi_i|. \quad (1.62)$$

Two cases are to be considered: either there exists a state $|\bar{\varphi}\rangle$ in \mathcal{V}_Q such that $P|\bar{\varphi}\rangle = 0$, or for any state $|\varphi\rangle$ in \mathcal{V}_Q , $P|\varphi\rangle \neq 0$.

- First case: If such a state $|\bar{\varphi}\rangle$ exists, its expansion as a linear combination of H 's eigenstates must include only terms proportional to $|\phi_{Q+1}\rangle$, $|\phi_{Q+2}\rangle$, etc. As a result evaluating H on $|\bar{\varphi}\rangle$ gives a value higher than E_{Q+1} , which in turn is higher than E_Q ,

$$\langle\bar{\varphi}|H|\bar{\varphi}\rangle \geq E_{Q+1} \geq E_Q. \quad (1.63)$$

Thus, the lemma is verified for $|\Psi\rangle = |\bar{\varphi}\rangle$.

- Second case: If the second case holds, then any two states $|\bar{\varphi}_1\rangle$ and $|\bar{\varphi}_2\rangle$ in \mathcal{V}_Q must be projected onto different functions in \mathcal{W}_Q (otherwise, $P(|\bar{\varphi}_1\rangle - |\bar{\varphi}_2\rangle)$ would cancel, contradicting the assumption). In other words, the application P that relates \mathcal{V}_Q and \mathcal{W}_Q is injective. Since both \mathcal{W}_Q and \mathcal{V}_Q have dimension Q and thanks to the Rank–nullity theorem, the function proves immediately bijective. As a result, there must exist a state $|\bar{\varphi}\rangle$ in \mathcal{V}_Q that P projects onto $|\phi_Q\rangle$,

$$P|\bar{\varphi}\rangle = a|\phi_Q\rangle \text{ with } a \neq 0. \quad (1.64)$$

Thus, the expansion of $|\bar{\varphi}\rangle$ as a linear combination of H 's eigenstates includes a term $a|\phi_Q\rangle$, along with other terms proportional to $|\psi_{Q+1}\rangle$, $|\psi_{Q+2}\rangle$, etc. These latter terms are grouped into a state $b|\Phi\rangle$, such that $|a|^2 + |b|^2 = 1$,

$$|\bar{\varphi}\rangle = a|\phi_Q\rangle + b|\Phi\rangle. \quad (1.65)$$

Evaluating H on $|\bar{\varphi}\rangle$ yields

$$\langle \bar{\varphi} | H | \bar{\varphi} \rangle = |a|^2 E_Q + |b|^2 \langle \Phi | H | \Phi \rangle = E_Q + |b|^2 (\langle \Phi | H | \Phi \rangle - E_Q) \geq E_Q \quad (1.66)$$

since $\langle \Phi | H | \Phi \rangle \geq E_Q$ due to $|\Phi\rangle$'s definition. Therefore, the lemma also holds for $|\Psi\rangle = |\bar{\varphi}\rangle$.

To complete the proof, we note that the highest eigenvalue of a finite-dimensional eigenvalue problem corresponds to the maximum expectation value of the corresponding operator,

$$\epsilon_Q \geq \langle \Psi | H | \Psi \rangle \geq E_Q. \quad (1.67)$$

This proves the last inequality in (1.60). The other inequalities are obtained by iterating the reasoning on the subspace \mathcal{V}_{Q-1} of all the states in \mathcal{V}_Q that are orthogonal to the eigenstate associated with ϵ_Q . \square

Theorem (1.60) reveals that, once the ground-state energy is obtained, the time-independent Schrödinger equation defines excited eigenstates by iterating the minimisation process of the energy expectation value over the residual vector subspace. Theorem (1.60) indicates that the procedure developed in the previous section, beyond providing approximations for the ground-state, also yields approximations for the excited eigenstates. Notice that, to obtain an approximation for the i^{th} eigenvalue, at least i trial states must be used. As before, non-linear variational parameters can be added to optimise the obtained upper bound. Note that the parameters optimising a given energy level are not necessarily the same as those optimising other energy levels.

1.2.3 Convergence of the Upper Bounds

Before concluding this discussion, let us examine a third theorem that describes the behaviour of these approximations as the number of trial states is increased. Let us denote by ϵ_1 to ϵ_Q the Q approximate eigenvalues obtained using Q trial states. Adding a $(Q+1)^{\text{th}}$ state to the trial set yields $Q+1$ new eigenvalues, denoted $\bar{\epsilon}_1$ to $\bar{\epsilon}_{Q+1}$. MacDonald demonstrated that this addition cannot worsen the approximations [24], meaning that

$$\bar{\epsilon}_1 \leq \epsilon_1 \leq \bar{\epsilon}_2 \leq \epsilon_2 \leq \dots \leq \bar{\epsilon}_Q \leq \epsilon_Q \leq \bar{\epsilon}_{Q+1}. \quad (1.68)$$

Since proving this result is more involved than the previous two theorems, the proof is omitted here. Interested readers are referred to reference [24] for MacDonald's original proof or to

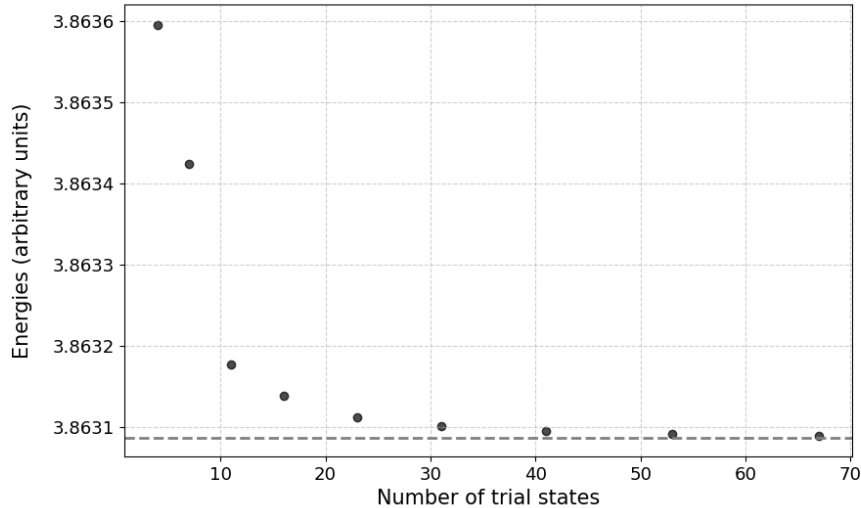


Figure 1.1: Illustration of the typical convergence behaviour obtained using variational theorems. An expansion in oscillator bases with a single non-linear variational parameter a is used to determine the ground-state energy of a system of three identical non-relativistic particles interacting via two-body linear interactions. Masses and parameters are chosen to reproduce energies from [25]. The optimisation of a is performed for seven oscillators (details on oscillator bases expansions are provided in Chapter 2), yielding $a = 1.446$. The converged result is indicated by the dashed gray line.

reference [23] for a more general and detailed derivation.

The above result illustrates the behaviour of the approximate upper bounds as the size of the trial set increases. When a small number of trial states is used, the upper bound can be relatively higher in energy. As more states are added, the approximation improves, gradually converging from above toward the true eigenenergy. In the limiting case of a complete set of trial states, diagonalisation of the infinite-dimensional Hamiltonian matrix yields the exact eigenvalues, in agreement with the matrix representation introduced at the end of Section 1.1.3. A typical example of convergence behaviour is shown on a ground state in Figure 1.1. This illustrative figure is taken from Chapter 2, where an approximation method based on the MacDonald theorem, known as the oscillator bases expansion, is explicitly discussed. Of course, the convergence rate strongly depends on the choice of the trial set and the specific Hamiltonian being solved. Certain trial sets are particularly well suited for specific classes of Hamiltonians, while others offer broader applicability, though potentially with some trade-off in efficiency. The closer the trial states resemble the true eigenstate, the faster the convergence. At the extreme, the exact eigenstate is included in the trial set, the approximation becomes exact and reduces to one state.

1.3 Miscellaneous Results

The final section of this introductory chapter is devoted to various theorems from non-relativistic quantum mechanics. These results will be primarily utilised in Chapter 3, where a second approximation method for the time-independent Schrödinger equation, known as the envelope theory, is developed. Despite their specific purpose in later discussions, these theorems are of a very general nature and merit inclusion in this chapter on the fundamentals of quantum mechanics. Notably, the first two theorems are often employed to assess the accuracy of other approximation methods, such as those based on the previously introduced variational theorems [23]. It illustrates that their applicability extends beyond the establishment of the envelope theory.

Hellmann-Feynman Theorem

Let us begin with the Hellmann-Feynman theorem. Consider a generic system consisting of an arbitrary number of particles in any number of dimensions. This system is governed by a Hamiltonian H which depends on a parameter λ . The Hellmann-Feynman theorem provides the following expression for the derivative of the energy eigenvalues of $H(\lambda)$, denoted $E(\lambda)$, with respect to λ

$$\frac{d}{d\lambda}E(\lambda) = \langle \phi(\lambda) | \frac{\partial}{\partial \lambda} H(\lambda) | \phi(\lambda) \rangle. \quad (1.69)$$

Above, $|\phi(\lambda)\rangle$ is the normalised eigenvector associated with the eigenvalue $E(\lambda)$.

Proof. This proof is inspired by the one provided in reference [23] – Given that $|\phi(\lambda)\rangle$ is an eigenvector of H , its energy expectation value simply equals the corresponding eigenvalue,

$$E(\lambda) = \langle \phi(\lambda) | H(\lambda) | \phi(\lambda) \rangle. \quad (1.70)$$

Differentiating both sides of this expression with respect to λ gives

$$\frac{d}{d\lambda}E(\lambda) = \langle \phi(\lambda) | \frac{\partial}{\partial \lambda} H(\lambda) | \phi(\lambda) \rangle + \langle \frac{\partial}{\partial \lambda} \phi(\lambda) | H(\lambda) | \phi(\lambda) \rangle + \langle \phi(\lambda) | H(\lambda) | \frac{\partial}{\partial \lambda} \phi(\lambda) \rangle \quad (1.71)$$

The first term on the right-hand side already matches the desired result. To complete the

proof, the remaining two terms must be shown to cancel,

$$\begin{aligned}
 & \left\langle \frac{\partial}{\partial \lambda} \phi(\lambda) \middle| H(\lambda) \middle| \phi(\lambda) \right\rangle + \left\langle \phi(\lambda) \middle| H(\lambda) \middle| \frac{\partial}{\partial \lambda} \phi(\lambda) \right\rangle \\
 &= E(\lambda) \left(\left\langle \frac{\partial}{\partial \lambda} \phi(\lambda) \middle| \phi(\lambda) \right\rangle + \left\langle \phi(\lambda) \middle| \frac{\partial}{\partial \lambda} \phi(\lambda) \right\rangle \right) \\
 &= E(\lambda) \frac{d}{d\lambda} \langle \phi(\lambda) | \phi(\lambda) \rangle = 0
 \end{aligned} \tag{1.72}$$

In the second and last lines, the Hermiticity of $H(\lambda)$ and the normalisation condition $\langle \phi(\lambda) | \phi(\lambda) \rangle = 1$ have been used, respectively. This completes the demonstration. \square

The Hellmann-Feynman theorem stands as a versatile tool. It can serve as a consistency check for analytical solutions, an accuracy measure for approximation methods, and even as a tool for proving other theorems. Both next results provide examples of the latter application.

Virial Theorem

The virial theorem also provides information about expectation values of energy eigenstates. Let us consider a N -body system in an arbitrary number of spatial dimensions, governed by a N -body Hamiltonian H generalising the structure from (1.12),

$$H = \sum_{i=1}^N T_i(|\mathbf{p}_i|) + \sum_{i=1}^N U_i(|\mathbf{s}_i|) + \sum_{i<j}^N V_{ij}(|\mathbf{r}_{ij}|). \tag{1.73}$$

Above, the shorthand notations $\mathbf{s}_i = \mathbf{r}_i - \mathbf{R}_{\text{CM}}$ and $\mathbf{r}_{ij} = \mathbf{r}_i - \mathbf{r}_j$ have been introduced. Compared to (1.12), the global kinetic energy has been decomposed into a sum over the kinetic energies of individual particles. This decomposition omits the centre-of-mass motion removal, but the theorem remains valid even when this removal is included [23]. Only one- and two-body interactions are considered. The virial theorem states that different expectation values taken on energy eigenstates satisfy the following relation,

$$\sum_{i=1}^N \left\langle p_i \frac{d}{dp_i} T_i(p_i) \right\rangle = \sum_{i=1}^N \left\langle s_i \frac{d}{ds_i} U_i(s_i) \right\rangle + \sum_{i<j}^N \left\langle r_{ij} \frac{d}{dr_{ij}} V_{ij}(r_{ij}) \right\rangle \tag{1.74}$$

where p_i , s_i and r_{ij} denotes $|\mathbf{p}_i|$, $|\mathbf{s}_i|$ and $|\mathbf{r}_{ij}|$, respectively.

Proof. This proof is inspired by the one provided in [26] – To begin, let us introduce a

dilatation of the position variables,

$$\bar{\mathbf{r}}_i = \frac{\mathbf{r}_i}{\lambda}, \quad \bar{\mathbf{p}}_i = \lambda \mathbf{p}_i \quad (1.75)$$

with $\lambda > 0$. This rescaling keeps the new position and momentum variables conjugate to each other. Of course, it also affects \mathbf{s}_i and \mathbf{r}_{ij} . Using the new variables, the system's Hamiltonian can be rewritten as

$$H(\mathbf{p}_i, \mathbf{r}_i) = H(\bar{\mathbf{p}}_i/\lambda, \lambda \bar{\mathbf{r}}_i) \quad (1.76)$$

This modification does not alter the spectrum of H , but it artificially introduces a parameter into H . It allows to apply the Hellmann-Feynman Theorem,

$$\frac{d}{d\lambda} E(\lambda) = \left\langle \frac{\partial}{\partial \lambda} H(\bar{\mathbf{p}}_i/\lambda, \lambda \bar{\mathbf{r}}_i) \right\rangle \quad (1.77)$$

where expectation values are computed for the eigenstate of H corresponding to $E(\lambda)$. However, since the introduction of λ is purely artificial and does not affect the spectrum, the left-hand side of (1.77) vanishes. Evaluating the right-hand side at $\lambda = 1$ yields the generalised virial theorem,

$$\left. \left\langle \frac{\partial}{\partial \lambda} H(\bar{\mathbf{p}}_i/\lambda, \lambda \bar{\mathbf{r}}_i) \right\rangle \right|_{\lambda=1} = 0. \quad (1.78)$$

Applying this result to the Hamiltonian (1.73), the expectation value is distributed on each term. Denoting $|\mathbf{p}_i| = p_i$, $|\mathbf{s}_i| = s_i$ and $|\mathbf{r}_{ij}| = r_{ij}$, one obtains

$$\left. \frac{\partial}{\partial \lambda} T(p_i/\lambda) \right|_{\lambda=1} = -p_i \frac{d}{dp_i} T(p_i), \quad (1.79a)$$

$$\left. \frac{\partial}{\partial \lambda} U(\lambda s_i) \right|_{\lambda=1} = s_i \frac{d}{ds_i} U(s_i), \quad (1.79b)$$

$$\left. \frac{\partial}{\partial \lambda} V(\lambda r_{ij}) \right|_{\lambda=1} = r_{ij} \frac{d}{dr_{ij}} V(r_{ij}). \quad (1.79c)$$

Combining equations (1.73), (1.78) and (1.79) yields the expected relation. \square

The virial theorem establishes relationships between expectation values of observables for the eigenstates of an Hamiltonian. For example, it allows to show that the eigenstates of the harmonic oscillator (1.51) satisfy

$$\sum_{i=1}^3 \frac{1}{m} \langle \mathbf{p}_i^2 \rangle = \sum_{i<j}^3 m\omega^2 \langle (\mathbf{r}_i - \mathbf{r}_j)^2 \rangle. \quad (1.80)$$

As already mentioned, beyond their formal significance, such relations can also serve as tools to assess the precision of approximate eigenstates.

Comparison Theorem

A third and final theorem will prove useful in further developments. Consider a generic many-body system in an arbitrary number of dimensions and consider two different Hamiltonians for this system, $H^{(1)}$ and $H^{(2)}$. Suppose that each Hamiltonian decomposes into a sum of a kinetic energy term, which depends only on momentum variables, and a potential energy term, which depends only on position variables. That is, if $H^{(1)} = T^{(1)} + V^{(1)}$ and $H^{(2)} = T^{(2)} + V^{(2)}$, and if the conditions $T^{(1)} \leq T^{(2)}$ for all momenta and $V^{(1)} \leq V^{(2)}$ for all positions hold, then the comparison theorem states that their corresponding energy spectra, $E_{\{\alpha\}}^{(1)}$ and $E_{\{\alpha\}}^{(2)}$, satisfy the same ordering,

$$E_{\{\alpha\}}^{(1)} \leq E_{\{\alpha\}}^{(2)}. \quad (1.81)$$

Above, $\{\alpha\}$ denotes the quantum numbers of both spectra.

Proof. This proof is inspired by the one provided in [27] – To start with, consider two Hamiltonians, $H^{(1)}$ and $H^{(2)}$, such that for any state $|\Psi\rangle$ the inequality

$$\langle \Psi | (H^{(2)} - H^{(1)}) | \Psi \rangle \geq 0. \quad (1.82)$$

holds. Next, define the following interpolating Hamiltonian

$$H(a) = (1 - a)H^{(1)} + aH^{(2)} \quad (1.83)$$

which continuously deforms $H^{(1)}$ into $H^{(2)}$ as a varies from 0 to 1. Applying the Hellmann-Feynman theorem to $H(a)$, one obtains

$$\frac{d}{da} E_{\{\alpha\}}(a) = \langle H^{(2)} - H^{(1)} \rangle \geq 0. \quad (1.84)$$

Above, $E_{\{\alpha\}}(a)$ denotes the eigenvalues of $H(a)$ and the expectation value is taken on the corresponding eigenstate. The right-hand side is non-negative due to the assumption (1.82). Since $E_{\{\alpha\}}(a)$ is an increasing function of a , it follows that

$$E_{\{\alpha\}}(0) = E_{\{\alpha\}}^{(1)} \leq E_{\{\alpha\}}(1) = E_{\{\alpha\}}^{(2)}. \quad (1.85)$$

To complete the proof, one has to verify that the Hamiltonians given in the theorem

statement satisfy (1.82). By separating the kinetic and potential contributions, one obtains

$$\langle \Psi | (H^{(2)} - H^{(1)}) | \Psi \rangle = \langle \Psi | (T^{(2)} - T^{(1)}) | \Psi \rangle + \langle \Psi | (V^{(2)} - V^{(1)}) | \Psi \rangle. \quad (1.86)$$

Since the potential functions satisfy $V^{(1)} \leq V^{(2)}$, expressing the second expectation value in the position representation ensures its non-negativity. Similarly, evaluating the first expectation value in the momentum representation guarantees its non-negativity as well. Consequently, the conditions are sufficient to establish (1.82), completing the proof. \square

The comparison theorem will serve as a tool to identify bounds for approximate spectra, particularly when using the envelope theory. This result concludes this non-exhaustive collection of noteworthy theorems in non-relativistic quantum mechanics.

This chapter in the context of a thesis

As an introduction to the field, this chapter does not present any original research results. Instead, it aims to establish the general framework within which the rest of the thesis is situated. As mentioned in the preface, the text is intended to be accessible to students beginning a Master's program focused on fundamental interactions. This chapter revisits key concepts that will be used throughout the document.

It also introduces a perspective less commonly found in the literature for approaching quantum mechanics: the variational theorem, not limited to ground states as it is often the case in introductory textbooks. Since this theorem plays a central role in the subsequent chapters, it seemed worthwhile to recall it in details here. In my view, the variational theorem reveals some particularly insightful aspects about how the Schrödinger equation's operates, and could be more widely used in both teaching and popularising physics. This chapter provided a fitting opportunity to explore this intuition.

Chapter 2

Oscillator Bases Expansions: a Versatile Resolution Method

Chapter 1, and more precisely Section 1.1, aimed to illustrate that solving the time-independent Schrödinger equation stands as a standard stage across various disciplines in physics, ranging from hadronic and nuclear to atomic physics. To achieve this task, numerous approximation methods have been developed, each possessing distinct strengths and limitations. A family of these, known as variational methods and based on the computation of Hamiltonian matrix elements on different trial states, has been outlined in Section 1.2. The current chapter focuses on one such method, named the oscillator bases expansion (OBE). Although generalisations for larger systems are possible, the discussion will focus on three-body systems. In that context, the OBE uses harmonic oscillator eigenstates with one or two non-linear variational parameters as trial functions [28]. This method enables to solve accurately a broad class of Hamiltonians, encompassing two-body interactions as well as non-relativistic and semi-relativistic kinematics. For that systems, the method, originally formulated only for two-body interactions, has recently been generalised in [29] to encompass the class of three-body forces introduced in Section 1.1.2. The OBE also easily manages conditions on the symmetry, the angular momentum and the parity of the desired solution. These features make the OBE particularly effective in hadronic physics, where semi-relativistic kinematics, well-defined angular momentum, and well-defined parity are often required [30, 31, 32, 33, 34].

This chapter builds upon and slightly expands the text from reference [29]. The subsequent sections are organized as follows. Section 2.1 elucidates the theoretical concepts related to the OBE for spinless particles. Section 2.1.1 reviews the three-body harmonic oscillator eigenstates and their essential properties. Section 2.1.2 recalls the Hamiltonian shape investigated in the current work and introduces suitable coordinates to only account for the internal motion.

Sections 2.1.3 and 2.1.4 describe the incorporation of symmetries into the bases and provide formulas for evaluating matrix elements, respectively. Section 2.2 enlarges the discussion to include the management of spin degrees-of-freedom. Section 2.3 examines the accuracy and computational complexity of the OBE. Finally, Section 2.4 offers concluding remarks and the chapter ends with some complementary sections that address subsidiary topics. Even though Chapter 1 did not specify the unit system used, natural units ($\hbar = 1$ and $c = 1$) will be assumed throughout this chapter and the remainder of this work.

2.1 The Theory of the Oscillator Bases Expansion

As already mentioned, the OBE relies on the MacDonald theorem, introduced in Equation (1.60). In brief, this theorem states that the i^{th} lowest eigenvalue of the Hamiltonian matrix, when restricted to a given set of orthonormal trial states $\{|\varphi_i\rangle\}$, provides an upper bound for the i^{th} lowest eigenvalue of the full Hamiltonian. The corresponding eigenvectors also serve as approximations for the true eigenvectors of H . Methods based on the MacDonald theorem involve two main computational steps: evaluating the Hamiltonian matrix elements $\langle\varphi_i|H|\varphi_j\rangle$ and diagonalising the resulting matrix. The accuracy of the upper bound is often refined by incorporating non-linear variational parameters into the trial states and by repeating the procedure for different parameter values. The most constraining upper bound, that is the lowest one, is then selected. In the three-body OBE, the trial states $|\varphi_i\rangle$ are chosen as eigenstates of the harmonic oscillator Hamiltonian and two non-linear variational parameters are included. This section develops an efficient procedure for computing the corresponding matrix elements, particularly for the case of three spinless particles.

2.1.1 The Harmonic Oscillator Eigenstates

Before evaluating the matrix elements, it is necessary to introduce the harmonic oscillator eigenstates as well as some of their properties. Specifying the harmonic oscillator Hamiltonian (1.51) for a generic pair of three-dimensional coordinates, denoted \mathbf{x} and \mathbf{y} , and omitting its parameters gives

$$H_{\text{oh}}(\mathbf{p}, \mathbf{q}, \mathbf{x}, \mathbf{y}) = \frac{\mathbf{p}^2}{2} + \frac{\mathbf{q}^2}{2} + \frac{\mathbf{x}^2}{2} + \frac{\mathbf{y}^2}{2}. \quad (2.1)$$

Here, \mathbf{p} and \mathbf{q} are the conjugate variables to \mathbf{x} and \mathbf{y} , respectively. These coordinates are supposed to be dimensionless. This Hamiltonian can be solved analytically using the separation

of variables method,

$$H_{\text{oh}}(\mathbf{p}, \mathbf{q}, \mathbf{x}, \mathbf{y}) = \left(\frac{\mathbf{p}^2}{2} + \frac{\mathbf{x}^2}{2} \right) + \left(\frac{\mathbf{q}^2}{2} + \frac{\mathbf{y}^2}{2} \right) = H_{\text{oh}}(\mathbf{p}, \mathbf{x}) + H_{\text{oh}}(\mathbf{q}, \mathbf{y}) \quad (2.2)$$

Since both partial Hamiltonians have the same structure, they share the same spectrum. The wave functions of the eigenstates can be found in any quantum mechanics textbooks [5, 6],

$$\begin{aligned} \varphi_{nlm}(\mathbf{r}) = R_{nl}(r)Y_{lm}(\hat{r}) \text{ with } R_{nl}(r) = \sqrt{\frac{2(n!)}{\Gamma(n+\ell+3/2)}} r^\ell e^{-r^2/2} L_n^{\ell+1/2}(r^2), \\ \text{and } E_{nlm} = 2n + \ell + \frac{3}{2}, \end{aligned} \quad (2.3)$$

with $n = 0, 1, \dots$ and $\ell = 0, 1, \dots$. Above, r and \hat{r} denote the modulus and angular components of the vector \mathbf{r} , respectively. The function Y_{lm} represents the standard spherical harmonics [35] and $L_n^{\ell+1/2}$ denotes the generalized Laguerre polynomials [36]. The use of spherical harmonics ensures that $\varphi_{nlm}(\mathbf{r})$ is an eigenstate of both the angular momentum Casimir operator and the third projection of the angular momentum associated with \mathbf{r} . The corresponding quantum numbers, ℓ and m , are often referred to as orbital quantum numbers. Notably, states with different m values are degenerated. The remaining quantum number, n , characterises the radial contribution to the energy and is thus known as the radial quantum number. The different φ_{nlm} wave functions are orthonormal.

With the separation of variables, the eigenfunctions for the full Hamiltonian, denoted $\Phi_{n_x \ell_x n_y \ell_y}^L(\mathbf{x}, \mathbf{y})$, are expressed as products of the eigenstates of the partial Hamiltonians. The corresponding eigenvalues, denoted $E_{n_x \ell_x n_y \ell_y}^L$, are given by the sum of the partial eigenvalues,

$$\Phi_{n_x \ell_x n_y \ell_y}^L(\mathbf{x}, \mathbf{y}) = [\varphi_{n_x \ell_x}(\mathbf{x})\varphi_{n_y \ell_y}(\mathbf{y})]_L \text{ and } E_{n_x \ell_x n_y \ell_y}^L = 2n_x + \ell_x + 2n_y + \ell_y + 3. \quad (2.4)$$

With this definition, the $\Phi_{n_x \ell_x n_y \ell_y}^L$ wave functions are orthogonal too. As suggested by the notation, n_x and ℓ_x (resp. n_y and ℓ_y) are interpreted as the radial and orbital quantum numbers associated with the coordinate \mathbf{x} (resp. \mathbf{y}). A combination of these quantum numbers that will frequently appear in the following discussions is Q , the number of quanta associated with Φ ,

$$Q = 2n_x + \ell_x + 2n_y + \ell_y. \quad (2.5)$$

In (2.4), the square brackets $[...]_L$ indicate that different third projections of angular momentum associated with the coordinates \mathbf{x} and \mathbf{y} are coupled to construct eigenstates of the total angular momentum operators, namely $L^2 = (\mathbf{L}_x + \mathbf{L}_y)^2$ and $L_z = (\mathbf{L}_x)_z + (\mathbf{L}_y)_z$. The corresponding

quantum numbers are denoted L and M , respectively. This recoupling is possible because the eigenstates (2.3) are degenerate in m . The coefficients involved in this recombination, denoted $\langle \ell_x m_x \ell_y m_y | LM \rangle$, are the well-known Clebsh-Gordan coefficients [35],

$$[\varphi_{n_x \ell_x}(\mathbf{x}) \varphi_{n_y \ell_y}(\mathbf{y})]_L = \sum_{m_x m_y} \langle \ell_x m_x \ell_y m_y | LM \rangle \varphi_{n_x \ell_x m_x}(\mathbf{x}) \varphi_{n_y \ell_y m_y}(\mathbf{y}). \quad (2.6)$$

Since Clebsh-Gordan coefficients are well-documented, their derivation and computation will not be detailed here¹. For the following discussions, it suffices to recall the standard rules for angular momentum coupling: the quantum numbers ℓ_x , ℓ_y and L must satisfy $|\ell_x - \ell_y| \leq L \leq \ell_x + \ell_y$. Definition (2.6) should be understood as a simple basis transformation, allowing one to switch from the common eigenstates of \mathbf{L}_x^2 , $(\mathbf{L}_x)_z$, \mathbf{L}_y^2 and $(\mathbf{L}_y)_z$ to those of L^2 , L_z , \mathbf{L}_x^2 and \mathbf{L}_y^2 . The latter basis is preferred because total angular momentum is an observable of interest, and because most Hamiltonians commute with both L^2 and L_z . In the notation $[\dots]_L$, the total angular momentum projection M has been omitted. This is because none of the matrix elements considered in the following sections explicitly depend on this quantum number².

The wave functions Φ are the ones used as trial functions in the oscillator bases expansion for three-body systems. Therefore, efficiently evaluating matrix elements such as

$$\langle \Phi_{n'_x \ell'_x n'_y \ell'_y}^L(\mathbf{x}, \mathbf{y}) | \mathcal{O}(\mathbf{x}, \mathbf{y}) | \Phi_{n_x \ell_x n_y \ell_y}^L(\mathbf{x}, \mathbf{y}) \rangle \quad \text{and} \quad \langle \Phi_{n'_x \ell'_x n'_y \ell'_y}^L(\mathbf{x}, \mathbf{y}) | \mathcal{O}(\mathbf{p}, \mathbf{q}) | \Phi_{n_x \ell_x n_y \ell_y}^L(\mathbf{x}, \mathbf{y}) \rangle \quad (2.7)$$

is a key objective of this method. The remainder of this section discusses properties of the harmonic oscillator eigenstates that will provide support in this regard.

Talmi's integral technique

In general, it is possible to reduce the aforementioned matrix elements to the evaluation of matrix elements on one-body harmonic oscillator eigenfunctions (2.3),

$$\langle \varphi_{n' \ell' m'}(\mathbf{r}) | \mathcal{O}(ar) | \varphi_{n \ell m}(\mathbf{r}) \rangle = \delta_{\ell' \ell} \delta_{m' m} \int r^2 dr R_{n' \ell'}(r) \mathcal{O}(ar) R_{n \ell}(r). \quad (2.8)$$

with a a real parameter which has been made explicit for further use. Because \mathcal{O} only depend on the modulus of \mathbf{r} , angular integrals are turned into Kronecker deltas using spherical harmonics

¹ Clebsh-Gordan coefficients play an important role in the theory of group representations, particularly in the decomposition of tensor product representations into irreducible representations. For further details, the reader is referred to [37].

² Since the quantum numbers m_x and m_y are summed over in the coupling, these are also naturally excluded from the left-hand side notation.

orthonormality, [35]. The remaining integral can be evaluated using the Talmi's integral technique [38],

$$\int r^2 dr R_{n'\ell}(r) \mathcal{O}(ar) R_{n\ell}(r) = \sum_{p=\frac{\ell+\ell'}{2}}^{n+n'+\frac{\ell+\ell'}{2}} B(n'\ell, n\ell, p) I_p(\mathcal{O}, a) \quad (2.9)$$

with

$$I_p(\mathcal{O}, a) = \frac{2}{\Gamma(p+3/2)} \int dr r^{2p+2} e^{-r^2} \mathcal{O}(ar). \quad (2.10)$$

In short, property (2.9) explicitly expresses the Laguerre polynomials from the $R_{n\ell}$ functions, allowing the left-hand side integral to be expanded as a sum of simpler ones, known as Talmi's integrals and denoted $I_p(\mathcal{O}, a)$. A closed formula for the $B(n'\ell; n\ell; p)$ coefficient is provided in [38]. Since these coefficients depend only on the quantum numbers within the set of trial states, they can be computed once, stored and subsequently retrieved whenever needed. For many functions \mathcal{O} (including cases of physical interest), the integrals $I_p(\mathcal{O}, a)$ admit analytical expressions, eliminating the need for numerical integration (see Complement 2.A). In all cases, the use of formulas (2.9) and (2.10) enables rapid and accurate evaluations of the matrix elements (2.8).

Momentum matrix element

The \mathcal{O} function in equation (2.8) depend solely on a position variable. Consequently, the direct application of Talmi's integral technique is not feasible when dealing with an operator that depends on momentum. However, as the Fourier transform of a one-body harmonic oscillator eigenfunctions remains a one-body harmonic oscillator eigenfunctions (up to a phase factor) [39],

$$\frac{1}{(2\pi)^{3/2}} \int d^3r e^{-i\mathbf{p}\mathbf{r}} \varphi_{n\ell m}(\mathbf{r}) = (-i)^{2n+\ell} \varphi_{n\ell m}(\mathbf{p}), \quad (2.11)$$

this technique can still be applied by switching to momentum representation. For quadratic functions of momentum, which are particularly relevant as they are associated with non-relativistic kinetic energy, the following relation can also be employed to simplify calculations [40, relation 3.10],

$$\begin{aligned} \langle \varphi_{n'\ell'm'}(\mathbf{r}) | \mathbf{p}^2 | \varphi_{n\ell m}(\mathbf{r}) \rangle &= \delta_{\ell'\ell} \delta_{m'm} \left((2n + \ell + 3/2) \delta_{n'n} \right. \\ &\quad \left. + \sqrt{n(n + \ell + 1/2)} \delta_{n'+1n} + \sqrt{n'(n' + \ell + 1/2)} \delta_{n'n+1} \right). \end{aligned} \quad (2.12)$$

Parity inversion and exchange of coordinates

Thanks to the properties of spherical harmonics [35, section 5.5.2], one can show that a parity inversion of the \mathbf{x} and \mathbf{y} coordinates in the $\Phi_{n_x \ell_x n_y \ell_y}^L(\mathbf{x}, \mathbf{y})$ functions simply produces additional real phase factors,

$$\Phi_{n_x \ell_x n_y \ell_y}^L(-\mathbf{x}, -\mathbf{y}) = (-1)^{\ell_x + \ell_y} \Phi_{n_x \ell_x n_y \ell_y}^L(\mathbf{x}, \mathbf{y}). \quad (2.13)$$

The \mathbf{x} and \mathbf{y} coordinates can also be exchanged. Using symmetry properties of Clebsch-Gordan coefficients [35, section 8.4.3], one can show that

$$\Phi_{n_x \ell_x n_y \ell_y}^L(\mathbf{y}, \mathbf{x}) = (-1)^{L - \ell_x - \ell_y} \Phi_{n_y \ell_y n_x \ell_x}^L(\mathbf{x}, \mathbf{y}). \quad (2.14)$$

Rotation of the coordinates

Instead of directly solving the Hamiltonian (2.1), one may try beforehand a change of coordinates. This Hamiltonian is symmetrical under the following coordinate transformation,

$$\begin{cases} \tilde{\mathbf{x}} = \cos \beta \mathbf{x} + \sin \beta \mathbf{y} \\ \tilde{\mathbf{y}} = -\sin \beta \mathbf{x} + \cos \beta \mathbf{y} \end{cases}. \quad (2.15)$$

As a consequence, all the functions $\Phi_{n_x \ell_x n_y \ell_y}^L(\tilde{\mathbf{x}}, \tilde{\mathbf{y}})$ are also eigenfunctions of (2.1) with $2n_x + \ell_x + 2n_y + \ell_y + 3$ as eigenvalue. This ensures that any $\Phi_{n_x \ell_x n_y \ell_y}^L(\tilde{\mathbf{x}}, \tilde{\mathbf{y}})$ can be expressed as a linear combination of $\Phi_{n'_x \ell'_x n'_y \ell'_y}^L(\mathbf{x}, \mathbf{y})$ functions that share the same energy eigenvalue than $\Phi_{n_x \ell_x n_y \ell_y}^L(\tilde{\mathbf{x}}, \tilde{\mathbf{y}})$,

$$\Phi_{n_x \ell_x n_y \ell_y}^L(\tilde{\mathbf{x}}, \tilde{\mathbf{y}}) = \sum_{n'_x \ell'_x n'_y \ell'_y} \langle n'_x \ell'_x n'_y \ell'_y; L | n_x \ell_x n_y \ell_y; L \rangle_{\beta} \Phi_{n'_x \ell'_x n'_y \ell'_y}^L(\mathbf{x}, \mathbf{y}) \quad (2.16)$$

where the summations on n'_x , ℓ'_x , n'_y and ℓ'_y are restricted to terms with a number of quanta equal to $2n_x + \ell_x + 2n_y + \ell_y$. This constraint ensures that the summation is finite. The coefficients denoted as $\langle n'_x \ell'_x n'_y \ell'_y; L | n_x \ell_x n_y \ell_y; L \rangle_{\beta}$ in equation (2.16) are known as Brody-Moshinsky coefficients with angle β . These can be computed recursively using the formula proposed in [41].

Passage to Hyperspherical coordinates

The Hamiltonian (2.1) can also be solved in hyperspherical coordinates [42]. The two three-dimensional \mathbf{x} and \mathbf{y} vectors are replaced by a single six-dimensional vector for which

hyperspherical coordinates are used [43, 42]. An hyperradius is defined

$$\rho^2 = \mathbf{x}^2 + \mathbf{y}^2, \quad (2.17)$$

as well as five hyperangles. Four among the five angles are simply chosen as the usual polar and azimuthal angles of the \mathbf{x} and \mathbf{y} vectors. These will therefore respectively be denoted θ_x , θ_y , φ_x and φ_y . The fifth angle, denoted α , is defined as follows³,

$$x = \rho \sin \alpha, \quad y = \rho \cos \alpha. \quad (2.18)$$

Because both x and y are positive definite, α lies in between 0 and $\pi/2$. For notation convenience, in the following, the set of angles $(\theta_x, \theta_y, \varphi_x, \varphi_y, \alpha)$ will be denoted as Ω . Switching to this system of coordinates, the harmonic oscillator Hamiltonian (2.1) in position representation reads

$$H_{\text{oh}} = -\frac{1}{2} \left(\frac{\partial^2}{\partial \rho^2} + \frac{5}{\rho} \frac{\partial}{\partial \rho} - \frac{1}{\rho^2} \Delta_{\Omega} \right) + \frac{\rho^2}{2}. \quad (2.19)$$

Above Δ_{Ω} is the hyperspherical Laplacian operator in six dimensions. The full expression of this operator is depicted in [43, 42]. Its eigenfunctions, known as hyperspherical harmonics, reads

$$\begin{aligned} \mathcal{Y}_K^{\ell_x \ell_y LM}(\Omega) &= N_K^{\ell_x \ell_y} \sin^{\ell_x} \alpha \cos^{\ell_y} \alpha P_n^{(\ell_x + \frac{1}{2}, \ell_y + \frac{1}{2})}(\cos 2\alpha) [Y_{\ell_x}(\theta_x, \varphi_x) Y_{\ell_y}(\theta_y, \varphi_y)]_L \\ \text{with } N_K^{\ell_x \ell_y} &= \left(\frac{2n!(K+2)(n+\ell_x+\ell_y+1)!}{\Gamma(n+\ell_x+3/2)\Gamma(n+\ell_y+3/2)} \right)^{1/2} \text{ and } n = \frac{K-\ell_x-\ell_y}{2} \end{aligned} \quad (2.20)$$

with the corresponding eigenvalue $K(K+4)$. Above, $P_n^{(a,b)}$ denotes a Jacobi polynomial [36]. The expression (2.19) is the one of a one-body harmonic oscillator Hamiltonian in a six-dimensional space. Separating the hyperradial and hyperangular parts of the equation, the following eigenfunctions are obtained [42],

$$\Psi_{NK}^{\ell_x \ell_y L}(\rho, \Omega) = \mathcal{R}_{NK}(\rho) \mathcal{Y}_K^{\ell_x \ell_y LM}(\Omega) \text{ with } \mathcal{R}_{NK}(\rho) = \sqrt{\frac{2(N!)}{\Gamma(K+N+3)}} e^{-\frac{\rho^2}{2}} \rho^K L_N^{K+2}(\rho^2), \quad (2.21)$$

the associated eigenvalues being $E_{NK}^{\ell_x \ell_y m_x m_y} = 2N + K + 3$. By construction, states $\Psi_{NK}^{\ell_x \ell_y L}$ have a total orbital angular momentum L as well as individual orbital angular momenta ℓ_x and ℓ_y .

Both sets of functions $\Psi_{NK}^{\ell_x \ell_y L}(\rho, \Omega)$ and $\Phi_{n_x n_y \ell_y}^L(\mathbf{x}, \mathbf{y})$ are eigenstates of the harmonic

³ This definition differs from the one used in [42]. To compare our relations with the ones from this reference, x and y have to be exchanged.

oscillator Hamiltonian, of the total orbital angular momentum operator and of the two individual angular momenta operators. Therefore, the $\Phi_{n_x \ell_x n_y \ell_y}^L(\mathbf{x}, \mathbf{y})$ functions can be written as a linear combination of all the $\Psi_{NK}^{\ell_x \ell_y L}(\rho, \Omega)$ functions with energy eigenvalue $E_{n_x \ell_x n_y \ell_y}^L$,

$$\Phi_{n_x \ell_x n_y \ell_y}^L(\mathbf{x}, \mathbf{y}) = \sum_{NK} \langle n_x n_y | NK \rangle_{\ell_x \ell_y} \Psi_{NK}^{\ell_x \ell_y L}(\rho, \Omega) \quad (2.22)$$

where the summations on N and K are restricted to terms where $2N + K = 2n_x + \ell_x + 2n_y + \ell_y$. The coefficients $\langle n_x n_y | NK \rangle_{\ell_x \ell_y}$ are defined by the following overlap integral,

$$\langle n_x n_y | NK \rangle_{\ell_x \ell_y} = \int d^3x d^3y \Psi_{NK}^{\ell_x \ell_y L}(\rho, \Omega)^* \Phi_{n_x \ell_x n_y \ell_y}^L(\mathbf{x}, \mathbf{y}). \quad (2.23)$$

In the following, these coefficients will be referred as hyperspherical coefficients. A closed formula to compute them is demonstrated in Complement 2.B.

2.1.2 Three-body Hamiltonians and Jacobi Coordinates

The aforementioned harmonic oscillator eigenstates will be used to solve three-body Hamiltonians of the form (1.12), which is restated below for reference,

$$H = T(\mathbf{p}_1, \mathbf{p}_2, \mathbf{p}_3) + V_{12}(r_{12}) + V_{13}(r_{13}) + V_{23}(r_{23}) + W\left(\sqrt{r_{12}^2 + r_{13}^2 + r_{23}^2}\right) \quad (2.24)$$

with $r_{ij} = |\mathbf{r}_i - \mathbf{r}_j|$.

As a reminder, variables \mathbf{r}_i and \mathbf{p}_i denote the position and momentum of the i -th particle in the system, respectively. Compared to (1.12), general two-body potentials V_{ij} and a three-body interaction W of the type announced in Section 1.1.2 are considered but one-body interactions have been omitted, these being less common. For the kinetic part of H , both non-relativistic (1.16) and semi-relativistic (1.17) kinematics can be considered.

To isolate the centre-of-mass motion in the Hamiltonian (2.24) requires to change of coordinates. For many-body systems, Jacobi coordinates are often used. [28, 44]. In the case of three non-relativistic particles, these replace the three individual positions by the centre-of-mass position, the relative position between particle 1 and 2 and the relative position between particle 3 and the centre-of-mass of particles 1 and 2. More precisely, for the current purpose, dimensionless Jacobi coordinates scaled with two variational parameters, denoted a and b , are

used,

$$a\mathbf{x} = \mathbf{r}_1 - \mathbf{r}_2, \quad b\mathbf{y} = \frac{m_1\mathbf{r}_1 + m_2\mathbf{r}_2}{m_{12}} - \mathbf{r}_3, \quad \mathbf{R} = \frac{m_1\mathbf{r}_1 + m_2\mathbf{r}_2 + m_3\mathbf{r}_3}{M}, \quad (2.25)$$

where m_{12} stands for $m_1 + m_2$. These dimensionless Jacobi coordinates were first introduced in nuclear physics [44], and have since been applied to hadronic physics as well [28]. Oscillator bases with a single scale parameter have also been employed in nuclear physics for systems of 2, 3, 4, and even N particles [40]. The momenta conjugate to \mathbf{x} , \mathbf{y} and \mathbf{R} are respectively given by

$$\frac{\mathbf{p}}{a} = \frac{m_2\mathbf{p}_1 - m_1\mathbf{p}_2}{m_{12}}, \quad \frac{\mathbf{q}}{b} = \frac{m_3(\mathbf{p}_1 + \mathbf{p}_2) - m_{12}\mathbf{p}_3}{M}, \quad \mathbf{P} = \mathbf{p}_1 + \mathbf{p}_2 + \mathbf{p}_3. \quad (2.26)$$

The interpretation of Jacobi coordinates in terms of centre-of-mass positions also applies for identical relativistic particles. However, in a relativistic treatment of systems with unequal masses, defining the centre-of-mass position requires knowing each particle's energy, making this task more complex. Nevertheless, although the interpretation of Jacobi coordinates no longer strictly holds in this context, the use of \mathbf{x} and \mathbf{y} coordinates to describe the internal motion remains valid. In both classical and relativistic mechanics, the condition $\mathbf{P} = \mathbf{0}$ ensures that eigenenergies are not affected by a possible global translational motion of the system. The only drawbacks of using Jacobi coordinates in relativistic contexts are potentially poorer convergence rates and inadequate resulting eigenstates⁴. The Hamiltonian (2.24) can explicitly be written in these Jacobi coordinates. The non-relativistic kinetic energies becomes

$$T_{\text{nr}}(\mathbf{p}, \mathbf{q}) = \frac{\mathbf{p}^2}{2\mu_p} + \frac{\mathbf{q}^2}{2\mu_q} \quad \text{with} \quad \mu_p = \frac{a^2 m_1 m_2}{m_{12}} \quad \text{and} \quad \mu_q = \frac{b^2 m_3 m_{12}}{M}, \quad (2.27)$$

the semi-relativistic one becomes

$$T_{\text{r}}(\mathbf{p}, \mathbf{q}) = \sqrt{\left(\frac{m_1}{m_{12}} \frac{\mathbf{q}}{b} + \frac{\mathbf{p}}{a}\right)^2 + m_1^2} + \sqrt{\left(\frac{m_2}{m_{12}} \frac{\mathbf{q}}{b} - \frac{\mathbf{p}}{a}\right)^2 + m_2^2} + \sqrt{\frac{\mathbf{q}^2}{b^2} + m_3^2}. \quad (2.28)$$

Above, the centre-of-mass motion has been manually cancelled by setting $\mathbf{P} = \mathbf{0}$. Finally, the arguments of both two-body and three-body interactions are modified,

$$V_{12}(|a\mathbf{x}|) + V_{13}\left(\left| -b\mathbf{y} - \frac{m_2}{m_{12}}a\mathbf{x} \right|\right) + V_{23}\left(\left| b\mathbf{y} - \frac{m_1}{m_{12}}a\mathbf{x} \right|\right), \quad (2.29)$$

⁴ The latter issue can be mitigated by employing the *point-form formalism* [45]

$$W \left(\sqrt{a^2 \left(1 + \frac{m_1^2 + m_2^2}{m_{12}^2} \right) \mathbf{x}^2 + 2b^2 \mathbf{y}^2 + 2ab \left(\frac{m_2 - m_1}{m_{12}} \right) \mathbf{x} \cdot \mathbf{y}} \right). \quad (2.30)$$

2.1.3 Setup of the bases

As the centre of mass motion has been removed in H , both the variables \mathbf{R} and \mathbf{P} do not enter in any parts of the Hamiltonian, thereby reducing the number of degrees of freedom to two. The remaining \mathbf{x} and \mathbf{y} coordinates can be used as a pair of three-dimensional coordinates on which harmonic oscillator eigenstates from Section 2.1.1 can depend. These functions will now be used to construct a concrete set of trial states whose features are in accordance with the system under consideration and the expectations of the user.

Orbital angular momentum and parity

First, in most problems, a solution with a given total orbital angular momentum is expected. To ensure that the provided approximation satisfies this requirement, the set of Φ functions is restricted to the ones whose L quantum number is in agreement with the expected total orbital angular momentum. Similarly, for some applications, a parity eigenstate is also expected. As the parity transformation, denoted Π , inverts the positions of each particles, its action on Jacobi coordinates is given by $\Pi^\dagger \mathbf{x} \Pi = -\mathbf{x}$ and $\Pi^\dagger \mathbf{y} \Pi = -\mathbf{y}$. Therefore, the action of the parity operator on the trial functions can directly be deduced from relation (2.13),

$$\Pi \Phi_{n_x \ell_x n_y \ell_y}^L(\mathbf{x}, \mathbf{y}) = \Phi_{n_x \ell_x n_y \ell_y}^L(-\mathbf{x}, -\mathbf{y}) = (-1)^{\ell_x + \ell_y} \Phi_{n_x \ell_x n_y \ell_y}^L(\mathbf{x}, \mathbf{y}). \quad (2.31)$$

The Φ functions are already parity eigenstates and the corresponding eigenvalue is given by the parity of $\ell_x + \ell_y$. Filling the set of trial states with even (resp. odd) sum of ℓ_x and ℓ_y ensure that the provided approximation will be a positive (resp. negative) parity eigenstate.

Symmetry under exchange of particles

As introduced in Section 1.1.4, in presence of identical particles, symmetries under the exchange of pairs of particles have to be introduced. The state of a system containing two identical particles must be either symmetric (for bosons) or anti-symmetric (for fermions) under their permutation. Let us choose particle 1 and 2 as the two identical particle and denote \mathbb{P}_{12} the operator that encodes their permutation. Acting on the Jacobi coordinates, this operator

reverses \mathbf{x} and lets \mathbf{y} unchanged,

$$\mathbb{P}_{12}^\dagger \mathbf{x} \mathbb{P}_{12} = -\mathbf{x}, \quad \mathbb{P}_{12}^\dagger \mathbf{y} \mathbb{P}_{12} = \mathbf{y}. \quad (2.32)$$

As a consequence, the action of \mathbb{P}_{12} on a Φ function can directly be obtained from a property similar to (2.13),

$$\mathbb{P}_{12} \Phi_{n_x \ell_x n_y \ell_y}^L(\mathbf{x}, \mathbf{y}) = \Phi_{n_x \ell_x n_y \ell_y}^L(-\mathbf{x}, \mathbf{y}) = (-1)^{\ell_x} \Phi_{n_x \ell_x n_y \ell_y}^L(\mathbf{x}, \mathbf{y}). \quad (2.33)$$

A Φ function is already an eigenstate of \mathbb{P}_{12} and the corresponding eigenvalue is given by the parity of its ℓ_x quantum number. In conclusion, in presence of two identical particles, the set of trial states must be filled with Φ functions of same ℓ_x parity (odd in presence of fermions and even in presence of bosons).

In presence of three identical particles, the situation is a bit more complicated. The state of the system must now be completely (anti)symmetric under any exchange of particles. Hopefully, because any permutation of three particles can be expressed in terms of two transpositions, it is sufficient to (anti)symmetrise on the exchange of particles 1 and 2 and of particles 2 and 3. For the first one, the task has already been done in the previous paragraph: a correct \mathbb{P}_{12} symmetry is ensured by considering only states of a given ℓ_x parity. The rest of the calculations considers this selection as carried out. The (anti)symmetrisation must now be performed on the exchange of particles 2 and 3, denoted \mathbb{P}_{23} . The action of this operator on Jacobi coordinates is given by

$$\mathbb{P}_{23}^\dagger \mathbf{x} \mathbb{P}_{23} = \frac{\mathbf{x}}{2} + \frac{b}{a} \mathbf{y}, \quad \mathbb{P}_{23}^\dagger \mathbf{y} \mathbb{P}_{23} = \frac{3a}{4b} \mathbf{x} - \frac{\mathbf{y}}{2}. \quad (2.34)$$

With such a coordinate transformation, the Φ functions will not be eigenstates of this operator. To obtain (anti)symmetric functions, one has to compute the matrix elements of the \mathbb{P}_{23} operator and to subsequently diagonalise it,

$$\begin{aligned} \langle \Phi_{n'_x \ell'_x n'_y \ell'_y}^{L'}(\mathbf{x}, \mathbf{y}) | \mathbb{P}_{23} | \Phi_{n_x \ell_x n_y \ell_y}^L(\mathbf{x}, \mathbf{y}) \rangle &= \langle \Phi_{n'_x \ell'_x n'_y \ell'_y}^{L'}(\mathbf{x}, \mathbf{y}) | \Phi_{n_x \ell_x n_y \ell_y}^L(\mathbf{x}', \mathbf{y}') \rangle \\ &\text{with } \mathbf{x}' = \frac{\mathbf{x}}{2} + \frac{b}{a} \mathbf{y} \text{ and } \mathbf{y}' = \frac{3a}{4b} \mathbf{x} - \frac{\mathbf{y}}{2}. \end{aligned} \quad (2.35)$$

It has been shown in [28] that the eigenstates of \mathbb{P}_{23} contain a finite number of Φ states only if $b = \sqrt{3}a/2$. Otherwise, the symmetry of the trial states can only be approximated. This leads to a trade-off between introducing a second non-linear variational parameter and preserving the symmetry to the trial states. Reference [28] concluded that prioritising symmetry is the preferable choice⁵. Assuming $b = \sqrt{3}a/2$, (2.34) becomes a rotation of coordinates as in (2.15)

and the \mathbb{P}_{23} matrix elements can be evaluated combining property (2.16) and the orthonormality of the oscillator eigenstates,

$$\langle \Phi_{n'_x \ell'_x n'_y \ell'_y}^{L'}(\mathbf{x}, \mathbf{y}) | \mathbb{P}_{23} | \Phi_{n_x \ell_x n_y \ell_y}^L(\mathbf{x}, \mathbf{y}) \rangle = \delta_{L'L} (-1)^{\ell'_x + \ell'_y + L} \langle n'_y \ell'_y n'_x \ell'_x; L' | n_x \ell_x n_y \ell_y; L \rangle_{\pi/6}. \quad (2.36)$$

By definition, the Brody-Moshinsky coefficient in this relation is zero if both number of quanta differs. As announced, if $b = \sqrt{3}a/2$, \mathbb{P}_{23} mixes together a finite number of states, the ones with the same total orbital angular momentum, the same parity and the same number of quanta. Therefore, to exactly get symmetrized states, it is sufficient to built the \mathbb{P}_{23} matrix up to an arbitrary number of quanta and to diagonalise it. The set of trial states can then be filled with all the obtained eigenvectors whose eigenvalue corresponds to the expected symmetry (namely +1 for three-boson systems and -1 for three-fermion systems). As a consequence, for three identical particles, the set Φ functions cannot be truncated randomly: all the Φ functions until a given number of quanta are necessarily involved in the calculations.

Convenient truncation for the bases

Except for systems of three identical particles, it seems that the set of oscillator eigenstates can be truncated everywhere. However, because property (2.16) will be used during the evaluation of matrix elements, a given Φ function will be decomposed as a linear combination of all the Φ functions that have the same number of quanta. Therefore, it is more convenient to include from the beginning all these functions in the calculations. So, even for systems of three different particles, the recommended sets of trial states contain all the Φ functions until a given number of quanta, denoted Q_{\max} . The higher Q_{\max} is, the more accurate the approximation produced by the set is but the larger the Hamiltonian matrix is.

Examples of trial sets

To illustrate the concepts discussed in this section, let us explicitly construct a few trial sets. First, consider a system made up three different particles for which a solution with total angular momentum $L = 1$ and negative parity is expected. Only states with a number of quanta less than three are included, setting $Q_{\max} = 3$. Within this set, trial states are ordered in ascending number of quanta,

$$\{\Phi_{0100}^1(\mathbf{x}, \mathbf{y}), \Phi_{0001}^1(\mathbf{x}, \mathbf{y}), \Phi_{1100}^1(\mathbf{x}, \mathbf{y}), \Phi_{0110}^1(\mathbf{x}, \mathbf{y}), \Phi_{1001}^1(\mathbf{x}, \mathbf{y}), \Phi_{0011}^1(\mathbf{x}, \mathbf{y}), \Phi_{0201}^1(\mathbf{x}, \mathbf{y}), \Phi_{0102}^1(\mathbf{x}, \mathbf{y})\}. \quad (2.37)$$

⁵ Let us also mention that the constraint $b = \sqrt{3}a/2$ restores the OBE to its original form [31, 30].

States with even numbers of quanta are forbidden by the parity constraint, while states that do not satisfy $|\ell_x - \ell_y| \leq 1 \leq \ell_x + \ell_y$ are excluded due to the angular momentum constraint.

As a second example, consider a system of two identical bosons and a different one. Here, a state with angular momentum $L = 0$ and positive parity is expected, and the break condition is set to $Q_{\max} = 4$. This yields the following set of trial states,

$$\{\Phi_{0000}^0(\mathbf{x}, \mathbf{y}), \Phi_{1000}^0(\mathbf{x}, \mathbf{y}), \Phi_{0010}^0(\mathbf{x}, \mathbf{y}), \Phi_{2000}^0(\mathbf{x}, \mathbf{y}), \Phi_{0020}^0(\mathbf{x}, \mathbf{y}), \Phi_{1010}^0(\mathbf{x}, \mathbf{y}), \Phi_{0202}^0(\mathbf{x}, \mathbf{y})\}. \quad (2.38)$$

States with odd numbers of quanta are excluded by the parity constraint, those with $\ell_x \neq \ell_y$ are ruled out by the angular momentum constraint, and finally, those with odd ℓ_x are forbidden by the symmetry constraint.

As a final example, consider a system of three identical bosons with expected angular momentum $L = 0$ and positive parity. For such a system, the trial set consists of eigenstates of \mathbb{P}_{23} . With $Q_{\max} = 4$, the resulting trial set is

$$\left\{ \Phi_{0000}^0(\mathbf{x}, \mathbf{y}), \frac{\Phi_{1000}^0(\mathbf{x}, \mathbf{y}) + \Phi_{0010}^0(\mathbf{x}, \mathbf{y})}{\sqrt{2}}, \frac{\sqrt{5}}{4} \Phi_{2000}^0(\mathbf{x}, \mathbf{y}) + \frac{\sqrt{5}}{4} \Phi_{0020}^0(\mathbf{x}, \mathbf{y}) + \sqrt{\frac{3}{8}} \Phi_{1010}^0(\mathbf{x}, \mathbf{y}), \right. \\ \left. \frac{\Phi_{2000}^0(\mathbf{x}, \mathbf{y}) + \Phi_{0020}^0(\mathbf{x}, \mathbf{y})}{4} - \sqrt{\frac{5}{24}} \Phi_{1010}^0(\mathbf{x}, \mathbf{y}) + \sqrt{\frac{2}{3}} \Phi_{0202}^0(\mathbf{x}, \mathbf{y}) \right\}. \quad (2.39)$$

Since states in this trial set are combinations of those from (2.38), the conditions on angular momentum and parity are preserved. Furthermore, all included states are symmetric under any particle exchange.

2.1.4 Calculation of Matrix Elements

The set of trial states being chosen, the matrix elements of the Hamiltonian have now to be evaluated. This goal will be completed thanks to the properties enumerated in section 2.1.1. Kinetic energies, two-body interactions and three-body interactions are considered separately.

Non-relativistic kinetic energy

Non-relativistic kinetics (2.27) are considered first. The following matrix elements have to be evaluated,

$$\langle \Phi_{n'_x \ell'_x n'_y \ell'_y}^{L'}(\mathbf{x}, \mathbf{y}) | \left(\frac{\mathbf{p}^2}{2\mu_p} + \frac{\mathbf{q}^2}{2\mu_q} \right) | \Phi_{n_x \ell_x n_y \ell_y}^L(\mathbf{x}, \mathbf{y}) \rangle \\ = \frac{1}{2\mu_p} \langle \Phi_{n'_x \ell'_x n'_y \ell'_y}^{L'}(\mathbf{x}, \mathbf{y}) | \mathbf{p}^2 | \Phi_{n_x \ell_x n_y \ell_y}^L(\mathbf{x}, \mathbf{y}) \rangle + \frac{1}{2\mu_q} \langle \Phi_{n'_x \ell'_x n'_y \ell'_y}^{L'}(\mathbf{x}, \mathbf{y}) | \mathbf{q}^2 | \Phi_{n_x \ell_x n_y \ell_y}^L(\mathbf{x}, \mathbf{y}) \rangle. \quad (2.40)$$

As both terms can be evaluated similarly, let us focus on the first one. To start with, Φ functions are expressed using relations (2.4) and (2.6). Because the \mathbf{p}^2 operator only acts on the \mathbf{x} part of the Φ function, the orthonormalisation of the φ function can be used to get rid of the \mathbf{y} dependence. In addition, considering that \mathbf{p}^2 is a scalar operator⁶, Clebsh-Gordan coefficients can be removed using results from [35, section 8.1.1],

$$\langle \Phi_{n'_x \ell'_x n'_y \ell'_y}^{L'}(\mathbf{x}, \mathbf{y}) | \mathbf{p}^2 | \Phi_{n_x \ell_x n_y \ell_y}^L(\mathbf{x}, \mathbf{y}) \rangle = \delta_{L'L} \delta_{n'_y n_y} \delta_{\ell'_y \ell_y} \delta_{\ell'_x \ell_x} \langle \phi_{n'_x \ell'_x 0}(\mathbf{x}) | \mathbf{p}^2 | \phi_{n_x \ell_x 0}(\mathbf{x}) \rangle. \quad (2.41)$$

Relation (2.12) can then be used to evaluate the residual matrix element. Collating with the analogous result for the \mathbf{q}^2 term, the following analytical expression for the kinetic energy matrix energy is obtained,

$$\begin{aligned} \langle \Phi_{n'_x \ell'_x n'_y \ell'_y}^{L'}(\mathbf{x}, \mathbf{y}) | \left(\frac{\mathbf{p}^2}{2\mu_p} + \frac{\mathbf{q}^2}{2\mu_q} \right) | \Phi_{n_x \ell_x n_y \ell_y}^L(\mathbf{x}, \mathbf{y}) \rangle \\ = \delta_{L'L} \delta_{\ell'_x \ell_x} \delta_{\ell'_y \ell_y} \left(\frac{\delta_{n'_y n_y}}{a^2} (K_p)_{n'_x n_x} + \frac{\delta_{n'_x n_x}}{b^2} (K_q)_{n'_y n_y} \right) \end{aligned} \quad (2.42)$$

with

$$\begin{aligned} (K_p)_{n'_x n_x} &= \frac{m_{12}}{2m_1 m_2} \left((2n_x + \ell_x + 3/2) \delta_{n'_x n_x} + \sqrt{n_x(n_x + \ell_x + 1/2)} \delta_{n'_x + 1 n_x} \right. \\ &\quad \left. + \sqrt{n'_x(n'_x + \ell_x + 1/2)} \delta_{n'_x n_x + 1} \right), \\ (K_q)_{n'_y n_y} &= \frac{M}{2m_{12} m_3} \left((2n_y + \ell_y + 3/2) \delta_{n'_y n_y} + \sqrt{n_y(n_y + \ell_y + 1/2)} \delta_{n'_y + 1 n_y} \right. \\ &\quad \left. + \sqrt{n'_y(n'_y + \ell_y + 1/2)} \delta_{n'_y n_y + 1} \right). \end{aligned} \quad (2.43)$$

The K_p and K_q matrices being independent of the a and b variational parameters, they can be computed once for all at the beginning of the optimisation. Let us also mention that if the three particles are identical and $b = \sqrt{3}a/2$, due to symmetry properties of the trial states, both terms from (2.40) proves to be equal, thereby simplifying calculations.

Two-body potential matrix elements

The two-body potentials divide in three terms, one for each pair of particles. The one related to particle 1 and 2 only depends on the \mathbf{x} coordinate. Using the same arguments than for relation (2.41) in the treatment of the non-relativistic kinetic energy, the \mathbf{y} coordinate and the

⁶ An operator is called scalar if it commutes with all the angular momentum operators. Especially, when a scalar operator acts on an angular momentum eigenstate, the resulting state retains this property.

Clebsh-Gordan coefficients can be eliminated

$$\begin{aligned} \langle \Phi_{n'_x \ell'_x n'_y \ell'_y}^{L'}(\mathbf{x}, \mathbf{y}) | V_{12}(a|\mathbf{x}|) | \Phi_{n_x \ell_x n_y \ell_y}^L(\mathbf{x}, \mathbf{y}) \rangle \\ = \delta_{L'L} \delta_{n'_y n_y} \delta_{\ell'_y \ell_y} \langle \varphi_{n'_x \ell'_x 0}(\mathbf{x}) | V_{12}(a|\mathbf{x}|) | \varphi_{n_x \ell_x 0}(\mathbf{x}) \rangle. \end{aligned} \quad (2.44)$$

The remaining matrix element can be evaluated using the Talmi's integral technology developed in Section 2.1.1.

Both other two-body interactions depend explicitly on the \mathbf{x} and \mathbf{y} coordinates, thereby making their evaluation less straightforward. Next developments focus on the V_{23} matrix elements,

$$\langle \Phi_{n'_x \ell'_x n'_y \ell'_y}^{L'}(\mathbf{x}, \mathbf{y}) | V_{23} \left(\left| b\mathbf{y} - \frac{m_1}{m_{12}} a\mathbf{x} \right| \right) | \Phi_{n_x \ell_x n_y \ell_y}^L(\mathbf{x}, \mathbf{y}) \rangle. \quad (2.45)$$

To evaluate these matrix elements, the \mathbf{x} and \mathbf{y} coordinates can be rotated as in relation (2.15). An angle β_1 is defined so that

$$\cos(\beta_1) = \frac{m_{12}}{\gamma_1} b, \quad \sin(\beta_1) = \frac{m_1}{\gamma_1} a. \quad (2.46)$$

with $\gamma_1 = \sqrt{b^2 m_{12}^2 + a^2 m_1^2}$. New $\tilde{\mathbf{x}}$ and $\tilde{\mathbf{y}}$ coordinates are obtained by rotating $-\mathbf{x}$ and \mathbf{y} with angle $-\beta_1$,

$$\tilde{\mathbf{x}} = \frac{m_{12}}{\gamma_1} \left(-b\mathbf{x} - \frac{m_1}{m_{12}} a\mathbf{y} \right), \quad \tilde{\mathbf{y}} = \frac{m_{12}}{\gamma_1} \left(-\frac{m_1}{m_{12}} a\mathbf{x} + b\mathbf{y} \right). \quad (2.47)$$

The angle and the rotation have been chosen so that the argument of the V_{23} function is colinear with the $\tilde{\mathbf{y}}$ coordinate. The inverse change of coordinates rotates $\tilde{\mathbf{x}}$ and $\tilde{\mathbf{y}}$ with angle β_1 to recover $-\mathbf{x}$ and \mathbf{y} . Using relations (2.13) and (2.16), the Φ functions can be rewritten in terms of $\tilde{\mathbf{x}}$ and $\tilde{\mathbf{y}}$,

$$\Phi_{n_x \ell_x n_y \ell_y}^L(\mathbf{x}, \mathbf{y}) = (-1)^{\ell_x} \sum_{\nu_x \lambda_x \nu_y \lambda_y} \langle \nu_x \lambda_x \nu_y \lambda_y; L | n_x \ell_x n_y \ell_y; L \rangle_{\beta_1} \Phi_{\nu_x \lambda_x \nu_y \lambda_y}^L(\tilde{\mathbf{x}}, \tilde{\mathbf{y}}). \quad (2.48)$$

When inserted in (2.45), equation (2.48) gives

$$\begin{aligned} \langle \Phi_{n'_x \ell'_x n'_y \ell'_y}^{L'}(\mathbf{x}, \mathbf{y}) | V_{23} \left(\left| b\mathbf{y} - \frac{m_1}{m_{12}} a\mathbf{x} \right| \right) | \Phi_{n_x \ell_x n_y \ell_y}^L(\mathbf{x}, \mathbf{y}) \rangle \\ = (-1)^{\ell_x + \ell'_x} \sum_{\nu_x \lambda_x \nu_y \lambda_y} \sum_{\nu'_x \lambda'_x \nu'_y \lambda'_y} \langle \nu'_x \lambda'_x \nu'_y \lambda'_y; L' | n'_x \ell'_x n'_y \ell'_y; L' \rangle_{\beta_1} \langle \nu_x \lambda_x \nu_y \lambda_y; L | n_x \ell_x n_y \ell_y; L \rangle_{\beta_1} \\ \langle \Phi_{\nu'_x \lambda'_x \nu'_y \lambda'_y}^{L'}(\tilde{\mathbf{x}}, \tilde{\mathbf{y}}) | V_{23} \left(\frac{\gamma_1}{m_{12}} |\tilde{\mathbf{y}}| \right) | \Phi_{\nu_x \lambda_x \nu_y \lambda_y}^L(\tilde{\mathbf{x}}, \tilde{\mathbf{y}}) \rangle \end{aligned} \quad (2.49)$$

which can be simplified using the same arguments than for V_{12} and for the non-relativistic kinetic energy,

$$\begin{aligned} & \langle \Phi_{n'_x \ell'_x n'_y \ell'_y}^{L'}(\mathbf{x}, \mathbf{y}) | V_{23} \left(\left| b\mathbf{y} - \frac{m_1}{m_{12}} a\mathbf{x} \right| \right) | \Phi_{n_x \ell_x n_y \ell_y}^L(\mathbf{x}, \mathbf{y}) \rangle \\ &= \delta_{L'L} (-1)^{\ell_x + \ell'_x} \sum_{\nu_x \lambda_x \nu_y \lambda_y \nu'_y \lambda'_y} \langle \nu_x \lambda_x \nu'_y \lambda'_y; L' | n'_x \ell'_x n'_y \ell'_y; L' \rangle_{\beta_1} \langle \nu_x \lambda_x \nu_y \lambda_y; L | n_x \ell_x n_y \ell_y; L \rangle_{\beta_1} \quad (2.50) \\ & \langle \varphi_{\nu'_y \lambda'_y 0}(\tilde{\mathbf{y}}) | V_{23} \left(\frac{\gamma_1}{m_{12}} |\tilde{\mathbf{y}}| \right) | \varphi_{\nu_y \lambda_y 0}(\tilde{\mathbf{y}}) \rangle. \end{aligned}$$

This formula, together with the Talmi's integral technique, allows for an efficient evaluation of V_{23} matrix elements. However, because β_1 explicitly depends on the a and b variational parameters, Brody-Moshinsky coefficients will have to be recomputed at each step of the optimisation.

The V_{13} matrix element can be evaluated using the same technique than for V_{23} . First, a β_2 angle is introduced so that

$$\cos(\beta_2) = \frac{m_{12}}{\gamma_2} b, \quad \sin(\beta_2) = \frac{m_2}{\gamma_2} a. \quad (2.51)$$

with $\gamma_2 = \sqrt{b^2 m_{12}^2 + a^2 m_2^2}$. New $\tilde{\mathbf{x}}$ and $\tilde{\mathbf{y}}$ coordinates are defined by rotating $-\mathbf{y}$ and \mathbf{x} with angle $-\beta_2$. The $\tilde{\mathbf{x}}$ coordinate appears to be proportional to the argument of V_{13} while relations (2.13), (2.14) and (2.16) are used to rewrite the states in terms of the new coordinates. Finally, simplifying the remaining matrix elements, a relation similar to (2.50) is obtained⁷,

$$\begin{aligned} & \langle \Phi_{n'_x \ell'_x n'_y \ell'_y}^{L'}(\mathbf{x}, \mathbf{y}) | V_{13} \left(\left| -b\mathbf{y} - \frac{m_2}{m_{12}} a\mathbf{x} \right| \right) | \Phi_{n_x \ell_x n_y \ell_y}^L(\mathbf{x}, \mathbf{y}) \rangle \\ &= \delta_{L'L} (-1)^{\ell_x + \ell'_x} \sum_{\nu_x \lambda_x \nu_y \lambda_y \nu'_x \lambda'_x} \langle \nu'_x \lambda'_x \nu_y \lambda_y; L' | n'_y \ell'_y n'_x \ell'_x; L' \rangle_{\beta_2} \langle \nu_x \lambda_x \nu_y \lambda_y; L | n_y \ell_y n_x \ell_x; L \rangle_{\beta_2} \quad (2.52) \\ & \langle \varphi_{\nu'_x \lambda'_x 0}(\tilde{\mathbf{x}}) | V_{13} \left(\frac{\gamma_2}{m_{12}} |\tilde{\mathbf{x}}| \right) | \varphi_{\nu_x \lambda_x 0}(\tilde{\mathbf{x}}) \rangle. \end{aligned}$$

Again, β_2 depends on a and b , forcing to recompute Brody-Moshinsky coefficients at each step of the optimisation. However, in presence of at least two identical particles (chosen as 1 and 2), relation (1.48) can be used to show that V_{23} and V_{13} matrix elements are equal. Therefore, the evaluation of one of these two matrix elements and the associated calculation of

⁷ The formula proposed in [28] differs a bit from the one presented here. The equivalence of the two formula can be shown using symmetry properties of Brody-Moshinsky coefficients.

Brody-Moshinsky coefficient can be avoided,

$$\langle V_{23} + V_{13} \rangle = 2 \langle V_{23} \rangle. \quad (2.53)$$

The same accounts for three identical particles: the three two-body potential matrix elements are shown to be equal and the single calculation of V_{12} is sufficient,

$$\langle V_{12} + V_{23} + V_{13} \rangle = 3 \langle V_{12} \rangle. \quad (2.54)$$

Semi-relativistic matrix elements

The semi-relativistic matrix elements can be computed by switching to momentum representation. Making use of relation (2.11), the evaluation of these matrix elements reduces to

$$\begin{aligned} & \langle \Phi_{n'_x \ell'_x n'_y \ell'_y}^{L'}(\mathbf{x}, \mathbf{y}) | T_r(\mathbf{p}, \mathbf{q}) | \Phi_{n_x \ell_x n_y \ell_y}^L(\mathbf{x}, \mathbf{y}) \rangle \\ &= i^{2n'_x + \ell'_x + 2n'_y + \ell'_y} (-i)^{2n_x + \ell_x + 2n_y + \ell_y} \int d^3p d^3q \left(\Phi_{n'_x \ell'_x n'_y \ell'_y}^{L'}(\mathbf{p}, \mathbf{q}) \right)^* T_r(\mathbf{p}, \mathbf{q}) \Phi_{n_x \ell_x n_y \ell_y}^L(\mathbf{p}, \mathbf{q}). \end{aligned} \quad (2.55)$$

The integral in the right-hand side is extremely similar to the ones evaluated for two-body matrix elements. The T_r function divides also in three terms. The third one only depends on the \mathbf{q} variable and can then be evaluated similarly to the V_{12} matrix element,

$$\begin{aligned} & i^{2n'_x + \ell'_x + 2n'_y + \ell'_y} (-i)^{2n_x + \ell_x + 2n_y + \ell_y} \int d^3p d^3q \left(\Phi_{n'_x \ell'_x n'_y \ell'_y}^{L'}(\mathbf{p}, \mathbf{q}) \right)^* \left(\frac{\mathbf{q}^2}{b^2} + m_3^2 \right)^{1/2} \Phi_{n_x \ell_x n_y \ell_y}^L(\mathbf{p}, \mathbf{q}) \\ &= (i)^{2n'_y + \ell'_y} (-i)^{2n_y + \ell_y} \delta_{L'L} \delta_{n'_x n_x} \delta_{\ell'_x \ell_x} \int d^3q \left(\phi_{n'_y \ell'_y 0}(\mathbf{q}) \right)^* \left(\frac{\mathbf{q}^2}{b^2} + m_3^2 \right)^{1/2} \phi_{n_y \ell_y 0}(\mathbf{q}). \end{aligned} \quad (2.56)$$

The front phase proves real as long as a given parity is implemented. The residual integral has the structure that Talmi's integral technique is able to evaluate (see Complement 2.A for an analytical formula). The two other terms can be evaluated following the same procedure than for the V_{23} and V_{13} two-body matrix elements. Let us consider the following term at first,

$$\int d^3p d^3q \left(\Phi_{n'_x \ell'_x n'_y \ell'_y}^{L'}(\mathbf{p}, \mathbf{q}) \right)^* \left(\left(\frac{m_1}{m_{12}} \frac{\mathbf{q}}{b} + \frac{\mathbf{p}}{a} \right)^2 + m_1^2 \right)^{1/2} \Phi_{n_x \ell_x n_y \ell_y}^L(\mathbf{p}, \mathbf{q}). \quad (2.57)$$

New $\tilde{\mathbf{p}}$ and $\tilde{\mathbf{q}}$ coordinates are defined by rotating \mathbf{p} and $-\mathbf{q}$ with angle $-\beta_1$. On the one hand, the $\tilde{\mathbf{p}}$ coordinate turns out to be proportional to the linear combination of \mathbf{p} and \mathbf{q} that occurs

in the matrix element,

$$\tilde{\mathbf{p}} = \eta_1 \left(\frac{m_1}{m_{12}} \frac{\mathbf{q}}{b} + \frac{\mathbf{p}}{a} \right) \quad \text{with} \quad \eta_1 = \frac{abm_{12}}{\sqrt{b^2m_{12}^2 + a^2m_1^2}}. \quad (2.58)$$

On the other hand the Φ functions can be rewritten in terms of the new coordinates making use of relations (2.13) and (2.16). Combining these results, eliminating the Clebsh-Gordan coefficients and proceeding to integration on $\tilde{\mathbf{q}}$, the aforementioned matrix element can be evaluated by computing⁸

$$\begin{aligned} & \int d^3p d^3q \left(\Phi_{n'_x \ell'_x n'_y \ell'_y}^{L'}(\mathbf{p}, \mathbf{q}) \right)^* \left(\left(\frac{m_1}{m_{12}} \frac{\mathbf{q}}{b} + \frac{\mathbf{p}}{a} \right)^2 + m_1^2 \right)^{1/2} \Phi_{n_x \ell_x n_y \ell_y}^L(\mathbf{p}, \mathbf{q}) \\ &= (-1)^{\ell_y + \ell'_y} \sum_{\nu'_x \lambda'_x \nu'_y \lambda'_y} \sum_{\nu_x \lambda_x \nu_y \lambda_y} \langle \nu'_x \lambda'_x \nu'_y \lambda'_y; L' | n'_x \ell'_x n'_y \ell'_y; L' \rangle_{\beta_1} \langle \nu_x \lambda_x \nu_y \lambda_y; L | n_x \ell_x n_y \ell_y; L \rangle_{\beta_1} \\ & \quad \delta_{\nu'_y \nu_y} \delta_{\lambda'_y \lambda_y} \int d^3\tilde{p} (\phi_{\nu'_x \lambda'_x 0}(\tilde{\mathbf{p}}))^* \left(\frac{\tilde{\mathbf{p}}^2}{\eta_1^2} + m_1^2 \right)^{1/2} \phi_{\nu_x \lambda_x 0}(\tilde{\mathbf{p}}). \end{aligned} \quad (2.59)$$

Once again the remaining integral can be evaluated using Talmi's integral technology. Finally, same tricks are used to compute the third matrix element,

$$\int d^3p d^3q \left(\Phi_{n'_x \ell'_x n'_y \ell'_y}^{L'}(\mathbf{p}, \mathbf{q}) \right)^* \left(\left(\frac{m_2}{m_{12}} \frac{\mathbf{q}}{b} - \frac{\mathbf{p}}{a} \right)^2 + m_2^2 \right)^{1/2} \Phi_{n_x \ell_x n_y \ell_y}^L(\mathbf{p}, \mathbf{q}). \quad (2.60)$$

New coordinates are defined by rotating \mathbf{p} and \mathbf{q} with angle $-\beta_2$ and, using the same arguments, the six-dimensional integral is reduced to⁸

$$\begin{aligned} & \int d^3p d^3q \left(\Phi_{n'_x \ell'_x n'_y \ell'_y}^{L'}(\mathbf{p}, \mathbf{q}) \right)^* \left(\left(\frac{m_2}{m_{12}} \frac{\mathbf{q}}{b} - \frac{\mathbf{p}}{a} \right)^2 + m_2^2 \right)^{1/2} \Phi_{n_x \ell_x n_y \ell_y}^L(\mathbf{p}, \mathbf{q}) \\ &= \sum_{\nu'_x \lambda'_x \nu'_y \lambda'_y} \sum_{\nu_x \lambda_x \nu_y \lambda_y} \langle \nu'_x \lambda'_x \nu'_y \lambda'_y; L' | n'_x \ell'_x n'_y \ell'_y; L' \rangle_{\beta_2} \langle \nu_x \lambda_x \nu_y \lambda_y; L | n_x \ell_x n_y \ell_y; L \rangle_{\beta_2} \\ & \quad \delta_{\nu'_y \nu_y} \delta_{\lambda'_y \lambda_y} \int d^3\tilde{p} (\phi_{\nu'_x \lambda'_x 0}(\tilde{\mathbf{p}}))^* \left(\frac{\tilde{\mathbf{p}}^2}{\eta_2^2} + m_2^2 \right)^{1/2} \phi_{\nu_x \lambda_x 0}(\tilde{\mathbf{p}}) \end{aligned} \quad (2.61)$$

with $\eta_2 = abm_{12}/\sqrt{b^2m_{12}^2 + a^2m_2^2}$ and where the remaining integrals can still be evaluated with Talmi's technique. In presence of two identical particles, thanks to symmetry properties of

⁸ The result in [28] slightly differs from the one presented here because, in this reference, parity conservation has been used to simplify the phases.

the states, this matrix element proves to be equal to the previous one, allowing to avoid its evaluation. In presence of three identical particles, the three matrix elements proves to be equal and only formula (2.56) is needed. Provided that a given parity is implemented, all matrix elements of T prove real.

Three-body potential matrix elements

Due to the $\mathbf{x} \cdot \mathbf{y}$ term in (2.30), three-body potential matrix elements seem harder to evaluate than the two-body ones. In general, handling such an expression, which depends on the angle between two coordinates, requires a multipole expansion. However in presence of at least two identical particles (chosen as 1 and 2), this term disappears thanks to the vanishing $m_2 - m_1$ coefficient,

$$\sqrt{a^2 \left(1 + \frac{m_1^2 + m_2^2}{m_{12}^2}\right) \mathbf{x}^2 + 2b^2 \mathbf{y}^2 + 2ab \left(\frac{m_2 - m_1}{m_{12}}\right) \mathbf{x} \cdot \mathbf{y}} = \sqrt{2b^2 \mathbf{y}^2 + 3/2a^2 \mathbf{x}^2}. \quad (2.62)$$

Under this assumption, the matrix elements can be evaluated naively, using directly the expressions (2.3) and (2.4) for the Φ functions,

$$\begin{aligned} & \langle \Phi_{n'_x \ell'_x n'_y \ell'_y}^{L'}(\mathbf{x}, \mathbf{y}) | W \left(\sqrt{2b^2 \mathbf{y}^2 + 3/2a^2 \mathbf{x}^2} \right) | \Phi_{n_x \ell_x n_y \ell_y}^L(\mathbf{x}, \mathbf{y}) \rangle \\ &= \delta_{\ell'_x \ell_x} \delta_{\ell'_y \ell_y} \int x^2 dx y^2 dy R_{n'_x \ell'_x}(x) R_{n'_y \ell'_y}(y) W \left(\sqrt{2b^2 y^2 + 3/2a^2 x^2} \right) R_{n_x \ell_x}(x) R_{n_y \ell_y}(y). \end{aligned} \quad (2.63)$$

Properties of Clebsh-Gordan coefficients [35, section 8.1.1] and spherical harmonics orthonormality relation [35, sections 5.1.4] have been used to get rid of the angular dependence. Within this approach, matrix elements are given by two-dimensional integrals, resulting in a considerably higher numerical cost than for the evaluation of matrix elements for two-body potentials.

However, if in addition the constraint on a and b for three identical particles is imposed, the argument of W proves to be proportional to the hyperradius defined in (2.17),

$$W \left(\sqrt{2b^2 \mathbf{y}^2 + 3/2a^2 \mathbf{x}^2} \right) = W \left(\sqrt{3/2} a \rho \right). \quad (2.64)$$

It is worth noting that this relation requires that $m_1 = m_2$ and $b = \sqrt{3}a/2$ but not that $m_2 = m_3$. Therefore, the following developments can also be used for systems of two identical particles provided that the second non-linear variational parameter is gave up. The matrix elements of a

function that only depends on the hyperradius can easily be evaluated using property (2.22),

$$\begin{aligned} & \langle \Phi_{n'_x \ell'_x n'_y \ell'_y}^{L'}(\mathbf{x}, \mathbf{y}) | W(\sqrt{3/2}a\rho) | \Phi_{n_x \ell_x n_y \ell_y}^L(\mathbf{x}, \mathbf{y}) \rangle \\ &= \sum_{N'K'NK} \langle n'_x n'_y | N'K' \rangle_{\ell'_x \ell'_y} \langle n_x n_y | NK \rangle_{\ell_x \ell_y} \langle \Psi_{N'K'}^{\ell'_x \ell'_y L'}(\rho, \Omega) | W(\sqrt{3/2}a\rho) | \Psi_{NK}^{\ell_x \ell_y L}(\rho, \Omega) \rangle. \end{aligned} \quad (2.65)$$

Expressions of Ψ functions are given in (2.21). In the remaining matrix elements, five of the six integrals are simplified using the orthogonality of hyperspherical harmonics [43, relation (3.24)] and Clebsh-Gordan properties [35, section 8.1.1]. The remaining integrals reads (volume element in hyperspherical coordinates is given in (2.95))

$$\begin{aligned} & \langle \Psi_{N'K'}^{\ell'_x \ell'_y L'}(\rho, \Omega) | W(\sqrt{3/2}a\rho) | \Psi_{NK}^{\ell_x \ell_y L}(\rho, \Omega) \rangle \\ &= \delta_{L'L} \delta_{\ell'_x \ell_x} \delta_{\ell'_y \ell_y} \delta_{K'K} \int d\rho \rho^5 \mathcal{R}_{N'K}(\rho) W(\sqrt{3/2}a\rho) \mathcal{R}_{NK}(\rho). \end{aligned} \quad (2.66)$$

This relation is extremely similar to relation (2.8) and can be evaluated using the same strategy, resulting in a modified Talmi's integral technique. The proof of the formula for $B(nl; n'l'; p)$ coefficients given in [38] is based on an explicit expression of Laguerre polynomials which encompasses both integers and half-integers indices, factorials having simply to be replaced by gamma functions [36]. Therefore, even if the half-integer $l + 1/2$ index in the Laguerre polynomial is replaced by an integer $K + 2$ index, this formula remains valid. It might have required an adaptation because normalisation coefficients from (2.3) and from (2.21) are different but these prove to cancel each other in the modified demonstration. As a consequence, the following formula is obtained for the integral from (2.66),

$$\begin{aligned} & \int d\rho \rho^5 \mathcal{R}_{N'K}(\rho) W(\sqrt{3/2}a\rho) \mathcal{R}_{NK}(\rho) \\ &= \sum_{p=\frac{2K+3}{2}}^{N'+N+\frac{2K+3}{2}} B(N'K + 3/2; NK + 3/2; p) I_p(W, \sqrt{3/2}a) \end{aligned} \quad (2.67)$$

with I_p defined in (2.10). Together, formulas (2.65), (2.66) and (2.67) allow for an efficient evaluation of three-body potential matrix elements. It as been numerically checked with different W that these ones provide the same results than relation (2.63).

This hyperspherical coefficient methodology has been specifically implemented to manage three-body forces in three-body systems. Nevertheless, it can be inexpensively generalised to systems of N identical particles. The corresponding developments are detailed in Complement 2.D.

Evaluation of Observables

The matrix element calculation techniques introduced in this section allow for evaluations of Hamiltonian matrix elements as well as expectation values of observables. Suppose that, using the MacDonald theorem, an approximation for an eigenstate of an Hamiltonian H is obtained,

$$|\Psi_{\text{approx}}^L\rangle = \sum_{n_x \ell_x n_y \ell_y} C_{n_x \ell_x n_y \ell_y} |\Phi_{n_x \ell_x n_y \ell_y}^L(\mathbf{x}, \mathbf{y})\rangle \quad (2.68)$$

where the summation is restricted to terms satisfying $2n_x + \ell_x + 2n_y + \ell_y \leq Q_{\text{max}}$, and the coefficients $C_{n_x \ell_x n_y \ell_y}$ result from the diagonalisation of H . The expectation value of an observable $\mathcal{O}(|\mathbf{r}_{ij}|)$ for this approximate state can be expressed in terms of matrix elements of $\mathcal{O}(|\mathbf{r}_{ij}|)$ evaluated on the trial states,

$$\begin{aligned} & \langle \Psi_{\text{approx}}^L | \mathcal{O}(|\mathbf{r}_{ij}|) | \Psi_{\text{approx}}^L \rangle \\ &= \sum_{n'_x \ell'_x n'_y \ell'_y} \sum_{n_x \ell_x n_y \ell_y} C_{n'_x \ell'_x n'_y \ell'_y}^* C_{n_x \ell_x n_y \ell_y} \langle \Phi_{n'_x \ell'_x n'_y \ell'_y}^L(\mathbf{x}, \mathbf{y}) | \mathcal{O}(|\mathbf{r}_{ij}|) | \Phi_{n_x \ell_x n_y \ell_y}^L(\mathbf{x}, \mathbf{y}) \rangle. \end{aligned} \quad (2.69)$$

Developing efficient procedures to evaluate matrix elements like those on the right-hand side has been one of the main focuses of this section. Consequently, once the approximate eigenstate is determined, evaluating an observable becomes no more complex than calculating an additional potential matrix. A similar argument applies to observables that depend on momentum variables or the hyperradius. Recall that, for three identical particles, the trial states themselves are linear combinations of Φ states. The situation remains analogous, but the coefficients $C_{n_x \ell_x n_y \ell_y}$ become combinations of those obtained during symmetrisation and the diagonalisation of the Hamiltonian matrix.

2.2 Including Spin Management

To extend the previous discussions and incorporate spin into the description, it is necessary to complement the spatial trial states introduced in Section 2.1.1 with spin states. Let us consider three particles with spin s_1 , s_2 and s_3 , respectively. Three-body spin states $|s_1 m_1; s_2 m_2; s_3 m_3\rangle$ were previously defined in Section 1.1.3. However, similar to the case of angular momentum, it is often preferable to use spin trial states with well-defined total spin quantum numbers. Individual spins can be coupled using a procedure analogous to that used for angular momentum in equation (2.6). In this case, two successive two-body couplings are required to obtain a total

spin for the trial states,

$$|((s_1 s_2)_{s_{12}} s_3)_S\rangle = \sum_{\substack{m_{12}, m_3, \\ m_2, m_1}} \langle s_{12} m_{12} s_3 m_3 | SM \rangle \langle s_1 m_1 s_2 m_2 | s_{12} m_{12} \rangle |s_1 m_1; s_2 m_2; s_3 m_3\rangle. \quad (2.70)$$

As with angular momentum, since none of the matrix elements considered in this work depend on the quantum number associated with the third total spin projection, S_z , it is omitted from the notation. The above construction is only possible for $s_{12} \in \{|s_1 - s_2|, \dots, s_1 + s_2\}$ and $S \in \{|s_{12} - s_3|, \dots, s_{12} + s_3\}$. Consequently, by fixing the spins s_1, s_2, s_3 and targeting a specific total spin S , only a finite number of three-body spin states can be constructed. These are the states for which $s_{12} \in \{|s_1 - s_2|, \dots, s_1 + s_2\}$ and $s_{12} \in \{|S - s_3|, \dots, S + s_3\}$. The spin trial states (2.70) can now complement the spatial trial states to form new trial sets,

$$|\Phi_{n_x \ell_x n_y \ell_y}^L; \chi_{s_{12}}^S\rangle = |[\varphi_{n_x \ell_x}(\mathbf{x}) \varphi_{n_y \ell_y}(\mathbf{y})]_L\rangle \otimes |((s_1 s_2)_{s_{12}} s_3)_S\rangle. \quad (2.71)$$

Depending on the problem, one may either retain the quantum numbers of \mathbf{S} and \mathbf{L} separately or combine them into quantum numbers of the total angular momentum $\mathbf{J} = (\mathbf{L} + \mathbf{S})$. In the latter case, the states $|\Phi_{n_x \ell_x n_y \ell_y}^L; \chi_{s_{12}}^S\rangle$ are further coupled using Clebsch-Gordan coefficients again. However, in the current work, the OBE will only be used in the former case, as only spin-spin interactions, such as those defined in (1.21), are considered.

Let us now turn to the evaluation of Hamiltonian matrix elements using the trial states (2.71). Since none of the corresponding Hamiltonian terms affect the spin degrees of freedom, all the formulas presented in Section 2.1.4 can be extended to the new trial state by simply adding Kronecker deltas for the spin quantum numbers, $\delta_{S'S} \delta_{s'_{12} s_{12}}$. However, spin-spin interaction potentials (1.21) depend on the spin part of the state. When evaluating the corresponding matrix elements, both factors in the potential act on the respective parts of the trial state as follows,

$$\begin{aligned} \langle \Phi_{n'_x \ell'_x n'_y \ell'_y}^{L'}; \chi_{s'_{12}}^{S'} | V_{ij}^{SS} | \Phi_{n_x \ell_x n_y \ell_y}^L; \chi_{s_{12}}^S \rangle \\ = \langle [\varphi_{n'_x \ell'_x}(\mathbf{x}) \varphi_{n'_y \ell'_y}(\mathbf{y})]_{L'} | V_{ij}(|\mathbf{r}_i - \mathbf{r}_j|) | [\varphi_{n_x \ell_x}(\mathbf{x}) \varphi_{n_y \ell_y}(\mathbf{y})]_L \rangle \\ \langle ((s_1 s_2)_{s'_{12}} s_3)_{S'} | \mathbf{S}_i \cdot \mathbf{S}_j | ((s_1 s_2)_{s_{12}} s_3)_S \rangle. \end{aligned} \quad (2.72)$$

The first factor on the right-hand side can be handled using the techniques from Section 2.1.4. The second factor is discussed in the following paragraphs.

Spin-Spin Interactions for Particles 1 and 2

Let us first focus on the contribution $\mathbf{S}_1 \cdot \mathbf{S}_2$. By construction, the trial spin states (2.70) are chosen as eigenstates of the Casimir operator associated with the total angular momentum of particles 1 and 2,

$$S_{12}^2 |((s_1 s_2)_{s_{12}} s_3)_S\rangle = s_{12}(s_{12} + 1) |((s_1 s_2)_{s_{12}} s_3)_S\rangle \text{ where } S_{12}^2 = (\mathbf{S}_{12})^2 = (\mathbf{S}_1 + \mathbf{S}_2)^2. \quad (2.73)$$

Since the spin of the three particles is definite from the outset, the trial spin states are also eigenstates of the individual spin Casimir operators. The dot product $\mathbf{S}_1 \cdot \mathbf{S}_2$ is conveniently related to these operators,

$$\mathbf{S}_1 \cdot \mathbf{S}_2 = \frac{1}{2} (S_{12}^2 - S_1^2 - S_2^2). \quad (2.74)$$

As a result, states $|((s_1 s_2)_{s_{12}} s_3)_S\rangle$ turn out to be eigenstates of the operator $\mathbf{S}_1 \cdot \mathbf{S}_2$, leading to the following diagonal matrix,

$$\begin{aligned} \langle ((s_1 s_2)_{s'_{12}} s_3)_{S'} | \mathbf{S}_1 \cdot \mathbf{S}_2 | ((s_1 s_2)_{s_{12}} s_3)_S \rangle \\ = \frac{1}{2} (s_{12}(s_{12} + 1) - s_1(s_1 + 1) - s_2(s_2 + 1)) \delta_{S'S} \delta_{s'_{12}s_{12}}. \end{aligned} \quad (2.75)$$

This expression allows for straightforward evaluations of spin-spin matrix elements corresponding to particles 1 and 2.

Spin-Spin interactions for particles 2 and 3

Computing spin matrix elements for interactions proportional to $\mathbf{S}_2 \cdot \mathbf{S}_3$ is more challenging, as the spin trial states (2.70) are not eigenstates of the S_{23}^2 Casimir operator. To address this difficulty, one can switch the coupling scheme and define states where particles 2 and 3 are coupled at first, instead of particles 1 and 2,

$$|(s_1 (s_2 s_3)_{s_{23}})_S\rangle = \sum_{\substack{m_{23}, m_1 \\ m_2, m_3}} \langle s_1 m_1 s_{23} m_{23} | SM \rangle \langle s_2 m_2 s_3 m_3 | s_{23} m_{23} \rangle |s_1 m_1; s_2 m_2; s_3 m_3\rangle \quad (2.76)$$

where $s_{23} \in \{|s_2 - s_3|, \dots, s_2 + s_3\}$ and $s_{23} \in \{|S - s_1|, \dots, S + s_1\}$. Since these two different sets of spin trial states span the exact same spin Hilbert space, they can be related through a change

of basis formula,

$$\begin{aligned} & |((s_1 s_2)_{s_{12}} s_3)_S\rangle \\ &= (-1)^{s_1+s_2+s_3+S} \sqrt{2s_{12}+1} \sum_{s_{23}} \sqrt{2s_{23}+1} \begin{Bmatrix} s_1 & s_2 & s_{12} \\ s_3 & S & s_{23} \end{Bmatrix} |((s_1 (s_2 s_3)_{s_{23}})_S)\rangle. \end{aligned} \quad (2.77)$$

The coefficients $\{\dots\}$ above are known as $6j$ symbols and, like Clebsh-Gordan coefficients, are well-documented [35]. Using the expansion (2.77) twice, matrix elements of $\mathbf{S}_2 \cdot \mathbf{S}_3$ are reported on the spin states from (2.76),

$$\begin{aligned} & \langle ((s_1 s_2)_{s'_{12}} s_3)_{S'} | \mathbf{S}_2 \cdot \mathbf{S}_3 | ((s_1 s_2)_{s_{12}} s_3)_S \rangle \\ &= \sqrt{2s'_{12}+1} \sqrt{2s_{12}+1} \sum_{s'_{23}} \sum_{s_{23}} \sqrt{2s'_{23}+1} \sqrt{2s_{23}+1} \begin{Bmatrix} s_1 & s_2 & s'_{12} \\ s_3 & S & s'_{23} \end{Bmatrix} \begin{Bmatrix} s_1 & s_2 & s_{12} \\ s_3 & S & s_{23} \end{Bmatrix} \\ & \quad \langle ((s_1 (s_2 s_3)_{s'_{23}})_{S'}) | \mathbf{S}_2 \cdot \mathbf{S}_3 | ((s_1 (s_2 s_3)_{s_{23}})_S) \rangle. \end{aligned} \quad (2.78)$$

The remaining matrix elements are evaluated using similar arguments as those used for $\mathbf{S}_1 \cdot \mathbf{S}_2$. Finally, one obtains

$$\begin{aligned} & \langle ((s_1 s_2)_{s'_{12}} s_3)_{S'} | \mathbf{S}_2 \cdot \mathbf{S}_3 | ((s_1 s_2)_{s_{12}} s_3)_S \rangle \\ &= \delta_{S'S} \sqrt{(2s'_{12}+1)(2s_{12}+1)} \sum_{s_{23}} \left(\frac{2s_{23}+1}{2} \right) \begin{Bmatrix} s_1 & s_2 & s'_{12} \\ s_3 & S & s_{23} \end{Bmatrix} \begin{Bmatrix} s_1 & s_2 & s_{12} \\ s_3 & S & s_{23} \end{Bmatrix} \\ & \quad (s_{23}(s_{23}+1) - s_2(s_2+1) - s_3(s_3+1)). \end{aligned} \quad (2.79)$$

Although slightly more intricate than the corresponding formula for particles 1 and 2, this result enables efficient evaluations of spin matrix elements.

Spin-Spin Interactions for Particles 1 and 3

The situation closely parallels the computation of matrix elements for particles 2 and 3. Once again, this problem is solved by switching to a different coupling scheme using a third set of spin states

$$|((s_1 s_3)_{s_{13}} s_2)_S\rangle = \sum_{\substack{m_{13}, m_2 \\ m_1, m_3}} \langle s_{13} m_{13} s_2 m_2 | SM \rangle \langle s_1 m_1 s_3 m_3 | s_{13} m_{13} \rangle |s_1 m_1; s_2 m_2; s_3 m_3\rangle \quad (2.80)$$

where $s_{13} \in \{|s_1 - s_3|, \dots, s_1 + s_3\}$ and $s_{13} \in \{|S - s_2|, \dots, S + s_2\}$. The corresponding change of basis formula also involves $6j$ symbols,

$$\begin{aligned} & |((s_1 s_2)_{s_{12}} s_3)_S\rangle \\ &= (-1)^{s_2 + s_3 + s_{12}} \sqrt{2s_{12} + 1} \sum_{s_{13}} (-1)^{s_{13}} \sqrt{2s_{13} + 1} \begin{Bmatrix} s_2 & s_1 & s_{12} \\ s_3 & S & s_{13} \end{Bmatrix} |((s_1 s_3)_{s_{13}} s_2)_S\rangle. \end{aligned} \quad (2.81)$$

By performing the same manipulations and using arguments similar to those used for $\mathbf{S}_2 \cdot \mathbf{S}_3$, one obtains the following formula,

$$\begin{aligned} & \langle ((s_1 s_2)_{s'_{12}} s_3)_{S'} | \mathbf{S}_1 \cdot \mathbf{S}_3 | ((s_1 s_2)_{s_{12}} s_3)_S \rangle \\ &= \delta_{S'S} (-1)^{s_{12} - s'_{12}} \sqrt{(2s'_{12} + 1)(2s_{12} + 1)} \sum_{s_{13}} \left(\frac{2s_{13} + 1}{2} \right) \begin{Bmatrix} s_2 & s_1 & s'_{12} \\ s_3 & S & s_{13} \end{Bmatrix} \begin{Bmatrix} s_2 & s_1 & s_{12} \\ s_3 & S & s_{13} \end{Bmatrix} \\ & \quad (s_{13}(s_{13} + 1) - s_1(s_1 + 1) - s_3(s_3 + 1)). \end{aligned} \quad (2.82)$$

This formula enables efficient evaluation of the corresponding spin matrix elements. Notably, as with spatial components, when two particles are identical, the matrix elements for $\mathbf{S}_1 \cdot \mathbf{S}_3$ and $\mathbf{S}_2 \cdot \mathbf{S}_3$ turn out to be equal. If all three particles are identical, all three spin-spin interaction matrix elements become equal. However, in these cases, the full trial states, including both spin and spatial components, must be symmetrised. This symmetrisation procedure is discussed in the remainder of this section.

Symmetrisation with Spin Degrees of Freedom

To complete the picture of spin degrees of freedom, the spin trial state must be symmetrised. As with spin-spin interactions, permutation operators act separately on both the spatial and spin components. Since spatial components were addressed in Section 2.1.3, only spin components remain to be discussed. To begin, the action of \mathbb{P}_{12} is examined. Using relation (2.70) and the properties of Clebsh-Gordan coefficients, one finds that

$$\mathbb{P}_{12} |((s_1 s_2)_{s_{12}} s_3)_S\rangle = (-1)^{s_1 + s_2 - s_{12}} |((s_1 s_2)_{s_{12}} s_3)_S\rangle \quad (2.83)$$

where $s_1 = s_2$, since at least particles one and two are identical. As with spatial degrees of freedom, the spin trial states are already either symmetric or anti-symmetric under the exchange of particles 1 and 2. Therefore, implementing symmetry into the trial set only requires selecting s_{12} values such that $2s - s_{12}$ has the expected parity. Notice that $(-1)^{2s - s_{12}}$ is always a real

number.

As with spatial components, the action of \mathbb{P}_{23} is not limited to the addition of a phase factor. For this reason, the \mathbb{P}_{23} matrix is constructed and subsequently diagonalised. In the presence of spin, the formula (2.36) must be supplemented with the following spin factor,

$$\langle \left((s_1 s_2)_{s'_{12}} s_3 \right)_{S'} | \mathbb{P}_{23} | \left((s_1 s_2)_{s_{12}} s_3 \right)_S \rangle = \langle \left((s_1 s_2)_{s'_{12}} s_3 \right)_{S'} | \left((s_1 s_3)_{s_{12}} s_2 \right)_S \rangle. \quad (2.84)$$

where $s_1 = s_2 = s_3$ for three identical particles. Using the change of basis formula (2.81) on the bra, the following result is obtained,

$$\begin{aligned} & \langle \left((s_1 s_2)_{s'_{12}} s_3 \right)_{S'} | \mathbb{P}_{23} | \left((s_1 s_2)_{s_{12}} s_3 \right)_S \rangle \\ &= \delta_{S'S} (-1)^{s_2+s_3+s'_{12}+s_{12}} \sqrt{(2s'_{12}+1)(2s_{12}+1)} \begin{Bmatrix} s_2 & s_1 & s'_{12} \\ s_3 & S & s_{12} \end{Bmatrix}. \end{aligned} \quad (2.85)$$

This formula provides the final ingredient necessary to handle spin degrees of freedom with the OBE. Constructing symmetrised trial states follows the same procedure as that introduced in Section 2.1.3, including the factor (2.85) when evaluating \mathbb{P}_{23} matrix elements.

2.3 Tests of the Method

The basis states having been chosen and the formulas for the matrix elements having been obtained, the method is ready for implementation. This section is devoted to various tests aimed at assessing the accuracy of the method. Tests are performed on systems for which other approximation methods, namely the hyperspherical harmonic expansion (HHE) and the Lagrange mesh method (LMM), can supply a very accurate point of comparison. Reviews of these two methods can be found in [46, 47] and in [48], respectively. These tests are designed to cover a diverse range of Hamiltonians including both non- and semi-relativistic kinematics, as well as two-body and three-body interactions. Comparisons are made with data from existing literature. The computational complexity of the OBE is discussed in Complement 2.C.

Throughout the following, a condensed notation $|\sigma; n; L^P\rangle$ is used to denote the eigenstates of the tested Hamiltonians. The label σ denotes the symmetry of the state (+1 for a symmetric state, -1 for an anti-symmetric state), P represents its parity (+ for an even state, - for an odd state) and L indicates its total angular momentum. Lastly, the non-zero integer n differentiates and orders the states according to their energy.

2.3.1 Tests with Two-body Interactions

To start with, let us perform tests on systems bound by two-body interactions, considering only non-relativistic kinematics at this stage. Two types of potentials are examined: power-law and Gaussian interactions. Let us first focus on power-law interacting systems,

$$V_{12}(r) = V_{23}(r) = V_{13}(r) = \frac{\beta}{|\beta|} \frac{r^\beta}{2}, \quad W(\rho) = 0. \quad (2.86)$$

For simplicity, interactions are assumed identical even in presence of different particles. The potential parameters are chosen to enable comparison with [25], which provides accurate solution of the corresponding Hamiltonians using HHE. Parameters and energies are provided in this reference in arbitrary units.

The first test considers three identical particles with unit masses. Seven ground state eigenenergies are evaluated for values of β ranging from -1 to 3 . Detailed results are provided only for the linear interaction case $\beta = 1$, and special attention is also given to the Coulomb interaction case $\beta = -1$. Figure 2.1 shows how the energy depends on the variational parameter a for $\beta = 1$ and for various values of Q_{\max} . As expected, one observes minima corresponding to the most accurate upper-bounds. The curve flattens as the number of quanta increases, suggesting that optimising a for a small basis and reusing the obtained value for larger bases does not significantly deteriorate the accuracy of the resulting upper-bound. Figure 2.2 illustrate the evolution of the upper-bound with increasing basis size after optimising a . As expected, the approximate eigenenergy decreases and converges to the value reported in [25]. Table 2.1 presents results across the full range of β values. For positive β the OBE reproduces the reference results with a relatively low number of quanta. The result is even exact for $\beta = 2$, as in this case, the potential (2.86) consists of a harmonic oscillator. It has been verified that the optimised eigenvector contains only a single trial state. On the other hand, for negative β and particularly for the Coulomb case $\beta = -1$, the OBE appears less accurate. This is because, even at $Q_{\max} = 20$, full convergence has not been totally reached, as illustrated in Figure 2.3. This behaviour highlights a general feature of the OBE: divergent potentials require more trial states to achieve a given level of accuracy. Even the method employed in [25], the HHE, does not achieve high precision for the Coulomb interaction, as the upper-bounds obtained using the OBE with more than 24 quanta lie slightly below the result from this reference. This is consistent with general observations regarding the HHE.

Energies for systems with different particles are also provided in [25]. A system of three bosons, where two have unit masses and the third has either a higher or a lower mass, denoted M , is considered. These particles interact via the same power-law potential given in (2.86). The

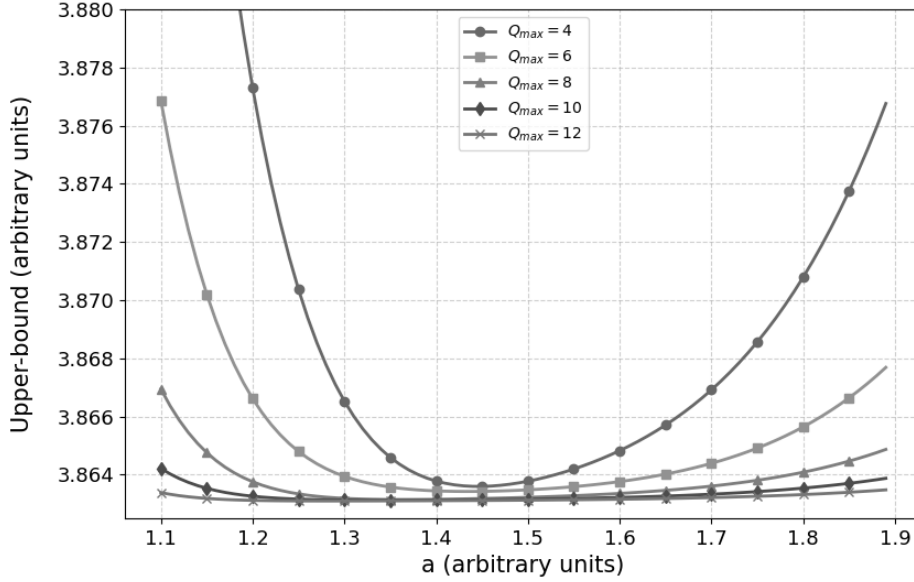
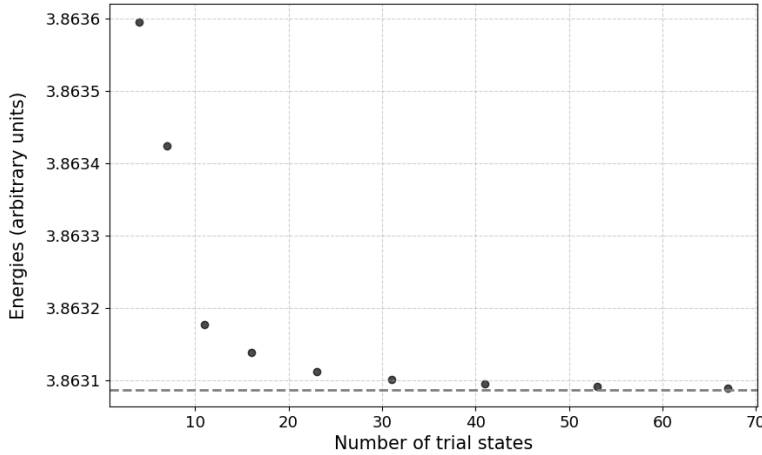


Figure 2.1: Upper-bounds obtained using the OBE are plotted depending on the variational parameter a . The ground state energy of three identical non-relativistic bosons interacting via (2.86) is considered. Arbitrary units are used: $m = 1$ and $\beta = 1$. Calculations are shown for various values of Q_{\max} .



Q_{\max}	N	E_{gs}
4	4	3.863 594
6	7	3.863 424
8	11	3.863 176
10	16	3.863 138
12	23	3.863 112
14	31	3.863 101
16	41	3.863 095
18	53	3.863 091
20	67	3.863 089

Figure 2.2: Figure and table showing different approximations obtained using the OBE as a function of the basis size. The ground state energy, E_{gs} , of three identical non-relativistic bosons interacting via (2.86) is considered. Arbitrary units are used: $m = 1$ and $\beta = 1$. The non-linear variational parameter a is optimised at $Q_{\max} = 4$, yielding $a = 1.4461$. In the figure, the converged result is indicated by the dashed gray line. The eigenenergy reported in [25] is 3.863 09.

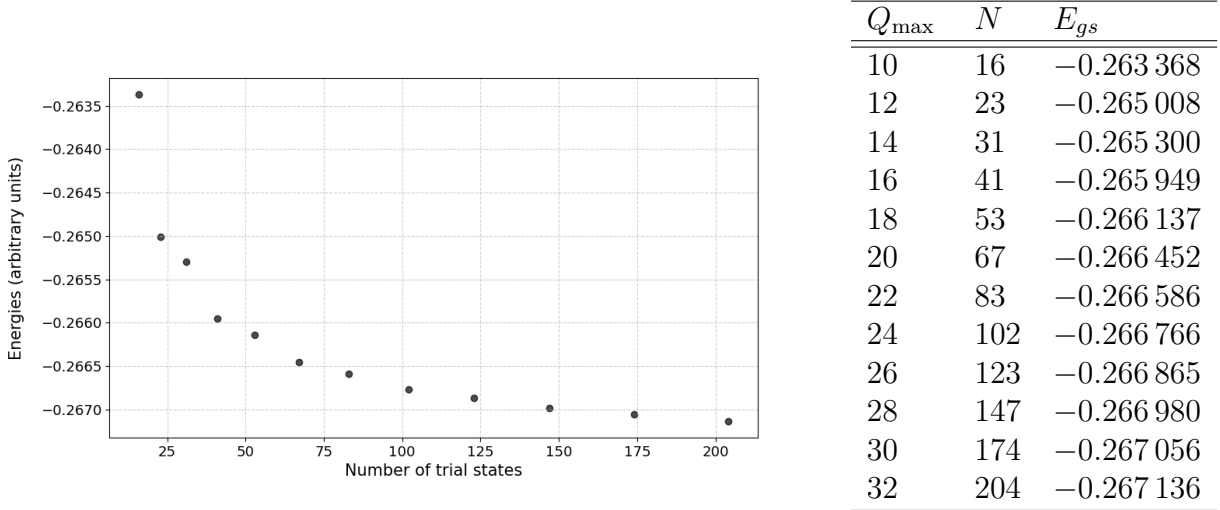


Figure 2.3: This figure and table shows different approximations obtained using the OBE as a function of the basis size. The ground state energy, E_{gs} , of three identical non-relativistic bosons interacting via (2.86) is considered. Arbitrary units are used: $m = 1$ and $\beta = -1$. The optimisation of the non-linear variational parameter a is performed at $Q_{\max} = 10$, yielding $a = 2.8422$. The eigenenergy reported in [25] is -0.26675 .

β	OBE	HHE [25]
-1.0	-0.266 45	-0.266 75
-0.5	-0.591 74	-0.591 73
0.1	1.880 18	1.880 19
0.5	2.916 53	2.916 54
1.0	3.863 09	3.863 09
2.0	5.196 15	5.196 15
3.0	6.155 91	6.155 91

Table 2.1: Ground state energies with $L = 0$, E_{gs} , in arbitrary units for three identical non-relativistic bosons interacting with potentials (2.86) and having unit masses are given depending on the potential parameter β . Results from the OBE and from HHE are compared. The maximum number of quanta used in the basis is $Q_{\max} = 20$, with a computed for $Q_{\max} = 10$.

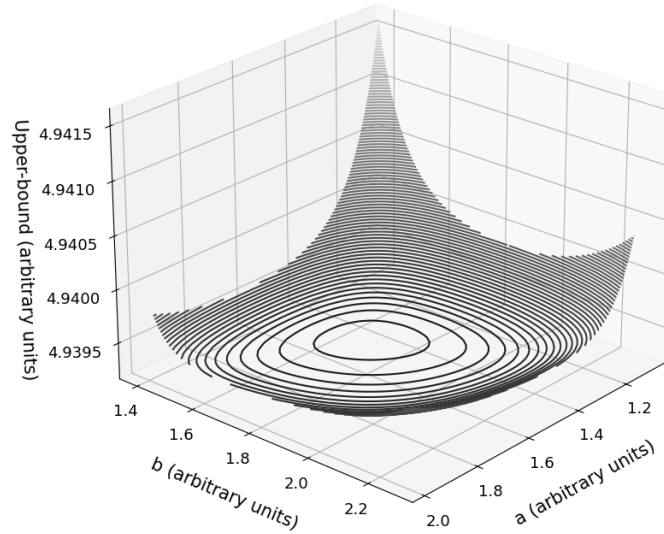


Figure 2.4: Upper-bounds obtained using the OBE are plotted depending on the variational parameters a and b . The ground state energy, E_{gs} , of three non-relativistic bosons interacting via (2.86) is considered. The first two identical bosons have unit masses, while the third one has $M = 0.2$. Linear interactions $\beta = 1$ are implemented. Calculation are shown for $Q_{\max} = 10$.

optimisation process for non-linear variational parameters a and b is illustrated in Figure 2.4 for $M = 0.2$ and $\beta = 1$. Results obtained using the OBE are compared to those from [25] in Table 2.2. Both methods show strong agreement on the ground state energy.

To illustrate the OBE with a more physical system, while still considering only two-body interactions, one may examine a system of three identical non-relativistic bosons interacting with Gaussian potentials,

$$V_{12}(r) = V_{23}(r) = V_{13}(r) = -V_0 e^{-r^2/R^2}, \quad W(\rho) = 0. \quad (2.87)$$

The parameters, taken from [10, 48], are given in atomic units: $V_0 = 1.227$ K, $R = 10.03$ at.u., $\rho_0 = 13.85$ at.u. and $m = 0.0231048$ (at.u.) $^{-2}$ K $^{-1}$. In references [10, 48], this potential serves as a first approximation for modelling Helium trimers. These references evaluate the ground state eigenenergies by mean of a LMM and a HHE, respectively. A more refined Hamiltonian, incorporating a three-body interaction, will be discussed later in this section. Table 2.3 presents the ground state energy obtained using the OBE for different basis sizes. The upper-bound converges to -0.1504 Kelvin, a value consistent with the result reported in [10, 48]. These references also indicates the presence of a weakly bound excited state at -2.467 millikelvin.

$M = 0.2$			$M = 5$		
β	OBE	HHE [25]	β	OBE	HHE [25]
-1	-0.1398	-0.1398	-1	-0.3841	-0.3848
0.1	1.9452	1.9452	0.1	1.8486	1.8486
1	4.9392	4.9392	1	3.4379	3.4379
2	7.5730	7.5730	2	4.3729	4.3729
3	9.7389	9.7389	3	5.0166	5.0166

Table 2.2: Ground state energies, E_{gs} , in arbitrary units for a system of three non-relativistic bosons interacting via the potential (2.86) are given depending on β . The first two identical bosons have unit masses, while the third has either $M = 0.2$ or $M = 5$. Results from the OBE and HHE [25] are compared. The maximal number of quanta used in basis is $Q_{\max} = 20$, with a optimised for $Q_{\max} = 10$.

Q_{\max}	N	E_{gs}
10	16	-0.1468
12	23	-0.1492
14	31	-0.1493
16	41	-0.1500
18	53	-0.1501
20	67	-0.1503
22	83	-0.1503
24	102	-0.1504

Table 2.3: Ground state energies, E_{gs} , for a system of three identical non-relativistic bosons interacting with potentials (2.87) are given in atomic units depending on the basis size, N . The optimisation on the non-linear variational parameter a has been performed at $Q_{\max} = 10$, yielding $a = 12.8625$ at.u. The ground state energy reported in [10] is -0.1504 K and -0.1504260932952 K in [48].

However, due to its weak binding, the OBE does not detect any excited state even for $Q_{\max} = 30$.

2.3.2 Tests with Three-body Interactions

Tests can now be performed on systems only bounded with three-body forces. At first, a system of three non-relativistic bosons interacting through an attractive three-body Gaussian potential is considered,

$$V_{12}(r) = V_{23}(r) = V_{13}(r) = 0, \quad W(\rho) = -3^{4/3} e^{-\rho^2/27}. \quad (2.88)$$

Unit masses are used. Parameters have been chosen to allow the comparison with results obtained in [48, p.87] using LMM in hyperspherical coordinates. Only the ground state energy

Q_{\max}	N	a	E_{gs}
6	7	1.6695	-1.739 737 863
8	11	1.6921	-1.739 828 778
10	16	1.6868	-1.739 828 773
12	23	1.6365	-1.739 830 590
14	31	1.6365	-1.739 830 808
16	41	1.6365	-1.739 830 913
18	53	1.6365	-1.739 830 929
20	67	1.6365	-1.739 830 936
22	83	1.6365	-1.739 830 937
24	102	1.6365	-1.739 830 938

Table 2.4: Ground state energies, E_{gs} , for a system of three identical non-relativistic bosons interacting with potentials (2.88) are given in arbitrary units depending on the basis size, N . For $Q_{\max} = 6, 8, 10, 12$, optimisation on the non-linear parameter a has been performed for $Q = Q_{\max}$. For $Q_{\max} > 12$, the a value is computed for $Q = 12$. The ground state energy reported in [48] is $-1.739 830 938$.

	OBE	LMM [48]
$ 1; 1; 0^+\rangle$	-1.739 830 938	-1.739 830 938
$ 1; 2; 0^+\rangle$	-0.552 311 353	-0.552 311 965
$ 1; 1; 2^+\rangle$	-0.373 040 428	-0.373 040 920

Table 2.5: Energies for the three lowest states for a system of three identical bosons interacting with potentials (2.88) in arbitrary units. Results from the OBE and from LMM [48] are compared. The maximal number of quanta used in the basis is $Q_{\max} = 24$ with a computed for $Q_{\max} = 12$.

is supplied in the text but equations can easily be implemented to produce excited energies too. The ground state energies given by the OBE for this system and for different sizes of the basis are compiled in Table 2.4. Various optimisations on a are conducted for small basis sizes to illustrate the stability of the optimum, even in the presence of three-body forces. Energies for the three lowest states from the OBE are compared to the ones from LMM in Table 2.5. The OBE is able to reproduce the energy spectrum up to nine to six digits depending on the energy level. Let us mention that the method used in [48] is particularly efficient for such a system whose potential only depends on the hyperradius variable (2.17). Hyperspherical equations become uncoupled and the system is entirely described by a single-variable hyperradial equation which is solved with the LMM.

In addition to Gaussian interactions, three-body power potentials can easily be implemented too. A system of three non-relativistic bosons interacting through a three-body Colombian

	OBE	LMM
$ 1; 1; 0^+\rangle$	-0.239 912 74	-0.239 999 98
$ 1; 2; 0^+\rangle$	-0.121 949 51	-0.122 448 97
$ 1; 1; 2^+\rangle$	-0.074 067 53	-0.074 074 07
$ 1; 3; 0^+\rangle$	-0.072 931 73	-0.074 074 07
$ 1; 1; 1^-\rangle$	-0.049 584 24	-0.049 586 78
$ 1; 1; 3^-\rangle$	-0.049 584 24	-0.049 586 78

Table 2.6: Energies in arbitrary units of the six lowest states for a system of three identical bosons interacting with potentials (2.89) in arbitrary units. Results from the OBE and from LMM are compared (see text). The maximal number of quanta used in basis is $Q_{\max} = 28$ with a computed for $Q = 16$.

potential is considered,

$$V_{12}(r) = V_{23}(r) = V_{13}(r) = 0, \quad W(\rho) = -\frac{3}{\rho}. \quad (2.89)$$

Unit masses are also used. This system is chosen to investigate the effect of a divergent potential rather than for its physical relevance. Nevertheless, a similar interaction was used in [13] to model the baryon spectrum. Accurate eigenenergies can again be obtained by solving equations from [48]. These are compared to results from the OBE in Table 2.6. Degeneracies between $|1; 3; 0^+\rangle$ and $|1; 1; 2^+\rangle$, as well as between $|1; 1; 1^-\rangle$ and $|1; 1; 3^-\rangle$ are observed in the spectrum. The first is inherent to the Coulombian shape and is not perfectly reproduced by the OBE due to a lack of convergence. The second occurs for any hyperradial potential and can be explained by the pure dependence of the system on the hyperradius. The aforementioned hyperradial equation which rules the dynamics of the system only depends on the K quantum number of the hyperspherical harmonic, thereby producing degeneracies in the spectrum. Concerning accuracy, the OBE seems less efficient than in the previous test. For two-body potential, it is already well-known that divergences deteriorate the accuracy of the OBE. This feature seems to apply for three-body forces too. More accurate results can of course be obtained by increasing the number of quanta.

2.3.3 Tests with Two- and Three-body Interactions

Physical systems, including both two- and three-body interactions can also be investigated. A first test is performed on a system of three non-relativistic identical bosons interacting with

$ 1; 1; 0^+\rangle$	OBE	HHE [49]	$ 1; 2; 0^+\rangle$	OBE	HHE [49]	$ 1; 1; 2^+\rangle$	OBE	HHE [49]
E	0.363	0.360	E	1.953	1.947	E	2.397	2.395
$\langle r \rangle$	1.368	1.367	$\langle r \rangle$	2.220	2.216	$\langle r \rangle$	2.368	2.366

Table 2.7: Energies and mean values in arbitrary units for the inter-particles distance of the three lowest states for a system of three identical bosons interacting with potentials (2.90). Results from the OBE and from HHE are compared. The maximal number of quanta used in basis is $Q_{\max} = 24$ with a computed for $Q = 12$.

two-body attractive Coulomb interactions and confined by a three-body linear potential,

$$V_{12}(r) = V_{23}(r) = V_{13}(r) = -\frac{1}{r}, \quad W(\rho) = \frac{1}{2}\rho. \quad (2.90)$$

A more sophisticated version of this potential is used for the description of baryonic bound states in [39]. Unit masses are used. The comparison is conducted with results from an HHE [49]. This time, energies and mean-values of the inter-particle distances are investigated for the three lowest states in Table 2.7. Symmetry properties ensure that this mean-value is independent of the chosen pair of particles. As already mentioned, for very divergent potentials, such as the Coulomb potential, the OBE often exhibits reduced accuracy. In the current test, the method proved to be able to provide energies and mean-values with three significant digits.

Finally, the system of three identical non-relativistic bosons that interacts through two-body attractive interactions (2.87) is extended, adding a three-body repulsive Gaussian interaction. The ground and first excited state energies for such a system are also provided in [48, p.87] and in [10]. These references use

$$V_{12}(r) = V_{23}(r) = V_{13}(r) = -V_0 e^{-r_{i2}^2/R^2}, \quad W(\rho) = W_0 e^{-\rho^2/\rho_0^2}. \quad (2.91)$$

with $V_0 = 1.227$ K, $W_0 = 0.279$ K, $R = 10.03$ at.u., $\rho_0 = 13.85$ at.u. and with masses of 0.0231048 (at.u.) $^{-2}$ K. $^{-1}$. In [10, 48], this potential is used to describe Helium trimers. The energy and mean-value of the inter-particle distance provided by the OBE, by the LMM and by the HHE are presented in Table 2.8. The ground state energy upper bound given by the OBE is in agreement with both other results. Mean-values were not computed in [10] but both OBE and LMM evaluations are compatible. In addition to the ground state, an excited state is mentioned in [10, 48]. Again, this state is so weakly bound that the OBE cannot provide any approximation for it, even up to 30 quanta.

One may continue to test the OBE with systems including spin-spin interactions or semi-relativistic kinematics. For instance, reference [28] demonstrates the use of the OBE in repro-

$ 1; 1; 0^+\rangle$	OBE	LMM [48]	HHE [10]
E (K)	-0.1263	-0.1264	-0.1264
$\langle r \rangle$ (a.u.)	17.4010	17.4707	N.A.

Table 2.8: Ground state energies, E , and mean values for the inter-particle distance, $\langle r \rangle$, are given in atomic units for a system of three identical bosons interacting with potentials (2.91). Results from the OBE, from the literature (LMM [48] and HHE [10]) are compared. For HHE, mean-value is not provided in the literature. The chosen maximal number of quanta in the basis is $Q_{\max} = 24$ with a computed for $Q = 12$.

ducing certain levels of the baryon spectrum by using semi-relativistic kinematics. However, to avoid an overflow of tests and because Chapter 5 is entirely dedicated to this topic, these additional applications are not covered in the current chapter⁹.

2.4 Conclusion: Why the OBE?

The OBE is a versatile and efficient approach for obtaining approximate eigenenergies and eigenfunctions in three-body systems. One of the key advantages of the OBE is its ability to easily handle both non- and semi-relativistic kinematics. Although not explicitly presented here, the formulas derived in this work can be generalized to accommodate arbitrary kinematics. Such Hamiltonians are encountered, for example, in atomic physics [50], hadronic physics [51] in quantum mechanics with a minimal length [52] and in fractional quantum mechanics [53]. In [29], the OBE originally designed for two-body interactions is extended to handle a specific class of three-body forces, thereby broadening its applicability. The method also allows for easy incorporation of symmetries, angular momentum, and parity quantum numbers into the obtained approximations.

Efficient computation of the corresponding matrix elements is achieved by decomposing the trial states into harmonic oscillator eigenstates within rotated or hyperspherical coordinates. The coefficients of these decompositions are evaluated through algebraic expressions. This strategy enables matrix element evaluations at a rate two orders of magnitude faster than using intensive numerical integrations. On the other hand, the OBE has been validated by comparing its approximations for the lowest eigenenergies and for the mean values of interparticle distances with results obtained using the HHE and the LMM. In short, the OBE proves to be a valuable compromise between accuracy, computational time and technical complexity.

These strengths make the OBE a valuable method, which has been used, for example, in

⁹ Although not presented in this document, the corresponding tests have been successfully conducted to validate the implementation used in the following.

hadronic physics, as demonstrated in references [30, 31, 32, 33, 34]. Moreover, the method can also be used to validate and assess the efficiency of other approximation strategies. For instance, the generalisation of the OBE to handle three-body forces has been used in [54] to evaluate the accuracy of the envelope theory, another approximation method discussed in the next chapter. In a current research, the OBE is also employed to evaluate the efficiency of the quark-diquark approximation in baryon spectroscopy.

Complement 2.A Analytical formulas for Talmi's integrals

This complement provides analytical expressions of Talmi's integrals (2.10) associated with the few \mathcal{O} functions that are used in this paper. For power potentials (including the linear and Coulomb potentials used in Section 2.3), these integrals are easily expressed in terms of Gamma functions,

$$I_p(\mathcal{O}(x) = \alpha x^\beta, a) = \alpha a^\beta \frac{\Gamma(p + 3/2 + \beta/2)}{\Gamma(p + 3/2)}. \quad (2.92)$$

Gaussian potentials (also employed in Section 2.3) admit analytical expressions as well,

$$I_p(\mathcal{O}(x) = \alpha e^{-\beta x^2}, a) = \alpha (1 + a^2 \beta)^{-3/2-p}. \quad (2.93)$$

The treatment of semi-relativistic kinetic energies in Section 2.1.4 relies on some Talmi's integrals that also possess analytical expressions [28],

$$I_p(\mathcal{O}(x) = \sqrt{x^2 + \alpha}, a) = a \left(\frac{\alpha}{a^2}\right)^{p+2} U\left(p + \frac{3}{2}, p + 3, \frac{\alpha}{a^2}\right), \quad (2.94)$$

where U denotes confluent hypergeometric functions of the second kind [36].

Complement 2.B Evaluation of the Hyperspherical coefficients

The hyperspherical coefficients introduced in Section 2.1 are defined in equation (2.23) as the overlap integral of two $\Phi_{n_x \ell_x n_y \ell_y}^L(\mathbf{x}, \mathbf{y})$ and $\Phi_{NK}^{\ell_x \ell_y L}(\rho, \Omega)$ functions. This Appendix is dedicated to development of a closed formula that allows for an efficient evaluation of these coefficients. First, the six-dimensional volume element can be turned into hyperspherical coordinates [43],

$$d^3x d^3y = \rho^5 \sin \theta_x \sin \theta_y (\sin \alpha)^2 (\cos \alpha)^2 d\rho d\theta_x d\varphi_x d\theta_y d\varphi_y d\alpha. \quad (2.95)$$

Using properties of spherical harmonics and Clebsh-Gordan coefficients [35, sections 5.1.4 and 8.1.1], this integral on Φ and Ψ functions reduces to an integral on R and \mathcal{R} functions,

$$\begin{aligned} \langle n_x n_y | NK \rangle_{\ell_x \ell_y} &= \iint \rho^5 R_{n_x \ell_x}(\rho \sin \alpha) R_{n_y \ell_y}(\rho \cos \alpha) \mathcal{R}_{NK}(\rho) N_K^{\ell_x \ell_y} \\ &\quad (\sin \alpha)^{\ell_x+2} (\cos \alpha)^{\ell_y+2} P_n^{(\ell_x+\frac{1}{2}, \ell_y+\frac{1}{2})}(\cos 2\alpha) d\rho d\alpha. \end{aligned} \quad (2.96)$$

Integrals over angular degrees of freedom yielded a value of 1. Let us remind that n is a notation shortcut for $(K - \ell_x - \ell_y)/2$. Substituting R and \mathcal{R} functions by their definitions (2.3) and (2.21), the integral becomes

$$\begin{aligned} \langle n_x n_y | NK \rangle_{\ell_x \ell_y} &= C \int_0^\infty d\rho \rho^{5+\ell_x+\ell_y+K} e^{-\rho^2} L_N^{K+2}(\rho^2) \int_0^{\pi/2} d\alpha (\sin \alpha)^{2\ell_x+2} (\cos \alpha)^{2\ell_y+2} \\ &\quad P_n^{(\ell_x+\frac{1}{2}, \ell_y+\frac{1}{2})}(\cos 2\alpha) L_{n_x}^{\ell_x+1/2}(\rho^2 \sin^2 \alpha) L_{n_y}^{\ell_y+1/2}(\rho^2 \cos^2 \alpha) \end{aligned} \quad (2.97)$$

where C is a factor that gathers all the normalisation coefficients,

$$C = N_K^{\ell_x \ell_y} \left(\frac{8(n_x!)(n_y!)(N!)}{\Gamma(n_x + \ell_x + 3/2)\Gamma(n_y + \ell_y + 3/2)\Gamma(K + N + 3)} \right)^{1/2}. \quad (2.98)$$

To get rid of the generalized Laguerre and Jacobi polynomials, one can replace them by their polynomial expressions [36, formulas 22.3.1 and 22.3.9],

$$L_n^a(x) = \sum_{i=0}^n (-1)^i \binom{n+a}{n-i} \frac{x^i}{i!}, \quad (2.99)$$

$$P_n^{(a,b)}(x) = \sum_{i=0}^n \binom{n+b}{n-i} \binom{n+a}{i} \left(\frac{x+1}{2} \right)^i \left(\frac{x-1}{2} \right)^{n-i}. \quad (2.100)$$

The symbol $\binom{x}{y}$ refers to the usual binomial coefficient defined in terms of gamma functions as

$$\binom{x}{y} = \frac{\Gamma(x+1)}{\Gamma(y+1)\Gamma(x-y+1)}. \quad (2.101)$$

Once these replacements are performed, the hyperspherical coefficients are expressed as a the result of four sums,

$$\begin{aligned}
 \langle n_x n_y | NK \rangle_{\ell_x \ell_y} &= C \sum_{s=0}^N \frac{(-1)^s}{s!} \binom{N+K+2}{N-s} \sum_{m=0}^n (-1)^{n-m} \binom{n+\ell_y+\frac{1}{2}}{n-m} \binom{n+\ell_x+\frac{1}{2}}{m} \\
 &\quad \sum_{i=0}^{n_x} \frac{(-1)^i}{i!} \binom{n_x+\ell_x+\frac{1}{2}}{n_x-i} \sum_{j=0}^{n_y} \frac{(-1)^j}{j!} \binom{n_y+\ell_y+\frac{1}{2}}{n_y-j} \\
 &\quad \int d\rho \rho^{5+\ell_x+\ell_y+K+2i+2j+2s} e^{-\rho^2} \int d\alpha (\sin \alpha)^{2(\ell_x+1+i+n-m)} (\cos \alpha)^{2(\ell_y+1+j+m)}.
 \end{aligned} \tag{2.102}$$

The integrals on ρ and α being decoupled, they can be evaluated and expressed in terms of gamma functions [36, formulas 6.2.1, 6.2.2, 7.4.4 and 7.4.5],

$$2 \int_0^\infty d\rho \rho^i e^{-\rho^2} = \Gamma\left(\frac{i+1}{2}\right), \tag{2.103}$$

$$2 \int_0^{\pi/2} d\alpha (\sin \alpha)^i (\cos \alpha)^j = \frac{\Gamma\left(\frac{i+1}{2}\right) \Gamma\left(\frac{j+1}{2}\right)}{\Gamma\left(\frac{i+j}{2} + 1\right)}. \tag{2.104}$$

This leads to the final expression,

$$\begin{aligned}
 \langle n_x n_y | NK \rangle_{\ell_x \ell_y} &= C \sum_{s=0}^N \frac{(-1)^s}{s!} \binom{N+K+2}{N-s} \sum_{m=0}^n (-1)^{n-m} \binom{n+\ell_y+\frac{1}{2}}{n-m} \binom{n+\ell_x+\frac{1}{2}}{m} \\
 &\quad \frac{(-1)^i}{i!} \binom{n_x+\ell_x+\frac{1}{2}}{n_x-i} \sum_{j=0}^{n_y} \frac{(-1)^j}{j!} \binom{n_y+\ell_y+\frac{1}{2}}{n_y-j} \\
 &\quad \frac{\Gamma\left(\frac{\ell_x+\ell_y+K}{2} + 3 + i + j + s\right) \Gamma\left(\ell_x + i + n - m + \frac{3}{2}\right) \Gamma\left(\ell_y + j + m + \frac{3}{2}\right)}{4 \Gamma(\ell_x + \ell_y + n + j + i + 3)}.
 \end{aligned} \tag{2.105}$$

This formula enables to compute accurately all the hyperspherical coefficients. It is consistent with the formula for $\langle n_x n_y | 0K \rangle_{\ell_x \ell_y}$ given in [42]. As the value of $2n_x + \ell_x + 2n_y + \ell_y$ increases, the number of coefficients to compute as well as the time needed to evaluate the four sums also increase. Nevertheless, since the hyperspherical coefficients does not depend of any parameters, they do not have to be recomputed every time. A single evaluation beforehand and the storage of the result in a data file allows to retrieve the coefficients efficiently. Using the Mathematica software, all the hyperspherical coefficients until $2n_x + \ell_x + 2n_y + \ell_y = 40$ have been computed in a few hours on a regular laptop computer. Both $\Phi_{n_x \ell_x n_y \ell_y}^L$ and $\Psi_{NK}^{\ell_x \ell_y L}$ sets of states from relation (2.22) being orthonormalised, hyperspherical coefficients satisfy the following probability

conservation relation,

$$\sum_{NK} \langle n_x n_y | NK \rangle_{\ell_x \ell_y}^2 = 1 \quad (2.106)$$

with the constraint $2N + K = 2n_x + \ell_x + 2n_y + \ell_y$ in the summations. This relation provides a useful consistency check to estimate the accuracy of the computed coefficients.

Complement 2.C Complexity Tests

One may wonder to what extent the use of Brody-Moshinsky and hyperspherical coefficients reduces the computational time required for evaluating Hamiltonian matrix elements. To investigate this, the management of three-body forces will be considered as an example. A comparison in runtime is conducted between the use of hyperspherical coefficients and naive numerical integrations of (2.63). This comparison involves a three-boson system with non-relativistic kinematics, unit masses, and a single attractive linear three-body potential, as defined below,

$$V_{12}(r) = V_{23}(r) = V_{13}(r) = 0, \quad W(\rho) = \frac{1}{2}\rho. \quad (2.107)$$

Ground-state evaluations, without optimisation of the variational parameter, are executed for different basis lengths (using Python3 for programming). The use of hyperspherical coefficients appears to reduce the runtime by approximately two orders of magnitude compared to performing intensive numerical integrations. The evaluation time as a function of the number of states in the basis roughly follows a power law with an exponent of 3.2. Given the duration for a specific basis size, this indicative fit provides an estimate of the time required for evaluations with an increased number of quanta. However, let us remind that hyperspherical coefficients have been precomputed and stored in advance, requiring only their retrieval during each run. This pre-computation is possible because hyperspherical coefficients are independent of the specific three-body interaction considered and the non-linear variational parameters a and b . The evaluation of hyperspherical coefficients using formula (2.105) seems to roughly follow a power law with an exponent of 2.0.

The situation differs slightly for two-body forces, where Brody-Moshinsky coefficients must be recomputed for each set of a and b values. In fact, evaluating these coefficients using the formulas (3.6)-(3.7) from [41] is significantly less computationally expensive than evaluating hyperspherical coefficients. Notably, for three identical particles, the process is further simplified, since only Brody-Moshinsky coefficients with an angle of $\pi/2$ are required. However, calculations involving only identical particles require a time-consuming symmetrisation step, which balances

the overall duration. To assess the evaluation time in the presence of two-body interactions, tests are conducted on systems of three particles interacting via two-body linear potentials,

$$V_{12}(r) = V_{23}(r) = V_{13}(r) = \frac{1}{2}r, \quad W(\rho) = 0. \quad (2.108)$$

Both a system of three identical bosons with unit masses and a system of two identical bosons with unit masses and a third particle with $M = 5$ are investigated. In the former case, the evaluation time as a function of the number of states in the basis roughly follows the same power law with an exponent of 3.2 as observed for three-body interactions. In the latter case, the evaluation time appears to follow a power law with an exponent of 2.3. In summary, compared to a more naive evaluation method, the use of Brody-Moshinsky coefficients for two-body interactions reduces the computational cost by at least the same magnitude as hyperspherical coefficients do for three-body forces.

This section also provides an opportunity to mention that hyperspherical coefficients can be used to handle systems containing two identical particles and one distinct particle. However, this approach necessitates forfeiting one of the two non-linear variational parameters, thereby reducing the accuracy of the resulting upper bounds. Despite this trade-off, the potential time savings during evaluations may enable the exploration of larger basis sizes. Thus, it remains unclear whether the use of hyperspherical coefficients will enhance overall accuracy. To address this question, a test is conducted on the ground state of a system involving two bosons of mass 1 and a third particle of mass 10, interacting through the three-body potential (2.107). Allocating 500 seconds for both methods, their respective accuracies are compared. Because the optimisation process duration depends on the inserted seed for a and b , in this test, the user has been assumed to possess the first digit of the optimised values of a and b . The results indicate that hyperspherical coefficients deliver a rapid and precise upper bound for the ground state while two-dimensional integrals struggles to achieve a commensurate level of accuracy even after 500 seconds. It turns out that, using the two-parameters method, the optimised value of b aligns in magnitude with $\sqrt{3}a/2$ for the chosen system. This feature can explain the low loss of accuracy upon setting from the beginning $b = \sqrt{3}a/2$.

Complement 2.D Possible generalisation

The OBE method, in its most general form, extends beyond systems with merely three particles. If the management of two-body forces for bigger systems is already well established in the literature [31], the hyperspherical coefficient method has initially been developed for systems

of three identical particles. However, this approach readily accommodates handling three-body forces within systems containing a greater number of identical particles. In these instances, the harmonic oscillator eigenstates are constructed by sequentially coupling the i^{th} Jacobi variable to the preceding $i - 1$ variables,

$$\Phi_{n_1 \ell_1 \dots n_{N-1} \ell_{N-1}}^{\ell_{12} \ell_{123} \dots L}(\mathbf{x}_1, \dots, \mathbf{x}_{N-1}) = \left[\dots \left[[\phi_{n_1 \ell_1}(\mathbf{x}_1) \phi_{n_2 \ell_2}(\mathbf{x}_2)]_{\ell_{12}} \phi_{\ell_3}(\mathbf{x}_3) \right]_{\ell_{123}} \dots \right]_L \quad (2.109)$$

where \mathbf{x}_i represents the i^{th} Jacobi coordinates within the N -body system. Consequently, any N -particle oscillator eigenstate encompasses a three-particle oscillator eigenstate. It allows to evaluate the matrix elements of the three-body interaction $W(\rho_{123})$ (with $\rho_{ijk}^2 = r_{ij}^2 + r_{ik}^2 + r_{jk}^2$) can be evaluated using hyperspherical coefficients,

$$\begin{aligned} \langle \Phi_{n'_1 \ell'_1 \dots n'_{N-1} \ell'_{N-1}}^{\ell'_{12} \ell'_{123} \dots L'} | W(\rho_{123}) | \Phi_{n_1 \ell_1 \dots n_{N-1} \ell_{N-1}}^{\ell_{12} \ell_{123} \dots L} \rangle &= \delta_{n'_3 n_3} \delta_{\ell'_3 \ell_3} \dots \delta_{n'_{N-1} n_{N-1}} \delta_{\ell'_{N-1} \ell_{N-1}} \delta_{\ell'_{123} \ell_{123}} \dots \delta_{L' L} \\ &\quad \langle \Phi_{n'_1 \ell'_1 n'_2 \ell'_2}^{\ell'_{12}}(\mathbf{x}_1, \mathbf{x}_2) | W(\rho_{123}) | \Phi_{n_1 \ell_1 n_2 \ell_2}^{\ell_{12}}(\mathbf{x}_1, \mathbf{x}_2) \rangle. \end{aligned} \quad (2.110)$$

Furthermore, thanks to the symmetry properties of the wave-function for N identical particles, all matrix elements associated with other triplets of particles are equal to those associated with particle 1, 2 and 3,

$$\begin{aligned} \forall i, j, k \in \{1, \dots, N\}, \langle \Phi_{n'_1 \ell'_1 \dots n'_{N-1} \ell'_{N-1}}^{\ell'_{12} \ell'_{123} \dots L'} | W(\rho_{ijk}) | \Phi_{n_1 \ell_1 \dots n_{N-1} \ell_{N-1}}^{\ell_{12} \ell_{123} \dots L} \rangle \\ = \langle \Phi_{n'_1 \ell'_1 \dots n'_{N-1} \ell'_{N-1}}^{\ell'_{12} \ell'_{123} \dots L'} | W(\rho_{123}) | \Phi_{n_1 \ell_1 \dots n_{N-1} \ell_{N-1}}^{\ell_{12} \ell_{123} \dots L} \rangle. \end{aligned} \quad (2.111)$$

This implies that all the necessary matrix element are derived without the need for new formula.

This chapter in the context of a thesis

This chapter covers one of the main topics I worked on during my PhD. The entire first six months were dedicated to implementing the method. It was initially intended to be used in conjunction with the helicity formalism to compute the three-gluon glueball spectrum. However, difficulties encountered during the research rendered this approach ineffective. Nevertheless, the resulting three-body code has been, and continues to be, extensively used within the research unit. It enabled us to easily test the accuracy of the resolution method discussed in the next chapter [54, 55], and it was used to study quark core dynamics in hybrid baryons, as part of a study led by L. Cimino [56]. It has also been applied in the context of two-gluon glueballs, allowing for a comparison between spectra obtained using spin versus helicity degrees of freedom for the gluons. More recently, it is being used by C. Tourbez to investigate the quark-diquark approximation in baryons (a topic briefly introduced in Part II), and it will support future work by J. Viseur in extending the study of hybrid baryons initiated by L. Cimino.

Beyond the implementation, the method was also extended to handle a specific class of K -body forces. In a collaborative effort with S. Youcef Khodja [29], we developed an efficient approach to compute three-body matrix elements on harmonic oscillator eigenstates, as introduced in this chapter. This extension was, of course, thoroughly tested.

Chapter 3

The Envelope Theory: a Step Toward Many-Body Systems

Most resolution methods for the time-independent Schrödinger equation in many-body quantum systems, including the OBE discussed in Chapter 2, rely on numerical computations. These methods tend to be highly accurate but require months of development and implementation. Their computational cost also increases with the number of particles, making the treatment of very large system highly challenging. In addition to these accurate but computationally expensive approximation methods, simpler techniques also warrant significant interest. Among such convenient approaches is the envelope theory (ET) [57, 58, 59, 60], also known as the auxiliary field method [61, 62]. The ET stands out as an easy-to-use approach with several advantages:

- (i) it can handle general Hamiltonians with non-standard kinematics in arbitrary dimensions;
- (ii) its computational cost is independent of the number of particles;
- (iii) in favourable cases, the approximate eigenvalues obtained via the ET can be proven analytical;
- (iv) in favourable cases, these approximate eigenvalues can prove to be either lower or upper bounds.

The fundamental idea behind this method is to replace the Hamiltonian H under study with auxiliary Hamiltonians \tilde{H} that are exactly solvable [62]. In practice, these auxiliary Hamiltonians are chosen to be many-body harmonic oscillators H_{ho} , which are exactly solvable for arbitrary dimensions [22, 63]. Ultimately, obtaining an approximate spectrum requires no more than solving a finite set of algebraic equations.

While the ET is generally reliable, its accuracy is difficult to assess due to the absence of convergence scheme. To address this limitation, various studies have been conducted. First, an improvement procedure for the method has been developed in [64, 65]. This enhancement is based on modifying the global harmonic oscillator quantum number and coupling the ET with an independent resolution method, the dominantly orbital state method (DOSM). This approach yields a second approximation, which is almost always more accurate than the original one. The difference between the two approximations provides an estimate of the accuracy level. Second, various tests of the method have been performed, comparing ET results with those obtained from accurate resolution methods [55, 54, 66, 67, 68]. These tests provide insights into the conditions under which the ET tends to be accurate. They demonstrated that the ET yields low relative errors for certain favourable systems, such as those with linear or Gaussian potentials, but exhibits lower accuracy for systems with Coulomb interactions. Although applying the improvement procedure sometimes allows for reasonably good results [64], in atomic spectra, both the ET and its improved version failed to reproduce binding energies accurately [65]. Two hypotheses, tested in [55], have been proposed to explain this limitation: the presence of a singularity in the potential, and the coexistence of attractive and repulsive components.

Regarding its applicability, the ET produces fairly accurate results for baryon spectra within the framework of potential models with QCD-inspired interactions [66]. The method has also been employed for hybrid mesons in [69]. The ET proves particularly useful in situations where the number of particles can be arbitrary large, such as in the large- N_c formulation of QCD [12, 70, 71, 72, 73, 74]¹. The method has also been used to explore a possible quasi Kepler's third law for quantum many-body systems [75, 76]. Additionally, the ET can serve to validate precise numerical calculations, as in [77], or provide quick estimates to supplement them (see Section 3.1.7). Lastly, in [78], the method was applied to the study exciton states, emphasising on its pedagogical value as an accessible analytical approximation technique.

This chapter builds upon and significantly expands the text from references [29]. Section 3.1 introduces the fundamental principles of the ET for systems of N identical particles. Section 3.1.1 develops the core concepts of the approximation method, while Section 3.1.2 and Section 3.1.3 present the main equations and properties essential for practical applications. Section 3.1.4 focuses on the improved version of the ET, and Section 3.1.5 explores some generalisations of the method. Additionally, Section 3.1.6 discusses approximations for observables. Finally, Section 3.1.7 examines tests and applications of the method. The second part of the chapter extends the ET to systems composed of different particles, following a structure similar to that used for identical particles. Given the increased complexity of calculations in this context, most

¹ In [69, 70, 71, 72, 73, 74], an earlier version of the ET was used without being named as such

derivations are deferred to the corresponding articles.

3.1 Envelope Theory for Systems of Identical Particles

Historically, the ET was first introduced by R.L. Hall as a geometrical technique that approximates a given Hamiltonian by "enveloping" its potential with exactly solvable ones [57, 58, 59, 60]. Independently and as a generalization of earlier works by Y.A. Simonov [79, 80], the method was rediscovered 20 years later by B. Silvestre-Brac, C. Semay and F. Buisseret under the name "auxiliary field method" [81, 82, 83, 84]. The equivalence of both approaches was demonstrated a few month later [85]. Although these two formulations complement each other, and most recent developments have been carried on within the auxiliary field framework, historical precedence dictates the retention of the oldest name. In this work, for pedagogical clarity and consistency with subsequent applications, the ET is introduced following the approach established by the auxiliary field method.

3.1.1 The envelope theory as an auxiliary field method

This section introduces the approximation underlying the ET using a simple system. Consider two non-relativistic with mass m and identical particles interacting with a generic two-body potential V ,

$$H = \frac{\mathbf{p}_1^2}{2m} + \frac{\mathbf{p}_2^2}{2m} - \frac{\mathbf{P}^2}{4m} + V(|\mathbf{r}_1 - \mathbf{r}_2|) \quad (3.1)$$

where $\mathbf{P} = \mathbf{p}_1 + \mathbf{p}_2$ is the total momentum of the system. The system is expressed in relative coordinates,

$$\mathbf{r} = \mathbf{r}_1 - \mathbf{r}_2, \quad \mathbf{R} = \frac{\mathbf{r}_1 + \mathbf{r}_2}{2}, \quad (3.2)$$

$$\mathbf{p} = \frac{\mathbf{p}_1 - \mathbf{p}_2}{2}, \quad \mathbf{P} = \mathbf{p}_1 + \mathbf{p}_2. \quad (3.3)$$

Above, \mathbf{p} and \mathbf{P} are conjugate to \mathbf{r} and \mathbf{R} , respectively. In these coordinates, the Hamiltonian of the system simplifies to

$$H = \frac{\mathbf{p}^2}{m} + V(r). \quad (3.4)$$

where $r = |\mathbf{r}|$. Analytical solutions for the spectrum of this Hamiltonian exist only for specific choices of V . Let us introduce one such analytically solvable potentials, given by $a\mathcal{V}(r)$, where

$a \in \mathbb{R}$. The corresponding Hamiltonian is denoted by $\mathcal{H}(a)$,

$$\mathcal{H}(a) = \frac{\mathbf{p}^2}{m} + a\mathcal{V}(r). \quad (3.5)$$

Its spectrum is denoted $\epsilon(a)$. The following construction may seem artificial at first, but its usefulness will become clear later. From V and \mathcal{V} , the following K function is defined,

$$K(x) = \frac{V'(x)}{\mathcal{V}'(x)} \quad (3.6)$$

where V' is the derivative of V with respect to its argument. The inverse function of K is denoted by J ,

$$J(K(x)) = x, \quad K(J(x)) = x. \quad (3.7)$$

Using J , an *auxiliary potential* $\tilde{V}(r, y)$ is constructed. It depends on an additional variable y ,

$$\tilde{V}(r, y) = y\mathcal{V}(r) + V(J(y)) - y\mathcal{V}(J(y)). \quad (3.8)$$

In the following, y is treated as a generic function of the position operator, and is referred to as an auxiliary field. The auxiliary potential is then used to define an auxiliary Hamiltonian \tilde{H} ,

$$\tilde{H}(y) = \frac{\mathbf{p}^2}{m} + \tilde{V}(r, y) \quad (3.9)$$

The key property of \tilde{H} is that it contains the solution of the original Hamiltonian. By choosing the auxiliary field as $y(r) = K(r)$ and using definitions (3.7), one recovers H from \tilde{H} . This choice of $y(r)$ corresponds to imposing a functional extremisation condition on the auxiliary Hamiltonian,

$$\left. \frac{\delta}{\delta y(r)} \tilde{H}(y) \right|_{y_0(r)} = 0 \quad \Leftrightarrow \quad y_0(r) = K(r). \quad (3.10)$$

Thus far, the description of the problem remains exact, though somewhat indirect. The auxiliary field method, later shown to be equivalent to the ET, suggests approximating the auxiliary field $y(r)$ as a simpler auxiliary real parameter y . This approximation reduces the auxiliary Hamiltonian to the exactly solvable form \mathcal{H} , up to additive terms depending only on y ,

$$\tilde{H}(y) = \mathcal{H}(y) + [V(J(y)) - y\mathcal{V}(J(y))]. \quad (3.11)$$

By assumption, the spectrum of $\tilde{H}(y)$, denoted $\tilde{\epsilon}(y)$, is analytical,

$$\tilde{\epsilon}(y) = \epsilon(y) + (V(J(y)) - y\mathcal{V}(J(y))). \quad (3.12)$$

The spectrum $\tilde{\epsilon}(y)$ provides an approximation of the true spectrum if the auxiliary parameter satisfies a condition analogous to the functional extremisation constraint (3.10). Since the field has become a parameter, this constraint simplifies to an extremisation on the spectrum of \tilde{H} ,

$$\left. \frac{\partial}{\partial y} \tilde{\epsilon}(y) \right|_{y_0} = 0. \quad (3.13)$$

As a result, choosing an exactly solvable potential \mathcal{V} and solving the above equation yield values $\epsilon(y_0)$ that approximate the true spectrum. Additionally, the eigenvectors of the auxiliary Hamiltonians can serve as approximations of the true eigenvectors. When both potentials V and \mathcal{V} are not overly complex, equation (3.13) can often be solved analytically. Otherwise, it can be handled numerically with minimal computational effort, typically requiring only a few hours of coding and a few seconds of runtime. A closer examination of (3.13) reveals an interesting property of the approximation frame: the extremum y_0 depends on the energy level. Consequently, the ET approximates the original Hamiltonian using a set of analytically solvable auxiliary Hamiltonians, where the parameter of each auxiliary Hamiltonian is tuned so that one of its energy levels approximates the corresponding level of the original Hamiltonian.

In the previous calculations, the approximation strategy was applied to a very simple system of two non-relativistic particles. A similar reasoning extends the ET variational equations (3.13) to systems of N identical particles in D dimensions with generic kinematics and interactions, provided that a suitable exactly solvable Hamiltonian is found. One such analytical Hamiltonian for many-body systems in arbitrary dimensions, already mentioned in Chapter 1, is the harmonic oscillator. In its most general form, this Hamiltonian enables the construction of ET for systems with different types of particles, one-body interactions, or even with K -body forces. To introduce the method gradually, let us focus on systems of N identical particles with two-body interactions. The following harmonic Hamiltonian is analytically solvable,

$$H_{\text{oh}} = \sum_{i=1}^N \frac{\mathbf{p}_i^2}{2\mu} - \frac{\mathbf{P}^2}{2N\mu} + \nu \sum_{i<j}^N |\mathbf{r}_i - \mathbf{r}_j|^2 \quad (3.14)$$

where, as before, $\mathbf{P} = \sum_i \mathbf{p}_i$ is the total momentum of the system. The explicit resolution of the N -body harmonic oscillator Hamiltonian is depicted in Complement 3.A. For $D > 1$ dimensions,

the corresponding spectrum takes the form

$$\epsilon_\alpha(\mu, \omega) = \sqrt{\frac{2N\nu}{\mu}} Q(\alpha) \quad \text{with} \quad Q(\alpha) = \sum_{i=1}^{N-1} (2n_i + \ell_i + D/2). \quad (3.15)$$

Above, α is a compact notation for the set of quantum numbers $\{n_1, \ell_1, \dots, n_{N-1}, \ell_{N-1}\}$. The quantum numbers n_i and ℓ_i correspond to the radial and orbital motion associated with the i^{th} N -body Jacobi coordinates (3.136). The summation runs up to $i = N - 1$, as the last Jacobi variable represent the centre-of-mass position, a degree-of-freedom that has been removed. The quantity $Q(\alpha)$, referred to as a global quantum number, encodes both the radial and orbital excitations of the system. For $D = 1$, where angular momentum is absent, $Q(\alpha)$ is replaced by $\sum_i (n_i + 1/2)$, with α now only labelling the radial quantum numbers $\{n_1, \dots, n_{N-1}\}$. Given this analytical spectrum, constructing an ET based on the harmonic oscillator to approximate N -body Hamiltonians of the form

$$H = \sum_{i=1}^N T(|\mathbf{p}_i|) + \sum_{i<j}^N V(|\mathbf{r}_i - \mathbf{r}_j|) \quad (3.16)$$

follows the same strategy as before but applied to each term of H_{oh} . Although the functions T and V are general, they must satisfy a few constraints, not overly restrictive and aligned with the physical interpretation of T and V (such as differentiability and positiveness of T) [86]. The centre-of-mass motion is assumed to be removed from H , either by explicit subtraction or by setting manually $\mathbf{P} = \mathbf{0}$. The role of auxiliary parameters is played by ν and $1/(2\mu)$. The following auxiliary Hamiltonian is introduced,

$$\tilde{H}(\mu, \nu) = \sum_{i=1}^N \left(\frac{\mathbf{p}_i^2}{2\mu} + T(G(\mu)) - \frac{G^2(\mu)}{2\mu} \right) + \sum_{i<j}^N (\nu |\mathbf{r}_i - \mathbf{r}_j|^2 + V(J(\nu)) - \nu J^2(\nu)). \quad (3.17)$$

where

$$G(x) = F^{-1}(x) \quad \text{with} \quad F(x) = \frac{x}{T'(x)}, \quad J(x) = K^{-1}(x) \quad \text{with} \quad K(x) = \frac{V'(x)}{2x}. \quad (3.18)$$

Different auxiliary parameters are not assigned to each particles because, this would be incompatible with (anti)symmetry condition of the state [61]. The spectrum of the auxiliary

Hamiltonians is given by

$$\tilde{\epsilon}_\alpha(\mu, \nu) = \sqrt{\frac{2N\nu}{\mu}} Q(\alpha) + N \left(T(G(\mu)) - \frac{G^2(\mu)}{2\mu} \right) + \frac{N(N-1)}{2} (V(J(\nu)) - \nu J^2(\nu)). \quad (3.19)$$

As before, an approximation for the spectrum of H is obtained by extremising the auxiliary spectrum with respect to the auxiliary parameters,

$$\left. \frac{\partial}{\partial \mu} \tilde{\epsilon}_\alpha(\mu, \nu) \right|_{\mu_0, \nu_0} = \left. \frac{\partial}{\partial \nu} \tilde{\epsilon}_\alpha(\mu, \nu) \right|_{\mu_0, \nu_0} = 0. \quad (3.20)$$

As expected, the extremal parameters μ_0 and ν_0 explicitly depend on α , meaning they vary with the energy level being approximated.

3.1.2 Compact equations

Although the variational equations of the ET (3.20) are usable, they present a few drawbacks, summarised as follows,

- analytical expressions for the intermediary functions G and J are required;
- computing the explicit derivatives of $\tilde{\epsilon}(\mu, \nu)$ can be tedious for complex G and/or J functions;
- the auxiliary parameters μ_0 and ν_0 , obtained during the resolution process, serve only to define the shape of the auxiliary Hamiltonians, limiting their broader interest.

All these issues are resolved by reformulating the variational equations into a more convenient form, known as *compact equations*. This reformulation yields a set of three algebraic equations that replace the variational ones in the search for an approximation of the spectrum of the Hamiltonian (3.16) [87, 88]²,

$$E = NT(p_0) + C_N^2 V(\rho_0), \quad (3.21a)$$

$$Np_0T'(p_0) = C_N^2 \rho_0 V'(\rho_0), \quad (3.21b)$$

$$Q(\alpha) = \sqrt{C_N^2} p_0 \rho_0, \quad (3.21c)$$

² In previous works, the parameter $r_0^2 = N^2 \langle (\mathbf{r}_i - \mathbf{R})^2 \rangle$, where \mathbf{R} denotes the centre of mass position, was used instead of ρ_0 to facilitate the treatment of one-body potentials. It can be shown that for identical particles both parameters are equivalent up to a multiplicative constant, $r_0^2 = C_N^2 \rho_0^2$. Since only two-body potential will be considered in this work, it is preferable to use ρ_0 .

where $C_N^2 = N(N-1)/2$ represents the number of particle pairs. The proof of the compact equations is deferred until after their full description. Solving equations (3.21) provides an expression for the approximated spectrum E in terms of the harmonic oscillator global quantum number $Q(\alpha)$. As a reminder, the latter is related to the internal radial and orbital quantum numbers, collectively denoted by α , through the following relationship,

$$Q(\alpha) = \sum_{i=1}^{N-1} \left(2n_i + \ell_i + \frac{D}{2} \right), \quad (3.22)$$

where D represents the dimensionality of the system. The two other unknowns obtained by solving (3.21), p_0 and ρ_0 , provide approximations of instructive expectation values within the system,

$$p_0^2 = \langle \mathbf{p}_i^2 \rangle, \quad \rho_0^2 = \langle |\mathbf{r}_i - \mathbf{r}_j|^2 \rangle. \quad (3.23)$$

Since all particles are identical, the subscripts i and j can be arbitrarily chosen from $\{1, \dots, N\}$. Because the above expectation values are not evaluated on the true eigenstates but rather on the eigenstates of the auxiliary Hamiltonians, they serve only as approximations of the exact values. The variables p_0 and ρ_0 are also related to the auxiliary parameters through the functions G and J ,

$$G(\mu_0) = p_0, \quad J(\rho_0) = r_0. \quad (3.24)$$

Equations (3.21) successfully addressed each of the three shortcomings of the variational equations (3.20). The equivalence between the compact and variational equations is demonstrated below. This proof relies on the miscellaneous theorems from Section 1.3.

Proof. A full description of the following proof can be found in [62], with a summary in [88] – Let us denote by $|\tilde{\varphi}_\alpha(\mu, \nu)\rangle$ the eigenstate of the auxiliary Hamiltonian $\tilde{H}(\mu, \nu)$ with quantum numbers α . Evaluated at the extremal auxiliary parameters $\mu_0(\alpha)$ and $\nu_0(\alpha)$, the state $|\tilde{\varphi}_\alpha(\mu_0(\alpha), \nu_0(\alpha))\rangle$ approximates the corresponding eigenstate of H . To simplify notation, the dependence on α of the auxiliary parameters is omitted in what follows. Applying the Hellmann-Feynman theorem (1.70) to evaluate the derivatives in (3.20), one obtains

$$\begin{aligned} \left. \frac{\partial}{\partial \mu} \tilde{\epsilon}_\alpha(\mu, \nu) \right|_{\mu_0, \nu_0} &= \langle \tilde{\varphi}_\alpha(\mu, \nu) | \frac{\partial}{\partial \mu} \tilde{H}(\mu, \nu) | \tilde{\varphi}_\alpha(\mu, \nu) \rangle \Big|_{\mu_0, \nu_0} = 0, \\ \left. \frac{\partial}{\partial \nu} \tilde{\epsilon}_\alpha(\mu, \nu) \right|_{\mu_0, \nu_0} &= \langle \tilde{\varphi}_\alpha(\mu, \nu) | \frac{\partial}{\partial \nu} \tilde{H}(\mu, \nu) | \tilde{\varphi}_\alpha(\mu, \nu) \rangle \Big|_{\mu_0, \nu_0} = 0. \end{aligned} \quad (3.25)$$

Expanding these equations using the definitions of $\tilde{H}(\mu, \nu)$ and $G(x)$ leads to

$$\langle \mathbf{p}_i^2 \rangle = G^2(\mu_0), \quad \langle |\mathbf{r}_i - \mathbf{r}_j|^2 \rangle = J^2(\nu_0). \quad (3.26)$$

Above, expectation values are taken with respect to the approximate eigenstate $|\tilde{\varphi}_\alpha(\mu_0, \nu_0)\rangle$, and they are independent of $i, j \in \{1, \dots, N\}$ due to symmetry arguments (see development (1.48) for a detailed calculation). Equations (3.26) address the third flaw mentioned earlier: through the functions G and J , the auxiliary parameters acquire a physical interpretation. Specifically, $G^2(\mu_0)$ approximates the expectation value of the squared individual momenta, while $J^2(\nu_0)$ approximates the expectation value of the squared relative distance. The term "approximate" is appropriate here, as these expectation values are computed on eigenstates of the auxiliary Hamiltonian, $|\tilde{\varphi}_\alpha(\mu_0, \nu_0)\rangle$. In the following, new variables p_0^2 and ρ_0^2 are introduced to represent $G^2(\mu_0)$ and $J^2(\nu_0)$, respectively.

Despite (3.26), solving for μ_0 and ν_0 via (3.20) remains a necessary step. The next developments aim to bypass their explicit computation. First, the approximate spectrum is expressed directly in terms of p_0 and ρ_0 ,

$$\begin{aligned} \epsilon_\alpha(\mu_0, \nu_0) &= \langle \varphi_\alpha(\mu_0, \nu_0) | \tilde{H}(\mu_0, \nu_0) | \varphi_\alpha(\mu_0, \nu_0) \rangle \\ &= NT(p_0) + \frac{N(N-1)}{2} V(\rho_0). \end{aligned} \quad (3.27)$$

To obtain (3.27), equations (3.26) are used to cancel equal terms. Second, two inequivalent identities are required to access p_0 and ρ_0 . A first one is obtained by applying the virial theorem (1.74) to $\tilde{H}(\mu_0, \nu_0)$, yielding

$$\frac{N}{\mu_0} p_0^2 = N(N-1) \nu_0 \rho_0^2. \quad (3.28)$$

Since the auxiliary Hamiltonian is a shifted harmonic oscillator, this result is analogous to equation (1.36). Using the definitions of G , H , J and K , one shows that

$$\mu_0 = \frac{p_0}{T'(p_0)}, \quad \nu_0 = \frac{V'(\rho_0)}{2\rho_0}. \quad (3.29)$$

Substituting these into (3.28) yields an equation depending only on p_0 and ρ_0 ,

$$Np_0T'(p_0) = \frac{N(N-1)}{2} \rho_0 V'(\rho_0). \quad (3.30)$$

To obtain a second independent relation between p_0 and ρ_0 , the spectrum (3.19) is revisited. Its expression simplifies for the extremal parameters,

$$\tilde{\epsilon}_\alpha(\mu_0, \nu_0) = \sqrt{\frac{2N\nu_0}{\mu_0}} Q(\alpha) + N \left(T(p_0) - \frac{p_0^2}{2\mu_0} \right) + \frac{N(N-1)}{2} (V(\rho_0) - \nu_0\rho^2) \quad (3.31)$$

Equations (3.29) are again used to eliminate the residual dependencies on μ_0 and ν_0 ,

$$\begin{aligned} \tilde{\epsilon}_\alpha(\mu_0, \nu_0) = \sqrt{N \frac{V'(\rho_0)}{\rho_0} \frac{T'(p_0)}{p_0}} Q(\alpha) + N \left(T(p_0) - \frac{p_0 T'(p_0)}{2} \right) \\ + \frac{N(N-1)}{2} \left(V(\rho_0) - \frac{\rho_0 V'(\rho_0)}{2} \right), \end{aligned} \quad (3.32)$$

and equation (3.27) allows for the elimination of the energy $\tilde{\epsilon}_\alpha(\mu_0, \nu_0)$,

$$\frac{Np_0 T'(p_0)}{2} + \frac{N(N-1)}{2} \frac{\rho_0 V'(\rho_0)}{2} = \sqrt{N \frac{V'(\rho_0)}{\rho_0} \frac{T'(p_0)}{p_0}} Q(\alpha). \quad (3.33)$$

Finally, substituting equation (3.30), one obtains

$$\sqrt{\frac{N(N-1)}{2}} p_0 \rho_0 = Q(\alpha) \quad (3.34)$$

This is a second independent equation that relates p_0 and ρ_0 . Equations (3.27), (3.30) and (3.34) together form the compact equations of the envelope theory. In most formulations, the approximate energy $\tilde{\epsilon}_\alpha(\mu_0, \nu_0)$ is simply denoted E , and the factor $N(N-1)/2$ is written as C_N^2 . \square

To illustrate the application of compact equations, a system of N identical particles with power-law kinetic energies and power-law two-body interactions is considered,

$$T(p) = A|p|^a, \quad V(x) = \frac{b}{|b|} B|x|^b. \quad (3.35)$$

where $A > 0$ and $a > 0$ are required for a well-defined kinetic energy [86], while $B > 0$ and $b \neq 0$ ensure the existence of bound states. Solving the compact equations for this system begins by

determining expressions for p_0 and ρ_0 from equations (3.21b) and (3.21c),

$$p_0 = \left(\frac{|b|BQ(\alpha)^b \left(\sqrt{C_N^2}\right)^{2-b}}{NaA} \right)^{1/(a+b)}, \quad \rho_0 = \left(\frac{NaAQ(\alpha)^a}{|b|B \left(\sqrt{C_N^2}\right)^{a+2}} \right)^{1/(a+b)}. \quad (3.36)$$

These expressions are then substituted into equation (3.21a) to obtain the approximated eigenenergies,

$$E = \frac{b}{|b|}(a+b) \left(\left(\frac{C_N^2 B}{a} \right)^a \left(\frac{NA}{|b|} \right)^b \left(\frac{Q(\alpha)}{\sqrt{C_N^2}} \right)^{ab} \right)^{1/(a+b)}. \quad (3.37)$$

Notably, if $b < 0$, the ET eigenenergies remain negative only if $b > -a$. For $b \leq -a$, the ET equations do not predict any physical bound states. By keeping the number of particles arbitrary, the ET provides analytical approximations for the energy spectrum, mean individual momentum, and mean relative distance with remarkably low computational cost. Accuracy tests of these ET approximations are deferred to Section 3.1.7.

3.1.3 Variational properties

Until now, the discussion has presented the ET as an auxiliary field method, but the term "envelope" in the original name remains to be elucidated. This can be achieved by examining the extremal auxiliary Hamiltonians and comparing them to the true Hamiltonian. The next discussion is structured as follows: at first, developments are framed within a proof environment, associated properties are subsequently summarised, emphasising practical aspects, and finally, results are illustrated on a concrete example.

Proof. A full description of the following proof can be found in [62], with a summary in [57, 68, 78] – Let us begin by reorganising the extremal auxiliary Hamiltonians,

$$\begin{aligned} \tilde{H}(\mu_0, \nu_0) &= \sum_{i=1}^N \left(\frac{\mathbf{p}_i^2}{2\mu_0} + T(G(\mu_0)) - \frac{G^2(\mu_0)}{2\mu_0} \right) + \sum_{i<j}^N (\nu_0 |\mathbf{r}_i - \mathbf{r}_j|^2 + V(J(\nu_0)) - \nu_0 J^2(\nu_0)) \\ &= \sum_{i=1}^N \left(T(p_0) + \frac{\mathbf{p}_i^2 - p_0^2}{2\mu_0} \right) + \sum_{i<j}^N (V(\rho_0) + \nu_0 (|\mathbf{r}_i - \mathbf{r}_j|^2 - \rho_0^2)) \\ &= \sum_{i=1}^N \tilde{T}(|\mathbf{p}_i|) + \sum_{i<j}^N \tilde{V}(|\mathbf{r}_i - \mathbf{r}_j|) \quad \text{where} \quad \tilde{T}(p) = T(p_0) + \frac{p^2 - p_0^2}{2\mu_0} \end{aligned} \quad (3.38)$$

$$\text{and} \quad \tilde{V}(x) = V(\rho_0) + \nu_0 (x^2 - \rho_0^2).$$

The last line explicitly separates \tilde{H} into individual auxiliary kinetic energies and pairwise auxiliary two-body potentials. The following argument is first presented for the auxiliary potentials. Let us evaluate the function $\tilde{V}(x)$ and its derivative at $x = \rho_0$,

$$\tilde{V}(\rho_0) = V(\rho_0), \quad \tilde{V}'(\rho_0) = 2\nu_0\rho_0 = V'(\rho_0). \quad (3.39)$$

The third equality follows from equation (3.29). Equations (3.39) demonstrate that $V(x)$ and $\tilde{V}(x)$ are tangent functions at the argument $x = \rho_0$. However, since in the ET the true Hamiltonian is not approximated by a single auxiliary Hamiltonian but rather by a set of them, it is not a single tangent auxiliary potential $\tilde{V}(x)$ that is constructed, but a collection of such potentials. This set, when represented graphically, tends to "envelope" the original potential. Figure 3.1 illustrates this envelope of auxiliary potentials for a system of three identical bosons with $V(x) = x/2$ and $T(p) = p^2/2$ (in arbitrary units). Similar reasoning shows that $T(p)$ and $\tilde{T}(p)$ are also tangent functions at $p = p_0$ and that the $\tilde{T}(p)$ kinetic energies likewise envelope the original function.

Beyond justifying the name of the method, this property has significant consequences. Once again, let us start with the potential term. First, the variable x is replaced by x^2 . This operation straightens the auxiliary potential, transforming its parabolic shape into a straight line. For the original potential, this variable transformation defines a new function, denoted b_V , such that $b_V(x^2) = V(x)$. Despite this reformulation, the auxiliary straight line remains tangent to the function b_V . It is straightforward to see that any line tangent to a concave (convex) function always lies above (below) it. Thus,

$$\forall x \in \mathbb{R}^+, b_V''(x) \leq 0 \implies \forall x \in \mathbb{R}^+, V(x) \leq \tilde{V}(x), \quad (3.40a)$$

$$\forall x \in \mathbb{R}^+, b_V''(x) \geq 0 \implies \forall x \in \mathbb{R}^+, V(x) \geq \tilde{V}(x). \quad (3.40b)$$

A similar argument applies to the kinetic energy, leading to analogous conclusions. Defining $b_T(p^2) = T(p)$, one obtains

$$\forall p \in \mathbb{R}^+, b_T''(p) \leq 0 \implies \forall p \in \mathbb{R}^+, T(p) \geq \tilde{T}(p), \quad (3.41a)$$

$$\forall p \in \mathbb{R}^+, b_T''(p) \geq 0 \implies \forall p \in \mathbb{R}^+, T(p) \leq \tilde{T}(p). \quad (3.41b)$$

These observations allow the use of the comparison theorem from Section 1.3, if the inequalities for T and V are consistent. If both b_V and b_T are either convex or concave, the approximation provided by the ET serves as either an upper or a lower bound for the true spectrum. If the second derivative of one of these functions vanishes, then the energy

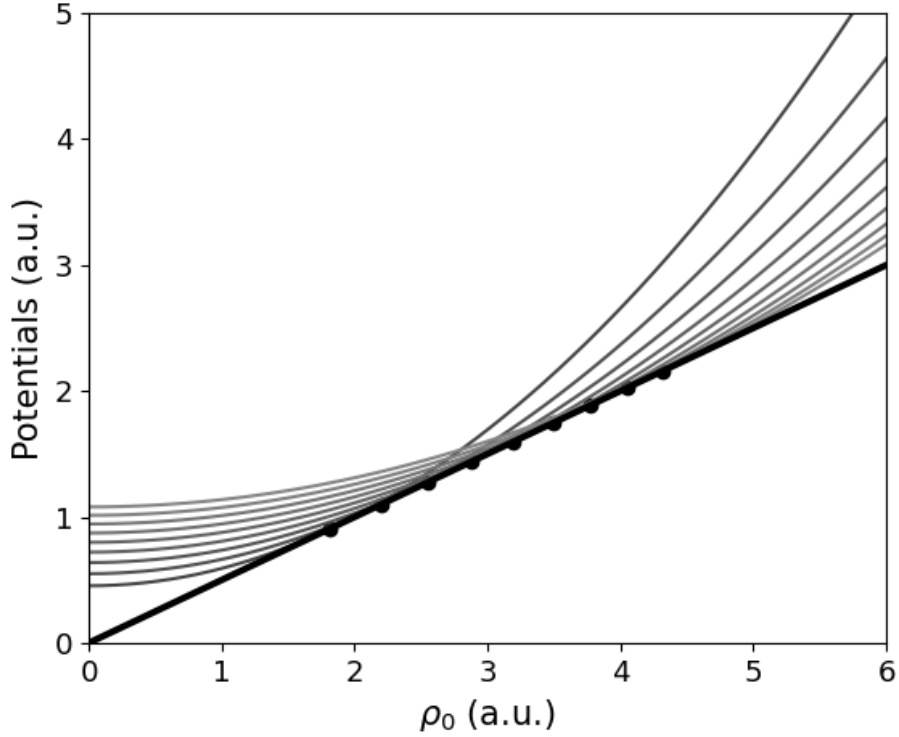


Figure 3.1: Illustration of the auxiliary potentials for linear two-body interactions. The system consists of three non-relativistic bosons of unit mass with $V(x) = x/2$ (in arbitrary units). The true potential is represented by a black line, while auxiliary potentials for increasing energy levels are plotted in shades of grey. The black dots indicate the contact points between the true potential and the auxiliary ones.

|| contribution of that part of H is exactly treated by the ET and should be ignored when assessing the variational character. If both second derivatives vanish, meaning that the true Hamiltonian itself is an harmonic oscillator, the ET provides the exact result. \square

To summarize, for certain favourable Hamiltonians, the energies approximated by the ET are either upper or lower bounds for the original energy spectrum [57, 58, 87]. To establish this, one must analyse the concavity of the following functions,

$$b_T(x) = T(\sqrt{x}), \quad (3.42)$$

$$b_V(x) = V(\sqrt{x}). \quad (3.43)$$

If both b_T and b_V are concave (convex) over \mathbb{R}_0^+ , the ET spectrum consists entirely of upper (lower) bounds. If the second derivative of one function vanishes, the variational character is determined by the other. If both second derivatives vanish, meaning that H corresponds to a

$\alpha > 2$	$\beta \geq 2$	lower bounds
	$\beta > 2$	lower bounds
$\alpha = 2$	$\beta = 2$	exact results
	$\beta < 2$	upper bounds
$\alpha < 2$	$\beta \leq 2$	upper bounds

Table 3.1: Variational properties of the ET approximations for N identical particles with power-law kinetic energies and power-law two-body interactions (3.35).

harmonic oscillator Hamiltonian, the ET provides the exact result. In other cases, no variational character can be guaranteed.

Continuing the example from previous section, one may ask whether the approximation (3.37) possesses a variational character. To analyse this, the concavity of the functions b_V and b_T is examined,

$$b_T''(p) = \frac{A}{4}a(a-2)p^{(a-4)/2}, \quad b_V''(x) = \frac{B}{4}|b|(b-2)x^{(b-4)/2}. \quad (3.44)$$

For certain ranges of a and b , the concavity of both functions aligns, ensuring a variational property for the ET approximations. These ranges and their corresponding interpretation are summarised in Table 3.1. For other values, the concavities are opposed, preventing any definitive conclusion regarding the variational character of the ET approximation.

3.1.4 Improvement of the envelope theory

The ET may lack accuracy for certain Hamiltonians. To address this limitation, a parameter ϕ can be introduced into the global quantum number $Q(\alpha)$,

$$\begin{aligned} Q_\phi(\alpha) &= \sum_{i=1}^{N-1} \left(\phi n_i + \ell_i + \frac{D + \phi - 2}{2} \right) \\ &= \phi \left[\sum_{i=1}^{N-1} \left(n_i + \frac{1}{2} \right) \right] + \left[\sum_{i=1}^{N-1} \ell_i + (N-1) \frac{D-2}{2} \right]. \end{aligned} \quad (3.45)$$

Notably, $Q_\phi(\alpha)$ generalises the previous global quantum number, as setting $\phi = 2$ recovers the original expression $Q(\alpha)$. The introduction of ϕ is inspired by [89], in which a universal effective quantum number for centrally symmetric two-body problems is proposed. Specifically, this reference suggests a well-defined separation of radial and angular contributions. Equation (3.45) extends this construction to N -body problems in an ad-hoc manner. While there is no rigorous

derivation justifying this generalisation, its effectiveness, particularly in improving the accuracy of the ET, supports its consideration.

One key advantage of expression (3.45) over (3.22) is that it partially breaks the strong degeneracy inherent to the harmonic oscillator Hamiltonian. With a well-calibrated strategy for determining ϕ , introducing such an additional parameter into the ET should enhance its accuracy. However, since the approximated energy is no longer an eigenvalue of an auxiliary harmonic oscillator, this improvement comes at the cost of losing the possible variational character.

Historically, the effectiveness of introducing ϕ was first tested by fitting this parameter to pre-existing results. For instance, ϕ was chosen to reproduce only the lowest energy eigenvalue, and the accuracy of the rest of the ET spectrum was then analysed. These tests proved conclusive: as expected, a value for ϕ that reproduced the ground state was found, and this value significantly improved, sometimes spectacularly, the accuracy of the rest of the spectrum [66]. However, since this technique requires prior knowledge of accurate energy values, one may question the relevance of approximating an energy level for which precise results already exist. Nonetheless, there are systems where only a few energy values are fully known, making this improved ET useful for exploring the inaccessible parts of the spectrum. Another approach is to fit ϕ for a particle number where numerical methods are efficient and then extend it to larger systems, assuming that ϕ depends only weakly on N . However, despite these arguments, at this stage, the introduction of ϕ remains a niche tool with limited practical applications.

To broaden its applicability, an *ab initio* procedure capable of determining ϕ without any prior knowledge has been developed. This approach relies on coupling the improved ET with another approximation method, the DOSM. This coupling is made possible by a semi-classical interpretation of the ET compact equations. These topics are addressed in the following sections.

A semi-classical interpretation for the ET equations

The compact equations (3.21) were derived using a fully quantum mechanical approach. However, they also bear a striking resemblance to classical formulations. Consider a system of N identical classical particles. To incorporate the symmetry constraints imposed by quantum mechanics, the system is assumed to move along a circular trajectory of radius d_0 , with each particle possessing the same momentum magnitude p_0 and being uniformly distributed along the orbit. Figure 3.2 illustrates this classical configuration. A generic kinetic energy function T and two-body interaction V are assumed, where T depends only on the magnitude of the particle momentum, and V depends on the magnitude of the relative distance. These assumptions align with those used to derive the compact equations (3.21).

Let us evaluate the total energy of this classical system, starting with kinetic energy. Since all

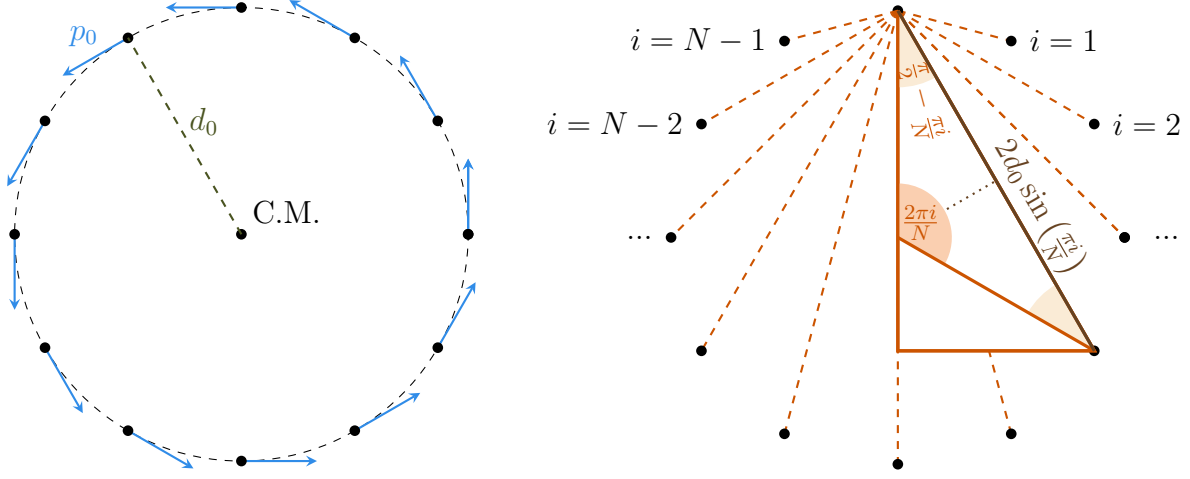


Figure 3.2: Schematic representation of a classical system governed by equations analogous to the compact equations of the ET. The left diagram defines key variables: the centre of mass (C.M.) coincides with the centre of rotation; all particles share the same momentum p_0 , and their distance from the centre is equal to d_0 . The right diagram illustrates the computation of the mean relative distance.

particles share the same momentum magnitude, the total kinetic energy consists of N identical terms, $T(p_0)$. The total potential energy, however, is more complex, since different particle pairs may have different separations. To approximate this contribution, the mean relative distance between particles, ρ_0 , is introduced. Evaluating the two-body potential at this average distance and multiplying by the number of particle pairs provides a reasonable estimate of the total potential energy. The total energy of the classical system is thus given by

$$E = NT(p_0) + C_N^2 V(\rho_0). \quad (3.46)$$

Despite being derived from a classical perspective, this expression is formally identical to the first compact equation of the ET. Next, the stability of this system can be analysed by equating the centrifugal force F_{cf} with the centripetal forces F_{cp} . The classical centrifugal contribution for a particle having an effective mass that depends on the momentum is discussed in [90, 91]. In the present case, it is given by

$$F_{cf} = p_0 T'(p_0) \frac{1}{d_0}. \quad (3.47)$$

The variables d_0 and ρ_0 can be related to each other using geometric considerations, as illustrated on the right panel of Figure 3.2,

$$\rho_0 = \frac{1}{N-1} \sum_{i=1}^{N-1} 2d_0 \sin\left(\frac{i\pi}{N}\right) = \frac{Nd_0}{C_N^2} \cot\left(\frac{\pi}{2N}\right). \quad (3.48)$$

This intricate expression can be approximated by $Nd_0 \approx \sqrt{C_N^2}\rho_0$, with an error of less than 10% for any number of particles [87]. Substituting d_0 into (3.47) gives

$$F_{cf} \approx \frac{Np_0T'(p_0)}{\sqrt{C_N^2}\rho_0}. \quad (3.49)$$

The centripetal force can again be estimated by assuming that the contribution from each of the $N - 1$ other particles can be approximated as a two-body interaction acting at the mean distance, $V'(\rho_0)$. However, since these contributions acts in a different directions, they must be projected along the diagonal of the circle. Referring again to Figure 3.2, one obtains

$$F_{cp} \approx V'(\rho_0) \sum_{i=1}^{N-1} \cos\left(\frac{\pi}{2} - \frac{i\pi}{N}\right) = V'(\rho_0) \sum_{i=1}^{N-1} \sin\left(\frac{i\pi}{N}\right) = V'(\rho_0) \cot\left(\frac{\pi}{2N}\right) \quad (3.50)$$

Applying the same approximation as before, this equation simplifies to

$$F_{cp} \approx \sqrt{C_N^2}V'(\rho_0). \quad (3.51)$$

Equating (3.49) and (3.51) yields an equation fully analogous to the second compact equation of the ET,

$$Np_0T'(p_0) = C_N^2\rho_0V'(\rho_0). \quad (3.52)$$

The third equation can be derived by classically evaluating the total angular momentum of the system, denoted L . Each particle follows a circular trajectory of radius d_0 with momentum p_0 , yielding an orbital angular momentum d_0p_0 . Summing over all particles gives

$$L = Nd_0p_0 \approx \sqrt{C_N^2}\rho_0p_0. \quad (3.53)$$

This equation closely resembles the third compact equation of the ET, with one key difference: instead of the global quantum number $Q(\alpha)$, which accounts for both radial and orbital motion, the classical equation involves only the total orbital angular momentum, L . This distinction is natural, given that the classical configuration under study does not include any radial motion. Therefore, the initial claim must be refined: the compact equations of the ET can be interpreted as describing a system of N classical particles orbiting on a circle, provided that any radial contribution is excluded from $Q(\alpha)$, including the associated zero-point energy. A separation between radial and orbital contributions naturally occurs in the generalised quantum number $Q_\phi(\alpha)$. By excluding the corresponding radial terms, the following purely orbital third compact

equation of the ET is constructed,

$$\lambda(\ell_1, \dots, \ell_{N-1}) = \sqrt{C_N^2 p_0 \rho_0}, \quad \text{where} \quad \lambda(\ell_1, \dots, \ell_{N-1}) = \sum_{i=1}^{N-1} \ell_i + (N-1) \frac{D-2}{2}. \quad (3.54)$$

The classical equation $L = \sqrt{C_N^2 \rho_0 p_0}$ can finally be identified with the above expression. To summarize, the classical set of equations (3.46), (3.52) and (3.53), which describes a system of N classical particles orbiting on a circle is equivalent to the purely orbital compact equations of the ET, where equation (3.54) replaces (3.21c). In the following, although both sets of equations are fully analogous, it is useful to distinguish the set derived from classical mechanics from the one obtained using the ET. The former will be referred to as the classical equations.

The DOSM for systems of N identical bodies

As its name suggests, the DOSM approximates states where orbital motion dominates over radial motion. More precisely, it suggests treating the radial excitation as a perturbation around a classical purely orbital motion. This method, originally formulated for two-body systems [92], can be extended to N bodies by using the aforementioned classical equations [64],

$$\tilde{E} = NT(\tilde{p}_0) + C_N^2 V(\tilde{\rho}_0), \quad (3.55a)$$

$$N\tilde{p}_0 T'(\tilde{p}_0) = C_N^2 \tilde{\rho}_0 V'(\tilde{\rho}_0), \quad (3.55b)$$

$$\lambda = \sqrt{C_N^2 \tilde{p}_0 \tilde{\rho}_0}. \quad (3.55c)$$

These equations approximate the total energy \tilde{E} , the mean distance $\tilde{\rho}_0$ and the mean momentum \tilde{p}_0 associated with the classical purely orbital motion described earlier. For convenience, in the following, any variable referring to a purely orbital motion is denoted with a tilde. This orbital motion can now be perturbed radially, which modifies the mean relative distances ρ_0 in the system by adding an increment $\Delta\rho_r \ll \rho_0$ to it,

$$\tilde{\rho}_0 \rightarrow \tilde{\rho}_0 + \Delta\rho_r. \quad (3.56)$$

Note that, even though it is referred to as an increment, $\Delta\rho_r$ can be both positive and negative. This radial perturbation also affects the momentum of the particles, but by construction, it lets the total angular momentum of the system unchanged. Therefore, after perturbation, \tilde{p}_0 is decomposed into two contributions: a radial one, denoted $p_r \ll \tilde{p}_0$, and a tangential one,

denoted p_0^* . The latter is used to preserve the total angular momentum of the system, so that

$$\lambda = \sqrt{C_N^2(\tilde{\rho}_0 + \Delta\rho_r)p_0^*}. \quad (3.57)$$

Combining both contributions, the impact of the radial perturbation is expressed as follows,

$$\tilde{p}_0 \rightarrow \sqrt{p_r^2 + p_0^{*2}} = \sqrt{p_r^2 + \frac{\lambda^2}{C_N^2(\tilde{\rho}_0 + \Delta\rho_r)^2}}. \quad (3.58)$$

Figure 3.3 illustrates this radial perturbation. Since $\Delta\rho_r \ll \tilde{\rho}_0$ and $p_r \ll \tilde{p}_0$, second-order Taylor expansions can be performed on equation (3.58). After a few calculations, the following replacement rule that initiates the radial perturbation is obtained,

$$\tilde{p}_0 \rightarrow \tilde{p}_0 \left(1 + \frac{p_r^2}{2\tilde{p}_0^2} - \frac{\Delta\rho_r}{\tilde{\rho}_0} + \frac{\Delta\rho_r^2}{\tilde{\rho}_0^2} \right). \quad (3.59)$$

The energy after the perturbation, E , is obtained by substituting the relations (3.56) and (3.59) into (3.55a). Again, second-order Taylor expansions are performed, yielding

$$\begin{aligned} E &= NT \left(\tilde{p}_0 \left(1 + \frac{p_r^2}{2\tilde{p}_0^2} - \frac{\Delta\rho_r}{\tilde{\rho}_0} + \frac{\Delta\rho_r^2}{\tilde{\rho}_0^2} \right) \right) + C_N^2 V(\tilde{\rho}_0 + \Delta\rho_r) \\ &= \tilde{E} + \left(\frac{NT'(\tilde{p}_0)}{2\tilde{p}_0} \right) p_r^2 + \left(\frac{N\tilde{p}_0 T'(\tilde{p}_0)}{\tilde{\rho}_0^2} + \frac{N\tilde{p}_0^2 T''(\tilde{p}_0)}{2\tilde{\rho}_0^2} + \frac{C_N^2 V''(\tilde{\rho}_0)}{2} \right) \Delta\rho_r^2. \end{aligned} \quad (3.60)$$

The first-order contributions cancel each other due to Equation (3.55b). This result provides the classical energy for a dominantly orbital state. The DOSM suggests quantising the radial motion. The energy increment due to the perturbation, $\Delta E = \tilde{E} - E$, is written, emphasising its dependence on p_r and $\Delta\rho_r$,

$$\begin{aligned} \Delta E &= \frac{p_r^2}{2\bar{m}} + \frac{\bar{k}\Delta\rho_r^2}{2} \text{ with } \bar{m} = \frac{\tilde{p}_0}{NT'(\tilde{p}_0)} \\ &\text{and } \bar{k} = \frac{2N\tilde{p}_0 T'(\tilde{p}_0)}{\tilde{\rho}_0^2} + \frac{N\tilde{p}_0^2 T''(\tilde{p}_0)}{\tilde{\rho}_0^2} + C_N^2 V'(\tilde{\rho}_0). \end{aligned} \quad (3.61)$$

Above, ΔE takes the form a one-dimensional harmonic oscillator Hamiltonian (both p_r and $\Delta\rho_r$ can be negative). For now, let us assume that variables p_r and $\Delta\rho_r$ are conjugate. This assumption will be re-examined later. The DOSM suggests considering this harmonic oscillator

Hamiltonian as a quantum operator and identifying the energy increment as its spectrum,

$$\Delta E = \sqrt{\frac{\bar{k}}{\bar{m}}} \left(n + \frac{1}{2} \right). \quad (3.62)$$

Here, the quantum number n globally encodes the radial excitation of the system. It should be distinguished from the n_i quantum numbers in the ET, which separately encodes the radial excitation associated with each Jacobi coordinate. Relating the n and the n_i quantum numbers is not straightforward. The easiest way to address this is by evaluating the N -body harmonic oscillator spectrum with the DOSM and to comparing the result to its analytical spectrum (3.15). After a few calculations, the DOSM provides the following approximate energy eigenvalues,

$$\tilde{E}_{\text{oh}} = E_{\text{oh}} + \Delta E_{\text{oh}} = \sqrt{\frac{N\nu}{\mu}} \left(\lambda + 2\sqrt{C_N^2} \left(n + \frac{1}{2} \right) \right). \quad (3.63)$$

Comparing with (3.15), it appears that the DOSM gives the exact result, provided that $\sqrt{C_N^2}(n + 1/2)$ is identified with $\sum_{i=1}^{N-1}(n_i + 1/2)$. It is a common feature of the DOSM to exactly reproduce the spectrum of the non-relativistic harmonic oscillator, even for purely radially excited states [93]. One might be surprised by the factor $\sqrt{C_N^2}$ that this identification introduces. In fact, it can be related to the assumption made regarding p_r and $\Delta\rho_r$. If, instead of $\Delta\rho_r$, the conjugate variable to p_r is taken to be $\sqrt{C_N^2}\Delta\rho_r$, this factor disappears from the relation that identifies n and $\{n_i\}$. Therefore, one can safely rescale the variable used to initiate the radial perturbation, provided that the quantum numbers are correctly identified at the end of the developments.

To summarize, the DOSM provides an approximation for the energy of dominantly orbital eigenstates. This approximation is obtained in two steps. First, \tilde{p}_0 and $\tilde{\rho}_0$ are determined by solving the purely orbital equations (3.55) for a given orbital excitation λ . Second, the orbital energy \tilde{E} is supplemented by a radial increment ΔE . The radial excitation is indicated by a global quantum number n and the increment is evaluated using the following formula,

$$\begin{aligned} \Delta E = \sqrt{\frac{\bar{k}}{\bar{m}}} \left(n + \frac{1}{2} \right) \quad \text{with } \bar{m} = \frac{\tilde{p}_0}{NT'(\tilde{p}_0)} \\ \text{and } \bar{k} = \frac{2N\tilde{p}_0T'(\tilde{p}_0)}{\tilde{\rho}_0^2} + \frac{N\tilde{p}_0^2T''(\tilde{p}_0)}{\tilde{\rho}_0^2} + C_N^2V'(\tilde{\rho}_0). \end{aligned} \quad (3.64)$$

The DOSM quantum numbers n and λ have been related to the quantum numbers from the ET

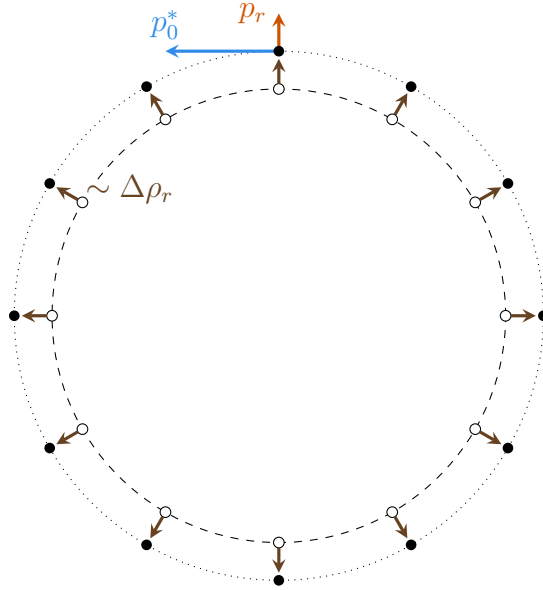


Figure 3.3: Schematic representation of the radial perturbation initiated while developing the DOSM for N -body systems. The perturbed momentum combines two contributions: a radial one, denoted p_r , and a tangential one, denoted p_0^* . The perturbed mean relative distance is also affected by an increment $\Delta\rho_r$.

as follows,

$$\sqrt{C_N^2}(n + 1/2) = \sum_{i=1}^{N-1} (n_i + 1/2), \quad \lambda = \sum_{i=1}^{N-1} \ell_i + (N - 1) \frac{D - 2}{2}. \quad (3.65)$$

Coupling the DOSM and the improved ET

The DOSM, as constructed in the previous section, is a self-sufficient method, that operates independently of the ET. However, the equations used by both methods are very similar, raising the possibility of coupling them. One key difference between the two methods is that the approximation given by the ET is valid for the entire spectrum, whereas the DOSM is specifically tuned to be particularly efficient for dominantly orbital states. Given this distinction, the following strategy is proposed. The ϕ parameter from the improved ET is chosen so that this method reproduces the spectrum of the DOSM for dominantly orbital states. By relying on the versatility of the ET approximation, the resulting expression for ϕ is then extended to the entire spectrum, including radially excited states.

To proceed with the matching of both methods, the equations of the improved ET must first be developed for dominantly orbital states. To start, let us rework $Q_\phi(\alpha)$ to introduce a

parameter that characterises the relative amount of orbital excitation, denoted as ϵ ,

$$\begin{aligned} Q_\phi(\alpha) &= \phi \left[\sum_{i=1}^{N-1} \left(n_i + \frac{1}{2} \right) \right] + \left[\sum_{i=1}^{N-1} \ell_i + (N-1) \frac{D-2}{2} \right] \\ &= \lambda \epsilon + \lambda \quad \text{with} \quad \lambda = \sum_{i=1}^{N-1} \ell_i + (N-1) \frac{D-2}{2} \quad \text{and} \quad \epsilon = \frac{\phi}{\lambda} \sum_{i=1}^{N-1} \left(n_i + \frac{1}{2} \right). \end{aligned} \quad (3.66)$$

For $\epsilon = 0$, the state under investigation is purely orbital, and the equations of the ET take a structure analogous to the classical questions,

$$\tilde{E} = N T(\tilde{p}_0) + C_N^2 V(\tilde{\rho}_0), \quad (3.67a)$$

$$N \tilde{p}_0 T'(\tilde{p}_0) = C_N^2 \tilde{\rho}_0 V'(\tilde{\rho}_0), \quad (3.67b)$$

$$\lambda(\ell_1, \dots, \ell_{N-1}) = \sqrt{C_N^2 \tilde{p}_0 \tilde{\rho}_0}, \quad (3.67c)$$

Since these are solutions to purely orbital equations, the energy, momentum and mean distance have been denoted with tildes. For $\epsilon \ll 1$, the state is dominantly orbital, and the variables, denoted E , p_0 and ρ_0 , are close to their purely orbital equivalents,

$$p_0 = \tilde{p}_0 + \Delta p \quad \text{with} \quad \Delta p \ll p_0, \quad (3.68a)$$

$$\rho_0 = \tilde{\rho}_0 + \Delta \rho \quad \text{with} \quad \Delta \rho \ll \rho_0, \quad (3.68b)$$

$$E = \tilde{E} + \Delta E \quad \text{with} \quad \Delta E \ll E_0, \quad (3.68c)$$

Substituting p_0 , ρ_0 and E into the ET compact equations allows to express ΔE in terms of the purely orbital variables and the quantum numbers ϵ and λ . First, Taylor expansions of the third compact equation provide an expression for Δp in terms of $\Delta \rho$,

$$\tilde{p}_0 + \Delta p = \tilde{p}_0 \left(1 + \epsilon + \frac{\Delta \rho}{\tilde{\rho}_0} \right). \quad (3.69)$$

This relation can then be substituted directly into the first compact equation. After a final series of Taylor expansions, the following expression is obtained for ΔE ,

$$\Delta E = N \tilde{p}_0 T'(\tilde{p}_0) \epsilon + \left(C_N^2 V'(\tilde{\rho}_0) - \frac{N \tilde{p}_0 T'(\tilde{p}_0)}{\tilde{\rho}_0} \right) \Delta \rho. \quad (3.70)$$

The terms in the large parentheses vanish due to equation (3.67b). Finally, an expression for

ΔE in terms of the expected quantities is obtained,

$$\Delta E = Np_0T'(p_0)\epsilon = Np_0T'(p_0)\frac{\phi}{\lambda}\sum_{i=1}^{N-1}\left(n_i + \frac{1}{2}\right). \quad (3.71)$$

This expression can now be compared to the one provided by the DOSM. Using (3.65) to relate n to $\{n_i\}$, equation (3.64) turns out very similar to (3.71),

$$\Delta E = \sqrt{\frac{\bar{k}}{C_N^2\bar{m}}}\sum_{i=1}^{N-1}\left(n_i + \frac{1}{2}\right). \quad (3.72)$$

The expression for ϕ is chosen so that both expressions give the same energy increment for dominantly orbital states,

$$\phi = \frac{\lambda}{N\tilde{p}_0T'(\tilde{p}_0)}\sqrt{\frac{\bar{k}}{C_N^2\bar{m}}}. \quad (3.73)$$

After some algebraic manipulation, a more compact expression is obtained,

$$\phi = \sqrt{2 + \frac{\tilde{p}_0T''(\tilde{p}_0)}{T'(\tilde{p}_0)} + \frac{\tilde{\rho}_0V''(\tilde{\rho}_0)}{V'(\tilde{\rho}_0)}}. \quad (3.74)$$

This is the aforementioned ab initio formula that can be used in the improved ET. From now on, the term "classical ET" will refer to the ET without the additional parameter ϕ , in contrast to the "improved ET" which computes and includes it using the above formula. The expression presented here is equivalent to the one in [64] but is more concise due to unnoticed simplifications [94].

Application example

For clarity, let us summarise the entire expression for ϕ in a single equation,

$$\phi = \sqrt{2 + \frac{\tilde{p}_0T''(\tilde{p}_0)}{T'(\tilde{p}_0)} + \frac{\tilde{\rho}_0V''(\tilde{\rho}_0)}{V'(\tilde{\rho}_0)}} \text{ where } \begin{cases} N\tilde{p}_0T'(\tilde{p}_0) = C_N^2\tilde{\rho}_0V'(\tilde{\rho}_0), \\ \sqrt{C_N^2\tilde{p}_0\tilde{\rho}_0} = \lambda(\ell_1, \dots, \ell_{N-1}) = \sum_{i=1}^{N-1}\left(\ell_i + \frac{D-2}{2}\right). \end{cases} \quad (3.75)$$

As can be seen, given an orbital excitation λ , obtaining ϕ requires first solving the above system of two equations to find \tilde{p}_0 and $\tilde{\rho}_0$. The equations in this system are fully analogous to the

second and third compact equations of the ET, with $Q(\alpha)$ replaced by λ . Consequently, if an analytical solution exists for the ET, \tilde{p}_0 and $\tilde{\rho}_0$ can be directly deduced from this solution. Otherwise, the system in (3.75) must be solved numerically. The computational cost of this operation is comparable to that of the classical ET itself. Once these variables are determined, ϕ can be computed and used in the generalised global quantum number $Q_\phi(\alpha)$,

$$Q_\phi(\alpha) = \phi \left[\sum_{i=1}^{N-1} \left(n_i + \frac{1}{2} \right) \right] + \lambda(\ell_1, \dots, \ell_{N-1}). \quad (3.76)$$

This new quantum number is then used in place of $Q(\alpha)$ in the compact equation of the ET. If an analytical solution exists, simply substituting this quantum number in the final expression is sufficient. Otherwise, compact equations must be solved numerically a second time. It is important to note that modifying $Q(\alpha)$ removes the guarantee of any variational character, if one exists.

To illustrate the calculation required by the improved ET, let us continue with the example from previous sections. Consider a system of N identical particles with power-law kinetic energies, $T(p) = Ap^a$, and power-law two-body interactions, $V(x) = Bx^b$. The classical ET provided the following expressions for E , p_0 and ρ_0 in Section 3.1.2,

$$p_0 = \left(\frac{NaAQ(\alpha)}{|b|B \left(\sqrt{C_N^2} \right)^{a+2}} \right)^{1/(a+b)}, \quad \rho_0 = \left(\frac{|b|BQ(\alpha)^b \left(\sqrt{C_N^2} \right)^{2-b}}{NaA} \right)^{1/(a+b)}, \quad (3.77)$$

$$E = \frac{b}{|b|} (a+b) \left(\left(\frac{C_N^2 B}{a} \right)^a \left(\frac{NA}{|b|} \right)^b \left(\frac{Q(\alpha)}{\sqrt{C_N^2}} \right)^{ab} \right)^{1/(a+b)}.$$

Determining \tilde{p}_0 and $\tilde{\rho}_0$ requires solving the same equations with λ replacing $Q(\alpha)$. This results in the following analogous expressions,

$$\tilde{p}_0 = \left(\frac{NaA\lambda}{|b|B \left(\sqrt{C_N^2} \right)^{a+2}} \right)^{1/(a+b)}, \quad \tilde{\rho}_0 = \left(\frac{|b|B\lambda^b \left(\sqrt{C_N^2} \right)^{2-b}}{NaA} \right)^{1/(a+b)}. \quad (3.78)$$

Substituting these expressions into the formulas for ϕ leads to significant simplifications. After a few algebraic manipulations, the following compact expression for ϕ is obtained,

$$\phi = \sqrt{a+b}. \quad (3.79)$$

In this special case, ϕ does not truly depend on λ . The above expression allows for the calculation of the new global quantum number $Q_\phi(\alpha)$, which can then be substituted into the compact equations. The following improved spectrum is obtained,

$$E = \frac{b}{|b|} (a+b) \left(\left(\frac{C_N^2 B}{a} \right)^a \left(\frac{NA}{|b|} \right)^b \left(\frac{Q_{\sqrt{a+b}}(\alpha)}{\sqrt{C_N^2}} \right)^{ab} \right)^{1/(a+b)}. \quad (3.80)$$

These eigenenergies are expected to be more accurate than the previous ones. Thanks to ϕ , the degeneracy of the ET spectrum has been partially raised. However, none of the variational interpretations from Section 3.1.3 holds any longer, as the quantum number of the harmonic oscillator has been modified. These statements are tested in the Section 3.1.7.

Before moving on, let us mention that, since the DOSM requires the concept of orbital angular momentum to exist, the ab initio improvement procedure can only be validated for $D > 1$. For systems in one dimension, no ab initio formula for an equivalent of ϕ has been developed.

3.1.5 Generalisations

Extensions of the ET and its improvement exist for systems of N identical particles interacting via Hamiltonians beyond (3.16). These generalisations allow for the inclusion of one-body potentials [62, 64] and/or a certain class of K -body forces [54, 88]. The ET has even been expanded to describe bound cyclic systems, as explored in [95]. These extensions are based on variations of the Hamiltonian (3.16) that remain analytically solvable. They lead to adapted compact equations, additional conditions for determining the variational character and, if developed, new formulas for the parameter ϕ . For detailed discussions of these modified ET, the reader is referred to the corresponding references. However, in order to illustrate how compact equations are affected and because the class of K -body interactions discussed in [88] generalises the three-body forces introduced in Section 1.12, the corresponding compact equations are presented in the present section. Detailed derivations are deferred to [54, 88].

Consider a system of N identical particles governed by the following general Hamiltonian,

$$H = \sum_{i=1}^N T(|\mathbf{p}_i|) + \sum_{\{i_1, \dots, i_k\}}^N W(r_{\{i_1, \dots, i_k\}}) \quad \text{where} \quad r_{\{i_1, \dots, i_k\}}^2 = \sum_{i < j}^{\{i_1, \dots, i_k\}} |\mathbf{r}_i - \mathbf{r}_j|^2. \quad (3.81)$$

As before, it is assumed that the centre-of-mass motion is removed from H . Above, $\{i_1, \dots, i_k\}$ denotes a specific set of K particles among the N available, and the sum $\sum_{\{i_1, \dots, i_k\}}^N$ runs over all possible sets of K particles in the system. It can be verified that for $K = 2$, the K -body

interaction terms reduce to the aforementioned two-body interactions, while for $N = K = 3$, they reduce to the three-body interactions introduced in Section (1.12). The ET provides an approximation for the spectrum of the Hamiltonian (3.81) by solving the following set of three compact equations [54, 88],

$$E = N T(p_0) + C_N^K W \left(\sqrt{C_K^2 \rho_0} \right), \quad (3.82a)$$

$$N p_0 T'(p_0) = C_N^K \sqrt{C_K^2 \rho_0} W' \left(\sqrt{C_K^2 \rho_0} \right), \quad (3.82b)$$

$$\sqrt{C_N^2} p_0 \rho_0 = Q(\alpha) = \sum_{i=1}^{N-1} \left(2n_i + \ell_i + \frac{D-2}{2} \right). \quad (3.82c)$$

Above, C_A^B is the binomial coefficient $A!/(B!(A-B)!)$. The unknowns p_0 and ρ_0 retain their previous interpretation (3.23) as approximations for the expectations values of momentum and relative distance. As expected, for $K = 2$, the compact equations (3.21) are recovered. Several K -body interactions can also be incorporated by duplicating the associated terms in equations (3.82a) and (3.82b).

Regarding the variational character of the approximation, a function $b_W(x)$ such that $b_W(x^2) = W(x)$ is introduced. The concavity of this function, together with the concavity properties of the other b -functions, determines whether the result provides an upper bound, a lower bound or simply an approximation to the true spectrum.

Finally, an adapted formula for ϕ has been obtained in reference [54] following similar calculation steps as previously detailed. It results in a very analogous expression,

$$\phi = \left(2 + \frac{\tilde{p}_0 T''(\tilde{p}_0)}{T'(\tilde{p}_0)} + \frac{\sqrt{C_k^2} \tilde{\rho}_0 V'' \left(\sqrt{C_k^2} \tilde{\rho}_0 \right)}{V' \left(\sqrt{C_k^2} \tilde{\rho}_0 \right)} \right)^{1/2} \quad (3.83)$$

$$\text{where } \begin{cases} N \tilde{p}_0 T'(\tilde{p}_0) = C_N^K \sqrt{C_K^2} \tilde{\rho}_0 V'(\sqrt{C_K^2} \tilde{\rho}_0), \\ \sqrt{C_N^2} \tilde{p}_0 \tilde{\rho}_0 = \lambda(\ell_1, \dots, \ell_{N-1}). \end{cases}$$

Again, for $K = 2$, the previous expression is recovered. This formula is again only valid for $D > 1$. The obtained parameter is to be used in the same modified global quantum number as for two-body interactions,

$$Q_\phi(\alpha) = \sum_{i=1}^{N-1} \left(\phi n_i + \ell_i + \frac{D + \phi - 2}{2} \right). \quad (3.84)$$

Of course, as for two-body forces, this modification of $Q(\alpha)$ with ϕ disrupts the variational character of the original ET, if it exists.

3.1.6 Approximations of eigenstates and relation with the OBE

As mentioned earlier, the ET can also be used to approximate eigenstates. However, obtaining and using these approximations is not as straightforward as with the spectrum. In this section, the associated calculations are illustrated for three-body systems, in line with the scope of this work. The development can easily be generalised to more particles.

First, a notation for the different approximate eigenstates provided by the ET must be introduced. They are specified by their symmetry σ , total angular momentum L , parity P and global quantum number $Q(\alpha)$,

$$|\sigma; Q^*(\alpha); L^P\rangle \quad \text{with} \quad Q^*(\alpha) = Q(\alpha) - 3 = 2n_1 + \ell_1 + 2n_2 + \ell_2. \quad (3.85)$$

Above, $Q^*(\alpha)$ replaces $Q(\alpha)$ for notational convenience and because $Q^*(\alpha)$ is directly related to the number of quanta defined in Section 2.1.3. As discussed while developing the basics of the ET in Section 3.1.1, the states $|\sigma; Q^*(\alpha); L^P\rangle$ are, by construction, symmetrised eigenstates of the auxiliary harmonic oscillators that have yet to be constructed. Since similar calculations have already been depicted in Section 2.1.3 for the OBE, this construction is discussed only briefly here.

Unsymmetrical eigenstates of the harmonic oscillator are explicitly constructed for a general number of particles in Complement 3.A. For three-body systems, these states are labelled by two radial, two orbital and two magnetic quantum numbers, and are denoted as $|\psi_{n_1\ell_1m_1n_2\ell_2m_2}(\mathbf{x}_1, \mathbf{x}_2)\rangle$. A given total angular momentum is assigned to these states using the usual coupling with Clebsch-Gordan coefficients,

$$|\psi_{n_1\ell_1n_2\ell_2}^L(\mathbf{x}_1, \mathbf{x}_2)\rangle = \sum_{m_1, m_2} \langle \ell_1 m_1 \ell_2 m_2 | LM \rangle |\psi_{n_1\ell_1m_1n_2\ell_2m_2}(\mathbf{x}_1, \mathbf{x}_2)\rangle, \quad (3.86)$$

where, as in Chapter 2, the quantum number M has been omitted in the left-hand side notation. One can show that these states are already parity eigenstates, with parity given by $P = (-1)^{\ell_1 + \ell_2}$. Symmetrised eigenstates are then written as definite linear combinations of eigenstates (3.86) sharing the same energy, parity and total angular momentum,

$$|\sigma; Q^*(\alpha); L^P\rangle = \sum_{n_1, \ell_1, n_2, \ell_2} C_{n_1\ell_1n_2\ell_2}^{LP\sigma} |\psi_{n_1\ell_1n_2\ell_2}^L(\mathbf{x}_1, \mathbf{x}_2)\rangle, \quad (3.87)$$

where the sum is constrained to terms with $2n_1 + \ell_1 + 2n_2 + \ell_2 = Q^*(\alpha)$ and $(-1)^{\ell_1+\ell_2} = (-1)^{Q^*(\alpha)} = P$. Procedures for explicitly determining the coefficients $C_{n_1 \ell_1 n_2 \ell_2}^{LP\sigma}$ are described in Section 2.1.3 and reference [54]. These coefficients are independent of the auxiliary parameters and need to be computed only once.

Notably, eigenstate approximations obtained from the OBE and the ET share the feature of being symmetrised harmonic oscillator eigenstates. As a reminder, the eigenvectors obtained using the OBE are decomposed as follows,

$$|\Psi_{\text{OBE}}\rangle = \sum_{Q^*=0}^{Q_{\max}} \sum_s d_s(Q^*) |\Phi_{n_x \ell_x n_y \ell_y}^L(\mathbf{x}, \mathbf{y})\rangle \quad (3.88)$$

where the states $|\Phi_{n_x \ell_x n_y \ell_y}^L(\mathbf{x}, \mathbf{y})\rangle$ are defined in equation (2.4) and where the sum over s accounts for all degrees of freedom other than the number of quanta. The coordinates \mathbf{x} and \mathbf{y} are dimensionless Jacobi coordinates, scaled by a single parameter a for three identical particles,

$$\mathbf{x} = \frac{\mathbf{x}_1}{a}, \quad \mathbf{y} = \frac{2\mathbf{x}_2}{\sqrt{3}a}. \quad (3.89)$$

Moreover, the parameter a is controlling the size of the harmonic oscillator used in the method. This role is analogous to that played by the variable ρ_0 in the ET. Owing to this similarity, the two variables can be related to each other [54],

$$\rho_0 = \sqrt{\frac{Q(\alpha)}{2}} a. \quad (3.90)$$

This equality, however, should be interpreted with caution. It indicates that, if the relation holds, the harmonic oscillator eigenstates constructed using the scale a in the OBE and those constructed using the scale ρ_0 in the ET are the same. Nevertheless, it should not be understood as a strict identity between the optimised variational parameter a and the solution of the ET equations ρ_0 . More broadly, the similarities between the OBE and the ET should not be construed as implying the equivalence of the two methods. They are built on fundamentally different approaches: the OBE approximates the true eigenstates using those of the harmonic oscillator, whereas the ET directly approximates the true Hamiltonian using harmonic oscillator ones. Although the ET variable ρ_0 and the variational parameter a are related, both methods determine these quantities using fundamentally different approaches.

Nevertheless, the similarity between the approximations from the ET and the OBE allows for an easy comparison. In the decomposition (3.88), there typically exists a value of Q^* for which $\sum_s |d_s(Q^*)|^2$ approaches 1. The corresponding number of quanta determines the value of

$Q^*(\alpha)$ to be used in the ET to obtain the corresponding approximation. It also quantifies the agreement between both methods: the closer the sum $\sum_s |d_s(Q^*)|^2$ is to 1, the more accurate the ET approximation becomes. Additionally, the more accurately equation (3.90) holds, the more both methods use the same scale, and the closer the resulting approximations are. This last observation leads to an interesting application of the ET. When optimizing the non-linear variational parameters with the OBE, selecting an initial guess for a can be somewhat challenging. Solving the ET equations can provide guidance: obtaining ρ_0 gives, via equation (3.90), an initial approximation for the optimised a value. While this equation does not generally yield the exact value, it provides a sufficiently accurate estimate to serve as an initial guess for a . This is particularly valuable since solving the ET equations numerically takes less than a second.

Finally, once the approximate eigenstates from the ET have been obtained in terms of harmonic oscillator eigenstates, approximating observables reduces to evaluating a few integrals of analytical integrands. Let us illustrate this in the case for a scalar observable \mathcal{O} . First, the symmetric state from the ET is decomposed using equation (3.87),

$$\begin{aligned} \langle \sigma; Q^*(\alpha); L^P | \mathcal{O} | \sigma; Q^*(\alpha); L^P \rangle = \\ \sum_{n'_1, \ell'_1, n'_2, \ell'_2} \sum_{n_1, \ell_1, n_2, \ell_2} C_{n'_1 \ell'_1 n'_2 \ell'_2}^{LP\sigma*} C_{n_1 \ell_1 n_2 \ell_2}^{LP\sigma} \langle \psi_{n'_1 \ell'_1 n'_2 \ell'_2}^L(\mathbf{x}_1, \mathbf{x}_2) | \mathcal{O} | \psi_{n_1 \ell_1 n_2 \ell_2}^L(\mathbf{x}_1, \mathbf{x}_2) \rangle \end{aligned} \quad (3.91)$$

Since \mathcal{O} does not act on angular degrees of freedom, the matrix elements on total angular momentum eigenstates simplify using Clebsch-Gordan properties,

$$\begin{aligned} \langle \psi_{n'_1 \ell'_1 n'_2 \ell'_2}^L(\mathbf{x}_1, \mathbf{x}_2) | \mathcal{O} | \psi_{n_1 \ell_1 n_2 \ell_2}^L(\mathbf{x}_1, \mathbf{x}_2) \rangle \\ = \delta_{\ell'_1 \ell_1} \delta_{\ell'_2 \ell_2} \langle \psi_{n'_1 \ell_1 n'_2 \ell_2 m_2}(\mathbf{x}_1, \mathbf{x}_2) | \mathcal{O} | \psi_{n_1 \ell_1 m_1 n_2 \ell_2 m_2}(\mathbf{x}_1, \mathbf{x}_2) \rangle \end{aligned} \quad (3.92)$$

where m_1 and m_2 can be chosen indifferently as the angular integrals from the matrix element on the right-hand side are trivial. Finally, the following expression is obtained

$$\begin{aligned} \langle \sigma; Q^*(\alpha); L^P | \mathcal{O} | \sigma; Q^*(\alpha); L^P \rangle = \\ \sum_{n'_1, n'_2} \sum_{n_1, n_2} \sum_{\ell_1, \ell_2} C_{n'_1 \ell_1 n'_2 \ell_2}^{LP\sigma*} C_{n_1 \ell_1 n_2 \ell_2}^{LP\sigma} \langle \psi_{n'_1 \ell_1 n'_2 \ell_2 m_2}(\mathbf{x}_1, \mathbf{x}_2) | \mathcal{O} | \psi_{n_1 \ell_1 m_1 n_2 \ell_2 m_2}(\mathbf{x}_1, \mathbf{x}_2) \rangle \end{aligned} \quad (3.93)$$

For simple cases, the residual matrix elements can be evaluated analytically using the properties of the harmonic oscillator eigenstates [54]. For more complex cases, numerical routines allow for reasonably fast evaluations.

3.1.7 Accuracy tests

The previous sections presented the ET as an easily applicable approximation method but whose accuracy proves difficult to predict. An improved version of the method exists and should improve overall accuracy, but quantifying this improvement remains elusive. Acquiring insights into the efficiency of the ET may help answer these questions. These are obtained by testing the ET on systems for which very accurate eigenenergies are accessible. References [54, 55, 66, 67] consist in gathering and analysing such tests. The current section goes over some of the results from these articles. The goal is to illustrate the main feature about the accuracy of the ET more than to provide an exhaustive review of the associated works. Especially, in accordance with the editorial policy of this document, tests are only preformed on three-body systems in three dimensions, although formulas are written for arbitrary numbers of particles N and dimensions D for the sake of generality. Tests involving larger systems of identical particles are proposed in references [64, 66, 67].

In general, only bosons will be considered, which implies that only combinations of quantum numbers $\{n_1, \ell_1, \dots, n_{N-1}, \ell_{N-1}\}$ that yield a symmetric harmonic oscillator eigenstate are permitted. Since the corresponding state is always symmetric, the ET approximation for the ground state of a bosonic system is simply obtained by setting $n_i = \ell_i = 0$ for all $i \in \{1, \dots, N-1\}$. For three particles, it results in a definite expression for the modified global quantum number,

$$Q_\phi^{BGS} = \phi + 1. \quad (3.94)$$

Let us remind that the initial quantum number is recovered by setting $\phi = 2$. The situation in presence of fermions is discussed in Complement 3.B. Finally, most tests are performed for non-relativistic kinematics, $T(p) = p^2/2m$. As arbitrary units are used, only unit masses are considered.

Power potential and the role of divergences

This first test aims to assess the accuracy of the formulas obtained while developing the method. Sections 3.1.2, 3.1.3 and 3.1.4 concludes by illustrating their formulas on a system of N identical bosons with power-law kinetic energies and power-law two-body interactions,

$$T(p) = Ap^a, \quad V(x) = \frac{b}{|b|} Bx^b. \quad (3.95)$$

As already mentioned, the current test will consider $N = 3$, $A = 1/2$ and $a = 2$. Only the ground state will be investigated. Concerning the interaction, b values ranging from -2 to 3

b	HHE [25]	OBE	ET	$[\delta]$	IET	$[\delta]$
-1.0	-0.266 75	-0.266 45	-0.125 00	[53%]	-0.281 25	[6%]
-0.5	-0.591 73	-0.591 74	-0.491 39	[17%]	-0.599 77	[1%]
0.1	1.880 19	1.880 18	1.914 06	[2%]	1.877 43	[< 1%]
0.5	2.916 54	2.916 53	3.082 03	[6%]	2.902 11	[< 1%]
1.0	3.863 09	3.863 09	4.088 52	[6%]	3.841 30	[< 1%]
2.0	5.196 15	5.196 15	5.196 15	[0%]	5.196 15	[0%]
3.0	6.155 91	6.155 91	5.683 94	[8%]	6.224 79	[1%]

Table 3.2: Ground state energies provided by the HHE from [25], the OBE, the ET and the improved ET (IET) for a system of three identical bosons of unit mass and interacting pairwise with potential $V(x) = b/(2|b|x^b)$. Arbitrary units are used. Relative differences with the OBE, denoted δ , are indicated in % for the ET and the improved ET. For the OBE, the maximum number of quanta used in the basis is $Q_{\max} = 20$, with a computed for $Q_{\max} = 10$.

and $B = 1/2$ are chosen to enable the comparison of the ET results with those from reference [25] and from the OBE. Some of the corresponding data were already presented in Section 2.3.1. Results are displayed on Table 3.2. For b positive, the accuracy of the ET is about a few percent of relative error while that of the improved version goes below or equal to 1%. As expected, both methods prove exact for $b = 2$, namely for harmonic interactions. The variational character predicted on Table 3.1 is verified for the ET, but not for the improved version. For b negative, the situation must be qualified. It seems that the more divergent the potential is, the less accurate the ET is. Although also slightly affected, the improved ET proves more resilient to this degradation. This conclusion is confirmed by the result from Figure 3.4. These tests use increasingly divergent power-law potentials $V(x) = -x^{-|b|}$ with $|b|$, until 1.75. Ground states are computed using the ET, the improved ET and the OBE. The ET provides reasonably accurate results for small $|b|$. However, as $|b|$ increases, the relative error also increases. When utilising the improved ET, the behaviour with respect to b is better reproduced. For values of b close to -2 , the accuracy of the improved ET results appears to decrease. It should be noted that for $b < -1$, the results obtained from the OBE should be interpreted with caution because convergence was not completely achieved.

These conclusions are general features with the ET: the more divergent the potential is, the less accurate proves the approximation, and turning to the improved ET can help mitigate this inaccuracy. It can be validated by testing the ET on other potentials in which a divergence can be controlled. For instance, a truncated Coulomb potential can be considered,

$$V(r) = -\frac{C}{\sqrt{r^2 + d^2}} \quad (3.96)$$

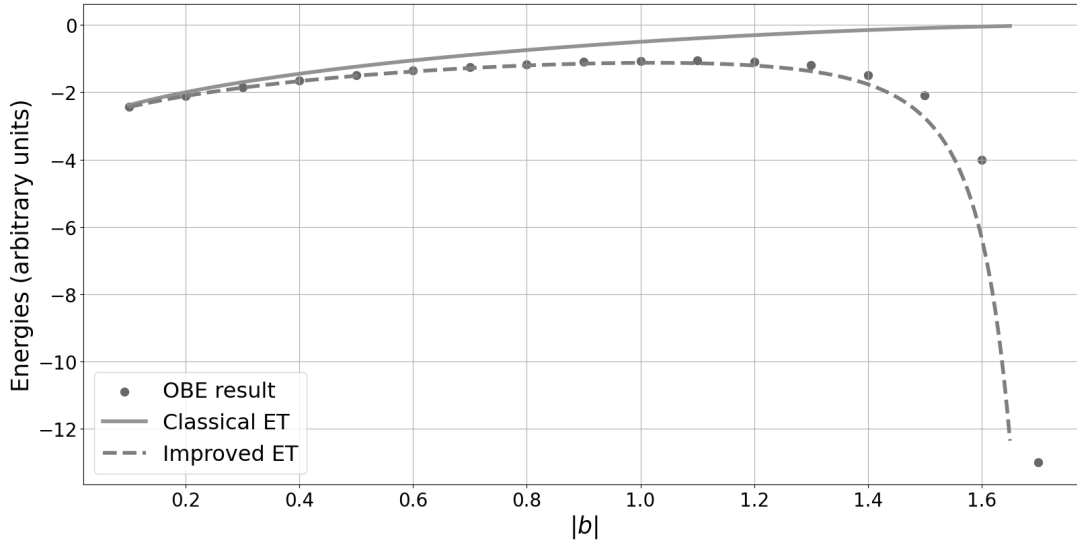


Figure 3.4: Ground state energies of a three-body system with $m = 1$ and a negative power potential $V(r) = -r^{-|b|}$ as a function of $|b|$. OBE results (dots), ET results (line) and improved ET results (dashed line). ET and improved ET results have been plotted with a line to easily distinguish them from the exact ones. For the OBE, a is computed for $Q_{\max} = 10$ while the maximum number of quanta used in the basis is $Q_{\max} = 26$.

with $C > 0$ and $d > 0$. Such a potential is commonly used to model electron-hole pairs, also known as excitons [96]. By applying equations (3.21b) and (3.21c), the following expression is obtained

$$\frac{mC}{N} \frac{(C_N^2)^2}{Q_\phi(\alpha)^2} \rho_0^4 = (\rho_0^2 + d^2)^{3/2}. \quad (3.97)$$

Since the solutions of this quartic equation are complicated to manipulate, numerical computations are preferred. It has been demonstrated that the classical ET provides upper bounds for this potential. In a previous study [78], the ET was employed to investigate this system, but only for two-body systems at $D = 1$. As the ET results are obtained through numerical calculations, the same applies to the improved ET. The conclusions drawn for this potential are similar to those of the previous example. As shown in Figure 3.5 for $C = 1$, the relative errors decrease as the divergence is smoothed, namely as d increases. Concerning the improved results, they better reproduce the dependence of energy on d . The loss of variational character is also manifest on Figure 3.5 for small d . A third example of increasingly divergent potential is depicted in reference [55].

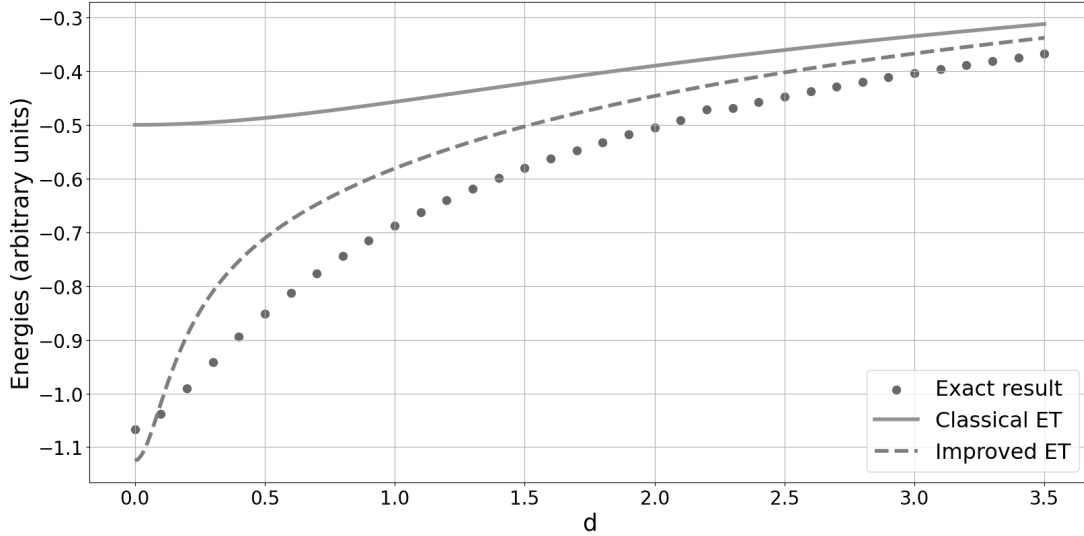


Figure 3.5: Ground state energy E of a three-body exciton system with $m = 1$ and $V(r) = -1/\sqrt{r^2 + d^2}$ as a function of d . OBE results (dots), ET results (solid line) and improved ET results (dashed line) are shown. ET and improved ET results have been plotted with a line to easily distinguish them from the OBE ones. For the OBE, a is computed for $Q_{\max} = 10$ while the maximum number of quanta used in the basis is $Q_{\max} = 26$.

Mixture of different variational characters

A second factor that may affect the ET accuracy is its variational character. When such a property can be established for the solution, it provides some guarantees regarding the quality of the approximation. Otherwise, the ET only asserts that the obtained values approach the true eigenenergies, without further details. To gain insights into the accuracy of the ET, situations with no variational interpretation need to be investigated. They arise, for instance, when a system involves two different interactions whose contributions to the variational character are opposed. Such configurations are found in physical systems, including atomic spectra. In the helium atom, for example, the attractive Coulomb interactions between the nucleus and the electrons coexist with the repulsive Coulomb interaction between the two electrons. These opposing contributions tend to impose contradictory variational characters, resulting in an ET spectrum whose accuracy is difficult to predict. Naturally, atomic systems involve two different types of particles, which requires deferring their description within the ET framework to Section 3.2.4.

Nevertheless, this situation can be replicated with identical particles by considering a potential consisting of two components: one providing an upper bound and the other a lower bound.

To control the variational character, multiplicative factors C and $1 - C$ are introduced. By continuously varying C from 0 to 1, one potential is switched on while the other is switched off. In other words, transitioning from $C = 0$ to $C = 1$ corresponds to a change in the variational character.

As an example to illustrate this approach, a potential combining cubic and linear interactions is considered. Referring to Table 3.1, the cubic potential $V(r) = \alpha r^3$ contributes to a lower bound due to its convex function $b_V(r) = \alpha r^{3/2}$. Conversely, the linear potential $V(r) = \beta r$ leads to an upper bound due to its concave function $b_V(r) = \beta r^{1/2}$. As a result, a potential combining both terms will, depending on the value of C , predominantly display one variational character or the other,

$$V(r) = \alpha C r^3 + \beta (1 - C) r. \quad (3.98)$$

When $C = 0$, $V(r)$ reduces to the linear potential and when $C = 1$, it reduces to the cubic potential. To compute the approximate spectrum, the compact equations (3.21) must be solved once again. It leads to a quintic equation,

$$\frac{N Q(N)^2}{m (C_N^2)^2} - 3\alpha C \rho_0^5 - \beta(1 - C)\rho_0^3 = 0, \quad (3.99)$$

which does not have a general analytical solution. Therefore, numerical computations are performed for both the ET and its improvement. The results are presented in Figure 3.6 for $\alpha = \beta = 1$ (in arbitrary units). As expected, when $C = 0$ (pure linear potential), the classical ET provides an upper bound for the energy, while when $C = 1$ (pure cubic potential), it provides a lower bound. In both cases, the improved ET yields noticeably more accurate results.

However, for intermediate values of C , the situation is more complex. The errors in evaluating the ground state due to the two components of the potential counterbalance each other, resulting in a more precise energy. Since the ET continuously transition from one variational character to the other, its results even match the exact ones at a specific value of C (in this case, approximately $C = 0.2$). However, due to the unpredictability of the crossover point, this feature is impractical to exploit. Regarding the improved ET, it appears less effective in the intermediate range of C values compared to the extremes. In general, the variational character serves as a safeguard, preventing the ET approximations from dropping too low or rising too high. In the absence of this variational guidance, the improved ET struggles to achieve higher accuracy. Concerning a hypothetical crossing of the improved curve with the exact results, the loss of the variational character implies that no general prediction can be made, although this feature does occur in the present example. In conclusion, it is not guaranteed that the improved ET will consistently outperform the classical ET in such situations. However, this result should

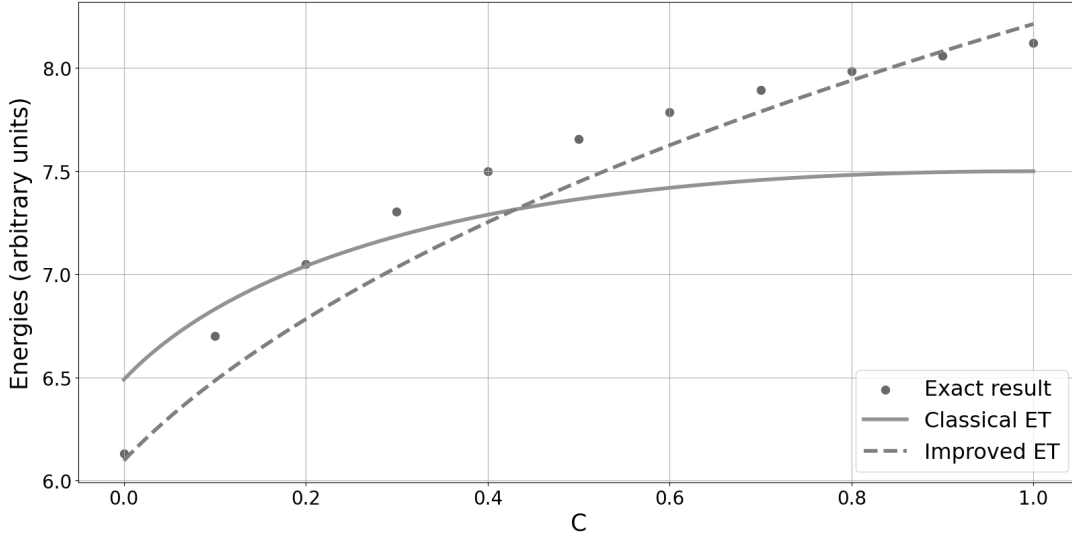


Figure 3.6: Energy E of a three-body system with $m = 1$ and a mixed cubic - linear potential $V(r) = Cr^3 + (1 - C)r$ as a function of C . OBE results (dots), ET results (solid line), and improved ET results (dashed line) are shown. For the OBE, a is computed for $Q_{\max} = 10$, while the maximum number of quanta used in the basis is $Q_{\max} = 26$.

be nuanced as the dashed curve more accurately reproduces the exact shape, and this analysis focuses exclusively on the bosonic ground state.

This first example is supplemented in reference [55] with two other potentials exhibiting similar variational characteristics. The conclusions are broadly consistent with those above: the ET proves to be fairly accurate on its own, and there is no guarantee that the improved ET will genuinely enhance accuracy. These tests also include more complex potential shapes, such as logarithmic and Gaussian interactions.

Three-body forces and observables

To close these illustrations of the ET, let us have a look at the generalisation to K -body forces introduced in Section 3.1.5. The associated approximation will be examined for a system of identical particles interacting with power-law K -body interactions,

$$T(p) = Ap^a, \quad W(\rho) = -\frac{b}{|b|}B\rho^b. \quad (3.100)$$

For now, the kinetic energy is kept arbitrary, but it will be shortly specified to the non-relativistic one ($a = 2$ and $A = 1/2m$). The generalised compact equations for K -body forces

being extremely similar to those for two-body interactions, the same accounts for their solutions,

$$p_0 = \left(\frac{|b|BQ(\alpha)^b C_N^K \left(\sqrt{C_K^2}\right)^b}{NaA \left(\sqrt{C_N^2}\right)^b} \right)^{1/(a+b)}, \quad \rho_0 = \left(\frac{NaAQ(\alpha)^a}{|b|B C_N^K \left(\sqrt{C_N^2}\right)^a \left(\sqrt{C_K^2}\right)^b} \right)^{1/(a+b)}, \quad (3.101)$$

$$E = \frac{b}{|b|} (a+b) \left(\left(\frac{C_N^K B}{a} \right)^a \left(\frac{NA}{|b|} \right)^b \left(\frac{\sqrt{C_K^2}}{\sqrt{C_N^2}} Q(\alpha) \right)^{ab} \right)^{1/(a+b)}. \quad (3.102)$$

Concerning the improved version, ϕ can be computed thanks to (3.83). Surprisingly, it results in the same value as for two-body interactions,

$$\phi = \sqrt{a+b}. \quad (3.103)$$

In the following, the accuracy of the ET approximations is investigated for three non-relativistic bosons with unit masses interacting through linear or Coulomb three-body forces. For both tests, ground states and excited eigenstates are examined. These examples are taken from reference [54].

Let us start with the linear case, $b = 1$ and $B = 1/2$. Using the OBE developed in Chapter 2, accurate eigenvalues and eigenfunctions are obtained for this potential. Table 3.3 compares the results from the ET and its improved version with those from the OBE. States from the ET and from the OBE are identified using the methodology described in Section 3.1.6. A parameter that indicates how well relation (3.90) holds is denoted by ν ,

$$\nu = \sqrt{\frac{Q(\alpha)}{2}} \frac{a}{\rho_0}. \quad (3.104)$$

The ratio associated with the dominant number of quanta in the eigenstates from the OBE, namely $\sum_s |d_s(Q^*)|^2$, is also provided and denoted $D(Q^*)$ for short. Examining the results, the accuracy of the ET is of the same order as for two-body interactions. As expected, there is a strong correlation between the proximity of ν and $D(Q^*)$ to 1 and the accuracy of the ET. The improvement procedure using the DOSM appears to be less effective for systems with three-body forces.

This analysis is confirmed by investigating the Coulomb case, with $b = -1$ and $B = 3$. Eigenenergies of this potential obtained with the OBE have already been displayed in Table 2.6. Table 3.4 compares the results given by the ET and the improved ET with those from

State	OBE	ET	$[\delta]$	IET	$[\delta]$	ν	$D(Q^*)$
$ 1; 0; 0^+\rangle$	2.753	2.835	[3.0%]	2.663	[3.3%]	1.09	0.97
$ 1; 2; 0^+\rangle$	3.795	3.985	[5.0%]	3.695	[2.6%]	1.10	0.94
$ 1; 2; 2^+\rangle$	3.915	3.985	[1.8%]	3.841	[1.9%]	1.06	0.97
$ 1; 3; 1^-\rangle$	4.434	4.500	[1.5%]	4.228	[4.7%]	1.02	0.99
$ 1; 3; 3^-\rangle$	4.434	4.500	[1.5%]	4.365	[1.6%]	1.02	0.99

Table 3.3: Energies in arbitrary units for the lowest states of a system of three identical bosons interacting through a linear three-body potential, $W(\rho) = \rho/2$. Results from the ET, the improved ET and the OBE are compared. Relative differences with respect to the OBE, denoted δ , are indicated in % for the ET and the improved ET. The parameters ν and $D(Q^*)$, which characterises the similarity between the ET and OBE approximations, are also provided. The maximal number of quanta used for the OBE is $Q_{\max} = 16$ with a computed for $Q = 10$.

State	OBE	ET	$[\delta]$	IET	$[\delta]$	ν	$D(Q^*)$
$ 1; 0; 0^+\rangle$	-0.240	-0.167	[30%]	-0.375	[56%]	1.36	0.89
$ 1; 2; 0^+\rangle$	-0.120	-0.060	[50%]	-0.167	[39%]	1.92	0.72
$ 1; 2; 2^+\rangle$	-0.074	-0.060	[19%]	-0.094	[27%]	1.22	0.90

Table 3.4: Energies in arbitrary units for the lowest states of a system of three identical bosons interacting through a Coulomb three-body potential, $W(\rho) = -3/\rho$. Results from the ET, the improved ET and the OBE are compared. Relative differences with respect to the OBE, denoted δ , are given in percent for the ET and the improved ET. Parameters ν and $D(Q^*)$, which characterise the similarity between ET and OBE approximations, are also provided. The maximal number of quanta used for the OBE is $Q_{\max} = 16$ with a computed for $Q = 10$.

Section 2.3.2. The ET approximation achieves a relatively low level of accuracy, similar to that for Coulomb two-body interactions. This poor accuracy is again explained by the divergent nature of the potential. The same correlation with ν and $D(Q^*)$ is observed. Once more, the improved ET struggles to achieve higher accuracy, likely for the same reasons.

Finally, let us briefly compare the approximations for a few observables obtained from the ET and the OBE. This analysis is performed using the same linear three-body potential as before. Table 3.5 presents results for different powers of the relative distance between particles. Due to its low accuracy for the spectrum, the improved ET is not included in this discussion. Notably, for $\langle |r_i - r_j|^2 \rangle$, obtaining an ET approximation requires no additional calculations, since ρ_0^2 directly gives this quantity. All the ET approximations obtained using the methodology from Section 3.1.6 prove to be quite accurate, with relative differences smaller than a few percent. Additional results can be found in reference [54].

State	$\langle r_i - r_j \rangle$			$\langle r_i - r_j ^2 \rangle$			$\langle r_i - r_j ^{-1} \rangle$		
	OBE	ET	$[\delta]$	OBE	ET	$[\delta]$	OBE	ET	$[\delta]$
$ 1; 0; 0^+\rangle$	2.035	2.011	[1.18%]	4.932	4.762	[3.45%]	0.633	0.633	[< 0.1%]
$ 1; 2; 0^+\rangle$	2.806	2.737	[2.46%]	9.863	9.410	[4.59%]	0.526	0.533	[1.33%]
$ 1; 2; 2^+\rangle$	2.867	2.846	[0.73%]	9.614	9.410	[2.12%]	0.446	0.446	[< 0.1%]
$ 1; 3; 1^-\rangle$	3.198	3.178	[0.63%]	12.217	12.00	[1.78%]	0.437	0.437	[< 0.1%]
$ 1; 3; 3^-\rangle$	3.292	3.272	[0.61%]	12.217	12.00	[1.78%]	0.367	0.367	[< 0.1%]

Table 3.5: Mean values for different powers of the relative distance between particles and for the lowest states of a system of three identical bosons interacting through a linear three-body potential, $W(\rho) = \rho/2$. Arbitrary units are used. Results from the ET and the OBE are compared, with relative differences from the OBE, denoted δ , given in %. The maximal number of quanta used for the OBE is $Q_{\max} = 16$ with a computed for $Q = 10$.

3.2 Envelope Theory for Systems of Different Particles

The previous description was restricted to systems of N identical particles. The ET can be extended to systems with different particles, as the harmonic oscillator Hamiltonian with varying masses and oscillator strengths remains analytically solvable [68]. The derivations follows relatively similar approach to that for identical particles. Therefore, for brevity, detailed calculations are omitted, and focus is placed on presenting and illustrating the resulting equations. Additionally, for simplicity, only two distinct particle types are considered. Further details on the ET for systems of different particles can be found in references [65, 68, 97].

3.2.1 Auxiliary fields for systems of different particles

Consider a system with N_a particles of type a and N_b particles of type b . Such a system will be referred to as a system of $N_a + N_b$ particles. The following harmonic oscillator Hamiltonian remains analytically solvable,

$$\begin{aligned}
H_{\text{oh}}^{\text{diff}}(\mu_a, \mu_b, \nu_{aa}, \nu_{bb}, \nu_{ab}) &= \sum_{i=1}^{N_a} \frac{\mathbf{p}_i^2}{2\mu_a} + \sum_{j=1}^{N_b} \frac{\mathbf{p}_j^2}{2\mu_b} + \sum_{i < i'=1}^{N_a} \nu_{aa} |\mathbf{r}_i - \mathbf{r}_{i'}|^2 \\
&+ \sum_{j < j'=1}^{N_b} \nu_{bb} |\mathbf{r}_j - \mathbf{r}_{j'}|^2 + \sum_{i=1}^{N_a} \sum_{j=1}^{N_b} \nu_{ab} |\mathbf{r}_i - \mathbf{r}_j|^2.
\end{aligned} \tag{3.105}$$

Here, \mathbf{p}_i and \mathbf{r}_i (\mathbf{p}_j and \mathbf{r}_j) denote the momentum and position of the i^{th} (j^{th}) particle of type a (b), respectively. As before, the centre-of-mass energy is implicitly removed by setting the total momentum of the system to zero manually, $\mathbf{P} = \sum_{i=1}^{N_a} \mathbf{p}_i + \sum_{j=1}^{N_b} \mathbf{p}_j = \mathbf{0}$. The solvability

of $H_{\text{oh}}^{\text{diff}}$ becomes evident when rewritten as the sum of three separated harmonic contributions,

$$H_{\text{oh}}^{\text{diff}} = H_a + H_b + H_{\text{CM}}. \quad (3.106)$$

Here, H_a describes the internal motion of the subsystem consisting of all particles of type a ,

$$H_a = \sum_{i=1}^{N_a} \frac{\mathbf{p}_i^2}{2\mu_a} - \frac{\mathbf{P}_a}{2M_a} + \sum_{i<i'=1}^{N_a} \left(\nu_{aa} + \frac{N_b}{N_a} \nu_{ab} \right) |\mathbf{r}_i - \mathbf{r}_{i'}|^2. \quad (3.107)$$

Above, $\mathbf{P}_a = \sum_{i=1}^{N_a} \mathbf{p}_i$ is the total momentum of subsystem a and $M_a = N_a \mu_a$ is its total mass. Similarly, H_b governs the internal motion of subsystem b ,

$$H_b = \sum_{j=1}^{N_b} \frac{\mathbf{p}_j^2}{2\mu_b} - \frac{\mathbf{P}_b}{2N_b \mu_b} + \sum_{j<j'=1}^{N_b} \left(\nu_{bb} + \frac{N_a}{N_b} \nu_{ab} \right) |\mathbf{r}_j - \mathbf{r}_{j'}|^2, \quad (3.108)$$

where $\mathbf{P}_b = \sum_{j=1}^{N_b} \mathbf{p}_j$ and $M_b = N_b \mu_b$. Finally, the term H_{CM} describes the relative dynamics between the two subsystems,

$$H_{\text{CM}} = \frac{\mathbf{p}^2}{2\mu} + N_a N_b \nu_{ab} \mathbf{r}^2. \quad (3.109)$$

Here, $\mathbf{p} = (M_b \mathbf{P}_a - M_a \mathbf{P}_b) / (M_a + M_b)$ is the relative momentum between the two subsystems³, $\mu = M_a M_b / (M_a + M_b)$ is the corresponding reduced mass, and $\mathbf{r} = \mathbf{R}_a - \mathbf{R}_b$ is the relative position between their centre-of-mass, defined as $\mathbf{R}_a = \sum_{i=1}^{N_a} \mathbf{r}_i / N_a$ and $\mathbf{R}_b = \sum_{j=1}^{N_b} \mathbf{r}_j / N_b$. With this decomposition (3.106), the spectrum of the Hamiltonian (3.105) is the sum of three well-known N -body harmonic oscillator spectra,

$$\begin{aligned} \epsilon_{\alpha_a, \alpha_b, n, \ell}(\mu_a, \mu_b, \nu_{aa}, \nu_{bb}, \nu_{ab}) &= Q(\alpha_a) \sqrt{\frac{2}{\mu_a} (N_a \nu_{aa} + N_b \nu_{ab})} \\ &+ Q(\alpha_b) \sqrt{\frac{2}{\mu_b} (N_b \nu_{bb} + N_a \nu_{ab})} + Q(n, \ell) \sqrt{\frac{2}{\mu} (N_a N_b \nu_{ab})}. \end{aligned} \quad (3.110)$$

Above, α_a (α_b) denotes the set of quantum numbers associated with the internal motion in the subsystem of particles a (b),

$$\alpha_a = \{n_1^a, \ell_1^a, \dots, n_{N_a-1}^a, \ell_{N_a-1}^a\}, \quad \alpha_b = \{n_1^b, \ell_1^b, \dots, n_{N_b-1}^b, \ell_{N_b-1}^b\}, \quad (3.111)$$

while n and ℓ correspond to the relative motion of the two centres of mass. The function Q retains its previous definition from the case of identical particles. Symmetry conditions on the

³ Note that, as $\mathbf{P} = \mathbf{0}$, one has $\mathbf{p} = \mathbf{P}_a = -\mathbf{P}_b$.

wave function constraint the possible values of $Q(\alpha_a)$ and $Q(\alpha_b)$, but no such constraint applies to $Q(n, \ell)$.

The exactly solvable Hamiltonian (3.105) enables the construction of an ET for a system of $N_a + N_b$ particles governed by the following general Hamiltonian,

$$H = \sum_{i=1}^{N_a} T_a(|\mathbf{p}_i|) + \sum_{j=1}^{N_b} T_b(|\mathbf{p}_j|) + \sum_{i < i'=1}^{N_a} V_{aa}(|\mathbf{r}_i - \mathbf{r}_{i'}|) + \sum_{j < j'=1}^{N_b} V_{bb}(|\mathbf{r}_i - \mathbf{r}_{i'}|) + \sum_{i=1}^{N_a} \sum_{j=1}^{N_b} V_{ab}(|\mathbf{r}_i - \mathbf{r}_j|). \quad (3.112)$$

Following a similar procedure as for a system of N identical particles, auxiliary Hamiltonians depending on five auxiliary parameters are constructed. Additional auxiliary parameters are unnecessary due to the symmetry conditions imposed on particles a and b , respectively. To simplify notation, the set of auxiliary parameters is denoted as $\gamma^{\text{aux}} = \{\mu_a, \mu_b, \nu_{aa}, \nu_{bb}, \nu_{ab}\}$, leading to the definition

$$\tilde{H}^{\text{diff}}(\gamma^{\text{aux}}) = H_{\text{oh}}^{\text{diff}}(\gamma^{\text{aux}}) + B^{\text{diff}}(\gamma^{\text{aux}}), \quad (3.113)$$

where the function B is given by

$$B(\gamma^{\text{aux}}) = N_a \left(T_a(G_a(\mu_a)) - \frac{G_a^2(\mu_a)}{2\mu_a} \right) + C_{N_a}^2 (V_{aa}(J_{aa}(\nu_{aa})) - \nu_{aa} J_{aa}^2(\nu_{aa})) + N_b \left(T_b(G_b(\mu_b)) - \frac{G_b^2(\mu_b)}{2\mu_b} \right) + C_{N_b}^2 (V_{bb}(J_{bb}(\nu_{bb})) - \nu_{bb} J_{bb}^2(\nu_{bb})) + N_a N_b (V_{ab}(J_{ab}(\nu_{ab})) - \nu_{ab} J_{ab}^2(\nu_{ab})). \quad (3.114)$$

Here, G_a , G_b , J_{aa} , J_{bb} and J_{ab} are defined as inverse functions of $x/T'_a(x)$, $x/T'_b(x)$, $V'_{aa}(x)/2x$, $V'_{bb}(x)/2x$ and $V'_{ab}(x)/2x$, respectively. Using the same arguments and methodology as for identical particles, an approximate spectrum of H is obtained by imposing extremisation conditions on spectrum of the auxiliary Hamiltonians with respect to auxiliary parameters,

$$\left. \frac{\partial}{\partial \mu_a} \tilde{\epsilon}_{\alpha_a, \alpha_b, n, \ell}(\gamma^{\text{aux}}) \right|_{\gamma^{\text{aux}} = \gamma_0^{\text{aux}}} = 0, \quad \left. \frac{\partial}{\partial \mu_b} \tilde{\epsilon}_{\alpha_a, \alpha_b, n, \ell}(\gamma^{\text{aux}}) \right|_{\gamma^{\text{aux}} = \gamma_0^{\text{aux}}} = 0, \quad (3.115a)$$

$$\left. \frac{\partial}{\partial \nu_{aa}} \tilde{\epsilon}_{\alpha_a, \alpha_b, n, \ell}(\gamma^{\text{aux}}) \right|_{\gamma^{\text{aux}} = \gamma_0^{\text{aux}}} = 0, \quad \left. \frac{\partial}{\partial \nu_{bb}} \tilde{\epsilon}_{\alpha_a, \alpha_b, n, \ell}(\gamma^{\text{aux}}) \right|_{\gamma^{\text{aux}} = \gamma_0^{\text{aux}}} = 0, \quad (3.115b)$$

$$\left. \frac{\partial}{\partial \nu_{ab}} \tilde{\epsilon}_{\alpha_a, \alpha_b, n, \ell}(\gamma^{\text{aux}}) \right|_{\gamma^{\text{aux}} = \gamma_0^{\text{aux}}} = 0, \quad (3.115c)$$

where

$$\tilde{\epsilon}_{\alpha_a, \alpha_b, n, \ell}(\gamma_{\text{aux}}) = \epsilon_{\alpha_a, \alpha_b, n, \ell}(\gamma_{\text{aux}}) + B(\gamma_{\text{aux}}). \quad (3.116)$$

The extremal auxiliary parameters γ_0^{aux} defines an extremal auxiliary Hamiltonian whose eigenenergy labelled by $\alpha_a, \alpha_b, n, \ell$ approximates an eigenenergy of the genuine Hamiltonian. As before, the extremisation conditions explicitly depend on the energy quantum numbers, leading to an approximation of the original Hamiltonian by a set of extremal auxiliary Hamiltonians.

3.2.2 Compact equations for $N_a + N_b$ particles

As in the case of identical particles, the five extremisation conditions, along with the energy formula, can be rewritten as a set of compact equations in which the functions G and J no longer appear, and the variables acquire a clear physical interpretation. Since the detailed derivation has already been presented for N identical particles, the final result is stated directly here. More details can be found in reference [97]. For systems of $N_a + N_b$ particles, the following seven compact equations hold

$$E = N_a T_a(p'_a) + N_b T_b(p'_b) + C_{N_a}^2 V_{aa}(\rho_{aa}) + C_{N_b}^2 V_{bb}(\rho_{bb}) + N_a N_b V_{ab}(\rho'_0), \quad (3.117a)$$

$$N_a T'_a(p'_a) \frac{p_a^2}{p'_a} = C_{N_a}^2 V'_{aa}(\rho_{aa}) \rho_{aa} + \frac{N_b}{N_a} C_{N_a}^2 V'_{ab}(\rho'_0) \frac{\rho_{aa}^2}{\rho_0^2}, \quad (3.117b)$$

$$N_b T'_b(p'_b) \frac{p_b^2}{p'_b} = C_{N_b}^2 V'_{bb}(\rho_{bb}) \rho_{bb} + \frac{N_a}{N_b} C_{N_b}^2 V'_{ab}(\rho'_0) \frac{\rho_{bb}^2}{\rho_0^2}, \quad (3.117c)$$

$$\frac{1}{N_a} T'_a(p'_a) \frac{P_0^2}{p'_a} + \frac{1}{N_b} T'_b(p'_b) \frac{P_0^2}{p'_b} = N_a N_b V'_{ab}(\rho'_0) \frac{R_0^2}{\rho_0^2}, \quad (3.117d)$$

$$Q(\alpha_a) = \sqrt{C_{N_a}^2 p_a \rho_{aa}}, \quad Q(\alpha_b) = \sqrt{C_{N_b}^2 p_b \rho_{bb}}, \quad Q(n, \ell) = P_0 R_0. \quad (3.117e)$$

where

$$p_a'^2 = p_a^2 + \frac{P_0^2}{N_a^2}, \quad p_b'^2 = p_b^2 + \frac{P_0^2}{N_b^2}, \quad \rho_0' = \frac{N_a - 1}{2N_a} \rho_{aa}^2 + \frac{N_b - 1}{2N_b} \rho_{bb}^2 + R_0^2. \quad (3.118)$$

The unknown variables are related to mean-values of observables,

$$p_a^2 = \langle \mathbf{p}_i^2 - \mathbf{P}_a^2 / N_a^2 \rangle, \quad p_b^2 = \langle \mathbf{p}_j^2 - \mathbf{P}_b^2 / N_b^2 \rangle, \quad P_0^2 = \langle \mathbf{p}^2 \rangle, \quad (3.119a)$$

$$\rho_{aa}^2 = \langle |\mathbf{r}_i - \mathbf{r}_{i'}|^2 \rangle, \quad \rho_{bb}^2 = \langle |\mathbf{r}_j - \mathbf{r}_{j'}|^2 \rangle, \quad R_0^2 = \langle \mathbf{r}^2 \rangle. \quad (3.119b)$$

Here, i, i' label any two particles of type a , and j, j' label any two particles of type b . The symmetry properties of the expected solution ensure that any choice of specific particle pairs

results in the same expectation value. Using definitions (3.118), one also obtain expectations values corresponding to the primed variables,

$$p_a'^2 = \langle \mathbf{p}_i^2 \rangle, \quad p_b'^2 = \langle \mathbf{p}_j^2 \rangle, \quad \rho_0'^2 = \langle |\mathbf{r}_i - \mathbf{r}_j|^2 \rangle. \quad (3.120)$$

These relations hold under the condition $\mathbf{P} = \mathbf{0}$. As verified in reference [97], the equations from Section 3.1.2 are recovered when all particles are considered identical. Regarding the variational properties, the situation is analogous to that described in Section 3.1.3. The two variational conditions from that Section are now replaced by five analogous conditions, which apply on the five arbitrary functions in the original Hamiltonian (3.112): T_a , T_b , V_{aa} , V_{bb} and V_{ab} .

The special case $N_b = 1$ is considered in the following and thus deserves explicit treatment. Under this assumption, based on their interpretation in terms of expectation values, the variables p_b and ρ_{bb} vanish, while variables P_0 and p_b' coincide. Consequently, the compact equations simplify to

$$E = N_a T_a(p_a') + T_b(P_0) + C_{N_a}^2 V_{aa}(\rho_{aa}) + N_a V_{ab}(\rho_0'), \quad (3.121a)$$

$$N_a T_a'(p_a') \frac{p_a'^2}{p_a'} = C_{N_a}^2 V_{aa}'(\rho_{aa}) \rho_{aa} + \frac{N_a - 1}{2} V_{ab}'(\rho_0') \frac{\rho_{aa}^2}{\rho_0'}, \quad (3.121b)$$

$$\frac{1}{N_a} T_a'(p_a') \frac{P_0^2}{p_a'} + T_b'(P_0) P_0 = N_a V_{ab}'(\rho_0') \frac{R_0^2}{\rho_0'}, \quad (3.121c)$$

$$Q(\alpha_a) = \sqrt{C_{N_a}^2 p_a \rho_{aa}}, \quad (3.121d)$$

$$Q(n, \ell) = P_0 R_0. \quad (3.121e)$$

where the definition of ρ_0' is slightly modified,

$$\rho_0' = \frac{N_a - 1}{2N_a} \rho_{aa}^2 + R_0^2. \quad (3.122)$$

The total motion is decomposed into an internal motion of the a -type particles, governed by equations (3.121b) and (3.121d), and a relative motion between the centre-of-mass of the a -particles and the single b -particle, described by equations (3.121c) and (3.121e). The interpretation of auxiliary parameters in terms of expectation values for $N_a + 1$ particles is given explicitly by

$$p_a^2 = \langle \mathbf{p}_i^2 - \mathbf{P}_a^2 / N_a^2 \rangle, \quad P_0^2 = \langle \mathbf{p}_b^2 \rangle = \langle \mathbf{P}_a^2 \rangle, \quad (3.123a)$$

$$\rho_{aa}^2 = \langle |\mathbf{r}_i - \mathbf{r}_{i'}|^2 \rangle, \quad R_0^2 = \langle |\mathbf{R}_a - \mathbf{r}_b|^2 \rangle. \quad (3.123b)$$

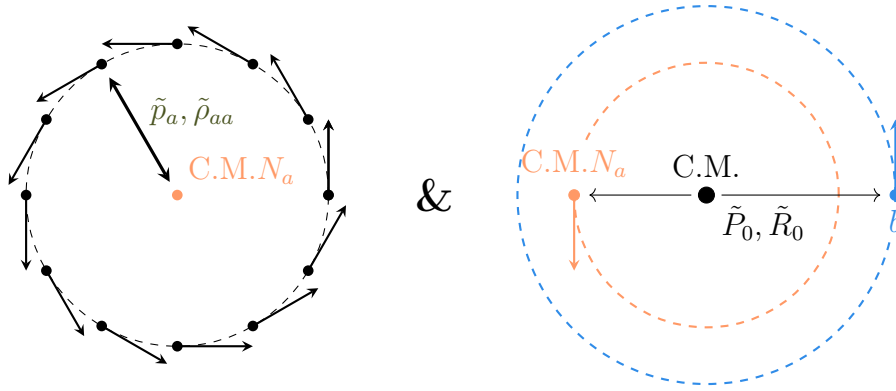


Figure 3.7: Illustration for the classical purely orbital motion used to develop a DOSM for systems of $N_a + 1$ particles. The abbreviations C.M. and C.M. N_a refer to the centre-of-mass associated with the entire system and the subsystem of particles a , respectively.

3.2.3 Improvement for $N_a + 1$ particles

The improvement procedure based on the DOSM can also be generalised for systems with different types of particles. However, as the complexity of the system increases, calculations, and especially Taylor developments, become progressively more involved. Therefore, the generalisation has only been developed explicitly for systems consisting of $N_a + 1$ particles. As with the compact equations, only the main calculations steps and final formulas are presented here. A complete description can be found in reference [65].

As a first step, a DOSM must be developed for systems of $N_a + 1$ particles. The construction follows the motion separation observed in equations (3.121). For purely orbital motions, equations (3.121b) and (3.121d) classically describe a system of N_a identical particles moving along a circular trajectory, uniformly distributed and possessing the same momentum. Additionally, equations (3.121c) and (3.121e) describe the classical relative circular motion of two different particles. One is assimilated to the centre-of-mass of the previous subsystem. This classical configuration is illustrated in Figure 3.7. It is important to note that this separation does not imply that both motions are uncorrelated: the interaction potential V_{ab} appears in both equations (3.121b) and (3.121c). As in Section 3.1.4, variables describing purely orbital motion are denoted with a tilde,

$$\tilde{E} = N_a T_a(\tilde{p}'_a) + T_b(\tilde{P}_0) + C_{N_a}^2 V_{aa}(\tilde{\rho}_{aa}) + N_a V_{ab}(\tilde{\rho}'_0), \quad (3.124a)$$

$$N_a T'_a(\tilde{p}'_a) \frac{\tilde{p}_a^2}{\tilde{p}'_a} = C_{N_a}^2 V'_{aa}(\tilde{\rho}_{aa}) \tilde{\rho}_{aa} + \frac{N_a - 1}{2} V'_{ab}(\tilde{\rho}'_0) \frac{\tilde{\rho}_{aa}^2}{\tilde{\rho}'_0}, \quad (3.124b)$$

$$\frac{1}{N_a} T'_a(\tilde{p}'_a) \frac{\tilde{P}_0^2}{\tilde{p}'_a} + T'_b(\tilde{P}_0) \tilde{P}_0 = N_a V'_{ab}(\tilde{\rho}'_0) \frac{\tilde{R}_0^2}{\tilde{\rho}'_0}, \quad (3.124c)$$

$$\sqrt{C_{N_a}^2 \tilde{p}_a \tilde{\rho}_{aa}} = \lambda_a(\ell_1, \dots, \ell_{N_a-1}) = \sum_{i=1}^{N_a-1} \ell_i + \frac{D-2}{2}, \quad (3.124d)$$

$$\tilde{P}_0 \tilde{R}_0 = \lambda_b(\ell) = \ell + \frac{D-2}{2}. \quad (3.124e)$$

Small radial excitations are then introduced for both motions. The perturbed variables p_a , ρ_{aa} , P_0 and R_0 are expressed in terms of increments p_r , $\Delta\rho_{aa}$, P_r and ΔR_0 in a manner analogous to that used for identical particles. After performing a series of Taylor expansions, the energy increment is obtained as

$$\Delta E \simeq \frac{1}{2\mu_a} \pi_r^2 + \frac{1}{2\mu_b} p_r^2 + \frac{k_a}{2} \Delta\rho^2 + \frac{k_b}{2} \Delta r^2 + \frac{k_c}{2} \Delta\rho \Delta r \quad (3.125)$$

where μ_a , μ_b , k_a , k_b and k_c are given in terms of the purely orbital variables,

$$\begin{aligned} \mu_a &= \frac{\tilde{p}'_a}{N_a T'_a(\tilde{p}'_a)}, \quad \mu_b = \left(\frac{T'_a(\tilde{p}'_a)}{N_a \tilde{p}'_a} + \frac{T'_b(\tilde{P}_0)}{\tilde{P}_0} \right)^{-1}, \\ k_a &= \frac{N_a T''_a(\tilde{p}'_a) \tilde{p}_a^4}{\tilde{\rho}_{aa}^2 \tilde{p}'_a{}^2} + \frac{N_a T'_a(\tilde{p}'_a) \tilde{p}_a^2}{\tilde{\rho}_{aa}^2} \left(\frac{3}{\tilde{p}'_a} - \frac{\tilde{p}_a^2}{\tilde{p}'_a{}^3} \right) + C_{N_a}^2 V''_{aa}(\tilde{\rho}_{aa}) \\ &\quad + \frac{(N_a - 1)^2 \tilde{\rho}_{aa}^2}{4 N_a \tilde{\rho}'_0{}^2} V''_{ab}(\tilde{\rho}'_0) + \frac{(N_a - 1)}{2} \left(\frac{1}{\tilde{\rho}'_0} - \frac{(N_a - 1) \tilde{\rho}_{aa}^2}{2 N_a \tilde{\rho}'_0{}^3} \right) V'_{ab}(\tilde{\rho}'_0), \\ k_b &= \frac{T''_a(\tilde{p}'_a) \tilde{P}_0^4}{N_a^3 \tilde{R}_0^2 \tilde{p}'_a{}^2} + \frac{T''_b(\tilde{P}_0) \tilde{P}_0^2}{\tilde{R}_0^2} + \frac{T'_a(\tilde{p}'_a) \tilde{P}_0^2}{N_a \tilde{R}_0^2} \left(\frac{3}{\tilde{p}'_a} - \frac{\tilde{P}_0^2}{N_a^2 \tilde{p}'_a{}^3} \right) \\ &\quad + \frac{2 T'_b(\tilde{P}_0) \tilde{P}_0}{\tilde{R}_0^2} + \frac{N_a \tilde{R}_0^2}{\tilde{\rho}'_0{}^2} V''_{ab}(\tilde{\rho}'_0) + N_a \left(\frac{1}{\tilde{\rho}'_0} - \frac{\tilde{R}_0^2}{\tilde{\rho}'_0{}^3} \right) V'_{ab}(\tilde{\rho}'_0), \\ k_c &= \frac{2 \tilde{p}_a^2 \tilde{P}_0^2}{N_a \tilde{p}'_a{}^2 \tilde{\rho}_{aa} \tilde{R}_0} \left(T''_a(\tilde{p}'_a) - \frac{T'_a(\tilde{p}'_a)}{\tilde{p}'_a} \right) + \frac{(N_a - 1) \tilde{\rho}_{aa} \tilde{R}_0}{\tilde{\rho}'_0{}^2} \left(V''_{ab}(\tilde{\rho}'_0) - \frac{V'_{ab}(\tilde{\rho}'_0)}{\tilde{\rho}'_0} \right). \end{aligned}$$

The expression (3.125) for ΔE is then interpreted as a quantum Hamiltonian to be solved. The spectrum of such a coupled harmonic oscillator can be found in reference [65, 98]. By following the procedure developed for identical particles, the associated quantum number are related to the n_i and ℓ_i quantum numbers through identification with the harmonic oscillator spectrum. Finally, the energy increment from the DOSM is given by

$$\Delta E = \sqrt{\frac{A}{C_{N_a}^2 \mu}} \sum_{i=1}^{N_a-1} \left(n_i + \frac{1}{2} \right) + \sqrt{\frac{B}{\mu}} \left(n + \frac{1}{2} \right) \quad (3.126)$$

where $\mu = \sqrt{\mu_a \mu_b}$ and

$$\begin{cases} A = \sqrt{\frac{\mu_b}{\mu_a}} k_a \\ B = \sqrt{\frac{\mu_a}{\mu_b}} k_b \end{cases} \quad \text{if } k_c = 0,$$

$$\begin{cases} A = \sqrt{\frac{\mu_b}{\mu_a}} k_a - \frac{k_c}{2} \\ B = \sqrt{\frac{\mu_a}{\mu_b}} k_b + \frac{k_c}{2} \end{cases} \quad \text{if } \epsilon = \frac{1}{k_c} \left(\sqrt{\frac{\mu_a}{\mu_b}} k_b - \sqrt{\frac{\mu_b}{\mu_a}} k_a \right) = 0,$$

$$\begin{cases} A = \sqrt{\frac{\mu_b}{\mu_a}} k_a - \frac{k_c}{2} \left(\frac{\epsilon}{|\epsilon|} \sqrt{1 + \epsilon^2} - \epsilon \right) \\ B = \sqrt{\frac{\mu_a}{\mu_b}} k_b + \frac{k_c}{2} \left(\frac{\epsilon}{|\epsilon|} \sqrt{1 + \epsilon^2} - \epsilon \right) \end{cases} \quad \text{if } \epsilon \neq 0.$$

The DOSM solution is now compared with the approximation given by the ET. A ϕ parameter is introduced in each global quantum number Q ,

$$Q(\alpha_a) = \phi_a \sum_{i=1}^{N_a} \left(n_i + \frac{1}{2} \right) + \lambda_a(\ell_1, \dots, \ell_{N_a}), \quad (3.127)$$

$$Q(n, \ell) = \phi_b \left(n + \frac{1}{2} \right) + \lambda_b(\ell), \quad (3.128)$$

and the ET equation are expanded near a purely orbital solution. The resulting expression for the energy increment due to the perturbation is

$$\Delta E = D_a \frac{\phi_a}{\lambda_a} \sum_{i=1}^{N_a} \left(n_i + \frac{1}{2} \right) + D_b \frac{\phi_b}{\lambda_b} \left(n + \frac{1}{2} \right). \quad (3.129)$$

where

$$D_a = T'_a(\tilde{p}'_a) \frac{N_a \tilde{p}'_a{}^2}{\tilde{p}'_a}, \quad D_b = T'_a(\tilde{p}'_a) \frac{\tilde{P}_0^2}{N_a \tilde{p}'_a} + T'_b(\tilde{P}_0) \tilde{P}_0.$$

Finally, ϕ_a and ϕ_b are chosen to match expressions (3.126) and (3.129),

$$\phi_a = \frac{\lambda_a}{D_a} \sqrt{\frac{A}{C_{N_a}^2 \mu}}, \quad \phi_b = \frac{\lambda_b}{D_b} \sqrt{\frac{B}{\mu}}. \quad (3.130)$$

Both the ET compact equations and the analytical expressions for ϕ_a and ϕ_b are significantly more intricate than those for N identical bodies. Except in very simple cases, deriving an analytical formula for the approximate spectrum proves impossible. However, to numerical

calculations remain feasible, with the computational cost being of the same order as for identical particles.

3.2.4 Tests of the ET for $N_a + 1$ particles

Finally, tests of the ET for systems of different particles are conducted. Since the case of identical particles has already been extensively discussed, only three tests are performed. Once again, in line with the scope of the present work, only three-particle systems, comprising two identical particles and a third distinct one, are considered. Given that $N_a = 2$, the internal motion within the subsystem of particles a is characterised by a single pair of quantum numbers, denoted n_a and ℓ_a in the following discussion. Furthermore, to emphasize the distinction, the quantum numbers that describe the relative motion with the particle b are denoted as n_b and ℓ_b . The three tests are drawn from reference [65].

Ultra-relativistic kinematics

To begin with, the ET and the improved ET are applied to ultra-relativistic massless particles interacting via harmonic potentials. Different interaction strengths are considered depending on the nature of the particle pair,

$$T_a(p) = T_b(p) = p, \quad V_{aa}(x) = x^2, \quad V_{ab}(x) = kx^2. \quad (3.131)$$

Arbitrary units are used. Calculations similar to those presented in Section 3.1.3 demonstrates that the ET provides upper bounds for such a system. For comparison, the eigenenergies of this three-body system are computed using the OBE. Additionally, reference [99] allows the eigenenergies to be inferred from those of a system of three non-relativistic particles interacting linearly. Based on results obtained by J.M. Richard using the method from [25], reference [65] derives very accurate eigenenergies for this Hamiltonian.

Two values of the interaction strength parameter are considered, $k = 0.1$ and $k = 10$. Energies for the ground state and two low-lying excited states with positive parity and zero total angular momentum are computed. Results for the ET, the improved ET, the OBE, and those from [65] are compared in Table 3.6 and Table 3.7. Approximations from the ET and the OBE are identified using the same methodology as for identical particles, while those from [65] and the OBE are matched based on the similarity of their energy values. For both tests, the ET provides energy eigenvalues with an accuracy of a few percent and, as expected, consistently yields upper bounds. With the improved version, the relative difference decreases to around

$(n_a, \ell_a, n_b, \ell_b)$	OBE	Ref. [65]	ET	$[\delta]$	IET	$[\delta]$
(0, 0, 0, 0)	5.288	5.288	5.597	[5.8%]	5.307	[0.4%]
(0, 0, 1, 0)	6.570	6.570	6.970	[6.1%]	6.571	[< 0.1%]
(0, 1, 0, 1)	7.513	7.515	7.868	[4.7%]	7.625	[1.5%]

Table 3.6: Low-lying eigenenergies for states with positive parity and zero total angular momentum for the system of three massless particles described in (3.131). The interaction strength is fixed at $k = 0.1$ (in arbitrary units). Results from the OBE, reference [65], the ET and the improved ET are compared. The relative differences from the OBE, denoted δ , are given in percent. The maximal number of quanta used for the OBE is $Q_{\max} = 16$ with a computed for $Q = 10$. The values for ϕ_a and ϕ_b provided by the improved ET were 1.76 and 1.79 for the three levels.

$(n_a, \ell_a, n_b, \ell_b)$	OBE	Ref. [65]	ET	$[\delta]$	IET	$[\delta]$
(0, 0, 0, 0)	14.505	14.506	15.353	[5.8%]	14.699	[1.3%]
(1, 0, 0, 0)	19.130	19.134	20.272	[6.0%]	19.291	[0.8%]
(0, 1, 0, 1)	20.335	20.340	21.580	[6.1%]	21.032	[3.4%]

Table 3.7: Low-lying eigenenergies for states with positive parity and zero total angular momentum for the system of three massless particles described in (3.131). The interaction strength is fixed at $k = 10$ (in arbitrary units). Results from the OBE, reference [65], the ET and the improved ET are compared. The relative differences from the OBE, denoted δ , are given in percent. The maximal number of quanta used for the OBE is $Q_{\max} = 16$ with a computed for $Q = 10$. The values of ϕ_a and ϕ_b given by the improved ET were 1.82 and 1.80 for the three levels.

1% or even lower. Notably, the first two states are symmetric under the exchange of the two identical particles, whereas the third state is antisymmetric.

Power potential

As a second test, systems of three non-relativistic particles interacting via power-law potentials are considered. The third particle being distinct from the first two is assigned a different mass,

$$T_a(p) = \frac{p^2}{2}, \quad T_b(p) = \frac{p^2}{2m}, \quad V_{aa}(x) = V_{ab}(x) = \frac{b}{|b|} \frac{x^b}{2}. \quad (3.132)$$

As before, arbitrary units are used. For this system, accurate energies for the ground state have already been obtained in Section 2.3.1 using the OBE. Two different masses were considered, $m = 0.2$ and $m = 5$. Results are now compared with those obtained using the ET and its improvement. For this system, the ET approximations exhibit varying variational properties depending on the value of b , following the same scheme as for identical particles. Energies are

$m = 0.2$						
b	OBE	ET	$[\delta]$	IET	$[\delta]$	(ϕ_a, ϕ_b)
-1.0	-0.1398	-0.0645	[53.8%]	-0.1316	[5.9%]	(1.07, 1.14)
0.1	1.9452	1.9804	[1.8%]	1.9489	[0.2%]	(1.55, 1.53)
1.0	4.9392	5.2278	[5.8%]	4.9687	[0.6%]	(1.79, 1.77)
2.0	7.5730	7.5730	[0%]	7.5730	[0%]	(2, 2)
3.0	9.7389	8.9925	[7.6%]	9.6703	[0.7%]	(2.16, 2.20)

Table 3.8: Ground-state eigenenergies for the system of three non-relativistic particles described in (3.132). The mass of the third particle is fixed at $m = 0.2$ (in arbitrary units). Results from the OBE, the ET, and the improved ET are compared. The relative differences from the OBE, denoted δ , are given in percent. The values of ϕ_a and ϕ_b are also provided. The maximal number of quanta used for the OBE is $Q_{\max} = 16$ with a computed for $Q = 10$.

$m = 5$						
b	OBE	ET	$[\delta]$	IET	$[\delta]$	(ϕ_a, ϕ_b)
-1.0	-0.3841	-0.1797	[53.2%]	-0.3029	[21.1%]	(1.05, 1.64)
0.1	1.8486	1.8820	[1.8%]	1.8568	[0.4%]	(1.48, 1.77)
1.0	3.4379	3.6386	[5.8%]	3.4753	[1.1%]	(1.74, 1.88)
2.0	4.3729	4.3729	[0%]	4.3729	[0%]	(2, 2)
3.0	5.0166	4.6320	[7.7%]	4.9693	[0.9%]	(2.20, 2.15)

Table 3.9: Ground-state eigenenergies for the system of three non-relativistic particles described in (3.132). The mass of the third particle is fixed at $m = 5$ (in arbitrary units). Results from the OBE, the ET, and the improved ET are compared. The relative differences from the OBE, denoted δ , are given in percent. The values for ϕ_a and ϕ_b are also provided. The maximal number of quanta used for the OBE is $Q_{\max} = 16$ with a computed for $Q = 10$.

compared in Table 3.8 ($m = 0.2$) and Table 3.9 ($m = 5$). For positive values of b , the accuracy of the ET and its improvement aligns with that observed in the previous test. However, for Coulomb interactions, its accuracy significantly decreases, likely due to the divergence of the interaction potential. In the case of $m = 0.2$, the improvement procedure restores reasonable accuracy. For $m = 5$, even this second calculation struggles to provide a truly accurate estimation.

Atomic systems

Finally, as anticipated in Section 3.1.7, atomic systems can also be investigated using the ET. In particular, the helium spectrum provides an interesting three-body systems to test the

accuracy of the ET. The helium Hamiltonian in atomic units⁴ is given by

$$H = \frac{\mathbf{p}_1^2}{2} + \frac{\mathbf{p}_2^2}{2} + \frac{\mathbf{p}_N^2}{2m} + \frac{1}{|\mathbf{r}_1 - \mathbf{r}_2|} - \frac{2}{|\mathbf{r}_N - \mathbf{r}_1|} - \frac{2}{|\mathbf{r}_N - \mathbf{r}_2|} \quad (3.133)$$

with $m = 4 \times 1836$, the mass of the helium nucleus. In this expression, \mathbf{p}_1 and \mathbf{r}_1 (and similarly \mathbf{p}_2 and \mathbf{r}_2) refer to the momentum and position of the first (second) electron, while \mathbf{p}_N and \mathbf{r}_N refer to the position and momentum of the nucleus.

Using the ET, an approximation for the ground-state energy of this system can be obtained. In this case, no variational interpretation can be ensured because the Hamiltonian (3.133) mixes attractive and repulsive interactions. For this system, the ET approximations can be directly compared to the experimental energy, namely 79 eV. While (3.133) is only an approximation of the true helium atom Hamiltonian (which, for instance, includes relativistic and spin-orbit corrections), the energy difference with this simpler version does not exceed a few percent. Therefore, the experimental result can be reliably used to assess the accuracy of the ET.

After implementation, the following approximate eigenenergies for the ET (E_{ET}) and its improvement (E_{iET}) are obtained,

$$E_{\text{ET}} = 33 \text{ eV}, \quad E_{\text{iET}} = 47 \text{ eV} \quad (\text{with } \phi_a = 1.21 \text{ and } \phi_b = 1.78). \quad (3.134)$$

Both approximations show particularly low accuracy. As before, the failure of the ET can be attributed to the presence of divergent interactions in the potential. The poor performance of the improvement procedure can be explained by the lack of variational character, as discussed in Section 3.1.7. Under this context, improving the ET using the DOSM proved notably less reliable, even for identical particles [55]. Another hypothesis, which has not yet been fully tested, is the mass asymmetry within the system. This may affect the efficiency of the improvement procedure, as already noted in Table 3.9.

3.3 Conclusion: why the ET?

The ET has proven to be a versatile, easily implementable, and reliable approximation method. It can handle systems consisting of N identical particles with generic kinematics, as well as one-body, two-body, and even a given type of K -body interactions. Additionally, it has been generalised to handle systems containing different types of particles with arbitrary kinematics and two-body interactions. For certain systems, the approximation obtained through

⁴ Energies in atomic units can be converted to eV by a factor of $\alpha^2 m_e = 27.21 \text{ eV}$.

the ET carries a variational interpretation. When higher precision is needed, an improvement procedure can be applied. A parameter is introduced into the ET quantum number and is determined by comparing the spectrum with the DOSM approximation. This procedure does not significantly increase the complexity of the original method. For systems with different types of particles, the improved ET has been developed specifically for systems with $N_a + 1$ particles.

Although predicting the performance of the ET remains challenging, various tests conducted on different systems have provided valuable insights. Notably, the presence of highly divergent potentials can reduce the accuracy of the ET. Furthermore, the improvement procedure may lose efficiency when contributions with opposing variational properties are mixed.

While the ET may not provide the highest accuracy, it stands out due to its generality and simplicity. In practice, its use requires solving only a set of three equations. For systems that are not overly complex, this resolution can often be carried out analytically, making it easy to vary system parameters or the number of particles. These advantages enable the ET to be applied in a wide range of contexts. It can certainly be used to validate the implementation of more precise numerical calculations [77], but it can also complement these numerical methods by providing easily obtainable approximations, as demonstrated in Section 3.1.6. Additionally, the method has been used to establish a quantum version of the quasi Kepler's third law [75, 76]. More recently, it has been used to determine upper-bounds for critical coupling constants [94]. The method aligns well with large- N approaches in quantum chromodynamics, where limits for large numbers of particles in bound states are of interest [70, 71, 72, 73, 74]. Lastly, the method was applied in a more classical manner to study hybrid mesons [69], and proposed for hybrid baryons in [56].

Complement 3.A The N identical body harmonic oscillator

This complement is devoted to the determination of the energy spectrum of the N identical body harmonic oscillator,

$$H_{\text{oh}} = \sum_{i=1}^N \frac{\mathbf{p}_i^2}{2\mu} - \frac{\mathbf{P}^2}{2N\mu} + \nu \sum_{i<j}^N |\mathbf{r}_i - \mathbf{r}_j|^2. \quad (3.135)$$

First, the centre-of-mass motion of the system can be removed by generalising the three-body Jacobi coordinates (2.100) for N identical bodies,

$$\mathbf{x}_i = \sum_{j=1}^i \frac{\mathbf{r}_j}{i} - \mathbf{r}_{i+1} \quad \text{for } i \in \{1, \dots, N-1\}, \quad \mathbf{x}_N = \sum_{j=1}^N \frac{\mathbf{r}_j}{N}. \quad (3.136)$$

Length dimensions have been kept. One recognises \mathbf{x}_N as the centre-of-mass position. Definition (3.136) can be rewritten into a matrix form,

$$\mathbf{x}_i = \sum_{j=1}^N U_{ij} \mathbf{r}_j \quad \text{with} \quad U = \begin{pmatrix} 1 & -1 & 0 & \cdots & 0 \\ 1/2 & 1/2 & -1 & \cdots & 0 \\ 1/3 & 1/3 & 1/3 & \cdots & 0 \\ \vdots & \vdots & \vdots & \ddots & \vdots \\ 1/N & 1/N & 1/N & \cdots & 1/N \end{pmatrix}. \quad (3.137)$$

With this formulation, obtaining the inverse transformation is a simple matter of matrix inversion. One can also show that momenta conjugated to \mathbf{x}_i , denoted $\boldsymbol{\pi}_i$ are obtained with the inverse transformation,

$$\boldsymbol{\pi}_i = \sum_{j=1}^N B_{ji} \mathbf{p}_j \quad \text{with} \quad B = U^{-1} = \begin{pmatrix} 1/2 & 1/3 & 1/4 & \cdots & 1/N & 1 \\ -1/2 & 1/3 & -1 & \cdots & 1/N & 1 \\ 0 & -2/3 & 1/3 & \cdots & 1/N & 1 \\ \vdots & \vdots & \vdots & \ddots & \vdots & \vdots \\ 0 & 0 & 0 & \cdots & (1-N)/N & 1 \end{pmatrix}. \quad (3.138)$$

Properties of the U and B matrix can be used to demonstrate the following two relations

$$\sum_{i=1}^N \mathbf{p}_i^2 - \frac{\mathbf{P}^2}{N} = \sum_{j=1}^{N-1} \frac{j+1}{j} \boldsymbol{\pi}_j^2 \quad \sum_{i < j} |\mathbf{r}_i - \mathbf{r}_j|^2 = \sum_{j=1}^{N-1} \frac{Nj}{j+1} \mathbf{x}_j^2. \quad (3.139)$$

Thanks to these intermediary results, the harmonic oscillator Hamiltonian can be rewritten in Jacobi coordinates,

$$H_{\text{oh}} = \sum_{i=1}^{N-1} h_i(\boldsymbol{\pi}_i, \mathbf{x}_i) \quad \text{with} \quad h_i(\boldsymbol{\pi}_i, \mathbf{x}_i) = \frac{(i+1)}{2i\mu} \boldsymbol{\pi}_i^2 + \frac{Ni\nu}{i+1} \mathbf{x}_i^2. \quad (3.140)$$

The full Hamiltonian is now separated as a sum of $N - 1$ one-body harmonic oscillator Hamiltonians h_i whose spectrum is well-documented,

$$h_i |\psi_{n_i \ell_i m_i}(\mathbf{x}_i)\rangle = \epsilon_{n_i \ell_i} |\varphi_{n_i \ell_i m_i}(\mathbf{x}_i)\rangle \quad \text{with} \quad \epsilon_{n_i \ell_i} = \sqrt{\frac{2N\nu}{\mu}} (2n_i + \ell_i + D/2) \quad (3.141)$$

Above, n_i and ℓ_i are positive integers, zero included. The $|\varphi_{n_i \ell_i m_i}(\mathbf{x}_i)\rangle$ states and the associated spectrum have already been depicted in Section 2.1.1 for unit masses, unit interaction constant and in three dimensions. With the separation of variables technique, the spectrum of the full N -body Hamiltonian is expressed as a sum of the one-body eigenenergies,

$$\epsilon(\mu, \nu) = \sqrt{\frac{2N\nu}{\mu}} \sum_{i=1}^{N-1} (2n_i + \ell_i + D/2), \quad (3.142)$$

and the total eigenstates are products of the individual eigenstates,

$$|\psi_{n_1 \ell_1 m_1 \dots n_{N-1} \ell_{N-1} m_{N-1}}(\mathbf{x}_1, \dots, \mathbf{x}_{N-1})\rangle = |\psi_{n_1 \ell_1 m_1}(\mathbf{x}_1)\rangle \otimes \dots \otimes |\psi_{n_{N-1} \ell_{N-1} m_{N-1}}(\mathbf{x}_{N-1})\rangle. \quad (3.143)$$

The quantum numbers n_i and ℓ_i indicates respectively the radial and orbital excitation associated with the i^{th} Jacobi coordinate. The total eigenstates $|\psi_{n_1 \ell_1 \dots n_{N-1} \ell_{N-1}}\rangle$ have a good parity $P = (-1)^{\ell_1 + \ell_2}$ but do not exhibit any symmetry under exchange of particles nor good angular momentum. These properties can be provided by combining different eigenstates with the same energy eigenvalue $\epsilon(\mu, \nu)$. Notice that this symmetry has to be implemented at the level of individual positions and not on Jacobi coordinates.

Complement 3.B The fermionic ground state with the ET

As mentioned in Section 3.1.7, using the ET, the bosonic ground state can easily be obtained by simply setting all the n_i and ℓ_i quantum numbers to zero. The corresponding harmonic oscillator eigenstate is naturally symmetric under any exchange of particles. Determining the fermionic ground state energy is, however, more involved. One must identify the lowest value of $Q(\alpha)$ that allows for the construction of an antisymmetric harmonic oscillator eigenstate. This challenge can be addressed using Pauli's exclusion principle, which states that, for Hamiltonians separable in individual coordinates, two fermions cannot have identical quantum numbers. However, in Complement 3.A, the independent oscillators are written in Jacobi coordinates, which precludes a straightforward application of this principle.

This obstacle is overcome by reference [100], where the N -body Harmonic oscillator is solved

by maintaining individual coordinates. The two-body harmonic interactions are transformed into one-body harmonic interactions in an exact manner, making the Hamiltonian separable. The resulting spectrum is consistent with the one obtained in Complement 3.A,

$$E = \sqrt{\frac{2N\nu}{\mu}} \left(\sum_{k=1}^N (2\nu_k + \lambda_k) - (2\mathcal{N} + \mathcal{L}) + (N-1)\frac{D}{2} \right). \quad (3.144)$$

Above, ν_k and λ_k are radial and orbital quantum numbers associated with individual positions, while \mathcal{N} and \mathcal{L} are quantum numbers related to the centre-of-mass motion. Magnetic quantum numbers μ_k and \mathcal{M} are also present but do not affect the spectrum. The centre-of-mass quantum numbers are constrained by the individual ones and, for a fermionic ground state, ultimately cancel out [101, p.3-4]. Since the quantum numbers are now directly tied to individual coordinates, Pauli's exclusion principle can be applied and the fermionic ground state energy is obtained by minimising equation (3.144) with each particle having distinct quantum number triplets $(\nu_k, \lambda_k, \mu_k)$. Analytical formulas for this fermionic ground state are provided in Reference [65], where the discussion is also expanded to include the improved ET.

This chapter in the context of a thesis

This chapter covers a topic that has been a primary matter for my master thesis, but a secondary topic in my PhD. At the end of my master, in the continuity of the generalisation of the ET initiated by L. Cimino [68, 97], I worked on extending the improvement of the ET for systems of N identical particles plus a different one [65]. In the future, this method is intended to be used in a study of hybrid baryons in the large- N formalism of quantum chromodynamics.

During my PhD, as mentioned at the end of the previous chapter, my contribution to the ET formalism was mainly to provide accurate results with the OBE in order to assess the ET accuracy [54, 55]. Most results of these studies have been introduced in Section 3.1.7. These tests enabled L. Cimino and me to identify the two typical behaviours mentioned in the main text.

Part II

Constituent Approaches of QCD and the Baryon Spectrum

Chapter 4

Hadronic Physics: From Discovery to Quantum Chromodynamics

This chapter introduces a special topic in which the technology presented in Part I provides significant support. Specifically, the chapter focuses on the study of a particular class of particles that have been observed from the early 20th century to the present day: the *hadrons*. Following a brief and non-exhaustive historical overview in Section 4.1, the classification of hadrons and the quark hypothesis are discussed in Section 4.2, following the framework established by M. Gell-Mann. The Section continues with an overview of the modern fundamental theory of the strong interaction, namely quantum chromodynamics, and concludes with a brief introduction to a current research topic: the exotic hadrons.

4.1 A short historical review of early hadron detections

Disclaimer: the following section is intended to provide a general overview of the emergence of hadron physics. The proposed summary does not claim to be exhaustive nor to present an entirely precise account of historical developments. Throughout the text, several pioneering works are cited for illustrative purposes, however this selection is likewise not comprehensive. For more in-depth analyses of hadron physics and its historical context, the reader is referred to references [102, 103].

This story of hadron physics begins in 1897 with the famous experimental discovery of the *electron* by J.J. Thomson [104]. Still considered as an elementary particle today, the electron marked the beginning of a new domain in physics: the study of elementary particles. With this discovery, the first constituent of matter was identified. Since atoms are electrically

neutral, the identification of the negatively charged electron suggested the existence of a positively charged counterpart. Thomson proposed that electrons were embedded in a positively charged medium, an idea known as the plum-pudding model [104]. Although now recognised as incorrect, Thomson's model was the first indication of positively charged components within atoms, later identified as *protons*.

Thomson's model was radically revised just a few years later, in 1911, by one of his students, E. Rutherford [105]. By bombarding a thin sheet of gold with alpha particles¹, Rutherford observed that the projectiles were occasionally deflected at large angles. To explain this experimental observation, he proposed that Thomson's diffuse positive charge was actually concentrated in a small central region, what came to be known as the atom nucleus². Rutherford calculated the expected cross-section for classical Coulomb scattering and successfully reproduced his experimental results. Remarkably, all observed nuclear masses appeared (approximately) as integer multiples of the lightest nucleus, that of hydrogen. In 1919, Rutherford identified this lightest nucleus as a fundamental building block of all other nuclei, and named it the *proton* [106]. The existence of multiple positively charged particles confined in a small space implied the existence of an attractive force strong enough to overcome electromagnetic repulsion. This was the first evidence of a new fundamental force, initially acting only between the components of the nucleus, known as the *strong interaction*. Particles subject to this force were eventually grouped (in 1962) under the name *hadrons*, in reference to their comparatively large mass (from the Ancient Greek ἄδρός, meaning "stout") [107].

Time went on, and, alongside experiments, theoretical physicists worked on explaining the dynamics that govern the behaviour of these new particles. In particular, they focused on understanding how atoms are structured and how they interact with the electromagnetic field. These theoretical efforts led to the development of quantum theory, whose modern formalism is outlined in Section 1.1. To name a few essential contributors, let us mention, in alphabetic order, N. Bohr, M. Born, L. de Broglie, P. Dirac, A. Einstein, W. Heisenberg, W. Pauli, M. Planck and E. Schrödinger. This list is far from exhaustive, and many other contributors also deserve recognition.

Another piece of the puzzle was revealed in 1932 by J. Chadwick, who discovered that atomic nuclei are also composed of neutral particles with a mass roughly equivalent to that of the proton [108]. The associated particle was called the *neutron* [106, 108] and became the second hadron to be experimentally detected. At the time, proton and neutrons were thought to be fundamental particles that, through their strong interactions, bound together to form nuclei.

¹ Previously identified by Rutherford as helium atoms stripped of their electrons.

² This hypothesis had previously been proposed by H. Nagaoka, but received little attention.

Electrons were then attracted to this nuclear structure by electromagnetic interactions, forming atoms on a larger scale. In addition to this trio, other particles, lighter than hadrons and insensitive to the strong interaction, were also postulated and observed.

- Electromagnetic radiations are carried by a fourth elementary particle, earlier postulated by M. Planck (in 1901) [109] and A. Einstein (in 1905) [110]. This particle was later named the *photon* in 1926 [106].
- Dirac's equations predicted the existence of a particle similar to the electron, but with a positive electric charge [111]. This particle was later observed by C.D. Anderson and named the *positron* [112]. The discovery of the positron introduced the concept of antiparticles: for every particle, there exists a corresponding antiparticle with the same mass but opposite charge.
- To explain the disintegration of certain nuclei, W. Pauli also introduced a light particle unaffected by both the strong and the electromagnetic interactions in 1930. This elusive particle, named the *neutrino* by E. Fermi³, would remain undetected until 1956 [113, 114].

The story of hadron physics takes a new turn in 1935 when H. Yukawa proposed a model in which the strong interaction between protons and neutrons is mediated by the exchange of massive particles [115]. These particles were predicted to have a mass intermediate between that of protons and electrons, which would explain the short range of the interaction. For this reason, they were named mesons (from the Greek μέσον, meaning "intermediate"). In 1937, the search for mesons encountered a false hope with the experimental discovery of a particle in the expected mass range [116]. However, this candidate soon turned out to resemble the electron more than Yukawa's meson. It was named the *muon* and, along with electrons, positrons and neutrinos, formed their own family of particles: the leptons (from the Greek λεπτός meaning "light").

The search for meson continued until 1947, when C. Powell observed two new charged particles with masses consistent with Yukawa's prediction [117]. These particles were named pions (as they were labelled with the Greek letter π), and their correspondence with Yukawa's hypothesis was soon validated. In 1950, the duo was joined by a third particle, neutral in charge and denoted π^0 [118]. Meanwhile, other hadrons, also subject to the strong interaction but lighter than protons and neutrons, were observed. Named kaons, they were included in the growing family of mesons. Notably, these latter particles exhibited unusually long lifetimes. This led

³ Fermi's model also introduced a second particle, called the anti-neutrino. Just as the positron is the antiparticle of the electron, the anti-neutrino is the antiparticle of the neutrino.

experimentalists to introduce a conserved quantity [119, 120] called *strangeness*, which will take a deeper significance in the next section.

In 1950, it was the proton and neutron family that expanded with the discovery of a third heavy particle, also sensitive to the strong interaction [121]. This new member was labelled with the Greek letter Λ and joined the protons and neutrons in a group named *baryons* (from the Greek βαρύς meaning "heavy") [120]. At this stage, the current classification is established: particles subject to the strong interactions are referred to as hadrons and are divided into two families. The baryons comprise the heavier particles, while the mesons encompass the comparatively lighter ones.

Things began to grow more complex from 1960 onward. At this point, physicists started discovering an increasing number of particles with hadron properties. This posed two main challenges to theorists. First, with a hundred of new hadrons being observed, there was a need to impose some order by classifying them into more restrictive families. Second, it became increasingly difficult to regard all these observed states as fundamental. Could such a variety be explained from a more ontologically parsimonious point of view? These questions were addressed between 1961 and 1964 by M. Gell-Mann through its hadron classification scheme and the formulation of the quark hypothesis. These concepts are discussed in the next section.

4.2 Hadron classification and the quark hypothesis

In much of the existing literature, for example in [18, 122, 123], the classification and structure of hadrons are presented with the quark hypothesis assumed from the outset. In contrast, the present section adopts a different perspective: it first aims to infer the existence of quarks based on the experimental hadron spectrum, and only then employs the quark hypothesis to explain hadronic properties. In a sense, this approach mirrors the one originally taken by M. Gell-Mann in the early 1960s [124, 125, 126, 127].

4.2.1 Hadron classification

To begin with, the question of classifying the seemingly disordered hadron zoology is investigated. Among the observed hadrons, and particularly the lightest ones, certain particles appear to share the same spin and parity, as well as very similar masses, despite differing electric charge.

For baryons, this is exemplified by the proton and neutron, or by the three sigma baryons [128],

$$m_{p^+} = 938 \text{ MeV}, \quad m_{n^0} = 939 \text{ MeV}; \quad (4.1)$$

$$m_{\Sigma^+} = 1189 \text{ MeV}, \quad m_{\Sigma^0} = 1193 \text{ MeV}, \quad m_{\Sigma^-} = 1197 \text{ MeV}. \quad (4.2)$$

For mesons, a similar pattern is seen in the three pions, the two kaons and the two anti-kaons [128],

$$m_{\pi^+} = 140 \text{ MeV}, \quad m_{\pi^0} = 135 \text{ MeV}, \quad m_{\pi^-} = 140 \text{ MeV}; \quad (4.3)$$

$$m_{K^+} = 494 \text{ MeV}, \quad m_{K^0} = 498 \text{ MeV}, \quad m_{\bar{K}^0} = 498 \text{ MeV}, \quad m_{K^-} = 494 \text{ MeV}. \quad (4.4)$$

In some cases, the width of the resonance⁴ makes it difficult to assign a sufficiently precise mass to distinguish between the different particles. This is the case, for example, with the four delta resonances, whose mass is measured at $(1232 \pm 2) \text{ MeV}$ [128].

This observation is reminiscent of the energy spectrum of the hydrogen atom. Due to the two possible projections of the electron spin, the hydrogen energy levels are nearly degenerated in pairs. Theoretically, this occurs because the dominant contribution to the Hamiltonian is invariant under transformations of the electron's spin state, while subleading corrections break this symmetry and lead to a splitting of these energy levels. By analogy, nearly degenerate hadrons can be viewed as different manifestations of a single quantum particle. For example, the proton and neutron are seen as two states of a single particle, the nucleon, distinguished by a new intrinsic degree of freedom. The formalism is directly copied from that of spin: a new intrinsic property, called *isospin*, is introduced, along with two associated operators, the isospin Casimir and the isospin projection operator. The eigenvalue of the Casimir operator, denoted I , determines the irreducible representation of $SU(2)$ that the state belongs to when it undergoes an isospin transformation. The eigenvalue of the isospin projection operator, denoted I_3 , distinguishes between the nearly degenerate states within that representation (the dimension of the corresponding invariant space is $2I + 1$). For instance, the nucleon forms an isospin doublet with $I = 1/2$, where the two isospin projections $I_3 = 1/2$ and $I_3 = -1/2$ correspond to the proton and the neutron, respectively. Tables 4.1 and 4.2 list selected baryons and mesons organised in different isospin multiplets, with their associated spin-parity J^P , mass, isospin I and isospin projection I_3 . Of course, from a dynamical perspective, isospin symmetry is only approximate, since states with different I_3 values generally differ in electric charge and

⁴ Experimentally, unstable particles are observed as "bump" structures in scattering cross-sections, referred to as resonances. These are typically characterised by a mean value, interpreted as the particle's mass, and a width, which is related to its life-time.

Multiplet	I	J^P	Mass	Label of the projections		
Nucleons	$\frac{1}{2}$	$\frac{1}{2}^+$	~ 940	$p^+ (I_3 = \frac{1}{2})$	$n^0 (I_3 = -\frac{1}{2})$	
Sigma	1	$\frac{1}{2}^+$	~ 1190	$\Sigma^+ (I_3 = 1)$	$\Sigma^0 (I_3 = 0)$	$\Sigma^- (I_3 = -1)$
Xi	$\frac{1}{2}$	$\frac{1}{2}^+$	~ 1310	$\Xi^0 (I_3 = \frac{1}{2})$	$\Xi^- (I_3 = -\frac{1}{2})$	
Lambda	0	$\frac{1}{2}^+$	~ 1115	$\Lambda^0 (I_3 = 0)$		
Delta	$\frac{3}{2}$	$\frac{3}{2}^+$	~ 1230	$\Delta^{++} (I_3 = \frac{3}{2})$	$\Delta^+ (I_3 = \frac{1}{2})$	$\Delta^0 (I_3 = -\frac{1}{2})$ $\Delta^- (I_3 = -\frac{3}{2})$
Sigma star	1	$\frac{3}{2}^+$	~ 1385	$\Sigma^{*+} (I_3 = 1)$	$\Sigma^{*0} (I_3 = 0)$	$\Sigma^{*-} (I_3 = -1)$
Xi star	$\frac{1}{2}$	$\frac{3}{2}^+$	~ 1530	$\Xi^{*0} (I_3 = \frac{1}{2})$	$\Xi^{*-} (I_3 = -\frac{1}{2})$	
Omega	0	$\frac{3}{2}^+$	~ 1670	$\Omega^- (I_3 = 0)$		

Table 4.1: Low-lying baryons grouped by isospin quantum numbers. The masses indicated are given in MeV, accurate to within a few MeV, with detailed isospin splittings omitted. Data are taken from reference [128].

do not have exactly the same energy. At the very least, this suggests that the electromagnetic interaction breaks isospin symmetry.

A close examination of Table 4.1 reveals that different isospin multiplets continue to share the same J^P quantum numbers. This observation motivates the extension of the hadron classification into larger families. In addition to their spin-parity, these multiplets also lie approximately in the same energy range, although the correspondence is more qualitative compared to that seen with isospin. This suggests the presence of a second, more approximate, symmetry underlying the hadron spectrum. This symmetry is known as the flavour symmetry, and the associated group is $SU(3)$. A detailed overview of this group, its properties and its applications in hadronic physics can be found in reference [123]. For the purposes of the present discussion, it suffices to recall the characteristics of the low-dimensional irreducible representations of $SU(3)$. They are summarised in Figure 4.1.

One can begin identifying the $SU(3)$ multiplets in the baryon and meson spectra by comparing the dimensionalities of the group representations with the number of available states. Furthermore, since flavour symmetry extends isospin symmetry, isospin multiplets should also be consistently embedded within the representation of $SU(3)$ (see horizontal lines in Figure 4.1). Based on this approach, the following structure of the spectra is suggested.

- The eight baryons with spin-parity $1/2^+$ correspond to an $SU(3)$ octet. As expected, they form an isospin singlet, two doublets and a triplet.
- The ten baryons with spin-parity $3/2^+$ correspond to an $SU(3)$ decuplet. As expected, they include an isospin singlet, a doublet, a triplet and a quadruplet.

Multiplet	I	J^P	Mass	Label of the projections		
Kaons	$\frac{1}{2}$	0^-	~ 495	$K^+ (I_3 = \frac{1}{2})$	$K^0 (I_3 = -\frac{1}{2})$	
Pions	1	0^-	~ 135	$\pi^+ (I_3 = 1)$	$\pi^0 (I_3 = 0)$	$\pi^- (I_3 = -1)$
Anti-Kaons	$\frac{1}{2}$	0^-	~ 495	$\bar{K}^0 (I_3 = \frac{1}{2})$	$K^- (I_3 = -\frac{1}{2})$	
Eta	0	0^-	~ 550	$\eta^0 (I_3 = 0)$		
Eta prime	0	0^-	~ 960	$\eta'^0 (I_3 = 0)$		

Kaons star	$\frac{1}{2}$	1^-	~ 890	$K^{*+} (I_3 = \frac{1}{2})$	$K^{*0} (I_3 = -\frac{1}{2})$	
Rho	1	1^-	~ 770	$\rho^+ (I_3 = 1)$	$\rho^0 (I_3 = 0)$	$\rho^- (I_3 = -1)$
Anti-Kaons star	$\frac{1}{2}$	1^-	~ 890	$\bar{K}^{*0} (I_3 = \frac{1}{2})$	$K^{*-} (I_3 = -\frac{1}{2})$	
Omega	0	1^-	~ 780	$\omega^0 (I_3 = 0)$		
Phi	0	1^-	~ 1020	$\phi^0 (I_3 = 0)$		

Table 4.2: Low-lying mesons grouped by isospin quantum numbers. The masses indicated are given in MeV, accurate to within a few MeV, with detailed isospin splittings omitted. Data are taken from reference [128].

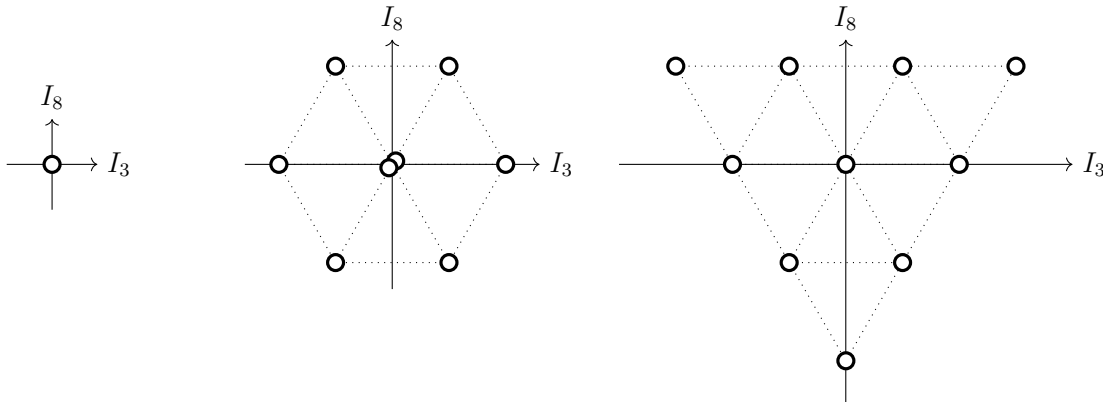


Figure 4.1: Schematic illustration of the singlet, octet and decuplet irreducible representations of $SU(3)$ (from left to right). Each white circle represents a state supporting the corresponding irreducible representation. The horizontal and vertical axes correspond to the eigenvalues of the third and eighth generators of $SU(3)$, respectively. Notably, the coordinate $(0,0)$ in the octet diagram is occupied by two distinct states, demonstrating that specifying I_3 and I_8 does not uniquely identify a state within the representation. It is also worth mentioning that horizontally aligned states form $SU(2)$ multiplets. The guiding idea behind hadron classification is to associate each experimentally observed hadron with the above group theory states.

- The nine mesons with spin-parity 0^- must be split into an $SU(3)$ octet and a separate singlet. As expected, the octet consists of one isospin singlet, two doublets and one triplet, while the $SU(3)$ singlet consist of a single isospin singlet. The identification of whether the η or the η' belongs to the octet is discussed in the next paragraph.
- The nine mesons with spin-parity 1^- are arranged analogously to those with 0^- . The identification of the ω and ϕ states is also addressed below.

The question of whether η or η' should be grouped with the $SU(3)$ octet is a subtle one. On one hand, these two particles share several properties: they have the same spin-parity, electric charge, total isospin, and isospin projection. On the other hand, flavour symmetry, which predicts two distinct states belonging to different $SU(3)$ multiplet, is only approximate, as evidenced, for instance, by differences in hadron masses. As a result, the physical η and η' states belong neither purely to the singlet nor to the octet. Instead, each is a mixture of the pure singlet and octet states with $I_3 = I_8 = 0$. Denoting these basis states as $|\eta_1\rangle$ and $|\eta_8\rangle$, the physical states $|\eta\rangle$ and $|\eta'\rangle$ can be parametrised as follows,

$$|\eta\rangle = \cos\theta |\eta_1\rangle + \sin\theta |\eta_8\rangle, \quad |\eta'\rangle = -\sin\theta |\eta_1\rangle + \cos\theta |\eta_8\rangle, \quad (4.5)$$

with $\theta \in [-\pi/2, \pi/2]$. A similar discussion applies to the ω and ϕ particles,

$$|\omega\rangle = \cos\bar{\theta} |\psi_1\rangle + \sin\bar{\theta} |\psi_8\rangle, \quad |\phi\rangle = -\sin\bar{\theta} |\psi_1\rangle + \cos\bar{\theta} |\psi_8\rangle. \quad (4.6)$$

Determining the values of θ and $\bar{\theta}$ requires further consideration and will not be discussed here [18, 123]. For reference, θ is observed to be in between -10° and -20° [122, 123], while $\bar{\theta}$ is around 35.4° [122].

Continuing the analysis of the hadron classification introduced above, particles within a given $SU(3)$ multiplet but belonging to different isospin multiplets are systematically distinguished by their strangeness⁵. More precisely, the strangeness S is found to be proportional to the eigenvalue of the eighth $SU(3)$ generator, I_8 , via the relation [122]

$$\frac{2}{\sqrt{3}}I_8 = B + S. \quad (4.7)$$

where $B = 1$ for baryons, $B = 0$ for mesons and $B = -1$ for anti-baryons (the latter are not discussed in this section). The sum $B + S$ is commonly referred to as the hypercharge, denoted

⁵ Strangeness is a conserved quantum number introduced to account for experimental observations. It was briefly introduced in Section 4.1.

by Y . It is empirically related to the electric charge Q (in unit of the elementary charge) through

$$Q = I_3 + \frac{Y}{2}. \quad (4.8)$$

The correspondence between the hadron spectrum and the $SU(3)$ multiplets is often illustrated using the diagrams in Figure 4.2, which synthesize the content of Tables 4.1-4.2 and Figure 4.1. At this stage, the classification of hadrons remains largely descriptive, highlighting the symmetries observed in experimental data. However, several important questions remain unanswered: Where do these multiplets originate? Why are baryons structured into octets and decuplets? Why are mesons arranged in singlets and octets? Why are the fundamental and sextet representations of $SU(3)$ seemingly absent from the spectrum? What is the origin of relation (4.8)? And why do mesons always have integer spin, while baryons have half-integer spin? All of these questions are addressed by Gell-Mann's quark hypothesis.

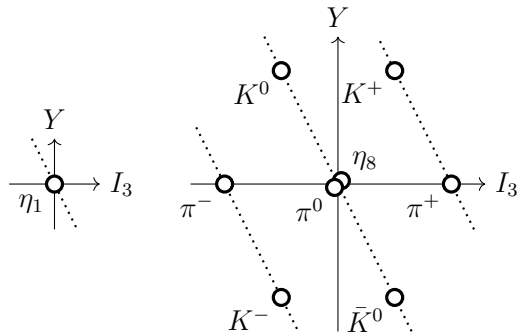
4.2.2 The quark hypothesis

To address the questions posed by the classification of hadrons, Gell-Mann proposed a bold hypothesis: hadrons are composed of more fundamental constituents. The total state $|q\rangle$ of its new particle, termed a quark, is assumed to include an additional contribution, denoted $|\mathcal{F}\rangle$ and referred to as the flavour component, in addition to its spatial and spin parts,

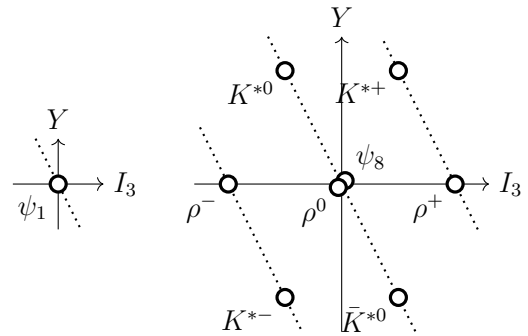
$$|q\rangle = |\psi(\mathbf{r})\rangle \otimes |sm_s\rangle \otimes |\mathcal{F}\rangle. \quad (4.9)$$

This flavour component is postulated to belong to a three-dimensional complex vector space that transforms under $SU(3)$ according to the fundamental representation of the group. A basis for this vector space is provided by group theory as the set of common eigenstates of I_3 and I_8 . These states are referred to as *up* (u), *down* (d) and *strange* (s) and are represented in the left part of Figure 4.3 using diagrams analogous to those introduced in the previous section. In addition to quarks, antiquarks are also assumed to exist. Their introduction follows the same logic as that of quarks, but this time employing the three-dimensional anti-fundamental representation of $SU(3)$. The basis flavour states for antiquarks are shown in the right side of Figure 4.3 and are denoted with an overbar.

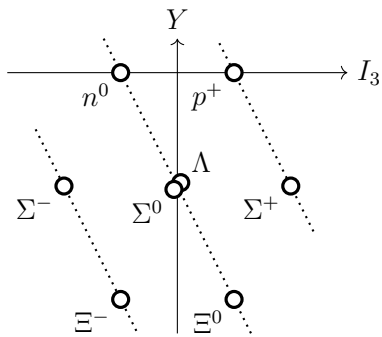
Quarks and antiquarks are treated as spin 1/2 fermions. Consequently, systems composed of multiple identical (anti)quarks are subjected to antisymmetrisation constraints. It should not be surprising that quarks of different flavours carry different electric charges as isospin symmetry, and more broadly flavour symmetry, is broken by the electromagnetic interaction. Concretely, u



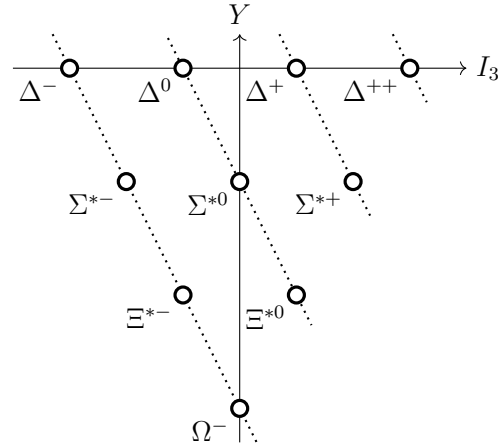
(a) Mesons with spin parity 0^- .



(b) Mesons with spin parity 1^- .



(c) Baryons with spin parity $\frac{1}{2}^+$.



(d) Baryons with spin parity $\frac{3}{2}^+$.

Figure 4.2: Association of the hadron spectrum from Tables 4.1 and 4.2 with the $SU(3)$ multiplets illustrated in Figure 4.1. Diagonal dotted lines illustrate the relation (4.8) for a given value of charge Q .

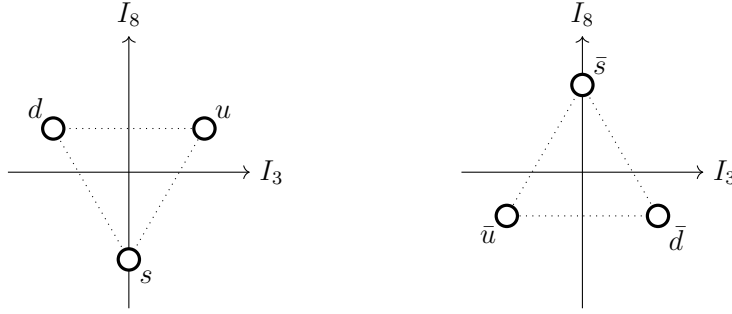


Figure 4.3: Schematic illustration of the fundamental (left) and anti-fundamental (right) representations of $SU(3)$. Each white circle represents a state supporting the corresponding irreducible representation and is associated with a possible flavour for the (anti)quark (either *up*, *down* or *strange*). The horizontal and vertical axes correspond to the eigenvalue of the third and eighth generators of $SU(3)$, respectively. The (anti)up and (anti)down states being horizontally aligned, they form $SU(2)$ doublet.

quarks have electric charge $Q = 2/3$, while d , s carry $Q = -1/3$. The charge of an antiquark is opposite to that of the corresponding quark. These assignments are consistent with equations (4.7) and (4.8).

In Gell-Mann's theory, the various hadrons observed experimentally are interpreted as bound states composed of specific numbers of quarks and/or antiquarks. In particular, baryons consist of three quarks, while mesons are composed of one quark and one antiquark. Hadron multiplets then arise from decomposing the corresponding many-body flavour space into irreducible representations of $SU(3)$. The procedure of decomposing a representation formed by tensor products of smaller ones is well-established in group theory. Without delving too deeply into mathematical details, let us illustrate the reasoning in the case of mesons. The case of baryons will be addressed more briefly thereafter.

The meson structure

Mesons are defined in the theory as bound states of one quark and one antiquark. The flavour component of the meson thus belongs to a nine-dimensional vector space. A naive basis for this space is obtained by performing all the possible tensor products of the individual flavour states,

$$\{|u\bar{u}\rangle, |u\bar{d}\rangle, |u\bar{s}\rangle, |d\bar{u}\rangle, |d\bar{d}\rangle, |d\bar{s}\rangle, |s\bar{u}\rangle, |s\bar{d}\rangle, |s\bar{s}\rangle\}. \quad (4.10)$$

By definition, (anti)quarks transform using the $SU(3)$ (anti)fundamental representation, denoted 3 ($\bar{3}$) in the following. As a result, the two-body state made of a quark and an antiquark transform with the corresponding tensor product representation, denoted $3 \otimes \bar{3}$. Group theory allows for

reorganising the nine dimensional space into two $SU(3)$ invariant subspaces⁶, one of dimension 8 and one of dimension 1, which transforms under $SU(3)$ using the octet and singlet representations, respectively. This sentence is often summed up by referring to the relation

$$3 \otimes \bar{3} = 8 \oplus 1. \quad (4.11)$$

Group theory also provides the precise combinations of flavour states (4.10) that realise the octet and singlet decomposition and fit with the diagrams displayed on figure 4.1. This second basis for the meson flavour component is illustrated on Figure 4.4. With this graph, one may already foresee the relation with the meson spectra displayed on Figures 4.2a and 4.2b.

The octet and singlet basis is particularly convenient for handling flavour-invariant quark dynamics. For simplicity, let us consider that this dynamics is modelled as in Chapter 1, through an $SU(3)$ -invariant Hamiltonian governing the quark system. Mesons are then defined as two-body eigenstates of the Hamiltonian. In this framework, the eight states of the octet are necessarily degenerate, as they are mutually connected by $SU(3)$ transformations. In contrast, the singlet state's energy should differ from that of the octet, as it resides in a separate invariant subspace. Even when the symmetry is only approximate, meaning the exact Hamiltonian includes correction terms that lift the degeneracy, the basis shown in Figure 4.4 remains useful. For example, in the hadronic context, flavour symmetry is evidently more approximate than isospin symmetry. Since the states in Figure 4.4 are chosen to form $SU(2)$ multiplets, the members of a given multiplet remain degenerate even when flavour symmetry-breaking corrections are taken into account (provided these corrections preserve isospin symmetry, as expected). In practice, even this residual symmetry is slightly broken, leading to a small energy splitting between levels with different I_3 eigenvalues.

The preceding discussion has focused on the flavour component of the quark-antiquark system. However, to construct the full mesonic states, the discussion should also consider the spin and spatial components. For a system of two spin-1/2 particles, two distinct total spin multiplets can be formed, one with total spin 0 and one with total spin 1,

$$\left\{ \begin{array}{l} |0, 0\rangle = \frac{1}{\sqrt{2}}(|\uparrow\downarrow\rangle - |\downarrow\uparrow\rangle), \\ |1, 1\rangle = |\uparrow\uparrow\rangle, \\ |1, 0\rangle = \frac{1}{\sqrt{2}}(|\uparrow\downarrow\rangle + |\downarrow\uparrow\rangle), \\ |1, -1\rangle = |\downarrow\downarrow\rangle, \end{array} \right. \quad (4.12)$$

⁶ An invariant subspace V for a group G is a vector subspace such that if any of its states is acted upon by any transformation from G , the resulting state stays in V .

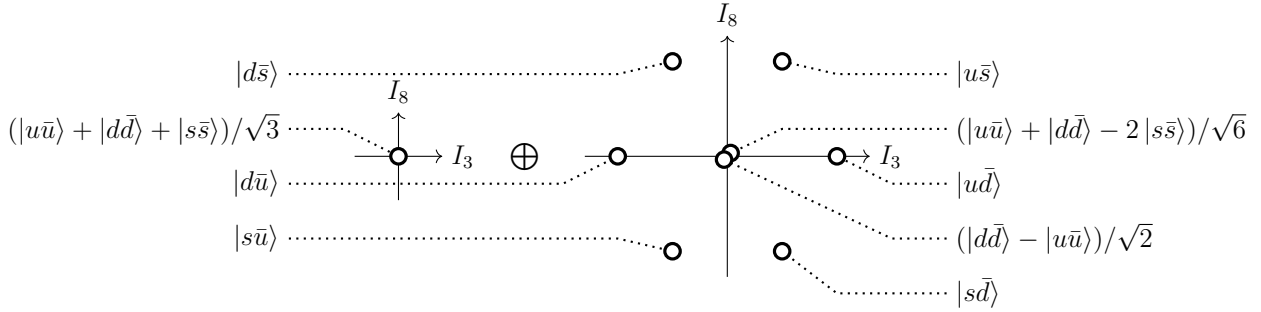


Figure 4.4: Flavour components for the decomposition in irreducible representation of the tensor product representation $3 \otimes \bar{3}$. The nine above states consist of a basis for the nine-dimensional vector space. The properties under $SU(3)$ of these states are well-established. Especially, the octet and singlet transform separately under $SU(3)$ and the basis states are I^2 , I_3 and I_8 eigenstates.

where $|SM\rangle$ denotes the total spin eigenstates, and $|\uparrow\downarrow, \downarrow\uparrow\rangle$ is a shorthand notation for the tensor product of individual spin states $|s_1 = 1/2, m_1 = \pm 1/2\rangle \otimes |s_2 = 1/2, m_2 = \pm 1/2\rangle$. The spatial component is obtained by solving the mesonic Hamiltonian. However, for low-lying meson states, the detailed spatial dependence is not required, as the system is assumed to remain in its spatial ground state. In particular, the total orbital angular momentum associated with the bound state is taken to be zero, so that the total angular momentum is fully determined by the spin degrees of freedom. With these considerations, Figures 4.2a and 4.2b can now be fully interpreted.

- Each pair of meson multiplets corresponds to a different spin configuration (4.12) of the quark-antiquark system. The total spin of the mesons reflects this distinction. The energy splitting arise from spin-dependent interactions within the mesonic Hamiltonian.
- Within Figure 4.2a or 4.2b, the meson states are differentiated by the flavour component of the quark-antiquark state. The specific flavour content is indicated in Figure 4.4. Each flavour multiplet is associated with a distinct energy, as they transform independently under the flavour symmetry group.
- The energy difference between the various states in $SU(3)$ multiplets results from flavour symmetry-breaking contributions to the Hamiltonian. Since these contributions preserve isospin symmetry, the degeneracy within the $SU(2)$ multiplets remains.
- Finally, smaller corrections to the mesonic Hamiltonian break the residual degeneracy within the $SU(2)$ multiplets, leading to slight energy differences among, for example, the three pion states.

The preceding description deliberately omitted certain aspects of the meson spectrum. In particular, beyond their flavour, isospin, spin and space quantum numbers, meson states are also characterised by specific parity and G -parity values. Parity is associated to the inversion of spatial coordinates and will be discussed in more detail in Part III. The G -parity operation combines charge conjugation \mathcal{C} , which transforms particles into their corresponding antiparticles, with a flavour rotation that reverses isospin projections, [123],

$$\mathcal{G} = \mathcal{C}e^{i\pi I_2}. \quad (4.13)$$

Above, I_2 denotes the second generator of the flavour symmetry group. Since the strong interaction is invariant under both parity and G -parity, it is natural to define meson states as eigenstates of these symmetry operators. This work is done in reference [123].

The baryon structure

As previously mentioned, the structure of the baryon spectrum will be discussed with less details. In Gell-Mann's theory, baryons are described as bound states of three quarks. Since quark's flavours transform with under fundamental representation of $SU(3)$, denoted by 3, the flavour component of a three-quark system transforms according to the tensor product representation $3 \otimes 3 \otimes 3$. This representation decomposes into one singlet, two octets and one decuplet,

$$3 \otimes 3 \otimes 3 = 1_{AS} \oplus 8_{MS} \oplus 8_{MA} \oplus 10_S. \quad (4.14)$$

The corresponding flavour-space basis is not explicitly listed here to avoid an unwieldy figure. Labels have been added to each multiplet to indicate their symmetry properties under particle exchange. A label S (AS) denotes that the states within the multiplet are (anti)symmetrical under the exchange of any two particles. A label MS (MA) indicates that the states are (anti)symmetrical under the exchange of the first two particles only. These are commonly referred to as mixed-symmetric and mixed-antisymmetric states, respectively. Turning to the spin degrees of freedom, the spin component of a system of three spin-1/2 particles decomposes into two spin doublets and one spin quadruplet,

$$\begin{cases} |\frac{1}{2}, \frac{1}{2}\rangle_{MS} = (|\uparrow\downarrow\uparrow\rangle + |\downarrow\uparrow\uparrow\rangle - 2|\uparrow\uparrow\downarrow\rangle)/\sqrt{6}, & \begin{cases} |\frac{1}{2}, \frac{1}{2}\rangle_{MA} = (|\uparrow\downarrow\uparrow\rangle - |\downarrow\uparrow\uparrow\rangle)/\sqrt{2}, \\ |\frac{1}{2}, -\frac{1}{2}\rangle_{MA} = (|\uparrow\downarrow\downarrow\rangle - |\downarrow\uparrow\downarrow\rangle)/\sqrt{2}, \end{cases} \end{cases} \quad (4.15a)$$

$$\begin{cases} |\frac{3}{2}, \frac{3}{2}\rangle_S = |\uparrow\uparrow\uparrow\rangle, \\ |\frac{3}{2}, \frac{1}{2}\rangle_S = (|\downarrow\uparrow\uparrow\rangle + |\uparrow\downarrow\uparrow\rangle + |\uparrow\uparrow\downarrow\rangle)/\sqrt{3}, \\ |\frac{3}{2}, -\frac{1}{2}\rangle_S = (|\uparrow\downarrow\downarrow\rangle + |\downarrow\uparrow\downarrow\rangle + |\downarrow\downarrow\uparrow\rangle)/\sqrt{3}, \\ |\frac{3}{2}, -\frac{3}{2}\rangle_S = |\downarrow\downarrow\downarrow\rangle \end{cases} \quad (4.15b)$$

using same notation as before. As indicated by the labels, the spin quadruplet is fully symmetrical under the exchange of any two particles, while the two spin doublets correspond to mixed-symmetric and mixed-antisymmetric states, respectively.

The principal difference from mesons is that baryons consist of three particles which are treated as identical in the current description. Consequently, the total state of the three-quark system must be antisymmetric under any quark exchange. Referring to the lowest-lying baryon decuplet in Figure 4.2d, this symmetry requirement introduces an unexpected obstacle. Since these baryons are spatial ground states, their spatial contributions are necessarily symmetric⁷. As they possess spin 3/2, their spin components, listed in equation (4.15), are also symmetric. Third, the flavour part of the state, as indicated in equation (4.14), is likewise symmetric. As a result, the total three-quark states for the low-lying baryon decuplet are fully symmetric under any quark exchange. This contradicts the spin-statistics theorem, which dictates that the total states of a system of identical fermions must be fully antisymmetric. The apparent contradiction implies that an additional structure, beyond space, spin, and flavour, must be present in the three-quark system.

This observation provided the first evidence for an additional component in quark states, known as the *colour* degree of freedom. Like flavour, colour is assumed to span a three-dimensional internal space and transforms under the fundamental representation of $SU(3)$. To avoid confusion, the colour group will hereafter be denoted by $SU(3)_c$, while the flavour group will be referred to as $SU(3)_f$. The basis colour states are conventionally labelled as *red*, *blue* and *green*⁸. This additional degree of freedom introduces a further constraint on hadronic states: they must be invariant under $SU(3)_c$. This requirement, often called the colour neutrality or whiteness condition, was historically linked to the emergence of the concept of quark confinement. Since quarks carry colour charge, they cannot exist in isolation but are always confined within

⁷ In full generality, an antisymmetric ground-state may be conceivable, particularly in systems involving fermions. The complete argument leading to the conclusion that the spatial component of baryons is symmetric is more nuanced. It involves comparing baryon and meson masses and observing that the energy difference is too small to account for difference in symmetry. The conclusion remains: the spatial components of the lowest-lying baryons must be symmetric.

⁸ As with flavour, the colour of an antiquark transforms under the anti-fundamental representation of $SU(3)_c$, with the corresponding states denoted *antired*, *antiblue* and *antigreen*.

hadrons. The discussion of confinement is deferred to the next section. Returning to baryons, let us now apply the whiteness condition. Quark colour transforms under the fundamental representation of $SU(3)_c$, so a three-quark colour state transforms according to the same tensor product representation introduced earlier in the context of $SU(3)_f$,

$$3 \otimes 3 \otimes 3 = 1_{AS} \oplus 8_{MS} \oplus 8_{MA} \oplus 10_S. \quad (4.16)$$

As expected, the only color-invariant state, namely the singlet, is antisymmetric under quark exchange. This resolves the tension with the spin-statistics theorem: the colour part of the baryon state is always antisymmetric, and therefore the remaining components of the three-quark state must be symmetric, as observed for the lowest-lying baryon decuplet.

Before concluding the discussion of baryons, the octet still needs to be accounted for. This is complicated by the fact that neither the spin-1/2 states nor the flavour octets individually exhibit an appropriate symmetry under quark exchange. However, by combining spin and flavour components with mixed symmetries, one can construct the following globally symmetric state,

$$\frac{1}{\sqrt{2}} (|1/2, 1/2\rangle_{MS} \otimes |\mathcal{F}\rangle_{MS} + |1/2, 1/2\rangle_{MA} \otimes |\mathcal{F}\rangle_{MA}). \quad (4.17)$$

Above, $|\mathcal{F}\rangle_{MS}$ and $|\mathcal{F}\rangle_{MA}$ refer to analogous basis states of the two flavour octets. This construction yields a globally symmetric space-spin-flavour component. When combined with the antisymmetric colour singlet, the resulting total three-quark state is fully antisymmetric, as required. The states obtained in this manner are finally identified with the lowest baryon octet.

4.3 Colour confinement and QCD

Let us return to the concept of colour charge, along with the related ideas of colour neutrality and quark confinement. There is much to be said about confinement, as it remains one of the most intriguing phenomena in particle physics. Numerous approaches based on different frameworks have been developed to deepen the understanding of its underlying mechanisms. Even today, significant theoretical effort continues to be devoted to this fundamental property of matter⁹. A commonly cited intuitive and qualitative explanation, often found in textbooks, suggests that quarks interact so strongly that, when separated, the energy interaction quickly surpasses the threshold for quark-antiquark pair creation. As a result, quarks effectively produce their own confinement partners, such that each becomes part of a colour neutral (white) state,

⁹ The issue is notably connected to one of the Millennium Prize Problems in Mathematics.

which interacts more weakly with its surroundings¹⁰. This intuitive picture connects the colour of quarks with the nature of their interactions. That idea gave rise to the theory of *quantum chromodynamics* (QCD). It is now regarded as the most fundamental framework for describing the strong interaction. While a detailed treatment of QCD slightly exceeds the scope of this work, it remains an indispensable topic in any discussion of hadronic physics.

Disclaimer: The following description aims to be as self-contained as possible, with a focus on outlining key aspects of QCD, including both its achievements and its limitations. References are also provided for readers who wish to explore specific topics in greater depth. For a general overview of the theory, one may refer, for example, to reference [129]. It should be emphasised that this is a conceptually demanding subject, which would easily warrant a dedicated treatment spanning hundreds of pages. The author apologises in advance if the discussion appears incomplete to some readers or challenging to others.

4.3.1 The QCD Lagrangian

The theory of QCD belongs to the broader class of quantum field theories (QFT). These theories are formulated using a Lagrangian framework rather than an Hamiltonian one, and place greater emphasis on field operators than on quantum states themselves. The interpretation of quantum fields can be subtle, and such interpretation is not essential for the present purposes. In brief, when a field operator associated with a particular configuration of a particle (for instance, the particle in a momentum eigenstate) acts on the lowest-energy state of the system, named as the vacuum, it produces a quantum state that is interpreted as containing the particle in that specific configuration. The QFT framework has proven to be a remarkably powerful tool for constructing standard theories of fundamental particles, as it enables the fully relativistic treatment of phenomena involving particle creations and disintegrations. Returning to the main topic, QCD is based on a Lorentz-invariant Lagrangian that is gauge invariant under the colour group $SU(3)_c$ [21, 130],

$$\mathcal{L}_{\text{QCD}} = \bar{\psi}_i(x_\mu) (i\gamma^\nu (D_\nu)_{ij} - m\delta_{ij}) \psi_j(x_\mu) - \frac{1}{4} F_{\nu\lambda}^a F^{a\nu\lambda} \quad (4.18)$$

¹⁰ A frequently drawn analogy is with atomic systems: although composed of electrically charged particles, atoms are overall electrically neutral. Colour charge is neutralised in hadrons, just as electric charge is neutralised in atoms. This analogy, however, is imperfect, since isolated electrons can be observed, whereas isolated coloured particles cannot. This latter feature is sometimes compared to permanent magnets, whose poles cannot be observed in isolation.

where

$$(D_\nu)_{ij} = \delta_{ij}\partial_\nu - \frac{ig}{2}A_\nu^a(x_\mu)(\lambda_a)_{ij}, \quad (4.19)$$

$$F_{\nu\lambda}^a = \partial_\nu A_\lambda^a(x_\mu) - \partial_\lambda A_\nu^a(x_\mu) + gf^{abc}A_\nu^b A_\lambda^c(x_\mu). \quad (4.20)$$

As summations over repeated indices i, j, a, b and c are implied, the position of colour indices is arbitrary. For spacetime indices, the Einstein convention is used. For simplicity, a single quark flavour is considered. Let us examine each component of this intricate expression in turn [21, 129], with an emphasis on physical aspects while setting aside certain mathematical subtleties.

- The symbol $\psi_i(x_\mu)$ with $i \in \{1, 2, 3\}$ denotes the three fields corresponding to the three colour states of quarks. Each $\psi_i(x_\mu)$ is a Dirac spinor field, meaning it inherently includes the two spin projections of both quarks and antiquarks. This compact formulation allows all four components to be treated simultaneously and facilitates the control of Lorentz invariance in the theory. The notation $\bar{\psi}_i(x_\mu)$ refers to the Dirac adjoint of $\psi_i(x_\mu)$ [21]. A deeper exploration of the underlying construction is omitted, as it is not essential to the present discussion. As noted, fields are functions of the four spacetime coordinates x_μ (Greek and Latin letters denote space-time and colour indices, respectively).
- The symbol $A_\nu^a(x_\mu)$ with $a \in \{1, \dots, 8\}$ denotes the eight vector fields associated with the eight bosons, called *gluons*, that mediate the colour interaction. This is analogous to quantum electrodynamics, where the electromagnetic interaction is mediated by the photon. However, unlike the photon, which is electrically neutral, gluons themselves carry colour charge, labelled by the index a , and can therefore interact with one another. The eight linearly independent colour charges for the gluons transform under the octet representation of $SU(3)_c$. The fields $A_\nu^a(x_\mu)$ are referred to as vector fields because they have four components, indexed by ν , corresponding to the four spacetime dimensions.
- The symbol $(D_\nu)_{ij}$ denotes the covariant derivative, a concept introduced to ensure local invariance of the Lagrangian under colour transformations. Notably, this same constraint leads to gluons transforming under the octet representation of $SU(3)_c$. The second term in the definition of $(D_\nu)_{ij}$ warrants closer inspection. It involves λ_a matrices, known as the Gell-Mann matrices, which are well-documented and tabulated [122, 129]. These matrices represent the eight generators of $SU(3)$ written in the fundamental representation. When inserted into the full Lagrangian, it yields a term

$$-\frac{ig}{2}\bar{\psi}_i(x_\mu)\gamma^\nu A_\nu^a(x_\mu)(\lambda_a)_{ij}\psi_j(x_\mu) \quad (4.21)$$

which is interpreted as describing interactions between (anti)quarks and gluons. Here, g is the strong coupling constant, and γ_μ represents the Dirac matrices. These matrices are well-established in the literature and facilitate the combination of Dirac spinors, their derivatives, and vector fields into Lorentz invariant quantities [21, 129].

- The symbol $F_{\nu\lambda}^a$ denotes the gluon field strength tensor. When inserted into the total Lagrangian, it generates terms that encode both the gluon dynamics [21],

$$-\frac{1}{2} (\partial_\nu A_\lambda^a(x_\mu) \partial^\nu A^{a\lambda}(x_\mu) - \partial_\lambda A_\nu^a(x_\mu) \partial^\lambda A^{a\nu}(x_\mu)), \quad (4.22)$$

and the gluon-gluon interactions [21],

$$-g f^{abc} \partial^\nu A^{a\lambda}(x_\mu) A_\nu^b A_\lambda^c(x_\mu) + \frac{g^2}{4} f^{abc} f^{ade} A_\nu^b A_\lambda^c(x_\mu) A^{d\nu} A^{e\lambda}(x_\mu). \quad (4.23)$$

In the interaction terms, the constants f^{abc} are antisymmetric and are called the structure constants of $SU(3)$. As with Gell-Mann and Dirac matrices, the structure constants are assumed to be well-documented and tabulated [122, 129].

- Above, m is a constant referred to as the *bare mass* of the quarks [131]. The origin of this appellation will be discussed further. The term in the Lagrangian associated with m is interpreted as providing mass to the quark. Notably, gluons do not have similar term and are, therefore, massless within the framework of QCD.

4.3.2 Perturbation theory and Feynman diagrams

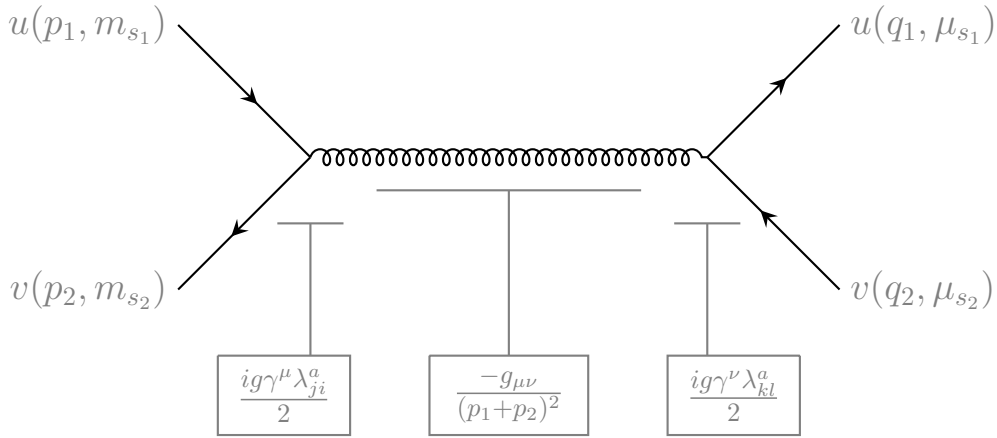
Accessing experimental predictions from a Lagrangian within the QFT framework is highly intricate, even in the simplest contexts. The formalism most commonly used to tackle this task is perturbation theory, developed by R. Feynman. For systems of particle interacting weakly enough, this formalism provides access to observables, such as the cross-sections of scattering processes, order by order in powers of the coupling constant. This is the well-known expansion in Feynman diagrams [129]. It enables the computation, for example, of the transfer matrix (from which cross-sections can be derived) for quark-antiquark elastic scattering at the first

order in the strong coupling constant [122, 130],

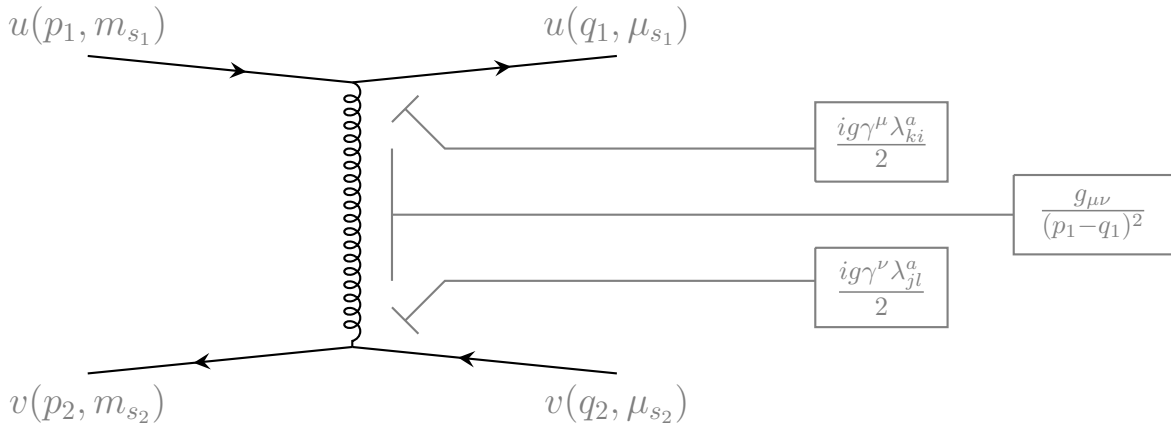
$$\begin{aligned}
\mathcal{T}(q_i(p_1, m_{s_1})\bar{q}_j(p_2, m_{s_2}) \rightarrow q_k(q_1, \mu_{s_1})\bar{q}_l(q_2, \mu_{s_2})) &= \frac{m^2}{(2\pi)^6 \sqrt{E_{p_1} E_{p_2} E_{q_1} E_{q_2}}} \\
&\left(\left(\bar{v}(p_2, m_{s_2}) \left(\frac{ig\gamma^\mu \lambda_{ji}^a}{2} \right) u(p_1, m_{s_1}) \right) \frac{-g_{\mu\nu}}{(p_1 + p_2)^2} \left(\bar{u}(q_1, \mu_{s_1}) \left(\frac{ig\gamma^\nu \lambda_{kl}^a}{2} \right) v(q_2, \mu_{s_2}) \right) \right. \\
&\quad \left. + \left(\bar{u}(q_1, \mu_{s_1}) \left(\frac{ig\gamma^\mu \lambda_{ki}^a}{2} \right) u(p_1, m_{s_1}) \right) \frac{g_{\mu\nu}}{(p_1 - q_1)^2} \left(\bar{v}(p_2, m_{s_2}) \left(\frac{ig\gamma^\nu \lambda_{jl}^a}{2} \right) v(q_2, \mu_{s_2}) \right) \right) \quad (4.24) \\
&= \frac{g^2 m^2}{(2\pi)^6 \sqrt{E_{p_1} E_{p_2} E_{q_1} E_{q_2}}} \left(\frac{1}{(p_1 + q_2)^2} \frac{\lambda_{ji}^a}{2} \frac{\lambda_{kl}^a}{2} \bar{u}(q_1, \mu_{s_1}) \gamma_\mu v(q_2, \mu_{s_2}) \bar{v}(p_2, m_{s_2}) \gamma^\mu u(p_1, m_{s_1}) \right. \\
&\quad \left. - \frac{1}{(p_1 - q_1)^2} \frac{\lambda_{ki}^a}{2} \frac{\lambda_{jl}^a}{2} \bar{u}(q_1, \mu_{s_1}) \gamma_\mu u(p_1, m_{s_1}) \bar{v}(p_2, m_{s_2}) \gamma^\mu v(q_2, \mu_{s_2}) \right).
\end{aligned}$$

Above, p and q denote the four-momenta with components ($E_p = \sqrt{m^2 + \mathbf{p}^2}$, \mathbf{p}) and $g_{\mu\nu}$ is the Minkowski metric (this document uses the signature $+ - - -$). Without going into too much detail, $u(p, m_s)$ and $v(p, m_s)$ are four-component spinors with momentum p and spin projection m_s associated with quarks and antiquarks, respectively [122, 129]. For reference, this formula is given in the Feynman gauge. The first equality is deliberately left unsimplified to illustrate the analogy with the Feynman diagrams in Figure 4.5. In their minimal interpretation, Feynman diagrams are considered as notational tools used to reconstruct cumbersome formulas easily. More ambitious interpretations of the formalism suggest that the true scattering processes undergone by the system is a quantum superposition of the different processes represented by each diagram in the expansion.

Going beyond first-order approximation introduces additional challenges, as naive calculations using Feynman diagrams predict divergent higher-order corrections. This issue is addressed through renormalisation procedures in the theory [21, 129]. In essence, counterterms are added to the Lagrangian so that their contributions cancel each divergence. The topic of renormalisation and its various schemes clearly extends beyond the scope of this document. However, it is worth mentioning the modified minimal subtraction ($\overline{\text{MS}}$) renormalisation scheme, as it reveals a key property of QCD. In this scheme, divergences are absorbed by introducing a dependence on the centre-of-mass energy in both the mass parameter of the Lagrangian and the coupling constant [21]. When applying this to QCD, the resulting energy dependence leads to a decrease in the coupling strength with increasing energy, as illustrated in Figure 4.6, reproduced from reference [132, 133]. This behaviour, known as asymptotic freedom, implies that quarks become less strongly bound at higher energies, thereby enabling the use of perturbation theory to study high-energy interactions, such as those occurring in proton-proton collisions [129]. In contrast, as the energy approaches the hadronic scale, the strong coupling constant increases and eventually



(a) Quark-antiquark annihilation diagram.



(b) One-gluon exchange diagram.

Figure 4.5: The two first-order Feynman diagrams for quark-antiquark scattering processes [122, 130]. These diagrams correspond to the expression given in equation (4.24). Contributions from the different components of the diagrams are indicated in gray.

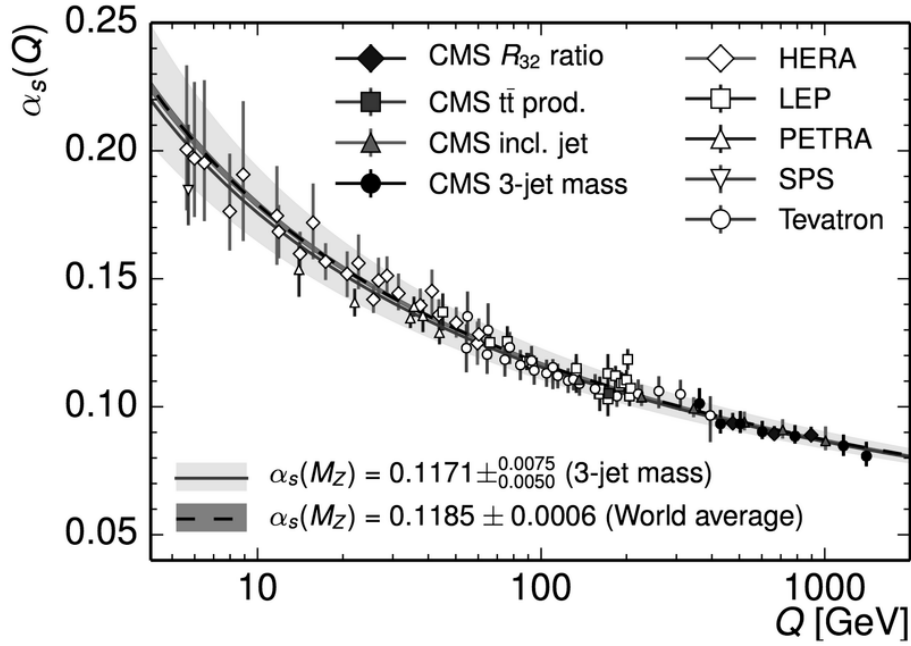


Figure 4.6: Experimental extraction of the strong coupling constant $\alpha_s = g^2/4\pi$ as a function of a relevant energy scale, denoted Q . Most often, this scale is chosen to be the centre-of-mass energy of the scattering event. Although the coupling constant is not itself an observable, its value can be inferred from measurements of observables that depend on it. The figure is reproduced from references [132, 133].

exceeds unity, at which point perturbation theory breaks down. Consequently, the Feynman diagrams shown in Figure 4.5 does not provide an accurate description of hadronic states. This increase in the coupling constant is consistent with the phenomenon of confinement mentioned earlier: at low momenta, and therefore at large distances due to Fourier transform relations, quarks become so tightly bound that they can no longer separate from one another.

4.3.3 Miscellaneous QCD properties and non-perturbative approaches

Another distinctive feature of QCD concerns the mass of quarks. The mass parameter in the Lagrangian, namely the bare mass m , indicates that quarks are inherently massive in the theory. For example, the bare masses of the u and d quark flavours typically lies between 3 and 5 MeV. This is significantly smaller than the nucleon mass, which is approximately 940 MeV. This stark contrast suggests that the majority of the proton's mass arises from the energy content of the proton. As previously mentioned, in the $\overline{\text{MS}}$ renormalisation scheme, the physical quark mass becomes decoupled from its bare mass. At low momenta, the interactions between quarks and gluonic fields lead to an increase in the effective quark mass, also known as the constituent-quark

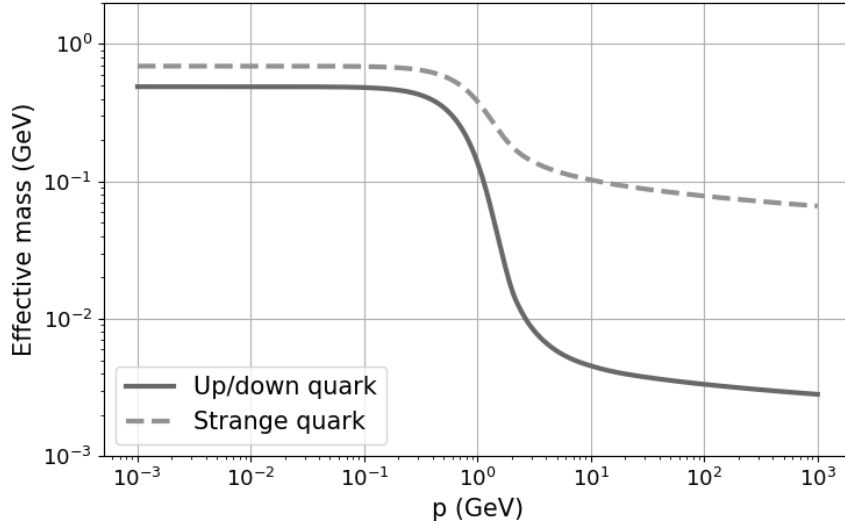


Figure 4.7: Effective quark mass as a function of the quark momentum modulus p , obtained by solving the SDE within the rainbow-ladder model [131]. At high momentum, the effective mass approaches the bare mass: approximately 3 MeV for up/down quarks and 65 MeV for strange quarks. At low momentum, the effective mass reaches its constituent value: around 500 MeV for up/down and 700 MeV for strange.

mass. This mass can be computed by solving the Schwinger-Dyson equations (SDE) for QCD [131]. These equations, sometimes referred to as the equations of motion for QFT, allow one to calculate the effective propagation properties of particles, even in the non-perturbative regime. The main challenge is that the SDE form an infinite tower of coupled equations, requiring a truncation scheme to render them solvable. Nevertheless, solving approximately the quark SDE is feasible and yields the momentum-dependent mass evolution shown in Figure 4.7. At large momentum, the quark mass approaches its bare value, consistent with the principle of asymptotic freedom. At low momentum, the mass increases and reaches its constituent value due to strong interactions with the gluonic field. Analogous but more technical calculations indicate that, despite being formally massless, gluons also acquire a dynamical mass due to their self-interactions [134].

Notably, as shown on figure 4.7 even the bare mass of the strange quark differs from that of the up and down quarks. This highlights the approximate nature of the $SU(3)_f$ flavour symmetry. Although not discussed so far, heavier quark flavours also exist, namely the *charm*, *bottom* and *top* quarks. Their inclusion expands the spectrum of possible hadrons, including those containing charm and bottom quarks. The top quark, however, is so massive that it decays almost immediately. This makes it difficult to identify its bound states. The heavier a quark is,

the more accurate a non-relativistic description becomes, and the less sensitive its bare mass is to dynamical mass generation effects.

Because perturbation theory fails to accurately describe the low-energy regime of QCD, physicists have turned to various alternative methods to access predictions directly derived from QCD. One such approach involves the Bethe-Salpeter equations which, when combined with the DSE, provide access to hadron spectra and to quantities analogous to hadron wave functions [131, 135]. Another widely used method is lattice QCD (LQCD), which formulates QCD on a finite-size space-time lattice. In this framework, observables can be expanded in powers of the inverse coupling constant, $\beta = 6/g^2$, which allows predictions to be made in the strong coupling regime. To remain consistent with continuum physics, smaller lattice spacings a require correspondingly larger values for β . By performing simulations for different (a, β) values, results can be extrapolated to the continuum limit, thereby enabling the inference of QCD predictions from lattice calculations. In practice, estimating observables in LQCD depends primarily on computational resources. One of the major achievements of LQCD has been the evaluation of the energy of the flux tube formed between a static quark-antiquark pair as a function of their separation [136]. This result is illustrated in Figure 4.8, where this string tension energy is plotted against the quark-antiquark distance. The figure is reproduced from reference [136]. Results from LQCD will serve as a reference for comparison in Part III. Of course, many other non-perturbative approaches to QCD deserve attention. However, since this topic lies somewhat beyond the scope of the present document, the discussion is concluded here.

4.3.4 Exotic particles

Following the previous brief exploration of QCD and its modern perspective on the concept of colour, let us return to the confinement condition introduced for baryons. While colour invariance was initially proposed to resolve symmetry inconsistencies in baryon wave functions, it also addresses a broader question: why do three-quark and quark-antiquark bound states exist, whereas, for example, two-quark bound states do not? As mentioned above, the answer lies in the condition of colour neutrality: both the tensor product representations $\bar{3} \otimes 3$ and $3 \otimes 3 \otimes 3$ contain a singlet state in their decomposition, as shown in equations (4.11) and (4.16), while that is not the case for the tensor product representation obtained with two quarks [18],

$$3 \otimes 3 = 6 \oplus \bar{3}. \quad (4.25)$$

Since this decomposition contains no singlet, such a system cannot form a colour-neutral state, and consequently, no observed hadron consists solely of two quarks. However, colour-

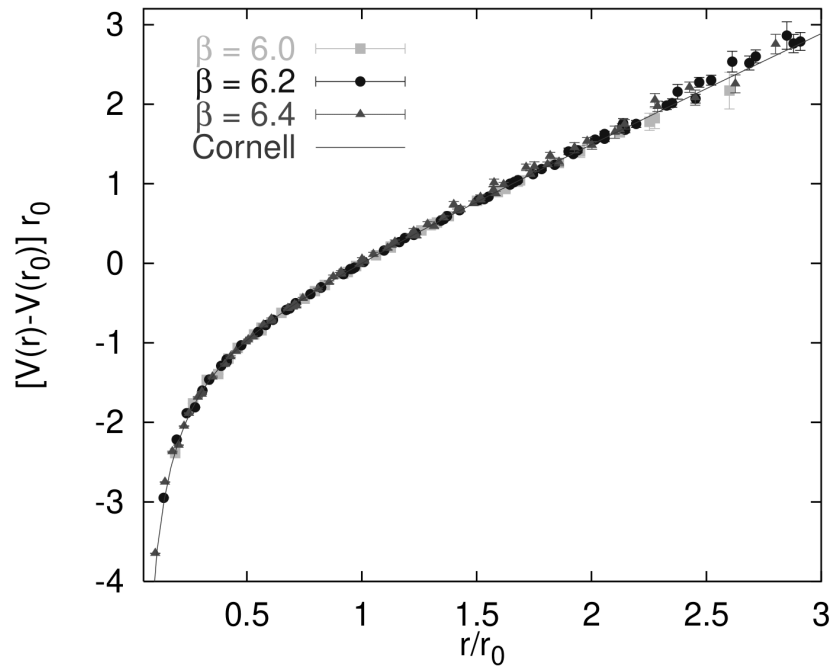


Figure 4.8: Energy of the flux tube generated by a static quark-antiquark pair computed using LQCD. Different point shapes correspond to different inverse coupling constants β (and thus different lattice spacing a). A fit with a Cornell potential (see Section 5.1) is shown for comparison. Distances are expressed in units of a given reference scale r_0 , defined in [136]. Energies are normalised such that $V(r_0) = 0$. The figure is reproduced from reference [136].

neutral combinations are not restricted to the conventional mesons and baryons. More *exotic* configurations can also yield $SU(3)_c$ singlet states [18, 103]. For example, one may consider systems comprising two quark and two antiquark, or four quark and one antiquark,

$$3 \otimes \bar{3} \otimes 3 \otimes \bar{3} = 1 \oplus \dots, \quad 3 \otimes 3 \otimes 3 \otimes 3 \otimes \bar{3} = 1 \oplus \dots \quad (4.26)$$

For brevity, only the first singlet term is shown in these decompositions. The resulting bound states are known as tetraquarks and pentaquarks, respectively. These exotic hadrons have been sought in high-energy experiments for decades. Recently, more and more evidences support the existence of heavy tetraquarks and pentaquarks states in experimental spectra [137]. Nonetheless, the internal quark distribution of these states remains a matter of ongoing debate. A central question is whether these particles form compact tetraquark/pentaquark states, or whether they are better described as loosely bound meson-meson or meson-baryon hadronic molecules.

The previous discussion of QCD also introduced another component that can be incorporated into the quark model: the gluon. Transforming under the octet representation of $SU(3)$, gluons can combine with quarks and antiquarks to form colour-neutral states. For instance, the following systems are allowed by the whiteness condition [18, 103],

$$3 \otimes \bar{3} \otimes 8 = 1 \oplus \dots, \quad 3 \otimes 3 \otimes 3 \otimes 8 = 1 \oplus \dots \quad (4.27)$$

These configurations correspond to hybrid mesons and hybrid baryons, respectively. Even more remarkably, QCD permits bound states composed entirely of gluons [3, 138],

$$8 \otimes 8 = 1_S \oplus \dots, \quad 8 \otimes 8 \otimes 8 = 1_S \oplus 1_{AS} \oplus \dots \quad (4.28)$$

For further use, the symmetry properties of the singlet components in these decompositions have been indicated. These purely gluonic states are referred to as glueball states, specifically two-gluon and three-gluon glueballs. The existence of particles composed entirely of gauge bosons is a unique and striking prediction of QCD. Despite their early theoretical prediction [1], glueball states have remained experimentally elusive, primarily due to their potential mixing with mesonic states. A detailed description of glueballs is presented in Part III.

This chapter in the context of a thesis

Like Chapter 1, the above text aimed to lay the foundations of the framework used in the chapters that follow. It provided a non-exhaustive overview of the key historical discoveries that gave rise to hadronic physics. It also traced the origin of the quark concept and its modern interpretation. Rather than being comprehensive, the goal was to introduce the essential concepts that will be used in the subsequent study of baryons and glueballs.

Perhaps the most original contribution of this chapter is Figure 4.7 in Section 4.3.3, which is not taken from any reference, but which I successfully reproduced myself during a doctoral training program on functional methods in QCD.

Chapter 5

The Baryon Spectrum : an Example of Three-body Bound States

This chapter builds upon the information provided in the previous one to develop a phenomenological formalism for exploring the hadron spectrum. Although the approach is neither *ab initio* nor Lorentz covariant, it allows access to various hadron properties with minimal conceptual and computational effort. Dynamical aspects are first addressed in Section 5.1, where a QCD-inspired effective Hamiltonian is constructed to describe the interaction between coloured particles. This Hamiltonian is then used to infer a baryon spectrum, which is compared with the experimental data in Section 5.2.

5.1 Modern constituent approaches

In this section, a phenomenological expression for the interaction between coloured particles is developed. The potential is separated into two main contributions: a short-range component arising from perturbative gluon exchanges, and a long-range confining component encoding the non-perturbative interactions between two separated colour charges.

5.1.1 Short-range QCD potential

Let us start by investigating the short-range behaviour. It is primarily governed by one-gluon-exchange processes between the two coloured particles. The corresponding potential can be inferred from the expression of the transfer matrix \mathcal{T}_{fi} . A key quantity in scattering theory is the scattering amplitude S_{fi} , whose modulus squared gives the probability for a given incoming state i to transition to a given outgoing state f . In relativistic theory, the transfer matrix and

the scattering amplitude are related. For instance, in two-to-two scattering of coloured spinors, the following relation holds [21],

$$\mathcal{S}_{fi} = \delta^3(\mathbf{p}_1 - \mathbf{q}_1)\delta^3(\mathbf{p}_2 - \mathbf{q}_2)\delta_{m_{s_1}\mu_{s_1}}\delta_{m_{s_2}\mu_{s_2}}\delta_{c_1d_1}\delta_{c_2d_2} + i(2\pi)^4\delta^4(P_f - P_i)\mathcal{T}_{fi}. \quad (5.1)$$

Above, \mathbf{p}_j , m_{s_j} and c_j (\mathbf{q}_j , μ_{s_j} and d_j) denote the three-momentum, spin projection and colour of the j^{th} incoming (outgoing) particle, respectively. In addition, P_i and P_f refer to the total four-momenta of the incoming and outgoing states. The scattering amplitude can also be computed from the Schrödinger equation in non-relativistic quantum mechanics. For the same scattering process as in (5.1) and at first order in perturbation theory, the non-relativistic scattering amplitude is given by [5]

$$\mathcal{S}_{fi} = \delta^3(\mathbf{p}_1 - \mathbf{q}_1)\delta^3(\mathbf{p}_2 - \mathbf{q}_2)\delta_{m_{s_1}\mu_{s_1}}\delta_{m_{s_2}\mu_{s_2}}\delta_{c_1d_1}\delta_{c_2d_2} - 2\pi i\delta^4(P_f - P_i)\mathcal{V}(\mathbf{q}). \quad (5.2)$$

Above, $\mathbf{q} = \mathbf{p}_1 - \mathbf{q}_1 = \mathbf{q}_2 - \mathbf{p}_2$ is the momentum transferred during the process. The function \mathcal{V} is the Fourier transform of the interaction potential in position representation $V(\mathbf{r})$,

$$\mathcal{V}(\mathbf{q}) = \int d^3r e^{i\mathbf{r}\cdot\mathbf{q}}V(\mathbf{r}). \quad (5.3)$$

The notation suggests that the potential depends only on the relative position between the particles, denoted \mathbf{r} . However, it may also depend on the spin and colour states, as well as on the particle momenta $\mathbf{p}_A = (\mathbf{p}_1 + \mathbf{q}_1)/2$ and $\mathbf{p}_B = (\mathbf{p}_2 + \mathbf{q}_2)/2$. By comparing equations (5.1) and (5.2), one easily finds

$$\mathcal{V}(\mathbf{q}) = -(2\pi)^3\mathcal{T}_{fi}. \quad (5.4)$$

As a result, the non-relativistic limit of the first-order transfer matrix provides the interaction potential in momentum space.

Equation (5.4) can be used to infer the non-relativistic interaction potential generated by a one-gluon-exchange process. For instance, the expression (4.24) for the transfer matrix can be used to deduce the potential between a quark and an antiquark bound within a meson. Mesonic states are colour singlets and must therefore possess a definite colour state, namely

$$\frac{1}{\sqrt{3}} (|r\rangle \otimes |\bar{r}\rangle + |b\rangle \otimes |\bar{b}\rangle + |g\rangle \otimes |\bar{g}\rangle) = \sum_{i,j \in \{r,g,b\}} \frac{\delta_{ij}}{\sqrt{3}} |i\rangle \otimes |\bar{j}\rangle, \quad (5.5)$$

where $\{|r\rangle, |b\rangle, |g\rangle\}$ and $\{|\bar{r}\rangle, |\bar{b}\rangle, |\bar{g}\rangle\}$ denote the individual colour and anticolour basis states, respectively. To obtain the meson-meson transfer matrix, contributions from equation (4.24)

with different incoming and outgoing colours must be combined,

$$\mathcal{T}_{\text{meson}} = \sum_{ij} \frac{\delta_{ij}}{\sqrt{3}} \sum_{kl} \frac{\delta_{kl}}{\sqrt{3}} \mathcal{T}(q_i(p_1, m_{s_1}) \bar{q}_j(p_2, m_{s_2}) \rightarrow q_k(q_1, \mu_{s_1}) \bar{q}_l(q_2, \mu_{s_2})). \quad (5.6)$$

Expression (4.24) splits in two terms, corresponding to the one-gluon-exchange and annihilation Feynman diagrams, respectively. Denoting these terms by \mathcal{T}_{OGE} and $\mathcal{T}_{\text{annih}}$, and using Gell-Mann matrices properties, one finds that

$$\sum_{ij} \frac{\delta_{ij}}{\sqrt{3}} \sum_{kl} \frac{\delta_{kl}}{\sqrt{3}} \mathcal{T}_{\text{OGE}} \sim \sum_{ij} \frac{\delta_{ij}}{\sqrt{3}} \sum_{kl} \frac{\delta_{kl}}{\sqrt{3}} \sum_a \frac{\lambda_{ki}^a}{2} \frac{\lambda_{jl}^a}{2} = \frac{4}{3}, \quad (5.7)$$

$$\sum_{ij} \frac{\delta_{ij}}{\sqrt{3}} \sum_{kl} \frac{\delta_{kl}}{\sqrt{3}} \mathcal{T}_{\text{annih}} \sim \sum_{ij} \frac{\delta_{ij}}{\sqrt{3}} \sum_{kl} \frac{\delta_{kl}}{\sqrt{3}} \sum_a \frac{\lambda_{ji}^a}{2} \frac{\lambda_{kl}^a}{2} = 0. \quad (5.8)$$

In a colour singlet configuration, the contribution from the annihilation Feynman diagram vanishes, while that from one-gluon-exchange is multiplied by a colour factor of 4/3. Once the expression for $\mathcal{T}_{\text{meson}}$ is obtained, applying equation (5.4) becomes a matter of algebraic manipulations. A detailed derivation can be found in reference [122], therefore, in the present discussion, the main calculation steps are only briefly sketched.

- The mesonic transfer matrix \mathcal{T} is expanded in the non-relativistic limit. Each contribution is expressed as a series in inverse powers of the quark masses, and terms of order $1/m^3$ and higher are neglected. This step primarily involves intricate Dirac spinor manipulations and Taylor expansions.
- Applying equation (5.4) allows identification of the non-relativistic interaction potential in momentum space. Pursuing the expansion in inverse powers of the quark masses yields an explicit expression for the potential in terms of the transferred momentum \mathbf{q} .
- Finally, the interaction potential as a function of the relative position \mathbf{r} is obtained by Fourier transforming the momentum-space potential.

The above methodology yields the quark-antiquark interaction in a mesonic state. Very similar developments can be used to derive the quark-quark interaction in a baryonic state. The resulting potential is similar to that obtained for mesons, with a few differences. First, the colour factor is affected. The colour state for a baryon is given by [130]

$$\sum_{i,j,k \in \{r,g,b\}} \frac{\epsilon_{ijk}}{\sqrt{6}} |i\rangle \otimes |j\rangle \otimes |k\rangle, \quad (5.9)$$

where ϵ_{ijk} is the fully antisymmetric Levi-Civita symbol, with $\epsilon_{rgb} = 1$. The resulting colour factor is

$$\sum_{ijk} \frac{\epsilon_{ijk}}{\sqrt{6}} \sum_{lmn} \frac{\epsilon_{lmn}}{\sqrt{6}} \sum_a \frac{\lambda_{li}^a}{2} \frac{\lambda_{mj}^a}{2} \delta_{kn} = -\frac{2}{3}, \quad (5.10)$$

which is notably negative. However, this negative sign is cancelled by an additional minus sign that appears when turning the antiquark into a quark. As a result, the one-gluon-exchange contribution in the baryon potential has the same sign as that for mesons but is simply reduced by a factor of two.

All these calculations lead to a structure commonly referred to as the Fermi-Breit potential, which is split into five distinct contributions,

$$V_{\text{Breit}}(\mathbf{r}) = V_{\text{Coulomb}} + V_{\text{Corr}} + V_{\text{Spin-Spin}} + V_{\text{Tensor}} + V_{\text{Spin-Orbit}}. \quad (5.11)$$

These terms are detailed in turn below. The first contribution, denoted V_{Coulomb} , dominates in non-relativistic systems,

$$V_{\text{Coulomb}} = -C \frac{\alpha_s}{r}. \quad (5.12)$$

Here, C is the aforementioned colour factor, whose value depends on the investigated colour singlet, $\alpha_s = g^2/4\pi$ is the strong coupling constant, and $r = |\mathbf{r}|$. One will recognise in this contribution an electrostatic potential weighted by the colour factor. Given the structural similarities between quantum electrodynamics and QCD, it is unsurprising to observe similar forms in the non-relativistic potentials they produce. Accounting for the term V_{Coulomb} constitutes the strict minimum necessary to implement a short range QCD contribution in a QCD-inspired hadron model. The second term, V_{Corr} , accounts for relativistic corrections to the Coulomb potential,

$$V_{\text{Corr}} = C\alpha_s \left(\frac{\pi}{2} \delta^3(\mathbf{r}) \left(\frac{1}{m_1^2} + \frac{1}{m_2^2} \right) + \frac{1}{2m_1 m_2} \left(\frac{\mathbf{p}_1 \cdot \mathbf{p}_2}{r} + \frac{(\mathbf{r} \cdot \mathbf{p}_1)(\mathbf{r} \cdot \mathbf{p}_2)}{r^3} \right) \right). \quad (5.13)$$

This term splits into a repulsive contact term and a Darwin term [139], the latter explicitly mixing momentum and spatial operators. Managing such corrections often proves cumbersome, particularly the Darwin term. Moreover, as these contributions usually result in small energy splittings, their omission can generally be compensated by fine-tuning phenomenological parameters in other terms. For these reasons, hadron models often prefer to omit these corrections. The third term, as its name suggests, accounts for interaction between spin components,

$$V_{\text{Spin-Spin}} = \frac{C\alpha_s}{m_1 m_2} \frac{8\pi}{3} \delta^3(\mathbf{r}) (\mathbf{S}_1 \cdot \mathbf{S}_2). \quad (5.14)$$

Above, \mathbf{S}_i refers to the spin operators of particle i . Unlike V_{Corr} , spin-spin interactions are expected to produce significant energy splittings by differentiating states according to the total spin of particles 1 and 2. Such interactions are commonly implemented in phenomenological models. However, $V_{\text{Spin-Spin}}$ also suffer from a major drawback: the contact term $\delta^3(\mathbf{r})$ can cause the eigenstates of the resulting Hamiltonian to collapse. This unpleasant feature might appear to question the validity of the approach taken here. Nevertheless, since the current calculations were performed only at first order, it is likely that higher-order corrections compensate for this inconvenience. To mitigate the collapse issue in practice, hadron models usually replace the Dirac delta function by finite-size functions that approach a delta in specific parameter limits. Usual examples of such functions include Yukawa and Gaussian forms,

$$f_{\text{Yuk.}}(r) = \lambda^2 \frac{e^{-\lambda r}}{4\pi r}, \quad f_{\text{Gauss.}}(r) = \left(\frac{\lambda}{\sqrt{\pi}} \right)^3 e^{-\lambda^2 r^2}. \quad (5.15)$$

The parameter λ is then phenomenologically tuned to best reproduce experimental data. Such replacements can be justified by considering that QCD renders point-like relativistic quarks and gluons delocalised through the dressing process [140, 141, 142]. The fourth term in V_{Breit} again involves spin operators but now couples them with the relative position, leading to a tensor interaction,

$$V_{\text{tensor}} = \frac{C\alpha_s}{m_1 m_2} \frac{1}{r^3} \left(\frac{3(\mathbf{S}_1 \cdot \mathbf{r})(\mathbf{S}_2 \cdot \mathbf{r})}{r^2} - \mathbf{S}_1 \cdot \mathbf{S}_2 \right). \quad (5.16)$$

This contribution breaks rotational invariance of the interaction. Tensor terms are sometimes incorporated into potential models, such as in reference [39]. However, due to their generally smaller magnitudes and complex management, they are often neglected in practice. The final term mixes spin and orbital angular momenta $\mathbf{r} \times \mathbf{p}_i$,

$$V_{\text{Spin-Orbit}} = \frac{C\alpha_s}{2} \frac{1}{r^3} \left(\frac{(\mathbf{r} \times \mathbf{p}_1) \cdot \mathbf{S}_1}{m_1^2} - \frac{(\mathbf{r} \times \mathbf{p}_2) \cdot \mathbf{S}_2}{m_2^2} + \frac{2}{m_1 m_2} ((\mathbf{r} \times \mathbf{p}_1) \cdot \mathbf{S}_2 - (\mathbf{r} \times \mathbf{p}_2) \cdot \mathbf{S}_1) \right). \quad (5.17)$$

This contribution is expected to play an important role by differentiating states according to their total angular momentum, orbital angular momenta, and spins. Nevertheless, it turns out that omitting spin-orbit contributions does not significantly deteriorate the resulting spectra. This might be explained by the existence of long-range spin-orbit contributions that compensate short-range ones. As with tensor interactions, some models explicitly include spin-orbit terms [39, 142] while others neglect them [45, 143, 144].

Beyond the contributions included in the Fermi-Breit potential, other short-range effects may

also be considered, such as Thomas precession [39]. Nevertheless, the above description provides a solid foundation for constructing QCD-inspired Hamiltonians capable of reproducing hadron spectra.

5.1.2 Long-range QCD potential

The long-range interaction is governed by complex gluon exchanges at low energies and therefore cannot be accessed through perturbative QCD. Historically, a widely used picture to describe quark-quark and quark-antiquark non-perturbative interactions suggests that coloured particles are connected by strings whose energy density increases linearly with their length. By integrating out the motion of the string, this picture leads to a linear long-range potential between the particles. Calculations in LQCD discussed in Section 4.3.3 permit to confirm this picture: the potential generated by two static colour charges is shown as a function of the particle separation in Figure 4.8. As expected, it exhibits a mixture of a short-range Coulombic behaviour and a long-range linear behaviour. The assumption of static particles implicitly relies on the fact that (anti)quarks evolve slowly enough to allow the gluonic field to continuously adapt to the new configuration [39].

Phenomenology and direct QCD calculations agree on the general behaviour of the long-range colour interaction, at least when only two particles are involved. What happens when three particles interact, as in baryons or three-gluon glueballs? For baryons, LQCD calculations support the picture in which each quark generates its own flux tube and the three tubes merge at a so-called Y junction [145, 146]. The position of their meeting point depends on the shape of the triangle formed by the quarks. Briefly, if one angle of this triangle is larger than 120° , the tubes meet at the corresponding apex, otherwise they meet at the point that minimises the total length of the flux tubes, known as the Toricelli point. Such junctions are illustrated on the left side of Figure 5.1. Mathematically, the potential can be written as

$$V_{qqq}(\mathbf{r}_1, \mathbf{r}_2, \mathbf{r}_3) \sim \begin{cases} |\mathbf{r}_j - \mathbf{r}_i| + |\mathbf{r}_k - \mathbf{r}_i| & \text{if the apex } \mathbf{r}_i \text{ is larger than } 120^\circ, \\ \min_{\mathbf{Y} \in \mathbb{R}^3} \sum_{i=1}^3 |\mathbf{r}_i - \mathbf{Y}| & \text{otherwise.} \end{cases} \quad (5.18)$$

where \mathbf{r}_i denotes the position of the i^{th} quark, and $i, j, k \in \{1, 2, 3\}$ with $i \neq j \neq k$ and $i \neq k$. Although this structure is well justified, it proves difficult to handle with many resolution methods, as it represents a genuine three-body interaction with a piecewise definition. For this



Figure 5.1: Comparison of different flux-tube configurations to model baryons. Static quarks are represented by black dots, and flux-tubes by straight lines. The Y junction and Δ junction are illustrated on the left and right, respectively. For each junction, three different relative positions of the static quarks are displayed.

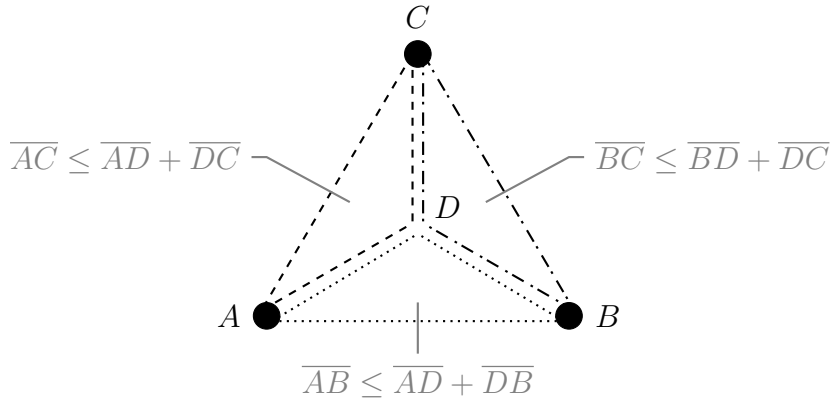


Figure 5.2: Length comparison between the Y and Δ junctions. In each of the three triangles, the length of the hypotenuse is smaller than the sum of the two other sides. By assembling the three triangles, the three hypotenuses reproduce the Δ shape, while the other sides together reproduce twice the Y shape.

reason, it is often approximated with a sum of two-body interactions, which are easier to handle,

$$\min_{\mathbf{Y} \in \mathbb{R}^3} \sum_{i=1}^3 |\mathbf{r}_i - \mathbf{Y}| \simeq \frac{1}{2} \sum_{i < j=1}^3 |\mathbf{r}_i - \mathbf{r}_j|. \quad (5.19)$$

This configuration is commonly called the Δ junction, as it consists of three flux-tubes forming a triangle. The corresponding junctions are illustrated on the right side of Figure 5.1. The $1/2$ factor must be introduced to obtain a reasonable approximation and can be justified geometrically. Using triangle inequalities, twice the total length of the flux tubes in the Y junction is bounded from below by the corresponding length in the Delta junction, as illustrated in Figure 5.2. Reference [147] demonstrates that including the $1/2$ factor yields good approximations of the energies obtained with a Y junction, and even suggests a more accurate factor of 0.54. There, the Y junction is also approximated by replacing the Toricelli point with the three-quark centre of mass. In that case, the three-body interaction (5.18) is replaced by three one-body interactions.

The above discussion explains how flux tubes adapt to a three-quark configuration. However, it did not address whether the string tension of the flux tubes is the same as in mesonic systems. It has been observed that the string tension scales with the $SU(3)$ quadratic Casimir F^2 associated with the particle's colour representation [148]. For a quark, this Casimir value is given by

$$\langle F^2 \rangle = \frac{1}{4} \sum_{a=1}^8 \langle \lambda_a^2 \rangle = \frac{4}{3}. \quad (5.20)$$

where the expectation value can be taken over any single-quark colour state. The calculation for an antiquark yields the same factor. The case of gluons will be discussed in Part III. This phenomenological Casimir-scaling hypothesis has been confirmed by LQCD calculations [149, 150, 151]. As a result, denoting the fundamental string tension by σ and applying Casimir scaling, the long-range behaviour of the colour interaction reads

$$V_{\bar{q}q}(\mathbf{r}_1, \mathbf{r}_2) = \frac{4}{3} \sigma |\mathbf{r}_1 - \mathbf{r}_2| \quad (5.21)$$

for mesons, and

$$V_{qqq}(\mathbf{r}_1, \mathbf{r}_2, \mathbf{r}_3) = \frac{4}{3} \sigma \begin{cases} |\mathbf{r}_j - \mathbf{r}_i| + |\mathbf{r}_k - \mathbf{r}_i| & \text{if the apex } \mathbf{r}_i \text{ is larger than } 120^\circ, \\ \min_{\mathbf{Y} \in \mathbb{R}^3} \sum_{i=1}^3 |\mathbf{r}_i - \mathbf{Y}| & \text{otherwise.} \end{cases} \quad (5.22)$$

for baryons. The latter is often approximated by

$$V_{qqq}(\mathbf{r}_1, \mathbf{r}_2, \mathbf{r}_3) = \frac{2}{3} \sigma \sum_{i < j=1}^3 |\mathbf{r}_i - \mathbf{r}_j|. \quad (5.23)$$

The long-range interaction discussed above still has a notable flaw: it rises indefinitely, whereas it is known that highly energetic flux tubes can break through quark-antiquark pair creation. To account for this saturation effect, some models modify the linear potential by introducing an exponential saturation,

$$V(r) = a(1 - e^{-br}), \quad (5.24)$$

where ab plays the role of the string tension, a sets energy saturation threshold, and b controls the sharpness of the transition [122]. This potential behaves linearly at short distances¹ and

¹ Strictly speaking, one should say "at short long-distances", since this section still discusses the long-range colour potential.

becomes constant as $r \rightarrow \infty$. Nevertheless, for low-lying hadrons, implementing such saturation does not significantly affect the spectrum.

5.1.3 Mid-range behaviour and kinematics

The two previous sections discussed the expected short-range and long-range behaviour of the colour potential, respectively. To reproduce the hadron spectrum with a potential model, an interaction consistent with these limiting expressions must be defined. The simplest interpolating potential simply superposes the Coulomb and linear interactions. This is the funnel (also known as Cornell) interaction,

$$V(r) = A\sigma r - \frac{C\alpha_s}{r} - B. \quad (5.25)$$

Above, C is the colour factor introduced in Section 5.1.1, and A denotes the value of the quadratic colour Casimir for mesons, or half of its value for baryons (only Δ junctions are considered for simplicity). The fundamental string tension, σ , is typically chosen around $0.15 - 0.18 \text{ GeV}^2$ [39, 152] while the strong coupling constant, α_s , is fixed around $0.4 - 0.5$ [142, 143, 152] (its momentum dependence discussed in Section 4.3.2 is often neglected). An additive constant, B , is also introduced. This constant is necessary to accurately reproduce the masses of low-energy hadrons. Its value depends on the system studied, it is typically about $0.1 - 0.3 \text{ GeV}$ for mesons [39, 143] and $0.4 - 0.6 \text{ GeV}$ for baryons² [39, 144]. This constant is consistent with LQCD calculations, since the potential obtained in Figure 4.8 is also defined up to an additive constant. Incidentally, the fit shown on that figure illustrates the comparison with a funnel-shaped potential. A definite explanation and ab initio calculation for this global energy rescaling remain difficult to obtain. Vacuum effects in QCD are often invoked [39, 130]. Other interpolating shapes have also been proposed, but they generally yield similar hadron masses [130]. In fact, a large number of potentials have been tested in the phenomenology of QCD [153]. For most of these, either the differences from the funnel potential are relatively small, or the potentials are tuned for specific hadronic systems. For these reasons, only the funnel potential will be used in the present calculations. Naturally, the funnel potential can be supplemented with any of the corrections discussed in Section 5.1.1.

Besides the interactions, one must also consider how kinetic energy is implemented in the model. Both non-relativistic and semi-relativistic kinetic energy expressions can be used, particularly for the heaviest quarks, but the semi-relativistic form proves more accurate [144, 154]. Furthermore, the issue of quark masses must be addressed. As discussed in Section 4.3.3, the effective mass of quarks depends on their momentum, transitioning from the bare mass at

² The value given here corresponds to a Δ -junction potential.

high momentum to a constituent mass at low momentum. Since the momentum distribution within a hadronic state is typically peaked at low momentum, the mass parameter is usually taken as the constituent mass in hadron models. Regarding flavour, most models assume exact isospin symmetry, and thus the up and down quarks are taken to have the same mass. By contrast, since the $SU(3)_f$ symmetry is a more approximate one, the strange quark is generally assigned a distinct constituent mass. Naturally, the charm and bottom quarks are also treated as distinct particles with their own masses. The typical orders of magnitude for the constituent masses are $0.2 - 0.3$ GeV for up/down quarks, $0.4 - 0.6$ GeV for strange quarks, $1.6 - 1.8$ GeV for charm quarks, and $5.0 - 5.3$ GeV for bottom quarks [39, 143].

5.2 The baryon spectrum

This section applies the methodology introduced earlier to compute a baryon spectrum. The Schrödinger-like equation is solved using the OBE described in Chapter 2. Model parameters are taken from references [144] for nucleons-like systems, and from [143, 155] for baryons in general. The computed results are compared with experimental data. Finally, the internal structure of the system is analysed by evaluating selected observables. Such calculations are used in current research to investigate the emergence of diquark substructures in certain baryons [30].

5.2.1 Nucleon-like baryons

The model proposed in reference [144] is used. In the notation introduced in Section 5.1, this corresponds to the following three-quark Hamiltonian,

$$H_{qqq} = \sum_{i=1}^3 \sqrt{\mathbf{p}_i^2 + m_i^2} + \sum_{i<j=1}^3 \left(\frac{2}{3} \sigma |\mathbf{r}_i - \mathbf{r}_j| - \frac{2}{3} \frac{\alpha_s}{|\mathbf{r}_i - \mathbf{r}_j|} - B_{qq} + \frac{4}{9} \frac{\alpha_s}{m_i m_j} \frac{\lambda^2 e^{-\lambda |\mathbf{r}_i - \mathbf{r}_j|}}{|\mathbf{r}_i - \mathbf{r}_j|} \mathbf{S}_i \cdot \mathbf{S}_j \right). \quad (5.26)$$

The parameter values are adopted from the corresponding reference: $\sigma = 0.182$ GeV², $\alpha_s = 0.57$, $\lambda = 0.533$ GeV, $B_{qq} = 0.409$ GeV and $m_u = m_d = 0.337$ GeV. The eigenvalues of the Hamiltonian (5.26) are presented in Table 5.1. First, energies obtained with the OBE are compared with those reported in reference [144]. While the two sets of values are generally in good agreement, some discrepancies remain. This differences likely stem from the difficulties the OBE encounters in accurately approximating the sharp divergence introduced by the Yukawa interactions. Interestingly, for N baryons, the discrepancies tend to diminish with increasing radial and

orbital excitations, presumably because the spatial wave functions become less concentrated near the origin. In some cases, particularly for all Δ baryons, the OBE results lie below those reported in reference [144], suggesting that the OBE may yield more accurate estimates. To mitigate the issue of divergences, the spin-spin interaction can be softened, by replacing the Yukawa function with a Gaussian profile, as suggested in Section 5.1.1. This approach is currently being explored in ongoing research. When compared with experimental data, the model reproduces the essential features of the low-lying baryon spectrum. This overall agreement is surprising, as the lightest quarks are expected to exhibit significant relativistic effects [39]. One notable limitation is the degeneracy in total angular momentum J for given values of orbital angular momentum L and spin S . This is illustrated in Figure 5.3. This degeneracy would be lifted by including spin-orbit contributions in the Hamiltonian (5.26).

The OBE also enables the evaluation of expectation values for various observables. Table 5.2 presents the mean interquark distance, $x = |\mathbf{r}_i - \mathbf{r}_j|$, and the mean distance between the centre of mass of a quark pair and the third particle, $y = |(\mathbf{r}_i + \mathbf{r}_j)/2 - \mathbf{r}_k|$. Due to the symmetry of the states, these distances are independent of the specific choice of indices i , j and k . The observables x and y allow for a classical representation of the quantum three-body system as a triangle, where the apices corresponds to the average positions of the constituent particles. An equilateral triangle configuration corresponds to a ratio $\langle x \rangle / \langle y \rangle \simeq 1.155$. This representation is admittedly quite reductive and does not account for the detailed internal quark distribution. Nevertheless, it offers a simple approximate illustration of the internal structure. In the present system, the deviations from this equilateral configuration are minimal, as expected from the symmetry constraints. Additional observables can also be investigated. For instance, reference [45] represents the spatial probability distributions of each baryon as functions of the moduli of both Jacobi coordinates. It also projects the eigenstates of (5.26) onto flavour multiplet states. These results are then used to establish a classification of physical baryon states within the baryon multiplets from Figures 4.2c and 4.2d in Section 4.2. Another notable example is provided in reference [144], which uses the same Hamiltonian to estimate decay widths of the baryons. The computational details are a bit too elaborate to summarise here, but the method involves evaluating a transition operator with the baryon wave function. While the results in these references were not obtained using the OBE, this method is fully capable of delivering comparable insights.

5.2.2 Broader baryon spectrum

Other quark flavours, such as strange and charm can of course also be used to construct baryon states. Such calculations are carried out, for example, in references [143, 155]. In these

$^{2S+1}L_J$	I^P	k	Particle's name	$E_{\text{exp.}}$ [128]	E_{OBE}	$E_{[144]}$
$^2S_{\frac{1}{2}}$	$\frac{1}{2}^+$	1	$N(939)$	0.939 (1)	0.959	0.939
$^2S_{\frac{1}{2}}$	$\frac{1}{2}^+$	2	$N(1440)$	1.440 (30)	1.612	1.578
$^2S_{\frac{1}{2}}$	$\frac{1}{2}^+$	3	$N(1710)$	1.710 (30)	1.869	1.860
$^4S_{\frac{3}{2}}$	$\frac{3}{2}^+$	1	$\Delta(1232)$	1.232 (2)	1.227	1.232
$^4S_{\frac{3}{2}}$	$\frac{3}{2}^+$	2	$\Delta(1600)$	1.570 (70)	1.850	1.855
$^2P_{\frac{1}{2}}$ or $^2P_{\frac{3}{2}}$	$\frac{1}{2}^-$	1	$N(1520)$ or $N(1535)$	1.515 (5) or 1.530 (15)	1.530	1.521
$^4P_{\frac{1}{2}}$ or $^4P_{\frac{3}{2}}$ or $^4P_{\frac{5}{2}}$	$\frac{1}{2}^-$	1	$N(1650)$ or $N(1675)$ or $N(1700)$	1.650 (15) or 1.672 (8) or 1.725 (75)	1.685	1.691
$^2P_{\frac{1}{2}}$ or $^2P_{\frac{3}{2}}$	$\frac{3}{2}^-$	1	$\Delta(1620)$ or $\Delta(1700)$	1.610 (20) or 1.710 (20)	1.616	1.621
$^2D_{\frac{3}{2}}$ or $^2D_{\frac{5}{2}}$	$\frac{1}{2}^+$	1	$N(1680)$ or $N(1720)$	1.685 (5) or 1.715 (35)	1.871	1.858

Table 5.1: Comparison between the experimental nucleon-like baryon spectrum $E_{\text{exp.}}$ [128] and the theoretical predictions from the model of reference [144]. Eigenenergies obtained using the OBE and those reported in [144] are listed in the columns E_{OBE} and $E_{[144]}$, respectively. All masses are given in GeV. The maximal number of quanta used for the OBE is $Q_{\text{max}} = 20$ with the non-linear variational parameter a computed for $Q = 10$. Some entries correspond to multiple particles due to degeneracies in the model spectrum with respect to the total angular momentum J . Experimental energies are taken as the Breit-Wigner masses given in [128], with uncertainties given in parentheses. As an exception, the energy of the $N(939)$ corresponds to the nucleon mass, and the uncertainty reflects the energy difference between its two isospin projections.

Particle's name	$\langle x \rangle$	$\langle y \rangle$	$\langle x \rangle / \langle y \rangle$
$N(939)$	2.2002	1.9128	1.151
$N(1440)$	3.1437	2.7334	1.150
$N(1710)$	3.5246	3.0875	1.142
$\Delta(1232)$	2.6863	2.3298	1.153
$\Delta(1600)$	3.5651	3.0916	1.153
$N(1520)$ or $N(1535)$	3.0206	2.6288	1.149
$N(1650)$ or $N(1675)$ or $N(1700)$	3.3437	2.9008	1.153
$\Delta(1620)$ or $\Delta(1700)$	3.1528	2.7343	1.153
$N(1680)$ or $N(1720)$	3.5128	3.0699	1.144

Table 5.2: Expectation values of two "observables" for low-lying baryons evaluated using the OBE on the Hamiltonian (5.26). The column $\langle x \rangle$ gives the mean distance between any two particles in the system. The column $\langle y \rangle$ gives the mean distance between centre of mass of any quark pair and the third particle. All distances are expressed in GeV^{-1} . The final column shows the ratio $\langle x \rangle / \langle y \rangle$. For reference, an equilateral mean configuration corresponds to $\langle x \rangle / \langle y \rangle \simeq 1.155$. The maximal number of quanta used for the OBE is $Q_{\max} = 20$ with the non-linear variational parameter a computed for $Q = 10$. Some rows correspond to multiple baryons due to degeneracies in the model with respect to the total angular momentum J .

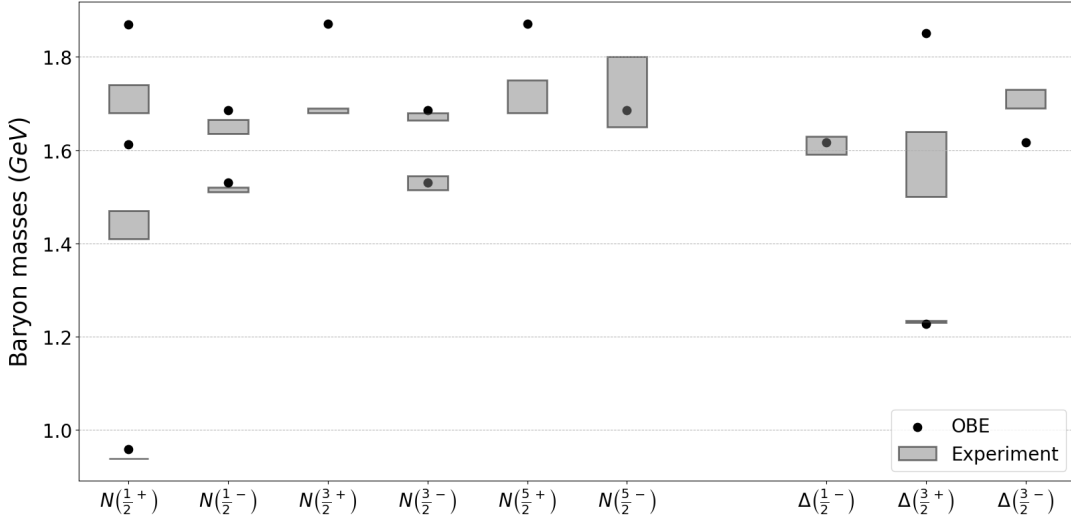


Figure 5.3: Graphical comparison between experimental nucleon-like baryon spectrum E_{exp} . [128] and theoretical predictions from the model presented in reference [144]. The plotted data correspond to the OBE results and experimental values listed in Table 5.1. Boxes indicate experimental results including the uncertainties.

works, non-relativistic kinematics are used and the set of parameters employed differs slightly from those used in [144],

$$H_{qqq} = \sum_{i=1}^3 \left(m_i + \frac{\mathbf{p}_i^2}{2m_i} \right) + \sum_{i<j=1}^3 \left(\frac{2}{3}\sigma|\mathbf{r}_i - \mathbf{r}_j| - \frac{2}{3}\frac{\alpha_s}{|\mathbf{r}_i - \mathbf{r}_j|} - B_{qq} + \frac{8}{3}\frac{\alpha_s}{m_i m_j} \frac{\lambda^2 e^{-\lambda|\mathbf{r}_i - \mathbf{r}_j|}}{|\mathbf{r}_i - \mathbf{r}_j|} \mathbf{S}_i \cdot \mathbf{S}_j \right), \quad (5.27)$$

with parameter values $\sigma = 0.139 \text{ GeV}^2$, $\alpha_s = 0.390$, $\lambda = 0.434 \text{ GeV}$, $B_{qq} = 0.457 \text{ GeV}$, $m_u = m_d = 0.337 \text{ GeV}$, $m_s = 0.6 \text{ GeV}$ and $m_c = 1.87 \text{ GeV}$. In addition to the kinematics and parameter differences, the interaction terms in Hamiltonian (5.27) are not entirely equivalent to those of equation (5.26), as the numerical factor in front of the spin-spin interactions is six times larger in (5.27). This choice is less consistent with the short-range behaviour expected from one-gluon-exchange processes. Nevertheless, this discrepancy can likely be absorbed into the potential parameters. The conventions from reference [143] are retained to facilitate comparison of results.

The eigenenergies obtained using the OBE are compared with those reported in [143, 155] and with experimental data from [128] in Tables 5.3. For most states, the results of [143] are less

accurate than those obtained using the OBE. In contrast, the predictions from [155] achieve a level of accuracy comparable to that of the OBE. As with nucleons, the simple potential model of equation (5.27) captures the main features of the baryon spectrum, as illustrated in Figure 5.4.

For these baryons, the investigation of potential diquark substructures becomes more pertinent, as symmetry constraints are relaxed. The last column of Table 5.3 presents the ratio $\langle x \rangle / \langle y \rangle$, where $\langle x \rangle$ denotes the mean distance between the two identical particles, and $\langle y \rangle$ the distance between their centre of mass and the third quark. As before, a ratio close to 1.155 characterizes an equilateral configuration, implying the absence of any diquark-like clustering. Compared to the results from Table 5.2, the baryons analysed in Table 5.3 deviate from this equilateral geometry, showing a relative increase in $\langle x \rangle$ (except for Λ). This trend is schematically depicted in Figure 5.5. In general, increasing the ratio indicates a tendency for the third quark to lie in between the two identical ones. Associating this third quark with one of the identical quarks forms a subsystem that resembles a diquark structure more closely than in the equilateral configuration. However, as seen in Figure 5.5, this effect remains modest in that particular case, and the diquark approximation is unlikely to provide a fully accurate description of the baryon spectrum or properties. For comparison, Table 5.4 presents results for baryons composed of two heavy quarks and a light one. In this case, the ratio $\langle x \rangle / \langle y \rangle$ is significantly smaller than 1.155, indicating the presence of a pronounced diquark substructure, as illustrated by the schematic diagrams in Figure 5.6. Heavy-heavy-light baryons are therefore likely to be better described by a quark-diquark approximation than the previously discussed particles.

5.3 Conclusion: why constituent approaches ?

Chapter 4 illustrated the diverse perspectives that have shaped hadron physics over time. From the early classification of hadron to the development of QCD via the quark hypothesis, the effort to explain the multitude of observed hadrons has driven decades of theoretical and experimental progress. Among the many frameworks currently employed to study hadrons, Chapter 5 introduced the basics of constituent approaches. These phenomenological and QCD-inspired methods are designed to retain essential physic features while requiring comparatively modest computational resources, even for complex systems. Initially developed to model the spectrum of conventional hadrons, constituent approaches have since been extended to more intricate systems, including exotic states [31, 156]. They are also used to explore subtler aspects of hadron structure, such as improving classification schemes [45] and computing decay rates [144]. The primary advantage of this framework lies in its conceptual simplicity and

Name & Content		$J^P(I)$	$E_{\text{exp. [128]}$	E_{OBE}	$E_{[143]}$	$E_{[155]}$	$\langle x \rangle$	$\langle y \rangle$	$\langle x \rangle / \langle y \rangle$
Λ	<i>nns</i>	$\frac{1}{2}^+(0)$	$1115.7 \pm 0.0 \pm 0.0$	1175	1196	N.A.	3.43	3.05	1.12
Σ	<i>nns</i>	$\frac{1}{2}^+(1)$	$1193.4 \pm 4.0 \pm 0.1$	1258	1281	N.A.	3.99	2.86	1.40
$\Sigma(1385)$	<i>nns</i>	$\frac{3}{2}^+(1)$	$1385.0 \pm 2.2 \pm 1.0$	1453	1477	N.A.	4.24	3.28	1.29
Λ_c	<i>nnc</i>	$\frac{1}{2}^+(0)$	$2286.5 \pm 0.0 \pm 0.1$	2316	2334	2300	3.37	2.62	1.29
$\Sigma_c(2455)$	<i>nnc</i>	$\frac{1}{2}^+(1)$	$2453.5 \pm 0.5 \pm 0.4$	2491	2511	2473	4.02	2.61	1.54
$\Sigma_c(2520)$	<i>nnc</i>	$\frac{3}{2}^+(1)$	$2518.0 \pm 0.5 \pm 2.3$	2563	2585	N.A.	4.13	2.75	1.50
Ω_c	<i>ssc</i>	$\frac{1}{2}^+(0)$	$2695.2 \pm 0.0 \pm 1.7$	2704	2717	2700	3.17	2.20	1.44
$\Omega_c(2770)$	<i>ssc</i>	$\frac{3}{2}^+(0)$	$2765.9 \pm 0.0 \pm 2.0$	2761	2776	N.A.	3.24	2.31	1.40

Table 5.3: Comparison between the experimental baryon spectrum $E_{\text{exp. [128]}$ and theoretical predictions from the model presented in reference [143]. Eigenenergies obtained using the OBE, as well as those reported in [143] and [155], are listed in the columns E_{OBE} , $E_{[143]}$ and $E_{[155]}$, respectively. All masses are given in MeV. Expectation values of two observables are also evaluated using the OBE: $\langle x \rangle$ denotes the mean distance between the two identical quarks, while $\langle y \rangle$ represents the mean distance between their centre of mass and the third particle. These distances are expressed in GeV^{-1} . The final column shows the ratio $\langle x \rangle / \langle y \rangle$. For reference, an equilateral mean configuration corresponds to $\langle x \rangle / \langle y \rangle \simeq 1.155$. The maximal number of quanta used for the OBE is $Q_{\text{max}} = 18$ with the non-linear variational parameters a and b computed for $Q = 8$. Two uncertainties are indicated for the experimental results: the first reflects the energy range covered by the isospin multiplet (0 indicates an isospin singlet), and the second represents the largest experimental uncertainty within the multiplet (0 indicates that all reported masses are more precise than the digits displayed).

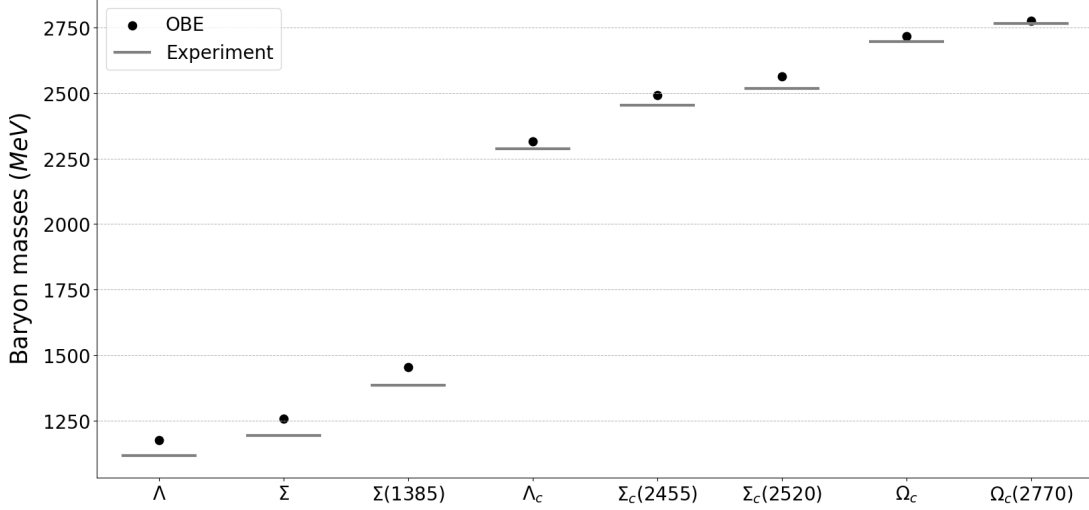


Figure 5.4: Graphical comparison between experimental baryon spectrum E_{exp} . [128] and theoretical predictions from the model presented in reference [143]. The plotted data correspond to the OBE results and experimental values listed in Table 5.3. Experimental uncertainties are not shown, as they are significantly smaller than the energy range displayed.

Name	Content	$J^P(I)$	$E_{\text{exp.}} [128]$	E_{OBE}	$\langle x \rangle$	$\langle y \rangle$	$\langle x \rangle / \langle y \rangle$
Ξ	ssn	$\frac{1}{2}^+ (\frac{1}{2})$	$1318.3 \pm 3.4 \pm 0.2$	1367	3.23	2.94	1.10
$\Xi(1530)$	ssn	$\frac{3}{2}^+ (\frac{1}{2})$	$1533.4 \pm 1.6 \pm 0.6$	1.571	3.43	3.41	1.01
Ξ_{cc}	ccn	$\frac{1}{2}^+ (\frac{1}{2})$	$3621.6 \pm ?? \pm 0.4$	3632	2.10	2.82	0.74
$\Xi_{cc}(?)$	ccn	$\frac{3}{2}^+ (\frac{1}{2})$	Unobserved	3.715	2.15	3.02	0.71

Table 5.4: Predictions for heavy-heavy-light baryon properties based on the model from reference [143]. When available, comparisons with experimental data E_{exp} . [128] are provided. Eigenenergies and observables are obtained using the OBE. Masses are expressed in MeV, and distances in GeV^{-1} . The column $\langle x \rangle$ denotes the mean distance between the two identical particles in the system, while $\langle y \rangle$ represents the mean distance between their centre of mass and the third particle. The final column shows the ratio $\langle x \rangle / \langle y \rangle$. For reference, an equilateral configuration corresponds to $\langle x \rangle / \langle y \rangle \simeq 1.155$. The maximal number of quanta used for the OBE is $Q_{\text{max}} = 18$ with the non-linear variational parameters a and b computed for $Q = 8$. Experimental uncertainties follow the same conventions as in Table 5.3. Interrogation marks indicate unknown quantities.

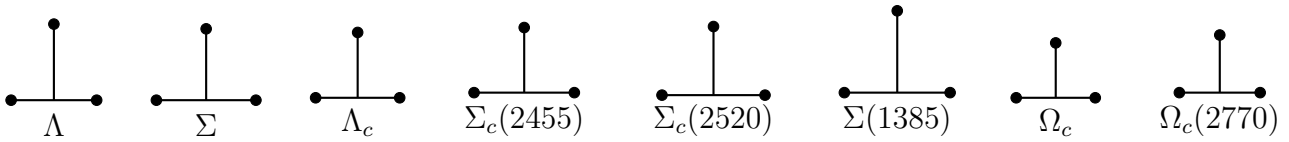


Figure 5.5: Schematic representations of the internal structures of baryons, as inferred from the expectation values evaluated in Table 5.3. In each diagram, the two identical quarks are positioned at the bottom. Diagrams are drawn to scale. In all cases, the presence of a well-defined internal diquark structure appears unlikely. Admittedly, this representation is only approximate and does not capture the detailed internal quark distribution.

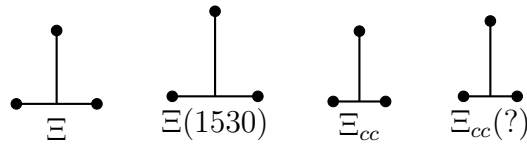


Figure 5.6: Schematic representations of the internal structures of baryons, as inferred from the expectation values in Table 5.4. In each diagram, the two identical quarks are positioned at the bottom. Diagrams are drawn to scale. In these systems, diquark substructures are more pronounced than in the previously considered cases. Admittedly, this representation is only approximate and does not capture the detailed internal quark distribution.

computational efficiency, especially when compared to more involved techniques such as LQCD or the Bethe-Salpeter equation.

Let us now highlight two current research directions pursued within the constituent quark model. First, this approach is used to evaluate the validity of the quark-diquark approximation across various baryon states. Preliminary results of this investigation were outlined at the end of Section 5.2. This methodology will subsequently be applied to support and expand upon a recent study of hybrid baryons [56]. Second, as noted, the constituent quark model can be adapted to study more exotic systems, including two- and three-gluon glueballs. This extension of the formalism proves non-trivial, as gluons are formally massless within QCD. However, the spin degrees of freedom of massless particles differ fundamentally from those of massive ones, necessitating a dedicated treatment. A suitable spin formalism for massless constituents must therefore be introduced to properly describe glueball dynamics. In addition to the theoretical interest and technical challenges involved, this subject also marks a first step toward reintroducing relativity into the constituent framework. For these reasons, the remainder of this document focuses on the study and modelling glueball systems.

This chapter in the context of a thesis

This Chapter has two main objectives. First, it introduces and justifies the key features of constituent approaches to QCD. Since this framework is central to the remainder of the document, its justification warrants a dedicated chapter. Once again, particular emphasis is placed on features that are essential for the developments that follow.

Second, the chapter present recent calculations carried out within the research unit, to which I contributed. I was involved in supervising C. Tourbez's Master thesis which, as mentioned in the above section, aims to evaluate the validity of the quark-diquark approximation in baryons. My contribution focused on obtaining accurate results for a full three-body description of the system using the OBE. These calculations open new perspectives for studying hybrid baryons using a quark-core plus gluon approach.

Part III

The Helicity Formalism and Glueball Spectroscopy

Chapter 6

Toward Relativistic Quantum Mechanics : the Helicity Formalism

The vast majority of prior developments have been carried out within a non-relativistic framework: the Schrödinger equation is inherently not Lorentz covariant, calculations were performed using Jacobi coordinates (2.25) in a naïve manner, and transformations between reference frames were treated without sufficient rigour. For instance, the Jacobi variable \boldsymbol{x} was universally interpreted as the relative distance between particles 1 and 2, regardless of the reference frame in which positions were defined. Additionally, the angular momentum between particle 1 and 2 was naively coupled with that of particle 3, even though these quantities were not necessarily defined in the same frame. While employing a semi-relativistic expression for the kinetic energy led to better agreement with experimental data for light particles, it does not address the underlying issues of covariance.

The remainder of this document seeks to develop a framework that partially remedies these shortcomings. The approach is based on the construction of Lorentz-covariant quantum states using Poincaré group (PG) transformations. In an effort to treat both massive and massless particles within a unified framework, the helicity formalism, originally developed by Jacob and Wick [157], is employed. As a motivation for these developments, the resulting formalism is subsequently applied to the study of two- and three-gluon glueballs. The existence of such hadrons was previously introduced in Section 4.3.4 and is discussed in greater detail in Chapter 7.

As a first step, this chapter introduces the helicity formalism for one- and two-body systems. This chapter builds upon and slightly expands the text from reference [158]. It is organised as follows. Section 6.1 introduces the PG, emphasizing the definitions and properties relevant to the subsequent application. Section 6.2 presents the helicity formalism for one-body systems,

detailing the basic properties of helicity states. Section 6.3 then extends the discussion to two-body systems. The treatment is kept general to ensure applicability to a broad range of systems. The application of the helicity technology in a constituent model framework, along with glueball-specific considerations, is deferred to the next Chapter.

6.1 The Poincaré group

The PG is the isometry group of the Minkowski spacetime. It includes spacetime translations, spacetime rotations, as well as parity and time-reversal operations. The well-known Lorentz group is obtained from the PG by excluding spacetime translations. Further removing spatial rotations, parity, and time-reversal yields the proper orthochronous Lorentz group. In the helicity formalism, the PG plays a dual role. First, operators from the Poincaré algebra (PA) are used to characterise particles states. Second, spacetime transformations are employed to set rest-frame states into motion and to construct two- and three-body states. For these reasons, it is helpful to begin with a brief review of the PA and the PG. Numerous sources offer comprehensive overviews of these theoretical concepts. Among the standard references in the field, the following paragraphs rely on [159] and [160].

6.1.1 The Poincaré algebra

The PA provides operators whose eigenstates serves as the building blocks for defining particle states. It consists of 10 generators, which can be grouped into three families. Four of these, denoted P_0 , P_1 , P_2 and P_3 , generate spacetime translations. These commute with each other,

$$\forall \mu, \nu \in \{0, 1, 2, 3\}, [P_\mu, P_\nu] = 0. \quad (6.1)$$

Throughout this work, Greek letters denote spacetime indices. As a reminder, the metric signature used is $+ - - -$. In the quantum context, the generators P_μ are associated with the four-momentum component operators. Three additional generators, denoted J_1 , J_2 and J_3 , generate spatial rotations. They obey the standard commutation relations of the $SO(3)$ algebra,

$$\forall i, j \in \{1, 2, 3\}, [J_i, J_j] = i \sum_k \epsilon_{ijk} J_k, \quad (6.2)$$

where ϵ is the fully antisymmetric Levi-Civita symbol. Roman letters are reserved for purely spatial indices, and the Einstein summation convention is applied only to spacetime indices. The rotation generators do not necessary commute with the P_μ generators. In quantum mechanics,

the J_i represent the components of total angular momentum. An alternative notation, using two indices, is sometimes employed: $J_1 = J^{23}$, $J_2 = J^{31}$, and $J_3 = J^{12}$, with $J^{ij} = -J^{ji}$. The final three generators, denoted K_1 , K_2 and K_3 , correspond to boosts along the three spatial directions. Although the full commutation relations are not required in this manuscript (interested readers may consult [159]), let us mention that $[K_3, J_3] = 0$. This implies that boosts along the z axis commute with rotations about the same axis. This property is frequently exploited in subsequent developments.

The 10 generators of the PA can be combined to define two Casimir operators, the squared four-momentum, P^2 , and the Pauli-Lubanski scalar, W^2 ,

$$P^2 = P_0^2 - P_1^2 - P_2^2 - P_3^2, \quad (6.3)$$

$$W^2 = W_0^2 - W_1^2 - W_2^2 - W_3^2 \text{ with } W_\mu = \frac{1}{2}\epsilon_{\mu\nu\rho\sigma}J^{\nu\rho}P^\sigma. \quad (6.4)$$

As Casimirs, these combinations are invariant under Poincaré transformations. To ensure a consistent definition across all observers, particle states are defined as eigenstates of these operators. This definition formally assigns each particle to a specific irreducible representation of the PG. The eigenvalue of P^2 is naturally interpreted as the square of the particle's mass. For massive states, the eigenvalue of W^2 is related to the spin of the particle. This can be seen by transforming to the particle's rest frame, where $P_0 = m$ and $P_i = 0$. In this frame, the spatial components of the Pauli-Lubanski vector reduce to $W_i = mJ_i$, and the Casimir becomes

$$W^2 = -m^2(J_1^2 + J_2^2 + J_3^2) = -m^2J^2, \quad (6.5)$$

where J^2 denotes the squared total angular momentum operator. In the rest frame of the particle, this angular momentum necessarily arises from the particle's intrinsic spin. The situation is more nuanced for massless particles. Physical massless particles, such as photons and gluons, satisfy $W^2 = 0$. For these cases, a different combination of generators becomes Lorentz invariant¹,

$$\Lambda = \frac{J_1P_1 + J_2P_2 + J_3P_3}{\sqrt{P_1^2 + P_2^2 + P_3^2}} = \frac{\mathbf{J} \cdot \mathbf{P}}{\sqrt{\mathbf{P}^2}}. \quad (6.6)$$

This operator, known as the helicity operator, represents the projection of spin along the direction of momentum. Although helicity is Lorentz invariant only for massless particles, its eigenstates can also be used to construct a complete set of states for massive particles, as will

¹ Strictly speaking, helicity is not fully Poincaré invariant, as it is reversed under parity. Since parity is a discrete transformation, it does not manifest within the PA.

be shown in Section 6.2.

6.1.2 Special Poincaré group transformations

In the following, specific elements of the PG will be used extensively, for instance, to set particles in motion or to relate different reference frames. This section introduces the notations adopted in the remainder of this work. An active viewpoint is assumed throughout.

Spatial rotations defined by Euler angles (α, β, γ) in the zyz convention are denoted $R(\alpha, \beta, \gamma)$. These can be expressed in terms of the PG generators of spatial rotations via the relation,

$$R(\alpha, \beta, \gamma) = e^{-i\alpha J_3} e^{-i\beta J_2} e^{-i\gamma J_3}. \quad (6.7)$$

In this notation, a rotation that aligns the z axis with a direction defined by polar and azimuthal angles (θ, ϕ) takes the form $R(\phi, \theta, \xi)$ where ξ is arbitrary. Two choices of ξ are commonly used: $\xi = 0$, named the 0 convention, and $\xi = -\phi$, named the $-\phi$ convention. When these rotations acts on four-vectors, such as four-momenta, their effect can be represented using matrices. For later use, the matrix representations of rotation $R(\phi, \theta, \xi)$ in both convention are given below,

$$R(\phi, \theta, 0) = \begin{pmatrix} \cos \theta \cos \phi & -\sin \phi & \sin \theta \cos \phi \\ \cos \theta \sin \phi & \cos \phi & \sin \theta \sin \phi \\ -\sin \theta & 0 & \cos \theta \end{pmatrix}, \quad (6.8)$$

$$R(\phi, \theta, -\phi) = \begin{pmatrix} \cos \theta \cos^2 \phi + \sin^2 \phi & \sin \phi \cos \phi (\cos \theta - 1) & \sin \theta \cos \phi \\ \sin \phi \cos \phi (\cos \theta - 1) & \cos \theta \sin^2 \phi + \cos^2 \phi & \sin \theta \sin \phi \\ -\sin \theta \cos \phi & -\sin \theta \sin \phi & \cos \theta \end{pmatrix}. \quad (6.9)$$

When acting on quantum states, rotations are implemented via a given unitary representation of the PG, denoted U . That is, while $R(\alpha, \beta, \gamma)$ denotes a group element, $U(R(\alpha, \beta, \gamma))$ denotes the corresponding operator acting on physical states. These rotations form the $SO(3)$ subgroup of the PG. This subgroup plays an important role in the study of the PG irreducible representations².

Lorentz boosts along the z axis, denoted L_z , will also be used extensively. Such unidirectional Lorentz boosts depend on a single parameter, commonly chosen to be the rapidity χ . In what follows, boosts that impart a momentum $p \geq 0$ along the z axis to a particle of mass $m > 0$

² This subgroup preserves the rest momentum of massive particles, namely $(m, 0, 0, 0)$. For that reason, it is commonly referred to as the little group for massive representations.

initially at rest are denoted $L_z(m, p)$. The corresponding rapidity is given by

$$\chi(m, p) = \tanh^{-1} \left(\frac{p}{\sqrt{m^2 + p^2}} \right) = \cosh^{-1} \left(\frac{\sqrt{m^2 + p^2}}{m} \right). \quad (6.10)$$

Naturally, specifying a unidirectional boost in terms of the pair (m, p) is not unique: many such pairs correspond to the same rapidity $\chi(m, p)$, and therefore to the same L_z transformation. However, this redundancy poses no issue for present purposes. The action of $L_z(m, p)$ on four-vectors is represented by the following matrix

$$L_z(m, p) = \begin{pmatrix} \cosh(\chi(m, p)) & 0 & 0 & \sinh(\chi(m, p)) \\ 0 & 1 & 0 & 0 \\ 0 & 0 & 1 & 0 \\ \sinh(\chi(m, p)) & 0 & 0 & \cosh(\chi(m, p)) \end{pmatrix}. \quad (6.11)$$

Since massless particles cannot be brought at rest, the case $m = 0$ requires separate treatment. The boost $L(0, p)$ refers to a transformation that imparts momentum $p > 0$ along z to a massless particle with an initial dimensionless four-momentum $(1, 0, 0, 1)$. Its matrix representation, which can be applied to four-vectors, is given by

$$L_z(0, p) = \begin{pmatrix} \frac{p^2+1}{2p} & 0 & 0 & \frac{p^2-1}{2p} \\ 0 & 1 & 0 & 0 \\ 0 & 0 & 1 & 0 \\ \frac{p^2-1}{2p} & 0 & 0 & \frac{p^2+1}{2p} \end{pmatrix}. \quad (6.12)$$

In line with the notation for rotations, the corresponding unitary operator acting on quantum states is denoted $U(L_z(m, p))$ for both massive and massless case. These unidirectional boosts also form a subgroup of the PG.

Rotations and boosts along the z direction can be composed to produce boosts in arbitrary directions. Two main combinations allow imparting momentum of magnitude p along a direction (θ, ϕ) to a massive particle initially at rest,

$$L(m, p, \theta, \phi) = R(\phi, \theta, 0)L_z(m, p)R(\phi, \theta, 0)^{-1}, \quad (6.13)$$

$$L_h(m, p, \theta, \phi) = R(\phi, \theta, 0)L_z(m, p). \quad (6.14)$$

The first definition applies a boost without inducing a net rotation, as the two outer rotations cancel each other. These will be referred to as *canonical boosts*. In contrast, the L_h boost induces both the expected boost and a net rotation of the state. This combination will be referred to as a *helicity boost*. For the massless particles, canonical boosts $L(0, p, \theta, \phi)$ cannot be used since a rest frame does not exist. In that case, only helicity boosts should be used to impart a momentum of magnitude p and direction (θ, ϕ) . Both definitions can be expressed in either the 0 or $-\phi$ convention. For canonical boosts, the choice of convention does not affect the resulting transformation: since rotations around and boosts along the z axis commute, both conventions yield the exact same Lorentz transformation. However, for helicity boosts, the convention must be specified as it alters the outcome. As before, the associated unitary operators acting on physical states are denoted by $U(L)$ and $U(L_h)$, respectively.

The final subgroup of the PG relevant for the following is the set of Lorentz transformations that leave the four-momentum $(1, 0, 0, 1)$ invariant. This subgroup is commonly referred to as the massless little group. It is isomorphic to $ISO(2)$, the group of isometries of the Euclidean plane. It is parametrised by two real numbers (α, β) , representing translations, and one angle θ , representing rotations. The action of an element $S(\alpha, \beta, \theta)$ of the massless little group on four-vectors is given by the matrix representation

$$S(\alpha, \beta, \theta) = \begin{pmatrix} 1 + \frac{1}{2}(\alpha^2 + \beta^2) & \alpha \cos \theta - \beta \sin \theta & \alpha \sin \theta + \beta \cos \theta & -\frac{1}{2}(\alpha^2 + \beta^2) \\ \alpha & \cos \theta & \sin \theta & -\alpha \\ \beta & -\sin \theta & \cos \theta & -\beta \\ \frac{1}{2}(\alpha^2 + \beta^2) & \alpha \cos \theta - \beta \sin \theta & \alpha \sin \theta + \beta \cos \theta & 1 - \frac{1}{2}(\alpha^2 + \beta^2) \end{pmatrix}. \quad (6.15)$$

It is straightforward to verify that for any values of (α, β, θ) , applying this matrix to the column four-vector $(1, 0, 0, 1)$ leaves it unchanged. The massless little group plays an major role in the classification of irreducible representations of the PG. As before, $S(\alpha, \beta, \theta)$ denotes the group element or its action on four-vectors, while $U(S(\alpha, \beta, \theta))$ denotes the corresponding operator acting on quantum states.

Finally, parity and time-reversal are discrete transformations that also belong to the PG. As they render the group non-simply connected, their treatment is often considered separately. In the following, parity is denoted by P , and its unitary representation acting on quantum states is denoted by Π . Parity commutes with rotations but reverses the direction of canonical boosts,

$$[P, R(\alpha, \beta, \gamma)] = 0, \quad PL(m, p, \theta, \phi) = L(m, p, \pi - \theta, \pi + \phi)P. \quad (6.16)$$

Time-reversal, on the other hand, will not be discussed in this work.

6.2 One-body Helicity States

To start with, let us focus on massive particles. As mentioned, these are classified according to their eigenvalue for both Casimir operators of the PG. Any state $|\psi; m; s\rangle$ such that

$$P^2 |\psi; m; s\rangle = m^2 |\psi; m; s\rangle \quad \text{and} \quad W^2 |\psi; m; s\rangle = -m^2 s(s+1) |\psi; m; s\rangle \quad (6.17)$$

is a possible state to describe a particle of mass m and spin s . To write the actual state of the particle, one has to resort to complete sets of states in which it can be decomposed. Two different complete sets will be introduced.

6.2.1 The one-body canonical states

The first set is filled with the common eigenstates of the third component of the Pauli-Lubanski vector W_3 and of the four P_μ operators. In the following, such common eigenstates, referred to as *one-body canonical states*, will be denoted $|m; p\theta\phi; sm_s\rangle$. The labels in the notation provides the eigenvalues of the aforementioned operators,

$$P^2 |m; p\theta\phi; sm_s\rangle = m^2 |m; p\theta\phi; sm_s\rangle, \quad (6.18a)$$

$$W^2 |m; p\theta\phi; sm_s\rangle = -m^2 s(s+1) |m; p\theta\phi; sm_s\rangle, \quad (6.18b)$$

$$P_0 |m; p\theta\phi; sm_s\rangle = \sqrt{m^2 + p^2} |m; p\theta\phi; sm_s\rangle, \quad (6.18c)$$

$$P_1 |m; p\theta\phi; sm_s\rangle = p \cos \phi \sin \theta |m; p\theta\phi; sm_s\rangle, \quad (6.18d)$$

$$P_2 |m; p\theta\phi; sm_s\rangle = p \sin \phi \sin \theta |m; p\theta\phi; sm_s\rangle, \quad (6.18e)$$

$$P_3 |m; p\theta\phi; sm_s\rangle = p \cos \theta |m; p\theta\phi; sm_s\rangle, \quad (6.18f)$$

$$W_3 |m; p\theta\phi; sm_s\rangle = m m_s |m; p\theta\phi; sm_s\rangle. \quad (6.18g)$$

Physically speaking, each p -canonical state has a definite mass, spin, four-momentum and spin projection along the z axis. The associated Lorentz-invariant orthonormality and completeness relations are written below,

$$\langle m; \bar{p}\bar{\theta}\bar{\phi}; s\bar{m}_s | m; p\theta\phi; sm_s \rangle = 2w \delta(p - \bar{p}) \delta(\phi - \bar{\phi}) \delta(\cos \theta - \cos \bar{\theta}) \delta_{m_s \bar{m}_s}, \quad (6.19)$$

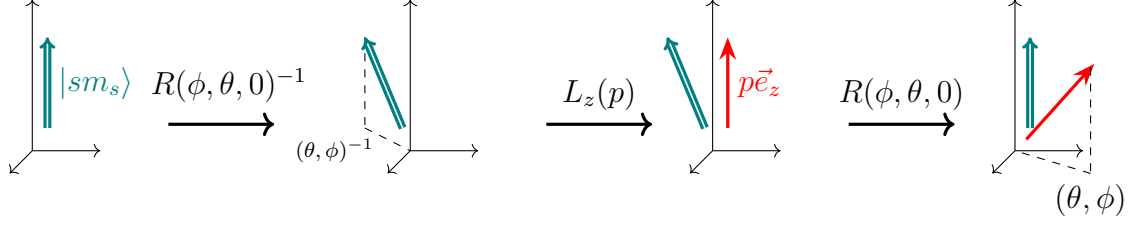


Figure 6.1: Graphic illustration for the definition (6.21) of one-body p -canonical states.

$$\sum_{m_s=-s}^s \int |m; p\theta\phi; sm_s\rangle \frac{d^3p}{2w} \langle m; p\theta\phi; sm_s| = \mathbf{1}, \quad (6.20)$$

where $w = \sqrt{m^2 + p^2}$. Normalisation conventions used in this document follow the ones from [160]. In the literature, one-body canonical states are often decomposed as the application of a so-called canonical boost on a rest state $|m; sm_s\rangle$,

$$\begin{aligned} |m; p\theta\phi; sm_s\rangle &= U(L(m, p, \theta, \phi)) |m; sm_s\rangle \\ &= U(R(\phi, \theta, 0)L_z(m, p)R(\phi, \theta, 0)^{-1}) |m; sm_s\rangle. \end{aligned} \quad (6.21)$$

By construction, rest states $|m; sm_s\rangle$ transform under rotations using the spin s irreducible representation of $SO(3)$. As a result, whenever applied on a rest state, rotations are concretely represented by the well-known Wigner D matrices [35],

$$U(R(\alpha, \beta, \gamma)) |m; sm_s\rangle = \sum_{m'_s=-s}^s D_{m'_s m_s}^s(\alpha, \beta, \gamma) |m; sm'_s\rangle. \quad (6.22)$$

Formula (6.21) provides an intuitive graphic interpretation for one-body canonical states which is illustrated in Figure 6.1. In the left-hand part of the diagram, the rest state is represented with a single green arrow which stands for its spin projection. The state is then subjected to a rotation and a boost which, notably, alter its momentum, represented by a red arrow. After successive transformations, as expected, the state ends with a momentum direction (θ, ϕ) and with a definite spin projection along the z axis. Apart from its visualisation use, this expression, combined with relation (6.21), also enables easy derivations of transformation rules under operations such as rotations, boosts and parity. The interested reader is referred to [161] for more details.

6.2.2 The one-body helicity states

Although one-body canonical states are abundantly used in quantum mechanics, especially in the non-relativistic limit, this set can not encompass massless particles. For this reason, a second set of state is introduced. The states are still chosen as the common eigenstates of the four P_μ generators but, instead of W_3 , these are taken as eigenstates of the helicity operator Λ . These states are named *one-body helicity states* and are denoted $|m; p\theta\phi; s\lambda\rangle$. Relations (6.18a) to (6.18f) remain true in terms of one-body helicity states, but (6.18g) is replaced by

$$\Lambda |m; p\theta\phi; s\lambda\rangle = \lambda |m; p\theta\phi; s\lambda\rangle. \quad (6.23)$$

States now have a definite spin projection along their momentum direction. The completeness and orthonormality relations for one-body helicity states are similar to that for one-body canonical states (same conventions are used),

$$\langle m; \bar{p}\bar{\theta}\bar{\phi}; s\bar{\lambda} | m; p\theta\phi; s\lambda \rangle = 2w \delta(p - \bar{p}) \delta(\phi - \bar{\phi}) \delta(\cos\theta - \cos\bar{\theta}) \delta_{\lambda\bar{\lambda}}, \quad (6.24)$$

$$\sum_{\lambda=-s}^s \int |m; p\theta\phi; s\lambda\rangle \frac{d^3p}{2w} \langle m; p\theta\phi; s\lambda| = \mathbf{1}. \quad (6.25)$$

As for canonical states, helicity ones can also be expressed in terms of a rest state on which boosts and rotations are applied,

$$\begin{aligned} |m; p\theta\phi; s\lambda\rangle &= U(L_h(m, p, \theta, \phi)) |m; s\lambda\rangle \\ &= U(R(\phi, \theta, 0) L_z(m, p)) |m; s\lambda\rangle. \end{aligned} \quad (6.26)$$

In comparison with relation (6.21), the canonical boost L has here been replaced by a helicity boost L_h . The graphic interpretation set up for relation (6.21) in Figure 6.1 can be adapted to fit with formula (6.26). The result is shown in Figure 6.2. Referring to the same graphical conventions, one can see that the state ends with a definite projection of the spin along the momentum direction instead of along the z axis. This feature is in agreement with the definition of the helicity operator. Before discussing the properties of one-body helicity states, let us draw the reader's attention to the fact that the 0 convention has been used in relation (6.26). Some other references consider the $-\phi$ convention [157, 159, 160],

$$|m; p\theta\phi; s\lambda\rangle_{-\phi} = U(R(\phi, \theta, -\phi) L_z(m, p)) |m; s\lambda\rangle. \quad (6.27)$$

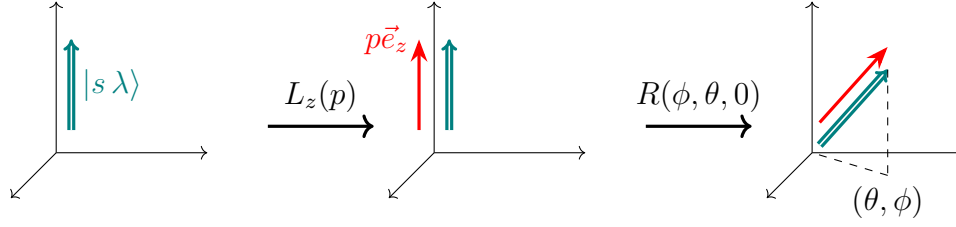


Figure 6.2: Graphic illustration for the definition (6.26) of one-body p -helicity states.

A priori, such a modified relation should result in a different definition for one-body helicity states. However, these two different definitions are shown to simply differ by a phase factor,

$$|m; p\theta\phi; s\lambda\rangle = e^{-i\lambda\phi} |m; p\theta\phi; s\lambda\rangle_{-\phi}. \quad (6.28)$$

Because physics is contained in the modulus squared of the state, this phase factor proves to be irrelevant in assessing a physical interpretation for one-body helicity states. Nevertheless, the user has to be conscious and consistent with the convention he employs, especially if he wants to superpose different helicity states. The current work will always use the zero convention.

The decomposition (6.26) also allows one to prove many properties about helicity states. Only a few of them will be recapped here. For more properties and demonstrations, the interested reader is referred to [157, 160, 161, 162]. The first property to be investigated is the transformation rule of helicity states under rotations. Simple algebra allows to show that

$$U(R(\alpha, \beta, \gamma)) |m; p\theta\phi; s\lambda\rangle = \pm e^{-i\xi\lambda} |m; p\theta'\phi'; s\lambda\rangle \quad (6.29)$$

where θ' , ϕ' and ξ satisfy $R(\phi', \theta', \xi) = R(\alpha, \beta, \gamma)R(\phi, \theta, 0)$. The phase $\exp(-i\xi\lambda)$ comes out while ensuring that the state, initially in 0 convention, ends in that same convention. Concerning the plus or minus sign, it is added to take into account the fact that, if at some point a 2π rotations is performed, it is to be identified to minus the identity for fermions. Property (6.29) is sometimes referred to as helicity rotational invariance, because the quantum number λ remains unchanged despite the rotation.

Secondly, the action of the parity transformation, Π , on one-body helicity states can be determined by making use of the commutation relations between parity, boosts and rotations. The following formula is obtained,

$$\Pi |m; p\theta\phi; s\lambda\rangle = \eta(-1)^{-s} |m; p(\pi - \theta)(\pi + \phi); s - \lambda\rangle. \quad (6.30)$$

Notice that the classical intuition that parity inverts particle's momentum and helicity is respected. Above, η refers to the intrinsic parity of the particle. This quantity defines how parity acts on the particle rest state,

$$\Pi |m; s\lambda\rangle = \eta |m; s\lambda\rangle. \quad (6.31)$$

It depends on the nature of the particle. In relation (6.30), both left- and right-hand side states are written in the zero convention. However, in many references, the right-hand side is written in a different convention, such as the π convention

$$\begin{aligned} |m; p(\pi - \theta)(\pi + \phi); s\lambda\rangle_\pi &= U(R(\pi + \phi, \pi - \theta, \pi))U(L_z(m, p)) |m; s\lambda\rangle \\ &= U(R(\phi, \theta, 0))U(R(0, \pi, 0))U(L_z(m, p)) |m; s\lambda\rangle \end{aligned} \quad (6.32)$$

or the opposite convention

$$\begin{aligned} |m; p(\pi - \theta)(\pi + \phi); s\lambda\rangle_- &= U(R(\phi, \theta, 0))U(L_{-z}(m, p)) |m; s - \lambda\rangle \\ \text{with } L_{-z}(m, p) &= R(0, \pi, 0)L_z(m, p)R(0, -\pi, 0). \end{aligned} \quad (6.33)$$

All these conventions being equal up to phase factors, they convey the same physical meaning,

$$\begin{aligned} |m; p(\pi - \theta)(\pi + \phi); s\lambda\rangle &= (-1)^\lambda |m; p(\pi - \theta)(\pi + \phi); s\lambda\rangle_\pi \\ &= (-1)^s |m; p(\pi - \theta)(\pi + \phi); s\lambda\rangle_-. \end{aligned} \quad (6.34)$$

These various conventions are introduced to simplify calculations that mixes helicity states with opposed directions. Such situations will for example be encountered in Section 6.3 where helicity states for two-body systems in their centre-of-mass frame (CoMF) are introduced.

Third, we focus on the application of a general Lorentz transformation L on an helicity state $|m; p\theta\phi; s\lambda\rangle$. The corresponding transformation rule reads as follows,

$$U(L) |m; p\theta\phi; s\lambda\rangle = \sum_{\lambda'=-s}^s D_{\lambda'\lambda}^s(\alpha_W, \beta_W, \gamma_W) |m; p'\theta'\phi'; s\lambda'\rangle. \quad (6.35)$$

Above, primed variables denote the components of the boosted momentum which are obtained by applying L on the initial four-momentum. In addition, $(\alpha_W, \beta_W, \gamma_W)$ denotes the Euler angles of a rotation R_W , named Wigner rotation, defined by the following combination of boosts,

$$R_W = (L_h(m, p', \theta', \phi'))^{-1} L L_h(m, p, \theta, \phi). \quad (6.36)$$

Relation (6.35) illustrates that, in general, the helicity of a massive state is not invariant under Lorentz transformations. The invariance of helicity under rotation (6.29) can be seen as a special case of property (6.35).

Finally, it is possible to switch from the one-body helicity basis to the one-body canonical one. Comparing relation (6.26) for helicity state to relation (6.21) for canonical state and using relation (6.22) provides the following transformation rule,

$$|m; p\theta\phi; s\lambda\rangle = \sum_{m_s=-s}^s D_{m_s\lambda}^s(\phi, \theta, 0) |m; p\theta\phi; sm_s\rangle. \quad (6.37)$$

This property allows the user to switch the complete set, based on its intended use.

Before closing this Section, let us insist on the fact that helicity states generalize very well to massless particles. In a common simplification of reality, massless particles are considered behaving as massive particles with only two spin projection, $+s$ and $-s$. This rule allows to infer the massless behaviour from the massive one. Complement 6.A goes beyond this simplification and provides more details about the distinction between massive and massless particles.

6.3 Two-body Helicity States

One-body helicity states (6.26) can be used to build a complete set of states for two-body systems. Because, in the following, these many-body states will be used to describe composite particles, we will focus on obtaining helicity states in the CoMF of the entire many-body system (the ECoMF). Properties of composite particles are most easily obtained in this frame: mass is given by the total energy of the state while spin is given by its total angular momentum. Before to dive into this description, let us shorten a bit notations. In the previous section, one-body states at rest were denoted $|m, sm_s\rangle$, a notation in which the mass, the spin and the spin projection of the particle were specified. In the following, the mass of the particle will be frequently omitted. By default, it will be assumed that the state $|s_i\lambda_i\rangle$ possesses the mass of the i^{th} particle. Similarly, in the following Sections, boosts along the z axis will be written without specifying any mass parameter. By default, this parameters will be supposed equal to the mass of the state on which the boost acts.

6.3.1 Helicity bases for two-body systems

Again, our analysis starts at the level of massive particle states. Differences in presence of massless particles will be discussed subsequently. Two particles are brought in their CoMF by

boosting them back-to-back,

$$|p\theta\phi; s_1\lambda_1 s_2\lambda_2\rangle = (-1)^{\lambda_2-s_2} U(R(\phi, \theta, 0)) [U(L_z(p)) |s_1\lambda_1\rangle \otimes U(R(0, \pi, 0)L_z(p)) |s_2\lambda_2\rangle] \quad (6.38a)$$

$$= (-1)^{\lambda_2-s_2} U(R(\phi, \theta, 0)L_z(p)) |s_1\lambda_1\rangle \otimes U(R(\pi + \phi, \pi - \theta, \pi)L_z(p)) |s_2\lambda_2\rangle. \quad (6.38b)$$

Above, p , θ and ϕ respectively denotes the modulus, the polar and the azimuthal angle of the momentum of the first particle in the ECoMF. Helicities λ_1 and λ_2 are defined in that same frame. The phase in front of the definition is mainly conventional [157] and results from the choice to assign to the one-body state with opposed momentum the opposite convention (6.33). Figure 6.3 schematically decomposes the successive transformations in definition (6.38a). By construction, states (6.38a) are eigenstates of particle 1 and 2 momentum operators. In the following, they will be referred to as *two-body p -helicity states*. Their orthonormalisation relation is

$$\langle \bar{p}\bar{\theta}\bar{\phi}; s_1\bar{\lambda}_1 s_2\bar{\lambda}_2 | p\theta\phi; s_1\lambda_1 s_2\lambda_2 \rangle = \frac{4W}{p} \delta(\bar{W} - W) \delta(\cos\bar{\theta} - \cos\theta) \delta(\bar{\phi} - \phi) \delta_{\bar{\lambda}_1\lambda_1} \delta_{\bar{\lambda}_2\lambda_2} \quad (6.39)$$

$$= \frac{4w_1(p)w_2(p)}{p^2} \delta(\bar{p} - p) \delta(\cos\bar{\theta} - \cos\theta) \delta(\bar{\phi} - \phi) \delta_{\bar{\lambda}_1\lambda_1} \delta_{\bar{\lambda}_2\lambda_2} \quad (6.40)$$

where $w_i(p)$ serves as a notation shortcut for $\sqrt{m_i^2 + p^2}$ and where $W = w_1(p) + w_2(p)$ is the total energy of the two-body state. If expression (6.38b) is more convenient for practical purposes, (6.38a) unveils that these states present a specific structure: they are obtained by rotating two-body states at rest with a reference orientation, here along the z axis,

$$|p; s_1\lambda_1 s_2\lambda_2\rangle = (-1)^{\lambda_2-s_2} (U(L_z(p)) |s_1\lambda_1\rangle \otimes U(R(0, \pi, 0)L_z(p)) |s_2\lambda_2\rangle). \quad (6.41)$$

A similar structure will reappear in the definition of helicity states for three-body systems in Chapter 8.

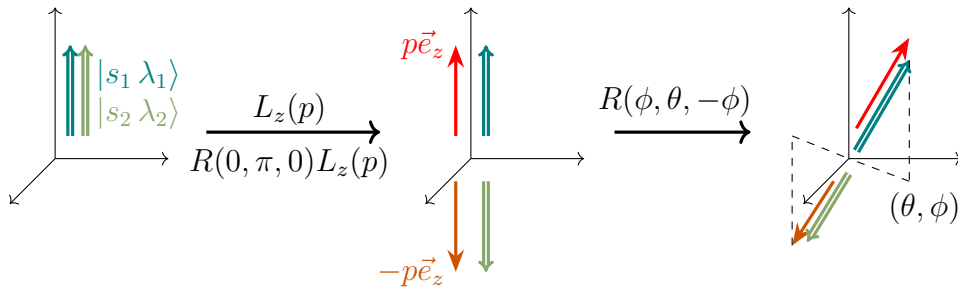


Figure 6.3: Schematic illustration for the definition of two-body p -helicity state (6.38a).

As already mentioned, states with a definite total angular momentum are expected. Such a property can be provided to two-body p -helicity states by weighting them with a Wigner D matrix and by integrating the result on angular degrees-of-freedom,

$$|p; JM; s_1 \lambda_1 s_2 \lambda_2\rangle = \sqrt{\frac{2J+1}{4\pi}} \int d\cos\theta d\phi D_M^{J*}{}_{\lambda_1-\lambda_2}(\phi, \theta, 0) |p\theta\phi; s_1 \lambda_1 s_2 \lambda_2\rangle. \quad (6.42)$$

In the following, these states will be referred to as *two-body J -helicity states*. The prefactor is introduced to ensure a standard normalisation,

$$\langle \bar{p}; \bar{J}\bar{M}; s_1 \bar{\lambda}_1 s_2 \bar{\lambda}_2 | p; JM; s_1 \lambda_1 s_2 \lambda_2 \rangle = \frac{4W}{p} \delta(\bar{W} - W) \delta_{\bar{J}J} \delta_{\bar{M}M} \delta_{\bar{\lambda}_1 \lambda_1} \delta_{\bar{\lambda}_2 \lambda_2} \quad (6.43)$$

$$= \frac{4w_1(p)w_2(p)}{p^2} \delta(\bar{p} - p) \delta_{\bar{J}J} \delta_{\bar{M}M} \delta_{\bar{\lambda}_1 \lambda_1} \delta_{\bar{\lambda}_2 \lambda_2}. \quad (6.44)$$

Of course, definition (6.42) is only relevant for $J \geq |\lambda_1 - \lambda_2|$. It can be shown that, under rotations, two-body J -helicity states follows the spin J irreducible representation of $SO(3)$ [161, 163], meaning that this state indeed has a total angular momentum J . For further use, let us mention that definition (6.42) can be inverted, expressing two-body p -helicity states as a linear combination of two-body J -helicity states [162],

$$|p\theta\phi; s_1 \lambda_1 s_2 \lambda_2\rangle = \sum_{J=|\lambda_1-\lambda_2|}^{\infty} \sum_{M=-J}^J \sqrt{\frac{2J+1}{4\pi}} D_M^J{}_{\lambda_1-\lambda_2}(\phi, \theta, 0) |p; JM; s_1 \lambda_1 s_2 \lambda_2\rangle. \quad (6.45)$$

Other properties of these states are abundantly described in the literature [152, 157, 160, 161, 162]. Their behaviour under parity and permutation of particles, denoted \mathbb{P}_{12} , will be reminded here for further use,

$$\Pi |p; JM; s_1 \lambda_1 s_2 \lambda_2\rangle = \eta_1 \eta_2 (-1)^{J-s_1-s_2} |p; JM; s_1 - \lambda_1 s_2 - \lambda_2\rangle, \quad (6.46)$$

$$\mathbb{P}_{12} |p; JM; s \lambda_1 s \lambda_2\rangle = (-1)^{J+2s} |p; JM; s \lambda_2 s \lambda_1\rangle. \quad (6.47)$$

Above, η_i is the intrinsic parity of the i^{th} particle. Symmetry having to be implemented only for identical particles, s_1 and s_2 have been taken equal each-other in relation (6.47). These two properties illustrate that two-body J -helicity states are neither parity eigenstates nor (anti)symmetric by themselves. Parity eigenstates are obtained by superposing states with opposed helicity signs. Non-normalised symmetric (anti-symmetric) states are obtained by

applying the two-body symmetriser \mathbb{S}_2 (anti-symmetriser \mathbb{A}_2),

$$\mathbb{S}_2 = \mathbb{1} + \mathbb{P}_{12}, \quad \mathbb{A}_2 = \mathbb{1} - \mathbb{P}_{12}. \quad (6.48)$$

As agreed, helicity states have been written in the zero convention. Switching the convention to the " $-\phi$ " one results in a different phase convention for p -helicity states. Nevertheless, provided that angles of the Wigner D matrix in definition (6.42) are adapted consequently, it can be shown that two-body J -helicity states are not affected.

In presence of massless particles, the results presented above remains correct up to a few adjustments. First in definition (6.38a)-(6.38b), the conventional phase has to be adapted to remove any spin occurrence, such a quantum number being formally undefined for massless particles. Following the usual misuse that massless particles have spin degrees-of-freedom with forbidden intermediary projections, it seems appropriate to replace s_2 by $|\lambda_2|$. Secondly, relations (6.46) and (6.47) only accounts for massive particles. It can be shown that, for massless ones, the factor $(-1)^{-s_1-s_2}$ has to be replaced by $(-1)^{\lambda_1+\lambda_2}$ while the $(-1)^{2s}$ factor from (6.47) has to be replaced by $(-1)^{2|\lambda_1|}$. Notice that, as long as helicities are integers, one can naively use massive relations with $\lambda_i = \pm s_i$ to deal with massless particles. The case of helicity states for two massless particles is also briefly discussed at the end of Complement 6.A.

Two-body p - and J -helicity states are not the two only complete sets able to describe two-body systems at rest. For massive particles, one can replace in definition (6.38b) each occurrences of p -helicity states by p -canonical ones. It results in the following definition for the so-called *two-body p -canonical states* [161],

$$\begin{aligned} |p\phi\theta; s_1 m_{s_1} s_2 m_{s_2}\rangle &= U(R(\phi, \theta, 0)L_z(p)R^{-1}(\phi, \theta, 0)) |s_1 m_{s_1}\rangle \\ &\otimes U(R(\pi + \phi, \pi - \theta, 0)L_z(p)R^{-1}(\pi + \phi, \pi - \theta, 0)) |s_2 m_{s_2}\rangle. \end{aligned} \quad (6.49)$$

These states are then used to define *two-body J -canonical states* through intermediary spin and spatial angular momentum couplings,

$$\begin{aligned} |p; JM; \ell s; s_1 s_2\rangle &= \sum_{m_\ell, m_s, m_{s_1}, m_{s_2}} (\ell m_\ell s m_s | JM)(s_1 m_{s_1} s_2 m_{s_2} | s m_s) \\ &\int d\cos\theta d\phi Y_{m_\ell}^\ell(\theta, \phi) |p\theta\phi; s_1 m_{s_1} s_2 m_{s_2}\rangle. \end{aligned} \quad (6.50)$$

Above, $(j_1 m_1 j_2 m_2 | j_3 m_3)$ refers to a Clebsh-Gordan coefficient and $Y_{m_\ell}^\ell(\theta, \phi)$ to a spherical harmonic. Because of the appearance of an orbital angular momentum quantum number ℓ , this definition is often used for in non-relativistic treatments. The interested reader will find a

description of properties about two-body canonical states in reference [161]. It is possible to relate two-body J -canonical states to two-body J -helicity states,

$$|p; JM; s_1 \lambda_1 s_2 \lambda_2\rangle = \sum_{s=|s_1-s_2|}^{s_1+s_2} \sum_{\ell=|J-s|}^{J+s} \sqrt{\frac{2\ell+1}{2J+1}} (s_1 \lambda_1 s_2 - \lambda_2 |s \lambda_1 - \lambda_2) \quad (6.51)$$

$$(\ell 0 s \lambda_1 - \lambda_2 |J \lambda_1 - \lambda_2) |p; JM; \ell s; s_1 s_2\rangle.$$

This relation allows to easily switch from one to the other set of states. For instance, it has been used in [152] to describe two-gluon glueballs in constituent approaches.

6.3.2 Decomposition of a physical two-body state in J -helicity states

Two-body J -helicity states can be used to model two-body composite particles. In the ECoMF, any two-body state with spin J and helicity quantum numbers can be decomposed as an integral on internal momentum degree-of-freedom of two-body p -helicity states. For two-body systems, the internal motion is ruled by the relative momentum $\mathbf{p} = (\mathbf{p}_1 - \mathbf{p}_2)/2$ whose modulus and angles have already been denoted p , θ and ϕ . Let us start by decomposing a generic two-body state in the ECoMF, denoted $|\Phi; s_1 \lambda_1 s_2 \lambda_2\rangle$, as a combination of two-body p -helicity states. Using the completeness relation of the latter, one gets

$$|\Phi; s_1 \lambda_1 s_2 \lambda_2\rangle = \int \frac{p^2 dp d\cos\theta d\phi}{4w_1(p)w_2(p)} \Phi(p, \theta, \phi) |p\theta\phi; s_1 \lambda_1 s_2 \lambda_2\rangle \quad (6.52)$$

where

$$\Phi(p, \theta, \phi) = \langle p\theta\phi; s_1 \lambda_1 s_2 \lambda_2 | \Phi; s_1 \lambda_1 s_2 \lambda_2 \rangle \quad (6.53)$$

is the two-body helicity-momentum wave function of the state. The Jacobian factor in (6.52) ensures consistence with the normalisation of two-body p -helicity states (6.40). Without additional requirements, this state has not the expected definite total angular momentum J . However, the definition of two-body J -helicity states proved that this property can be supplied by imposing the angular dependence of $\Phi(p, \theta, \phi)$,

$$\Phi_M^J(p, \theta, \phi) = \sqrt{\frac{2J+1}{4\pi}} \Psi(p) D_{M \lambda_1 - \lambda_2}^{J*}(\phi, \theta, 0). \quad (6.54)$$

The function $\Psi(p)$ can be understood as a radial helicity-momentum wave function. Replacing Φ by Φ_M^J in expression (6.52) results in the decomposition of a generic two-body helicity state

with total angular momentum J , denoted $|\Psi; JM; s_1 \lambda_1 s_2 \lambda_2\rangle$, in two-body J -helicity states,

$$|\Psi; JM; s_1 \lambda_1 s_2 \lambda_2\rangle = \int \frac{p^2 dp}{4w_1(p)w_2(p)} \Psi(p) |p; JM; s_1 \lambda_1 s_2 \lambda_2\rangle. \quad (6.55)$$

States $|\Psi; JM; s_1 \lambda_1 s_2 \lambda_2\rangle$ can be used to model spin J two-body composite particles. If the composite state is made of identical particles or is expected to possess a parity quantum-number, the above discussion has to be slightly adapted. The structure (6.55) still applies but two-body J -helicity states in the right-hand side have to be replaced by parity and/or symmetry eigenstates which are obtained using properties (6.46) and (6.47). Concerning normalisation, states $|\Psi; JM; s_1 \lambda_1 s_2 \lambda_2\rangle$ are expected to have a unit normalisation,

$$\langle \Psi; JM; s_1 \lambda_1 s_2 \lambda_2 | \Psi; JM; s_1 \lambda_1 s_2 \lambda_2 \rangle = 1. \quad (6.56)$$

Using expression (6.55) and orthonormalisation of two-body J -helicity states (6.44), one can transfer this normalisation condition to the $\Psi(p)$ wave function,

$$\int \frac{p^2 dp}{4w_1(p)w_2(p)} |\Psi(p)|^2 = 1. \quad (6.57)$$

For convenience, it is worth introducing a modified radial helicity-momentum wave function, denoted $\Xi(p)$ that includes the Jacobian factors from (6.57),

$$\Xi(p) = \frac{p \Psi(p)}{2\sqrt{w_1(p)w_2(p)}}. \quad (6.58)$$

In terms of $\Xi(p)$, the normalisation condition (6.57) significantly simplifies

$$\int dp |\Xi(p)|^2 = 1, \quad (6.59)$$

while (6.55) has to be slightly adapted,

$$|\Psi; JM; s_1 \lambda_1 s_2 \lambda_2\rangle = \int \frac{p dp}{2\sqrt{w_1(p)w_2(p)}} \Xi(p) |p; JM; s_1 \lambda_1 s_2 \lambda_2\rangle. \quad (6.60)$$

Notice that, Ψ having to remain finite for all p , Ξ must necessary cancel at $p = 0$ for massive particles. Further tests show that this condition stays required in the massless case.

Complement 6.A Helicity states for massless particles

In Sections 6.2 and 6.3, massive particle states were discussed. For massless ones, the Pauli-Lubanski Casimir is identically zero and helicity proves to be Lorentz invariant. As a result, a general massless state $|\phi; 0; \lambda\rangle$ stays by definition eigenstate of the squared-momentum operator but with a null eigenvalue. It is also defined as eigenstate of the helicity operator,

$$P^2 |\psi; 0; \lambda\rangle = 0 |\psi; 0; \lambda\rangle, \quad \Lambda |\psi; 0; \lambda\rangle = \lambda |\psi; 0; \lambda\rangle. \quad (6.61)$$

If helicity is truly Lorentz invariant, it is nevertheless reversed by a parity transformation, meaning that massless states always come by pairs, one with helicity λ and the other one with helicity $-\lambda$. This feature justifies the aforementioned simplification of reality: although spin is not formally defined in the massless case, these two states with same nature but opposed helicities are often considered as the two facets of a spin λ particle whose intermediary projections are forbidden. This is the case when someone consider left-handed and right-handed photons as a unique spin 1 particle whose 0 projection is forbidden.

To describe the actual state of a massless particle, complete orthonormal sets are again necessary. Since massless particles have no rest frame, the corresponding states are defined as eigenstates of the helicity operator, and only the p -helicity states are suitable to describe them. These are eigenstates of the exact same operators than massive ones but with zero as eigenvalue for both Casimir operators,

$$P^2 |0; p\theta\phi; s\lambda\rangle = 0 |0; p\theta\phi; s\lambda\rangle, \quad W^2 |0; p\theta\phi; s\lambda\rangle = 0 |0; p\theta\phi; s\lambda\rangle. \quad (6.62)$$

Above, s rather specifies which values λ can take than is a true quantum number. Massless p -helicity states significantly differ from massive ones in the sense that, because massless particles cannot be taken at rest, relation (6.26) cannot remain valid for these. A similar relation can nevertheless be obtained by turning the rest state into another reference state having a more suitable four-momentum for massless particles. Choosing this reference four-momentum as $k = (1, 0, 0, 1)$ and denoting the associated reference state $|0; s\lambda\rangle$, the adapted relation reads

$$\begin{aligned} |0; p\theta\phi; s\lambda\rangle &= U(L_h(0, p, \theta, \phi)) |0; s\lambda\rangle \\ &= U(R(\phi, \theta, 0)L_z(0, p)) |0; s\lambda\rangle. \end{aligned} \quad (6.63)$$

Notice that, because $|0; s\lambda\rangle$ has a unit spatial momentum along the z axis, this state proves to be eigenstate of both W_3 and Λ , these two operators being equal in the current circumstances.

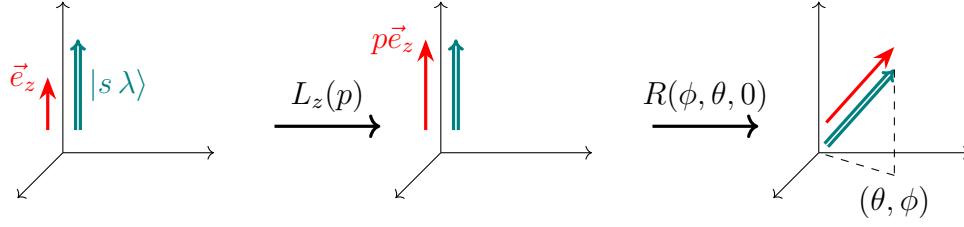


Figure 6.4: Graphic illustration for the definition (6.63) of massless one-body p -helicity states.

Because of this adaptation, the graphic interpretation of massive p -helicity states must slightly be adapted, the initial state having a non-zero spatial momentum. The new diagram is shown in Figure 6.4. Apart from this modification in the initial state, both diagrams are to be understood similarly.

Let us now focus on the adaptation of properties (6.31) and (6.35) to massless particles. First, as the definition of intrinsic parity (6.31) relies on rest states, it must be adapted for a massless reference state. Applying parity on this state reverses its non-zero spatial momentum and, as already mentioned, opposes the helicity quantum number. It results in the following relation for the action of parity on a reference state,

$$\Pi |0; s\lambda\rangle = \eta U(R(0, \pi, 0)) |0; s - \lambda\rangle \quad (6.64)$$

where η is defined as the intrinsic parity of the massless particle. This modification considered, one can roughly follow the same calculation steps than in the massive case to demonstrate that

$$\Pi |0; p\theta\phi; s\lambda\rangle = \eta(-1)^\lambda |0; p(\pi - \theta)(\pi + \phi); s - \lambda\rangle. \quad (6.65)$$

Formula (6.65) replaces (6.30) in presence of massless particles. The discussion of relation (6.35) must also partially be revised. In the massive case, the Wigner rotations R_W defined in relation (6.36) is shown to belong to $SO(3)$, namely the massive little group. Setting $m = 0$, the combination (6.36) turns out to no longer belong to the massive little group but to the massless one, $ISO(2)$. Therefore, the transformation is no longer parameterised by Euler angles but by three $ISO(2)$ parameters, such as the α , β and θ parameters suggested in reference [159], and the action of R_W on physical states is no longer provided by $SU(2)$ Wigner D matrices but instead reduces to [164]

$$D_{\lambda'\lambda}^s(\alpha_W, \beta_W, \theta_W) = e^{i\theta_W\lambda} \delta_{\lambda'\lambda}. \quad (6.66)$$

The $\delta_{\lambda'\lambda}$ factor ensures that, as expected for massless states, the helicity quantum number remains invariant while boosting the state. This replacement done, relation (6.35) can be freely

used even while dealing with massless particles. Although R_W is no longer a true spatial rotation, this transformation is still called Wigner rotation through misuse of language.

As already mentioned in the main text, helicity states for two massless bodies behave quite similarly to those of massive ones. The demonstrations are very similar to their massive counterparts, with the main differences generally arising from the phase factor in definition (6.38), which must be adapted by replacing s_2 with $|\lambda_2|$. The one-body parity transformation rule (6.30) must also be replaced by the massless version (6.65). The rest of the demonstrations remain analogous to the massive case since the reference helicity states for the massless particles, $|0; s\lambda\rangle$, are also J_3 eigenstates.

This chapter in the context of a thesis

This chapter introduces the second major topic of my PhD thesis: the helicity formalism. It lays the groundwork by providing a self-contained overview, and presenting a broad set of key concepts and properties. While the results discussed are not original at this stage, they are essential for preparing the developments that follow and the application to two- and three-gluon glueballs.

Chapter 7

Two-gluon Glueballs: Set Up of a Methodology

One of the earliest predictions of Quantum Chromodynamics (QCD) is the existence of colour-singlet pure-gauge states, introduced in Section 4.3.4 as glueballs [1]. Despite this theoretical prediction, a consensus on their properties and definitive experimental evidence remain elusive. Two-gluon glueball states have been extensively studied both theoretically [3, 165] and experimentally [2, 165]. Theoretical results have been obtained using various phenomenological approaches, functional methods, and LQCD. On the experimental side, notable experimental efforts by collaborations such as PANDA, Crystal Barrel, WA102 or BESIII continue the search for these states. In contrast, three-gluon glueballs have received relatively little attention due to the technical complexity involved. On the theory side, the LQCD spectrum is expected to include three-gluon states [166, 167, 168, 169]. Experimentally, the possible observation of odderon exchange at TOTEM is still debated [170].

This Chapter aims to describe two-gluon systems within the framework of constituent models. Constituent gluons transform under $SU(3)_c$ with its octet (or adjoint) representation, denoted 8, leading to the following decompositions for two- and three-gluon systems [138]

$$8 \otimes 8 = 1_S \oplus \dots \qquad 8 \otimes 8 \otimes 8 = 1_S \oplus 1_{AS} \oplus \dots \qquad (7.1)$$

These decompositions indicate the possibility of forming bound states of two and three constituent gluons, so-called two- and three-gluon glueballs, in constituent approaches. The dynamics of these bound states are implemented using a phenomenological but QCD inspired Hamiltonian. Properties of constituent particles often differ from their QCD counterparts (for instance, as mentioned in Section 4.3.3, constituent quarks are often treated as heavier than their QCD

equivalents). For two-gluon glueballs, it has been shown in reference [152] that constituent gluons have to be considered as massless particles with helicity degrees-of-freedom in order to reproduce results from LQCD calculations. A more detailed description of constituent gluon properties is deferred to later section.

Although studies of two-gluon glueballs within constituent approaches already exists in the literature [171, 51, 152], the further extension to three-gluon glueballs necessitates introducing a methodology better suited for three-gluons systems. This Chapter applies the helicity formalism to compute the spectrum of two-gluon glueballs. As for the previous chapter, it builds upon the text from reference [158]. Section 7.1 develops a general methodology to perform bound-state calculations within the helicity formalism. Subsequently, Section 7.2 applies this methodology to the description of two-gluon glueballs.

7.1 Calculations with physical two-body states

The following developments aims to evaluate matrix elements of observables, such as Hamiltonians, on composite particle states. It focuses on unsymmetrical two-body J -helicity states (6.60) but can easily be adapted to symmetrised odd/even helicity states. States (6.60) being written in momentum representation, observables that depends on momentum variables prove to be easier to evaluate. Let us consider an observable $\mathcal{O}(\hat{p})$ that only depends on the modulus of the relative momentum (only spherically symmetric variables are investigated). Let us evaluate $\mathcal{O}(\hat{p})$ on $|\Psi; JM; \lambda_1 \lambda_2\rangle$,

$$\langle \Psi; JM; s_1 \bar{\lambda}_1 s_2 \bar{\lambda}_2 | \mathcal{O}(\hat{p}) | \Psi; JM; s_1 \lambda_1 s_2 \lambda_2 \rangle = \int \frac{\bar{p} d\bar{p}}{2\sqrt{w_1(\bar{p})w_2(\bar{p})}} \frac{p dp}{2\sqrt{w_1(p)w_2(p)}} \Xi(\bar{p})^* \Xi(p) \langle \bar{p}; JM; s_1 \bar{\lambda}_1 s_2 \bar{\lambda}_2 | \mathcal{O}(\hat{p}) | p; JM; s_1 \lambda_1 s_2 \lambda_2 \rangle. \quad (7.2)$$

Two-body J -helicity states being by construction eigenstates of p , the action of $\mathcal{O}(p)$ reduces to a simple scalar multiplication. Using orthonormality relation (6.44), one gets

$$\langle \Psi; JM; s_1 \bar{\lambda}_1 s_2 \bar{\lambda}_2 | \mathcal{O}(\hat{p}) | \Psi; JM; s_1 \lambda_1 s_2 \lambda_2 \rangle = \delta_{\lambda_1 \bar{\lambda}_1} \delta_{\lambda_2 \bar{\lambda}_2} \int dp |\Xi(p)|^2 \mathcal{O}(p). \quad (7.3)$$

A similar expression accounts for symmetrised odd/even helicity state as long as these are correctly orthonormalised.

The evaluation of operators that depend on position variables proves to be more difficult to handle. Let us consider $\mathcal{O}(\hat{r})$ an operator that only depend on the modulus of the relative position (again, the emphasis is put on spherically symmetric observables), one may require to

evaluate it on the composite particle state,

$$\begin{aligned} & \langle \Psi \bar{J} \bar{M}; s_1 \bar{\lambda}_1 s_2 \bar{\lambda}_2 | \mathcal{O}(\hat{r}) | \Psi; JM; s_1 \lambda_1 s_2 \lambda_2 \rangle = \\ & \int \frac{\bar{p} d\bar{p}}{2\sqrt{w_1(\bar{p})w_2(\bar{p})}} \frac{p dp}{2\sqrt{w_1(p)w_2(p)}} \Xi(\bar{p})^* \Xi(p) \langle \bar{p}; \bar{J} \bar{M}; s_1 \bar{\lambda}_1 s_2 \bar{\lambda}_2 | \mathcal{O}(\hat{r}) | p; JM; s_1 \lambda_1 s_2 \lambda_2 \rangle. \end{aligned} \quad (7.4)$$

Above, different total angular momenta J and \bar{J} were considered. This modification has been implemented for further use while studying the case of three-body systems. Two-body J -helicity states being not position eigenstate, the evaluation of $\mathcal{O}(\hat{r})$ on $|\bar{p}; JM; s_1 \lambda_1 s_2 \lambda_2\rangle$ requires more developments than the evaluation of $\mathcal{O}(\hat{p})$. Let us first switch of basis and develop two-body J -helicity states into the canonical basis using relation (6.51),

$$\begin{aligned} & \langle \bar{p}; \bar{J} \bar{M}; s_1 \bar{\lambda}_1 s_2 \bar{\lambda}_2 | \mathcal{O}(\hat{r}) | p; JM; s_1 \lambda_1 s_2 \lambda_2 \rangle = \\ & \sum_{\bar{s}=|s_1-s_2|}^{s_1+s_2} \sum_{\bar{\ell}=|J-\bar{s}|}^{J+\bar{s}} \mathcal{C}_{\bar{\ell}\bar{s};\bar{\lambda}_1\bar{\lambda}_2}^{\bar{J};s_1s_2} \sum_{s=|s_1-s_2|}^{s_1+s_2} \sum_{\ell=|J-s|}^{J+s} \mathcal{C}_{\ell s;\lambda_1\lambda_2}^{J;s_1s_2} \langle \bar{p}; \bar{J} \bar{M}; \bar{\ell} \bar{s}; s_1 s_2 | \mathcal{O}(\hat{r}) | p; JM; \ell s; s_1 s_2 \rangle \end{aligned} \quad (7.5)$$

with the following notation shortcut

$$\mathcal{C}_{\ell s;\lambda_1\lambda_2}^{J;s_1s_2} = \sqrt{\frac{2\ell+1}{2J+1}} (s_1 \lambda_1 s_2 - \lambda_2 | s \lambda_1 - \lambda_2) (\ell 0 s \lambda_1 - \lambda_2 | J \lambda_1 - \lambda_2). \quad (7.6)$$

The problem now reduces to the evaluation of $\mathcal{O}(\hat{r})$ on the more traditional canonical states. Using the definition (6.50) of two-body J -canonical states in terms of p -ones, one obtains

$$\begin{aligned} & \langle \bar{p}; \bar{J} \bar{M}; \bar{\ell} \bar{s}; s_1 s_2 | \mathcal{O}(\hat{r}) | p; JM; \ell s; s_1 s_2 \rangle \\ & = \sum_{\bar{m}'_\ell \bar{m}'_s \bar{m}'_{s_1} \bar{m}'_{s_2}} (\bar{\ell} \bar{m}'_\ell \bar{s} \bar{m}'_s | \bar{J} \bar{M}) (s_1 \bar{m}'_{s_1} s_2 \bar{m}'_{s_2} | \bar{s} \bar{m}'_s) \int d\cos\bar{\theta}' d\bar{\phi}' Y_{\bar{m}'_\ell}^{\bar{\ell}*}(\bar{\theta}', \bar{\phi}') \\ & \quad \sum_{m'_\ell m'_s m'_{s_1} m'_{s_2}} (\ell m'_\ell s m'_s | JM) (s_1 m'_{s_1} s_2 m'_{s_2} | s m'_s) \int d\cos\theta' d\phi' Y_{m'_\ell}^\ell(\theta', \phi') \\ & \quad \langle \bar{p} \bar{\theta}' \bar{\phi}'; s_1 \bar{m}'_{s_1} s_2 \bar{m}'_{s_2} | \mathcal{O}(\hat{r}) | p \theta' \phi'; s_1 m'_{s_1} s_2 m'_{s_2} \rangle \end{aligned} \quad (7.7)$$

Because spin degrees-of-freedom are uncorrelated from spatial ones in canonical states and because the observable $\mathcal{O}(\hat{r})$ does not affect them, the right-hand side residual matrix elements are proportional to $\delta_{\bar{m}'_{s_1} m'_{s_1}} \delta_{\bar{m}'_{s_2} m'_{s_2}}$. Concerning spatial degrees-of-freedom, the action of the

observable can be evaluated using a result from reference [172]¹,

$$\begin{aligned} & \langle \bar{p}\bar{\theta}'\bar{\phi}'; s_1\bar{m}'_{s_1} s_2\bar{m}'_{s_2} | \mathcal{O}(\hat{r}) | p\theta'\phi'; s_1m'_{s_1} s_2m'_{s_2} \rangle \\ &= \delta_{\bar{m}'_{s_1}m'_{s_1}} \delta_{\bar{m}'_{s_2}m'_{s_2}} 4\sqrt{w_1(\bar{p})w_2(\bar{p})w_1(p)w_2(p)} \sum_{\ell''m''_\ell} Y_{m''_\ell}^{\ell''}(\bar{\theta}', \bar{\phi}') Y_{m''_\ell}^{\ell''*}(\theta', \phi') \mathcal{O}_{\ell''}(\bar{p}, p) \end{aligned} \quad (7.8)$$

where

$$\mathcal{O}_\ell(\bar{p}, p) = \frac{2}{\pi} \int_0^\infty j_\ell(\bar{p}r) \mathcal{O}(r) j_\ell(pr) r^2 dr, \quad (7.9)$$

$j_\ell(x)$ being spherical Bessel functions. Making use of spherical harmonics and Clebsh-Gordan coefficients properties, one gets

$$\begin{aligned} & \langle \bar{p}; \bar{J}\bar{M}; \bar{\ell}\bar{s}; s_1s_2 | \mathcal{O}(\hat{r}) | p; JM; \ell s; s_1s_2 \rangle \\ &= 4\sqrt{w_1(\bar{p})w_2(\bar{p})w_1(p)w_2(p)} \mathcal{O}_\ell(\bar{p}, p) \delta_{\bar{J}J} \delta_{\bar{M}M} \delta_{\bar{\ell}\ell} \delta_{\bar{s}s}. \end{aligned} \quad (7.10)$$

This expression is inserted in (7.5) and leads to the following formula for the evaluation of $\mathcal{O}(\hat{r})$ on two-body J -helicity states,

$$\begin{aligned} & \langle \bar{p}; \bar{J}\bar{M}; s_1\bar{\lambda}_1 s_2\bar{\lambda}_2 | \mathcal{O}(\hat{r}) | p; JM; s_1\lambda_1 s_2\lambda_2 \rangle \\ &= \delta_{\bar{J}J} \delta_{\bar{M}M} \sum_{s=|s_1-s_2|}^{s_1+s_2} \sum_{\ell=|J-s|}^{J+s} \mathcal{C}_{\bar{\ell}s; \bar{\lambda}_1 \bar{\lambda}_2}^{J; s_1 s_2} \mathcal{C}_{\ell s; \lambda_1 \lambda_2}^{J; s_1 s_2} 4\sqrt{w_1(\bar{p})w_2(\bar{p})w_1(p)w_2(p)} \mathcal{O}_\ell(\bar{p}, p). \end{aligned} \quad (7.11)$$

Finally, back to the state for the composite particle, expression (7.4) becomes

$$\begin{aligned} & \langle \Psi; \bar{J}\bar{M}; s_1\bar{\lambda}_1 s_2\bar{\lambda}_2 | \mathcal{O}(\hat{r}) | \Psi; JM; s_1\lambda_1 s_2\lambda_2 \rangle \\ &= \delta_{\bar{J}J} \delta_{\bar{M}M} \sum_{s=|s_1-s_2|}^{s_1+s_2} \sum_{\ell=|J-s|}^{J+s} \mathcal{C}_{\bar{\ell}s; \bar{\lambda}_1 \bar{\lambda}_2}^{J; s_1 s_2} \mathcal{C}_{\ell s; \lambda_1 \lambda_2}^{J; s_1 s_2} \int p dp \bar{p} d\bar{p} \Xi(\bar{p})^* \Xi(p) \mathcal{O}_\ell(\bar{p}, p). \end{aligned} \quad (7.12)$$

As expected due to angular momentum conservation, matrix elements for central potentials are proportional to $\delta_{\bar{J}J} \delta_{\bar{M}M}$. Moreover, as soon as non-zero, these are also independent of the total angular momentum projection M . The evaluation of position matrix elements on symmetrised odd/even helicity states only differs from the one on two-body J -helicity by the coefficients of the expansion in canonical states. Relation (7.12) remains valid provided that the expression (7.6) for \mathcal{C} coefficients is correctly adapted.

¹ The result from [172] must slightly be adapted in two different ways. Firstly, our normalisation conventions being different, a kinematic factor have been added. Secondly, a property of Legendre polynomials is used to get spherical harmonics back.

Analytical expressions of $\mathcal{O}_\ell(\bar{p}, p)$ for different potentials are given in [172]. For instance, in presence of a Yukawa potential $\mathcal{O}(r) = -\alpha e^{-\eta r}/r$, one gets

$$\mathcal{O}_\ell(\bar{p}, p) = -\frac{\alpha}{\pi \bar{p} p} Q_\ell \left(\frac{\bar{p}^2 + p^2 + \eta^2}{2\bar{p} p} \right) \quad (7.13)$$

with $Q_\ell(x)$ a second kind Legendre function [36]. This expression can be naively plugged into the integral from (7.12) without any extra precaution, even for $\eta = 0$. As a result, the treatment of Coulomb interactions only require the evaluation of the following integrals,

$$\int p dp \bar{p} d\bar{p} \Xi(\bar{p})^* \Xi(p) \mathcal{O}_\ell(\bar{p}, p) = -\frac{\alpha}{\pi} \int dp d\bar{p} \Xi(\bar{p})^* \Xi(p) Q_\ell \left(\frac{\bar{p}^2 + p^2}{2\bar{p} p} \right). \quad (7.14)$$

Although they present a logarithmic divergence for $p = \bar{p}$, Gaussian quadrature allows for a reasonably efficient evaluation of these integrals. This is even easier by introducing a new set of coordinates,

$$v = \bar{p} + p, \quad \bar{v} = \bar{p} - p, \quad dvd\bar{v} = 2dpd\bar{p}. \quad (7.15)$$

As a result, equation (7.14) becomes

$$\begin{aligned} & \int p dp \bar{p} d\bar{p} \Xi(\bar{p})^* \Xi(p) \mathcal{O}_\ell(\bar{p}, p) \\ &= -\frac{\alpha}{2\pi} \int_0^\infty dv \int_{-v}^v d\bar{v} \Xi \left(\frac{v + \bar{v}}{2} \right)^* \Xi \left(\frac{v - \bar{v}}{2} \right) Q_\ell \left(\frac{v^2 + \bar{v}^2}{v^2 - \bar{v}^2} \right). \end{aligned} \quad (7.16)$$

The situation is more delicate concerning linear potentials. The Fourier transform of these potentials are not traditional functions but are distributions [173]. To overcome this difficulty, the \mathcal{O}_ℓ function associated to this potential is defined by screening the linear potential with a decreasing exponential,

$$\mathcal{O}(r) = \lambda r = \lim_{\eta \rightarrow 0} \lambda r e^{-\eta r} = -\lim_{\eta \rightarrow 0} \frac{\partial^2}{\partial \eta^2} \left(-\lambda \frac{e^{-\eta r}}{r} \right). \quad (7.17)$$

The second equality relates the linear potential to a derivative of the Yukawa potential whose \mathcal{O}_ℓ function is provided above. Using this relation, before taking the limit for η , one gets

$$\begin{aligned} \mathcal{O}_\ell^\eta(\bar{p}, p) &= \frac{\lambda}{\pi \bar{p} p} \frac{\partial^2}{\partial \eta^2} (Q_\ell(z_\eta)) \quad \text{with } z_\eta = \frac{\bar{p}^2 + p^2 + \eta^2}{2\bar{p} p} \\ &= \frac{\lambda}{\pi \bar{p} p} \frac{\partial}{\partial \eta} \left(\frac{\eta Q'_\ell(z_\eta)}{p\bar{p}} \right) = \frac{\lambda}{\pi} \left(\frac{Q'_\ell(z_\eta)}{(p\bar{p})^2} + \eta^2 \frac{Q''_\ell(z_\eta)}{(p\bar{p})^3} \right) \end{aligned} \quad (7.18)$$

where Q'_ℓ and Q''_ℓ denotes the first and second derivatives of Q_ℓ with respect to its argument. The limit on η is taken after integration and has to be considered carefully to ensure a finite result. Reference [173] develops formulas for this matrix element with arbitrary ℓ ,

$$\begin{aligned} & \lim_{\eta \rightarrow 0} \int p dp \bar{p} d\bar{p} \Xi(\bar{p})^* \Xi(p) \mathcal{O}_\ell^\eta(\bar{p}, p) \\ &= \frac{\lambda}{\pi} \int_0^\infty d\bar{p} \Xi(\bar{p})^* P \int_0^\infty \left(\frac{4\bar{p}^2 \Xi(\bar{p})}{(\bar{p}^2 - p^2)^2} + Q'_\ell \left(\frac{p^2 + \bar{p}^2}{2p\bar{p}} \right) \frac{\Xi(p)}{p\bar{p}} \right) dp \end{aligned} \quad (7.19)$$

where P denotes the Cauchy principal value of the integral. The left-hand side of relation (7.19) presents an apparent difference with its equivalent in [173]. This is because what is called $V_\eta^\ell(p, \bar{p})$ in [173] is actually equal to $p\bar{p} \mathcal{O}_\ell^\eta(\bar{p}, p)$. Integrals from (7.19) are quite difficult to handle, mainly due to the Cauchy principal value. To overcome this problem, coordinates (7.15) are again introduced. Performing the change, (7.19) becomes

$$\begin{aligned} & \lim_{\eta \rightarrow 0} \int p dp \bar{p} d\bar{p} \Xi(\bar{p})^* \Xi(p) \mathcal{O}_\ell^\eta(\bar{p}, p) \\ &= \frac{\lambda}{\pi} \int_0^\infty dv P \int_{-v}^v d\bar{v} \Xi \left(\frac{v + \bar{v}}{2} \right)^* \left(\frac{(v + \bar{v})^2}{2v^2\bar{v}^2} \Xi \left(\frac{v + \bar{v}}{2} \right) + Q'_\ell \left(\frac{v^2 + \bar{v}^2}{v^2 - \bar{v}^2} \right) \frac{2\Xi \left(\frac{v - \bar{v}}{2} \right)}{v^2 - \bar{v}^2} \right). \end{aligned} \quad (7.20)$$

With these coordinates, the Cauchy principal value in the integration on \bar{v} can naturally be taken into account by performing a Gauss-Legendre quadrature with an even number of points [173, 174]. Formulas (7.16) and (7.20) allows for an efficient evaluation of matrix elements with (7.12). Complement 7.A illustrates the calculation of Hamiltonian matrix-elements using formulas (7.3), (7.16) and (7.20).

7.2 Two-gluon Glueballs

The previous Section introduced a way to compute matrix elements on two-body helicity states. In the current Section, this formalism is applied to the description of glueballs in the framework of constituent approaches. Glueballs are modelled as colourless bound states of several constituent gluons. The latter are considered as bosons with helicity degrees of freedom $\lambda = \pm 1$ and negative intrinsic parity. The mass of the constituent gluon remains a controversial subject. Although formally massless, the QCD gluon has proven to acquire a dynamical mass in the non-perturbative regime [134, 175, 176, 177, 178, 179, 180]. This incited some studies to consider a massive kinetic energy for constituent gluons (with a mass around 0.5 GeV) [142, 181]. On the other hand, reference [152] tends to indicate that the challenge in modelling glueballs

consists more in the correct use of the helicity formalism than in the choice of the kinematics. In addition, it has already been observed in other constituent approaches that a modification in the kinematics of the system can be absorbed in modifications of the parameters from the potential [182]. For these reasons, the current work will consider an ultra-relativistic kinetic energy for the constituent gluon. This Section limits the discussion to two-gluon bound states that produces the so-called two-gluon glueballs. The colourless constraint on the wave function implies for two-gluon glueballs a positive charge conjugation and a symmetric colour part of the state [138]. Gluons having a bosonic nature, the spin-space part of the two-body state must also be symmetrical.

To start with, let us focus on the construction of symmetrical two-body J -helicity states with $\lambda_i = \pm 1$ and having a definite parity. Making use of properties (6.46) and (6.47), reference [152] constructs four sets of such symmetric parity eigenstates,

$$|p; S_+; J^P = (2k)^+\rangle = \frac{1}{\sqrt{2}}(|p; JM; +1 + 1\rangle + |p; JM; -1 - 1\rangle), \quad (7.21a)$$

$$|p; S_-; J^P = (2k)^-\rangle = \frac{1}{\sqrt{2}}(|p; JM; +1 + 1\rangle - |p; JM; -1 - 1\rangle), \quad (7.21b)$$

$$|p; D_+; J^P = (2k + 2)^+\rangle = \frac{1}{\sqrt{2}}(|p; JM; +1 - 1\rangle + |p; JM; -1 + 1\rangle), \quad (7.21c)$$

$$|p; D_-; J^P = (2k + 3)^+\rangle = \frac{1}{\sqrt{2}}(|p; JM; +1 - 1\rangle - |p; JM; -1 + 1\rangle). \quad (7.21d)$$

with $k \in \mathbb{N}$. For readability, s_1 and s_2 labels have been omitted from the notation. One can show that these states are correctly orthonormalised. In each of the four sets, parity and signature of J had to be constrained to ensure a correct symmetry of the state. In addition, the constraint $J \geq |\lambda_1 - \lambda_2|$ in definition (6.42) forbade the occurrence of total angular momenta smaller than two in $|D_\pm; J^P\rangle$ sets. The linear combinations of helicity states (7.21a) to (7.21d) can be expanded in terms of two-body J -canonical states making use of (6.51). This calculation has been performed in reference [152]. The resulting expansions are displayed in Table 7.1.

As suggested in Chapter 6, these two-gluon states $|p; S_\pm/D_\pm; J^P\rangle$ are integrated on their momentum degree-of-freedom to produce a generic glueball state,

$$|\Psi; S_\pm/D_\pm; J^P\rangle = \int \frac{dp}{2} \Xi(p) |p; S_\pm/D_\pm; J^P\rangle, \quad (7.22)$$

where $\Xi(p)$ satisfy the normalisation condition (6.59). Compared to (6.60), expression (7.22) replaces $\sqrt{w_1(p)w_2(p)}$ by p because both gluons are assumed to be massless. One can now go back over the demonstration of relations (7.3) and (7.12) to generalise them for the symmetrical

$$\begin{aligned}
|p; S_+; (2k)^+\rangle &= \sqrt{\frac{2}{3}} |p; {}^1 2k_{2k}\rangle - \sqrt{\frac{2k(2k+1)}{3(4k-1)(4k+3)}} |p; {}^5 2k_{2k}\rangle \\
&\quad + \sqrt{\frac{k(2k-1)}{(4k+1)(4k-1)}} |p; {}^5 2k - 2_{2k}\rangle + \sqrt{\frac{(k+1)(2k+1)}{(4k+3)(4k+1)}} |p; {}^5 2k + 2_{2k}\rangle, \\
|p; S_-; (2k)^-\rangle &= \sqrt{\frac{2k}{4k+1}} |p; {}^3 2k - 1_{2k}\rangle - \sqrt{\frac{2k+1}{4k+1}} |p; {}^3 2k + 1_{2k}\rangle, \\
|p; D_+; (2k+2)^+\rangle &= \sqrt{\frac{(k+2)(2k+3)}{(4k+3)(4k+5)}} |p; {}^5 2k_{2k+2}\rangle + \sqrt{\frac{6(k+2)(2k+1)}{(4k+3)(4k+7)}} |p; {}^5 2k + 2_{2k+2}\rangle \\
&\quad + \sqrt{\frac{(k+1)(2k+1)}{(4k+5)(4k+7)}} |p; {}^5 2k + 4_{2k+2}\rangle, \\
|p; D_-; (2k+3)^+\rangle &= -\sqrt{\frac{2k+5}{4k+7}} |p; {}^5 2k + 2_{2k+3}\rangle - \sqrt{\frac{2(k+1)}{4k+7}} |p; {}^5 2k + 4_{2k+3}\rangle.
\end{aligned}$$

Table 7.1: Expansion of symmetrised parity eigenstate two-body J -helicity states in canonical J -helicity states from [152]. A condensed notation for J -canonical states has been used, $|p; {}^{2s+1}l_J\rangle = |p; JM; ls; s_1 s_2\rangle$.

$|\Psi; S_{\pm}/D_{\pm}; J^P\rangle$ states. On the one hand, the generalisation of (7.3) is immediate. Symmetrical states being similarly orthonormalised, the demonstration does not require any modification and one gets,

$$\langle \Psi; S_{\pm}/D_{\pm}; J^P | \mathcal{O}(\hat{p}) | \Psi; S_{\pm}/D_{\pm}; J^P \rangle = \int dp |\Xi(p)|^2 \mathcal{O}(p). \quad (7.23)$$

Kinetic energy matrix elements that mix states with different labels are shown to cancel. Because states are naturally written in momentum space, angular momentum does not play any role in the calculation. It results in a left-hand side of equation (7.23) independent of S/D and J . This was not the case in [152] where calculations were performed in coordinate space. On the other hand, relation (7.12) requires a slight modification. Because symmetrised states satisfies a different expansion in canonical states, coefficients $\mathcal{C}_{\ell s; \lambda_1 \lambda_2}^{J; s_1 s_2}$ from relation (7.12) have to be replaced by the expansion coefficients from Table 7.1. Denoting the latter $\mathcal{C}_{\ell s}^J$, one gets the following analogue to (7.12),

$$\begin{aligned}
&\langle \Psi; S_{\pm}/D_{\pm}; J^P | \mathcal{O}(\hat{r}) | \Psi; S_{\pm}/D_{\pm}; J^P \rangle \\
&= \sum_{s=0}^2 \sum_{\ell=|J-s|}^{J+s} (\mathcal{C}_{\ell s}^J)^2 \int pdp \bar{p} d\bar{p} \Xi(\bar{p})^* \Xi(p) \mathcal{O}_{\ell}(\bar{p}, p).
\end{aligned} \quad (7.24)$$

These two formulas can now be used to concretely compute a glueball spectrum by means of a variational approach (see Section 1.2). A Gaussian shape supplemented by a p factor that cancels at $p = 0$ is suggested as a trial helicity-momentum wave function,

$$\Xi_a(p) = Ape^{-ap^2}. \quad (7.25)$$

In the following, the approximation provided by this trial state will be referred to as the *single Gaussian approximation* (SGA). To enable comparison, the Hamiltonian considered is the same as the one in [152],

$$\mathcal{H}_{\text{GB}} = 2\sqrt{p^2} + \frac{9\sigma_m}{4}r - 3\frac{\alpha_s}{r} \quad (7.26)$$

where $\alpha_s = 0.450$ is the strong coupling constant and $\sigma_m = 0.185 \text{ GeV}^2$ is the mesonic string tension. Compared to the fundamental string tension σ introduced in Section 5.1.2, one has $\sigma_m = 4\sigma/3$. As a reminder, the factor $9/4$ comes from the Casimir scaling hypothesis [151] (for gluons in the adjoint representation, $\langle F^2 \rangle = 3$) and the factor 3 corresponds to the colour charge associated to a pair of constituent gluons in a colour singlet. This factor will be detailed in greater depth in Complement 9.B. Instanton contributions², added in [152] to split the degeneracy of the lowest states, are not considered at first. Masses obtained using the SGA for the low-lying angular momenta are displayed in the second column of Table 7.2. These results are compared to energies from reference [152] (instanton contributions are manually removed). At first sight, both values seem incompatible. Energies from the SGA, a variational method supposed to provide upper bounds, lies below the ones from reference [152], where a very accurate resolution method has been used (namely, the Lagrange mesh method [184]). This incompatibility is left noticing that reference [152] solves the same Hamiltonian using a fundamentally different approach. First of all, the total orbital angular momentum of the system is evaluated on the symmetric parity eigenstates from Table 7.1. The matrix obtained in this way turns out to be diagonal with respective diagonal elements $J(J+1) + 2$ for $|p; S_{\pm}, J^P\rangle$ states and $J(J+1) - 2$ for $|p; D_{\pm}, J^P\rangle$ states. Consequently, reference [152] suggests to replace the $|p; S_{\pm}/D_{\pm}, J^P\rangle$ states by canonical ones with effective angular momenta ℓ_{eff} such that

$$\ell_{\text{eff}}(\ell_{\text{eff}} + 1) = J(J + 1) \pm 2. \quad (7.27)$$

The Hamiltonian matrix is then evaluated on these effective canonical states rather than on

² Instantons are classical solutions to the Euclidean equations of motion in non-Abelian gauge theories. In QCD, they reflect the topologically non-trivial structure of the vacuum and contribute to non-perturbative phenomena such as tunnelling between different vacuum sectors [183]. In most of the present work, instanton effects are not considered.

State	$E_{\text{or.SGA}}$	$[\delta]$	$E_{\text{mod.SGA}}$	$[\delta]$	Ref [152]
$ \Psi; S_+, 0^+\rangle$	1.769	[19%]	2.216	[2%]	2.174
$ \Psi; S_-, 0^-\rangle$	2.216	[2%]	2.216	[2%]	2.174
$ \Psi; D_+, 2^+\rangle$	2.279	[12%]	2.651	[2%]	2.588
$ \Psi; S_+, 2^+\rangle$	3.060	[1%]	3.194	[4%]	3.077
$ \Psi; S_-, 2^-\rangle$	3.043	[1%]	3.194	[4%]	3.077
$ \Psi; D_-, 3^+\rangle$	3.297	[1%]	3.393	[4%]	3.254
$ \Psi; D_+, 4^+\rangle$	3.897	[3%]	3.981	[6%]	3.768
$ \Psi; S_+, 4^+\rangle$	4.150	[5%]	4.204	[6%]	3.961
$ \Psi; S_-, 4^-\rangle$	4.139	[4%]	4.204	[6%]	3.961

Table 7.2: Comparison of two-gluon glueball spectra. Upper bounds obtained with the original SGA, $E_{\text{or.SGA}}$, are compared to the modified SGA, $E_{\text{mod.SGA}}$, and to the spectrum from [152] for which instanton contributions have been removed for the comparison. Energy results are provided in GeV. Relative differences with [152], δ , are indicated in square brackets.

the true two-body helicity states. Mimicking this strategy with the SGA give rise to the fourth column of Table 7.2. Such calculations require the evaluation of second kind Legendre functions for non-integer ℓ values. As expected, this modified SGA provides upper bounds of the energies from [152].

Results from the original SGA are compared with LQCD results in Table 7.3 and in Figure 7.1. First of all, one notices that most of the masses provided by the original SGA lies below the ones from [152]. Nevertheless, in most of the case, relative differences between both methods lies around a few percent. The main exception to this claim occurs for the 0^+ state. In reference [152], 0^+ and 0^- states proves to be degenerated thereby requiring the introduction of instanton interactions to split both levels. The original SGA naturally raises this degeneracy. It does not mean that instanton does not contribute in the glueball spectrum but that their effects maybe overestimated by the use of the method from [152]. All results seem in global agreement with LQCD results [167, 166, 168, 169], no matter which methodology is used.

It can be worth considering an extension of the SGA by incorporating a second Gaussian trial wave function (7.25) within the variational approach [23]. This second Gaussian is independent of the first and is characterized by its own variational parameter, b . The single Hamiltonian matrix element to compute in the SGA is replaced by the evaluation of 2 by 2 Hamiltonian and

State	$E_{\text{or.SGA}}$	LQCD [166]	LQCD [168]
$ \Psi; S_+, 0^+\rangle$	1.769	$1.710 \pm 0.050 \pm 0.080$	$1.475 \pm 0.030 \pm 0.065$
$ \Psi; S_-, 0^-\rangle$	2.216	$2.560 \pm 0.035 \pm 0.120$	$2.250 \pm 0.060 \pm 0.100$
$ \Psi; D_+, 2^+\rangle$	2.279	$2.390 \pm 0.030 \pm 0.120$	$2.150 \pm 0.030 \pm 0.100$
$ \Psi; S_+, 2^+\rangle$	3.060	N.A.	$2.880 \pm 0.100 \pm 0.130$
$ \Psi; S_-, 2^-\rangle$	3.043	$3.040 \pm 0.040 \pm 0.150$	$2.780 \pm 0.050 \pm 0.130$
$ \Psi; D_-, 3^+\rangle$	3.297	$3.670 \pm 0.050 \pm 0.180$	$3.385 \pm 0.090 \pm 0.150$
$ \Psi; D_+, 4^+\rangle$	3.897	N.A.	$3.640 \pm 0.090 \pm 0.160$
$ \Psi; S_+, 4^+\rangle$	4.150	N.A.	N.A.
$ \Psi; S_-, 4^-\rangle$	4.139	N.A.	N.A.

Table 7.3: Comparison of two-gluon glueball spectra. Upper bounds obtained with the original SGA are compared to some LQCD results from [166, 168]. A supplementary LQCD calculations [169] that predicts a $|\Psi; D_+, 4^+\rangle$ state of $3.650 \pm 0.060 \pm 0.180$ GeV can be mentioned. Energy results are provided in GeV.

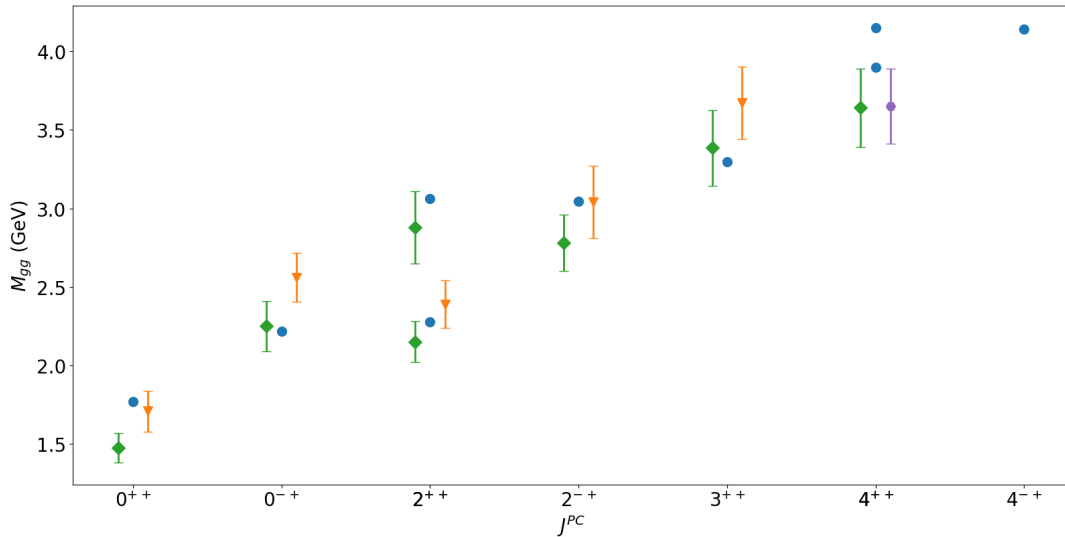


Figure 7.1: Comparison of two-gluon glueball spectra. Upper bounds obtained with the SGA (blue circles) are compared to LQCD results from [166] (orange triangles), [168] (green diamonds) and [169] (purple hexagon).

State	$E_{\text{or.SGA}}$	E_{DGA}	Ref [152]	LQCD [166, 167]	LQCD [168]
$ \Psi_1; S_+, 0^+\rangle$	1.769	1.668	2.174	$1.710 \pm 0.050 \pm 0.080$	$1.475 \pm 0.030 \pm 0.065$
$ \Psi_2; S_+, 0^+\rangle$	N.A.	2.808	2.993	$2.670 \pm 0.180 \pm 0.130$	$2.755 \pm 0.070 \pm 0.120$
$ \Psi_1; S_-, 0^-\rangle$	2.216	2.202	2.174	$2.560 \pm 0.035 \pm 0.120$	$2.250 \pm 0.060 \pm 0.100$
$ \Psi_2; S_-, 0^-\rangle$	N.A.	3.069	2.993	$3.640 \pm 0.060 \pm 0.180$	$3.370 \pm 0.150 \pm 0.150$
$ \Psi_1; D_+, 2^+\rangle$	2.279	2.241	2.588	$2.390 \pm 0.030 \pm 0.120$	$2.150 \pm 0.030 \pm 0.100$
$ \Psi_2; D_+, 2^+\rangle$	N.A.	3.249	3.325	N.A.	N.A.
$ \Psi_1; S_+, 2^+\rangle$	3.060	3.042	3.077	N.A.	$2.880 \pm 0.100 \pm 0.130$
$ \Psi_2; S_+, 2^+\rangle$	N.A.	3.852	3.732	N.A.	N.A.
$ \Psi_1; S_-, 2^-\rangle$	3.043	3.042	3.077	$3.040 \pm 0.040 \pm 0.150$	$2.780 \pm 0.050 \pm 0.130$
$ \Psi_2; S_-, 2^-\rangle$	N.A.	3.845	3.732	$3.890 \pm 0.040 \pm 0.190$	$3.480 \pm 0.140 \pm 0.160$
$ \Psi_1; D_-, 3^+\rangle$	3.297	3.295	3.254	$3.670 \pm 0.050 \pm 0.180$	$3.385 \pm 0.090 \pm 0.150$
$ \Psi_2; D_-, 3^+\rangle$	N.A.	4.067	3.882	N.A.	N.A.

Table 7.4: Comparison of two-gluon glueball spectra. Upper bounds obtained with the original SGA, $E_{\text{or.SGA}}$, are compared to the DGA, E_{DGA} , and to the spectrum from [152] from which instanton contributions have been removed for the comparison. Labels Ψ_1 and Ψ_2 respectively refer to the fundamental and to the first excited state. Some LQCD results from [166, 167, 168] are added as points of comparison. Energy results are provided in GeV.

overlap matrices, which form the core of a generalised eigenvalue problem,

$$\begin{pmatrix} \langle \Psi_a | \mathcal{H}_{\text{GB}} | \Psi_a \rangle & \langle \Psi_a | \mathcal{H}_{\text{GB}} | \Psi_b \rangle \\ \langle \Psi_b | \mathcal{H}_{\text{GB}} | \Psi_a \rangle & \langle \Psi_b | \mathcal{H}_{\text{GB}} | \Psi_b \rangle \end{pmatrix} \begin{pmatrix} C_1 \\ C_2 \end{pmatrix} = E \begin{pmatrix} \langle \Psi_a | \Psi_a \rangle & \langle \Psi_a | \Psi_b \rangle \\ \langle \Psi_b | \Psi_a \rangle & \langle \Psi_b | \Psi_b \rangle \end{pmatrix} \begin{pmatrix} C_1 \\ C_2 \end{pmatrix} \quad (7.28)$$

where $|\Psi_a\rangle$ serves as a shorthand for any symmetric helicity states $|\Psi; S_{\pm}/D_{\pm}; J^P\rangle$, with a being the non-linear variational parameter considered. This double Gaussian approximation (DGA) serves two purposes: to assess the accuracy of the SGA, and to explore first radially excited states. The non-linear variational parameters of each Gaussian, denoted a and b above, are treated as independent, and optimisation is performed on both. Results are presented in Table 7.4. For all considered states, the energy difference between the SGA and DGA does not exceed 0.1 GeV (it even decreases to below 0.01 GeV for high angular momenta). These findings suggest that the SGA is sufficiently accurate to study low-lying two-gluon glueball states. For radially excited states, as expected, the DGA results aligns in magnitude with those from reference [152].

Complement 7.A Examples of calculations in momentum space

To simplify, evaluations will be performed on pure two-body canonical states. Three different two-body systems will be considered,

$$\mathcal{H}_{\text{Coul}}(p, r) = \frac{p^2}{2\mu} - \frac{g}{r}, \quad (7.29)$$

$$\mathcal{H}_{\text{lin}}(p, r) = \frac{p^2}{2\mu} + \lambda r, \quad (7.30)$$

$$\mathcal{H}_{\text{Ful}}(p, r) = \sqrt{m_1^2 + p^2} + \sqrt{m_2^2 + p^2} + Ar - \frac{\kappa}{r}, \quad (7.31)$$

with $\mu = m_1 m_2 / (m_1 + m_2)$ denoting the reduced mass. For convenience, in all cases, both particles are chosen with equal non-zero masses, $m_1 = m_2 = m$ and $\mu = m/2$. Natural units are used. Hamiltonian matrix elements will be computed for a Gaussian-like Ξ helicity wave function with one parameter,

$$\Xi_a(p) = 2 \left(\frac{(2a)^3}{\pi} \right)^{1/4} p e^{-ap^2}. \quad (7.32)$$

Above, the constant has been fixed to ensure that the condition (6.59) holds. The variational theorem (1.53) ensures that, for any angular momentum ℓ and for all value of the parameter a , this matrix element consist of an upper-bound for the ground state energy with angular momentum ℓ of the corresponding Hamiltonian. This approximated eigenenergy is the one referred as SGA in Section 7.2.

Concerning kinetic energies, the integral from relation (7.3) can be solved analytically for both non- and semi-relativistic kinematics,

$$|A|^2 \int dp p^2 e^{-2ap^2} \frac{p^2}{2\mu} = \frac{3}{8} \frac{1}{a\mu}, \quad (7.33)$$

$$|A|^2 \int dp p^2 e^{-2ap^2} 2\sqrt{m^2 + p^2} = \sqrt{\frac{8a}{\pi}} m^2 e^{am^2} K_1(am^2). \quad (7.34)$$

Above K_n refers to a modified Bessel function of second kind. Potential matrix elements are managed using relations (7.14) and (7.20) from previous sections. As already mentioned, numerical integration methods based on Gauss-Legendre quadrature are used.³ Results for the

³ For both potentials, to compute matrix elements using (7.16) and (7.20), Gauss-Legendre quadratures

ℓ	E_{exact}	E_{SGA}	a_{opt}
0	-0.50	-0.42	0.89
1	-0.25	-0.12	3.16
2	-0.125	-0.05	6.99

Table 7.5: Spectra comparison for the Coulomb Hamiltonian (7.29). Upper bounds obtained with the SGA, (E_{SGA}), are compared to the analytical spectrum from [186], E_{exact} , for various angular momenta ℓ . Optimised values of the variational parameter, a_{opt} are also displayed in the fourth column. Arbitrary units are used: $m = 2$ and $g = 1$.

potential and the kinetic energy are then gathered to compute Hamiltonian matrix-elements and the obtained upper bounds are minimised on the variational parameter a . With a single trial state, this method only provides approximations for the lowest state of a given angular momentum ℓ .

Let us now focus on the results of the three tests. The Table 7.5 displays the upper bounds obtained for the Hamiltonian $\mathcal{H}_{\text{Coul}}$. For this test, the mass m of the particles has been fixed to 2 while the constant of the Coulomb potential g has been fixed to 1, both in arbitrary units. One will notice that the obtained upper bounds are far from accurate, especially for $\ell = 3$. This is a regular feature when using a Gaussian trial wave function to solve a divergent potential. One can check that turning the trial wave function into the exact one for the $\ell = 0$ ground state [185],

$$\Xi^{\text{Coul}}(p) \propto \frac{p}{(1+p^2)^2}, \quad (7.35)$$

allows to exactly reproduce its eigenenergy, as expected. Concerning the pure linear Hamiltonian \mathcal{H}_{lin} , results in arbitrary units are displayed in Table 7.6 for unit masses and linear potential constant. An analytical spectrum for $\ell = 0$ is provided in [130]. For $\ell > 0$, the SGA is compared to the spectrum provided by another approximation method, the Lagrange-mesh method [184]. One can see that a single Gaussian provides a quite accurate upper bound for the $\ell = 0$ ground state. For $\ell > 0$, as expected, the very accurate results provided by the Lagrange-mesh method lies below those obtained with the SGA. Finally, the Hamiltonian \mathcal{H}_{Ful} is investigated. This Hamiltonian has been used in [154] to model bottomonium and charmonium systems. Table 7.7 compares the results obtained with the SGA to the spectrum provided in the reference. In both cases and for each ℓ values, the single Gaussian upper-bound achieves an accuracy below 2%.

with 1000 points are used for integrals on \bar{v} while integrals on v are handled with a change of variables $v = v_t/(1 - v_t)$ and only 300 points. Integrals on v turn out to be clearly less sensitive than the ones on \bar{v} .

ℓ	E_{exact}	E_{LM}	E_{SGA}	a_{opt}
0	2.338	2.338	2.345	0.960
1	N.A.	3.361	3.472	0.648
2	N.A.	4.248	4.556	0.494

Table 7.6: Spectra comparison for the linear Hamiltonian (7.30). Upper bounds obtained with the SGA, (E_{SGA}), are compared to the analytical spectrum from [130] for $\ell = 0$ (E_{exact}) and to the spectrum from the Lagrange mesh method [184] for various angular momenta, (E_{LM}). Optimised values of the variational parameter, a_{opt} are also displayed in the fourth column. Arbitrary units are used : $m = 1$ and $\lambda = 1$.

ℓ	E_{exact}	E_{SGA}	$[\varepsilon]$	a_{opt}	ℓ	E_{exact}	E_{SGA}	$[\varepsilon]$	a_{opt}
0	9.448	9.499	[0.5%]	0.391	0	3.067	3.094	[0.9%]	1.383
1	9.900	9.920	[0.2%]	0.450	1	3.504	3.531	[0.8%]	1.141
2	10.150	10.204	[0.5%]	0.397	2	3.811	3.886	[2%]	0.903

Table 7.7: Spectra comparison for Fulcher’s Hamiltonian \mathcal{H}_{Ful} [154] (bottomonium at left, charmonium at right). Upper bounds obtained with the SGA, (E_{SGA}), are compared to the spectrum from [130] for various angular momenta ℓ . Optimised values of the variational parameter, a_{opt} are also displayed in the fourth column. Energy results and a values are respectively provided in GeV and GeV^{-1} . Relative errors ε are indicated in square brackets.

This chapter in the context of a thesis

This chapter revisits the two-gluon glueball spectrum through an innovative approach. As mentioned earlier, studies applying the helicity formalism to two-gluon glueballs already exist in the literature. However, the methodology presented here refines that description and, incidentally, proposes a general framework for treating systems with multiple constituent gluons. The calculations are carried out directly in momentum space, with controllable accuracy through the addition of Gaussian functions in the approximation. Both eigenenergies and eigenstates are obtained, and the comparison with LQCD results indicates agreement, taking into account the associated uncertainties.

Chapter 8

Three-body Helicity Formalism: A Technical Extension

Previous chapters successfully developed a relativistic framework for studying two-body systems. Incidentally, this framework enabled reproducing the low-lying positive charge conjugation glueball spectrum. To access states with negative charge conjugation, however, a glueball must contain at least a third gluon. This requirement motivates the extension of the previous methodology to three-body systems, with the goal of inferring the three-gluon glueball spectrum.

This chapter introduces the helicity formalism for three-body systems, while glueball-specific considerations are deferred to the next chapter. As in the two-body case, efforts are made to produce complete sets of three-body helicity states possessing a total angular momentum J in the ECoMF. These sets of three-body states will then be used to decompose the state of composite particles at rest. There are two main approaches to defining helicity states in three-body systems, each with its own strengths and weaknesses. Accordingly, the chapter is divided into two parts. Section 8.1 presents the first definition for helicity states, which offers convenient parity and symmetry properties. Section 8.2 introduces an alternative definition, better suited for computing two-body interaction matrix elements. Globally, this chapter relies more heavily on supplementary material, as derivations of key properties are relegated to the complements. These demonstrations are somewhat more technical than the main text, but they warrant attention, as such developments are often missing from the literature. This chapter still builds upon the text from reference [158].

8.1 Berman's Definition

Berman's three-body helicity states definition is based on the observation that, in their CoMF, any set of three particles always lies and moves in a given plane. This feature allows the following geometrical construction for the tensorial product of three one-body helicity states in the ECoMF [161, 187],

$$\begin{aligned}
 |\alpha\beta\gamma; w_1w_2w_3; \lambda_1\lambda_2\lambda_3\rangle = & U(R(\alpha, \beta, \gamma)) [U(R(\phi_1, \pi/2, 0)L_z(p_1)) |s_1\lambda_1\rangle \\
 & \otimes U(R(\phi_2, \pi/2, 0)L_z(p_2)) |s_2\lambda_2\rangle \\
 & \otimes U(R(\phi_3, \pi/2, 0)L_z(p_3)) |s_3\lambda_3\rangle]
 \end{aligned} \tag{8.1}$$

where p_i and ϕ_i are fixed combinations of particle's energies, w_1 , w_2 and w_3 ,

$$p_i = \sqrt{w_i^2 - m_i^2}, \quad \cos \varphi_{ij} = \frac{p_k^2 - p_i^2 - p_j^2}{2p_i p_j}, \tag{8.2}$$

$$\phi_1 = \varphi_{13} - \pi/2, \quad \phi_2 = \varphi_{13} + \varphi_{12} - \pi/2, \quad \phi_3 = 3\pi/2. \tag{8.3}$$

Above, φ_{ij} angles are always to be taken in between 0 and π . Individual masses and spins are not reminded in the notation for the sake of conciseness. As for two-body p -helicity states, definition (8.1) can be decomposed in two pieces. Inside the square brackets, reference momenta are provided to each of the three particles using helicity convention. Their modulus are defined so that the i -th particle has an energy w_i , while their direction is chosen so that it respects four conditions.

1. Each momentum lies in the xy plane.
2. The sum of the momenta is the null vector.
3. The momentum of the third particle is along the y direction toward negatives.
4. The cross product of the momenta of particle 1 and 2 is along the z axis toward positives.

All these conditions are ensured by definitions (8.2) and (8.3). This define what will be thereafter named *Berman's reference state* and denoted as follows,

$$\begin{aligned}
 |w_1w_2w_3; \lambda_1\lambda_2\lambda_3\rangle = & U(R(\phi_1, \pi/2, 0)L_z(p_1)) |s_1\lambda_1\rangle \otimes U(R(\phi_2, \pi/2, 0)L_z(p_2)) |s_2\lambda_2\rangle \\
 & \otimes U(R(\phi_3, \pi/2, 0)L_z(p_3)) |s_3\lambda_3\rangle.
 \end{aligned} \tag{8.4}$$

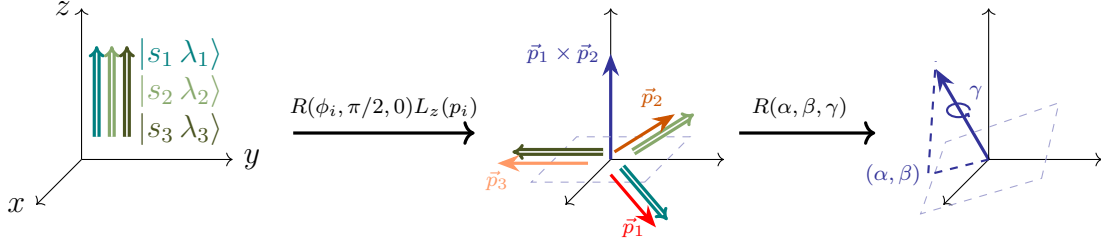


Figure 8.1: Visual interpretation for the definition of Berman's p -helicity states (8.1).

Once the reference state is built, in a second phase, this state is rotated with Euler angles (α, β, γ) to give its orientation to the plane in which lies the three particles. This decomposition provides its interpretation to the angles (α, β, γ) , these are the angles of the normal to particles' plane. A visual interpretation of the aforementioned structure is proposed in Figure 8.1. States defined in (8.1) will be thereafter referred to as *Berman's p -helicity states*.¹ These satisfies the following orthonormality relation [161, 187],

$$\begin{aligned} \langle \bar{\alpha} \bar{\beta} \bar{\gamma}; \bar{w}_1 \bar{w}_2 \bar{w}_3; \bar{\lambda}_1 \bar{\lambda}_2 \bar{\lambda}_3 | \alpha \beta \gamma; w_1 w_2 w_3; \lambda_1 \lambda_2 \lambda_3 \rangle &= 8 \delta(w_1 - \bar{w}_1) \delta(w_2 - \bar{w}_2) \delta(w_3 - \bar{w}_3) \\ &\delta(\alpha - \bar{\alpha}) \delta(\cos \beta - \cos \bar{\beta}) \delta(\gamma - \bar{\gamma}) \delta_{\lambda_1 \bar{\lambda}_1} \delta_{\lambda_2 \bar{\lambda}_2} \delta_{\lambda_3 \bar{\lambda}_3}. \end{aligned} \quad (8.5)$$

Normalisation announced in [161] differ from this one by a multiplicative constant. It is due to a different choice of convention for normalisation of one-body helicity states (as a reminder, the convention used here is the one of [160]).

The definition (8.1) introduces three-body helicity states with defined directions for the momenta and therefore no good total angular momentum. It is as straightforward as for two-body J -helicity states to combine these states to overcome this deficiency [161, 187],

$$\begin{aligned} |JM\mu; w_1 w_2 w_3; \lambda_1 \lambda_2 \lambda_3 \rangle &= \sqrt{\frac{2J+1}{8\pi^2}} \int d\alpha d\cos\beta d\gamma D_{M\mu}^{J*}(\alpha, \beta, \gamma) |\alpha \beta \gamma; w_1 w_2 w_3; \lambda_1 \lambda_2 \lambda_3 \rangle \\ &= \sqrt{\frac{2J+1}{8\pi^2}} \int d\alpha d\cos\beta d\gamma D_{M\mu}^{J*}(\alpha, \beta, \gamma) U(R(\alpha, \beta, \gamma)) |w_1 w_2 w_3; \lambda_1 \lambda_2 \lambda_3 \rangle. \end{aligned} \quad (8.6)$$

States defined hereinabove will be referred to as *Berman's J -helicity states* and satisfy the

¹ This name refers to one of the authors of a pioneer work using this definition [187]. Conventions in this work slightly differs from the ones used here, the third particle being taken along the x -axis towards negatives. For completeness, let us also mention the names of J.Werle and M.Jacob that abundantly contributed to this definition too [187, 188].

following orthonormality relation [161],

$$\langle \bar{J}\bar{M}\bar{\mu}; \bar{w}_1\bar{w}_2\bar{w}_3; \bar{\lambda}_1\bar{\lambda}_2\bar{\lambda}_3 | JM\mu; w_1w_2w_3; \lambda_1\lambda_2\lambda_3 \rangle = 8\delta(w_1 - \bar{w}_1)\delta(w_2 - \bar{w}_2)\delta(w_3 - \bar{w}_3) \delta_{J\bar{J}}\delta_{M\bar{M}}\delta_{\mu\bar{\mu}}\delta_{\lambda_1\bar{\lambda}_1}\delta_{\lambda_2\bar{\lambda}_2}\delta_{\lambda_3\bar{\lambda}_3}. \quad (8.7)$$

This relation can also be compared to the results in reference [188], where different orientation conventions are used, and in reference [187], where an expression only including space degrees-of-freedom is provided. In addition to the total angular momentum J and its projection M , a third quantum number μ is produced. This quantum number corresponds to the projection of the total angular momentum along the normal to the plane [161]. Even if the direction of this normal is not fixed due to the integration on the (α, β, γ) angles. The projection of J along the normal to the plane is well-defined. One may wonder if the choice to set up the reference state in the xy plane really matters, the angles of this plane being integrated in Berman's J -helicity states anyway. It is demonstrated in Complement 8.A that a modification of this reference plane truly impact the definition of Berman's J -helicity states,

$$|JM\mu; w_1w_2w_3; \lambda_1\lambda_2\lambda_3\rangle = \sum_{\mu'=-J}^J D_{\mu\mu'}^J(\bar{R}^{-1}) |JM\mu'; w_1w_2w_3; \lambda_1\lambda_2\lambda_3\rangle_{\bar{R}} \quad (8.8)$$

where the state denoted $|JM\mu; w_1w_2w_3; \lambda_1\lambda_2\lambda_3\rangle_{\bar{R}}$ is built from a different initial configuration, with the rotation \bar{R} relating the reference planes used to define the states on either side of equation (8.8). The change of reference plane modified the definition of the μ quantum number.

The action of parity and permutation operators on Berman's states can be investigated. As for one- and two-body helicity states, Berman's J -helicity states are not parity eigenstates by themselves [161],

$$\Pi |JM\mu; w_1w_2w_3; \lambda_1\lambda_2\lambda_3\rangle = \eta_1\eta_2\eta_3(-1)^{-s_1-s_2-s_3-\mu} |JM\mu; w_1w_2w_3; -\lambda_1 - \lambda_2 - \lambda_3\rangle. \quad (8.9)$$

Above, η_i is still the intrinsic parity of the i^{th} particle. To get parity eigenstates, linear combinations of Berman's J -helicity states that mixes helicity signs have to be considered. Concerning permutations of particles, let \mathbb{P}_{ij} be the operator that represents exchange operations between particles i and j . Berman's J -helicity states are not eigenstates of permutations but

$$\mathbb{P}_{12} |JM\mu; w_1w_2w_3; \lambda_1\lambda_2\lambda_3\rangle = (-1)^{J+\mu+\lambda_1+\lambda_2-\lambda_3} |JM - \mu; w_2w_1w_3; \lambda_2\lambda_1\lambda_3\rangle, \quad (8.10a)$$

$$\mathbb{P}_{13} |JM\mu; w_1w_2w_3; \lambda_1\lambda_2\lambda_3\rangle = (-1)^{J-\mu-\lambda_1-\lambda_2-\lambda_3} e^{-i\varphi_{13}\mu} |JM - \mu; w_3w_2w_1; \lambda_3\lambda_2\lambda_1\rangle, \quad (8.10b)$$

$$\mathbb{P}_{23} |JM\mu; w_1w_2w_3; \lambda_1\lambda_2\lambda_3\rangle = (-1)^{J+\mu+\lambda_1-\lambda_2-\lambda_3} e^{i\varphi_{23}\mu} |JM - \mu; w_1w_3w_2; \lambda_1\lambda_3\lambda_2\rangle, \quad (8.10c)$$

where expressions of φ_{ij} are given in (8.2). The relation for \mathbb{P}_{12} can be found in [161, 187] but results for \mathbb{P}_{13} and \mathbb{P}_{23} are new. The proof of (8.10b) is given in Complement 8.A. This proof can easily be adapted to demonstrate (8.10c). It has been checked that above relations are consistent with S_3 multiplication table,

$$\mathbb{P}_{23} = \mathbb{P}_{12}\mathbb{P}_{13}\mathbb{P}_{12}. \quad (8.11)$$

Non-normalised symmetric (anti-symmetric) states can be obtained by applying the three-body symmetriser \mathbb{S}_3 (anti-symmetriser \mathbb{A}_3) on each Berman's J -helicity state (8.6),

$$\mathbb{S}_3 = \mathbf{1} + \mathbb{P}_{12} + \mathbb{P}_{13} + \mathbb{P}_{12}\mathbb{P}_{13}\mathbb{P}_{12} + \mathbb{P}_{13}\mathbb{P}_{12} + \mathbb{P}_{12}\mathbb{P}_{13}, \quad (8.12)$$

$$\mathbb{A}_3 = \mathbf{1} - \mathbb{P}_{12} - \mathbb{P}_{13} - \mathbb{P}_{12}\mathbb{P}_{13}\mathbb{P}_{12} + \mathbb{P}_{13}\mathbb{P}_{12} + \mathbb{P}_{12}\mathbb{P}_{13}. \quad (8.13)$$

Symmetric and antisymmetric parity eigenstates for three-gluon systems are built in Section 9.3.

8.1.1 Decomposition of a physical three-body state in Berman's J -helicity states

In the same way as for two-body systems, any three-body bound state in the ECoMF with spin J and with helicity quantum numbers can be decomposed as an integral on the internal momentum degrees-of-freedom of Berman's p -helicity states. But contrary to the two-body case, this integral can be written in many possible variables. As an example, Jacobi coordinates have already been introduced. These coordinates, denoted \mathbf{x} and \mathbf{y} , complemented with the centre-of-mass position, \mathbf{R} , were used in the Chapters 2 and 3 to deal with many-body bound states. For three identical bodies, in terms of individual positions, they reads

$$\mathbf{x} = \mathbf{x}_1 - \mathbf{x}_2, \quad \mathbf{y} = \frac{\mathbf{x}_1 + \mathbf{x}_2}{2} - \mathbf{r}_3, \quad \mathbf{R} = \frac{\mathbf{x}_1 + \mathbf{x}_2 + \mathbf{r}_3}{3}. \quad (8.14)$$

Berman's states being momentum eigenstates, Jacobi coordinates will take part in the following through their conjugated momenta,

$$\mathbf{p}_x = \frac{\mathbf{p}_1 - \mathbf{p}_2}{2}, \quad \mathbf{p}_y = \frac{\mathbf{p}_1 + \mathbf{p}_2 - 2\mathbf{p}_3}{3}, \quad \mathbf{P} = \mathbf{p}_1 + \mathbf{p}_2 + \mathbf{p}_3, \quad (8.15)$$

where \mathbf{P} is the total momentum of the system. This choice of coordinates has the advantage that it does not bring any Jacobian compared to individual momenta,

$$d^3p_1 d^3p_2 d^3p_3 = d^3P d^3p_x d^3p_y. \quad (8.16)$$

Another possible system of coordinates that may be used consists of three angles that describe the plane in which the momenta lies as well as the three momentum length. One will recognize in this set of coordinates the α , β , γ , p_1 , p_2 and p_3 variables used in Berman's definition of p -helicity states (8.1). Equivalently, one can replace the p_i variables by the w_i ones, these being related each other through relation (8.2). In the following, these coordinates will be called *pseudo-momentum perimetric coordinates* (PMP-coordinates), in analogy with position perimetric coordinates, used, for instance, in [189]. The full change of coordinates from Jacobi to PMP is not mandatory for the sake of this discussion. Let us simply mention that, for three massless particles, the modulus of Jacobi coordinates can be related to w_i variables as follows

$$p_x^2 = (2w_1^2 + 2w_2^2 - w_3^2)/4, \quad p_y^2 = w_3^2, \quad (8.17)$$

and that, between these variables, a non-trivial Jacobian has to be taken into account,

$$d^3p_x d^3p_y = w_1 w_2 w_3 dw_1 dw_2 dw_3 d\alpha d\cos\beta d\gamma. \quad (8.18)$$

This relation can be demonstrated by considering the intermediary system of coordinates that supplements α , β , γ with the respective moduli of \mathbf{p}_x and \mathbf{p}_y as well as the angle between these two vectors, denoted $\cos\theta_{xy}$ [189].

Out of the two possible sets of coordinates, the momentum perimetric ones clearly fits better with Berman's definition of helicity states. Making use of the completeness relation of Berman's p -helicity states, a generic three-body helicity state in the ECoMF, $|\Phi; \lambda_1 \lambda_2 \lambda_3\rangle$, is naturally decomposed in coordinates w_1 , w_2 , w_3 , α , β and γ ,

$$|\Phi; \lambda_1 \lambda_2 \lambda_3\rangle = \int \frac{dw_1 dw_2 dw_3 d\alpha d\cos\beta d\gamma}{8} \Phi(\alpha, \beta, \gamma, w_1, w_2, w_3) |\alpha\beta\gamma; w_1 w_2 w_3; \lambda_1 \lambda_2 \lambda_3\rangle \quad (8.19)$$

where

$$\Phi(\alpha, \beta, \gamma, w_1, w_2, w_3) = \langle \alpha\beta\gamma; w_1 w_2 w_3; \lambda_1 \lambda_2 \lambda_3 | \Phi; \lambda_1 \lambda_2 \lambda_3 \rangle \quad (8.20)$$

is the three-body helicity-momentum wave function of the state. Above, w_1 and w_2 are integrated along the set of positive real while w_3 is bounded by $|w_1 - w_2|$ and $w_1 + w_2$ so that $\mathbf{P} = \mathbf{0}$ is possible. This relation is the three-body equivalent to the two-body decomposition (6.52). Here again, this state has not the expected definite total angular momentum J . But reminding Berman's definition of J -helicity states, this property can be supplied to the state by imposing

the angular dependence of $\Phi(\alpha, \beta, \gamma, w_1, w_2, w_3)$,

$$\Phi_{M\mu}^J(\alpha, \beta, \gamma, w_1, w_2, w_3) = \sqrt{\frac{2J+1}{8\pi^2}} \Psi(w_1, w_2, w_3) D_{M\mu}^{J*}(\alpha, \beta, \gamma). \quad (8.21)$$

Replacing Φ by $\Phi_{M\mu}^J$ in expression (8.19) results in the decomposition of a generic three-body helicity state with total angular momentum J , denoted $|\Psi; JM\mu; \lambda_1\lambda_2\lambda_3\rangle$, in Berman's J -helicity states,

$$|\Psi; JM\mu; \lambda_1\lambda_2\lambda_3\rangle = \int \frac{dw_1 dw_2 dw_3}{8} \Psi(w_1, w_2, w_3) |JM\mu; w_1 w_2 w_3; \lambda_1 \lambda_2 \lambda_3\rangle. \quad (8.22)$$

Imposing a unit normalisation for $|\Psi; JM\mu; \lambda_1\lambda_2\lambda_3\rangle$ and making use the orthonormalisation of Berman's J -helicity (8.7) allows to infer the normalisation condition on $\Psi(w_1, w_2, w_3)$,

$$\langle \Psi; JM\mu; \lambda_1\lambda_2\lambda_3 | \Psi; JM\mu; \lambda_1\lambda_2\lambda_3 \rangle = \int \frac{dw_1 dw_2 dw_3}{8} |\Psi(w_1, w_2, w_3)|^2 = 1. \quad (8.23)$$

States $|\Psi; JM\mu; \lambda_1\lambda_2\lambda_3\rangle$ can be used to model spin J three-body composite particles made of three constituents. Although the aforementioned developments considered three identical particles, they can be easily generalised to three different particles. The same commentary than for two-body systems (cf. Section 6.3.2) about symmetry and parity applies. In presence of identical particles and/or if a parity quantum-number is expected, Berman's J -helicity states have to be replaced by parity and/or symmetry eigenstates which can be obtained using properties (8.9) to (8.10c). This construction will be performed in the special case of three-gluon systems in Chapter 9.

8.2 Wick's definition

Next to Berman's proposal to define three-body helicity states, Wick suggests another scheme based on an intermediate two-body coupling. First, following relation (6.42), particles 1 and 2 are coupled in a two-body J -helicity state at rest,

$$\begin{aligned} & |p_{12}; j_{12}\lambda_{12}; s_1\lambda'_1 s_2\lambda'_2\rangle \\ &= \sqrt{\frac{2j_{12}+1}{4\pi}} \int d\cos\theta_{12} d\phi_{12} D_{\lambda_{12}\lambda'_1-\lambda'_2}^{j_{12}*}(\phi_{12}, \theta_{12}, 0) |p_{12}\theta_{12}\phi_{12}; s_1\lambda'_1 s_2\lambda'_2\rangle. \end{aligned} \quad (8.24)$$

Above, p_{12} , θ_{12} and ϕ_{12} respectively denotes the momentum modulus, polar and azimuthal angle of particle 1 in the CoMF of particles 1 and 2 (12-CoMF). Helicities λ'_1 and λ'_2 are also defined

in this frame. By construction, states defined by equation (8.24) possess a definite total angular momentum for particles 1 and 2, denoted j_{12} . The third particle is then taken into account. The subsystem of particle 1 and 2 is considered as a composite particle of spin j_{12} , of spin projection λ_{12} and of mass $m_{12}(p_{12})$ with

$$m_{12}(p_{12}) = \sqrt{p_{12}^2 + m_1^2} + \sqrt{p_{12}^2 + m_2^2}. \quad (8.25)$$

This mass is necessarily non-zero. The composite particle is then coupled with the third particle in the same way it has been done for particles 1 and 2. Because masses of the different states are less explicit than before, these quantities are temporary brought back in the notation of the boosts along the z axis. The composite particle and the third one are boosted in their own CoMF, which coincide with the ECoMF,

$$\begin{aligned} |p\theta\phi; j_{12}\lambda_{12}s_3\lambda_3; p_{12}s_1\lambda'_1s_2\lambda'_2\rangle &= (-1)^{\lambda_3-s_3} U(R(\phi, \theta, 0)L_z(m_{12}(p_{12}), p)) |p_{12}; j_{12}\lambda_{12}; s_1\lambda'_1s_2\lambda'_2\rangle \\ &\otimes U(R(\pi + \phi, \pi - \theta, \pi)L_z(m_3, p)) |s_3\lambda_3\rangle. \end{aligned} \quad (8.26)$$

Above, p , θ and ϕ respectively denotes the modulus, the polar and the azimuthal angle of the momentum of the composite particle in the ECoMF. By construction, this momentum is opposite to that of the third particle, both thereby having the same modulus. For this reason, in the following, the notation p_3 will supplant p . States (8.26) will be referred to as *Wick's p -helicity states*. Even if quantum numbers that describe the internal motion of the subsystem have been included in the notations, definition (8.26) has the exact same structure than (6.38a). Therefore, a total angular momentum can be provided to the whole system by integrating on momentum angles as well,

$$\begin{aligned} |p_3; JM; j_{12}\lambda_{12}s_3\lambda_3; p_{12}s_1\lambda'_1s_2\lambda'_2\rangle \\ = \sqrt{\frac{2J+1}{4\pi}} \int d\cos\theta d\phi D_{M\lambda_{12}-\lambda_3}^{J*}(\phi, \theta, 0) |p_3\theta\phi; j_{12}\lambda_{12}s_3\lambda_3; p_{12}s_1\lambda'_1s_2\lambda'_2\rangle. \end{aligned} \quad (8.27)$$

These three-body helicity states will be referred as *Wick's J -helicity states*. Their orthonormality relation is the following,

$$\begin{aligned} \langle \bar{p}_3; \bar{J}\bar{M}; \bar{j}_{12}\bar{\lambda}_{12}s_3\bar{\lambda}_3; \bar{p}_{12}s_1\bar{\lambda}'_1s_2\bar{\lambda}'_2 | p_3; JM; j_{12}\lambda_{12}s_3\lambda_3; p_{12}s_1\lambda'_1s_2\lambda'_2\rangle \\ = \frac{8W(p_{12}, p_3)}{p_3 p_{12}} \delta(\bar{W} - W) \delta(\bar{m}_{12} - m_{12}) \delta_{\bar{J}J} \delta_{\bar{M}M} \delta_{\bar{j}_{12}j_{12}} \delta_{\bar{\lambda}_{12}\lambda_{12}} \delta_{\bar{\lambda}'_1\lambda'_1} \delta_{\bar{\lambda}'_2\lambda'_2} \delta_{\bar{\lambda}_3\lambda_3}. \end{aligned} \quad (8.28)$$

Above, W is the total energy of the three-body system in its CoMF,

$$W(p_{12}, p_3) = \sqrt{m_{12}(p_{12})^2 + p_3^2} + \sqrt{m_3^2 + p_3^2}. \quad (8.29)$$

As mentioned above, p_{12} is defined in the 12-CoMF, whereas p_3 is a momentum in the ECoMF. Relation (8.28) is to be compared to the one provided in reference [163]. Both are not directly equivalent because the definition of Wick's J -helicity states from this reference differs by an additional $(p_3 p_{12}/W m_{12})^{1/2}/4$ kinematic factor from ours. For further use, this relation is specified for the case of three massless particles. In that case, the relations between p_{12} , p_3 , m_{12} and W simplifies

$$\begin{cases} W = p_3 + \sqrt{4p_{12}^2 + p_3^2}, \\ m_{12} = 2p_{12} \end{cases} \iff \begin{cases} p_3 = (W^2 - m_{12}^2)/(2W), \\ p_{12} = m_{12}/2 \end{cases} \quad (8.30)$$

As a result, in the massless case, relation (8.28) is shown to become

$$\begin{aligned} & \langle \bar{p}_3; \bar{J}\bar{M}; \bar{j}_{12}\bar{\lambda}_{12}s_3\bar{\lambda}_3; \bar{p}_{12}s_1\bar{\lambda}'_1s_2\bar{\lambda}'_2 | p_3; JM; j_{12}\lambda_{12}s_3\lambda_3; p_{12}s_1\lambda'_1s_2\lambda'_2 \rangle \\ &= \frac{2^5 W^2}{(W^2 - m_{12}^2)m_{12}} \delta(\bar{W} - W) \delta(\bar{m}_{12} - m_{12}) \delta_{\bar{J}J} \delta_{\bar{M}M} \delta_{\bar{j}_{12}j_{12}} \delta_{\bar{\lambda}_{12}\lambda_{12}} \delta_{\bar{\lambda}'_1\lambda'_1} \delta_{\bar{\lambda}'_2\lambda'_2} \delta_{\bar{\lambda}_3\lambda_3}. \end{aligned} \quad (8.31)$$

For the current purpose, this relation will prove more comfortable to use in terms of p_3 and p_{12} , these variables being directly momenta of particles in different frames,²

$$\begin{aligned} & \langle \bar{p}_3; \bar{J}\bar{M}; \bar{j}_{12}\bar{\lambda}_{12}s_3\bar{\lambda}_3; \bar{p}_{12}s_1\bar{\lambda}'_1s_2\bar{\lambda}'_2 | p_3; JM; j_{12}\lambda_{12}s_3\lambda_3; p_{12}s_1\lambda'_1s_2\lambda'_2 \rangle \\ &= \frac{4\sqrt{p_3^2 + 4p_{12}^2}}{p_3 p_{12}} \delta(\bar{p}_3 - p_3) \delta(\bar{p}_{12} - p_{12}) \delta_{\bar{J}J} \delta_{\bar{M}M} \delta_{\bar{j}_{12}j_{12}} \delta_{\bar{\lambda}_{12}\lambda_{12}} \delta_{\bar{\lambda}'_1\lambda'_1} \delta_{\bar{\lambda}'_2\lambda'_2} \delta_{\bar{\lambda}_3\lambda_3}. \end{aligned} \quad (8.32)$$

Whereas Berman's J -helicity states (8.6) allows for an easy implementation of symmetry through relations (8.9) to (8.10c), Wick's states, thanks to the intermediary two-body coupling, are more convenient to compute matrix elements for operators related to the internal motion. To exploit the advantages of both definitions, a relationship between the two different sets of

² The Jacobian determinant related to this change is $dW dm_{12} = 2W(p_{12}, p_3)/\sqrt{p_3^2 + 4p_{12}^2} dp_3 dp_{12}$.

states can be constructed,

$$\begin{aligned}
|JM\mu; w_1 w_2 w_3; \lambda_1 \lambda_2 \lambda_3\rangle &= \sum_{\lambda'_1, \lambda'_2} D_{\lambda'_1 \lambda_1}^{s_1} (R_W^1) D_{\lambda'_2 \lambda_2}^{s_2} (R_W^2) e^{i(2s_2+2s_3+\lambda'_2-\lambda'_1-\mu)\pi/2} \\
&\sum_{j_{12}=|\lambda'_1-\lambda'_2|}^{\infty} \sum_{\lambda_{12}=-j_{12}}^{j_{12}} e^{i\lambda_{12}\pi/2} \sqrt{\frac{2j_{12}+1}{2}} d_{\lambda_{12} \lambda'_1-\lambda'_2}^{j_{12}}(\pi/2 - \phi_{12}) d_{\mu \lambda_{12}-\lambda_3}^J(\pi/2) \quad (8.33) \\
&|p_3; JM; j_{12} \lambda_{12} s_3 \lambda_3; p_{12} s_1 \lambda_1 s_2 \lambda_2\rangle.
\end{aligned}$$

A demonstration of this property is provided in Complement 8.B. Above, ϕ_{12} is the azimuthal angle of the first particle in the 12-CoMF where the momentum of the third particle is along the y axis towards negatives. This quantity, as well as every other dynamical quantity in this relation, is to be understood as depending on w_1 , w_2 and w_3 . Rotations R_W^1 and R_W^2 are Wigner rotations given by the following combinations of boosts and rotations,

$$\begin{aligned}
R_W^1 &= (R(\phi_{12}, \pi/2, 0) L_z(m_1, p_{12}))^{-1} L_3 (R(\phi_1, \pi/2, 0) L_z(m_1, p_1)), \\
R_W^2 &= (R(\pi + \phi_{12}, \pi/2, 0) L_z(m_2, p_{12}))^{-1} L_3 (R(\phi_2, \pi/2, 0) L_z(m_2, p_2)).
\end{aligned} \quad (8.34)$$

where $L_3 = R(3\pi/2, \pi/2, 0) L_z(m_{12}, p_3) R^{-1}(3\pi/2, \pi/2, 0)$. The fact that helicities of particle 1 and 2 are summed in the formula keeps track that helicities λ_i and λ'_i are not defined in the same frame. The appearance of an infinite sum over j_{12} is also an expected feature. To obtain a given total angular momentum J , one can always choose an arbitrarily large relative angular momentum between particle 1 and 2 and then compensate it with the relative angular momentum between this subsystem and the third particle. Let us mention that formula (8.33) looks rather similar to a result obtained by Wick in [163]. In this reference, Wick rewrites its states in a more symmetrical way, closer to Berman's definition but where the yz plane is chosen as reference. This rewriting introduces two Wigner rotations and a Wigner d -matrix which depends on a dynamical angle. The formula introduced in the current work presents the same components supplemented by a second Wigner D -matrix that rotates the reference plane, in accordance with property (8.8). Formula (8.33) can be seen as a descendant to Wick's rewriting.

In Chapter 9, formula (8.33) will be used to describe systems of three massless gluons. For massless particles, both previous Wigner rotations simplify following expression (6.66). The

change of basis formula reduces to

$$\begin{aligned}
 |JM\mu; w_1 w_2 w_3; \lambda_1 \lambda_2 \lambda_3\rangle &= e^{i(2s_2+2s_3+\lambda_2-\lambda_1-\mu)\pi/2} e^{i(\theta_1\lambda_1+\theta_2\lambda_2)} \\
 &\sum_{j_{12}=|\lambda_1-\lambda_2|}^{\infty} \sum_{\lambda_{12}=-j_{12}}^{j_{12}} e^{i\pi\lambda_{12}/2} \sqrt{\frac{2j_{12}+1}{2}} d_{\lambda_{12}\lambda_1-\lambda_2}^{j_{12}}(\pi/2 - \phi_{12}) d_{\mu\lambda_{12}-\lambda_3}^J(\pi/2) \\
 &|p_3; JM; j_{12}\lambda_{12}s_3\lambda_3; p_{12}s_1\lambda_1s_2\lambda_2\rangle.
 \end{aligned} \tag{8.35}$$

As expected, since helicity is Lorentz invariant for massless particles, the corresponding quantum numbers are no longer summed. Values for both θ_i angles are founded by applying the methodology suggested in reference [164]. These two angles are shown to cancel and the phase factor reduces,

$$e^{i(2s_2+2s_3+\lambda_2-\lambda_1-\mu)\pi/2} e^{i(\theta_1\lambda_1+\theta_2\lambda_2)} = (-1)^{s_3+s_2} e^{i(\pi/2)(\lambda_2-\lambda_1-\mu)}. \tag{8.36}$$

This phase is manifestly independent of the w_1 , w_2 or w_3 energies. In the case of massless particles, the expression of ϕ_{12} , p_{12} and p_3 in terms of w_1 , w_2 and w_3 also simplifies,

$$\cos(\pi/2 - \phi_{12}) = (w_1 - w_2)/w_3, \quad 2p_{12} = \sqrt{(w_1 + w_2)^2 - w_3^2}, \quad p_3 = w_3. \tag{8.37}$$

Inverting these relations, one gets

$$w_1 = (\sqrt{4p_{12}^2 + w_3^2} + uw_3)/2, \quad w_2 = (\sqrt{4p_{12}^2 + w_3^2} - uw_3)/2, \quad w_3 = p_3, \tag{8.38}$$

where $u = \cos(\pi/2 - \phi_{12}) = \sin\phi_{12}$. A consistency check of formula (8.35) is provided in Complement 8.B.

Complement 8.A Properties of Berman's States

This Appendix is devoted to the demonstration of some properties about Berman's states missing in the literature. Let us start with property (8.8), which is about the modification of the reference plane in the definition of Berman's J helicity states. For the sake of conciseness, in the following, $R(\alpha, \beta, \gamma)$ will be denoted R and $d\alpha d\cos\beta d\gamma$ will be denoted dR . First, an arbitrary rotation \bar{R} is artificially introduced in (8.6). The \bar{R} rotation is applied on the reference

state $|w_1 w_2 w_3; \lambda_1 \lambda_2 \lambda_3\rangle$ while its inverse is composed with the rotation R ,

$$|JM\mu; w_1 w_2 w_3; \lambda_1 \lambda_2 \lambda_3\rangle = \sqrt{\frac{2J+1}{8\pi^2}} \int dR D_{M\mu}^{J*}(R) U(R\bar{R}^{-1}) U(\bar{R}) |w_1 w_2 w_3; \lambda_1 \lambda_2 \lambda_3\rangle. \quad (8.39)$$

Turning the integration on R Euler angles into an integration on $R\bar{R}^{-1}$ Euler angles, one gets

$$|JM\mu; w_1 w_2 w_3; \lambda_1 \lambda_2 \lambda_3\rangle = \sum_{\mu'=-J}^J D_{\mu'\mu}^{J*}(\bar{R}) \sqrt{\frac{2J+1}{8\pi^2}} \int d(R\bar{R}^{-1}) D_{M\mu'}^{J*}(R\bar{R}^{-1}) U(R\bar{R}^{-1}) (U(\bar{R}) |w_1 w_2 w_3; \lambda_1 \lambda_2 \lambda_3\rangle). \quad (8.40)$$

In the right-hand side of this equation, one recognize the definition of a Berman's J helicity state whose reference state would have been tilted with the rotation \bar{R} . Denoting this state $|JM\mu'; w_1 w_2 w_3; \lambda_1 \lambda_2 \lambda_3\rangle_{\bar{R}}$, one finally gets formula (8.8),

$$|JM\mu; w_1 w_2 w_3; \lambda_1 \lambda_2 \lambda_3\rangle = \sum_{\mu'=-J}^J D_{\mu\mu'}^J(\bar{R}^{-1}) |JM\mu'; w_1 w_2 w_3; \lambda_1 \lambda_2 \lambda_3\rangle_{\bar{R}}. \quad (8.41)$$

This property can be used to relate different conventions for Berman's states. In reference [187], Berman's reference states are defined considering the momentum of the third particle as opposite to the x axis in [187] while it is opposite to the y axis in the current work. In light of the previous developments, these two definitions for Berman's J -helicity states have a chance to differ each-other. The rotation \bar{R} that conveys from one convention to the other one brings the y axis along the x one, meaning

$$\bar{R} = R(0, 0, -\pi/2). \quad (8.42)$$

Applying the aforementioned relation to this case, one gets

$$\begin{aligned} |JM\mu; w_1 w_2 w_3; \lambda_1 \lambda_2 \lambda_3\rangle &= \sum_{\mu'=-J}^J D_{\mu\mu'}^J(0, 0, \pi/2) |JM\mu'; w_1 w_2 w_3; \lambda_1 \lambda_2 \lambda_3\rangle_{[187]} \\ &= i^{-\mu} |JM\mu; w_1 w_2 w_3; \lambda_1 \lambda_2 \lambda_3\rangle_{[187]}, \end{aligned} \quad (8.43)$$

where the notation $|\dots\rangle_{[187]}$ refers to an helicity state that uses conventions from [187]. Although both states have the same physical meaning, they differ by their phase conventions.

The action of \mathbb{P}_{13} on Berman's J -helicity states also deserves a few explanations. The interest of symmetry being limited to the study of identical particles, spins and masses of the three particles will be supposed equal, $s_1 = s_2 = s_3 = s$ and $m_1 = m_2 = m_3 = m$. Calculations have first to be performed at the p -helicity states level. The permutation operator exchanges the

states of particle 1 and 3,

$$\begin{aligned} \mathbb{P}_{13} |\alpha\beta\gamma; w_1 w_2 w_3; \lambda_1 \lambda_2 \lambda_3\rangle &= U(R(\alpha, \beta, \gamma)) (U(R(\phi_3, \pi/2, 0) L_z(p_3)) |s\lambda_3\rangle \\ &\otimes U(R(\phi_2, \pi/2, 0) L_z(p_2)) |s\lambda_2\rangle \\ &\otimes U(R(\phi_1, \pi/2, 0) L_z(p_1)) |s\lambda_1\rangle). \end{aligned} \quad (8.44)$$

It is not clear if the left-hand side of this equation fits with the structure of a Berman's p -helicity states because for now relations (8.2) and (8.3) are not verified. This difficulty can be overcome by the insertion of a rotation $R(\varphi_{13}, -\pi, 0)$. The angles are chosen to mimic the action of \mathbb{P}_{13} on the momenta, as illustrated on Fig. 8.2. Algebraically, one gets,

$$\begin{aligned} \mathbb{P}_{13} |\alpha\beta\gamma; w_1 w_2 w_3; \lambda_1 \lambda_2 \lambda_3\rangle &= U(R(\alpha, \beta, \gamma) R(\varphi_{13}, -\pi, 0)) \\ &\quad (U(R(0, \pi, -\varphi_{13}) R(\phi_3, \pi/2, 0) L_z(p_3)) |s\lambda_3\rangle \\ &\otimes U(R(0, \pi, -\varphi_{13}) R(\phi_2, \pi/2, 0) L_z(p_2)) |s\lambda_2\rangle \\ &\otimes U(R(0, \pi, -\varphi_{13}) R(\phi_1, \pi/2, 0) L_z(p_1)) |s\lambda_1\rangle). \end{aligned} \quad (8.45)$$

The $SO(3)$ multiplication law can be used to reduce the previous expression

$$R(\alpha, \beta, \gamma) R(\varphi_{13}, -\pi, 0) = R(\pi + \alpha, \pi - \beta, -(\pi + \gamma + \varphi_{13})), \quad (8.46)$$

$$R(0, \pi, -\varphi_{13}) R(\phi, \pi/2, 0) = R(\pi + \varphi_{13} - \phi, \pi/2, \pi) \quad (\forall \phi \in \mathbb{R}). \quad (8.47)$$

With these relations the action of \mathbb{P}_{13} on $|\alpha\beta\gamma; W w_1 w_2; \lambda_1 \lambda_2 \lambda_3\rangle$ becomes,

$$\begin{aligned} \mathbb{P}_{13} |\alpha\beta\gamma; w_1 w_2 w_3; \lambda_1 \lambda_2 \lambda_3\rangle &= U(R(\pi + \alpha, \pi - \beta, -(\pi + \gamma + \varphi_{13}))) (U(R(\pi + \varphi_{13} - \phi_3, \pi/2, \pi) L_z(p_3)) |s\lambda_3\rangle \\ &\otimes U(R(\pi + \varphi_{13} - \phi_2, \pi/2, \pi) L_z(p_2)) |s\lambda_2\rangle \\ &\otimes U(R(\pi + \varphi_{13} - \phi_1, \pi/2, \pi) L_z(p_1)) |s\lambda_1\rangle). \end{aligned} \quad (8.48)$$

This relation can be even further simplified using expression (8.3) for ϕ_1 , ϕ_2 and ϕ_3 ,

$$\begin{aligned} \mathbb{P}_{13} |\alpha\beta\gamma; w_1 w_2 w_3; \lambda_1 \lambda_2 \lambda_3\rangle &= U(R(\pi + \alpha, \pi - \beta, -(\pi + \gamma + \varphi_{13}))) (U(R(\varphi_{13} - \pi/2, \pi/2, \pi) L_z(p_3)) |s\lambda_3\rangle \\ &\otimes U(R(3\pi/2 - \varphi_{12}, \pi/2, \pi) L_z(p_2)) |s\lambda_2\rangle \\ &\otimes U(R(3\pi/2, \pi/2, \pi) L_z(p_1)) |s\lambda_1\rangle) \end{aligned} \quad (8.49)$$

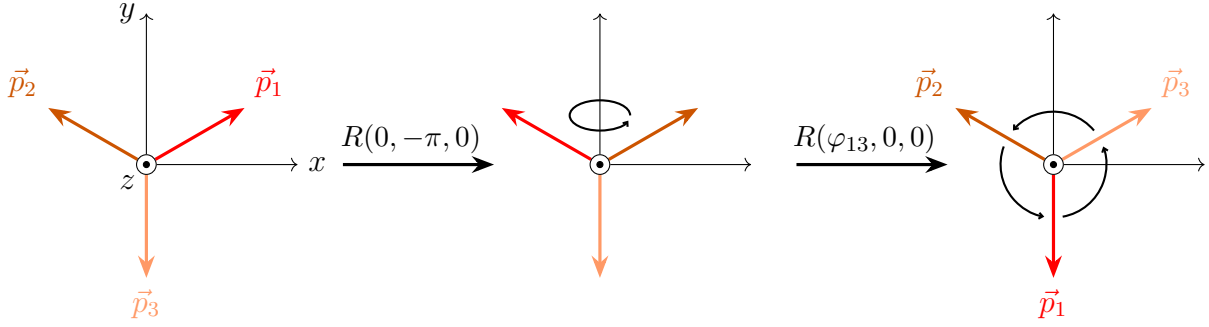


Figure 8.2: Diagram justifying the role of $R(\varphi_{13}, -\pi, 0)$ in the application of \mathbb{P}_{13} on Berman's states.

$$\begin{aligned}
 &= U(R(\pi + \alpha, \pi - \beta, -(\pi + \gamma + \varphi_{13}))) (U(R(\varphi_{13} - \pi/2, \pi/2, \pi)L_z(p_3)) |s\lambda_3\rangle \\
 &\quad \otimes U(R(\varphi_{13} + \varphi_{23} - \pi/2, \pi/2, \pi)L_z(p_2)) |s\lambda_2\rangle \quad (8.50) \\
 &\quad \otimes U(R(3\pi/2, \pi/2, \pi)L_z(p_1)) |s\lambda_1\rangle).
 \end{aligned}$$

Last equality makes use of $\varphi_{12} + \varphi_{23} + \varphi_{13} = 2\pi$. The three angles in the reference state now satisfy relations (8.2) and (8.3) with w_1 and w_3 exchanged. To definitely obtain a true p -helicity state, the π rotations around the z axis have to be absorbed in the $|s\lambda_i\rangle$. This operation produces three $(-1)^{-\lambda_i}$ phase factors,

$$\begin{aligned}
 &\mathbb{P}_{13} |\alpha\beta\gamma; w_1w_2w_3; \lambda_1\lambda_2\lambda_3\rangle \\
 &= (-1)^{-\lambda_1-\lambda_2-\lambda_3} |(\pi + \alpha)(\pi - \beta)(-\pi - \gamma - \varphi_{13}); w_3w_2w_1; \lambda_3\lambda_2\lambda_1\rangle. \quad (8.51)
 \end{aligned}$$

Now that the relation has been written for Berman's p -helicity states, the corresponding relation for Berman's J -helicity states can be obtained,

$$\begin{aligned}
 &\mathbb{P}_{13} |JM\mu; w_1w_2w_3; \lambda_1\lambda_2\lambda_3\rangle \\
 &= \sqrt{\frac{2J+1}{8\pi^2}} \int d\alpha d\cos\beta d\gamma D_{M\mu}^{J*}(\alpha, \beta, \gamma) \mathbb{P}_{13} |\alpha\beta\gamma; w_1w_2w_3; \lambda_1\lambda_2\lambda_3\rangle \\
 &= (-1)^{-\lambda_1-\lambda_2-\lambda_3} \sqrt{\frac{2J+1}{8\pi^2}} \int d\alpha d\cos\beta d\gamma D_{M\mu}^{J*}(\alpha, \beta, \gamma) \\
 &\quad |(\pi + \alpha)(\pi - \beta)(-\pi - \gamma - \varphi_{13}); w_3w_2w_1; \lambda_3\lambda_2\lambda_1\rangle. \quad (8.52)
 \end{aligned}$$

The integration variables can be changed to fit with the new angles in the p -helicity state,

$$\begin{aligned}
 & \mathbb{P}_{13} |JM\mu; w_1 w_2 w_3; \lambda_1 \lambda_2 \lambda_3\rangle \\
 &= (-1)^{-\lambda_1 - \lambda_2 - \lambda_3} \sqrt{\frac{2J+1}{8\pi^2}} \int d\alpha' d\cos\beta' d\gamma' D_{M\mu}^{J*}(\alpha' - \pi, \pi - \beta', -\pi - \gamma' - \varphi_{13}) \\
 & \quad |\alpha' \beta' \gamma'; w_3 w_2 w_1; \lambda_3 \lambda_2 \lambda_1\rangle.
 \end{aligned} \tag{8.53}$$

Making use of Wigner D matrices properties [35], the aforementioned relation can be reduced,

$$\begin{aligned}
 & \mathbb{P}_{13} |JM\mu; w_1 w_2 w_3; \lambda_1 \lambda_2 \lambda_3\rangle \\
 &= (-1)^{-\lambda_1 - \lambda_2 - \lambda_3} \sqrt{\frac{2J+1}{8\pi^2}} \int d\alpha' d\cos\beta' d\gamma' ((-1)^{J-\mu} e^{-i\varphi_{13}\mu} D_{M-\mu}^{J*}(\alpha', \beta', \gamma')) \\
 & \quad |\alpha' \beta' \gamma'; w_3 w_2 w_1; \lambda_3 \lambda_2 \lambda_1\rangle \\
 &= (-1)^{J-\mu - \lambda_1 - \lambda_2 - \lambda_3} e^{-i\varphi_{13}\mu} |JM - \mu; w_3 w_2 w_1; \lambda_3 \lambda_2 \lambda_1\rangle.
 \end{aligned} \tag{8.54}$$

This closes the demonstration of the property. The action of \mathbb{P}_{23} is demonstrated in a similar way.

Complement 8.B Proof of the change of basis formula

This Appendix is dedicated to the derivation of relation (8.33). It is divided in three parts. First, Berman's p -helicity states are restructured to include a state for particle 1 and 2 in their CoMF. Then, this rewriting is used to prove the change of basis formula. Finally, a consistency check concerning normalisation of the states is suggested.

Rewriting of p -helicity states

To fit with Wick's structure, particle 1 and 2 in Berman's states are to be brought in their own CoMF. This operation is performed on the reference states (8.4) at first. The boost that transitions between the ECoMF and the 12-CoMF is the one that imparts a momentum \mathbf{p}_3 to a particle of mass m_{12} initially at rest. It writes down as follows

$$L_3 = R(3\pi/2, \pi/2, 0) L_z(m_{12}, p_3) R^{-1}(3\pi/2, \pi/2, 0). \tag{8.55}$$

This L_3 boost can be artificially inserted into the definition of Berman's reference states (8.4),

$$\begin{aligned}
 & |w_1 w_2 w_3; \lambda_1 \lambda_2 \lambda_3\rangle \\
 &= U(L_3^{-1} L_3) \left[U(R(\phi_1, \pi/2, 0) L_z(p_1)) |s_1 \lambda_1\rangle \otimes U(R(\phi_2, \pi/2, 0) L_z(p_2)) |s_2 \lambda_2\rangle \right] \\
 & \quad \otimes U(R(\phi_3, \pi/2, 0) L_z(p_3)) |s_3 \lambda_3\rangle \quad (8.56) \\
 &= U(L_3^{-1}) \left[U(L_3) U(R(\phi_1, \pi/2, 0) L_z(p_1)) |s_1 \lambda_1\rangle \otimes U(L_3) U(R(\phi_2, \pi/2, 0) L_z(p_2)) |s_2 \lambda_2\rangle \right] \\
 & \quad \otimes U(R(\phi_3, \pi/2, 0) L_z(p_3)) |s_3 \lambda_3\rangle.
 \end{aligned}$$

Inside the brackets, both particle 1 and particle 2 are subjected to the L_3 boost. The subsequent development focuses on the first particle but the same applies to the second one. The expression to simplify results from applying a Lorentz boost on a one-body helicity state (6.26),

$$U(L_3) U(R(\phi_1, \pi/2, 0) L_z(p_1)) |s_1 \lambda_1\rangle = U(L_3) |p_1 \pi/2 \phi_1; s_1 \lambda_1\rangle_0. \quad (8.57)$$

For further clarification, the third angle convention is written as an index. The situation is the one handled by property (6.35),

$$U(L_3) |p_1 \pi/2 \phi_1; s_1 \lambda_1\rangle_0 = \sum_{\lambda'_1} D_{\lambda'_1 \lambda_1}^{s_1}(R_W^1) |p_{12} \theta_{12} \phi_{12}; s_1 \lambda'_1\rangle_0. \quad (8.58)$$

By construction, after applying the L_3 boost, the momentum ends in the 12-CoMF. Corresponding coordinates have been denoted p_{12} , θ_{12} and ϕ_{12} , in agreement with notations from Wick's definition (8.24). Because momenta in the reference state are chosen to lie in the xy plane and because L_3 is a boost along the y axis, boosted momenta remain in that same plane. As a consequence, the polar angle θ_{12} is shown to be identically equal to $\pi/2$. Concerning expressions of p_{12} and ϕ_{12} in terms of the energies w_1 , w_2 and w_3 , these are obtained by evaluating different Lorentz invariant combinations of four-momenta³ in both the 12-CoMF and the ECoMF. This allows to show that

$$2p_{12} = \sqrt{(w_1 + w_2)^2 - w_3^2}, \quad \cos(\pi/2 - \phi_{12}) = \frac{w_1 - w_2}{w_3}. \quad (8.59)$$

The Wigner rotation R_W^1 is obtained by specifying expression (6.36) to the current situation,

$$R_W^1 = (R(\phi_{12}, \pi/2, 0) L_z(m_1, p_{12}))^{-1} L_3 (R(\phi_1, \pi/2, 0) L_z(m_1, p_1)). \quad (8.60)$$

³ Namely $(\mathbf{P}_1 + \mathbf{P}_2)^2$, $(\mathbf{P}_1 + \mathbf{P}_3)^2$ and $(\mathbf{P}_1 + \mathbf{P}_2 + \mathbf{P}_3)^2$.

This expression for R_W^1 and the knowledge of each particle masses and energies theoretically allow to determine the parameters for the Wigner rotation and to deduce the corresponding D matrix. The same calculation is applied to the second particle. By collecting the results, the following intermediate expression is obtained for the three-body reference state,

$$\begin{aligned}
 |w_1 w_2 w_3; \lambda_1 \lambda_2 \lambda_3\rangle &= \sum_{\lambda'_1, \lambda'_2} D_{\lambda'_1 \lambda_1}^{s_1} (R_W^1) D_{\lambda'_2 \lambda_2}^{s_2} (R_W^2) \\
 &\left(U(L_3)^{-1} \left[|p_{12}(\pi/2)(\phi_{12}); s_1 \lambda'_1\rangle_0 \otimes |p_{12}(\pi/2)(\pi + \phi_{12}); s_2 \lambda'_2\rangle_0 \right] \right. \\
 &\quad \left. \otimes |p_3(\pi/2)\phi_3; s_3 \lambda_3\rangle_0 \right). \tag{8.61}
 \end{aligned}$$

Above, the definition of one-body helicity state (6.26) has also been used for the last particle. By using the definition of L_3 , its invert can be written as

$$L_3^{-1} = R(5\pi/2, \pi/2, 0) L_z(m_{12}, p_3) R^{-1}(5\pi/2, \pi/2, 0). \tag{8.62}$$

The boost L_3^{-1} proves to fit the definition of a canonical boost (6.21). An helicity boost would be more convenient to subsequently construct helicity states. To perform the conversion, the rotation on the right can be absorbed into both one-body helicity states, using the invariance of helicity under rotations (6.29),

$$R^{-1}(5\pi/2, \pi/2, 0) |p_{12}(\pi/2)(\phi_{12}); s_1 \lambda'_1\rangle_0 = e^{i\xi_1 \lambda'_1} |p_{12}(\pi/2 - \phi_{12})(3\pi/2); s_1 \lambda'_1\rangle_0, \tag{8.63}$$

$$R^{-1}(5\pi/2, \pi/2, 0) |p_{12}(\pi/2)(\pi + \phi_{12}); s_2 \lambda'_2\rangle_0 = e^{i\xi_2 \lambda'_2} |p_{12}(\pi/2 + \phi_{12})(5\pi/2); s_2 \lambda'_2\rangle_\pi. \tag{8.64}$$

Because in definition (8.24) the second particle is considered as opposed to the first one, it is brought in the π convention instead of the 0 one. Above, the expressions for the polar and azimuth angles from the right-hand side state are obtained by applying $R^{-1}(5\pi/2, \pi/2, 0)$ on both particle momenta. Concerning ξ_1 and ξ_2 , their values are obtained by explicitly multiplying both rotations that provide their angles to the one-body helicity states by $R^{-1}(5\pi/2, \pi/2, 0)$,

$$\begin{aligned}
 R^{-1}(5\pi/2, \pi/2, 0) R(\phi_{12}, \pi/2, 0) &= R(3\pi/2, \pi/2 - \phi_{12}, \pi/2), \\
 R^{-1}(5\pi/2, \pi/2, 0) R(\pi + \phi_{12}, \pi/2, 0) &= R(5\pi/2, \pi/2 + \phi_{12}, -\pi/2).
 \end{aligned} \tag{8.65}$$

Noticing that ϕ_{12} itself lies in between $-\pi/2$ and $\pi/2$, these two formulas have been tuned so that the second Euler angle of both combined rotations lies in between 0 and π . The combined rotations are neither in the 0 nor in the π convention. This issue is resolved by adding the suitable rotation around the z axis. After acting on the helicity state, this results in a simple

phase factor,

$$e^{i\lambda'_1\xi_1} = e^{-i\lambda'_1\pi/2}, \quad e^{i\lambda'_2\xi_2} = e^{3i\lambda'_2\pi/2}. \quad (8.66)$$

At this stage, the reference state has been restructured as follows,

$$\begin{aligned} & |w_1w_2w_3; \lambda_1\lambda_2\lambda_3\rangle \\ &= \sum_{\lambda'_1, \lambda'_2} D_{\lambda'_1 \lambda_1}^{s_1} (R_W^1) D_{\lambda'_2 \lambda_2}^{s_2} (R_W^2) e^{-i(\lambda'_1 - 3\lambda'_2)\pi/2} \left(U(R(5\pi/2, \pi/2, 0)) L_z(m_{12}, p_3) \right) \\ & \quad \left[|p_{12}(\pi/2 - \phi_{12})(3\pi/2); s_1\lambda'_1\rangle_0 \otimes |p_{12}(\pi/2 + \phi_{12})(5\pi/2); s_2\lambda'_2\rangle_\pi \right] \\ & \quad \otimes |p_3(\pi/2)(3\pi/2); s_3\lambda_3\rangle_0. \end{aligned} \quad (8.67)$$

Two small modifications remain to be performed. First, the third particle is for now in the 0 convention but, because the momentum of particle 3 will be considered as opposed, its third angle convention should be changed to the π one, thereby adding a $e^{i\lambda_3\pi}$ phase factor. Lastly, the state inside the brackets can be rewritten as a two-body helicity state (6.38b). This only requires an additional phase $(-1)^{s_2 - \lambda'_2}$. The final expression for the reference state is

$$\begin{aligned} |w_1w_2w_3; \lambda_1\lambda_2\lambda_3\rangle &= \sum_{\lambda'_1, \lambda'_2} D_{\lambda'_1 \lambda_1}^{s_1} (R_W^1) D_{\lambda'_2 \lambda_2}^{s_2} (R_W^2) e^{i(2s_2 + \lambda'_2 - \lambda'_1 + 2\lambda_3)\pi/2} \\ & \quad \left(U(R(5\pi/2, \pi/2, 0)) L_z(m_{12}, p_3) \right) |p_{12}(\pi/2 - \phi_{12})(3\pi/2); s_1\lambda'_1 s_2\lambda'_2\rangle \\ & \quad \otimes |p_3(\pi/2)(3\pi/2); s_3\lambda_3\rangle_\pi. \end{aligned} \quad (8.68)$$

This expression has the desired structure: particles 1 and 2 are coupled in their own CoMF, and this subsystem is boosted towards the ECoMF to be coupled with the third particle.

Rewriting of J -helicity states

Now that an intermediary coupling has been added in Berman's p -helicity states, the development of Berman's J -helicity states in Wick's J -helicity states can be performed. By inserting relation (8.68) into the definition (8.6), the following expression is obtained,

$$\begin{aligned}
 |JM\mu; w_1 w_2 w_3; \lambda_1 \lambda_2 \lambda_3\rangle &= \sqrt{\frac{2J+1}{8\pi^2}} \sum_{\lambda'_1, \lambda'_2} D_{\lambda'_1 \lambda_1}^{s_1} (R_W^1) D_{\lambda'_2 \lambda_2}^{s_2} (R_W^2) e^{i(2s_2 + \lambda'_2 - \lambda'_1 + 2\lambda_3)\pi/2} \\
 &\int d\alpha d\cos\beta d\gamma D_{M\mu}^{J*}(\alpha, \beta, \gamma) U(R(\alpha, \beta, \gamma)) \left(U(R(5\pi/2, \pi/2, 0)) L_z(m_{12}, p_3) \right. \\
 &\left. |p_{12}(\pi/2 - \phi_{12})(3\pi/2); s_1 \lambda'_1 s_2 \lambda'_2\rangle \otimes |p_3(\pi/2)(3\pi/2); s_3 \lambda_3\rangle_\pi \right). \tag{8.69}
 \end{aligned}$$

To fit with Wick's definition, eigenstates of the total angular momentum relative to particle 1 and 2 would be preferable to the current $|p_{12}(\pi/2 - \phi_{12})(3\pi/2); s_1 \lambda'_1 s_2 \lambda'_2\rangle$. Such two-body states are related to each-other by relation (6.45). By omitting some passive coefficients for brevity, the following expression is obtained,

$$\begin{aligned}
 |JM\mu; w_1 w_2 w_3; \lambda_1 \lambda_2 \lambda_3\rangle &= \sum_{\lambda'_1, \lambda'_2} [\dots] \int d\alpha d\cos\beta d\gamma (\dots) \\
 &\sum_{j_{12}=|\lambda'_1 - \lambda'_2|}^{\infty} \sum_{\lambda_{12}=-j_{12}}^{j_{12}} \sqrt{\frac{2j_{12}+1}{4\pi}} D_{\lambda_{12} \lambda'_1 - \lambda'_2}^{j_{12}}(3\pi/2, \pi/2 - \phi_{12}, 0) U(R(\alpha, \beta, \gamma)) \\
 &\left(U(R(5\pi/2, \pi/2, 0)) L_z(m_{12}, p_3) |p_{12}; j_{12} \lambda_{12}; \lambda'_1 \lambda'_2\rangle \otimes |p_3(\pi/2)(3\pi/2); s_3 \lambda_3\rangle_\pi \right). \tag{8.70}
 \end{aligned}$$

The structure of the state inside the large parentheses almost follows the pattern of Wick's p -helicity states (8.26). The main difference lays in the rotation that acts on the two-body state. It involves a $5\pi/2$ rotation around the z -axis where a rotation in between 0 and 2π is expected. For bosonic states, 2π rotations are identified to the identity and can freely be ignored. For fermionic states, these rotations give rise to minus signs which have to be taken into account. Both cases can be taken into account at once by adding a $(-1)^{2\lambda'_1 + 2\lambda'_2}$ factor. A $(-1)^{\lambda_3 - s_3}$ phase factor has also to be added to truly correspond to Wick's p -helicity state definition,

$$\begin{aligned}
 |JM\mu; w_1 w_2 w_3; \lambda_1 \lambda_2 \lambda_3\rangle &= \sum_{\lambda'_1, \lambda'_2} [\dots] \int d\alpha d\cos\beta d\gamma (\dots) \sum_{j_{12}=|\lambda'_1 - \lambda'_2|}^{\infty} \sum_{\lambda_{12}=-j_{12}}^{j_{12}} \sqrt{\frac{2j_{12}+1}{4\pi}} \\
 &D_{\lambda_{12} \lambda'_1 - \lambda'_2}^{j_{12}}(3\pi/2, \pi/2 - \phi_{12}, 0) U(R(\alpha, \beta, \gamma)) (-1)^{2\lambda'_1 + 2\lambda'_2 + s_3 - \lambda_3} \\
 &|p_3(\pi/2)(\pi/2); j_{12} \lambda_{12} s_3 \lambda_3; p_{12} s_1 \lambda'_1 s_2 \lambda'_2\rangle. \tag{8.71}
 \end{aligned}$$

A second use of relation (6.45) allows to replace this state with defined momenta by a sum of states with defined total angular momentum,

$$\begin{aligned}
 |JM\mu; w_1 w_2 w_3; \lambda_1 \lambda_2 \lambda_3\rangle &= \sum_{\lambda'_1, \lambda'_2} [\dots] \int d\alpha d\cos\beta d\gamma (\dots) \\
 &\sum_{j_{12}=|\lambda'_1-\lambda'_2|}^{\infty} \sum_{\lambda_{12}=-j_{12}}^{j_{12}} \{\dots\} \sum_{\bar{J}=|\lambda_{12}-\lambda_3|}^{\infty} \sum_{\bar{M}=-\bar{J}}^{\bar{J}} \sqrt{\frac{2\bar{J}+1}{4\pi}} D_{\bar{M} \lambda_{12}-\lambda_3}^{\bar{J}}(\pi/2, \pi/2, 0) \\
 &U(R(\alpha, \beta, \gamma)) |p_3; \bar{J}\bar{M}; j_{12}\lambda_{12}s_3\lambda_3; p_{12}s_1\lambda'_1 s_2\lambda'_2\rangle.
 \end{aligned} \tag{8.72}$$

Dots have again been used to replace passive coefficients in the expression. The relation can still be simplified. To start with, the transformation rule of angular momentum eigenstates under rotations [159, 160] is used to eliminate the $U(R(\alpha, \beta, \gamma))$ operator,

$$\begin{aligned}
 |JM\mu; w_1 w_2 w_3; \lambda_1 \lambda_2 \lambda_3\rangle &= \sum_{\lambda'_1, \lambda'_2} [\dots] \int d\alpha d\cos\beta d\gamma (\dots) \\
 &\sum_{j_{12}=|\lambda'_1-\lambda'_2|}^{\infty} \sum_{\lambda_{12}=-j_{12}}^{j_{12}} \{\dots\} \sum_{\bar{J}=|\lambda_{12}-\lambda_3|}^{\infty} \sum_{\bar{M}=-\bar{J}}^{\bar{J}} \sqrt{\frac{2\bar{J}+1}{4\pi}} D_{\bar{M} \lambda_{12}-\lambda_3}^{\bar{J}}(\pi/2, \pi/2, 0) \\
 &\sum_{M'=-\bar{J}}^{\bar{J}} D_{M'\bar{M}}^{\bar{J}}(\alpha, \beta, \gamma) |p_3; \bar{J}M'; j_{12}\lambda_{12}s_3\lambda_3; p_{12}s_1\lambda'_1 s_2\lambda'_2\rangle.
 \end{aligned} \tag{8.73}$$

Aforementioned passive coefficients will be reintroduced one after the others. Brackets, curly brackets and parentheses are used consistently to trace their origin. The (α, β, γ) dependence is confined in two Wigner D matrices,

$$\begin{aligned}
 |JM\mu; w_1 w_2 w_3; \lambda_1 \lambda_2 \lambda_3\rangle &= \sum_{\lambda'_1, \lambda'_2} [\dots] \sum_{j_{12}=|\lambda'_1-\lambda'_2|}^{\infty} \sum_{\lambda_{12}=-j_{12}}^{j_{12}} \{\dots\} \sum_{\bar{J}=|\lambda_{12}-\lambda_3|}^{\infty} \sum_{\bar{M}=-\bar{J}}^{\bar{J}} \sqrt{\frac{2\bar{J}+1}{4\pi}} D_{\bar{M} \lambda_{12}-\lambda_3}^{\bar{J}}(\pi/2, \pi/2, 0) \\
 &\sum_{M'=-\bar{J}}^{\bar{J}} \left(\int d\alpha d\cos\beta d\gamma (D_{M\mu}^{J*}(\alpha, \beta, \gamma)) D_{M'\bar{M}}^{\bar{J}}(\alpha, \beta, \gamma) \right) \\
 &|p_3; \bar{J}M'; j_{12}\lambda_{12}s_3\lambda_3; p_{12}s_1\lambda'_1 s_2\lambda'_2\rangle.
 \end{aligned} \tag{8.74}$$

The orthogonality of Wigner D matrices [35] can now be used. It produces three Kronecker deltas that eliminate three sums among the six,

$$\begin{aligned}
 & |JM\mu; w_1 w_2 w_3; \lambda_1 \lambda_2 \lambda_3\rangle \\
 &= \left[\sqrt{\frac{2J+1}{8\pi^2}} \right] \sum_{\lambda'_1, \lambda'_2} [\dots] \sum_{j_{12}=|\lambda'_1-\lambda'_2|}^{\infty} \sum_{\lambda_{12}=-j_{12}}^{j_{12}} \{ \dots \} \sqrt{\frac{2J+1}{4\pi}} D_{\mu \lambda_{12}-\lambda_3}^J(\pi/2, \pi/2, 0) \\
 & \qquad \qquad \qquad \frac{8\pi^2}{2J+1} |p_3; JM; j_{12} \lambda_{12} s_3 \lambda_3; p_{12} s_1 \lambda'_1 s_2 \lambda'_2\rangle.
 \end{aligned} \tag{8.75}$$

At this stage, reintroducing all the passive coefficients, the following expression has been obtained,

$$\begin{aligned}
 |JM\mu; w_1 w_2 w_3; \lambda_1 \lambda_2 \lambda_3\rangle &= \sqrt{2\pi} \sum_{\lambda'_1, \lambda'_2} \left[D_{\lambda'_1 \lambda_1}^{s_1} (R_W^1) D_{\lambda'_2 \lambda_2}^{s_2} (R_W^2) e^{i(2s_2+\lambda'_2-\lambda'_1+2\lambda_3)\pi/2} \right] \\
 & \sum_{j_{12}=|\lambda'_1-\lambda'_2|}^{\infty} \sum_{\lambda_{12}=-j_{12}}^{j_{12}} \left\{ (-1)^{2\lambda'_1+2\lambda'_2+s_3-\lambda_3} \sqrt{\frac{2j_{12}+1}{4\pi}} D_{\lambda_{12} \lambda'_1-\lambda'_2}^{j_{12}}(3\pi/2, \pi/2 - \phi_{12}, 0) \right\} \\
 & \qquad \qquad \qquad D_{\mu \lambda_{12}-\lambda_3}^J(\pi/2, \pi/2, 0) |p_3; JM; j_{12} \lambda_{12} s_3 \lambda_3; p_{12} s_1 \lambda'_1 s_2 \lambda'_2\rangle.
 \end{aligned} \tag{8.76}$$

Complex numbers inside the summation can be made explicit by turning complex Wigner D matrices into real d matrices and phases [35, section 4.3],

$$\begin{aligned}
 & D_{\lambda_{12} \lambda'_1-\lambda'_2}^{j_{12}}(3\pi/2, \pi/2 - \phi_{12}, 0) D_{\mu \lambda_{12}-\lambda_3}^J(\pi/2, \pi/2, 0) \\
 & \qquad \qquad \qquad = e^{-i(3\lambda_{12}+\mu)\pi/2} d_{\lambda_{12} \lambda'_1-\lambda'_2}^{j_{12}}(\pi/2 - \phi_{12}) d_{\mu \lambda_{12}-\lambda_3}^J(\pi/2).
 \end{aligned} \tag{8.77}$$

Compiling phase factors and noticing that λ_{12} and $\lambda'_1 - \lambda'_2$ have the same integer or half-integer nature, one gets the final expression,

$$\begin{aligned}
 |JM\mu; w_1 w_2 w_3; \lambda_1 \lambda_2 \lambda_3\rangle &= \sum_{\lambda'_1, \lambda'_2} D_{\lambda'_1 \lambda_1}^{s_1} (R_W^1) D_{\lambda'_2 \lambda_2}^{s_2} (R_W^2) e^{i(2s_2+2s_3+\lambda'_2-\lambda'_1-\mu)\pi/2} \\
 & \sum_{j_{12}=|\lambda'_1-\lambda'_2|}^{\infty} \sum_{\lambda_{12}=-j_{12}}^{j_{12}} e^{i\lambda_{12}\pi/2} \sqrt{\frac{2j_{12}+1}{2}} d_{\lambda_{12} \lambda'_1-\lambda'_2}^{j_{12}}(\pi/2 - \phi_{12}) d_{\mu \lambda_{12}-\lambda_3}^J(\pi/2) \\
 & \qquad \qquad \qquad |p_3; JM; j_{12} \lambda_{12} s_3 \lambda_3; p_{12} s_1 \lambda'_1 s_2 \lambda'_2\rangle.
 \end{aligned} \tag{8.78}$$

Normalisation consistence

To confirm relations (8.33) and (8.35), one may try to deduce the orthonormalisation of Berman's J -helicity states from the one of Wick's J -helicity states. This subsection is devoted

to this consistency check supposing three massless particles. The scalar product of two arbitrary Berman's J -helicity states is evaluated by making use of relation (8.35) while Wick's states orthonormalisation (8.32) is assumed. After a few algebra, one gets

$$\begin{aligned}
 & \langle \bar{J}\bar{M}\bar{\mu}; \bar{w}_1\bar{w}_2\bar{w}_3; \bar{\lambda}_1\bar{\lambda}_2\bar{\lambda}_3 | JM\mu; w_1w_2w_3; \lambda_1\lambda_2\lambda_3 \rangle \\
 &= \frac{4\sqrt{p_3^2 + 4p_{12}^2}}{p_3p_{12}} \delta(\bar{p}_3 - p_3)\delta(\bar{p}_{12} - p_{12}) \delta_{\bar{J}J}\delta_{\bar{M}M}\delta_{\bar{\lambda}_1\lambda_1}\delta_{\bar{\lambda}_2\lambda_2}\delta_{\bar{\lambda}_3\lambda_3} e^{i(\bar{\mu}-\mu)\pi/2} \\
 & \quad \sum_{j_{12}=|\lambda_1-\lambda_2|}^{\infty} \sum_{\lambda_{12}=-j_{12}}^{j_{12}} \frac{2j_{12}+1}{2} d_{\lambda_{12}\lambda_1-\lambda_2}^{j_{12}}(\pi/2 - \bar{\phi}_{12}) d_{\lambda_{12}\lambda_1-\lambda_2}^{j_{12}}(\pi/2 - \phi_{12}) \\
 & \quad \quad \quad d_{\bar{\mu}\lambda_{12}-\lambda_3}^J(\pi/2) d_{\mu\lambda_{12}-\lambda_3}^J(\pi/2).
 \end{aligned} \tag{8.79}$$

Let us remind that a dependence on the energy variable w_1 (\bar{w}_1) is hidden inside the ϕ_{12} ($\bar{\phi}_{12}$) angle. Comparing with the announced orthonormalisation of Berman's J -helicity states, the remaining summations on j_{12} and λ_{12} are expected to produce a Kronecker delta in μ and a Dirac delta in w_1 . Using properties of d matrices [35], these summations can be reduced analytically,

$$\begin{aligned}
 & \sum_{j_{12}=|\lambda_1-\lambda_2|}^{\infty} \sum_{\lambda_{12}=-j_{12}}^{j_{12}} \frac{2j_{12}+1}{2} d_{\lambda_{12}\lambda_1-\lambda_2}^{j_{12}}(\bar{u}) d_{\lambda_{12}\lambda_1-\lambda_2}^{j_{12}}(u) d_{\bar{\mu}\lambda_{12}-\lambda_3}^J(\pi/2) d_{\mu\lambda_{12}-\lambda_3}^J(\pi/2) \\
 & \quad \quad \quad = \delta(u - \bar{u}) \delta_{\mu\bar{\mu}}.
 \end{aligned} \tag{8.80}$$

where the shorter notation u for the variable $\cos(\pi/2 - \phi'_1)$ has been used. Dirac deltas on p_3 , p_{12} and u can also be turned into Dirac deltas on w_1 , w_2 and w_3 using (8.38),

$$\delta(\bar{u} - u)\delta(\bar{p}_{12} - p_{12})\delta(\bar{p}_3 - p_3) = \frac{2p_3p_{12}}{\sqrt{4p_{12}^2 + p_3^2}} \delta(\bar{w}_1 - w_1)\delta(\bar{w}_2 - w_2)\delta(\bar{w}_3 - w_3). \tag{8.81}$$

As a result, one get the expected orthonormalisation of Berman's J -helicity states,

$$\begin{aligned}
 \langle \bar{J}\bar{M}\bar{\mu}; \bar{w}_1\bar{w}_2\bar{w}_3; \bar{\lambda}_1\bar{\lambda}_2\bar{\lambda}_3 | JM\mu; w_1w_2w_3; \lambda_1\lambda_2\lambda_3 \rangle &= 8 \delta(\bar{w}_1 - w_1)\delta(\bar{w}_2 - w_2)\delta(\bar{w}_3 - w_3) \\
 & \quad \delta_{\bar{J}J}\delta_{\bar{M}M}\delta_{\bar{\mu}\mu}\delta_{\bar{\lambda}_1\lambda_1}\delta_{\bar{\lambda}_2\lambda_2}\delta_{\bar{\lambda}_3\lambda_3}.
 \end{aligned} \tag{8.82}$$

This chapter in the context of a thesis

This chapter reviews and extends the state of the art in the three-body helicity formalism. While not exhaustive, neither with respect to Berman's nor Wick's definitions, it offers an innovative perspective by developing a change of basis formula that enables transitions between both complete sets of states. As a second key contribution, the chapter presents a detailed analysis of the symmetry properties of Berman's state. Both results are introduced along with their corresponding derivations.

These complex developments are motivated by the goal of the thesis: generalising the methodology introduced in Chapter 7 to the case of three-gluon glueballs.

Chapter 9

Three-gluon Glueballs: Broadening the Spectrum

With the framework of three-body helicity states now established, this final chapter applies it to the case of three-gluon glueballs. Following a methodology analogous to that used in the two-gluon case, the helicity formalism is employed to derive the spectrum of three-gluon glueball states. However, due to the presence of two distinct bases, additional internal degrees of freedom, and multiple relevant CoMF, the resulting calculations are considerably more technical than those for two-body systems. In the interest of completeness and reproducibility, detailed expressions are provided throughout. Nevertheless, the reader is encouraged to maintain focus on the overarching methodology, which remains largely consistent with that of the two-body case.

The developments in this chapter are organized into three main sections. In Section 9.1, symmetry and parity are implemented in Berman's basis, yielding a complete set of states suitable for describing three-gluon bound states. This basis is then used to construct trial states designed to reasonably approximate the true three-gluon glueball states. In Section 9.2, a method is developed for computing matrix elements on these trial states. Finally, in Section 9.3, the Hamiltonian matrix elements are evaluated on the trial states to extract the corresponding glueball spectrum. Section 9.4 concludes the chapter with perspectives on refining the current calculations and investigating additional properties beyond the mass spectrum.

9.1 Berman's basis for three-gluon systems

Let us start with the acquisition of symmetric parity eigenstates from Berman's J -helicity states. Dealing with three spin 1 massless particles, the helicity quantum number λ_i can only

take two values, -1 and $+1$. Therefore, there are only eight possible triplets of helicities $(\lambda_1, \lambda_2, \lambda_3)$. In Berman's definition, any consistent set of J, M, μ, w_1, w_2, w_3 quantum numbers can be built from each of these triplets. In other words, for any given energy and angular momentum quantum numbers, eight three-gluon J -helicity states can be obtained :

$$\begin{aligned} & |JM\mu; w_1w_2w_3; + + +\rangle, |JM\mu; w_1w_2w_3; - - +\rangle, |JM\mu; w_1w_2w_3; - + +\rangle, \\ & |JM\mu; w_1w_2w_3; - + -\rangle, |JM\mu; w_1w_2w_3; + - +\rangle, |JM\mu; w_1w_2w_3; + - -\rangle, \\ & |JM\mu; w_1w_2w_3; + + -\rangle, |JM\mu; w_1w_2w_3; - - -\rangle. \end{aligned} \quad (9.1)$$

For shortness, only the sign of helicities have been kept in the notation. Let us start by implementing parity quantum numbers in these eight states. Considering that gluons have negative intrinsic parity and using relation (8.9), the eight states (9.1) can be recombined into eight parity eigenstates,

$$\begin{aligned} & |JM\mu; w_1w_2w_3; + + +\rangle + |JM\mu; w_1w_2w_3; - - -\rangle, \\ & |JM\mu; w_1w_2w_3; - + +\rangle + |JM\mu; w_1w_2w_3; + - -\rangle, \\ & |JM\mu; w_1w_2w_3; + - +\rangle + |JM\mu; w_1w_2w_3; - + -\rangle, \\ & |JM\mu; w_1w_2w_3; + + -\rangle + |JM\mu; w_1w_2w_3; - - +\rangle, \\ & |JM\mu; w_1w_2w_3; + + +\rangle - |JM\mu; w_1w_2w_3; - - -\rangle, \\ & |JM\mu; w_1w_2w_3; - + +\rangle - |JM\mu; w_1w_2w_3; + - -\rangle, \\ & |JM\mu; w_1w_2w_3; + - +\rangle - |JM\mu; w_1w_2w_3; - + -\rangle, \\ & |JM\mu; w_1w_2w_3; + + -\rangle - |JM\mu; w_1w_2w_3; - - +\rangle. \end{aligned} \quad (9.2)$$

Their parity eigenvalue is $(-1)^{-\mu}$ for the four left states and $(-1)^{1-\mu}$ for the four right ones. In addition to parity, symmetry is also to be implemented. Depending on the expected charge conjugation of the system, three-gluon states have to be symmetrised (negative charge conjugation) or anti-symmetrised (positive charge conjugation) [138]. Applying both the symmetriser and the anti-symmetriser on the eight states (9.2) provides states with a definite symmetry under exchange of particles. The result of these applications is presented in Table 9.1. Fixing respectively $\sigma = +1$ or $\sigma = -1$ provides symmetric or anti-symmetric states. Because permutation operators change the sign of μ , (anti-)symmetric states mix different states with opposite μ quantum numbers. To avoid any redundancy, μ must be understood as positive in Table 9.1.

$$\begin{aligned}
& (|JM\mu; w_1w_2w_3; + + +\rangle + |JM\mu; w_1w_2w_3; - - -\rangle) \\
& + \sigma(-1)^{J+\mu+1} (|JM - \mu; w_2w_1w_3; + + +\rangle + |JM - \mu; w_2w_1w_3; - - -\rangle) \\
& + \sigma(-1)^{J+\mu+1} e^{-i\varphi_{13}\mu} (|JM - \mu; w_3w_2w_1; + + +\rangle + |JM - \mu; w_3w_2w_1; - - -\rangle) \\
& + \sigma(-1)^{J+\mu+1} e^{i\varphi_{23}\mu} (|JM - \mu; w_1w_3w_2; + + +\rangle + |JM - \mu; w_1w_3w_2; - - -\rangle) \\
& + e^{-i\varphi_{13}\mu} (|JM\mu; w_2w_3w_1; + + +\rangle + |JM\mu; w_2w_3w_1; - - -\rangle) \\
& + e^{i\varphi_{23}\mu} (|JM\mu; w_3w_1w_2; + + +\rangle + |JM\mu; w_3w_1w_2; - - -\rangle)
\end{aligned}$$

$$\begin{aligned}
& (|JM\mu; w_1w_2w_3; - + +\rangle + |JM\mu; w_1w_2w_3; + - -\rangle) \\
& + \sigma(-1)^{J+\mu+1} (|JM - \mu; w_2w_1w_3; + - +\rangle + |JM - \mu; w_2w_1w_3; - + -\rangle) \\
& + \sigma(-1)^{J+\mu+1} e^{-i\varphi_{13}\mu} (|JM - \mu; w_3w_2w_1; + + -\rangle + |JM - \mu; w_3w_2w_1; - - +\rangle) \\
& + \sigma(-1)^{J+\mu+1} e^{i\varphi_{23}\mu} (|JM - \mu; w_1w_3w_2; - + +\rangle + |JM - \mu; w_1w_3w_2; + - -\rangle) \\
& + e^{-i\varphi_{13}\mu} (|JM\mu; w_2w_3w_1; + + -\rangle + |JM\mu; w_2w_3w_1; - - +\rangle) \\
& + e^{i\varphi_{23}\mu} (|JM\mu; w_3w_1w_2; + - +\rangle + |JM\mu; w_3w_1w_2; - + -\rangle)
\end{aligned}$$

$$\begin{aligned}
& (|JM\mu; w_1w_2w_3; + + +\rangle - |JM\mu; w_1w_2w_3; - - -\rangle) \\
& + \sigma(-1)^{J+\mu+1} (|JM - \mu; w_2w_1w_3; + + +\rangle - |JM - \mu; w_2w_1w_3; - - -\rangle) \\
& + \sigma(-1)^{J+\mu+1} e^{-i\varphi_{13}\mu} (|JM - \mu; w_3w_2w_1; + + +\rangle - |JM - \mu; w_3w_2w_1; - - -\rangle) \\
& + \sigma(-1)^{J+\mu+1} e^{i\varphi_{23}\mu} (|JM - \mu; w_1w_3w_2; + + +\rangle - |JM - \mu; w_1w_3w_2; - - -\rangle) \\
& + e^{-i\varphi_{13}\mu} (|JM\mu; w_2w_3w_1; + + +\rangle - |JM\mu; w_2w_3w_1; - - -\rangle) \\
& + e^{i\varphi_{23}\mu} (|JM\mu; w_3w_1w_2; + + +\rangle - |JM\mu; w_3w_1w_2; - - -\rangle)
\end{aligned}$$

$$\begin{aligned}
& (|JM\mu; w_1w_2w_3; - + +\rangle - |JM\mu; w_1w_2w_3; + - -\rangle) \\
& + \sigma(-1)^{J+\mu+1} (|JM - \mu; w_2w_1w_3; + - +\rangle - |JM - \mu; w_2w_1w_3; - + -\rangle) \\
& + \sigma(-1)^{J+\mu+1} e^{-i\varphi_{13}\mu} (|JM - \mu; w_3w_2w_1; + + -\rangle - |JM - \mu; w_3w_2w_1; - - +\rangle) \\
& + \sigma(-1)^{J+\mu+1} e^{i\varphi_{23}\mu} (|JM - \mu; w_1w_3w_2; - + +\rangle - |JM - \mu; w_1w_3w_2; + - -\rangle) \\
& + e^{-i\varphi_{13}\mu} (|JM\mu; w_2w_3w_1; + + -\rangle - |JM\mu; w_2w_3w_1; - - +\rangle) \\
& + e^{i\varphi_{23}\mu} (|JM\mu; w_3w_1w_2; + - +\rangle - |JM\mu; w_3w_1w_2; - + -\rangle)
\end{aligned}$$

Table 9.1: Combinaisons of Berman's J helicity states that present a given parity and symmetry. Depending on whether σ is chosen to be $+1$ or -1 the state is symmetric or anti-symmetric. The parity eigenvalue of the two first sets of states is $(-1)^{-\mu}$ while it is $(-1)^{1-\mu}$ for the two last one.

9.1.1 Three-gluon glueball states

The eight states from Table 9.1 will now be used to construct states that model J^{PC} three-gluon glueballs. The procedure for this construction was outlined at the end of Section 8.1. Specifically, this involves replacing $|JM\mu; w_1 w_2 w_3; \lambda_1 \lambda_2 \lambda_3\rangle$ in the right-hand side of equation (8.22) with one of the states from Table 9.1. Due to their similarities, states from the first and third lines from Table 9.1 can be treated together, as can those from the second and fourth sets. Notably, due to symmetrization, each glueball state combines multiple Berman's states where the energy variables w_1 , w_2 and w_3 appear in different orders. This difference can be transferred to the $\Psi(w_1, w_2, w_3)$ wave function by appropriately exchanging integration variables. The resulting combinations are presented in Table 9.2. At this stage, the normalisation of the symmetrised states is not guaranteed.

Table 9.2 shows that any J^{PC} quantum numbers can, in principle, be realized by a three-gluon system. However, it may be reasonable to assume that low-lying glueball states correspond to symmetric helicity-momentum wave functions,

$$\forall i, j, k \in \{1, 2, 3\}, \Psi(w_i, w_j, w_k) = \Psi(w_1, w_2, w_3). \quad (9.3)$$

Imposing this symmetry reduces the states in Table 9.2 to those in Table 9.3. Unlike the general case, states with a symmetric helicity-momentum wave function exhibit a selection rule for $\mu = 0$. Specifically, when $\sigma(-1)^J = 1$, terms involving $+\mu$ systematically cancel those with $-\mu$. This implies that states with $\mu = 0$ and negative (positive) charge conjugation only exist for odd (even) J values. Since the following discussions primarily consider states with negative charge conjugation, $\mu = 0$ will always imply an odd J . This feature highlights two interesting properties of the spectrum. First, because the even value $J = 0$ can only be achieved by setting $\mu = 0$, no state with symmetric wave function, null total angular momentum and negative charge conjugation can be constructed. Colour-singlet two-gluon states have only positive charge conjugation, therefore a 0^{--} bound state of pure glue would either contradict hypothesis (9.3) or require at least four constituent gluons, a requirement consistent with group theory arguments [138]. Secondly, negative charge conjugation states with $J = 2$ must at least have $\mu = 1$. Qualitatively, one may suppose that higher μ projection of the total angular momentum would result in higher energy states. If this is correct, the $\mu = 0$ selection rule would push $J = 2$ states to higher masses.

This analysis is supported by glueball spectrum calculations from other approaches. For instance, Figure 9.1, taken from reference [167], shows glueball masses calculated using LQCD. In this spectrum, the first 0^{P-} state appears above 4.5 GeV, significantly higher than the

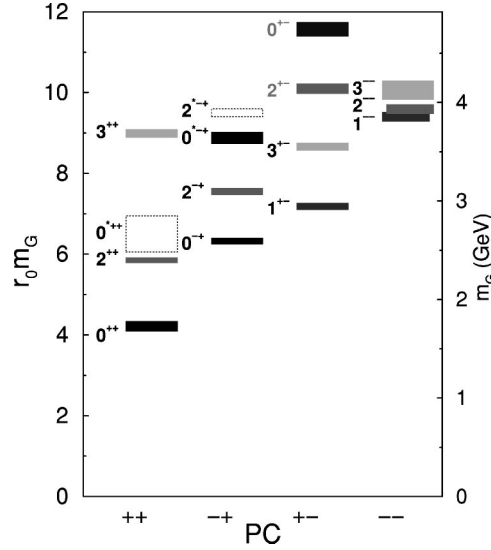


Figure 9.1: Glueball spectrum obtained using LQCD. The picture is taken from reference [167].

lowest J^{P-} state, which lies below 3 GeV. This aligns with the preceding analysis. The $J = 0$ state may be interpreted as a first four-gluon state or a three-gluon state with a non-symmetric helicity-momentum wave function $\Psi(w_1, w_2, w_3)$. Beyond $J = 0$, the hierarchy of even states follows the expected pattern: the $J = 1$ and $J = 3$ states, which allow $\mu = 0$, appear in order, while the $J = 2$ state is shifted to higher energies. However, the situation for odd states remains less clear. Further discussion is deferred until quantitative results are obtained.

States from Table 9.2 and 9.3 are also consistent with results from references [190] and [191]. In Reference [190], it is argued that no general selection rules govern the decay of a particle into three massless spin-1 particles. This is consistent with the absence of selection rules in Table 9.2. Reference [191] refines this discussion for symmetric decays into three photons, concluding that such a decay is not possible for $J = 0$ particles. This agrees with the analysis of states from Table 9.3. Moreover, the helicity triplets combinations constructed in [191] closely resemble those in the current work. For this reason, the labels A'_2 and A''_2 from reference [191] have been adopted in Table 9.2 and 9.3 to distinguish these states.

9.1.2 Low-lying three-gluon Glueballs with negative charge conjugation

The current description of the glueball spectrum has remained qualitative. To move toward quantitative analysis, the methodology based on the variational theorem, applied to two-gluon glueballs in Chapter 7, will be extended to three-gluon glueballs. This approach involves, on one hand, constructing a set of trial states designed to approximate three-gluon glueballs

$$\begin{aligned}
& |\Psi; A'_2; JM; C = -\sigma; P = \pm(-1)^\mu\rangle \\
&= \int \frac{dw_1 dw_2 dw_3}{8} \left(\Psi(w_1, w_2, w_3) + e^{-i\varphi_{23}\mu} \Psi(w_3, w_1, w_2) + e^{i\varphi_{13}\mu} \Psi(w_2, w_3, w_1) \right) \\
&\quad (|JM\mu; w_1 w_2 w_3; + + +\rangle \pm |JM\mu; w_1 w_2 w_3; - - -\rangle) \\
& -\sigma(-1)^{J+\mu} \int \frac{dw_1 dw_2 dw_3}{8} \left(\Psi(w_2, w_1, w_3) + e^{-i\varphi_{13}\mu} \Psi(w_3, w_2, w_1) + e^{i\varphi_{23}\mu} \Psi(w_1, w_3, w_2) \right) \\
&\quad (|JM - \mu; w_1 w_2 w_3; + + +\rangle \pm |JM - \mu; w_1 w_2 w_3; - - -\rangle)
\end{aligned}$$

$$\begin{aligned}
& |\Psi; A''_2; JM; C = -\sigma; P = \pm(-1)^\mu\rangle \\
&= \int \frac{dw_1 dw_2 dw_3}{8} \left(\Psi(w_1, w_2, w_3) (|JM\mu; w_1 w_2 w_3; - + +\rangle \pm |JM\mu; w_1 w_2 w_3; + - -\rangle) \right. \\
&\quad + e^{-i\varphi_{23}\mu} \Psi(w_3, w_1, w_2) (|JM\mu; w_1 w_2 w_3; + + -\rangle \pm |JM\mu; w_1 w_2 w_3; - - +\rangle) \\
&\quad \left. + e^{i\varphi_{13}\mu} \Psi(w_2, w_3, w_1) (|JM\mu; w_1 w_2 w_3; + - +\rangle \pm |JM\mu; w_1 w_2 w_3; - + -\rangle) \right) \\
& -\sigma(-1)^{J+\mu} \int \frac{dw_1 dw_2 dw_3}{8} \\
&\quad \left(\Psi(w_2, w_1, w_3) (|JM - \mu; w_1 w_2 w_3; + - +\rangle \pm |JM - \mu; w_1 w_2 w_3; - + -\rangle) \right. \\
&\quad + e^{-i\varphi_{13}\mu} \Psi(w_3, w_2, w_1) (|JM - \mu; w_1 w_2 w_3; + + -\rangle \pm |JM - \mu; w_1 w_2 w_3; - - +\rangle) \\
&\quad \left. + e^{i\varphi_{23}\mu} \Psi(w_1, w_3, w_2) (|JM - \mu; w_1 w_2 w_3; - + +\rangle \pm |JM - \mu; w_1 w_2 w_3; + - -\rangle) \right)
\end{aligned}$$

Table 9.2: Total angular momentum, parity and charge conjugation eigenstates for three-gluon systems. A generic helicity-momentum wave function $\Psi(w_1, w_2, w_3)$ is considered. Labels A'_2 and A''_2 differentiate the two symmetrical combinations of helicity triplets possible. These labels are inspired by the notations in reference [191] and originate from crystallography [192].

$$\begin{aligned}
& |\Psi; A'_2; JM; C = -\sigma; P = \pm(-1)^\mu\rangle \\
&= \int \frac{dw_1 dw_2 dw_3}{8} \Psi(w_1, w_2, w_3) (1 + e^{-i\varphi_{23}\mu} + e^{i\varphi_{13}\mu}) \\
&\quad (|JM\mu; w_1 w_2 w_3; + + +\rangle \pm |JM\mu; w_1 w_2 w_3; - - -\rangle) \\
&\quad -\sigma(-1)^{J+\mu} \int \frac{dw_1 dw_2 dw_3}{8} \Psi(w_1, w_2, w_3) (1 + e^{-i\varphi_{13}\mu} + e^{i\varphi_{23}\mu}) \\
&\quad (|JM - \mu; w_1 w_2 w_3; + + +\rangle \pm |JM - \mu; w_1 w_2 w_3; - - -\rangle)
\end{aligned}$$

$$\begin{aligned}
& |\Psi; A''_2; JM; C = -\sigma; P = \pm(-1)^\mu\rangle \\
&= \int \frac{dw_1 dw_2 dw_3}{8} \Psi(w_1, w_2, w_3) \left((|JM\mu; w_1 w_2 w_3; - + +\rangle \pm |JM\mu; w_1 w_2 w_3; + - -\rangle) \right. \\
&\quad \left. + e^{-i\varphi_{23}\mu} (|JM\mu; w_1 w_2 w_3; + + -\rangle \pm |JM\mu; w_1 w_2 w_3; - - +\rangle) \right. \\
&\quad \left. + e^{i\varphi_{13}\mu} (|JM\mu; w_1 w_2 w_3; + - +\rangle \pm |JM\mu; w_1 w_2 w_3; - + -\rangle) \right) \\
&\quad -\sigma(-1)^{J+\mu} \int \frac{dw_1 dw_2 dw_3}{8} \\
&\quad \Psi(w_1, w_2, w_3) \left((|JM - \mu; w_1 w_2 w_3; + - +\rangle \pm |JM - \mu; w_1 w_2 w_3; - + -\rangle) \right. \\
&\quad \left. + e^{-i\varphi_{13}\mu} (|JM - \mu; w_1 w_2 w_3; + + -\rangle \pm |JM - \mu; w_1 w_2 w_3; - - +\rangle) \right. \\
&\quad \left. + e^{i\varphi_{23}\mu} (|JM - \mu; w_1 w_2 w_3; - + +\rangle \pm |JM - \mu; w_1 w_2 w_3; + - -\rangle) \right)
\end{aligned}$$

Table 9.3: Total angular momentum, parity and charge conjugation eigenstates for three-gluon systems. A symmetric helicity-momentum wave function $\Psi(w_1, w_2, w_3)$ is considered. Labels A'_2 and A''_2 differentiate the two possible symmetrical combinations of helicity triplets. These labels are inspired by the notations in reference [191] and originate from crystallography [192].

accurately and, on the other, evaluating Hamiltonian matrix elements on this set. For the former, appropriate trial helicity-momentum wave functions Ψ must be chosen. For the latter, formulas to compute matrix elements on three-body helicity states are required. This subsection addresses both these tasks for the low-lying three-gluon glueball states with negative charge conjugation and with a symmetric Ψ function. Angular momenta up to $J = 3$ and μ projections up to $\mu = 1$ are considered. To keep equations concise, reduced notations are introduced for Berman's J -helicity states and for the three-body helicity states defined in (8.22),

$$|\lambda_1\lambda_2\lambda_3\rangle_\mu^J = |JM\mu; w_1w_2w_3; \lambda_1\lambda_2\lambda_3\rangle, \quad |\Psi; \lambda_1\lambda_2\lambda_3\rangle_\mu^J = |\Psi; JM\mu; \lambda_1\lambda_2\lambda_3\rangle. \quad (9.4)$$

In $|\lambda_1\lambda_2\lambda_3\rangle_\mu^J$, the order of energy labels is tacitly assumed to be always $w_1w_2w_3$. For clarity in plain text, three-body states defined in equation (8.22) will be referred to as *unsymmetrical states*, while those from Table 9.3 will be referred to as *symmetrical states*. Symmetrical states corresponding to the above-named low-lying three-gluon glueballs can be made explicit using these notations. Considering $\mu = 0$, the following states are obtained,

$$|\Psi; A'_2; \mu = 0; J^{PC} = (2k+1)^{\pm-}\rangle = \frac{1}{\sqrt{2}} \left(|\Psi; +++\rangle_0^{2k+1} \pm |\Psi; ---\rangle_0^{2k+1} \right), \quad (9.5)$$

$$\begin{aligned} |\Psi; A''_2; \mu = 0; J^{PC} = (2k+1)^{\pm-}\rangle = \frac{1}{\sqrt{6}} \left(|\Psi; -++\rangle_0^{2k+1} \pm |\Psi; +- -\rangle_0^{2k+1} \right. \\ \left. + |\Psi; ++ -\rangle_0^{2k+1} \pm |\Psi; -- +\rangle_0^{2k+1} \right. \\ \left. + |\Psi; +- +\rangle_0^{2k+1} \pm |\Psi; -+ -\rangle_0^{2k+1} \right) \end{aligned} \quad (9.6)$$

where $k \in \mathbb{N}$ (even angular momenta are forbidden for $\mu = 0$). Notations of the states have slightly been adapted in comparison with those from Table 9.3. Considering $\mu = \pm 1$, the following states are obtained,

$$\begin{aligned} |\Psi; A'_2; |\mu| = 1; J^{PC} = J^{\mp-}\rangle = \left(|\Psi(1 + e^{-i\varphi_{23}} + e^{i\varphi_{13}}); +++\rangle_1^J \right. \\ \left. \pm |\Psi(1 + e^{-i\varphi_{23}} + e^{i\varphi_{13}}); ---\rangle_1^J \right. \\ \left. + (-1)^J |\Psi(1 + e^{-i\varphi_{13}} + e^{i\varphi_{23}}); +++\rangle_{-1}^J \right. \\ \left. \pm (-1)^J |\Psi(1 + e^{-i\varphi_{13}} + e^{i\varphi_{23}}); ---\rangle_{-1}^J \right), \end{aligned} \quad (9.7)$$

$$\begin{aligned}
|\Psi; A_2''; |\mu| = 1; J^{PC} = J^{\mp-}\rangle = \frac{1}{\sqrt{12}} & \left(|\Psi; - + +\rangle_1^J \pm |\Psi; + - -\rangle_1^J + |\Psi e^{i\varphi_{13}}; + - +\rangle_1^J \right. \\
& \pm |\Psi e^{i\varphi_{13}}; - + -\rangle_1^J + |\Psi e^{-i\varphi_{23}}; + + -\rangle_1^J \pm |\Psi e^{-i\varphi_{23}}; - - +\rangle_1^J \\
& + (-1)^J (|\Psi; + - +\rangle_{-1}^J \pm |\Psi; - + -\rangle_{-1}^J + |\Psi e^{i\varphi_{23}}; - + +\rangle_{-1}^J \\
& \left. \pm |\Psi e^{i\varphi_{23}}; + - -\rangle_{-1}^J + |\Psi e^{-i\varphi_{13}}; + + -\rangle_{-1}^J \pm |\Psi e^{-i\varphi_{13}}; - - +\rangle_{-1}^J) \right). \tag{9.8}
\end{aligned}$$

In general, symmetrical states are linear combinations of unsymmetrical ones whose helicity-momentum wave function is potentially modified by an additional kinematic factor introduced during the symmetrisation process. In (9.5), (9.6) and (9.8), square root factors have been added to ensure that symmetric states are normalised as long as unsymmetrical ones are. The question of the normalisation of equation (9.7) is deferred to Section 9.3.

9.1.3 Selection of trial helicity-momentum wave functions

Let us start by selecting a suitable structure to use for trial helicity-momentum wave functions $\Psi(w_1, w_2, w_3)$. The most convenient choice is probably a Gaussian shaped wave function for which calculations are reasonably simple and which often offers great convergence properties. Symmetrical states (9.5) to (9.8) being linear combinations of unsymmetrical ones, this discussion takes place at the level of the latter. Gaussians may be constructed using different sets of coordinates, thereby leading to non-equivalent structures. The most straightforward choice is probably to consider a Gaussian shaped helicity-momentum wave function in PMP-coordinates,

$$\Psi_{\text{PMP}}(w_1, w_2, w_3) = A e^{-a((w_1-b)^2+(w_2-b)^2+(w_3-b)^2)}. \tag{9.9}$$

Above, A is a normalisation constant used to ensure that (8.23) is respected. If an expansion with more than one trial state is to be used, for instance adapting equation (7.28), the normalisation condition is replaced by the evaluation of an overlap matrix [23]. In that case, the constant A can be omitted. The structure (9.9) incorporates two non-linear variational parameters, a and b . The former encodes the spreading in energy and has dimensions of inverse energy squared. The latter encodes the position of the energy peak and has energy dimension. Different constant for each terms in the exponential cannot be used to keep the trial wave function symmetrical. The choice of wave function is, of course, arbitrary, and many modifications can be proposed. After several tests, adding a square root factor $\sqrt{8w_1w_2w_3}$ in front of the Gaussian was found to improve convergence. As a result, the following trial wave function is suggested,

$$\Psi_{a,b}(w_1, w_2, w_3) = A \sqrt{8w_1w_2w_3} e^{-a((w_1-b)^2+(w_2-b)^2+(w_3-b)^2)}, \tag{9.10}$$

and the corresponding unsymmetrical state reads

$$|\Psi_{\text{PMP}}; \lambda_1 \lambda_2 \lambda_3 \rangle_\mu^J = A \int \frac{dw_1 dw_2 dw_3}{8} \sqrt{8w_1 w_2 w_3} e^{-a((w_1-b)^2 + (w_2-b)^2 + (w_3-b)^2)} |\lambda_1 \lambda_2 \lambda_3 \rangle_\mu^J. \quad (9.11)$$

Further calculations will require to switch for the system of coordinates depicted in relation (8.38), namely $u = \sin(\phi_{12})$, p_{12} and p_3 . In these new coordinates, $\Psi_{a,b}(w_1, w_2, w_3)$ becomes

$$\Psi_{a,b}(u, p_{12}, p_3) = A \sqrt{p_3 (8p_{12}^2 + 2p_3^2 (1 - u^2))} e^{-\frac{a}{2}(6b^2 - 4b(\sqrt{4p_{12}^2 + p_3^2} + p_3) + 4p_{12}^2 + 3p_3^2)} e^{-\frac{a}{2}u^2 p_3^2}. \quad (9.12)$$

One can already anticipate why this system of coordinates will be helpful: the variable u is by definition the cosine of the angle that occurs in the change of basis formula (8.35), while the variable p_{12} is the relative momentum between particle 1 and 2 in their CoMF, a variable of great interest for the evaluation of two-body potential matrix elements. Symmetric states from equations (9.7) and (9.8) supplement the helicity-momentum wave function with kinematics factors that depend on the angles φ_{ij} defined in (8.2). To complete the picture of the wave function, these additional kinematic factors should be made explicit in u, p_{12}, p_3 coordinates,

$$\begin{aligned} \cos \varphi_{12} &= \frac{(1 - u^2) p_3^2 - 4p_{12}^2}{(1 - u^2) p_3^2 + 4p_{12}^2}, & \cos \varphi_{13} &= -\frac{u \sqrt{4p_{12}^2 + p_3^2} + p_3}{\sqrt{4p_{12}^2 + p_3^2} + up_3}, \\ \cos \varphi_{23} &= \frac{u \sqrt{4p_{12}^2 + p_3^2} - p_3}{\sqrt{4p_{12}^2 + p_3^2} - up_3}. \end{aligned} \quad (9.13)$$

On one hand, in states (9.7), the following combinations of φ_{ij} appear,

$$1 + e^{\pm i\varphi_{13}} + e^{\mp i\varphi_{23}} = \frac{(1 - u^2)(p_3^2 - 2\sqrt{(4p_{12}^2 + p_3^2)p_3^2}) + 4p_{12}^2}{(1 - u^2)p_3^2 + 4p_{12}^2} \mp i \frac{4p_{12}u\sqrt{(1 - u^2)p_3^2}}{(1 - u^2)p_3^2 + 4p_{12}^2}. \quad (9.14)$$

On the other hand, in states (9.8), φ_{ij} angles are taken in complex exponential,

$$\begin{aligned} e^{i\varphi_{13}} &= -\frac{u \sqrt{4p_{12}^2 + p_3^2} + p_3}{\sqrt{4p_{12}^2 + p_3^2} + up_3} + i \frac{2p_{12}\sqrt{1 - u^2}}{\sqrt{4p_{12}^2 + p_3^2} + up_3}, \\ e^{i\varphi_{23}} &= \frac{u \sqrt{4p_{12}^2 + p_3^2} - p_3}{\sqrt{4p_{12}^2 + p_3^2} - up_3} + i \frac{2p_{12}\sqrt{1 - u^2}}{\sqrt{4p_{12}^2 + p_3^2} - up_3}. \end{aligned} \quad (9.15)$$

9.2 Evaluation of matrix elements

To acquire an approximate energy spectrum by using the variational theorem (1.53) requires the evaluation of Hamiltonian matrix elements on trial states. Therefore, it requires deriving

formulas for performing such calculations on symmetrical states. Since symmetrical states decompose as linear combinations of unsymmetrical ones (see equations (9.5) to (9.8)), establishing formulas for the latter will give support to the evaluation of matrix elements for the former. The extension to symmetrical states will be discussed further in the next subsection.

9.2.1 Evaluation on unsymmetrical states

Because helicity states are momentum eigenstates, the evaluation of kinetic energy operators is the most straightforward to perform. To encompass many different kinematics at once, a generic $T(w_1, w_2, w_3)$ kinetic energy is considered for now. This function is only supposed to depend on the three w energies and not on the angles α, β, γ . First, definition (8.22) can be used for both the bra and the ket,

$$\begin{aligned} \int \frac{d\bar{w}_1 d\bar{w}_2 d\bar{w}_3}{8} \frac{dw_1 dw_2 dw_3}{8} \bar{\Psi}^*(\bar{w}_1, \bar{w}_2, \bar{w}_3) \Psi(w_1, w_2, w_3) \\ \bar{\mu} \langle \bar{\Psi}; \bar{\lambda}_1 \bar{\lambda}_2 \bar{\lambda}_3 | T | \Psi; \lambda_1 \lambda_2 \lambda_3 \rangle_{\mu}^J = \int \frac{d\bar{w}_1 d\bar{w}_2 d\bar{w}_3}{8} \frac{dw_1 dw_2 dw_3}{8} \bar{\Psi}^*(\bar{w}_1, \bar{w}_2, \bar{w}_3) \Psi(w_1, w_2, w_3) \\ \bar{\mu} \langle \bar{\lambda}_1 \bar{\lambda}_2 \bar{\lambda}_3 | T | \lambda_1 \lambda_2 \lambda_3 \rangle_{\mu}^J. \end{aligned} \quad (9.16)$$

Berman's J -helicity states being eigenstates of the three w energies, the evaluation of $T(w_1, w_2, w_3)$ on these comes down to a simple scalar multiplication,

$$\begin{aligned} \bar{\mu} \langle \bar{\Psi}; \bar{\lambda}_1 \bar{\lambda}_2 \bar{\lambda}_3 | T | \Psi; \lambda_1 \lambda_2 \lambda_3 \rangle_{\mu}^J = \int \frac{d\bar{w}_1 d\bar{w}_2 d\bar{w}_3}{8} \frac{dw_1 dw_2 dw_3}{8} \bar{\Psi}^*(\bar{w}_1, \bar{w}_2, \bar{w}_3) \Psi(w_1, w_2, w_3) \\ T(w_1, w_2, w_3) \bar{\mu} \langle \bar{\lambda}_1 \bar{\lambda}_2 \bar{\lambda}_3 | \lambda_1 \lambda_2 \lambda_3 \rangle_{\mu}^J. \end{aligned} \quad (9.17)$$

Finally, using the orthonormalisation relation of Berman's J -helicity states, three Dirac deltas are produced and removes the integrations on bar variables,

$$\begin{aligned} \bar{\mu} \langle \bar{\Psi}; \bar{\lambda}_1 \bar{\lambda}_2 \bar{\lambda}_3 | T | \Psi; \lambda_1 \lambda_2 \lambda_3 \rangle_{\mu}^J \\ = \delta_{\bar{\mu}\mu} \delta_{\bar{\lambda}_1 \lambda_1} \delta_{\bar{\lambda}_2 \lambda_2} \delta_{\bar{\lambda}_3 \lambda_3} \int \frac{dw_1 dw_2 dw_3}{8} \bar{\Psi}^*(w_1, w_2, w_3) \Psi(w_1, w_2, w_3) T(w_1, w_2, w_3). \end{aligned} \quad (9.18)$$

As a reminder, both w_1 and w_2 vary from 0 to $+\infty$ while w_3 varies between $|w_1 - w_2|$ and $w_1 + w_2$. This formula allows for reasonably easy evaluations of kinetic energy matrix elements on unsymmetrical states.

Let us turn to the two-body potential. For symmetric states, matrix elements of the three two-body interactions are shown to be equal each-other. As a result, computing a single two-body interaction matrix elements, and multiplying it by three, is sufficient to evaluate the entire potential energy of the system. Because the current goal is to perform evaluations on such

symmetric states, calculations will only be developed for the interaction between particles 1 and 2. One may expect to re-use the method set up to compute potential matrix elements for two-body systems. To do so, the trial states have to be developed in Wick's helicity basis in order to introduce two-body sub-couplings. From definition (8.22), one can use the expansion (8.35) to develop the state in Wick's helicity basis,

$$|\Psi; \lambda_1 \lambda_2 \lambda_3\rangle_\mu^J = e^{i(\pi/2)(\lambda_2 - \lambda_1 - \mu)} \sum_{j_{12}=|\lambda_1 - \lambda_2|}^{\infty} \sum_{\lambda_{12}=-j_{12}}^{j_{12}} i^{\lambda_{12}} \sqrt{\frac{2j_{12} + 1}{2}} d_{\mu \lambda_{12} - \lambda_3}^J(\pi/2) \int \frac{dw_1 dw_2 dw_3}{8} \Psi(w_1, w_2, w_3) d_{\lambda_{12} \lambda_1 - \lambda_2}^{j_{12}}(\pi/2 - \phi_{12}) |p_3; JM; j_{12} \lambda_{12} \lambda_3; p_{12} \lambda_1 \lambda_2\rangle. \quad (9.19)$$

For the sake of readability, summation ranges are omitted in the next expressions. For further convenience, variables u , p_{12} and p_3 are introduced in the integral (see relations (8.38) and (8.81)),

$$|\Psi; \lambda_1 \lambda_2 \lambda_3\rangle_\mu^J = e^{i(\pi/2)(\lambda_2 - \lambda_1 - \mu)} \sum_{j_{12}} \sum_{\lambda_{12}} i^{\lambda_{12}} \sqrt{\frac{2j_{12} + 1}{2}} d_{\mu \lambda_{12} - \lambda_3}^J(\pi/2) \int \frac{p_3 p_{12} du dp_{12} dp_3}{4\sqrt{4p_{12}^2 + p_3^2}} \Psi(u, p_{12}, p_3) d_{\lambda_{12} \lambda_1 - \lambda_2}^{j_{12}}(\arccos u) |p_3; JM; j_{12} \lambda_{12} \lambda_3; p_{12} \lambda_1 \lambda_2\rangle. \quad (9.20)$$

As a reminder, integration ranges are -1 to 1 for u while it is 0 to ∞ for both p_3 and p_{12} . Because this important result is relatively cumbersome, the following notation shortcuts are introduced,

$$\mathcal{C}_{J\mu; \lambda_1 \lambda_2 \lambda_3}^{j_{12} \lambda_{12}} = e^{i(\pi/2)(\lambda_2 - \lambda_1 - \mu + \lambda_{12})} \sqrt{\frac{2j_{12} + 1}{2}} d_{\mu \lambda_{12} - \lambda_3}^J(\pi/2), \quad (9.21)$$

$$\Psi_{\lambda_{12} \lambda_1 - \lambda_2}^{j_{12}}(u, p_{12}, p_3) = \Psi(u, p_{12}, p_3) d_{\lambda_{12} \lambda_1 - \lambda_2}^{j_{12}}(\arccos u). \quad (9.22)$$

The above \mathcal{C} coefficients should not be confused with those for two-body systems, defined in relation (7.6). The difference should be clear depending on the context and looking at the index structure. With these notations, equation (9.20) shortens,

$$|\Psi; \lambda_1 \lambda_2 \lambda_3\rangle_\mu^J = \sum_{j_{12}} \sum_{\lambda_{12}} \mathcal{C}_{J\mu; \lambda_1 \lambda_2 \lambda_3}^{j_{12} \lambda_{12}} \int \frac{p_3 p_{12} du dp_{12} dp_3}{4\sqrt{4p_{12}^2 + p_3^2}} \Psi_{\lambda_{12} \lambda_1 - \lambda_2}^{j_{12}}(u, p_{12}, p_3) |p_3; JM; j_{12} \lambda_{12} \lambda_3; p_{12} \lambda_1 \lambda_2\rangle. \quad (9.23)$$

This formula will be very helpful to evaluate two-body potential matrix elements associated with particle 1 and 2. This interaction, denoted \mathcal{O} , is supposed to solely depend on the relative

distance between these two particles, $r_{12} = |\mathbf{r}_1 - \mathbf{r}_2|$. This distance is assumed to be defined in the (12)-CoMF. First, equation (9.23) is used on both the bra and the ket,

$$\begin{aligned} \langle \bar{\Psi}; \bar{\lambda}_1 \bar{\lambda}_2 \bar{\lambda}_3 | \mathcal{O}(r_{12}) | \Psi; \lambda_1 \lambda_2 \lambda_3 \rangle_\mu^J &= \sum_{\bar{j}_{12}} \sum_{\bar{\lambda}_{12}} \sum_{j_{12}} \sum_{\lambda_{12}} \left(\mathcal{C}_{J\bar{\mu}; \bar{\lambda}_1 \bar{\lambda}_2 \bar{\lambda}_3}^{j_{12} \lambda_{12}} \right)^* \mathcal{C}_{J\mu; \lambda_1 \lambda_2 \lambda_3}^{j_{12} \lambda_{12}} \\ &\int \frac{\bar{p}_3 \bar{p}_{12} d\bar{u} d\bar{p}_{12} d\bar{p}_3}{4\sqrt{4\bar{p}_{12}^2 + \bar{p}_3^2}} \left(\bar{\Psi}_{\bar{\lambda}_{12} \bar{\lambda}_1 - \bar{\lambda}_2}^{j_{12}}(\bar{u}, \bar{p}_{12}, \bar{p}_3) \right)^* \int \frac{p_3 p_{12} du dp_{12} dp_3}{4\sqrt{4p_{12}^2 + p_3^2}} \Psi_{\lambda_{12} \lambda_1 - \lambda_2}^{j_{12}}(u, p_{12}, p_3) \quad (9.24) \\ &\langle \bar{p}_3; JM; \bar{j}_{12} \bar{\lambda}_{12} \bar{\lambda}_3; \bar{p}_{12} \bar{\lambda}_1 \bar{\lambda}_2 | \mathcal{O}(r_{12}) | p_3; JM; j_{12} \lambda_{12} \lambda_3; p_{12} \lambda_1 \lambda_2 \rangle. \end{aligned}$$

By doing so, the evaluation of $\mathcal{O}(r_{12})$ on Berman's J -helicity states comes down to its evaluation on Wick's J -helicity states. The latter, thanks to the intermediary coupling in Wick's definition, consists of evaluating on $\mathcal{O}(r_{12})$ on two-body J -helicity states. Dividing up the normalisation factor from (8.32) between both state and ensuring a normalisation for two-body states consistent with Chapter 6, one gets

$$\begin{aligned} &\langle \bar{p}_3; JM; \bar{j}_{12} \bar{\lambda}_{12} \bar{\lambda}_3; \bar{p}_{12} \bar{\lambda}_1 \bar{\lambda}_2 | \mathcal{O}(r_{12}) | p_3; JM; j_{12} \lambda_{12} \lambda_3; p_{12} \lambda_1 \lambda_2 \rangle \\ &= \frac{\sqrt{4\bar{p}_3^2 + 4\bar{p}_{12}^2} \sqrt{4p_3^2 + 4p_{12}^2}}{\sqrt{4\bar{p}_3 \bar{p}_{12}} \sqrt{4p_3 p_{12}}} \delta(\bar{p}_3 - p_3) \delta_{\bar{\lambda}_3 \lambda_3} \langle \bar{p}_{12}; \bar{j}_{12} \bar{\lambda}_{12}; \bar{\lambda}_1 \bar{\lambda}_2 | \mathcal{O}(r_{12}) | p_{12}; j_{12} \lambda_{12}; \lambda_1 \lambda_2 \rangle. \quad (9.25) \end{aligned}$$

Because r_{12} is defined in the (12)-CoMF, the residual matrix elements on two-body states can be computed by using formulas developed in Section 7.1. For central potentials, it has proven to cancel for $\bar{j}_{12} \neq j_{12}$ or $\bar{\lambda}_{12} \neq \lambda_{12}$ in equation (7.11). It has also been enhanced in this section that these matrix elements, as soon as non-zero, does not truly dependent on the total angular momentum projection λ_{12} . Equation (9.25) can be plugged into equation (9.24),

$$\begin{aligned} \langle \bar{\Psi}; \bar{\lambda}_1 \bar{\lambda}_2 \bar{\lambda}_3 | \mathcal{O}(r_{12}) | \Psi; \lambda_1 \lambda_2 \lambda_3 \rangle_\mu^J &= \delta_{\bar{\lambda}_3 \lambda_3} \sum_{j_{12}} \sum_{\lambda_{12}} \left(\mathcal{C}_{J\bar{\mu}; \bar{\lambda}_1 \bar{\lambda}_2 \bar{\lambda}_3}^{j_{12} \lambda_{12}} \right)^* \mathcal{C}_{J\mu; \lambda_1 \lambda_2 \lambda_3}^{j_{12} \lambda_{12}} \\ &\int \frac{p_3 \sqrt{\bar{p}_{12} p_{12}} d\bar{u} d\bar{p}_{12} du dp_{12} dp_3}{4\sqrt{p_3^2 + 4\bar{p}_{12}^2} 4\sqrt{p_3^2 + 4p_{12}^2}} \left(\bar{\Psi}_{\bar{\lambda}_{12} \bar{\lambda}_1 - \bar{\lambda}_2}^{j_{12}}(\bar{u}, \bar{p}_{12}, p_3) \right)^* \Psi_{\lambda_{12} \lambda_1 - \lambda_2}^{j_{12}}(u, p_{12}, p_3) \quad (9.26) \\ &\langle \bar{p}_{12}; j_{12} \lambda_{12}; \bar{\lambda}_1 \bar{\lambda}_2 | \mathcal{O}(r_{12}) | p_{12}; j_{12} \lambda_{12}; \lambda_1 \lambda_2 \rangle. \end{aligned}$$

The lower boundary in the summation on j_{12} must now fulfill both the constraints $j_{12} \geq |\lambda_1 - \lambda_2|$

and $j_{12} \geq |\bar{\lambda}_1 - \bar{\lambda}_2|$. This integral can be reorganised as follows,

$$\begin{aligned} \int p_3 dp_3 \int \frac{d\bar{p}_{12}}{2} \frac{dp_{12}}{2} \tilde{\Psi}(\bar{p}_{12}, p_3; j_{12}, \lambda_{12}, \bar{\lambda}_1 - \bar{\lambda}_2; \bar{\Psi}^*) \tilde{\Psi}(p_{12}, p_3; j_{12}, \lambda_{12}, \lambda_1 - \lambda_2; \Psi) \\ \left(\mathcal{C}_{J\bar{\mu}; \bar{\lambda}_1 \bar{\lambda}_2 \lambda_3}^{j_{12} \lambda_{12}} \right)^* \mathcal{C}_{J\mu; \lambda_1 \lambda_2 \lambda_3}^{j_{12} \lambda_{12}} \end{aligned} \quad (9.27)$$

$$\langle \bar{p}_{12}; j_{12} \lambda_{12}; \bar{\lambda}_1 \bar{\lambda}_2 | \mathcal{O}(r_{12}) | p_{12}; j_{12} \lambda_{12}; \lambda_1 \lambda_2 \rangle$$

where

$$\tilde{\Psi}(p_{12}, p_3; j_{12}, \lambda_{12}, \Delta\lambda; \Psi) = \frac{\sqrt{p_{12}}}{2\sqrt{4p_{12}^2 + p_3^2}} \int du \Psi_{\lambda_{12} \Delta\lambda}^{j_{12}}(u, p_{12}, p_3) \quad (9.28)$$

and where the product of three-body \mathcal{C} coefficients can be made a bit more explicit,

$$\begin{aligned} \left(\mathcal{C}_{J\bar{\mu}; \bar{\lambda}_1 \bar{\lambda}_2 \lambda_3}^{j_{12} \lambda_{12}} \right)^* \mathcal{C}_{J\mu; \lambda_1 \lambda_2 \lambda_3}^{j_{12} \lambda_{12}} &= e^{i\frac{\pi}{2}((\lambda_2 - \bar{\lambda}_2) + (\bar{\lambda}_1 - \lambda_1) + (\bar{\mu} - \mu))} \frac{2j_{12} + 1}{2} d_{\bar{\mu} \lambda_{12} - \lambda_3}^J(\pi/2) d_{\mu \lambda_{12} - \lambda_3}^J(\pi/2) \\ &= (-1)^{(\lambda_2 - \bar{\lambda}_2)/2 + (\bar{\lambda}_1 - \lambda_1)/2 + (\bar{\mu} - \mu)/2} \frac{2j_{12} + 1}{2} d_{\bar{\mu} \lambda_{12} - \lambda_3}^J(\pi/2) d_{\mu \lambda_{12} - \lambda_3}^J(\pi/2). \end{aligned} \quad (9.29)$$

In equation (9.27), the function $\tilde{\Psi}$ acts like an unnormalised two-body helicity-momentum wave function that would depend on three parameters (a , b and p_3). Therefore, the evaluation of the integrals on p_{12} and \bar{p}_{12} is fully analogous to what has been done to compute potential matrix elements for two-body systems.

Equations (9.27) to (9.29) are key formulas for the current work as they allow computation of two-body potential matrix elements on three-body helicity states. However, these formulas involves the evaluation of an infinite series of four dimensional integrals. Even when truncating this series, calculating such a large number of integrals remains a significant challenge. Gaining deeper insight into the components of this formula may help mitigate this complexity. Complement 9.A is dedicated to this analysis.

9.2.2 Evaluation on symmetrical states

The previous subsection worked at obtaining formulas to compute Hamiltonian matrix elements on unsymmetrical states. In the current one, this technology is used to generalise calculations to symmetric states. Starting with kinetics, a formula for both symmetric states having $\mu = 0$ can easily be obtained thanks to the absence of mixing between helicities in (9.18). The situation is even simpler because non-zero terms prove to be independent of the actual

value of λ_1 , λ_2 or λ_3 . Only a single integral has to be evaluated,

$$\begin{aligned} \langle \bar{\Psi}; A'_2; 0; (2k+1)^{\pm-} | T | \Psi; A'_2; 0; (2k+1)^{\pm-} \rangle &= \langle \bar{\Psi}; A''_2; 0; (2k+1)^{\pm-} | T | \Psi; A''_2; 0; (2k+1)^{\pm-} \rangle \\ &= \int \frac{dw_1 dw_2 dw_3}{8} \bar{\Psi}^*(w_1, w_2, w_3) \Psi(w_1, w_2, w_3) T(w_1, w_2, w_3). \end{aligned} \quad (9.30)$$

Concerning states based on $\mu = \pm 1$, the presence of Kronecker deltas in (9.18) still simplifies the evaluation of kinetic energy. For the A'_2 states, see equation (9.7), due to the additional kinematic factors arising from the symmetrisation, the result requires the evaluation of a slightly different integral,

$$\begin{aligned} \langle \bar{\Psi}; A'_2; 1; J^{\mp-} | T | \Psi; A'_2; 1; J^{\mp-} \rangle \\ = \int \frac{dw_1 dw_2 dw_3}{2} \bar{\Psi}^*(w_1, w_2, w_3) \Psi(w_1, w_2, w_3) |1 + e^{-i\varphi_{13}} + e^{i\varphi_{23}}|^2 T(w_1, w_2, w_3). \end{aligned} \quad (9.31)$$

For the A''_2 states, see equation (9.8), the kinetic energy matrix elements are again provided by the previous integral,

$$\begin{aligned} \langle \bar{\Psi}; A''_2; 1; J^{\mp-} | T | \Psi; A''_2; 1; J^{\mp-} \rangle \\ = \int \frac{dw_1 dw_2 dw_3}{8} \bar{\Psi}^*(w_1, w_2, w_3) \Psi(w_1, w_2, w_3) T(w_1, w_2, w_3). \end{aligned} \quad (9.32)$$

For each symmetric state, kinetic energy matrix elements can be evaluated in a single integral. Notice that equations (9.30) to (9.32) allows to infer formulas for the overlap between symmetrical states by plugging $T(w_1, w_2, w_3) = 1$.

Let us move on to the case of two-body potential. Due to the $\delta_{\bar{\lambda}_3 \lambda_3}$ factor in (9.27), some matrix elements on unsymmetrical states are directly shown to cancel. For state (9.5), the resulting expression only requires to evaluate two matrix elements,

$$\begin{aligned} \langle \bar{\Psi}; A'_2; 0; (2k+1)^{\pm-} | \mathcal{O}(r_{12}) | \Psi; A'_2; 0; (2k+1)^{\pm-} \rangle \\ = \frac{1}{2} \left(\begin{matrix} 2k+1 \\ 0 \end{matrix} \langle \bar{\Psi}; + + + | \mathcal{O}(r_{12}) | \Psi; + + + \rangle_0^{2k+1} + \begin{matrix} 2k+1 \\ 0 \end{matrix} \langle \bar{\Psi}; - - - | \mathcal{O}(r_{12}) | \Psi; - - - \rangle_0^{2k+1} \right). \end{aligned} \quad (9.33)$$

One can immediately observe that potential matrix elements for these states are parity de-generated. Concerning state (9.6), this sum is composed of twelve matrix elements including

non-diagonal ones,

$$\begin{aligned}
& \langle \bar{\Psi}; A_2''; 0; (2k+1)^{\pm-} | \mathcal{O}(r_{12}) | \Psi; A_2''; 0; (2k+1)^{\pm-} \rangle \\
&= \frac{1}{6} \left(\begin{aligned} & {}^{2k+1}_0 \langle \bar{\Psi}; -++ | \mathcal{O}(r_{12}) | \Psi; -++ \rangle_0^{2k+1} + {}^{2k+1}_0 \langle \bar{\Psi}; +-+ | \mathcal{O}(r_{12}) | \Psi; +-+ \rangle_0^{2k+1} \\ & + {}^{2k+1}_0 \langle \bar{\Psi}; --+ | \mathcal{O}(r_{12}) | \Psi; --+ \rangle_0^{2k+1} + {}^{2k+1}_0 \langle \bar{\Psi}; -+- | \mathcal{O}(r_{12}) | \Psi; -+- \rangle_0^{2k+1} \\ & + {}^{2k+1}_0 \langle \bar{\Psi}; +- - | \mathcal{O}(r_{12}) | \Psi; +- - \rangle_0^{2k+1} + {}^{2k+1}_0 \langle \bar{\Psi}; +++ | \mathcal{O}(r_{12}) | \Psi; +++ \rangle_0^{2k+1} \end{aligned} \right) \quad (9.34) \\
&+ \frac{1}{3} \left(\begin{aligned} & {}^{2k+1}_0 \langle \bar{\Psi}; +-+ | \mathcal{O}(r_{12}) | \Psi; -++ \rangle_0^{2k+1} + {}^{2k+1}_0 \langle \bar{\Psi}; +- - | \mathcal{O}(r_{12}) | \Psi; -+- \rangle_0^{2k+1} \\ & \pm {}^{2k+1}_0 \langle \bar{\Psi}; --+ | \mathcal{O}(r_{12}) | \Psi; -++ \rangle_0^{2k+1} \pm {}^{2k+1}_0 \langle \bar{\Psi}; --+ | \mathcal{O}(r_{12}) | \Psi; +-+ \rangle_0^{2k+1} \\ & \pm {}^{2k+1}_0 \langle \bar{\Psi}; -+- | \mathcal{O}(r_{12}) | \Psi; +++ \rangle_0^{2k+1} \pm {}^{2k+1}_0 \langle \bar{\Psi}; +++ | \mathcal{O}(r_{12}) | \Psi; +- - \rangle_0^{2k+1} \end{aligned} \right).
\end{aligned}$$

Finally, concerning states with $\mu = \pm 1$, calculations will only be illustrated with $|\Psi; A_2'; 1; J^{\pm\pm}\rangle$ because it is less cumbersome to decompose than $|\Psi; A_2''; 1; J^{\pm\pm}\rangle$,

$$\begin{aligned}
& \langle \bar{\Psi}; A_2'; 1; J^{\mp-} | \mathcal{O}(r_{12}) | \Psi; A_2'; 1; J^{\mp-} \rangle \\
&= \left(\begin{aligned} & {}^J_1 \langle (1 + e^{i\varphi_{13}} + e^{-i\varphi_{23}}) \bar{\Psi}; +++ | \mathcal{O}(r_{12}) | (1 + e^{i\varphi_{13}} + e^{-i\varphi_{23}}) \Psi; +++ \rangle_1^J \\ & + {}^J_1 \langle (1 + e^{i\varphi_{13}} + e^{-i\varphi_{23}}) \bar{\Psi}; --- | \mathcal{O}(r_{12}) | (1 + e^{i\varphi_{13}} + e^{-i\varphi_{23}}) \Psi; --- \rangle_1^J \\ & + {}^J_{-1} \langle (1 + e^{-i\varphi_{13}} + e^{i\varphi_{23}}) \bar{\Psi}; +++ | \mathcal{O}(r_{12}) | (1 + e^{-i\varphi_{13}} + e^{i\varphi_{23}}) \Psi; +++ \rangle_{-1}^J \\ & + {}^J_{-1} \langle (1 + e^{-i\varphi_{13}} + e^{i\varphi_{23}}) \bar{\Psi}; --- | \mathcal{O}(r_{12}) | (1 + e^{-i\varphi_{13}} + e^{i\varphi_{23}}) \Psi; --- \rangle_{-1}^J \\ & + 2(-1)^J {}^J_1 \langle (1 + e^{i\varphi_{13}} + e^{-i\varphi_{23}}) \bar{\Psi}; +++ | \mathcal{O}(r_{12}) | (1 + e^{-i\varphi_{13}} + e^{i\varphi_{23}}) \Psi; +++ \rangle_{-1}^J \\ & + 2(-1)^J {}^J_1 \langle (1 + e^{i\varphi_{13}} + e^{-i\varphi_{23}}) \bar{\Psi}; --- | \mathcal{O}(r_{12}) | (1 + e^{-i\varphi_{13}} + e^{i\varphi_{23}}) \Psi; --- \rangle_{-1}^J \end{aligned} \right) \quad (9.35)
\end{aligned}$$

In general, the symmetry properties depicted in Complement 9.A facilitate in evaluating these matrix elements. They show that part of those on unsymmetrical states are strictly equal, while some others involve the same integrals but combine them differently (see equation (9.27)). This significantly reduces the overall computational cost. This is especially true if the helicity-momentum wave function Ψ is even in u . Apart from diagonal matrix elements, symmetric states are also shown to mix with each other. For instance, mixtures between $|\Psi; A_2'; 0; (2k)^{\pm-}\rangle$

and $|\Psi; A_2''; 0; (2k)^\pm\rangle$ are given by

$$\begin{aligned} \langle \bar{\Psi}; A_2'; 0; (2k+1)^\pm | \mathcal{O}(r_{12}) | \Psi; A_2''; 0; (2k+1)^\pm \rangle &= \frac{1}{\sqrt{12}} \\ & \left(\begin{aligned} & {}^{2k+1}_0 \langle \bar{\Psi}; + + + | \mathcal{O}(r_{12}) | \Psi; - + + \rangle_0^{2k+1} + {}^{2k+1}_0 \langle \bar{\Psi}; + + + | \mathcal{O}(r_{12}) | \Psi; + - + \rangle_0^{2k+1} \\ & \pm {}^{2k+1}_0 \langle \bar{\Psi}; + + + | \mathcal{O}(r_{12}) | \Psi; - - + \rangle_0^{2k+1} + {}^{2k+1}_0 \langle \bar{\Psi}; - - - | \mathcal{O}(r_{12}) | \Psi; + - - \rangle_0^{2k+1} \\ & \pm {}^{2k+1}_0 \langle \bar{\Psi}; - - - | \mathcal{O}(r_{12}) | \Psi; + + - \rangle_0^{2k+1} + {}^{2k+1}_0 \langle \bar{\Psi}; - - - | \mathcal{O}(r_{12}) | \Psi; - + - \rangle_0^{2k+1} \end{aligned} \right). \end{aligned} \quad (9.36)$$

However, it will be shown in the next section that this mixing is quite small for three-gluon glueballs and only affects masses very slightly.

9.3 Determination of the low-lying Glueball Spectrum

Trial states and formulas set up all along the previous sections will now be used to compute a true mass spectrum for 1^\pm three-gluon glueballs. It will require to evaluate matrix elements of a Hamiltonian that should model three-gluon glueballs. This work considers the following structure for the latter,

$$H = T(w_1, w_2, w_3) + V(r_{12}) + V(r_{13}) + V(r_{23}). \quad (9.37)$$

with $r_{ij} = |\mathbf{r}_i - \mathbf{r}_j|$. Different kinematics T can be envisaged for gluons. Although these particles are formally massless, they acquire a constituent mass in some potential models. In the following, calculations will be performed considering ultra-relativistic kinematics,

$$T(w_1, w_2, w_3) = w_1 + w_2 + w_3. \quad (9.38)$$

Concerning potential, funnel interactions will be assumed,

$$V(r) = \sigma_m r - \frac{3\alpha_s}{2r}. \quad (9.39)$$

Above, σ_m is the meson string tension, generally set around 0.185 GeV^2 , and α_s is the strong coupling constant. In the following, the latter is fixed at 0.450 (as in Chapter 7 and reference [152]). The mesonic string tension is used as confinement constant because each gluon is supposed to provide both a 3 and a $\bar{3}$ flux tube. The six flux tubes join two by two in a Δ shape, as illustrated in Figure 9.2. Because each junction connects 3 and $\bar{3}$ flux tubes, the meson string tension has not to be rescaled. The factor $3/2$ is the colour factor corresponding with three

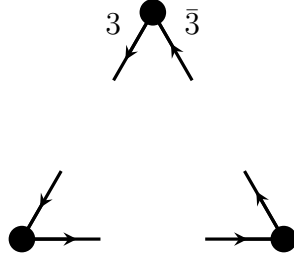


Figure 9.2: Schematic representation of the Δ junction modelling three-gluon glueballs in the current work. Gluons bounds two by two by pooling 3 and $\bar{3}$ flux tubes.

gluons in a colour singlet. The use of this potential and its comparison with a Y junction is explained in Complement 9.B. To avoid reproducing many evaluations for different mesonic string tensions σ_m , dimensionless variables are introduced by rescaling the current ones with the square-root of the string tension,

$$\mathbf{w}_i = w_i/\sqrt{\sigma_m}, \quad \mathbf{r}_{ij} = \sqrt{\sigma_m} r_{ij}. \quad (9.40)$$

Dimensionless equivalent for p_3 and p_{12} are also defined

$$\mathfrak{p}_3 = p_3/\sqrt{\sigma_m}, \quad \mathfrak{p}_{12} = p_{12}/\sqrt{\sigma_m}. \quad (9.41)$$

Because u is already dimensionless, it remains unchanged. Relation (8.38) still relates variables $\mathbf{w}_1, \mathbf{w}_2, \mathbf{w}_3$ and $u, \mathfrak{p}_{12}, \mathfrak{p}_3$. Using these new coordinates, a dimensionless version \mathbb{H} of the Hamiltonian (9.37) is introduced,

$$\mathbb{H} = H/\sqrt{\sigma_m} = \mathbb{T}(\mathbf{w}_1, \mathbf{w}_2, \mathbf{w}_3) + \mathbb{V}(\mathbf{r}_{12}) + \mathbb{V}(\mathbf{r}_{13}) + \mathbb{V}(\mathbf{r}_{23}) \quad (9.42)$$

where

$$\mathbb{T}(\mathbf{w}_1, \mathbf{w}_2, \mathbf{w}_3) = \mathbf{w}_1 + \mathbf{w}_2 + \mathbf{w}_3, \quad \mathbb{V}(\mathbf{r}) = \mathbf{r} - \frac{3\alpha_s}{2\mathbf{r}}. \quad (9.43)$$

This Hamiltonian will be evaluated on different symmetric trial states. To start with, a single trial state is considered. As a reminder, the reasonable trial wave function that had been chosen is

$$\Psi_{a,b}(w_1, w_2, w_3) = A\sqrt{8w_1w_2w_3}e^{-a((w_1-b)^2+(w_2-b)^2+(w_3-b)^2)}. \quad (9.44)$$

For states (9.5) and (9.6), this trial wave function remains unmodified. For states (9.7) and (9.8), it has to be multiplied by different kinematic factors to ensure the right symmetry properties. In the following, calculations will be made explicit for a generic kinematic factor, denoted

$\Gamma(w_1, w_2, w_3)$. These trial wave functions are to be turned into the new dimensionless coordinate system. The change simply rescales the a parameter by a factor σ_m and modify the value of the normalisation constant A ,

$$\mathbf{a} = \sigma_m a, \quad \mathbf{b} = b/\sqrt{\sigma_m}, \quad \mathbb{A} = \sigma_m^{\frac{3}{2}} A. \quad (9.45)$$

The rescaling factor for the normalisation constant has been chosen to eliminate the dimensions of the wave function. The use of a dimensionless wave function also suggests to rescale Berman's and Wick's bases to make them dimensionless,

$$|JM\mu; \mathbf{w}_1 \mathbf{w}_2 \mathbf{w}_3; \lambda_1 \lambda_2 \lambda_3\rangle = \sigma^{\frac{3}{4}} |JM\mu; w_1 w_2 w_3; \lambda_1 \lambda_2 \lambda_3\rangle, \quad (9.46)$$

$$|\mathbf{p}_3; JM; j_{12} \lambda_1 \lambda_2 \lambda_3; \mathbf{p}_{12} \lambda_1 \lambda_2\rangle = \sigma^{\frac{3}{4}} |p_3; JM; j_{12} \lambda_1 \lambda_2 \lambda_3; p_{12} \lambda_1 \lambda_2\rangle. \quad (9.47)$$

All the formulas set up to evaluate matrix elements can now be switched to the new coordinates. Taking every change into account, all the rescaling factors cancels each others. As a result, each formula can be naively turned into dimensionless coordinates by replacing A , a , w_i , p_3 and/or p_{12} by their dimensionless counterpart.

At first, let us investigate the normalisation of the symmetric trial states. For states (9.5), (9.6) and (9.8), the normalisation constant A is fixed by imposing the normalisation of the unsymmetrical trial states, implying that $\Psi_{a,b}$ must satisfy (8.23). Switching to dimensionless coordinates, one has to evaluate the following integral,

$$|\mathbb{A}|^2 = \left(\int d\mathbf{w}_1 d\mathbf{w}_2 d\mathbf{w}_3 \mathbf{w}_1 \mathbf{w}_2 \mathbf{w}_3 e^{-2a((\mathbf{w}_1 - \mathbf{b})^2 + (\mathbf{w}_2 - \mathbf{b})^2 + (\mathbf{w}_3 - \mathbf{b})^2)} \right)^{-1}, \quad (9.48)$$

where both \mathbf{w}_1 and \mathbf{w}_2 are integrated between 0 and ∞ while \mathbf{w}_3 is integrated between $|\mathbf{w}_1 - \mathbf{w}_2|$ and $\mathbf{w}_1 + \mathbf{w}_2$. Generic multidimensional integration techniques provide fast and accurate evaluations of \mathbb{A} . As inferred from (9.31), the situation is slightly more complicated for state (9.7) due to the additional kinematic factor. For the A'_2 state, the normalization involves the integral

$$|\mathbb{A}|^2 = \left(4 \int d\mathbf{w}_1 d\mathbf{w}_2 d\mathbf{w}_3 \mathbf{w}_1 \mathbf{w}_2 \mathbf{w}_3 e^{-2a((\mathbf{w}_1 - \mathbf{b})^2 + (\mathbf{w}_2 - \mathbf{b})^2 + (\mathbf{w}_3 - \mathbf{b})^2)} |1 + e^{-i\varphi_{13}} + e^{i\varphi_{23}}|^2 \right)^{-1}. \quad (9.49)$$

It is possible to evaluate these two integrals numerically, with any desired accuracy.

The evaluation of kinetic energy matrix elements is analogous to the normalisation. States (9.5), (9.6) and (9.8) requires to evaluate a single three-dimensional integral, as demonstrated in relations (9.30) and (9.32). For the current trial wave function, it equates to compute the

following integral

$$\langle \mathbb{T} \rangle = |\mathbb{A}|^2 \int d\mathbf{w}_1 d\mathbf{w}_2 d\mathbf{w}_3 \mathbf{w}_1 \mathbf{w}_2 \mathbf{w}_3 e^{-2a((\mathbf{w}_1 - \mathbf{b})^2 + (\mathbf{w}_2 - \mathbf{b})^2 + (\mathbf{w}_3 - \mathbf{b})^2)} (\mathbf{w}_1 + \mathbf{w}_2 + \mathbf{w}_3). \quad (9.50)$$

On the other hand, kinetic energy matrix elements for state (9.7) are provided by relation (9.31), which complements the integrand with a kinematic factor,

$$\begin{aligned} \langle \Psi_{a,b}; A'_2; \pm; 1^{\pm-} | \mathbb{T} | \Psi_{a,b}; A'_2; \pm; 1^{\pm-} \rangle = \\ 4|\mathbb{A}|^2 \int d\mathbf{w}_1 d\mathbf{w}_2 d\mathbf{w}_3 \mathbf{w}_1 \mathbf{w}_2 \mathbf{w}_3 e^{-2a((\mathbf{w}_1 - \mathbf{b})^2 + (\mathbf{w}_2 - \mathbf{b})^2 + (\mathbf{w}_3 - \mathbf{b})^2)} \\ |1 + e^{-i\varphi_{13}} + e^{i\varphi_{23}}|^2 (\mathbf{w}_1 + \mathbf{w}_2 + \mathbf{w}_3). \end{aligned} \quad (9.51)$$

It remains to evaluate potential matrix elements. As already mentioned, thanks to the symmetry of the state, the evaluation for the interaction between particles 1 and 2 is sufficient to infer the full potential energy of the Δ junction,

$$\langle \mathbb{V}(r_{12}) + \mathbb{V}(r_{13}) + \mathbb{V}(r_{23}) \rangle = 3 \langle \mathbb{V}(r_{12}) \rangle. \quad (9.52)$$

Relations (9.33), (9.34) and (9.35) reduce evaluations on symmetric states to several evaluations on unsymmetrical states, eventually with additional kinematic factors. The latter evaluations can be performed using formula (9.27). Specifying for the current trial wave function and using variables u , p_{12} and p_3 defined in equation (8.37), one gets

$$\begin{aligned} \int \mathfrak{p}_3 d\mathfrak{p}_3 \int \frac{d\bar{\mathfrak{p}}_{12}}{2} \frac{d\mathfrak{p}_{12}}{2} \tilde{\Psi}_{a,b}^*(\bar{\mathfrak{p}}_{12}, \mathfrak{p}_3; j_{12}, \lambda_{12}, \bar{\lambda}_1 - \bar{\lambda}_2; \bar{\Gamma}) \tilde{\Psi}_{a,b}(\mathfrak{p}_{12}, \mathfrak{p}_3; j_{12}, \lambda_{12}, \lambda_1 - \lambda_2; \Gamma) \\ \langle \bar{\mathfrak{p}}_{12}; j_{12} \lambda_{12}; \bar{\lambda}_1 \bar{\lambda}_2 | \mathbb{V}(r_{12}) | \mathfrak{p}_{12}; j_{12} \lambda_{12}; \lambda_1 \lambda_2 \rangle \end{aligned} \quad (9.53)$$

where

$$\begin{aligned} \tilde{\Psi}_{a,b}(\mathfrak{p}_{12}, \mathfrak{p}_3; j_{12}, \lambda_{12}, \Delta\lambda; \Gamma) = \mathbb{A} \frac{\sqrt{\mathfrak{p}_{12}\mathfrak{p}_3}}{2\sqrt[4]{4\mathfrak{p}_{12}^2 + \mathfrak{p}_3^2}} e^{-\frac{a}{2}(6\mathfrak{b}^2 - 4\mathfrak{b}(\sqrt{4\mathfrak{p}_{12}^2 + \mathfrak{p}_3^2} + \mathfrak{p}_3) + 4\mathfrak{p}_{12}^2 + 3\mathfrak{p}_3^2)} \\ \int_{-1}^1 du \sqrt{8\mathfrak{p}_{12}^2 + 2\mathfrak{p}_3^2(1-u^2)} d_{\lambda_{12} \Delta\lambda}^{j_{12}}(\arccos u) e^{-\frac{a}{2}\mathfrak{p}_3^2 u^2} \Gamma(u, \mathfrak{p}_{12}, \mathfrak{p}_3). \end{aligned} \quad (9.54)$$

These integrals must be evaluated. Performing efficient numerical integrations requires to slightly modify the variables and to refine the definition of $\tilde{\Psi}$. First, because the integral on \mathfrak{p}_3 will be performed using a generalised Gauss-Laguerre quadrature, the variable \mathfrak{p}_3 is modified as

follows

$$x = 3\mathfrak{a}\mathfrak{p}_3^2, \quad \mathfrak{p}_3 = \sqrt{\frac{x}{3\mathfrak{a}}}, \quad \mathfrak{p}_3 d\mathfrak{p}_3 = \frac{dx}{6\mathfrak{a}}. \quad (9.55)$$

After replacement and a bit of reorganisation, the integrals to evaluate become

$$|\mathbb{A}|^2 \sqrt{\frac{2}{(6\mathfrak{a})^3}} \int \sqrt{x} e^{-x} dx \int \frac{d\bar{\mathfrak{p}}_{12}}{2} \frac{d\mathfrak{p}_{12}}{2} \Theta_{\mathfrak{a},\mathfrak{b}}(\bar{\mathfrak{p}}_{12}, x; j_{12}, \lambda_{12}, \bar{\lambda}_1 - \bar{\lambda}_2; \bar{\Gamma}^*) \quad (9.56)$$

$$\Theta_{\mathfrak{a},\mathfrak{b}}(\mathfrak{p}_{12}, x; j_{12}, \lambda_{12}, \lambda_1 - \lambda_2; \Gamma) \langle \bar{\mathfrak{p}}_{12}; j_{12}\lambda_{12}; \bar{\lambda}_1\bar{\lambda}_2 | \mathbb{V}(\mathfrak{r}_{12}) | \mathfrak{p}_{12}; j_{12}\lambda_{12}; \lambda_1\lambda_2 \rangle$$

with a function Θ that replaces $\tilde{\Psi}$,

$$\Theta_{\mathfrak{a},\mathfrak{b}}(\mathfrak{p}_{12}, x; j_{12}, \lambda_{12}, \Delta\lambda; \Gamma) = \mathcal{F}_{\mathfrak{a},\mathfrak{b}}(\mathfrak{p}_{12}, x) \int du \mathcal{K}_{\mathfrak{a}}(u, \mathfrak{p}_{12}, x; j_{12}, \lambda_{12}, \Delta\lambda; \Gamma) \quad (9.57)$$

where

$$\mathcal{F}_{\mathfrak{a},\mathfrak{b}}(\mathfrak{p}_{12}, x) = \frac{\sqrt{\mathfrak{p}_{12}}}{2^4 \sqrt{4\mathfrak{p}_{12}^2 + \frac{x}{3\mathfrak{a}}}} e^{-\frac{\mathfrak{a}}{2}(6\mathfrak{b}^2 - 4\mathfrak{b}(\sqrt{4\mathfrak{p}_{12}^2 + x/(3\mathfrak{a})} + \sqrt{x/(3\mathfrak{a})}) + 4\mathfrak{p}_{12}^2)} \quad (9.58)$$

and where

$$\mathcal{K}_{\mathfrak{a}}(u, \mathfrak{p}_{12}, x; j_{12}, \lambda_{12}, \Delta\lambda; \Gamma) = \sqrt{8\mathfrak{p}_{12}^2 + \frac{2x}{3\mathfrak{a}}(1-u^2)} d_{\lambda_{12}\Delta\lambda}^{j_{12}}(\arccos u) e^{-\frac{x}{6}u^2} \Gamma\left(u, \mathfrak{p}_{12}, \sqrt{x/(3\mathfrak{a})}\right). \quad (9.59)$$

Symmetry properties of Θ under modifications of indices λ_{12} and $\Delta\lambda$ are the same as the ones of $\tilde{\Psi}$. They are compiled in Complement 9.A. Integrals (9.56) and (9.57) can be computed using a series of Gauss quadratures. The following procedure is applied.

- Choose a definite number of points to use in each of the integrals on x , \mathfrak{p}_{12} , $\bar{\mathfrak{p}}_{12}$ and u . Notice that the integrals on \mathfrak{p}_{12} and $\bar{\mathfrak{p}}_{12}$ will be turned into integrals on $\mathfrak{v} = \mathfrak{p}_{12} + \bar{\mathfrak{p}}_{12}$ and $\bar{\mathfrak{v}} = \mathfrak{p}_{12} - \bar{\mathfrak{p}}_{12}$, as suggested in Section 7.1. Because the integral on $\bar{\mathfrak{v}}$ is the most sensitive, it is recommended to assign the greatest number of points to it.
- Accuracies being chosen, identify the different x values and \mathfrak{p}_{12} values at which an evaluation of the function Θ will be required and perform all the necessary evaluations. Gauss-Legendre quadrature works very well for the integral on u . The result is stored for further use.
- For each x value, compute the two-body matrix elements in the same way it has been

done in Chapter 7. Thanks to the previous step, two-body wave functions Θ have already been tabulated. Again, the result is stored for further use.

- At this stage, only the integral on x remains. Perform this last integral by using the evaluations of two-body matrix elements stored during the last step. As already mentioned, a Gauss-Laguerre quadrature is the most adapted.

For each value of j_{12} and λ_{12} , that is for each term in the sum in equation (9.53), four integrals are evaluated numerically. Since the sum extends to $j_{12} \rightarrow \infty$, the number of necessary integrals would be infinite. In practice, the sum on j_{12} is truncated at a given level, denoted j_{\max} . Plugging the computed integrals into equation (9.53) allows for an approximate evaluation of two-body potential matrix elements on unsymmetrical trial states. Because of the multiple quadratures and because of this truncation, the exactness of the evaluation cannot be guaranteed. The matrix elements on unsymmetrical states can be combined following expressions (9.33) to (9.36) in order to compute those on symmetrical trial states. To get the full potential energy, the factor 3 from equation (9.52) is not to be forgotten. Once potential matrix elements on symmetrical states have been computed, the contribution from kinetic energy is added, and the Hamiltonian matrix elements are obtained. This calculation is repeated for many different couples (\mathbf{a}, \mathbf{b}) and only the minimum value is retained as an approximation for the true spectrum.

Since these states are the simplest to handle, convergence properties are illustrated using $|\Psi_{a,b}; A'_2; 0; 1^{\pm-}\rangle$ and $|\Psi_{a,b}; A''_2; 0; 1^{\pm-}\rangle$. All the following evaluations will be performed with $\alpha_s = 0.450$ [152]. To start with, calculations are performed for various numbers of points used in the different quadratures. All these computations employ for now the same cut-off at $j_{12} = 20$. The minimisation process is executed for each configuration. The results are summarized in Table 9.4. As expected, the integrals over u and x converge with as few as 30 points. While slightly more sensitive, the integral on \mathbf{v} does not require more than 50 points for sufficient accuracy in the current context. The key parameter for ensuring precision is the number of points used in the integral over \mathbf{v} . Using 100 points, the energy stabilizes to two significant digits. The search for a minimum in the variational parameters can also be illustrated. Figure 9.3 shows energy evaluations over a range of (\mathbf{a}, \mathbf{b}) pairs. Clear minima are observed for each state. Lastly, the convergence of the sum over j_{12} can be examined by repeating evaluations with various cut-off values. The result is displayed in Figure 9.4. Although the convergence behaviour differs slightly between states, a reasonable convergence is achieved in all cases. Notice that the j_{12} convergence can also be assessed by calculating normalisation by means of equation (9.53), substituting $\mathbb{V}(r_{12})$ with the identity operator.

Before to move on to the determination of a complete spectrum, the mixing between different

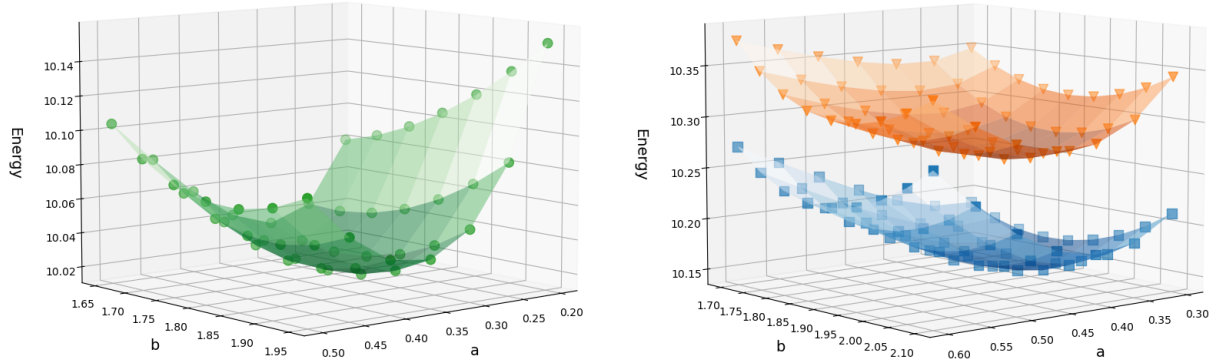


Figure 9.3: Plot of Hamiltonian matrix element for a single trial state depending on the non-linear variational parameters \mathfrak{a} and \mathfrak{b} . Left : a symmetric state $|\Psi_{\mathfrak{a},\mathfrak{b}}; A'_2; 0; 1^{\pm-}\rangle$ is considered. Right : symmetric states $|\Psi_{\mathfrak{a},\mathfrak{b}}; A''_2; 0; 1^{\pm-}\rangle$ are considered (even with orange triangles and odd with blue squares). Quadrature with 30 points have always been used except for $\bar{\mathfrak{v}}$ where 100 points have been used. A cut-off $j_{\max} = 20$ has been chosen.

symmetric states is to be investigated. This issue will be illustrated using $|\Psi_{\mathfrak{a},\mathfrak{b}}; A'_2; 0; 1^{+-}\rangle$ and $|\Psi_{\mathfrak{a},\mathfrak{b}}; A''_2; 0; 1^{+-}\rangle$. Without allowing for mixing, approximate energies are simply obtained by evaluating the Hamiltonian on each state separately,

$$E_{A'_2;0} = 10.020, \quad E_{A''_2;0} = 10.269. \quad (9.60)$$

Introducing mixing between these state requires the evaluation of off-diagonal Hamiltonian matrix elements and solving the corresponding eigenvalue problem. The off-diagonal matrix elements of the kinetic energy cancel, while those for the potential are calculated using formula (9.36). The splitting is found to be maximal when both states share the same variational parameters. The resulting optimal eigenvalues of the Hamiltonian matrix are

$$E_1 = 9.9902, \quad E_2 = 10.3319. \quad (9.61)$$

As shown, the mixing slightly affects the energies, but this effect does not exceed 1% of the original value. Mixing with states of higher mass is expected to have an even smaller impact due to the increasing energy gap. Consequently, the following calculations will be performed using pure symmetric states.

A concrete three-gluon glueball spectrum can now be computed. Again, $\alpha_s = 0.450$ is used. Calculations are performed with a cut-off at $j_{12} = 20$ for the summation and with 30 points for each quadrature, except for $\bar{\mathfrak{v}}$ where 100 points are used. Full optimisations of the variational parameters \mathfrak{a} and \mathfrak{b} are performed. The states $|\Psi_{\mathfrak{a},\mathfrak{b}}; A'_2; 0; J^{\pm-}\rangle$, $|\Psi_{\mathfrak{a},\mathfrak{b}}; A''_2; 0; J^{\pm-}\rangle$

For $ \Psi; A'_2; 0; 1^{\pm-}\rangle$:		For $ \Psi; A''_2; 0; 1^{+-}\rangle$:		For $ \Psi; A''_2; 0; 1^{--}\rangle$:	
$(N_u, N_v, N_{\bar{v}}, N_x)$	Energy	$(N_u, N_v, N_{\bar{v}}, N_x)$	Energy	$(N_u, N_v, N_{\bar{v}}, N_x)$	Energy
(30, 30, 30, 30)	9.9499	(30, 30, 30, 30)	10.1793	(30, 30, 30, 30)	10.0566
(50, 30, 30, 30)	9.9499	(50, 30, 30, 30)	10.1793	(50, 30, 30, 30)	10.0566
(100, 30, 30, 30)	9.9499	(100, 30, 30, 30)	10.1793	(100, 30, 30, 30)	10.0566
(30, 50, 30, 30)	9.9536	(30, 50, 30, 30)	10.1817	(30, 50, 30, 30)	10.0616
(30, 100, 30, 30)	9.9536	(30, 100, 30, 30)	10.1817	(30, 100, 30, 30)	10.0616
(30, 30, 50, 30)	9.9895	(30, 30, 50, 30)	10.2297	(30, 30, 50, 30)	10.1097
(30, 30, 100, 30)	10.0202	(30, 30, 100, 30)	10.2689	(30, 30, 100, 30)	10.1512
(30, 30, 30, 50)	9.9499	(30, 30, 30, 50)	10.1793	(30, 30, 30, 50)	10.0566
(30, 30, 30, 100)	9.9499	(30, 30, 30, 100)	10.1793	(30, 30, 30, 100)	10.0566

Table 9.4: Evaluations of the glueball masses in unit of $\sqrt{\sigma}$ for different numbers of points for the quadratures. For $|\Psi; A'_2; 0; 1^{\pm-}\rangle$, energies are given for $(\mathbf{a}, \mathbf{b}) = (0.35, 1.8)$. For $|\Psi; A'_2; 0; 1^{+-}\rangle$, energies are given for $(\mathbf{a}, \mathbf{b}) = (0.45, 1.95)$. For $|\Psi; A'_2; 0; 1^{--}\rangle$, energies are given for $(\mathbf{a}, \mathbf{b}) = (0.35, 1.9)$. A cut-off at $j_{12} = 20$ has been used.

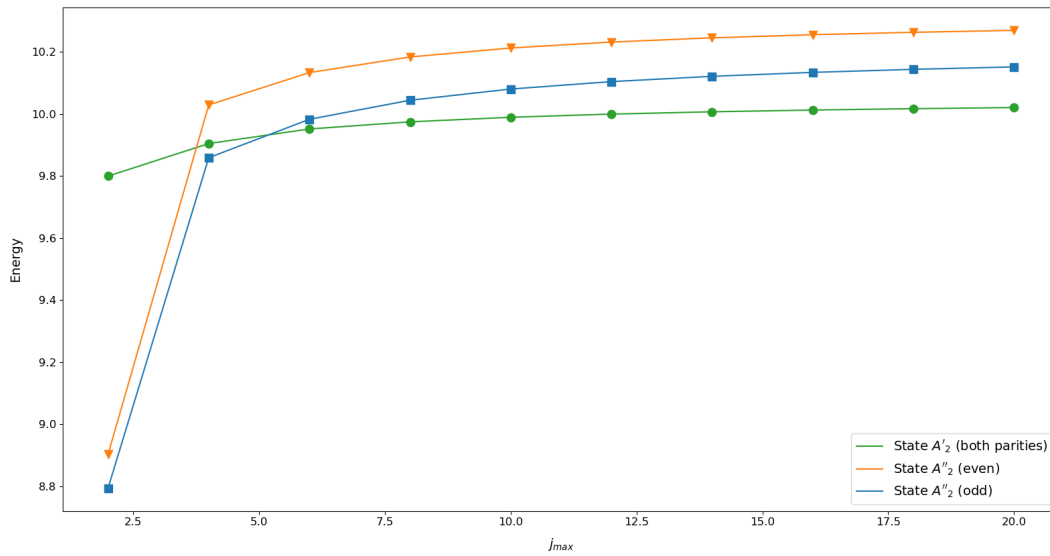


Figure 9.4: Evolution of the lowest three-gluon glueball masses depending on the cut-off for the sum in j_{12} . Results for $|\Psi_{a,b}; A'_2; 0; 1^{\pm-}\rangle$ use $(\mathbf{a}, \mathbf{b}) = (0.35, 1.8)$ and are displayed with green circles. Results for $|\Psi_{a,b}; A''_2; 0; 1^{+-}\rangle$ use $(\mathbf{a}, \mathbf{b}) = (0.45, 1.95)$ and are displayed with orange triangles. Results for $|\Psi_{a,b}; A''_2; 0; 1^{--}\rangle$ use $(\mathbf{a}, \mathbf{b}) = (0.35, 1.9)$ and are displayed with blue squares.

and $|\Psi_{a,b}; A'_2; 1; J^{\pm-}\rangle$ are investigated up to $J = 3$. However, states $|\Psi_{a,b}; A''_2; 1; J^{\pm-}\rangle$ are not considered, as they involve significantly more computations of matrix elements on unsymmetrical states, leading to a substantial increase in computational cost. The resulting three-gluon glueball masses, expressed in unit of $\sqrt{\sigma}$, are presented in Table 9.5. For comparison, Figure 9.6 displays these masses alongside results from LQCD. Masses are normalized to the lowest state, 1^{+-} . Several observations support a relatively good agreement between the current calculation and LQCD results [166, 167].

- The lowest 1^{+-} and 3^{+-} three-gluon glueballs obtained using the helicity formalism appear at the correct energy. However, the helicity formalism predicts a pair of states, whereas LQCD predicts only a single state [166, 167].
- The lowest 2^{+-} glueball is found with the same hierarchy in both approaches. However, its energy is 10% lower using the helicity formalism. Unlike the lowest 1^{+-} and 3^{+-} , the 2^{+-} does not exhibit a nearby secondary state, but this is an artifact resulting from the omission of $|\Psi_{a,b}; A''_2; 1; J^{\pm-}\rangle$ states in the analysis. The 10% discrepancy may be explained by this omission : including $|\Psi_{a,b}; A''_2; 1; 2^{+-}\rangle$ could slightly shift the 2^{+-} average energy. It may also stem from the simplicity of the Hamiltonian used, which does not account for spin interactions.
- For negative parity, the first excited 1^{--} state predicted by the helicity formalism appears similar to the lowest 1^{--} observed in LQCD. As for 2^{+-} , the relative energy is around 5% too low. This discrepancy can likely be explained with the same arguments as for the 2^{+-} state.
- Finally, a 3^{--} state analogous to the one observed in LQCD is also predicted. In this case, energies from the helicity formalism and LQCD are in good agreement.

On the other hand, the spectrum depicted by the helicity formalism does not fully align with the LQCD results. In particular, the helicity formalism predicts states that are not observed in LQCD. Overall, the helicity spectrum appears to exhibit near- parity degeneracy, whereas the LQCD spectrum clearly separates into two distinct columns.

- Low-lying 1^{--} and 3^{--} three-gluon glueballs are predicted by the helicity formalism. These states appear, roughly speaking, at the same energy than their positive parity counterparts. According to [166, 167], in LQCD, the lowest 1^{--} and 3^{--} lie well above the lowest 1^{+-} and 3^{+-} .

- On the positive parity side, the helicity formalism predicts 1^{+-} and 3^{+-} states in the vicinity of the lowest 2^{+-} glueball. Again, such states are absent in references [166, 167].

Several explanations can be proposed for this discrepancy. On the one hand, constituent approaches are known to sometimes overestimate the number of resonances. However, this effect typically impacts excited states rather than low-lying ones. On the other hand, it is possible that LQCD methods have missed a few states due to the challenges in interpreting the signal and in performing the continuum limit. For example, it seems that a more recent study of LQCD results observes an excited 1^{+-} glueball state whose energy is consistent with the one obtained using the helicity formalism [193].

For two-gluon glueballs, which lies in the $C = +$ part of the spectrum, it is already known that helicity degrees of freedom are necessary to reproduce the lattice spectrum [152]. It would be interesting to compare the $C = -$ glueball spectrum obtained with helicity degrees of freedom in the present model to the $C = -$ spectrum obtained when longitudinal spin components for the gluon are included. Fortunately, such results have already been published [194, 142]. However, the Hamiltonian considered in these studies includes spin interactions. To ensure a fair comparison, eigenenergies from the dimensionless Hamiltonian (9.42) are computed considering three spin-1 particles and using the OBE developed in Chapter 2 [28, 29]. Figure 9.5 illustrates the comparison. Energies are again given in units of the lowest 1^{+-} state. LQCD results from reference [193] are also included. It is immediately apparent that the spectrum computed with spin degrees of freedom exhibits several flaws.

- Positive parity states are all degenerate, whereas LQCD predicts a definite hierarchy for the lowest J^{+-} glueball states. In particular, spin degrees of freedom predict a low-lying 0^{+-} glueball, which LQCD calculations place at a higher energy.
- On the negative parity side, the 1^{--} and 3^{--} spin eigenstates share the same energy, while the 2^{--} state lies significantly higher. In contrast, LQCD calculations predict nearly degenerated states with a soft ordering in ascending total angular momentum.

On the other hand, using helicity degrees of freedom better reproduces the overall spectrum, apart from the aforementioned inaccuracies and extra states. As with two-gluon glueballs [152], it appears that constituent gluons should be treated as particles endowed with massless helicity quantum numbers.

The previous analysis focused on the relative spectrum. To obtain a genuine energy spectrum requires to fix the mesonic string tension σ_m . The best agreement with LQCD results is achieved for a value of $\sigma_m = 0.086\text{GeV}^2$, which seems a factor 2 smaller compared to the values found in

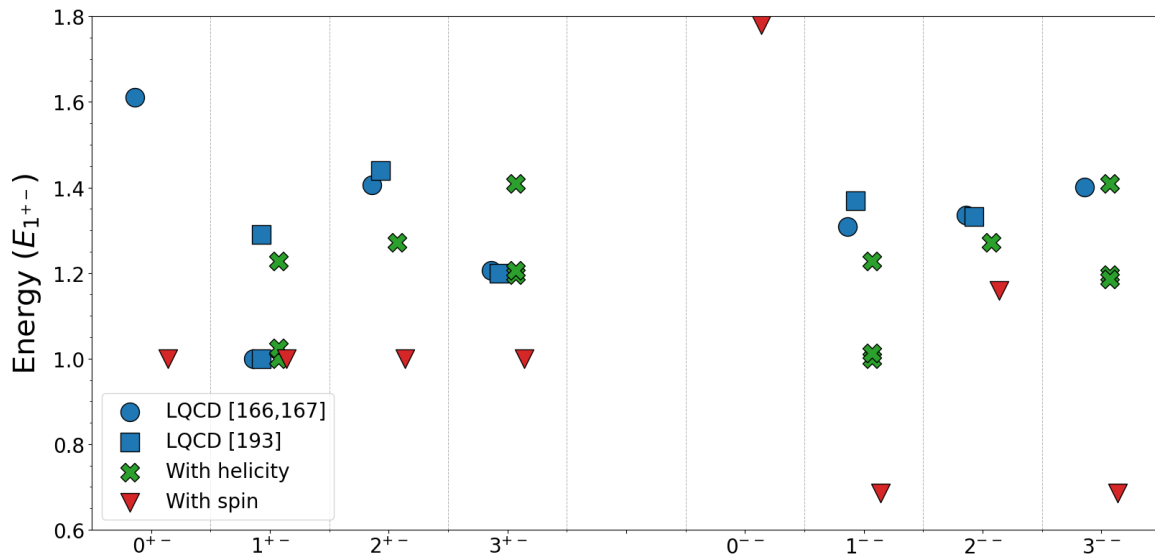


Figure 9.5: Comparison of low-lying negative charge conjugation glueball spectra computed using different approaches. Blue dots and squares represent the results from the LQCD calculations from references [166, 167] and [193], respectively. Red triangles correspond to results obtained by considering three spin-1 particles governed by the Hamiltonian (9.42). Finally, green crosses are obtained by considering helicity degrees of freedom for the constituent gluons. Masses are normalized to the 1^{+-} state.

State	Opt. b	Opt. a	E
$ \Psi; A'_2; 0; 1^{\pm-}\rangle$	1.80	0.35	10.020
$ \Psi; A''_2; 0; 1^{+-}\rangle$	1.95	0.45	10.269
$ \Psi; A''_2; 0; 1^{--}\rangle$	1.90	0.35	10.151
$ \Psi; A'_2; 0; 3^{\pm-}\rangle$	2.25	0.55	11.990
$ \Psi; A''_2; 0; 3^{+-}\rangle$	2.30	0.55	12.090
$ \Psi; A''_2; 0; 3^{--}\rangle$	2.25	0.50	11.881
$ \Psi; A'_2; 1; 1^{\mp-}\rangle$	2.40	0.6	12.305
$ \Psi; A'_2; 1; 2^{\mp-}\rangle$	2.40	0.6	12.742
$ \Psi; A'_2; 1; 3^{\mp-}\rangle$	2.65	0.95	14.113

Table 9.5: Display of the dimensionless three-gluon glueball spectrum obtained by using the three-body helicity formalism. Energies are given in unit of $\sqrt{\sigma}$. Only a single trial state is considered and the optimisation on variational parameters **a** and **b** is performed. Calculations are performed until $J = 3$ and $|\mu| = 1$. Only one of the two states with $|\mu| = 1$ is considered (namely, A'_0). All integrals are computed with 30 point, except for those on \bar{v} which use 100 points. The sum in j_{12} is truncated at $j_{12} = 20$.

the literature (see for instance [39, 144, 152, 156]). This issue can be addressed by reasonably modifying the Hamiltonian (9.37). In baryon studies, it is common to complement the potential with a constant term, particularly when dealing with light quarks [39]. Replacing the potential (9.39) with

$$V(r) = \sigma r - \frac{3\alpha_s}{2r} + C \quad (9.62)$$

were $\sigma = 0.150\text{GeV}^2$, $\alpha_s = 0.450$ and $C = -0.375\text{GeV}$ results in the spectrum displayed in Figure 9.7. The agreement between absolute spectra is as good as that for relative spectra, and the parameters used are more consistent with values typically found in the literature. It is also important to notice that the methodology employed in this work inherently provides approximate results. This approximate character may also explain the discrepancies observed in both spectra.

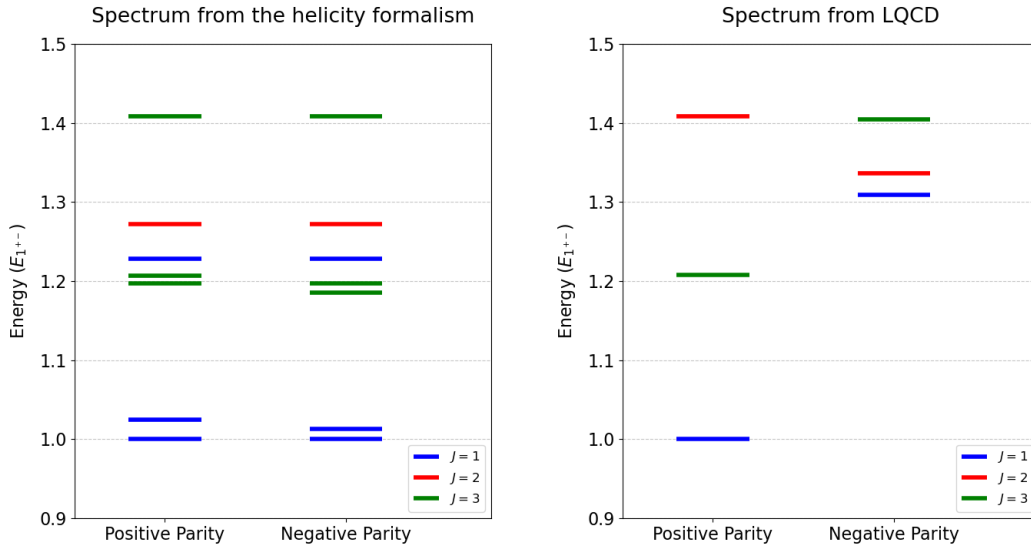


Figure 9.6: Comparison of glueball spectra obtained using the helicity formalism (left, this work) and LQCD (right, references [166, 167]). In both cases, spectra are provided in unit of the lowest mass. Concerning calculations with the helicity formalism, a strong coupling constant $\alpha_s = 0.450$ has been used.

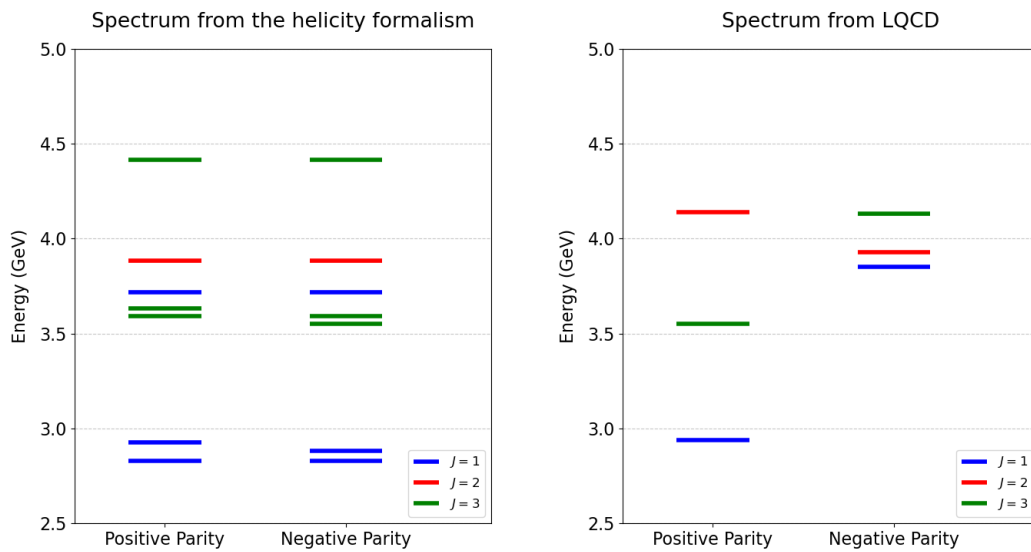


Figure 9.7: Comparison of glueball spectra obtained using the helicity formalism with the modified potential (9.62) (left, this work) and quenched LQCD (right, references [166, 167]). In both cases, spectra are provided in GeV.

9.4 Outlooks for the glueball spectrum

The previous chapters illustrated that the framework of constituent approaches combined with the two- and three-body helicity formalism enables to explore the two- and three-gluon glueball spectra. Especially, a definite methodology able to infer a spectrum for helicity states and based on the variational theorem has been set up for both two- and three-body systems.

Concerning two-gluon glueballs, the spectrum obtained using the helicity formalism is compatible with LQCD calculations. This agreement gives credit in the method and motivated the generalisation to three-gluon glueballs. Although similar calculations are already present in the literature [51, 152, 171], the perspective introduced in Chapter 7 proves different, and enables a more straightforward generalisation to three-gluon systems.

The situation concerning three-gluon glueballs is less conclusive. In units of the meson string tension, the helicity formalism proves able to reproduce the spectrum from LQCD with a satisfying accuracy but predicts supplementary states whose origin remains elusive. The comparison with calculations involving three spin-1 particles favoured the use of helicity degrees of freedom. When comparing spectra in physical units, a mesonic string tension too low by a factor of 2 compared to its standard value is to be used. This flaw can be overcome by adding a constant term in the potential in agreement with the potential used in baryons [39]. Although it allows to use parameter values in their physical range, it slightly deteriorates the agreement with LQCD. In addition, this parameter was not necessary to describe two-gluon glueballs.

Additional research may help unveiling the origin of these discrepancies. Improvements about the accuracy of the resolution method in the case of three-gluon glueballs may give credit to the spectrum obtained using the helicity formalism. Including more trial states in the resolution to test the convergence, truly implementing the possibility of mixing between the different symmetrical states, increasing the number of points in the quadrature or increasing the cut-off in j_{12} are all trails to reach this goal. Hamiltonian (9.37) may also be refined and complemented, for instance, with spin-based interactions. A more detailed study of the role of three-body forces could also be considered. This may help to decide whether the extra states predicted by the current methodology are artifacts of the resolution method or not.

Setting aside the question of the extra states, the solutions obtained using the helicity formalism may also yield additional insights into glueball properties. For instance, effort could be directed toward evaluating observables beyond the energy, such as decay rates.

Complement 9.A Symmetry considerations about equation (9.27)

First of all, let us have a quick look at coefficients (9.29),

$$\begin{aligned} & \left(\mathcal{C}_{J\bar{\mu};\bar{\lambda}_1\bar{\lambda}_2\bar{\lambda}_3}^{j_{12}\lambda_{12}} \right)^* \mathcal{C}_{J\mu;\lambda_1\lambda_2\lambda_3}^{j_{12}\lambda_{12}} \\ &= (-1)^{(\lambda_2-\bar{\lambda}_2)/2+(\bar{\lambda}_1-\lambda_1)/2+(\bar{\mu}-\mu)/2} \frac{2j_{12}+1}{2} d_{\bar{\mu}\lambda_{12}-\lambda_3}^J(\pi/2) d_{\mu\lambda_{12}-\lambda_3}^J(\pi/2). \end{aligned} \quad (9.63)$$

These coefficients are easily shown to stay real, independently of the spin of the particles. If μ or $\bar{\mu}$ is null, properties of Wigner d matrices allows to show that, as long as $J - \lambda_{12} + \lambda_3$ is an odd number, the whole coefficient cancels [35]. Because λ_3 belongs to $\{+1, -1\}$ and because the total angular momentum of a symmetric state with $\mu = 0$ must be odd, whenever μ or $\bar{\mu}$ is null, all terms with odd λ_{12} cancel, thereby avoiding evaluating them.

The dependency on helicity quantum numbers of the $\tilde{\Psi}$ function (9.28) can be investigated. The symmetry properties of Wigner d matrices allow to equate different evaluations of $\tilde{\Psi}$. Following equalities immediately comes out of these symmetry properties,

$$\begin{aligned} \tilde{\Psi}(\dots; j_{12}, \lambda_{12}, \Delta\lambda; \dots) &= \tilde{\Psi}(\dots; j_{12}, -\Delta\lambda, -\lambda_{12}; \dots) = (-1)^{\lambda_{12}} \tilde{\Psi}(\dots; j_{12}, -\lambda_{12}, -\Delta\lambda; \dots) \\ &= (-1)^{\lambda_{12}} \tilde{\Psi}(\dots; j_{12}, \Delta\lambda, \lambda_{12}; \dots). \end{aligned} \quad (9.64)$$

Other symmetries require Ψ to be an even function of u . In that case, performing the change of variables $u \rightarrow -u$ allows to show that

$$\begin{aligned} \tilde{\Psi}(\dots; j_{12}, \lambda_{12}, \Delta\lambda; \dots) &= (-1)^{j_{12}} \tilde{\Psi}(\dots; j_{12}, -\lambda_{12}, \Delta\lambda; \dots) = (-1)^{j_{12}} \tilde{\Psi}(\dots; j_{12}, -\Delta\lambda, \lambda_{12}; \dots) \\ &= (-1)^{j_{12}+\lambda_{12}} \tilde{\Psi}(\dots; j_{12}, \Delta\lambda, -\lambda_{12}; \dots) = (-1)^{j_{12}+\lambda_{12}} \tilde{\Psi}(\dots; j_{12}, \lambda_{12}, -\Delta\lambda; \dots). \end{aligned} \quad (9.65)$$

The assumption that requires Ψ to be even is consistent with the trial shape (9.12). However, it may be invalidated if kinematic factors such as those from relations (9.14) and (9.15) need to be included in order to ensure the symmetry of the state. Regardless of this precaution, relations (9.64) and/or (9.65) allow for the recycling of most evaluations of $\tilde{\Psi}$, thereby reducing computational cost. These eight symmetry relations can even show that $\tilde{\Psi}$ cancels for some combinations of quantum numbers, such as for $\Delta\lambda = 0$, λ_{12} even and j_{12} odd.

Finally, the matrix element on two-body J -helicity states appearing in the integrand from equation (9.27) is also to be analysed. Its dependence on helicity quantum numbers can be investigated by means of formula (7.11) from Section 7.1. Using properties of Clebsh-Gordan

coefficients, it can be shown that

$$\mathcal{C}_{l_{12}s_{12};\lambda_1\lambda_2}^{j_{12};11} = (-1)^{s_{12}} \mathcal{C}_{l_{12}s_{12};-\lambda_2-\lambda_1}^{j_{12};11} = (-1)^{l_{12}-j_{12}} \mathcal{C}_{l_{12}s_{12};-\lambda_1-\lambda_2}^{j_{12};11} \quad (9.66)$$

where \mathcal{C} coefficients are those defined in Section 7.1. Applying this result to equation (7.11) reveals that certain helicity quadruplets $(\lambda_1, \lambda_2, \bar{\lambda}_1, \bar{\lambda}_2)$ yield identical values. Specifically, these quadruplets can be grouped into five families, within which matrix elements on two-body J -helicity states are equal each-other. These families are displayed in Table 9.6. Let us also mention that, again in view of (7.11), these matrix elements are real-valued. This allows to freely exchange the bra and the ket,

$$\langle \bar{p}_{12}; j_{12}\lambda_{12}; \bar{\lambda}_1\bar{\lambda}_2 | \mathcal{O}(r_{12}) | p_{12}; j_{12}\lambda_{12}; \lambda_1\lambda_2 \rangle = \langle p_{12}; j_{12}\lambda_{12}; \lambda_1\lambda_2 | \mathcal{O}(r_{12}) | \bar{p}_{12}; j_{12}\lambda_{12}; \bar{\lambda}_1\bar{\lambda}_2 \rangle. \quad (9.67)$$

Observations about $\tilde{\Psi}$ and about the two-body matrix elements are to be combined to deduce symmetry properties of the whole integral from (9.27). Simplifications occur depending on the assumptions made on Ψ and $\bar{\Psi}$.

A special case of prime importance in the following concerns Ψ and $\bar{\Psi}$ being two equal real functions which are even for u . These assumptions imply two symmetry properties at the level of the integrals. First, the equality and reality hypothesis allows to freely exchange $\Delta\lambda$ and $\Delta\bar{\lambda}$ by exchanging both integration variables. On the other hand, the hypothesis about the parity in u implies that the sign of each $\Delta\lambda$ can be flipped, at worst, at the cost of a phase factor $(-1)^{j_{12}+\lambda_{12}}$. These two properties implies that integrals line up with the five families of helicity quadruplets from Table 9.6, except for the 5th family in which quadruplets above and below the dashed line differ by a $(-1)^{j_{12}+\lambda_{12}}$ phase factor. Each evaluation of an integral from (9.27) for a given helicity quadruplet provides a value valid for any other quadruplet in the same family, potentially up to a minus sign.

Apart from this special case, a second simplification turns out relevant for the upcoming developments. In the first family from Table 9.6, both $\Delta\lambda$ and $\Delta\bar{\lambda}$ are always zero. As a result and without further conditions, calculations for both helicity quadruplet in this family will yield identical values for integrals. This result will prove valuable, as the two helicity quadruplets in question are precisely those encountered during calculations with A_2'' states.

Complement 9.B Potential for three-gluon glueballs

The confining interactions between three gluons can be described in two main geometries. From the perspective discussed in the main text, each gluon generates two flux tubes that

1 st family	(+, +, +, +) (-, -, -, -)			
2 nd family	(+, +, -, -) (-, -, +, +)			
3 rd family	(-, +, -, +) (+, -, +, -)			
4 th family	(+, -, -, +) (-, +, +, -)			
5 th family	(+, -, +, +)	(+, +, +, -)	(+, -, -, -)	(-, -, +, -)
	(-, +, +, +)	(+, +, -, +)	(-, +, -, -)	(-, -, -, +)

Table 9.6: Table of the different helicities quadruplets $(\lambda_1, \lambda_2, \bar{\lambda}_1, \bar{\lambda}_2)$ that give rise to the same matrix element on two-body J -helicity states $\langle \bar{p}_{12}; j_{12} \lambda_{12}; \bar{\lambda}_1 \bar{\lambda}_2 | \mathcal{O}(r_{12}) | p_{12}; j_{12} \lambda_{12}; \lambda_1 \lambda_2 \rangle$.

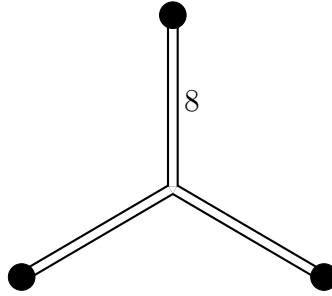


Figure 9.8: Schematic representation of a Y junction modelling three-gluon glueballs. The three gluons bound at once by pooling their three 8 flux tubes.

transform with the fundamental and the anti-fundamental representation of $SU(3)$. These flux tubes merge pairwise, in a so-called Δ junction. Alternatively, each gluon can be viewed as producing a single flux tube in the adjoint representation of $SU(3)$. In that case, the three flux tubes merge in a so-called Y junction [142], as illustrated in Figure 9.8. The Y junction consists in a genuine three-body interaction. In contrast with baryons, for glueballs, the Δ junction is not necessary an approximation of the Y one as both can be obtained by combining flux tubes in a globally colour-neutral configuration. Differences between Y and Δ junctions are discussed in [85, 195], with the conclusions favouring the Δ junction.

For comparison, let us consider here a Y junction. In this configuration, the interaction potential used in constituent approaches writes down as follows,

$$V(\mathbf{r}_1, \mathbf{r}_2, \mathbf{r}_3) = \min_{\mathbf{Y}} \sum_{i=1}^3 \sigma \langle F_i^2 \rangle |\mathbf{r}_i - \mathbf{Y}| + \sum_{i < j}^3 \frac{\alpha_s \langle F_i \cdot F_j \rangle}{|\mathbf{r}_i - \mathbf{r}_j|}. \quad (9.68)$$

Here, σ is the fundamental string tension, and α_s is the strong coupling constant. In agreement with the notations from Section 5.1.2, the factor $\langle F_i^2 \rangle$ corresponds to the $SU(3)$ Casimir operator acting on the i^{th} particle. Including this factor in the confining potential was referred to as the

Casimir scaling hypothesis in this section [150, 151, 149]. For flux tubes transforming under the fundamental or the anti-fundamental representation of $SU(3)$, this factor is shown to equal $4/3$, while for flux tubes transforming with the adjoint representation of $SU(3)$, it is shown to equal 3. The one-gluon exchange term includes a factor $\langle F_i \cdot F_j \rangle$ which combines the $SU(3)$ generators of particles i and j . In Section 5.1.1, it was computed using Gell-Mann matrices, as in equation (5.7). Its value can also be deduced from those of the Casimir,

$$\langle F_i \cdot F_j \rangle = \frac{\langle (F_i + F_j)^2 \rangle - \langle F_i^2 \rangle - \langle F_j^2 \rangle}{2}, \quad (9.69)$$

where $(F_i + F_j)^2$ is the $SU(3)$ Casimir operator for the pair of particles i and j . Substituting these factors for a system of three gluons leads to the following expression,

$$V(\mathbf{r}_1, \mathbf{r}_2, \mathbf{r}_3) = 3\sigma \min_{\mathbf{Y}} \sum_{i=1}^3 |\mathbf{r}_i - \mathbf{Y}| - \sum_{i<j}^3 \frac{3\alpha_s}{2|\mathbf{r}_i - \mathbf{r}_j|}. \quad (9.70)$$

The Y junction introduces a genuine three-body interaction, which is incompatible with the formalism developed in the current work. As proposed in reference [147], this three-body interaction can be approximated by three effective two-body interactions with a rescaling parameter close to $1/2$. The interaction then becomes

$$V(\mathbf{r}_1, \mathbf{r}_2, \mathbf{r}_3) = \frac{3}{2}\sigma \sum_{i<j}^3 |\mathbf{r}_i - \mathbf{r}_j| - \sum_{i<j}^3 \frac{3\alpha_s}{2|\mathbf{r}_i - \mathbf{r}_j|}. \quad (9.71)$$

To compare this with the potential (9.39) used in the Δ junction, one must relate the mesonic and the fundamental string tensions. For mesons, the Casimir scaling factor is $4/3$ for both the quark and the anti-quark flux tubes,

$$\sigma_m = \frac{4}{3}\sigma. \quad (9.72)$$

Expressing the interaction potential in terms of the mesonic string tension gives

$$V(\mathbf{r}_1, \mathbf{r}_2, \mathbf{r}_3) = \frac{9}{8}\sigma_m \sum_{i<j}^3 |\mathbf{r}_i - \mathbf{r}_j| - \sum_{i<j}^3 \frac{3\alpha_s}{2|\mathbf{r}_i - \mathbf{r}_j|}. \quad (9.73)$$

This potential differs from the Δ junction potential (9.39) by a factor of $9/8$. This factor, a little higher than 1, slightly increases the overall energy of the glueball if Y junction is considered. This conclusion aligns with the LQCD arguments from reference [195]. For this reason, a Δ junction is preferred in the present work.

This chapter in the context of a thesis

This final chapter concludes the document by reviewing the core innovative results obtained during my PhD thesis. All results presented in this section are original and directly address the central research question that guided the work [158]. These calculations also open the way to exploring properties beyond the glueball spectrum, which could serve as the basis of future research.

Conclusion and Outlooks

As a concluding section, let us briefly revisit the central thread that has run throughout this document. The journey began within the framework of non-relativistic quantum mechanics. After a short review of the formalism, a key tool for solving its equations, the variational theorem, was introduced. From this technique emerged the oscillator bases expansion (OBE) [29], a concrete and general method capable of solving the Hamiltonians encountered in the subsequent chapters. In the present work, the method was developed explicitly for three-body systems, in line with the scope of this document. Larger systems were addressed using the second resolution method explored herein, the envelope theory (ET). This user-friendly technique allows for the computation of approximate spectra in N -body systems at particularly low computational cost [65]. With some experience and intuition, gained by applying the method to various systems, the ET proves to be a reliable tool when fully precise energies are not required [54, 55]. This concluded the chapters devoted to general quantum mechanics.

The next two chapters focused the physics of hadrons. Following a brief historical overview, the classification of hadrons and their interpretation in terms of quarks were discussed. The concepts of flavour and colour were introduced following the historical sequence of their discovery. The chapter then offered a concise review of QCD, emphasising key features of the theory rather than delving into the technicalities of QFT. Topics such as the gluonic field, the one-gluon exchange transfer matrix, the running coupling constant, dynamical mass generation, the potentials derived from lattice QCD (LQCD), and the existence of exotic states were all briefly covered to provide a comprehensive overview of the low-energy QCD landscape. The subsequent chapter leveraged this background to establish a framework for studying hadrons, namely the constituent models. In these, hadrons are treated as bound states of constituent quarks and/or gluons governed by a phenomenological QCD-inspired Hamiltonian. After a detailed justification of this Hamiltonian, the framework was applied to baryons, illustrating its use by reproducing the experimental spectrum and examining the baryon internal structure.

In the third and final part, constituent approaches were applied to the study of glueballs. The framework was adapted to better accommodate special relativity and extended to handle

massless particles. This was done by employing the helicity formalism. Two-gluon states with definite symmetry properties were decomposed using a Lorentz covariant helicity basis. The variational theorem was then applied to evaluate the spectrum of the phenomenological Hamiltonian in the two-gluon centre of mass frame (CoMF). A comparison with LQCD results showed good agreement between the two approaches [158]. The remainder of the text focused on extending the model to three-gluon glueballs. This endeavour was more technical due to the additional degrees of freedom, the interplay between multiple reference frames, and the presence of two distinct helicity bases. After developing and reviewing the three-body helicity formalism, a spectrum for three-gluon glueballs was obtained. In this case, the agreement with LQCD was less definitive than for two-gluon systems. The global energy correspondence was more qualitative, and some states predicted by the model were not observed in LQCD. Nevertheless, the use of helicity formalism clearly improved the overall spectrum compared to traditional spin-based models [158]. It is also hoped that enhancing the resolution methods and refining the phenomenological Hamiltonian could improve this agreement. Beyond energy spectra, both two- and three-gluon calculations also offer access to eigenstates, which can be used to infer additional glueball properties.

Echoing to the introduction, I hope the reader is convinced that the initial objective, *studying of two-gluon and three-gluon glueballs within constituent models*, has been successfully addressed during this thesis. Of course, many open questions remain, and several future directions can be envisaged in the short- and medium-term to deepen the understanding of glueball properties. Although only briefly mentioned here, experimental efforts are currently underway to detect glueballs in particle accelerators. Achieving theoretical consensus across models and frameworks would provide a robust foundation for experimentalists in interpreting their data. This work contributes to that broader scientific effort. More generally, the tools developed herein can be applied to a range of other problems in hadronic physics. In the short term, the OBE will be used to investigate the internal structure of baryons, particularly in testing the validity of the diquark hypothesis. In the medium term, the OBE combined with the helicity formalism will be used to study hybrid baryons. These prospects, along with continued investigation into glueballs, suggest a promising future for constituent approaches in hadronic physics.

List of Abbreviations

12-CoMF	Centre-of-mass frame of particles 1 and 2
at.u.	Atomic units
CoMF	Centre-of-Mass frame
DGA	Double Gaussian approximation
DOSM	Dominantly orbital state method
ECoMF	Centre-of-Mass frame of the entire many-body system
ET	Envelope theory
HHE	Hyperspherical harmonic expansions
LMM	Lagrange mesh method
LQCD	Lattice quantum chromodynamics
$\overline{\text{MS}}$	Modified minimal subtraction
OBE	Oscillator bases expansions
PA	Poincaré algebra
PG	Poincaré group
PMP-coordinates	Pseudo-momentum perimetric coordinates
QCD	Quantum chromodynamics
QFT	Quantum field theory
SDE	Schwinger-Dyson equations
SGA	Single Gaussian approximation

Bibliography

- [1] H. Fritzsche and M. Gell-Mann. «Current Algebra: Quarks and What Else?» *eConf C720906V2* (1972), 135 (cited on pages vii, 156, 201).
- [2] V. Crede and C.A. Meyer. «The Experimental Status of Glueballs». *Prog. Part. Nucl. Phys.* 63 (2009), 74 (cited on pages vii, 201).
- [3] V. Mathieu, N. Kochelev, and V. Vento. «The Physics of Glueballs». *Int. J. Mod. Phys. E* 18 (2009), 1 (cited on pages vii, 156, 201).
- [4] BESIII Collaboration. «Determination of Spin-Parity Quantum Numbers of $X(2370)$ as 0^{-+} from $J/\psi \rightarrow \gamma K_S^0 K_S^0 \eta'$ ». *Phys. Rev. Lett.* 132 (2024), 181901 (cited on page vii).
- [5] D.J. Griffiths and D.F. Schroeter. *Introduction to Quantum Mechanics*. Cambridge: Cambridge University Press, 2018 (cited on pages ix, 3, 6, 19, 21, 35, 160).
- [6] C. Cohen-Tannoudji, B. Diu, and F. Laloë. *Quantum Mechanics*. Weinheim: Wiley-VCH, 2020 (cited on pages ix, 3, 6, 8, 14, 19, 35).
- [7] J.J. Sakurai and J. Napolitano. *Modern Quantum Mechanics*. Cambridge: Cambridge University Press, 2021 (cited on pages ix, 3).
- [8] F. Gieres. «Mathematical surprises and Dirac's formalism in quantum mechanics». *Rep. Prog. Phys.* 63 (2000), 1893 (cited on page 4).
- [9] M. Blau. *Symplectic Geometry and Geometric Quantization*. 1992 (cited on page 5).
- [10] M. Gattobigio, A. Kievsky, and M. Viviani. «Spectra of helium clusters with up to six atoms using soft-core potentials.» *Phys. Rev. A* 84 (2011), 052503 (cited on pages 8, 9, 62, 63, 66, 67).
- [11] S. Ishikawa. «Three-Body Potentials in α -Particle Model of Light Nuclei». *Few-Body Syst.* 58 (2017), 37 (cited on page 8).
- [12] F. Buisseret, C.T. Willemyns, and C. Semay. «Many-Quark Interactions: Large- N Scaling and Contribution to Baryon Masses». *Universe* 8 (2022), 311 (cited on pages 8, 9, 76).

- [13] M. Ferraris et al. «A three-body force model for the baryon spectrum». *Phys.Lett.B* 364 (1995), 231 (cited on pages 8, 9, 65).
- [14] V. Dmitrašinović. «Cubic Casimir operator of $SU_C(3)$ and confinement in the nonrelativistic quark model». *Phys.Lett.B* 499 (2001), 135 (cited on pages 8, 9).
- [15] S. Pepin and F. Stancu. «Three-body confinement force in hadron spectroscopy». *Phys. Rev. D* 65 (2002), 054032 (cited on pages 8, 9).
- [16] B. Desplanques et al. «The baryonic spectrum in a constituent quark model including a three-body force». *Z.Phys.A* 343 (1992), 331 (cited on page 8).
- [17] W. Pauli. «Über den Zusammenhang des Abschlusses der Elektronengruppen im Atom mit der Komplexstruktur der Spektren». *Z. Physik* 31 (1952), 765 (cited on page 10).
- [18] F.E. Close. *An Introduction to Quarks and Partons*. London: Academic Press, 1979 (cited on pages 12, 134, 138, 154, 156).
- [19] F. Stancu. *Group Theory in Subnuclear Physics*. Oxford: Oxford Science Publications, 1996 (cited on page 12).
- [20] A. Khare. *Fractional Statistics and Quantum Theory*. London: World Scientific, 2005 (cited on page 17).
- [21] M. Srednicki. *Quantum Field Theory*. Cambridge: Cambridge University Press, 2007 (cited on pages 17, 147–150, 160).
- [22] C. Semay and C.T. Willemyns. «Some specific solutions to the translation-invariant N -body harmonic oscillator Hamiltonian». *J.Phys.Commun* 5 (2021), 115002 (cited on pages 20, 75).
- [23] Y. Suzuki and K. Varga. *Stochastic Variational Approach to Quantum-Mechanical Few-Body Problems*. Heidelberg: Springer Berlin, 1998 (cited on pages 20, 24, 26–28, 210, 249).
- [24] J.K.L. MacDonald. «Successive Approximations by the Rayleigh-Ritz Variation Method». *Phys. Rev.* 43 (1933), 830 (cited on pages 23, 25).
- [25] J.L. Basdevant, A. Martin, and J.M. Richard. «Improved bounds on many-body Hamiltonians (II). Baryons from mesons in the quark model». *Nucl. Phys. B.* 343 (1990), 69 (cited on pages 26, 59–63, 105, 120).
- [26] Y. Ipekoğlu and S. Turgut. «An elementary derivation of the quantum virial theorem from Hellmann-Feynman theorem». *Eur. Phys. J.* 37 (2016), 045405 (cited on page 28).

- [27] C. Semay. «General comparison theorem for eigenvalues of a certain class of Hamiltonians». *Phys. Rev. A* 83 (2011), 024101 (cited on page 30).
- [28] B. Silvestre-Brac et al. *Quantum three body problems using harmonic oscillator bases with different sizes*. Internal report ISN 0066. 2020. arXiv: 2003.11028 [quant-ph] (cited on pages 33, 40, 41, 43, 48, 50, 66, 68, 267).
- [29] C. Chevalier and S. Youcef Khodja. «Three-Body Forces in Oscillator Bases Expansion». *Few-Body Syst.* 65 (2024), 86 (cited on pages 33, 67, 74, 76, 267, 277).
- [30] S. Fleck, B. Silvestre-Brac, and J.M. Richard. «Search for diquark clustering in baryons». *Phys. Rev. D* 38 (1988), 1519 (cited on pages 33, 44, 68, 168).
- [31] C. Semay and B. Silvestre-Brac. «Diquonia and potential models». *Z.Phys.C* 61 (1994), 271 (cited on pages 33, 44, 68, 72, 173).
- [32] C. Semay, F. Brau, and B. Silvestre-Brac. «Pentaquarks $uudd\bar{s}$ with One Color Sextet Diquark». *Phys. Rev. Lett.* 94 (2005), 062001 (cited on pages 33, 68).
- [33] E. Klempt and B.C. Metsch. «Multiplet classification of light-quark baryons». *Eur.Phys.J.A* 48 (2012), 127 (cited on pages 33, 68).
- [34] S. Noh, W. Park, and S.H. Lee. «Doubly heavy tetraquarks, $qq'\bar{Q}\bar{Q}'$, in a nonrelativistic quark model with a complete set of harmonic oscillator bases». *Phys. Rev. D* 103 (2021), 114009 (cited on pages 33, 68).
- [35] V.K. Khersonskii, A.N. Moskalev, and D.A. Varshalovich. *Quantum Theory Of Angular Momentum*. Singapore: World Scientific Publishing Co., 1988 (cited on pages 35–38, 46, 51, 52, 56, 69, 188, 231, 237, 238, 272).
- [36] M. Abramowitz and I.A. Stegun. *Handbook of Mathematical Functions with Formulas, Graphs, and Mathematical Tables*. New York: Dover Publications, Inc., 1964 (cited on pages 35, 39, 52, 68–70, 205).
- [37] W.-K. Tung. *Group Theory in Physics*. London: World Scientific, 1985 (cited on page 36).
- [38] T.A. Brody, G. Jacob, and M. Moshinsky. «Matrix Elements In Nuclear Shell Theory». *Nucl.Phys.* 17 (1960), 16 (cited on pages 37, 52).
- [39] S. Capstick and N. Isgur. «Baryons in a relativized quark model with chromodynamics». *Phys. Rev. D* 34 (1986), 2809 (cited on pages 37, 66, 163, 164, 167–169, 269, 271).
- [40] M. Moshinsky. *The Harmonic Oscillator in Modern Physics: from Atoms to Quarks*. New York: Gordon and Breach, Science Publishers, Inc., 1969 (cited on pages 37, 41).

- [41] B. Silvestre-Brac. «The cluster model and the generalized Brody-Moshinsky coefficients». *J.Physique* 46 (1985), 1087 (cited on pages 38, 71).
- [42] J. Raynal and J. Revai. «Transformation Coefficients in the Hyperspherical Approach to the Three-Body Problem». *Nuovo Cimento A (1965-1970)* 68 (1970), 612 (cited on pages 38, 39, 70).
- [43] T.K. Das. *Hyperspherical Harmonics Expansion Techniques*. New Delhi: Springer, 2016 (cited on pages 39, 52, 68).
- [44] P. Nunberg, D. Prospero, and E. Pace. «An application of a new harmonic-oscillator basis to the calculation of trinucleon ground-state observables». *Nucl.Phys.A* 285 (1977), 58 (cited on pages 40, 41).
- [45] T. Melde, W. Plessas, and B. Sengl. «Quark-model identification of baryon ground and resonant states». *Phys. Rev. D* 77 (2008), 114002 (cited on pages 41, 163, 169, 173).
- [46] A. Kievsky et al. «A high-precision variational approach to three- and four-nucleon bound and zero-energy scattering states». *J.Phys.G: Nucl.Part.Phys.* 35 (2008), 063101 (cited on page 58).
- [47] L.E. Marcucci et al. «The Hyperspherical Harmonics Method: A Tool for Testing and Improving Nuclear Interaction Models». *Front.Phys.* 8 (2020), 69 (cited on page 58).
- [48] D. Baye. «The Lagrange-mesh method». *Phys. Rep.* 565 (2015), 1 (cited on pages 58, 62–67).
- [49] J. Dohet-Eraly. Private communication. 2024 (cited on page 66).
- [50] V. Ariel Altschul, A. Fraenkel, and E. Finkman. «Effects of band nonparabolicity on twodimensional electron gas». *J.Appl.Phys.* 71 (1992), 4382 (cited on page 67).
- [51] A. Szczepaniak et al. «Glueball spectroscopy in a relativistic many-body approach to hadronic structure». *Phys. Rev. cLett.* 76 (1996), 2011 (cited on pages 67, 202, 271).
- [52] F. Brau. «Minimal length uncertainty relation and the hydrogen atom». *J.Phys.A:Math.Gen.* 32 (1999), 7691 (cited on page 67).
- [53] N. Laskin. «Fractional Schrödinger equation». *Phys. Rev. E* 66 (2002), 056108 (cited on page 67).
- [54] L. Cimino et al. «Tests of the Envelope Theory for Three-Body Forces». *Few-body Syst.* 65 (2024), 20 (cited on pages 68, 74, 76, 99, 100, 102–104, 110, 111, 127, 277).
- [55] L. Cimino et al. «Accuracy tests of the envelope theory». *Results Phys.* 58 (2024), 107470 (cited on pages 74, 76, 104, 106, 109, 123, 127, 277).

- [56] L. Cimino, C.T. Willemyns, and C. Semay. «Quark core-gluon model for heavy hybrid baryons». *Phys. Rev. D* 110 (2024), 034032 (cited on pages 74, 124, 176).
- [57] R.L. Hall. «Energy trajectories for the N -boson problem by the method of potential envelopes». *Phys. Rev. D* 22 (1980), 2062 (cited on pages 75, 77, 85, 87).
- [58] R.L. Hall. «A geometrical theory of energy trajectories in quantum mechanics». *J. Math. Phys.* 24 (1983), 324 (cited on pages 75, 77, 87).
- [59] R.L. Hall. «Kinetic potentials in quantum mechanics». *J. Math. Phys.* 25 (1984), 2708 (cited on pages 75, 77).
- [60] R.L. Hall, W. Lucha, and F.F. Schöberl. «Relativistic N -boson systems bound by pair potentials $V(r_{ij}) = g(r_{ij}^2)$ ». *J. Math. Phys.* 45 (2004), 3086 (cited on pages 75, 77).
- [61] B. Silvestre-Brac et al. «The quantum \mathcal{N} -body problem and the auxiliary field method». *J. Math. Phys.* 51 (2010), 032104 (cited on pages 75, 80).
- [62] B. Silvestre-Brac, C. Semay, and F. Buisseret. «The Auxiliary Field Method in Quantum Mechanics». *J. Math. Phys.* 4 (2012), P120601 (cited on pages 75, 82, 85, 99).
- [63] R.L. Hall and B. Schwesinger. «The complete exact solution to the translation-invariant N -body harmonic oscillator problem». *J. Math. Phys.* 20 (1979), 2481 (cited on page 75).
- [64] C. Semay. «Improvement of the envelope theory with the dominantly orbital state method». *Eur. Phys. J. Plus* 130 (2015), 156 (cited on pages 76, 92, 97, 99, 104).
- [65] C. Chevalier et al. «Improvement of the Envelope Theory for Systems with Different Particles». *Few-Body Syst.* 63 (2022), 40 (cited on pages 76, 112, 117, 118, 120, 121, 127, 277).
- [66] C. Semay. «Numerical Tests of the Envelope Theory for Few-Boson Systems». *Few-Body Syst.* 56 (2015), 149 (cited on pages 76, 89, 104).
- [67] C. Semay and L. Cimino. «Tests of the Envelope Theory in One Dimension». *Few-Body Syst.* 60 (2019), 64 (cited on pages 76, 104).
- [68] C. Semay, L. Cimino, and C. Willemyns. «Envelope theory for systems with different particles». *Few-Body Syst.* 61 (2020), 19 (cited on pages 76, 85, 112, 127).
- [69] C. Semay, F. Buisseret, and B. Silvestre-Brac. «Towers of hybrid mesons». *Phys. Rev. D* 79 (2009), 094020 (cited on pages 76, 124).
- [70] C. Semay et al. «Baryonic mass formula in large N_c QCD versus quark model». *Phys. Rev. D* 75 (2007), 096001 (cited on pages 76, 124).

- [71] C. Semay, F. Buisseret, and F. Stancu. «Mass formula for strange baryons in large N_c QCD versus quark model». *Phys. Rev. D* 76 (2007), 116005 (cited on pages 76, 124).
- [72] C. Semay and F. Buisseret. «Charm and bottom baryon masses in the combined $1/N_c$ and $1/m_Q$ expansion versus the quark model». *Phys. Rev. D* 78 (2008), 076003 (cited on pages 76, 124).
- [73] F. Buisseret and C. Semay. «Light baryon masses in different large- N_c limits». *Phys. Rev. D* 82 (2010), 056008 (cited on pages 76, 124).
- [74] F. Buisseret, N. Matagne, and C. Semay. «Spin contribution to light baryons in different large- N limits». *Phys. Rev. D* 85 (2012), 036010 (cited on pages 76, 124).
- [75] C. Semay and C. Willemyns. «Equivalent period for a stationary quantum system». *Results. Phys.* 14 (2019), 102476 (cited on pages 76, 124).
- [76] C. Semay and C.T. Willemyns. «Quasi Kepler's third law for quantum many-body systems». *Eur. Phys. J. Plus* 136 (2021), 342 (cited on pages 76, 124).
- [77] Y. Chargui, A. Dhabbi, and A. Trabelsi. «Exact analytical treatment of the asymmetrical spinless Salpeter equation with a Coulomb-type potential». *Phys. Scr.* 90 (2015), 015201 (cited on pages 76, 124).
- [78] C. Semay and M. Balcaen. «The envelope theory as a pedagogical tool». *Eur. J. Phys.* 44 (2023), 035401 (cited on pages 76, 85, 106).
- [79] Y.A. Simonov. «Regge trajectories from QCD». *Phys. Lett. B* 226 (1989), 151 (cited on page 77).
- [80] Y.A. Simonov. «Baryon Regge trajectories from the area law of the Wilson loop». *Phys. Lett. B* 228 (1989), 413 (cited on page 77).
- [81] B. Silvestre-Brac, C. Semay, and F. Buisseret. «Auxiliary fields as a tool for computing analytical solutions of the Schrödinger equation». *J. Phys. A: Math. Theor.* 41 (2008), 275301 (cited on page 77).
- [82] B. Silvestre-Brac, C. Semay, and F. Buisseret. «Extensions of the auxiliary field method to solve Schrödinger equations». *J. Phys. A: Math. Theor.* 41 (2008), 425301 (cited on page 77).
- [83] B. Silvestre-Brac, C. Semay, and F. Buisseret. «Semirelativistic Hamiltonians and the Auxiliary Field Method». *Int. J. Mod. Phys. A* 24 (2009), 4695 (cited on page 77).

- [84] B. Silvestre-Brac, C. Semay, and F. Buisseret. «The auxiliary field method and approximate analytical solutions of the Schrödinger equation with exponential potentials». *J. Phys. A: Math. Theor.* 42 (2009), 245301 (cited on page 77).
- [85] F. Buisseret, C. Semay, and B. Silvestre-Brac. «Some equivalences between the auxiliary field method and envelope theory». *J. Math. Phys.* 50 (2009), 032102 (cited on pages 77, 274).
- [86] C. Semay and L. Ducobu. «Quantum and classical probability distributions for arbitrary Hamiltonians». *Eur. J. Phys.* 37 (2016), 045403 (cited on pages 80, 84).
- [87] C. Semay and C. Roland. «Approximate solutions for N -body Hamiltonians with identical particles in D dimensions». *Res. Phys.* 3 (2013), 231 (cited on pages 81, 87, 91).
- [88] C. Semay and G. Sicorello. «Many-Body Forces with the Envelope Theory». *Few-Body Syst.* 59 (2018), 119 (cited on pages 81, 82, 99, 100).
- [89] A.A. Lobashev and N.N. Trunov. «A universal effective quantum number for centrally symmetric problems». *J. Phys. A* 42 (2009), 345202 (cited on page 88).
- [90] V. Ariel. *Effective Mass and Energy-Mass Relationship*. 2012. arXiv: 1205.3995 [physics.gen-ph]. URL: <https://arxiv.org/abs/1205.3995> (cited on page 90).
- [91] C. Semay. «Bounds for Hamiltonians with arbitrary kinetic parts». *Res. Phys.* 2 (2012), 114 (cited on page 90).
- [92] M.G. Olsson. «Universal behavior in excited heavy-light and light-light mesons». *Phys. Rev. D* 55 (1997), 5479 (cited on page 92).
- [93] C. Semay and F. Buisseret. «Two- and three-body calculations within the dominantly orbital state method». *Phy. Lett. A* 377 (2013), 1826 (cited on page 94).
- [94] C. Tourbez, C. Semay, and C. Chevalier. «Upper bounds for critical coupling constants for binding some quantum many-body systems». *Eur. Phys. J. Plus* 140 (2025), 520 (cited on pages 97, 124).
- [95] C. Semay and F. Buisseret. «Bound Cyclic Systems with the Envelope Theory». *Few-body Syst.* 58 (2017), 151 (cited on page 99).
- [96] F. Grasselli. «Variational approach to the soft-Coulomb potential in low-dimensional quantum systems». *Am. J. Phys.* 85 (2017), 834 (cited on page 106).
- [97] L. Cimino and C. Semay. «Compact Equations for the Envelope Theory». *Braz. J. Phys* 52 (2022), 45 (cited on pages 112, 115, 116, 127).

- [98] D.N. Makarov. «Coupled harmonic oscillators and their quantum entanglement.» *Phys. Rev. E* 97 (2018), 042203 (cited on page 118).
- [99] I. Salom and V. Dmitrašinović. «Relativistic Three-Body Harmonic Oscillator». *Lie Theory and Its Applications in Physics*. Ed. by V. Dobrev. Vol. 335. Springer Proceedings in Mathematics & Statistics. Springer Singapore, 2020, 473 (cited on page 120).
- [100] J.M. Lévy-Leblond. «Generalized uncertainty relations for many-fermion system.» *Phys. Lett. A* 26 (1968), 540 (cited on page 126).
- [101] A. de-Shalit and I. Talmi. *Nuclear Shell Theory*. London: Academic Press, 1963 (cited on page 127).
- [102] Y. Nambu. *Quarks: Frontiers in Elementary Particle Physics*. Singapore: World Scientific, 1985 (cited on page 131).
- [103] J. Richard. *Introduction à la physique des hadrons: symétries, structure et dynamique*. Paris: EDP Sciences, 2021 (cited on pages 131, 156).
- [104] J.J. Thomson. *The Corpuscular Theory of Matter*. New York: Charles Scribner's Sons, 1907 (cited on pages 131, 132).
- [105] E. Rutherford. «LXXIX. The scattering of α and β particles by matter and the structure of the atom». *The London, Edinburgh, and Dublin Philosophical Magazine and Journal of Science* 21 (1911), 669 (cited on page 132).
- [106] C.T. Walker and G.A. Slack. «Who Named the -ON's?» *Am. J. Phys.* 38 (1970), 1380 (cited on pages 132, 133).
- [107] L.B. Okun. «The theory of weak interaction». *1962 International Conference on High-Energy Physics at CERN*. Ed. by J. Prentki. 1962, 845 (cited on page 132).
- [108] J. Chadwick. «Possible Existence of a Neutron». *Nature* 129 (1932), 312 (cited on page 132).
- [109] M. Plank. «Über das Gesetz der Energieverteilung im Normalspectrum». *Ann. Physik* 2 (1901), 553 (cited on page 133).
- [110] A. Einstein. «Über einen die Erzeugung und Verwandlung des Lichtes betreffenden heuristischen Gesichtspunkt». *Ann. Physik* 322 (1905), 132 (cited on page 133).
- [111] P.A.M. Dirac. «The quantum theory of the electron». *Proc. R. Soc. Lond. A* 117 (1928), 610 (cited on page 133).
- [112] C.D. Anderson. «The Positive Electron». *Phys. Rev.* 43 (6 1933), 491–494 (cited on page 133).

- [113] L.M. Brown. «The idea of the neutrino». *Phys. Today* 31 (1978), 23 (cited on page 133).
- [114] C.L. Cowan et al. «Detection of the Free Neutrino: a Confirmation». *Science* 124 (1956), 103 (cited on page 133).
- [115] H. Yukawa. «On the Interaction of Elementary Particles». *Proc. Phys.-Math. Soc. Jpn.* 17 (1935), 48 (cited on page 133).
- [116] J.C. Street and E.C. Stevenson. «New Evidence for the Existence of a Particle of Mass Intermediate Between the Proton and Electron». *Phys. Rev.* 52 (1937), 1003 (cited on page 133).
- [117] C.M.G. Lattes, G.P.S. Occhialini H. Muirhead, and C.F. Powell. «Processes involving charged mesons». *Nature* 159 (1947), 694 (cited on page 133).
- [118] R. Bjorklund et al. «High Energy Photons from Proton-Nucleon Collisions». *Phys. Rev.* 77 (1950), 213 (cited on page 133).
- [119] A. Pais. «Some Remarks on the V -Particles». *Phys. Rev.* 86 (1952), 663 (cited on page 134).
- [120] T. Nakano and K. Nishijima. «Charge Independence for V -particles». *Progr. Theor. Phys.* 10 (1953), 581 (cited on page 134).
- [121] V. D. Hopper and S. Biswas. «Evidence Concerning the Existence of the New Unstable Elementary Neutral Particle». *Phys. Rev.* 80 (1950), 1099. DOI: 10.1103/PhysRev.80.1099 (cited on page 134).
- [122] D. R. Entem et al. *The Constituent Quark Model*. 2025. arXiv: 2504.07897 [hep-ph]. URL: <https://arxiv.org/abs/2504.07897> (cited on pages 134, 138, 148–151, 161, 166).
- [123] C. Amsler. *The Quark Structure of Hadrons: An Introduction to the Phenomenology and Spectroscopy*. Cham: Springer, 2018 (cited on pages 134, 136, 138, 144).
- [124] M. Gell-Mann. *The Eightfold Way: A Theory of strong interaction symmetry*. Internal report CTSL-20. 1961 (cited on page 134).
- [125] Y. Ne'eman. «Derivation of strong interactions from a gauge invariance». *Nuclear Physics* 26 (1961), 222 (cited on page 134).
- [126] M. Gell-Mann. «A schematic model of baryons and mesons». *Phys. Lett.* 8 (1964), 214 (cited on page 134).
- [127] G. Zweig. *An $SU(3)$ model for strong interaction symmetry and its breaking*. Internal report CERN-TH-412. 1964 (cited on page 134).

- [128] S. Navas et al. «Review of Particle Physics». *Phys. Rev. D* 110 (2024), 030001 (cited on pages 135–137, 170, 172, 174, 175).
- [129] W. Greiner and A. Schäfer. *Quantum chromodynamics*. Berlin: Springer, 1994 (cited on pages 147–150).
- [130] W. Lucha, F.F. Schöberl, and D. Gromes. «Bound states of quarks». *Phys. Rep.* 200 (1991), 127 (cited on pages 147, 150, 151, 161, 167, 214, 215).
- [131] G. Eichmann et al. «Baryons as relativistic three-quark bound states». *Prog. Part. Nucl. Phys.* 91 (2016), 1 (cited on pages 149, 153, 154).
- [132] CMS Collaboration. «Measurement of the inclusive 3-jet production differential cross section in proton–proton collisions at 7 TeV and determination of the strong coupling constant in the TeV range». *Eur. Phys. J. C* 75 (2015), 186 (cited on pages 150, 152).
- [133] S. Bethke. «Results from ATLAS and CMS: Strong Interactions and New Physics». *Proceedings of 54th International Winter Meeting on Nuclear Physics — PoS(BORMIO2016)*. Vol. 272. 2016, 042 (cited on pages 150, 152).
- [134] J.M. Cornwall. «Dynamical mass generation in continuum quantum chromodynamics». *Phys. Rev. D* 26 (1982), 1453 (cited on pages 153, 206).
- [135] R. Williams, C.S. Fischer, and W. Heupel. «Light mesons in QCD and unquenching effects from the 3PI effective action». *Phys. Rev. D* 93 (2016), 034026 (cited on page 154).
- [136] G.S. Bali. «QCD forces and heavy quark bound states». *Physics Reports* 343 (2001), 1 (cited on pages 154, 155).
- [137] N. Hüsken, E.S. Norella, and I. Polyakov. *A Brief Guide to Exotic Hadrons*. to appear in *Mod. Phys. Lett. A*. 2025. arXiv: 2410.06923 [hep-ph]. URL: <https://arxiv.org/abs/2410.06923> (cited on page 156).
- [138] N. Boulanger et al. «Constituent gluon interpretation of glueballs and gluelumps». *Eur. Phys. J. A* 38 (2008), 317 (cited on pages 156, 201, 207, 242, 244).
- [139] C.G. Darwin. «LI. The dynamical motions of charged particles». *Philos. Mag.* 39 (1920), 537 (cited on page 162).
- [140] F. Brau and C. Semay. «Light meson spectra and instanton-induced forces». *Phys. Rev. D* 58 (1998), 034015 (cited on page 163).
- [141] F. Brau, C. Semay, and B. Silvestre-Brac. «Unified meson-baryon potential». *Phys. Rev. C* 66 (2002), 055202 (cited on page 163).

- [142] V. Mathieu, C. Semay, and B. Silvestre-Brac. «Semirelativistic potential model for three-gluon glueballs». *Phys. Rev. D* 77 (2008), 094009 (cited on pages 163, 167, 206, 267, 274).
- [143] R.K. Bhaduri, L.E. Cohler, and Y. Nogami. «A Unified Potential for Mesons and Baryons». *Nuovo Cimento A* 65 (1981), 376 (cited on pages 163, 167–169, 172, 174, 175).
- [144] L. Theußl et al. «Hadronic decays of N and Δ resonances in a chiral quark model». *Eur. Phys. J. A* 12 (2001), 91 (cited on pages 163, 167–170, 172, 173, 269).
- [145] T.T. Takahashi et al. «Three-Quark Potential in $SU(3)$ Lattice QCD». *Phys. Rev. Lett.* 86 (2001), 18 (cited on page 164).
- [146] T.T. Takahashi et al. «Detailed analysis of the three-quark potential in $SU(3)$ lattice QCD». *Phys. Rev D* 65 (2002), 114509 (cited on page 164).
- [147] B. Silvestre-Brac et al. «The baryonic Y -shape confining potential energy and its approximants». *Eur. Phys. J. C* 32 (2003), 385 (cited on pages 165, 275).
- [148] F. Buisseret, V. Mathieu, and C. Semay. «Glueball phenomenology and the relativistic flux tube model». *Phys. Rev. D* 80 (2009), 074021 (cited on page 166).
- [149] P. Bicudo, M. Cardoso, and O. Oliveira. «Study of the gluon-quark-antiquark static potential in $SU(3)$ lattice QCD». *Phys. Rev. D* 77 (2008), 091504 (cited on pages 166, 275).
- [150] G.S. Bali. «Casimir scaling of $SU(3)$ static potentials». *Phys. Rev. D* 62 (2000), 114503 (cited on pages 166, 275).
- [151] C. Semay. «About the Casimir scaling hypothesis». *Eur. Phys. J. A* 22 (2004), 353 (cited on pages 166, 209, 275).
- [152] V. Mathieu, F. Buisseret, and C. Semay. «Gluons in glueballs: Spin or helicity?» *Phys. Rev. D* 77 (2008), 114022 (cited on pages 167, 194, 196, 202, 206–210, 212, 257, 262, 267, 269, 271).
- [153] M. Sreelakshmi and A. Ranjan. «Models and potentials in hadron spectroscopy». *J. Phys. G: Nucl. Part. Phys.* 50 (2023), 073001 (cited on page 167).
- [154] L.P. Fulcher. «Matrix representation of the nonlocal kinetic energy operator, the spinless Salpeter equation and the Cornell potential». *Phys. Rev. D* 50 (1994), 447 (cited on pages 167, 214, 215).
- [155] B. Silvestre-Brac. «Spectrum and Static Properties of Heavy Baryons». *Few-Body Systems* 20 (1996), 1 (cited on pages 168, 169, 172–174).

- [156] F. Giannuzzi. «Heavy pentaquark spectroscopy in the diquark model». *Phys. Rev. D* 99 (2019), 094006 (cited on pages 173, 269).
- [157] M. Jacob and G.C. Wick. «On the General Theory of Collisions for Particles with Spin». *Ann. Phys.* 7 (1959), 404 (cited on pages 181, 189, 190, 193, 194).
- [158] Cyrille Chevalier and Vincent Mathieu. *Two- and Three-gluon Glueballs within the Helicity Formalism*. To appear in *Phys. Rev. D*. 2025. arXiv: 2503.15146 [hep-ph]. URL: <https://arxiv.org/abs/2503.15146> (cited on pages 181, 202, 217, 276, 278).
- [159] S. Weinberg. *The Quantum Theory of Fields*. New York: Cambridge University Press, 1995 (cited on pages 182, 183, 189, 199, 236).
- [160] A.D. Martin and T.D. Spearman. *Elementary Particle Theory*. Amsterdam: North-Holland Publishing Co., 1970 (cited on pages 182, 188–190, 194, 219, 236).
- [161] S.-U. Chung. *Spin formalisms*. CERN-71-08. 1971 (cited on pages 188, 190, 194–196, 218–221).
- [162] D.R. Giebink. «Relativity and spin in one-, two- and three-body systems». *Phys. Rev. C* 32 (1985), 502 (cited on pages 190, 194).
- [163] G.C. Wick. «Angular Momentum States for Three Relativistic Particles». *Ann. Phys.* 18 (1962), 65 (cited on pages 194, 225, 226).
- [164] N.H. Lindner, A. Peres, and D.R. Terno. «Wigner’s little group and Berry’s phase for massless particles». *J. Phys. A* 36 (2003), 449 (cited on pages 199, 227).
- [165] F.J. Llanes-Estrada. «Glueballs as the Ithaca of meson spectroscopy». *Eur. Phys. J. Spec. Top* 230 (2021), 1575 (cited on page 201).
- [166] Y. Chen et al. «Glueball spectrum and matrix elements on anisotropic lattices». *Phys. Rev. D* 73 (2006), 014516 (cited on pages 201, 210–212, 266–268, 270).
- [167] C.J. Morningstar and M. Peardon. «Glueball spectrum from an anisotropic lattice study». *Phys. Rev. D* 60 (1999), 034509 (cited on pages 201, 210, 212, 244, 245, 266–268, 270).
- [168] H.B. Meyer and M.J. Teper. «Glueball Regge trajectories and the pomeron: a lattice study». *Phys. Lett. B* 605 (2005), 344 (cited on pages 201, 210–212).
- [169] D.Q. Liu and J.M. Wu. «The first calculation for the mass of the ground 4^{++} glueball state on lattice». *Mod. Phys. Lett. A* 17 (2002), 1419 (cited on pages 201, 210, 211).
- [170] V. Petrov and N. Tkachenko. *Odderon: Lost or/and Found?* 2022. arXiv: 2201.06948 [hep-ph]. URL: <https://arxiv.org/abs/2201.06948> (cited on page 201).

- [171] A.P. Szczepaniak and E.S. Swanson. «The low-lying glueball spectrum». *Phys. Lett. B* 577 (2003), 61 (cited on pages 202, 271).
- [172] D. Eyre and J.P. Vary. «Solving momentum-space integral equations for quarkonia spectra with confining potentials». *Phys. Rev. D* 34 (1986), 3467 (cited on pages 204, 205).
- [173] H. Hersbach. «Relativistic linear potential in momentum space». *Phys. Rev. D* 47 (1993), 3027 (cited on pages 205, 206).
- [174] J.W. Norbury, D.E. Kahana, and K.M. Maung. «Confining potential in momentum space». *Can. J. Phys.* 70 (1992), 86 (cited on page 206).
- [175] A. Cucchieri et al. «Just how different are the $SU(2)$ and $SU(3)$ Landau-gauge propagators in the infrared regime?» *Phys. Rev. D* 76 (2007), 114507 (cited on page 206).
- [176] A.C. Aguilar, D. Binosi, and J. Papavassiliou. «Gluon and ghost propagators in the Landau gauge: Deriving lattice results from Schwinger-Dyson equations». *Phys. Rev. D* 78 (2008), 025010 (cited on page 206).
- [177] A. C. Aguilar and J. Papavassiliou. «Gluon mass generation without seagull divergences». *Phys. Rev. D* 81 (2010), 034003 (cited on page 206).
- [178] A.C. Aguilar et al. «Gluon mass scale through nonlinearities and vertex interplay». *Phys. Rev. D* 100 (2019), 094039 (cited on page 206).
- [179] M.Q. Huber. «Correlation functions of Landau gauge Yang-Mills theory». *Phys. Rev. D* 101 (2020), 114009 (cited on page 206).
- [180] M. N. Ferreira and J. Papavassiliou. *Gluon mass scale through the Schwinger mechanism*. 2025. arXiv: 2501.01080 [hep-ph]. URL: <https://arxiv.org/abs/2501.01080> (cited on page 206).
- [181] W.-S. Hou, C.-S. Luo, and G.-G. Wong. «Glueball states in a constituent gluon model». *Phys. Rev. D* 64 (2001), 014028 (cited on page 206).
- [182] C. Semay and B. Silvestre-Brac. «Comparison between relativistic, semirelativistic, and nonrelativistic approaches of quarkonium». *Phys. Rev. D* 46 (1992), 5177 (cited on page 207).
- [183] M. Shifman. *Instantons in Gauge Theories*. Singapore: World Scientific Publishing Co., 1994 (cited on page 209).
- [184] C. Semay et al. «Semirelativistic Lagrange mesh Calculations». *Phys. Rev. E* 64 (2001), 016703 (cited on pages 209, 214, 215).

- [185] S. Flügge. *Practical Quantum Mechanics*. Berlin: Springer, 1994 (cited on page 214).
- [186] R.J. Yáñez, W. Van Assche, and J.S. Dehesat. «Position and momentum information entropies of the D -dimensional harmonic oscillator and hydrogen atom». *Phys. Rev. A* 50 (1994), 3065 (cited on page 214).
- [187] S.M. Berman and M. Jacob. «Systematics of Angular and Polarization Distributions in Three-Body Decays». *Phys. Rev.* 139B (1965), 1023 (cited on pages 218–221, 228).
- [188] J. Werle. «Relativistic Partial Wave Expansions for Multi-Particle Processes». *Phys. Lett.* 4 (1963), 127 (cited on pages 219, 220).
- [189] M. Hesse. «Three-body bound-state calculations by the Lagrange-mesh method: Selection of a coordinate system». *Phys. Rev. E* 65 (2002), 046703 (cited on page 222).
- [190] D.C. Peaslee. «Absolute Selection Rules for Meson Decay». *Helv. Phys. Acta* 23 (1950), 845 (cited on page 245).
- [191] F.G. Fumi and L. Wolfenstein. «Allowed Final States for Annihilation into Three Photons». *Phys. Rev.* 90 (1953), 498 (cited on pages 245–247).
- [192] M. Hamermesh. *Group Theory and Its Application to Physical Problems*. New York: Dover Publications, Inc., 1989 (cited on pages 246, 247).
- [193] A. Athenodorou and M. Teper. «The glueball spectrum of $SU(3)$ gauge theory in $3 + 1$ dimensions». *J. High Energ. Phys.* 2020 (2020), 172 (cited on pages 267, 268).
- [194] F.J. Llanes-Estrada, P. Bicudo, and S.R. Cotanch. « J^{--} Oddballs and a Low Odderon Intercept». *Phys. Rev. Lett.* 96 (2006), 081601 (cited on page 267).
- [195] M. Cardoso and P. Bicudo. «First study of the three-gluon static potential in lattice QCD». *Phys. Rev. D* 78 (2008), 074508 (cited on pages 274, 275).